Seismic Ground Motion in Large Urban Areas

Edited by
Giuliano F. Panza
Ivanka Paskaleva
Concettina Nunziata

2004

Birkhäuser Verlag
Basel · Boston · Berlin

Reprint from Pure and Applied Geophysics
(PAGEOPH), Volume 161 (2004), No. 5/6

Editors

Giuliano F. Panza
Università degli Studi di Trieste
Dipartimento di Scienze della Terra
Via Weiss 4
34127 Trieste
Italy

e-mail: panza@dst.univ.trieste.it

Ivanka Paskaleva
Central Laboratory of Seismic Mechanics
and Earthquake Engineering
CLSMEE, BAS
Acad. G. Bonchev St., Bl. 3
1113 Sofia
Bulgaria

e-mail: paskalev@geophys.bas.bg

The Abdus Salam International Center for
Theoretical Physics, SAND group
Strada costiera 11
34100 Trieste
Italy

Concettina Nunziata
Università di Napoli Federico II
Dipartimento di Geofisica e Vulcanologia
Largo San Marcellino, 10
80138 Napoli
Italy

e-mail: conunzia@unina.it

A CIP catalogue record for this book is available from the Library of Congress,
Washington D.C., USA

Bibliographic information published by Die Deutsche Bibliothek:
Die Deutsche Bibliothek lists this publication in the Deutsche Nationalbibliographie; deatailed bibliographic data is available in the internet at <http://dnb.ddb.de>

ISBN-13:978-3-7643-7042-8 e-ISBN-13:978-3-0348-7355-0
DOI: 10.1007/978-3-0348-7355-0

www.birkhauser.ch

Contents

Pure appl. geophys. 161 (2004) 943–948
0033–4553/04/060943–06
DOI 10.1007/s00024-004-2485-6

Pure and Applied Geophysics

Preface

The Earth's population is expanding at a rate of 1.45% annually and has a strong tendency to pool in ever-larger and more complex urban settings. Governments at all levels and the scientific community must recognize that most of humanity will soon be living in cities. Each of the urban areas on our planet has a unique set of urban systems related to security, energy, water, nutrition, economics, and the environment. In the future the urban "system of systems" will become more vulnerable to the hazards of natural events such as earthquakes. The recent earthquakes prove again that for the urban areas to be safe and sustainable it is necessary to implement long-range urban planning and risk assessment tools that rely on an accurate and multidisciplinary urban modeling. We still need and must develop tools as hazard's scenarios, and subsequently we should map the parameters necessary for long-range improvement planning of the cities, which will play the role of infrastructure "keys." The challenge of urban hazard mapping is to predict the ground-motion effects related to various source, path and site characteristics not just at a single site but also over an extended region, and do so with an acceptable level of reliability. The difficulty of this challenge is manifested in the spatially irregular patterns of damage that are typically observed after major earthquakes.

This volume summarizes the main results achieved in the framework of the UNESCO-IUGS-IGCP project 414 "Realistic Modelling of Seismic Input for Megacities and Large Urban Areas," centered at the Abdus Salam International Center for Theoretical Physics. It addresses the problems of pre-disaster orientation like hazard prediction, risk assessment, and hazard mapping, in connection with seismic activity. The unequal distribution of damage and casualties from earthquakes, which often affects urban areas, gives rise to problems that are still a challenge that has fostered numerous studies on the estimation of the seismic ground motion before the occurrence of a damaging earthquake. This task requires the detailed knowledge of both the subsurface structure within the city and of the probable location and characteristics of seismic sources around it. On the other hand one must use theoretical methods and related computer codes that allow us the realistic and reliable simulation of the expected seismic ground motion. These numerical simulations play an important role, especially in areas of complex geology, and they can provide realistic synthetic waveforms at places where no recordings are available. Synthetics are compared with observations wherever

instrumental data are available. During recent years, several methods have been proposed for the theoretical estimation of the seismic response at a specific site.

This volume contains results obtained using tools which enable us to estimate realistic amplification effects in complex structures, exploiting the available knowledge relative to geotechnical, lithological and geophysical parameters, topography of the medium, tectonic, historical data, and seismotectonic models. The ground motion modeling technique applied in most of the papers proves that it is possible to investigate the local effects even at large epicentral distances, too often neglected event, taking into account both the seismic source and the propagation path effects.

This collection gathers original studies which offer quantitative information required for the design, construction and retrofitting of the built environment. In particular, these studies have a long-lasting impact on the reduction of the environmental hazard associated with the seismically active regions, and contribute to the definition of the source and response spectra to be used in the mosaic of the studied world seismic regions.

The accurate knowledge of subsoil structures and probable complex source mechanisms is used to study the local site effects in large urban areas and Megacities like: Algiers, Alexandria, Beijing, Bucharest, Cairo, Delhi, Napoli, Santiago de Cuba, Sofia, Thessaloniki and Zagreb. Alongside, a comparison with traditional methods for seismic microzoning is made for selected regions and cities.

The seismic microzoning of ***Santiago de Cuba***, by Alvarez *et al.* "Seismic microzoning of Santiago de Cuba: An approach by SH waves modelling" is performed using synthetic SH-waves seismograms calculated along four profiles in the basin of the city. The modeling is accomplished using a hybrid approach (modal summation for the path from the source to the local profile and finite differences for the local profile) for a maximum frequency of 1 Hz. An intention to reappraise the seismic potential of the geologic structures in the site of ***Algiers*** and its surroundings is presented by Harbi *et al.* "Seismicity and tectonic structures in the site of Algiers and its surroundings." The compilation of a working earthquake catalogue is made using all events reported in the available documentation and the tectonic setting of the zone under investigation. The available fault plane solutions are summarized taking into account the results of studies of the most recent earthquakes of the area. The paper highlights the great interest in the detailed and timely assessment of the seismic hazard of Algiers and its surroundings which is made possible by the realistic modeling of the scenario seismic input. The study by El Alami *et al.* "Seismicity of Morocco for the period of 1987–1994", analyzes the recent seismicity for ***Morocco*** and for the Northern Morocco Seismic Network (NMSNET). Mouayn *et al.* "Coda duration magnitude for the north of Morocco" developed and tested the first empirical coda-duration magnitude (MD). The probabilistic seismic hazard analysis for the eastern Rift area in northern Morocco by Ait Brahim *et al.* "Using active faults and seismicity

for the strong motion modeling in the eastern rif (northern Morocco)" is established on the basis of the seismicity database and marine seismic reflection profiles. A selected attenuation relationship is used to construct peak-ground acceleration contour maps for specific return periods and typical economic lifetimes of structures. The microzonation study by Parvez *et al.* "Microzonation and site specific ground motion modelling for Delhi city" in *Delhi Metropolitan City* by 2-D modeling of SH and P-SV waves is performed with a hybrid technique, based on the modal summation and the finite-difference scheme. Complete realistic seismograms are computed along two geological cross sections. Two earthquake sources (July 15, 1720, I = IX MM, M = 7.4, and August 27, 1960, M = 6.0) are used in the modeling. The main focus of the El Sayed *et al.*, paper "Seismicity and seismic hazard in ALEXANDRIA and its surroundings" is the modeling of the May 28, 1998 earthquake which occurred in the ***Egyptian coastal zone*** in the vicinity of Alexandria. To mitigate the seismic hazard effects in Alexandria City, different scenarios are constructed using the deterministic approach. Ground motion parameters and frequencies of their peaks are calculated for different focal mechanisms. The study carried out about the most vulnerable area along the Nile valley Cairo – Faiyoum "The Nile valley of Egypt: A major active graben that magnifies seismic waves" if different from the previous one "Seismicity and seismic hazard in ALEXANDRIA and its surroundings" shows that the loose soft alluvial sediments of the Nile Canyon are the main factors for potential damage, because they may strongly amplify the ground motion (e.g., the peak-ground acceleration, PGA, can increase by a factor varying from 3 to 13). Herak *et al.* "Amplification of horizontal strong ground motion in Zagreb (Croatia) for realistic earthquake scenarios" deal with the amplification of horizontal strong ground motion in ***Zagreb*** for realistic earthquake scenarios along a selected profile with a quite complex local geology. The examination of the complete synthetic waveforms, corresponding to a suite of sixteen, realistically chosen, source mechanisms, shows that, even for variations of the order of commonly observed uncertainties of dip and rake angles of the causative fault, both PGA and response spectra (RS) vary at some sites by more than a factor of two. An important result common to several papers, and well described in the Zagreb case study, is that, especially for strongly laterally heterogeneous structures, *local effects must be determined for each of the relevant sources, taking all associated uncertainties into account as completely as possible.* In the paper "Seismic ground motion in ***Napoli*** for the 1980 Irpinia earthquake" by Nunziata, the seismo-stratigraphic cross sections have been defined for studying local site seismic effects. Such study has been made with an hybrid approach (mode summation for the path from the source, and the finite-difference method for the local profile). Synthetic seismograms are validated with the 1980 Irpinia earthquake; a good example of strong shaking for Napoli, recorded 10 km from the modeled sites. Taking into account the stratigraphies and the available shear-

wave velocity profiles, six seismo-stratigraphic zones have been recognized in Napoli. From the computed realistic P-SV and SH-wave seismograms it is concluded that the pyroclastic soil cover causes an increase of the signal's amplitudes, and the spectral amplification ranges between 2 and 3 at about 1–3 Hz. In particular, at the historical center, characterized by several cavities, the frequency of the maximum spectral amplification is very close to the eigenfrequencies of the buildings heavily damaged by the 1980 earthquake. The paper by Nunziata *et al.* "Seismic characterization of Neapolitan soils" discusses a synthesis of literature and original shear-wave velocity measurements carried out at ***Napoli***. Detailed seismic wave velocity profiles versus depth have been obtained in typical lithostratigraphies with FTAN and Hedghegog methods by using Rayleigh surface waves recorded in refraction seismic surveys. A strong scattering of shear-wave velocity has resulted, even in the same formation, which suggests making measurements for each evaluation of response analysis or, alternatively, to make a parametric study which considers the wide range of variability of the Neapolitan pyroclastic products which are, practically, sands, from a geotechnical point of view, with different percentage of welding. The mapping of the seismic ground motion in ***Bucharest***, due to large intermediate-depth Vrancea earthquakes, is the result of Cioflan *et al.* studies "Deterministic approach for the seismic microzonation of Bucharest." As controlling records the accelerograms of the Magurele station, low-pass filtered at 1.0 Hz, of the three last major strong ($M_w > 6$) Vrancea earthquakes are considered. The hybrid method is used considering the double-couple seismic source approximation, scaled for the intermediate depth, and relatively simple regional (bedrock) and local structural models. The presence of alluvial sediments and the possible variation of the scenario event require the use of all three components of motion for a reliable determination of the seismic input. A new seismic microzonation map has been constructed. The scope of Moldoveanu *et al.* work "Microzonation of Bucharest: State-of-the-art" is to formulate a state-of-the-art of the microzonation of Bucharest. The statistics based on the historical records show that, in Vrancea, about three destructive subcrustal earthquakes ($M \sim 7.0$) occur each century. In these circumstances, the seismic microzonation of the city is important information to be considered by the decision-makers in order to establish the appropriate level of preparedness to the earthquake threat.

The seismic zoning for ***Thessaloniki*** by Triantafyllidis *et al.* is carried out in two parts. The paper "Part I: Theoretical site response estimation for microzoning purposes" estimates the theoretical site response along seven cross sections for several double-couple sources using the hybrid method. Synthetic accelerograms up to a maximum frequency of 6 Hz for all components of motion are calculated. The discussed cases confirm that the geometry and depth of the rock basement, along with the impedance contrast, are responsible for ground amplification phenomena such as edge effects and generation and entrapment of local surface

waves. In the paper "Part II: Comparison of theoretical and experimental site effects" the reliability and the quality of the theoretically estimated ground responses is tested with observed data. The comparison validates the synthetic modeling and demonstrates that in cases of complex geometries, the use of at least 2-D numerical simulations is required in order to evaluate reliable site effects. The realistic modeling of seismic wave ground motion and the estimation of site effects in ***Beijing*** City is done by Ding *et al.* in the papers "Realistic modeling of seismic wave ground motion in Beijing City" and "Estimation of site effects in Beijing City." In the paper "Realistic modeling of seismic wave ground motion in Beijing City," advanced algorithms for the calculation of synthetic seismograms in laterally heterogeneous anelastic media have been applied to model the ground motion in Beijing City. The synthetic signals are compared with the few available seismic recordings (1998, Zhangbei earthquake) and with the distribution of the observed macroseismic intensity (1976, Tangshan earthquake). In the paper "Estimation of site effects in Beijing City" the database of 3-D geophysical structures for Beijing City has been built up to model the seismic ground motion in the City, caused by the 1976 Tangshan and the 1998 Zhangbei earthquakes. The hybrid method, which combines the modal summation and the finite-difference algorithms, is employed in the simulation. The numerical results show that the thick Tertiary and Quaternary sediments are responsible of the severe amplification of the seismic ground motion. Such a result is well correlated with the abnormally high macroseismic intensity zone (Xiji area) associated to the 1976 Tangshan earthquake and with the records in Beijing, associated to the 1998 Zhangbei earthquake. The city of ***Sofia*** is exposed to a high seismic risk. The paper by Paskaleva *et al.* "Expert assessment of the displacement provoked by seismic events: Case study for the Sofia metropolitan area" combines the recent tectonic and geological information to characterize and estimate displacements using expert assessment. The lack of instrumental recordings for Sofia fostered the studies by Slavov *et al.* "Deterministic earthquake scenarios for the city of Sofia" to compute realistic synthetic seismic signals, due to several earthquake scenarios along chosen geological profiles crossing the city.

Acknowledgements

This volume has been made possible by the dedicated work of numerous reviewers whose time, conscientious efforts and scientific expert judgment have been oriented to improve the quality of this issue. As such Alptekin, Ansal, Aoudia, Benouar, Bielik, Borcherdt, Bruchev, Celebi, Dineva, Ding, Dobroka, El-Sayed, Frangov, Gao, Gaur, Ghafory-Ashtiany, Graves, Gusev, Herak, Jordanovski, Khosrow, Lindholm, Marmureanu, Mohan, Mollaioli, Paskaleva, Pitilakis, Radovanovic,

Radulian, Rangelow, Ranguelov, Sanò, Talaganov, Tezcan, Trifunac, Yanoskaya, Wu are warmly thanked for willingly accepting the above responsibility and providing competent reviews.

The Editors dedicate this issue to Dr. Attia El-Sayed who passed away on February 11, 2003.

Giuliano F. Panza
Dipartimento di Scienze della Terra
Via Weiss, 4
and
"Abdus Salam"
International Center for Theoretical Physics
SAND group
34127 Trieste
Italy
E-mail: panza@dst.units.it

Ivanka Paskaleva
CLSMEE-BAS
Acad. G. Bonchev 3
1113 Sofia
Bulgaria
E-mail: Paskalev@server.geophys.bas.bg

Concettina Nunziata
Dipartimento di Geofisica e Vulcanologia
Largo San Marcellino, 10
80138-Napoli
Italy
E-mail: conunzia@unina.it

Pure appl. geophys. 161 (2004) 949–967
0033–4553/04/060949–19
DOI 10.1007/s00024-003-2502-1

Pure and Applied Geophysics

Seismicity and Tectonic Structures in the Site of Algiers and its Surroundings: A Step Towards Microzonation

A. HARBI[1], S. MAOUCHE[1], A. AYADI[1,4], D. BENOUAR[2], G. F. PANZA[3,4] and H. BENHALLOU[1,5]

Abstract—We intend to reappraise the seismogenic potential of the geologic structures in the site of Algiers and its surroundings. A compilation of a working earthquake catalogue is first made using all events reported in all previous documentation available. However for the sake of homogeneity and a certain degree of reliability of the data, only revised seismic events with epicenter coordinates, magnitude and/or intensity are included. A tectonic setting of the zone under investigation and available fault plane solutions are presented. The results obtained in previous seismological studies of the most recent earthquakes of the area are also discussed. The findings highlight the great interest to be taken in the detailed and timely assessment of the seismic hazard of Algiers and its surroundings which is made possible by the realistic modelling of the scenario seismic input.

Key words: Algiers, seismicity, tectonics, earthquakes catalogue.

Introduction

Most of the northern Algerian cities lie in earthquake-prone zones. Algiers, Constantine, Oran, Guelma, Chlef (formerly El Asnam), M'sila and other important cities have been affected by damaging earthquakes in the last two centuries. Meanwhile the effect on earthquake risk of rapid urban growth is not well appreciated. The reduction of seismic risk requires a detailed microzonation of the urban areas and this must be preceded by a realistic seismic hazard assessment. For this purpose we analyze the tectonics and seismic potential in the Algiers area, taking into account the results obtained in previous research works carried out after the largest seismic events which occurred in Algiers. The identification of active faults, as

[1] Centre de Recherche en Astronomie, Astrophysique et Geophysique, BP. 63, Bouzaréah, Alger, Algeria.
[2] University of Algiers (USTHB), Civil Engineering Dpt., Alger, Algeria.
[3] Dipartimento di Scienze della Terra, Universita' di Trieste, Italy.
[4] The Adus Salam International Centre for Theoretical Physics, SAND Group, Trieste, Italy.
[5] Faculté des Sciences de la Terre de l'Aménagment du Territoire et de la Géographie, USTHB, Alger, Algeria.

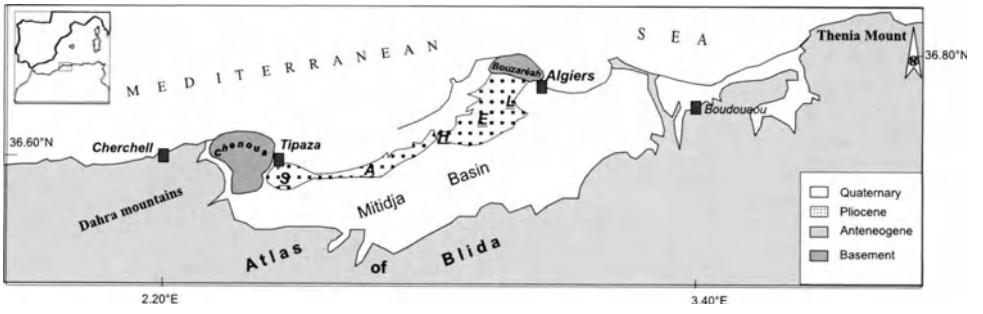

Figure 1
Geologic scheme of Algiers area showing the Sahel anticline.

earthquake sources, is essential for seismic hazard evaluation. Therefore a tectonic setting of the region under study is presented and used to complement a working earthquake catalogue. The catalogue includes all earthquakes reported in the literature, to which it has been possible to assign, after careful revision, geographical coordinates and magnitude or intensity.

For the city of Algiers, the research area considered is defined within a radius of 100 km between latitude 36°–37.75° north and longitude 2°–4° east. Algiers city is located in the Sahel[1], a narrow land strip which extends from Algiers to Tipaza in the west and from Algiers to Boudouaou in the east, about 120 km long. Wide about 20 km in the east and only few kilometers in the west, the Sahel presents a smoothly broken relief. This morphostructural unit is bounded, to the north by the Mediterranean Sea, to the south by the Mitidja plain, to the east by the volcanic mount of Thenia and to the west by the Dahra mountains. All these geographic entities surrounding the Sahel of Algiers are seismically active.

Generally, authors distinguish the western Sahel called the Sahel anticline of Algiers which runs for about 70 km from Tipaza to Algiers (Fig. 1) and the eastern Sahel located between Algiers and Boudouaou. According to the seismic history of the region, the western Sahel is more seismically active. It experienced many seismic events of moderate size ($M \leq 6$). Historically, the Algiers area has been affected by earthquakes located in three clearly defined zones: Cheliff zone, Cherchell zone and Blida zone (Fig. 2). These zones were delineated in a preliminary investigation based on existing catalogues (BENOUAR, 1993; MOKRANE *et al.*, 1994) and taking into account the coincidence of areas with particular seismic activity as well as geological characteristics. This delimitation corresponds to the seismogenic zoning focused only on the area under consideration and is nearly similar to that proposed by AOUDIA *et al.*, (2000) on a larger scale within the framework of the Algerian territory hazard assessment.

[1] The name Sahel means littoral and indicates a flat or slightly wavy coastal region, which is not very high.

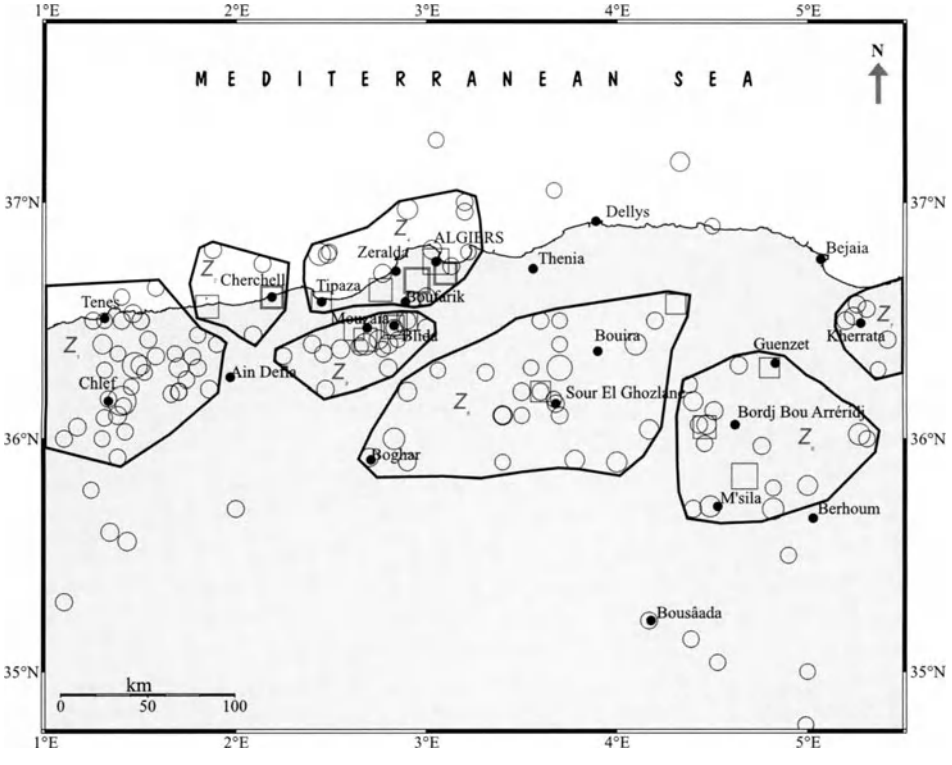

Figure 2
Seismogenic zones in central Algeria, Z_1: Cheliff zone, Z_2: Cherchell zone, Z_3: Blida zone, Z_4: Algiers Sahel zone, Z_5: Sour El Ghozlane zone, Z_6: M'sila zone, Z_7: Kherrata zone. This figure represents the seismicity of intensity I ≥ VI MSK before 1900 (earthquake data are from MOKRANE *et al.*, 1994) and of magnitude $M \geq 4.0$ from 1900 to 1990 (earthquake data are from BENOUAR, 1993).

The Earthquake Catalogue

The lack of a homogeneous catalogue reverting far enough in time (few centuries) constitutes an obstacle for an efficient seismic hazard assessment at any site. Hence, it is a basic need to provide for the Algiers region an earthquake catalogue containing data as reliable as possible. As stated by several authors (VOGT, 1991; AMBRASEYS and FINKEL, 1993), the uncritical use of standard earthquake listings for tectonic interpretation and hazard evaluation is unwise.

Fairly informative catalogues or listings of Algerian earthquakes (HÉE, 1919–1935,1924, 1925, 1932, 1933, 1936–1939, 1950; ROTHÉ, 1950; GRANDJEAN, 1954; ROUSSEL, 1973; BENHALLOU, 1985) exist but they are often inhomogeneous and not easily usable for different reasons. The most recent ones, that of BENOUAR (1993) which covers the twentieth century and that of MOKRANE *et al.*, (1994) dealing with the 1365–1992 period try to compensate for these drawbacks. However, these

earthquake catalogues must be homogenized and regularly updated. A recent study (HARBI, 2001) merged these catalogues for the northeast of Algeria [33°N–38°N, 4°E–9.5°E]. In the framework of the present study, the homogenization is extended to the region [36°N–37.75°N, 2°E–4°E].

Due to the heterogeneity in the quality and quantity of the macroseismic information and of the instrumental data sources, the earthquake catalogue is subdivided into three time windows: 1) before 1830; 2) 1830–1900, 3) 1900–2000. The CRAAG, ISC and USGS/NEIC data files are merged in the compiled catalogue in order to up date it until 2000.

Seismicity of the pre-1830 Period

This period corresponds to the pre-colonization era when Algeria was under the Ottoman empire. The available sources (MILNE, 1911; AMBRASEYS and VOGT, 1988; MOKRANE *et al.*, 1994; BOUDIAF, 1996) allowed to gather 70 seismic events from 1365 to 1825 for the region under consideration. However, the review of these events was impossible because of the lack of information. For this period only AMBRASEYS and VOGT (1988), who list about 37 events in the study region, report macroseismic information for 17 earthquakes, estimate the epicenter coordinates for five shocks and allocate the intensity only for the earthquake of 3 February 1716.[2]

On the other hand, it would be hazardous to take into consideration the estimated data reported in BOUDIAF (1996) and USGS/NEIC (1994) (see the following section) without a critical analysis. Indeed, the study of the seismic events occurred during the pre-colonization period, requiring painstaking and elaborate research in the historical documents and ancient manuscripts available in libraries and religious institutions in Algeria. In a preliminary investigation, OUSSADOU (2001) succeeded to check the majority of the earthquakes quoted by AMBRASEYS and VOGT (1988) and MILNE (1911) and even to improve the precision of the dates of occurrence of some shocks. Nevertheless, the retrieved information is not sufficiently consistent for a careful and deep study of these earthquakes. Therefore, at this early stage of research the seismicity of this period is not considered.

Seismicity of the 1830–1900 Period

In its first go, the catalogue includes 321 estimates for 213 seismic events and covers the time period 1833–1899. In the eighteen century, the proliferation of local newspapers contributed largely to the survival of macroseismic information, and enabled us to confirm a total of 130 seismic events. USGS/NEIC data files quote 21 other seismic events and BOUDIAF (1996) quotes 10 events. In the catalogues of USGS/NEIC (1994), and BOUDIAF (1996) the macroseismic locations are system-

[2] For this event, AMBRASEYS and VOGT (1988) adopt an epicenter in the Cheliff plain (to the SW of the region under study) and allocate intensity VII MSK at Algiers.

atically defined for each seismic event, however there is no indication of the criteria followed by the authors when assigning the epicenter location and intensity. On the other side, ROTHÉ (1950), ROUSSEL (1973), BENHALLOU (1985) and MOKRANE *et al.*, (1994) catalogues define sporadically the macroseismic locations. For the 1830–1900 period, the USGS/NEIC (1994) and BOUDIAF (1996) listings contain macroseismic epicenters that can induce several errors in the seismotectonic interpretation and/or seismic hazard assessment for a given site. For example, in BOUDIAF (1996) all earthquakes with epicenter in Algiers are located offshore or at about 40 km to the south of Algiers, i.e., near Blida. Blida belongs to the Blidean Atlas and not to the Sahel of Algiers. The same error in assigning coordinates recurs for all given earthquakes with epicenters in Blida, Cherchell, Boufarik and others. Similarly, some seismic events given in the USGS/NEIC (1994) catalogue are mislocated (are located offshore). From these observations it is evident how much attention must be paid to handling macroseismic data which must be examined carefully and meticulously.

The analysis of the seismicity is in progress. The retrieval and collection of the macroseismic information permits reconstruction of certain significant events that affected globally the Mitidja basin. This is particularly true at its southern boundary, in the Blidean Atlas, to the west of Algiers, in the Cherchell region, or to the southeast, in the Sour El Ghozlane region. These zones seem to have been seismically quite active during this period. Regarding the Sahel of Algiers, as suggested by the macroseismic effects reported, one can note (in spite of a stated permanent activity) that the seismicity during this period of time was of low magnitude.

Seismicity of the Post-1900 Period

This period has been quite well investigated by BENOUAR (1993) whose catalogue (from 1900 to 1990) contains five earthquakes located in the region under consideration, which have been studied or revised on the basis of reliable information (macroseismic and instrumental).

Similarly, one can find in the MOKRANE *et al.* (1994) catalogue (from 1365 to 1992) 28 macroseismic studies, based on first-hand sources such as questionnaires collected by C.R.A.A.G., which is in charge of seismological observation and monitoring in Algeria. Additional valuable and significant information about the seismicity of the 1990–1996 period is given in SEBAI (1997). ISC, USGS/NEIC and CRAAG files are used to up date the earthquake catalogue until 2000. It seems that BENOUAR (1993) and MOKRANE *et al.*, (1994) did not use Hée and Grandjean catalogues. In fact, 194 seismic events mentioned only in HÉE (1919–1935,1924, 1925, 1932, 1933, 1936–1939, 1950) listings and 74 only by GRANDJEAN (1954) were omitted in recent studies (BENOUAR, 1993; MOKRANE *et al.*, 1994). These earthquakes are contained in press reports which referred to "Le Bulletin Météorologique de l'Observatoire d'Alger".

For the post-1900 time period, 23 events considered to have a magnitude equal to or greater than 4.0 (Table 1) within the Sahel of Algiers were identified. The largest events occurred in the Sahel of Algiers during the last two decades (Oued Djer earthquake of 31 October 1988, $m_b = 5.3$; Mont Chenoua earthquake of 29 October 1989, $m_b = 5.7$; Tipaza earthquake of 09 February 1990, $m_b = 5$ and Algiers of 04 September 1996, $m_b = 5.3$).

Seismicity Analysis of Algiers Area

On the basis of the reported seismic events in the updated catalogue, several maps illustrating the seismicity of the Algiers area have been produced. Figure 3 represents the seismicity of the considered zone from 1839 to 2000. In the Sahel of Algiers, it can be noticed that the highest seismic activity is situated in the western part of this

Table 1

Date	Time (h/m/s)	Lat. (°N)	Long. (°E)	*M*	I (MSK)	Site	Remark	Reference
27/11/1923	19.50.20	36.73	3.13	4.4	4	Maison Carrée		(1)
05/11/1924	18.54.31	36.60	3.00	4.8S, 5.2b	8	Ben Chabane		(1)
06/11/1924	17.58.12	36.65	2.90	4.2S	7	Ben Chabane	A	(1)
06/11/1924	22.59.58	36.65	2.90	4.7S	6	Ben Chabane	A	(1)
04/03/1931	05.36.40	36.70	2.77	4.8	8	Camp Chenes	O	(1), (2)
28/05/1940	10.15.36	36.80	3.03	5S	–	N. Alger.	O	(1)
25/10/1949	0.0.0	37.00	3.20	4.4	6	N. Alger	O, M	(1)
13/03/1960	05.15.04	36.96	3.20	4.4S	5	Cap Matifou	O	(1), (2)
04/09/1978	13.36.00	36.59	2.93	4.1S, 4.2b	–	W. Khemis Khechna		(1)
30/06/1981	02.43.58	37.26	3.05	4.1S, 4.2b	–	Mediterranean	O	(1)
01/12/1982	06.21.06	36.79	3.22	4.1S, 4.3b		Bordj El Bahri	O	(1)
29/10/1989	19.09.13	36.62	2.33	6.0S, 5.7b	8	Chenoua Mount	O	(1), (2)
29/10/1989	19.20.49	36.63	2.47	4.0	6	Tipaza	A, O	(1)
29/10/1989	19.21.52	36.74	2.44	5.7S, 5.6b	7	Chenoua Mount	A, O	(1)
29/10/1989	19.43.59	36.64	2.47	4.0b	–	Tipaza	A, O	(3)
04/11/1989	20.08.05	36.69	2.39	4.1S, 4.1b	–	N. Nador	A, O	(1)
05/11/1989	11.38.18	36.72	2.42	4.5S, 4.7b	–	Chenoua Mount	A, O	(1)
22/11/1989	20.37.48	36.71	2.49	4.3b	–	Chenoua Mount	A, O	(3)
05/02/1990	07.17.45	36.72	2.47	4.0S, 4.2b	–	Chenoua Mount	O	(1)
09/02/1990	09.31.47	36.40	2.52	4.7S, 5.0b	5	Tipaza	O	(1), (4)
09/02/1990	09.13.19	36.87	2.48	3.7S, 4.0b		N. Tipaza	A, O	(3), (4)
12/04/1990	22.47.53	36.79	2.49	4.1S, 4.7b		N. Tipaza	O	(1)
04/09/1996	04.14.03	36.90	2.81	5.3S, 5.3b	7	N. Ain Benian	O	(3), (4)

References: (1) BENOUAR (1993); (2) MOKRANE *et al.* (1994); (3) ISC catalogue;[1] (4) SEBAÏ (1997).
In the column of remarks: A = aftershock, M = macroseismic epicenter, O = offshore epicenter.
In the column of magnitude M: S = Surface-wave magnitude, b = body-wave magnitude.

[1] http://www.isc.ac.uk

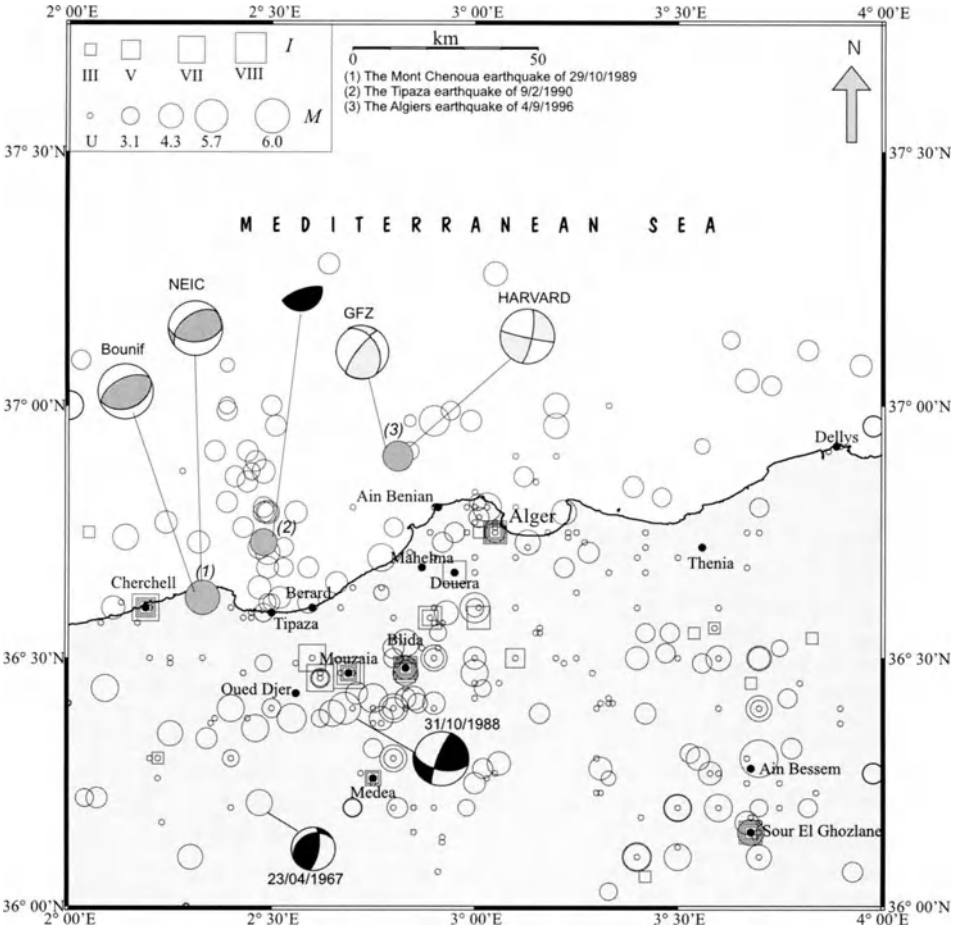

Figure 3
The spatial distribution of earthquakes (only main seismic events) from 1839 to 2000 (square: pre-1900 period, circle: post-1900 period, *u* for unknown magnitude). Focal mechanism solution of the earthquake of 23/4/1967 is from GIRARDIN *et al.* (1977), those of 31/10/1988 and 9/2/1990 are Harvard CMT solutions. The different fault plane solutions drawn in gray correspond respectively to the Mont Chenoua earthquake of 29/10/1989 (in dark gray) and the Algiers earthquake of 4/9/1996 (in light grey).

morphological structure. Another prominent characteristic that is drawn from this study is the presence of many events located offshore as well as the concentration of seismic swarms in at least four zones as reported in a preliminary investigation (Fig. 2). From west to east, the seismogenic zones of Cherchell, Blidean Atlas, Sahel of Algiers and Sour El Ghozlane area are clearly delineated. The earthquakes in the region under consideration are of moderate magnitude. Few earthquakes of the post-1900 time period are of magnitude equal to or greater than 5.0 as depicted by Figure 4. The strongest events occurred early (Ben Chaabane earthquake of 5/11/1924,

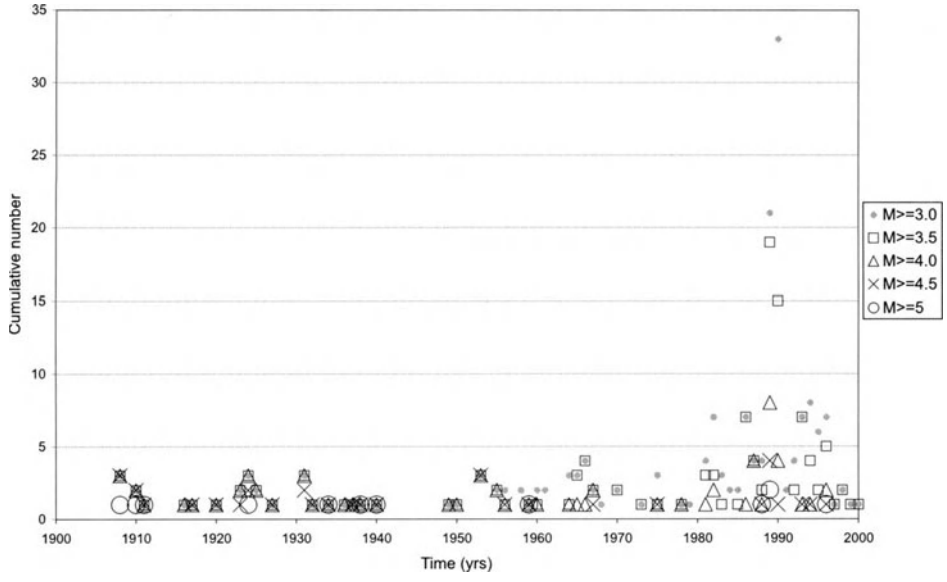

Figure 4
The cumulative number of earthquakes with M equal or larger than 3.0, 3.5, 4.0, 4.5 and 5.0, respectively, as a function of time during the post-1900 period for the zone under investigation.

$M_s = 5.2$) and at the end of the 20th century (Oued Djer earthquake of 31/10/1988, $M_s = 5.6$; Chenoua earthquake of 29/10/1989, $M_s = 5.7$; Algiers earthquake of 4/9/1996, $M_s = 5.3$). The time period between the first and the last events is characterized by a quasi-permanent seismic activity of low magnitude. The lack of seismic data (in Figure 4) between 1940 and 1950 corresponds to events of undefined magnitude. The increasing number of seismic events in the two last decades is due to microseismic surveys carried out after the large events of the Chenoua-Tipaza earthquake of 29/10/1989 and the Algiers earthquake of 4/9/1996. Seismic events corresponding to the Tipaza earthquake of 9/2/1990 ($M_s = 4.7$) and its 55 aftershocks.[3] (of magnitude equal to or greater than 3.0) were recorded when the Algerian Seismological Network was still in operation. This activity and the location of Algiers near the most active seismogenic zones in Algeria (the Cheliff basin which experienced the well known earthquake of 10/10/1980 ($M_s = 7.3$) in El Asnam) make the seismic hazard of Algiers quite relevant. Therefore serious actions must be taken for a realistic assessment of the seismic hazard of the area. This can be done, taking advantage of the precious information contained in previous studies (BENHALLOU, 1985; BENOUAR, 1993; MOKRANE *et al.*, 1994; SEBAÏ, 1997; HARBI, 2001) pertaining to the large earthquakes which occurred as far as Jijel to the east and Tenes to the west, which were felt in Algiers with intensities varying from III to VII MSK.

[3] In fact 220 aftershocks of $M \geq 1$ were recorded according to SEBAÏ (1997).

Focal Mechanisms

For the definition of the source mechanisms at this stage of the research, only published fault plane solutions are adopted. With the exception of the solution given in GIRARDIN *et al.* (1977) which was calculated by considering polarities, all the remaining focal mechanisms were deduced by using inversion methods (BOUNIF *et al.*, 1999; GFZ, CSEM and Harvard solutions). Other fault plane solutions are reported in SEBAÏ (1997) who calculated 30 focal mechanisms of aftershocks of the Tipaza earthquake of 9/2/1990 and 5 composite focal mechanism solutions obtained for several groups of aftershocks of the Algiers earthquake of 4/9/1996 (see Appendix). Taking into consideration these results as well as those represented in Figure 3, one can say that the focal mechanisms suggest that reverse faulting is the predominant mode of seismic deformation in the Sahel of Algiers, and this result is in agreement with the stress regime in the Ibero-Maghrebian region (UDIAS and BUFORN, 1991).

Seismotectonic Framework

Various approaches permitted to enlighten, at best, the seismotectonic framework of the region under study and particularly that of the Sahel of Algiers. Seismological studies of the most recent earthquakes that affected the Algiers area allowed identification of the tectonic features responsible for the seismic activity. Other methods are used for the same purpose such as geological studies, morphological analysis, analysis of aerial and satellite photographs, digital elevation models, study of the marine terraces as well as of the hydrographic network. As a matter of fact, none of the recent seismic events generated surface ruptures as clear as it would permit them to associate, unambiguously, to a precise fault. However, several authors presented hypotheses and arguments regarding the tectonic activity of the region.

Tectonics and Seismological Analyses

The Mitidja basin including the Sahel of Algiers is more or less well known from a geological point of view. In fact several studies (tectonics, neotectonics, distribution of terraces, hydrographic network, etc.) have been devoted to it (FICHEUR, 1896; GLANGEAUD, 1927, 1932; AYMÉ, 1952, 1956; AYMÉ and MAGNÉ, 1953; LEPVRIER and MAGNÉ, 1975; BONNETON, 1977; MEGHRAOUI, 1988; SAOUDI, 1989; BELHAÏ *et al.*, 1990; BOUDIAF, 1996). The Sahel of Algiers is an active fold structure, 70-km long, from Tipaza to Algiers, asymmetric and inclined to the south with an average topographic offset of 200 m (MEGHRAOUI, 1988). This fault-related fold constitutes three fault segments: the northeastern, the central and the western segments. The recent tectonic activity of this structure is attested by its global morphology and its interaction with the hydrographic network on the one hand and on the other hand by

the relation between the uplifted marine and alluvial terraces which are deformed on the sides of the Sahel anticline.

In the Mitidja basin, rivers (commonly called oued) that originated from the Atlas do cross the plain south to north. One notes that this network passes around tectonic obstacles at the foot of the Sahel anticline before flowing into the sea (Figure 5). This configuration testifies in favor of the evolution of the hydrographic network according to tectonic and obviously to pluviometric conditions. Hence the position and origin of the Haloula Lake are of tectonic nature. The barrier of the Sahel fault-related fold calls to mind the relation of the Sara El Maarouf fault-related fold and the formation of the Bir Saf-Saf Lake in the Cheliff basin. None of the waterways takes the exact shape of the basin in the synclinal axis as suggested by its morphology. This observation would be in relation with tectonic structures in the NW–SE direction. The similarity between the geometry of the Sahel anticline and that of the Sara El Maarouf fault-related fold favors the presence of a blind fault on the south limb of the Sahel. In the zone of Mahelma, the aerial photograph shows a fault of 6-km long affecting the quaternary terraces and trending in the NE-SW direction. Furthermore, a cross section (Fig. 6a) of the Mitidja basin, made by MAOUCHE and HADDOUM (2001) by using boreholes and local drilling well data, shows the geometry of fold with a blind fault on the south limb. Moreover, these authors draw a geological map showing the distribution of the Quaternary deposits in the Mitidja basin as well as the most characteristic neotectonic features of the region (Fig. 6b).

The seismological analyses are based on seismological studies (fault plane solutions, aftershocks, etc.) and on field observations made after an earthquake. They particularly concern the Mont-Chenoua earthquake of 29/10/1989 (MEGHRAOUI, 1991; AFFROUN and AZIZI, 1992; BEZZEGHOUD *et al.*, 1990), the Tipaza earthquake of 9/2/1990 (SEBAÏ *et al.*, 1997; SEBAÏ, 1997) and the Algiers earthquake of 4/9/1996 (SEBAÏ *et al.*, 1997; SEBAÏ, 1997; MAOUCHE *et al.*, 1998; MAOUCHE, 2002). The information useful for our purpose and the most striking results are summarized in the Appendix.

Discussion

The Mont Chenoua earthquake is the largest recorded event that occurred in the Sahel of Algiers. The source of this seismic event was identified by MEGHRAOUI (1991). In spite of its size ($M_s = 4.7$) and the macroseismic effects it induced ($I_{max} = V$ MSK), the Tipaza earthquake of 9/2/1990 thanks to the quality of the available data, provides precious elements to the seismotectonic interpretation of the Sahel of Algiers. According to SEBAÏ (1997), the gap observed between the two swarms of aftershocks (Fig. 7) may be interpreted as a migration of the seismicity. We rather think that the gap could be modeled by a fault with variable dip. The first ramp, dipping 60° toward the NW, is followed by a flat and finally by a second ramp,

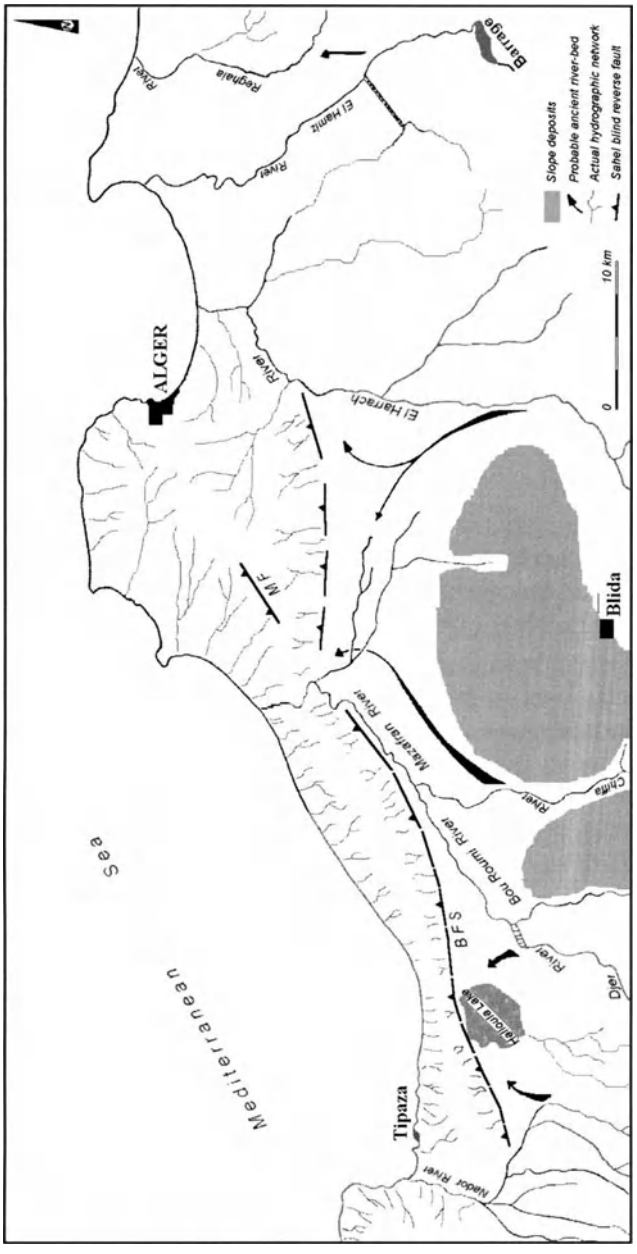

Figure 5
Drainage network of the Sahel of Algiers (after MAOUCHE and HADDOUM, 2001), BFS: Blind Fault of the Sahel of Algiers (after MEGHRAOUI, 1988), MF: the Mahelma fault.

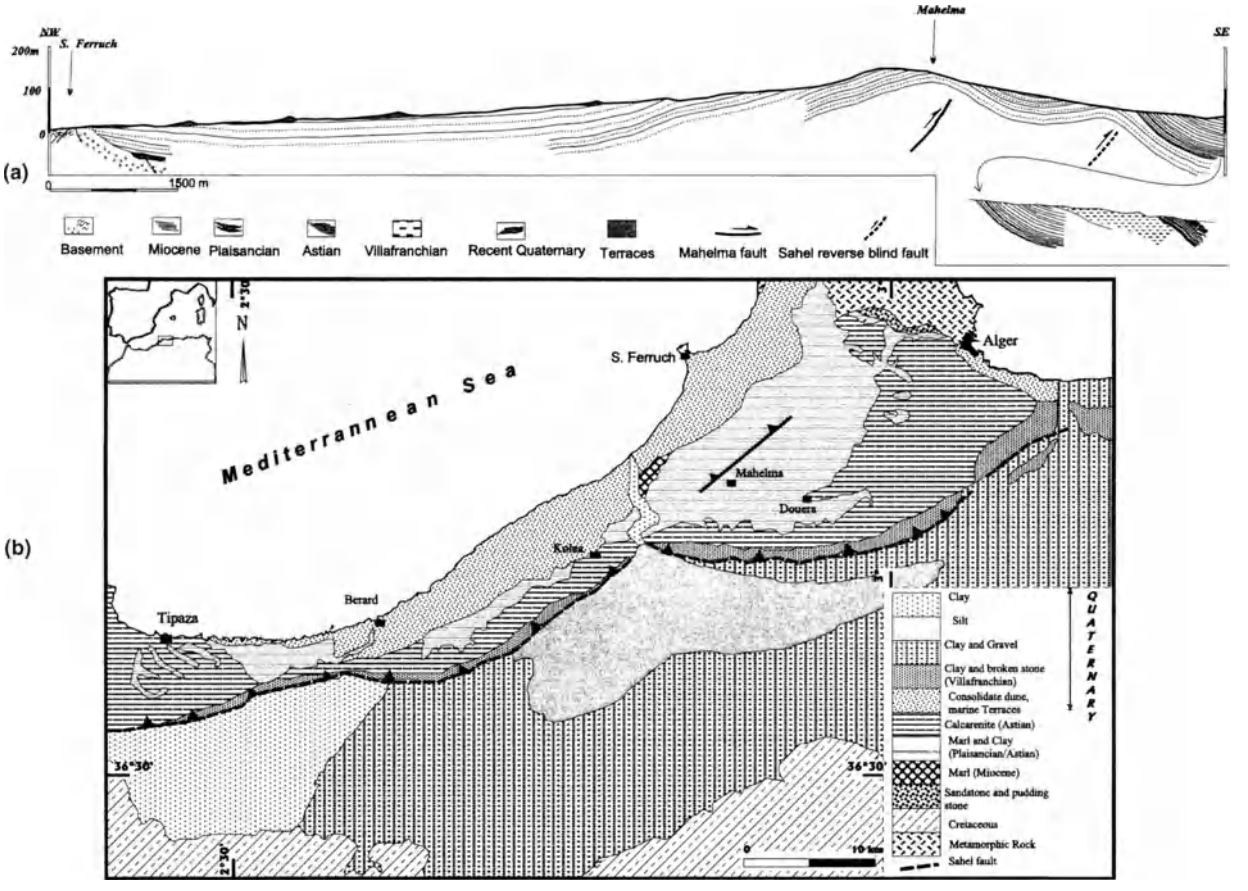

Figure 6
(a) NW-SE cross section of the Algiers Sahel (from MAOUCHE and HADDOUM, 2001); (b) synthetic geological map showing the Plio-Quaternary deposits at the Algiers Sahel, dashed line represents the reverse blind fault of the Sahel anticline (after MAOUCHE and HADDOUM, 2001).

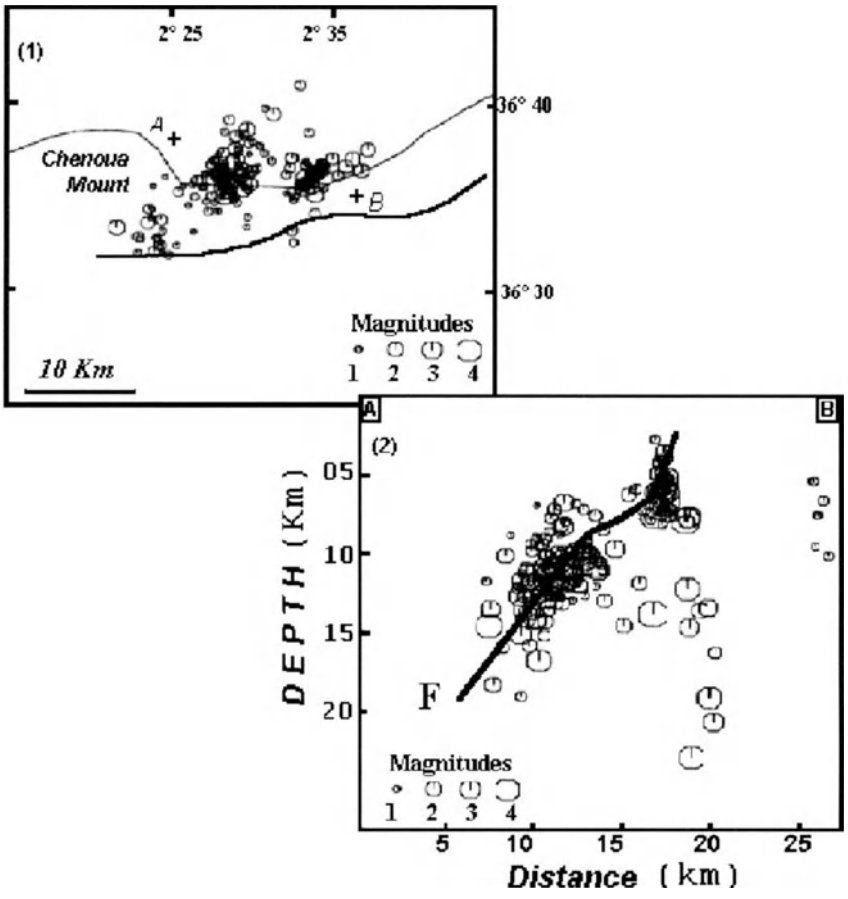

Figure 7
(1) Distribution of the best-located aftershocks' hypocenters of the Tipaza earthquake of 9.2.1990. Solid line represents the south limit of the Sahel anticline, A-B indicate the position of the cross section presented in (2). (2) A schematic representation of the fault *F* showing the geometry of ramp and flat (after SEBAÏ, 1997 and MAOUCHE, 2002).

parallel to the first one, and whose top is situated at 10 km of depth in the vicinity of Tipaza. Other conclusions may be inferred from the focal mechanisms determined by SEBAÏ (1997) for 30 aftershocks. Figure 8 shows the distribution of *P* and *T* axes of these mechanisms which display a NW–SE stress direction that is in agreement with other results given in UDIAS and BUFORN (1991) and, BEZZEGHOUD and BUFORN (1999). The small dip of the pressure axes shows that the stress is subhorizontal. In this case, the active structure generating this earthquake would be a reverse fault trending in the NE–SW direction.

The results of a comparison of the respective distribution of aftershocks of the Mont Chenoua earthquake of 29/10/1989 and the Tipaza earthquake of 9/2/1990

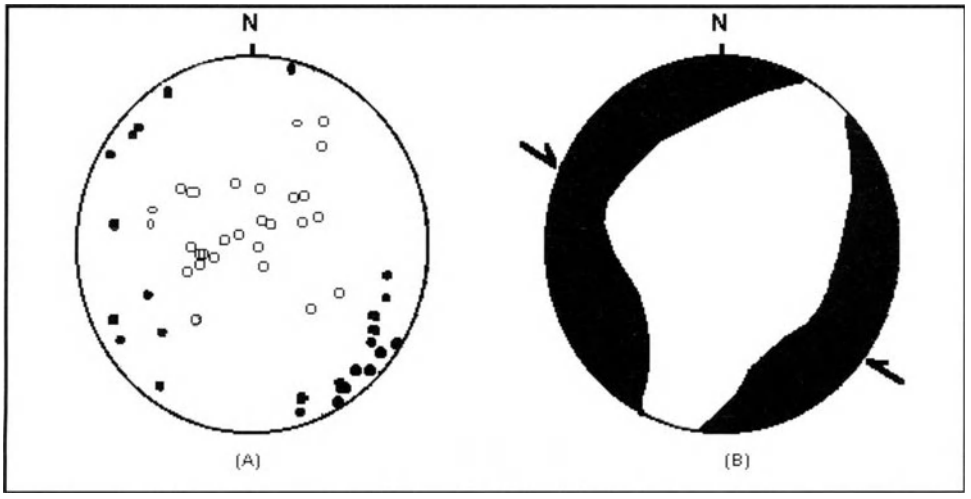

Figure 8
(A) Stereographic projection (Schmidt, lower hemisphere) of the *P* and *T* axes related to the aftershocks of the Tipaza earthquake of 9.2.1990. (B) Stress field, black: compression, white: distension (after MAOUCHE, 2002).

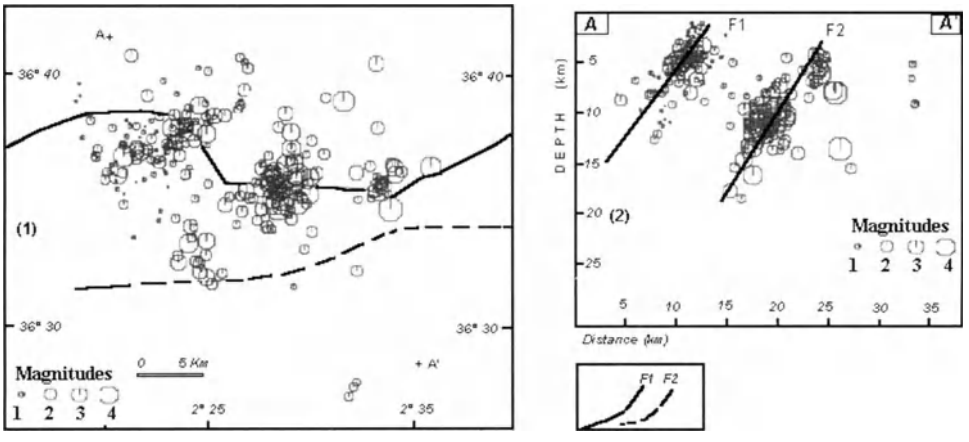

Figure 9
(1) Distribution of the aftershocks' hypocenters of, respectively, the Mont Chenoua earthquake of 29.10.1989 (to the left) and Tipaza earthquake of 9.2.1990 (to the right) (modified from SEBAÏ, 1997). Dashed line represents the south limit of the Sahel anticline, A-A′ indicate the position of the cross section presented in (2). (2) Hypocenters of the same aftershocks projected onto the vertical plane A-A′ along the NW–SE direction. The locket represents the probable relation between faults F1 and F2 (after MAOUCHE, 2002).

made by SEBAÏ (1997) are summarized in the Appendix. Figure 9 illustrates this comparison and shows to the left the spatial distribution of aftershocks and to the right the hypocenters projection on a vertical plane following a cross section

perpendicular to the extension of the aftershocks swarm. This projection identifies two possible planes of parallel blind reverse faults (F1 and F2), striking N45° with a dip of 60° toward the NW. In this case, the westernmost fault (F1) would probably be older than the fault F2 and piggyback thrust propagation is observed.

The Algiers earthquake of 4/9/1996 highlights another structural feature in the Sahel of Algiers, however the quality of the data available pertinent to this earthquake, localized offshore (CRAAG, USGS), is limited. The surface ruptures observed at the marine terraces and constituting cracks parallel to the coastline, for about 6 km along the shore with an apparent normal movement, are difficult to interpret due to the absence of scratches. Taking into account the results obtained by SEBAÏ (1997), and MAOUCHE and HADDOUM (2001), one can ascribe this earthquake to the presence of a tectonic element on the Ain Benian[4] margin and parallel to the coastline.

Conclusions

The seismic potential in the Algiers area can have destructive effects despite the relatively low intensities. In fact, the seismicity in the Algiers area is shallow and the geological setting is characterized by marly, sandy or marine sedimentary materials which make this zone very sensitive even to a moderate seismic input. The historical seismicity of the Algiers Sahel prior to 1830 is still under review but preliminary results suggest that much of the damage was concentrated in the coastal localities. Two types of seismotectonic sources are suggested in this zone: 1) blind reverse faulting evidenced by morphological indications as deformed terraces and density of drainage pattern; 2) offshore faults to be identified by reflection profiles analysis and which could have been the source of the last destructive earthquake in Algiers (4/9/1996). Accordingly with historical records, the Algiers area has been affected by earthquakes located in three clearly defined zones (Cheliff, Cherchell and Blida), which increased the vulnerability of the elements at risk in the city.

The topographic relief, the geological structures and their seismic potential, the type of soil in the site of Algiers, the concentration of the population (about 3 millions inhabitants) and of the governmental institutions, the conformity of the urban planning to emergencies, the vulnerability of old and new structures, make a detailed deterministic study of the possible seismic input mandatory in order to avoid a disastrous toll after the next relevant earthquake. The national or local authorities,

[4] Algiers earthquake is also called Ain Benian earthquake since the most damage was recorded in this city.

the earthquake engineering and the disaster mitigation planning organizations have to take practical and effective preparedness and prevention measures for the city of Algiers and its surroundings. Most of the structures in Algiers and its surroundings have a high vulnerability and very low and variable resistance to earthquake loads. Most of these buildings have suffered considerable deterioration through ageing, past earthquakes, rain and, particularly, neglect and lack of proper repairs. We believe that the rehabilitation of buildings should concern the strengthening of the structural and the non-structural systems so that they can resist future earthquake disasters. As urbanization rapidly continues, Algiers, as many other cities, is faced with the challenge of developing in a way that should be environmentally, socially and economically sustainable. Natural disasters mitigation constitutes a necessity for urban inhabitants; an obligation for governments and a strategic resource for investment promoters.

Earthquake hazard assessment should be an integral part of any strategy or policy for local and regional development.

Acknowledgements

This research, partly supported by CRAAG, was conducted within the framework of the UNESCO/IUGS/IGCP project 414 and represents a first step towards the microzonation of Algiers. The homogenization and analysis of the earthquake catalogue as well as the microzonation of Algiers are ongoing within the framework of the UNESCO/IUGS/IGCP project 457. Our thanks go to Dr. Sebaï Amal for providing useful documents. Dr. Abdelkrim Aoudia and an anonymous reviewer are gratefully acknowledged for critically reading the manuscript and helpful suggestions for its improvement.

Appendix

The Mt. Chenoua Earthquake of 29/10/1989	The Tipaza Earthquake of 9/2/1990	The Algiers Earthquake of 4/9/1996
	Macroseismic Observations	
The affected area localized between Tipaza and Cherchell is delineated by the VIII, VII and VI (MSK) isoseismals (1).	This event of I_{max} = V MSK affected the area between Bérard and Staoueli. The elongation of this isoseismal in the NE-SW direction is in good agreement with the aftershocks distribution (5).	The isoseismal VII(MSK) = I_{max} strikes in the NNW-SSE direction, in agreement with the aftershocks distribution (4). The global shape of isoseismals VI, V and IV is in the ENE-SSW direction.

Appendix (contd.)

The Mt. Chenoua Earthquake of 29/10/1989	The Tipaza Earthquake of 9/2/1990	The Algiers Earthquake of 4/9/1996
	Focal Mechanism	
Reverse fault in the ENE-WSW direction (1). The strike of the fault plane (focal mechanism) correlates with the aftershocks distribution (2).	The focal mechanism of the main shock (Harvard solution) corresponds to a reverse fault remarkably compatible with the aftershocks distribution (5). Half of the calculated fault plane solutions (for 30 aftershocks) correspond to reverse faults (5).	The focal mechanism of the main shock as well as those of five composite focal mechanisms calculated exhibit reverse faults with strike-slip component (5).
	Aftershocks Analysis	
The aftershock distribution is elongated in a NE-SW direction and occupies a large area in the Mont Chenoua and offshore zone (1). It outlines a fault of 10-km long and 5.8-km wide (3). Seismic events concentrate in a zone approximately 15-km long and 10-km wide. At depth, aftershocks are distributed between the surface and 20 km with a notable cluster between 5 km and 10 km (1).	The majority of aftershocks is concentrated to the north of the Sahel anticline. Three swarms striking NE-SW are observed; the first two (respectively from Tipaza to the sea and in the Nador region) identify a fault 20-km long, and the third one identifies a fault 10-km long, near Bérard to the east of Tipaza, parallel to the first one (5).	The aftershocks distribution identifies a fault 20-km long, striking in the NNW-SSE direction (4). However at the end of this line, another direction (E-W) is noted making this zone more complex (7). The transverse projection seems to indicate a dip of 40° toward WSW (4).
	Geological Effects	
Coseismic surface breaks with 4.0 km of fault length and 7.0 cm of vertical displacement, consisting of cracks and fissures, appeared on the southern side of Mt. Chenoua (1).	No geological effects.	No surface ruptures but some landslides and rockfalls were induced in the coastal region of Ain Benian along 6 kilometers (6).
	Interpretation of Authors	
This earthquake has reactivated the westernmost fold segment of the Sahel anticline (1).	The heterogeneity of the fault plane solutions obtained emphasises the complexity of the tectonics in this region. The distribution of aftershocks of the Mt. Chenoua earthquake as well as those of the Tipaza earthquake show clearly two distinct NE-SW seismogenic faults 8 km apart (5).	The difference observed in the direction of isoseismals is certainly due the geological nature of the Bouzaréah basement. The induced geological effects are due to the ground shaking (7). The aftershock distribution suggests the existence of a continental fault with offshore continuation (5 & 6).

Numbers in brackets correspond to the following references:
(1) MEGHRAOUI (1991)
(2) BEZZEGHOUD *et al.* (1990)
(3) AFROUN and AZIZI (1992)
(4) SEBAÏ *et al.* (1997)
(5) SEBAÏ (1997)
(6) MAOUCHE *et al.* (1998)
(7) MAOUCHE, (2002)

References

AFFROUN, N. and AZIZI, D., *Analyse des répliques du séisme du mont Chenoua (Algérie) du 29 octobre 1989 (M = 6.0)* (Mémoire d'Ingéniorat d'état, IST/USTHB, Alger, Algérie, 1992).

AMBRASEYS N. N. and VOGT, J. (1988), *Material for the Investigation of the Seismicity of the Region of Algiers*, European Earthq. Eng. *3*, 16–29.

AMBRASEYS, N. N. and FINKEL, C., *Material for the investigation of the seismicity of the Eastern Mediterranean Region during the period 1690–1710.* In *Materials of the CEC Project: Review of Historical Seismicity in Europe* (ed. M. Stucchi) (CNR, 1993), pp. 173–194.

AOUDIA, A., VACCARI, F., SUHADOLC, P., and MEGHRAOUI M. (2000), *Seismogenic Potential and Earthquake Hazard Assessment in the Tell Atlas of Algeria*, JOSE *4*, 79–88.

AYMÉ, A., *Le Quaternaire littoral des environs d'Alger*, Actes du Congrès Panafricain de Préhistoire, IIe session (Alger 1952), pp. 242–246.

AYMÉ, A. and MAGNÉ, J. M. (1953), *Etude des terrains néogènes de la cluse du Mazafran*, Travaux des collaborateurs, Bull. n°1, fasc. *11*, pp. 129–150

AYMÉ, A. (1956), *Modifications récentes survenues dans le réseau hydrographique du Sahel pendant le Quaternaire*, B. S. H. N. Afr. Du Nord, t. XLVII, pp. 50–56.

BELHAÏ, D., MERLE, O., and SAADALLAH, A. (1990), *Transpression dextre à l'Eocène supérieur dans la chaîne des Maghrébides (massif du Chenoua, Algérie)*, C. R. Acad. Sci. Paris *310*, Série II, 795–800.

BENHALLOU, H., *Les Catastrophes Séismiques de la Région d'Echéliff dans le contexte de la Séismicité Historique de l'Algérie*, Thèse de Doctorat Es-Sciences, IST-USTHB, Alger, Algeria, 1985.

BENOUAR, D., *The seismicity of Algeria and Adjacent Regions During the Twentieth Century*, Ph.D. Thesis, Imperial College of Science, Technology and Medicine, University of London, 1993, 712 pp.

BEZZEGHOUD, M., BOUNIF, M. A., BOUGHACHA, M. S., and BENHALLOU, H., *Résultats préliminaires sur le séisme du Mont Chenoua (Algérie, M = 6.0) du 29 Octobre 1989*, 8ème Séminaire National des Sciences de la Terre, 16–18 Décembre, Constantine, 1990.

BEZZEGHOUD, M. and BUFORN, E. (1999), *Source Parameters of the 1992 Mellila (Spain, $M_w = 4.8$), 1994 Alhoceima (Morocco, $M_w = 5.8$), and 1994 Mascara (Algeria, $M_w = 5.7$), Earthquakes and Seismotectonic Implications*, BSSA *89*, 2, 99, 359–372.

BONNETON, J. R., *Géologie de la zone de contact entre la Mitidja et l'Atlas de Blida au sud d'Alger*, Thèse de Doctorat, 3ème cycle, Univ. Pierre et Marie Curie, Paris, 1977.

BOUDIAF, A., *Etude sismotectonique de la région d'Alger et de la Kabylie (Algérie) : Utilisation des modèles numériques de terrain (MNT) et de télédetection pour la reconnaissance des structures tectoniques actives : contribution à l'évaluation de l'aléa sismique*, Thèse de Doctorat, Université de Montpellier II, France, 1996.

BOUNIF, A., BEZZEGHOUD, M., DORBATH, L., LEGRAND, D., RIVERA, L., DESCHAMPS, A., and PHILIPP, H. (1999). *The Chenoua (Algeria) earthquake of October 29, 1989*, Geophys. J. Int., submitted.

FICHEUR, M. E. (1896), *Aperçu Sommaire sur les Terrains Néogènes du Sahel d'Alger*, B. S. G. F. , 3ème Série, XXIV, 973–981.

GIRARDIN, N., Hatzfeld, D., and Guiraud, R. (1977), *La sismicité du Nord de l'Algérie*, C.R. somm. Soc. Géol. Fr., fasc. 2, 95–100.

GLANGEAUD, L. (1927), *Contribution à l'étude stratigraphique du Pliocène et du Quaternaire de la région littorale à l'Ouest d'Alger*, Bull. de la Soc. D'Hist. Nat. De l'Af. du Nord, XVII, 27–32.

GLANGEAUD, L. (1932), *Etude géologique de la région littorale de la provence d'Alger*, Bull. Soc. Géol. Algérie, 2ème Série, n. 8, 350–598.

GRANDJEAN, A. (1954), *Séismes d'Algérie de 1940 à 1950 inclus*, Ann. Inst. Phys. Globe, Strasbourg, 3ème Partie, Géophysique, VII, 83 (Le Puy).

HARBI, Assia, *Analyse de la sismicité et mise en évidence d'accidents actifs dans le Nord-Est Algérien*, Magister Thesis , USTHB, Alger, 2001, 195 pp.

HÉE, A. (1924), *Note sur le tremblement de terre du 05 novembre*, Annuaire Institut de Physique du Globe de Strasbourg, 2ème Partie, Séismologie, 95–98.

HÉE, A. (1919, 1935), Annuaire de l'Institut de Physique du Globe de Strasbourg, 2ème Partie, Séismologie.

HÉE, A. (1936, 1939), Annales de l'Institut de Physique du Globe de Strasbourg, Nouvelle série, 2ème Partie, Séismologie, I, IV.

HÉE, A. (1925), *La fréquence des tremblements de Terre en Algérie 1911-1924*, Monogr. Bur. Centr. Seismol. Inter., Série B (2), 111–154.

HÉE, A. (1932), *La séismicité de l'Afrique du Nord, 1911-1931*, Matériaux pour l'Etude des Calamités, Genève *4* (28), 291–296.

HÉE, A. (1933), *La fréquence des tremblements de terre en Algérie,1911-1932*, Monogr. Bur. Centr. Seism. Intern., 99 pp.

HÉE, A. (1950), *Catalogue des séismes algériens de 1850 à 1911*, Ann. Inst. Phys. Globe, Strasbourg, 6, 41–49, Strasbourg.

LEPVRIER, C. and MAGNÉ, J. (1975), *Le Néogène « post-nappes » du Tell septentrional à l'Ouest d'Alger*, B. S. G. F. (7), XVII, n. 4, 612–619.

MAOUCHE, S., BENOUAR, D., HARBI, A., and BENHALLOU H. (1998), *The Algiers (Algeria) Earthquake of 4 September 1996*, Europ. Earth. Engin., *XII*, n.1.

MAOUCHE, S. and HADDOUM, A., La sismicité de l'Algérois: Aspect tectonique. Procceding du *11ème Séminaire National des Sciences de la Terre*, Tlemcen, 28–30 Octobre, 2001.

MAOUCHE, S., *Etude sismotectonique dans l'Algérois et les zones limitrophes de Cherchell-Gouraya*, Magister Thesis, FSTGAT/USTHB, Alger 2002.

MEGHRAOUI, M., *Géologie des zones sismiques du nord de l'Algérie: Paléosismologie, Tectonique Active et Synthèse Sismotectonique*, Thèse de Doctorat es Sciences, Université de Paris sud, Centre d'Orsay, 1988, 356 pp.

MEGHRAOUI, M. (1991), *Blind Reverse Faulting System Associated with the Mont Chenoua-Tipaza Earthquake of 29 October 1989 (North-Central Algeria)*, Terra Nova *3*, 84–93.

MILNE, J., *Catalogue of Destructive Earthquakes*, Report of the 18th Meeting of BAAS, Portsmouth, London, U.K., 1911, pp. 649–740.

MOKRANE, A., AIT MESSAOUD, A., SEBAÏ, A., AYADI, A., BEZZEGHOUD, M., and BENHALLOU, H., *Les séismes en Algérie de 1365 à 1992*. Publication du Centre de Recherche en Astronomie, Astrophysique et Géophysique, Département: Etudes et Surveillance Sismique, ESS, C.R.A.A.G, Alger-Bouzaréah, 1994, 277 pp.

OUSSADOU, F., *Contribution à la sismotectonique de l'Algérie occidentale par la sismicité, les mécanismes au foyer, les mesures de déformation et la tectonique générale*, Magister Thesis, FSTGAT/USTHB, Alger, 2002.

ROTHÉ, J. P. (1950), *Les séismes de Kherrata et la séismicité de l'Algérie*, Bull. Serv. Cart. Geol. Algérie, 4ème Série, Géophysique *3*.

ROUSSEL, J. (1973), *Les zones actives et la fréquence des séismes en Algérie 1716-1970*, *Bull. Soc. Hist. Natur. Afrique du Nord. 64* (3), 2 pp. 11–227.

SAOUDI, N., *Pliocene et Pleistocene inférieur et moyen du Sahel occidental d'Alger*, ENAG, 1989, 174 pp.

SEBAÏ, A., *Analyse sismologique des séismes récents du Sahel d'Alger*, Magister Thesis, IST-USTHB, Alger, 1997, 178 pp.

SEBAÏ, A., MAOUCHE, S., DERAMCHI, A., FERKOUL, A., and Haned, S., *Du récent séisme d'Alger du 04 sptembre 1996 (M = 5.7)*, Proceeding du Séminaire Maghrébin sur la Réduction du Risque Sismique, Oran, 1997.

UDIAS, A. and BUFORN, E. (1991), *Regional Stresses on the Eurasia Africa Plate Boundary Derived from Focal Mechanisms of Large Earthquakes*, Pure Appl. Geophys. *136*, 433–448.

USGS/NEIC, *Epic User's Guide, Retrieval Software for the Global Hypocenter Data Base* – (CD-ROM, Version 3.0, September 1994).

VOGT, J. (1991), *Some glimpses at historical seismology*, Tectonophysics *193*, 1–7.

(Received February 20, 2002, accepted September 3, 2002)

Pure appl. geophys. 161 (2004) 969–982
0033–4553/04/060969–14
DOI 10.1007/s00024-003-2503-0

Pure and Applied Geophysics

Seismicity of Morocco for the Period 1987–1994

S. O. El Alami[1], B. Tadili[1], L. Aït Brahim[2], and I. Mouayn[2]

Abstract— A seismic data file of 3,740 earthquakes from January 1987 to December 1994 has been elaborated for Morocco and the border regions, with 10 main events registering magnitudes from 5 to 5.6. Such seismicity is particularly important for Morocco as the released seismic energy constitutes a considerable part of the total energy radiated during the 20th century. Relative seismicity maps confirm the persistence of the major features of the seismicity of Morocco. An important seismic activity is observed in the Alboran region continental crust, which absorbs the maximum deformation resulting from the convergence of the African and Iberian plates. However, in the longitude window 3.5°– 6° W at depths of 25 to 50 km, a seismic gap zone seems to take place. An explanation of this phenomenon may be provided by the slab breakoff model. Even if the seismicity of Morocco remains moderate, heavy damage is observed when the magnitude of earthquakes exceeds 4.5, especially in the case of traditional buildings.

Key words: Seismicity, hazard, gap, aftershocks, 87–94, Morocco.

Introduction

During its history Morocco has experienced destructive earthquakes. The first important one occurred in the 9th Century, and it was violently felt from Tangier to Tlemcen (Algeria). In 1045–1046, a violent earthquake caused the death of several people, and significant damage in Fes (El Mrabet *et al.*, 1991). In 1522 Fes city was nearly destroyed by a violent earthquake, with damage observed in an area of 160 km^2 around Fes. In 1624, again in Fes city, an important earthquake (I = VIII) caused 1500 to 2500 deaths, as reported by the chronicles. This earthquake caused significant material damage and touched several other localities, including Meknes and Baddis (El Mrabet *et al.*, 1991).

The Lisbon earthquake in 1755 is considered the most significant earthquake in human history. With its oceanic origin (area of the Corringe bank), it was felt over a vast part of North Africa and throughout western Europe (Levret, 1991). Damage in Morocco was considerable; there were several thousand deaths and partial destruction of many localities, among them Meknes (I = VIII), Fes (I = VII), and

[1] Institut Scientifique, Département de Physique du Globe, BP 703, Rabat, Maroc.
E-mails: elalami@israbat.ac.ma, tadili@israbat.ac.ma

[2] Faculté des Sciences, Département de Géologie, Rabat, R.P., Maroc. E-mails: aitbrahi@fsr.ac.ma, mouaynissam@hotmail.com

Marrakech (I = VII). All the localities on the Atlantic coast from Tangier (I = VII to VIII) to Agadir were seriously affected by the combined effect of the earthquake and the tsunami (EL ALAMI and TINTI, 1991).

The most destructive earthquake in Morocco in the 20th century was the Agadir earthquake of February 29, 1960, with magnitude $m_b = 5.8$, epicentral intensity $I_0 = X$ (MSK), and an estimated released energy of 10^{20} ergs. This is the equivalent energy produced by the explosion of about 2500 tons of TNT. Loss of human life and the amount of materials were catastrophic: more than 12000 deaths and about 290 million dollars in damage, with near destruction of some districts of the city. We attribute this damage mainly to two factors:

1 — The focus of the earthquake was located at a depth of 1.3 to 3 km below the city of Agadir (Rothé in DUFFAUD *et al.*, 1962). CHERKAOUI and MEDINA (1988) assigned a focal depth of 1.4 km after revision of the macroseismic data.

2 — Agadir is situated on plio-quaternary sediments 200 m thick called plain of Souss, which caused a site amplification effect (BARD, 1985; CHERKAOUI and MEDINA, 1988).

On February 28, 1969, an earthquake ($M = 7.3$) located at the same zone as the Lisbon earthquake was felt in Morocco. It caused the death of 6 people at Salé situated in front of Rabat (I = VI to VII). At Safi (I = VI to VII) material damage was observed (BEN SARI, 1978; CHERKAOUI, 1991).

The first studies of the seismicity of Morocco appeared in 1932 with HÉE's (1932) works, and subsequently many catalogues were published (see Table 1). ROUX (1934)

Table 1

The main seismic catalogues concerning Morocco

Period	Covered region	Number of events	Author
1911–1933	North Africa	–	HÉE (1932)
1901–1933	(25°–45°) N , (5°E–20°W)	–	GALBIS (1932, 1940)
historical events and 1901–1933	Morocco	–	ROUX (1934)
1904–1946	The World	–	GUTENBERG and RICHTER (1954)
1901–1961	(35°–44°) N , (5°E–20°W)	–	MUNUERA (1963)
1901–1955	Europe and Mediterranean basin	–	KARNIK (1969)
1919–1967	(28°–37°) N , (0°–14°) W	360	DUVERGÉ (1969)
1901–1975	(28°–38°) N , (0°–19°) W	810	BENSARI (1978)
1972–1975	(30°–40°) N , (4°–12°) W	–	HATZFELD (1978)
1976–1978	(30°–40°) N , (4°–12°) W	–	FROGNEUX (1980)
1901–1984	(21°–38°) N , (0°–20°) W	4091	CHERKAOUI (1988)
1901–1989	(21°–38°) N , (0°–20°) W	5989	TADILI and RAMDANI (1991)
1987–1994	(21°–38°) N , (0°–20°) W	3740	Our study

elaborated the first catalogue pertaining to the past and contemporary seismicity of Morocco (up to 1933), in which for the first time Arabic documents were used and important informations regarding historical earthquakes (before 1900) was given. The MUNUERA (1963) catalogue reported, for the first time, geographic coordinates of epicentres, magnitudes, and empirical formulas used to calculate magnitudes from intensities for seismic events. In the KARNIK (1969) catalogue, valid for some countries in Europe and the Mediterranean basin, both instrumental and macroseismic data were used to determine the epicentre locations, and to estimate magnitudes. HATZFELD (1978) as well as BEN SARI (1978) used HYPO 71 program for the determination of the epicentre locations. Magnitudes were computed either using amplitudes or signal durations. For their studies on the seismic risk and seismotectonics north of Morocco, TADILI and RAMDANI (1991) used a catalogue with events from 1901 to 1989, essentially based on the Spanish Bulletin of the National Geographic Institute (IGN, Madrid).

The first Moroccan seismic station (Fig. 1) was installed in 1937 by the scientific Institute of Rabat. Three more stations were added between 1964 and 1968, after the Agadir earthquake in 1960. Thereafter 12 additional stations were installed between 1971 and 1981. Since 1981, the PAMERAR project entitled "Project of Assessment and

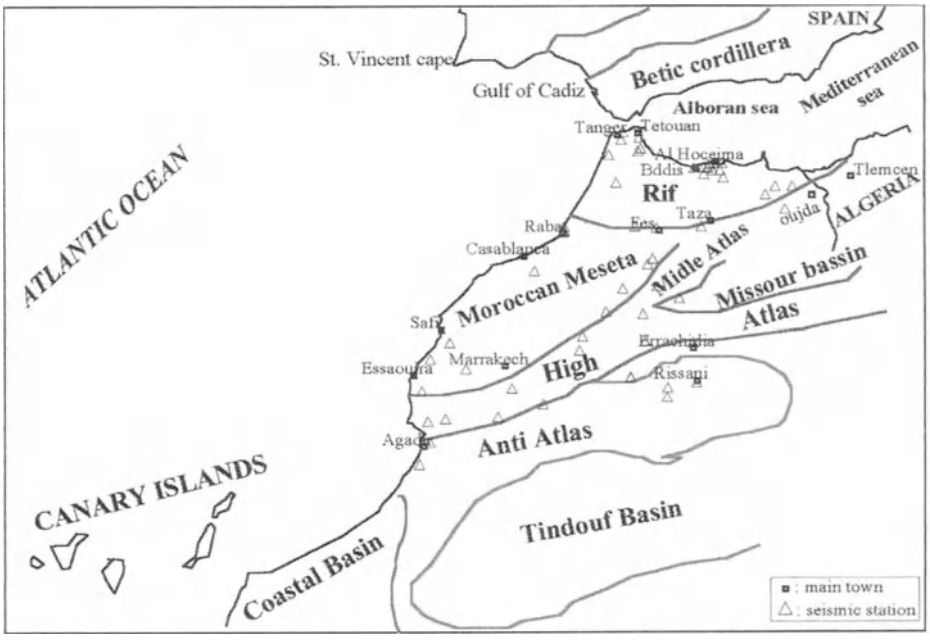

Figure 1
Schematic tectonic map of Morocco and the south of Spain and Portugal, with the seismic national network. Around Al Hoceima is shown the seismic network recording the aftershocks of the 26 May 1994 Al Hoceima earthquake, for 14 days.

Mitigation of Earthquake Risk in the Arab Region" contributed considerably to extend the National seismological network. This network is run by the National Centre of the Co-ordination and Planning of the Scientific and Technical Research, and is currently composed of several types of stations: telemetered, portable, and broadband seismic stations.

From January 1987 to December 1994, a seismic data file of 3740 earthquakes was prepared for Morocco and the border regions, with 10 main events reaching magnitudes $5 \leq M \leq 5.6$. Seismicity in Morocco for this period is particularly relevant as the released seismic energy constituted a considerable part of the total energy radiated during the 20th century in Morocco.

Seismicity of Morocco over the Period 1987–1994

The Seismic Data File

In order to study the seismic activity of Morocco for the period 1987 to 1994, we elaborated a data file of 3740 seismic events, of which 358 events were provided by yearly seismological bulletins of the Earth Physics Department (Département de physique du globe DPG, Rabat). The authors' contribution (Fig. 2a) consists of the data processing, with the program HYPO71 (LEE and LAHR, 1975) for 536 seismic events recorded by:

— Permanent seismological networks of DPG and CNCPRST.
— Safi-Essaouira local seismic network, installed from 1986 to 1991, on behalf of National Office of Electricity (ONE).
— Temporary networks installed in order to record the aftershocks of : 1) the Essaouira earthquake of 1988 (EL ALAMI *et al.*, 1989); 2) the Agadir earthquake of 1992 (EL ALAMI *et al.*, 1992); 3) the Al Hoceima earthquake of 1994 (EL ALAMI *et al.*, 1998).

The determination of an earthquake is defined by: origin time, latitude, longitude, depth, rms, erz (error on the depth in km), erh (error in km from epicentre), magnitude (M_d) and number of phases or used stations. Data from international centres consist of 2742 events from the SSIS (Seccio de sismologia e inginiera, Espagne), 53 events from the ISC (International Seismological Centre, Great Britain), 4 events from the NEIC (National Earthquake Information Centre), 18 events from LIS (Lisbone, Instituto geofisico do infante, Portugal), and 29 events from the CNCPRST (Centre National de Coordination et planification de la recherche scientifique et technique, Maroc). This file is conceived for the period of January 1, 1987 to December 31, 1994, for the zone located between latitudes (20°–38°)N and longitudes (0°– 20°)W.

The mean rms obtained for the entire data set is 0.56. For the SSIS data the rms is 0.56, and 0.42 for the data provided by the authors, while the rms for the DPG data

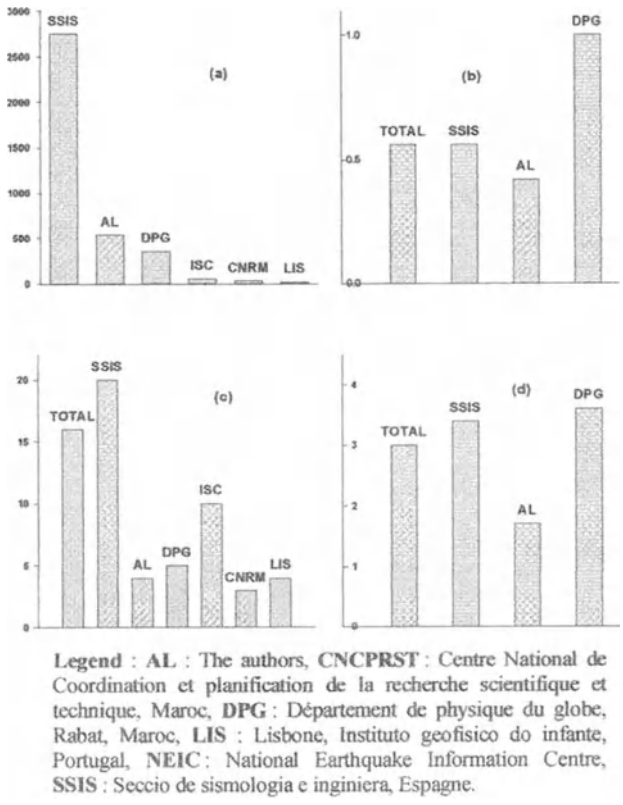

Figure 2
Characteristics of seismic data file. **a**: Data Source distribution, **b**: data rms distribution, **c**: observation mean number distribution, **d**: depth mean error distribution.

is near 1.0 (Fig. 2b). For all the sources of data used in this study, the mean number of observations used is 16 (Fig. 2c). The mean error over the depth erz is about 3 km for the entire data set (Fig.2d), 3.4 for the SSIS data and 1.7 for our contribution. The mean erh is about 3 km for the entire data set.

Seismicity Maps of Morocco for the Period 1987–1994

The knowledge of geographical distribution of earthquakes in a given region is of primary interest for studying seismicity. When correlated with geological structures, this constitutes a basic work for developing a seismotectonic map (RAMDANI, 1991; EL ALAMI, 1998), which can be used to elaborate a seismic hazard map (CHERKAOUI, 1991; TADILI, 1991). Thus, any territory development work at the national or regional scale, must take into account the results of these studies.

The seismicity map of Morocco for the period of 1987–1994 is shown in Fig. 3. 3740 seismic events are reported without any restriction. We note the persistence of

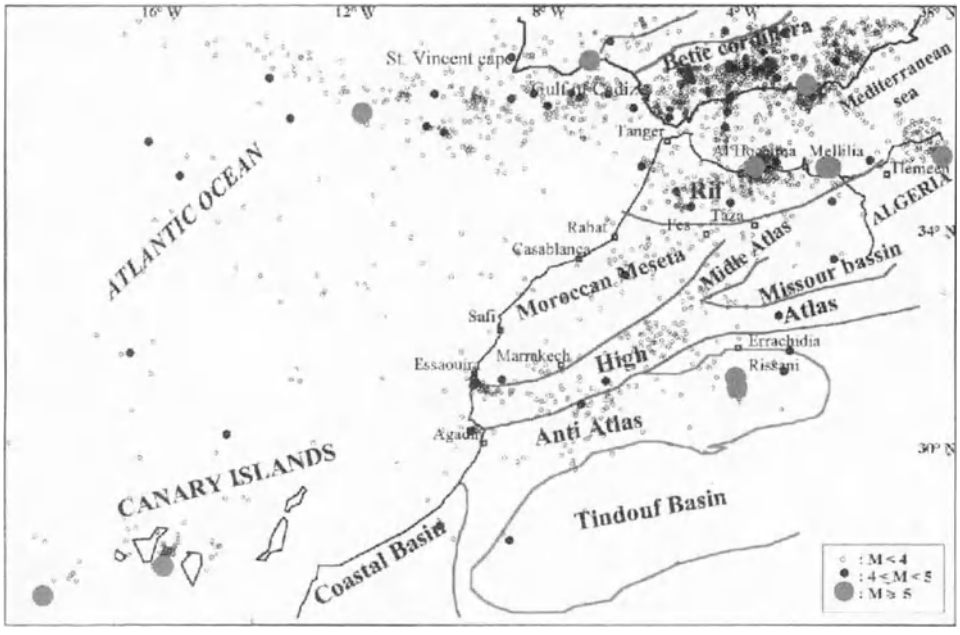

Figure 3
Seismicity of Morocco and border regions for the period 1987–1994, 3740 seismic events are reported.

the main features of the seismicity of Morocco (BEN SARI, 1978; HATZFELD, 1978; CHERKAOUI, 1991; RAMDANI, 1991; TADILI, 1991), such as the location of the majority of the epicentres in the Rif and the Alboran Sea. Overall, we can distinguish four principal seismic zones (Fig. 3): 1— southwest of the St. Vincent cape. 2— the Gulf of Cadiz. 3— the oval Betico-Rifain (the southeast of Spain, Alboran Sea and Rif). 4— the Atlasic zone. Nevertheless, the Canary Islands area must not be ignored, since it can constitute a veritable seismic danger potential source for the south coast of Morocco.

General Tectonic Setting of the Alboran Region

From the geodynamic point of view, the major problems that have been extensively discussed during the last two decades are those relative to the deep mechanisms that originated the Alboran Sea, and the real limit between Africa and Iberia. A large outline of the previous ideas can be found in recent papers published by MEGHRAOUI *et al.* (1996) and CALVERT *et al.* (1997), thus, we review here only the main points.

With respect to the vertical motions, three mechanisms have been proposed for the origin of the Alboran basin: (i) passive subsidence related to *in situ* cooling of a

thermal dome (e.g., WEIJERMAARS, 1988); (ii) delamination of a thickened lithosphere (PLATT and WISSERS, 1989; MORLEY, 1992; SEBER, 1995), and (iii) orogene collapse related to body forces (DEWEY, 1988). These vertical motions, which can be quantified through a subsidence analysis (WATTS *et al.*, 1992), do not seem to be reflected by the actual seismicity, perhaps with the exception of the deep earthquakes (600 km) recorded near Granada in southern Spain, which are thought to reflect stress release within a fragment of subducted lithosphere (e.g., BUFORN *et al.*, 1991).

Similarly, different models were proposed to explain the tectonics of the area in the context of the horizontal motions, i.e., the convergence between north-western Africa and Iberia, to which the observed seismicity is strongly related.

Seismicity around the Alboran Sea

From the seismic data file of Morocco for the period of 1987– 1994, concerning the geographical area located at (34° to 38°) N and (0.5° to 11°) W, we selected 1964 events which have rms ≤ 1, erz ≤ 5 km and erh ≤ 5 km (Fig. 4a). The analysis of the seismicity of this region suggested many interesting observations:

— The 1964 event locations are projected on the latitude-depth plane (cross section oriented NS) and represented in Figure 4b. This representation shows an important seismic activity, mostly at depths lower than 30 km. This range of depths corresponds to the continental crust which absorbs the maximum deformation resulting from the convergence of the African and Iberian plates (Fig. 5). We also observe a zone of intermediate-depth seismic activity from the Betic coast to the Rif coast in the window latitude (35.5°– 37°) N, which spans into the upper mantle depths reaching a maximum of 120 km. This intermediate depth seismic activity accounts for the majority of the sub crustal earthquakes in this region (Fig. 4a). The Betic crust is characterized by a high seismic activity within these latitudes (BUFORN *et al.*, 1988; SEBER *et al.*, 1996). This is an argument for the existence of a previous subduction zone in which the African plated plunged beneath the Iberian plate.

— A window of data in Figure 4a with longitudes of 3.5°– 6° W is represented in Figure 4c. We can observe the existence of a seismic gap zone between the Alboran Sea and the Gulf of Cadiz, at depths from 25 to 50 km, already studied by SEBER (1996) and interpreted as the result of a lithospheric delamination area. A detailed explanation of this seismic Gap zone is provided by the Slab breakoff model given by MAURY *et al.* (2000). In this model, the lithospheric delamination caused in the subduction period permitted the flow ascension of asthenospheric material through the tear of the down going slab. This caused the melting of the overlying lithospheric mantle in the subduction zone and thinning of the lithosphere through thermal erosion. As the asthenospheric material

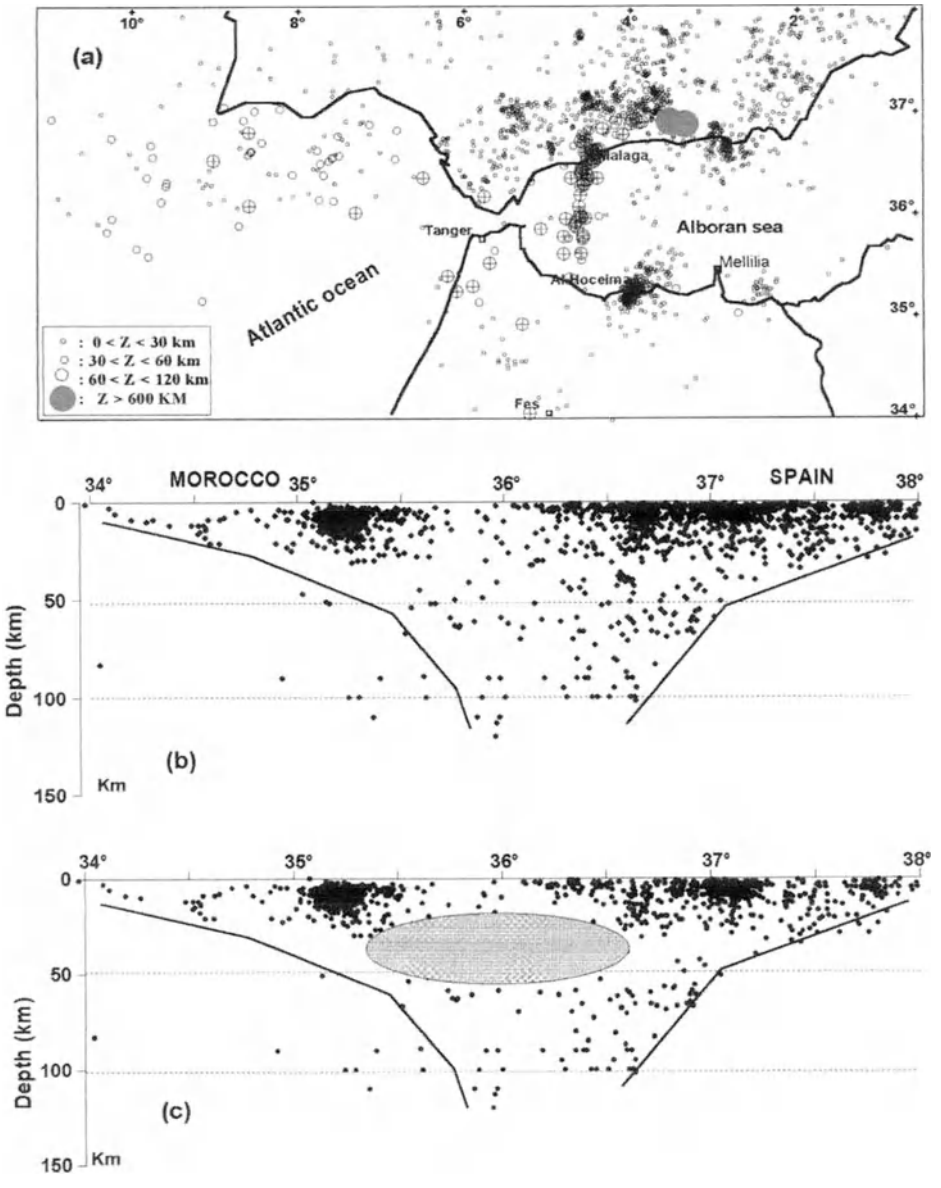

Figure 4

(**a**) Seismicity of the north of Morocco and border regions throughout 1987–1994. Only events (1964) with rms ≤ 1, erz ≤ 5 km, and erh ≤ 5 km are represented; (**b**) NS cross section projection of the 1964 events of Figure 3a; (**c**) NS cross section projection of the 1964 events of Figure 3a, however only events in the window longitude 3.5°–6°W are shown.

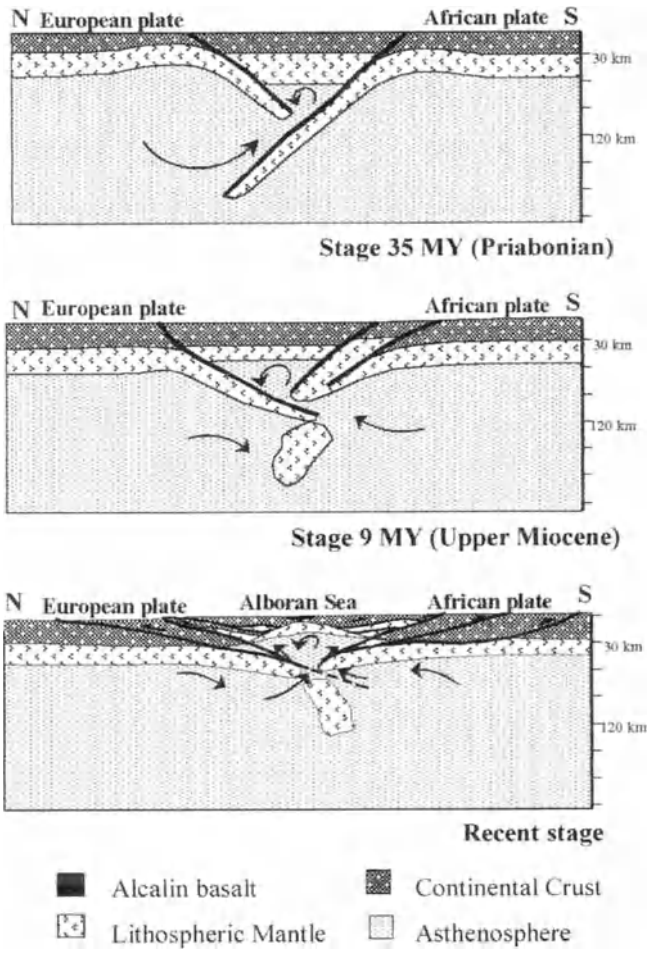

Figure 5
Proposed geodynamic model to explain the existence of a seismic gap zone from 25 to 50 km, and the intermediate-depth seismicity in the Alboran sea.

ascended through the window in the slab, partial melting occurred at the uprising boundary between asthenosphere and lithosphere, creating the Gap zone (Fig. 5). The presence of this nonseismic zone is consistent with the occurrence of low density asthenospheric material at shallower depths as interpreted by the gravity modelling of an isostatic anomaly of up to −120 mGal in the Rif region (SEBER, 1996). This Gap zone beneath the Alboran Sea coincides with extremely low *Pn* velocities (7.5– 7.9 km/s) in the uppermost mantle (HATZFELD and BEN SARI, 1977).

Our proposed geodynamic model (Fig. 5) is roughly the same model proposed by SEBER (1996), with minor modifications.

Table 2

Significant earthquakes in the 1987–1994 time period

Date	Hour	Lat. N (°)	Lon. W (°)	Rms	Depth	Erz	Erh	Ns	M_b (SSIS)	Source	M_d (DPG)
09/04/88	20:27:25.2	31.277	9.688	0.6	13	3	6	10	4.7	DPG	4.6
21/11/88	10:19:6.8	31.315	9.757	1.2	*	4	*	42	4.3	SSIS	4.6
09/05/89	2:30:37.4	27.947	16.200	0.4	36	5	2	8	5.2	SSIS	*
20/12/89	04:15:05	37.225	7.390	0.7	23	1	2	64	5.0	SSIS	4.7
21/03/91	13:32:0.5	27.405	18.682	0.3	40	7	11	8	5.1	SSIS	5.3
12/03/92	13:5:56.1	35.272	2.532	0.9	8	2	3	73	5.3	SSIS	5.2
05/04/92	21:50:57	30.444	9.742	1.1	0	10	*	5	3.7	AL	4.7
23/10/92	09:11:8.6	31.220	4.357	0.8	7	4	4	65	5.3	SSIS	5.2
30/10/92	10:44:1.8	31.412	4.383	0.6	21	3	3	66	5.1	SSIS	5.2
23/05/93	7:40:56.4	35.273	2.425	0.8	6	2	2	78	5.4	SSIS	5.1
23/12/93	14:22:35.4	36.780	2.937	0.9	8	1	2	85	5.0	SSIS	4.7
26/05/94	8:26:53.8	35.280	3.990	1.4	13	2	3	57	5.6	AL	5.6
18/08/.94	1:13:7.3	35.478	0.142	0.8	5	4	5	88	5.7	SSIS	*

Significant Earthquakes through 1987–1994

During recent years seismic activity showed a net fresh outbreak, particularly in the period 1987–1994, considered as the most important period for the seismicity of Morocco (Fig. 2), from the beginning of the 20th century. The seismic energy released during this period is very considerable, and 10 seismic events (Table 2) with magnitude $M \geq 5$ were recorded. Events from 1900 to 1986, with $M \geq 5$ obtained from the seismic catalogue of CHERKAOUI (1988) completed by the 1987–1994 data, are represented in the histogram in Figure 6. We found that the maximum period separating two successive earthquakes with $M \geq 5$ is about 7 years. The period of 1992–1994 is marked by an important seismic activity, with 7 events attaining magnitude $5 \leq M \leq 5.6$.

The Essaouira crisis is the result of the occurrence of two successive earthquakes, both with magnitude $M_d = 4.6$, that is the earthquakes of April 9, 1988 (JEBLI, and

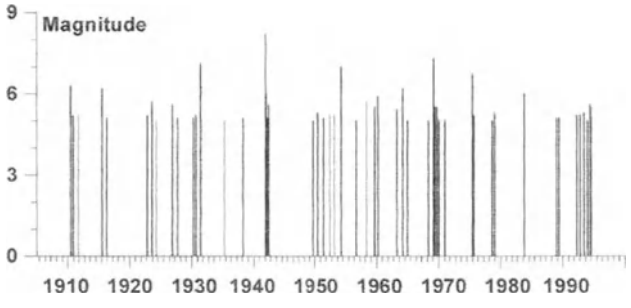

Figure 6
Distribution of earthquakes with magnitudes $M \geq 5$ related to the 1900–1994 time period.

RAMDANI, 1988), and November 21, 1988 (EL ALAMI *et al.*, 1989). The two epicentres were located at Sidi Bourja (25 km SE of Essaouira) a few kilometres from each other, with an epicentral intensity $I_0 =$ VI (MSK) for both events. They caused moderate material damages specially in the south of Essaouira. The focal mechanism of the November 21, 1988 earthquake corresponded to a sliding, with the tension axis oriented NW-SE to N-S. On April 5, 1992, on the southern border of the high Atlas, at 21h 17 min, the Agadir region, was shaken by an earthquake with a magnitude $M_d =$ 4.7. This epicentre was located at 30.41° N and 9.74° W. The earthquake was decidedly felt by the population of Agadir city. Its intensity is estimated V to VI on the MSK scale (EL ALAMI *et al.*, 1992). This shallow earthquake with its small number of aftershocks was located in the Agadir Bay. The focal mechanism corresponds to a strike-slip reverse fault with pressure axis oriented N-S. The town of Rissani is located at the southeast border of the High Atlas Mountain belt which extends from Atlantic Morocco to Tunisia over more than 2000 km however is rarely more than 100-km wide. Despite the very low seismicity level in the Rissani region, the city was shaken successively by two violent earthquakes of magnitude 5.2 in 1992, October 23 at 09:11 and October 30 at 11:43. The epicentre intensity was estimated about VI - VII (MSK) (JEBLI and EL ALAMI, 1992). The earthquake of October 30 resulted in one death and substantial material damage. Focal mechanisms correspond to a transverse fault with principal stress trending NW-SE.

Since the installation of the Moroccan seismological network, the Al Hoceima earthquake of May 26, 1994 (08 h 27 min) was considered as the most violent earthquake recorded in Morocco, after the Agadir event of February 29, 1960. Its magnitude (M_d) reached the value of 5.6, and its maximum intensity was estimated VIII to IX (EMS scale 1992). The epicentre was located at 35.28° N and 3.99° W. Its seismic moment *Mo* was estimated 9.17×10^{17} Nm (NEIC) or 1×10^{18} Nm (Harvard). This earthquake caused two deaths and important material damage, principally in many villages in the southwest of Al Hoceima city, where more then 70% of the structures are traditional (without reinforced concrete). In the south of Al Hoceima, thousands of aftershocks were recorded for 14 days following the main shock, and only 512 were determined (EL ALAMI *et al.*, 1998). The focal mechanisms determined from the main shock and 7 aftershocks indicated show the predominance of strike-slip faults with either normal or reverse components.

Lastly, there are certain earthquakes located in the border regions of Morocco which may represent a potential seismic risk:

- events of March 12, 1992 ($M_b =$ 5.3) and May 23, 1993 ($M_b =$ 5.4) in the open sea of the town of Nador (90 km in the east of Al Hoceima).
- event of August 18, 1994 ($M_b =$ 5.7) located in the northeast of Oujda.
- event of May 9, 1989 ($M_b =$ 5.2) located in the Canary Islands.
- events of December 12, 1989 ($M_b =$ 5.2) and December 23, 1993 ($M_b =$ 5.0), located in the south of Spain.

Conclusion

In the context of the studies of seismicity of Morocco encompassing the 1987–1994 time period, we elaborated a data file of 3740 seismic events with a mean rms of 0.56 and mean erz and erh of 3 km. The averaged number of observations used for the epicentre determination is 16. The analysis of the obtained histograms and seismicity maps suggests the following main results:

1) The persistence of the major features of the seismicity of Morocco as described before (BEN SARI, 1978; HATZFELD, 1978; CHERKAOUI, 1991; RAMDANI, 1991; TADILI, 1991). The majority of the epicentres is generally located in the Rif, and the Alboran Sea. At least five important seismic zones can be distinguished: the southwest of the St. Vincent Cape, the Gulf of Cadiz, the oval Betico-Rifain (the southeast of Spain, Alboran Sea and Rif), the Atlasic domain, and the Canary Islands region.
2) An important seismic activity is confined at depths from 0 to about 30 km. This range of depths corresponds to the continental crust which absorbs the maximum deformation resulting from the convergence of the African and Iberian plates. Focuses at depth between 50 and 120 km were also observed in the window latitude of 35.5°–37° N. This is an argument for the existence of a previous subduction zone in which the African plate plunged beneath the Iberian plate. Hypocentres at these depths occurred in a rectangular area trending NNE– SSW with the majority of them in the European side.
3) In the window longitude of 3.5°– 6° W, we clearly observed the existence of a seismic gap zone between the Alboran Sea and the Gulf of Cadiz, at depths ranging from 25 to 50 km studied by SEBER (1996), and interpreted as the result of a lithospheric delamination area. A detailed explanation of this seismic Gap zone is provided by the Slab breakoff model given by MAURY *et al.* (2000).
4) 1987–1994 is a period that marked the seismicity of Morocco, with the occurrence of 10 seismic events registering a magnitude $M \geq 5$. After the Agadir earthquake of 29 February, 1960, the Al Hoceima earthquake of 26 May, 1994 ($M_d = 5.6$, $I =$ VIII to IX on EMS scale) is the most violent event recorded in Morocco.
5) The focal mechanisms determined for the significant earthquakes during the period 1987–1994 show the predominance of stress trending NW-SE to N-S. This is perfectly compatible with the actual compression N–S, related to the convergence between the Africa and Iberian plates.

In general, moderate damage was observed when the magnitude exceeded 4.5, however this depends also on the focal depth, the geological properties of the affected sites, and especially on the application or non-application of the seismic building code. Even if Morocco is situated in a moderate seismicity zone, the seismic risk remains very important because of the inferior quality of the majority of existing buildings. They were not envisioned to resist even moderate earthquakes. In fact, 90% of earthquake victims lived in such buildings. The Agadir earthquake is the best example.

REFERENCES

BARD, P. Y., *Les effets de site d'origine structurale: Principaux résultats expérimentaux et méthodes.* In *Génie parasismique* (ed. Davidovici, V.) (Presses de l'Ecole Nationale des Ponts et chaussées, Paris 1985) pp. 223–238.

BEN SARI, D., *Connaissance géophysique du Maroc* (Thèse de Doctorat es-sciences, Univ., Grenoble 1978).

BUFORN, E., UDIAS, A., MEZCUA, J. and MADARIAGA, R. (1991), *A Deep Earthquake Under South Spain, 8 March 1990*, Bull. Seismol. Soc. Am. *81*, 4, 403–1407.

BUFORN , E., UDIAS , A., and MEZCUA (1988), *Seismicity and Focal Mechanisms in South* Spain, Bull. Seismol. Soc. Am. *78*, 2008–2224.

CALVERT , A., FRANSISCO , G., DOGAN , S., MUAWIA , B., NACER , J., AOMAR , I., and AHMED , D. (1997), *An Intergrated Geophysical Ivestigation of Recent Seismicity in the Al-Hoceima Region of North Morocco*, Bull. Seismol. Soc. Am. *87*, 3, 637–651.

CHERKAOUI, T. E., *Fichier des séismes du Maroc et des régions limitrophes: 1901–1984,* (Trav. Inst. Scien., Rabat 1988).

CHERKAOUI, T. E. and MEDINA, F. (1988), *Révision des données macrosismiques et du mécanisme au foyer du séisme d'Agadir du 29 février 1960*, Revue de Géographie marocaine *12*, Nouvelle Série, *1*, 51–62.

CHERKAOUI, T. E., *Contribution à l'étude de l'aléa sismique au Maroc* (Thèse d'Université Joseph Fourier, Grenoble 1991).

DEWEY , J. (1988), *Extensional Collapse of Orogens* , Tectonics *7*, 1123–1139.

DUVERGÉ (1969)

DUFFAUD, F., ROTHÉ, J. P., DEBRACH, J., ERIMESCO, P., CHOUBERT, G., and FAURE-MURET, A., *Le séisme d'Agadir du 29 février 1960.* (Notes et Mém. 154 Serv. Géol., Maroc 1962) Duvergé, J., *La séismicité du Maroc; Le séisme d'Agadir et la protection parasismique,* (Dip. Ing. Géoph.; Inst. Phys. Globe, Univ., Strasbourg 1969).

EL ALAMI, S. O., RAMDANI, F., MEDINA, F., and JEBLI, H. (1989), *Le séisme d'Essaouira du 21 nov 1988; carte des isoséistes, étude des répliques et mécanisme au foyer*, Bull. Inst. Sci. Rabat *13*, 43–50.

EL ALAMI, S. O. and TINTI , S. (1991), *A Preliminary Evaluation of the Tsunami Hazards in the Moroccan Coasts*, Inter. J. Tsunami Soc. *9*, 1, 31–38.

EL ALAMI, S. O., MEDINA, F., and JEBLI , H. (1992), *Etude du séisme d'Agadir du 5 avril 1992*, GAIA, Portugal *5*, 1–5.

EL ALAMI, S. O., TADILI, B., CHERKAOUI, T. E., MEDINA, F., RAMDANI, M., AÏT BRAHIM, L., and HARNAFI, M. (1998), *Al Hoceima Earthquake of May 26, 1994, and Its Aftershocks. Seismotectonic Study*, Annali di Geofisica *41*, 4, 519–538.

EL MRABET, T., LEVRET, A., RAMDANI, M., and TADILI, B. (1991), *Historical Seismicity in Morocco: Methodological Aspect and Cases of Multidisciplinary Evaluation, in* «*Seismici, Seismotectonics and Seismic Risk of the Ibero-Maghrebian Region*», serie monografia, Publ. I.G.N. *8*, 115– 129.

FROGNEUX, M., *La sismicité marocaine de 1972 à 1978. Etude des paramètres à la source des séismes proches* (Thèse de 3ème cycle, Univ. Grenoble 1980).

GALBIS R J., *Catalogo sismico de la zona comprendida entre los meridianos 5°E y 20°W de Greenwich y los paralelos 45° y 25°* (N I. Inst. Geogr. y Catastral, Madrid 1932)

GALBIS, R J., *Catalogo sismico de la zona comprendida entre los meridianos 5°E y 20°W de Greenwich y los paralelos 45° y 25°* (N. II. Inst. Geogr. y Catastral, Madrid 1940).

GUTENBERG, B. and RICHTER, C. F., *Seismicity of the Earth and Associate Phenomena* (Princeton University Press 2nd Ed. 1954).

HATZFELD, D. and BEN SARI D. (1977), *Grands profils sismiques dans la région de l'arc de Gibraltar*, Bull. Soc. Geol. France *7*, 749–756.

HATZFELD, D., *Etude sismotectonique de la zone de collision ibéro-maghrébine* (Thèse de Doctorat d'Etat, Univ. Grenoble 1978).

HEE, A. (1932), *La séismicité dans l'Afrique du Nord de 1911 à 1931*, Matériaux pour l'étude des calamités, Genève, *28*, 291–337.

JEBLI, H. and RAMDANI, F. (1988), *Le tremblement de terre du 9 avril 1988 au Sud d'Essaouira : Etude macrosismique*, Bull. Inst. Sci. Rabat *12*, 55–57.

JEBLI, H. and EL ALAMI, S. O., *Le séisme de Rissani du 23 octobre 1992, étude macrosismique* (Institut Scientifique, Rabat 1992).

KARNIK , V., *Seismicity of the European Area. Part I* (Reidl Pub. Co., Dordrecht 1969).

LEE, W. H. and LAHR, J. E. (1975), *HYPO71 a Computer Program for Determining Hypocenter, Magnitude and First Motion Pattern of Local Earthquakes*, U.S. Geol. Surv. Open-file report, 75– 331.

LEVRET, A., *Macrosismisité historique et contemporaine du Maroc en vue de l'évaluation de l'aléa sismique sur le site de Sidi Boulebra in "étude de sites et de faisabilité d'une centrale électroncleaire au Maroc"* (Office national de l'Electricité, Casablanca 1991)

MAURY, R. C., FOURCADE, S., COULON, C., EL AZZOUZI, M., BELLON, H., COUTELLE, A., OUABADI, A., SEMROUD, B., MEGARTSI, M., Cotton, J., BELANTEUR, O., LOUNI-HACINI, A., PIQUÉ, A., CAPDEVILA, R., HERNANDEZ, J., and RÉHAULT, J-P. (2000), *Post-collisionnal neogene magmatism of the Mediterranean Maghreb Margin: A consequence of slab breakoff* (C.R. Acad. Sci. Paris, Earth and Planetary Sciences,) *331*, 159–173.

MEGHRAOUI, M., MOREL, J. L., ANDRIEUX, J., and DAHMANI, M. (1996), *Tectonique plio-quaternaire de la chaîne tello-rifaine et de la mer d'Alboran. Une zone complexe de convergence continent-continent.* Bull. Soc. Géol. Fr. *167*, 1, 141–157.

MUNUERA, J. M., *Datos basicos para un estudio de sismisidad en el area de la peninsula ibérica* (Mem. Geogr.Y Catastral, XXXII, Madrid 1963).

MORLEY , C. K. (1992), *Notes on Neogene Basin History of the Western Alboran Sea and its Implications for the Tectonic Evolution of the Rif-Betic Orogenic Belt*, J. Struct. Geol. *14*, 1, 57– 65.

PEATT, J. P. and WISSERS, R. L. M. (1989), *Extensional Collapse of Thickened Continental Lithosphere: A Working Hypothesis for the Alboran Sea and Gibraltar Arc*, Geology *17*, 540–543.

RAMDANI, M., *Etude sismotectonique du Nord du Maroc* (Thèse de Doctorat es Sciences; Fac. des Sc., Univ. Mohammed I, Oujda 1991).

ROUX, G. (1934), *Notes sur les tremblements de terre ressentis au Maroc avant 1933*, Mém. Soc. Scien. Nat. Maroc *XXXIX*, 42–71.

SEBER, D., *Lithospheric and Upper Mantle Structure beneath Northern Morocco and Central Syria* (Ph. D. Thesis, Cornell University 1995).

SEBER D., BARAZANGI, M., IBNBRAHIM, A., and DEMNATI, A. (1996), *Geophysical Evidence for Lithospheric Délamination beneath the Alboran Sea and Rif-Betic Mountains*, Nature *379*, 785–790.

TADILI, B., *Etude du risque sismique au Nord du Maroc* (Thèse de Doctorat es Sciences; Fac. des Sc., Univ. Mohammed I, Oujda 1991) .

TADILI, and RAMDANI, (1991)

WATTS *et al.* (1992)

WEIJERMAARS, R. (1988). *Neogene Tectonics in the Western Mediterranean May Have Caused the Messinian Salinity Crisis and an Associated Glacial Event*, Tectonophysics *148*, 211–219.

(Received December 12, 2001, accepted January 16, 2003)

Pure appl. geophys. 161 (2004) 983–1002
0033–4553/04/060983–20
DOI 10.1007/s00024-003-2504-z

Pure and Applied Geophysics

The Nile Valley of Egypt: A Major Active Graben that Magnifies Seismic Waves

A. EL-SAYED[1,2,†], F. VACCARI[1,3], and G. F. PANZA[1,4]

Abstract—The Nile valley and the Nile delta are part of the active rift that is probably connected with the Red Sea tectonism. This zone is characterized by small-to-moderate size earthquakes that have caused extremely severe damage to recent and historical constructions. The most vulnerable area along the Nile valley is the one of Cairo-Faiyoum. Small local and large distant earthquakes could be a source of huge socio-economic damage in this area. The loose soft alluvial sediments of the Nile Canyon are the main factor behind this potential damage because they may greatly amplify the ground motion, as demonstrated by strong ground motion modelling. The largest amplification is generally concentrated along the edges of the graben and occurs at frequencies between 1 Hz and 2 Hz. This may explain the huge damage caused by distant earthquakes during recent and historical times. The distribution of intensity values during the events of 1926 and 1992 is well correlated with the modelled spatial distribution of the spectral amplification.

Key words: Egypt, seismicity, Nile valley, and Nile delta.

1. Introduction

The rapid growth in the Egyptian population is generally concentrated in the urbanized areas within the Nile valley and its delta, where most of the Egyptian sensitive structures and archaeological sites are located. Those urban areas are the zones most vulnerable to earthquakes, mainly due to the presence of the soft sediments of the Nile filling the Nile Canyon. That is because the unconsolidated surficial sediments can amplify earthquake ground motion, resulting in damage to structures far from the epicenter of the earthquake. The 1985 Michoacan, Mexico, and 1989 Loma Prieta earthquakes are recent reminders for the site effect of the local geological conditions.

To map the areas where amplification is likely to occur and to convey this information to emergency managers and community officials is important for the

[1] Department of Earth Sciences, Trieste University, Trieste, Italy.
[2] Department of Geology, Mansoura University, Mansoura, Egypt.
[3] Istituto Nazionale di Geofisica e Vulcanologia – Osservatorio Vesuviano, Naples, Italy.
[4] The Abdus Salam International Center for Theoretical Physics, SAND Group, Trieste, Italy.
† Dr. El-Sayed passed away in Mansoura on February 11, 2003.

planning of earthquake mitigation. Moreover, the awareness coming from pre-event modelling of strong ground motion is essential in (1) land use planning, (2) reducing business vulnerability, (3) retrofitting buildings, (4) producing guidelines for new constructions and (5) assisting in infrastructure upgrading.

The Nile valley is a large elongated Oligo-Miocene rift, trending N-S as an echo for the Red Sea rifting. During the Pliocene-Quaternary the Nile valley filled the Eonile Canyon with loose sediments that extended to a few hundreds of meters (EL-GAMILI, 1982; SAID, 1981). River deposits in this canyon include clay, sand and gravel (SAID, 1981). This geologic setting makes the settlements within the valley vulnerable to both distant and local earthquakes. In this study we will consider the Cairo-Faiyoum area as a pilot example. It is the most populated settlement along the valley and in entire Egypt, and in the past it has been affected by local (e.g., the 778, 1303, 1847 and 1992 events) and distant events (e.g., the 1926 earthquake in the Hellenic arc and the 1995 earthquake in the Gulf of Aqaba).

The spatial distribution of earthquakes (Fig. 1) and the associated damages raised the following questions: (1) must the Nile valley be considered a seismically active zone?, (2) why do small local and large distant earthquakes have a relatively large effect on the Cairo-Faiyoum area? Our main purpose in this study is to answer these questions, and to account for them in the seismic hazard estimation. This has been achieved by reviewing the history, origin and seismicity of the Nile valley region as well as modelling the effects of the Nile Canyon sediments on seismic waves propagation.

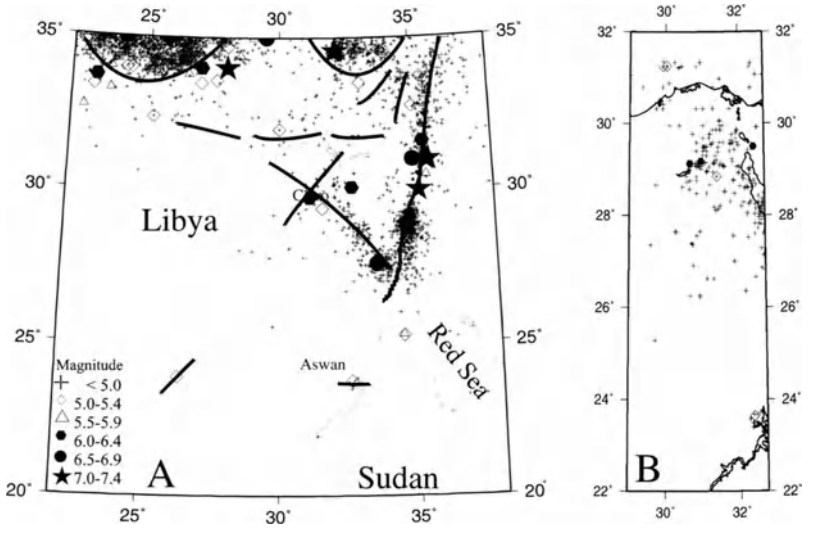

Figure 1
Distribution of earthquake epicenters in and around Egypt in the time period 1900–2001. Lines denote the major tectonic elements that are reported in the studied area (modified from KEBEASY, 1990 and MESHERF, 1990).

2. Origin of the Nile Valley

The origin of the Nile valley has been a subject of controversy. BEADNELL (1901) and SANDFORD (1934) advocated that the Nile valley is of erosional origin. On the other hand, many authors (e.g., SIEBERG, 1932; SAID, 1981; EL-GAMILI, 1982; KEBEASY, 1990; MESHERF, 1990; KULHANEK *et al.*, 1993) consider it of tectonic origin. The tectonic origin of the Nile valley is supported by the fault scarps bordering the cliffs of the Nile valley, by the numerous faults recognized on its sides (EL-GAMILI, 1982; SAID 1981, 1990) and by the focal mechanisms of the most recent earthquakes (NRIAG, 2001). Moreover, recent studies indicate that the Nile valley of Egypt occupied the marginal part of two tectonic zones (the Eastern Desert and the inner part of the Neogene-Quaternary platform), and it is considered as a barrier that prevented the extension of the activity of the East African orgenic belt to the west (SAID, 1990).

SAID (1981) studied the evolution of the Nile River from its sediments in the Eonile Canyon since the late Miocene (Messinian) age and he identified five episodes affected by meteorological and tectonic activity. The most intense seismic activities reported in the Nile valley are related to the tectonic activity of the Red Sea axial zone (SAID, 1981; ROSS and SCHLEE, 1973) and with the eastern Mediterranean recent tectonism (HSU *et al.*, 1973). No evidence of major faulting or seismic activity is known from northern Egypt since the early Miocene (SAID, 1981), although the valley extends along a seismo-active zone (SIEBERG, 1932; MAAMOUN *et al.*, 1984; KEBEASY, 1990).

3. Seismic Activity

The location of Egypt, at the intersection of ancient and important continental and maritime routes, made it a country of a long and relatively well documented history, preserved in a variety of sources. AMBRASEYS *et al.* (1994) subdivided the earthquake history in Egypt into three periods representing the pre-Islamic, Islamic and instrumental periods.

The distribution of earthquake activity in the pre-Islamic period depends mainly on papyri and archeological evidence provided by temples and monuments themselves. The difficulty in this period is that most of the material for the study of ancient Egypt contains no explicit mention of earthquakes (FAULKNER, 1969). A few well documented reports of earthquake-induced damage are found in San El-Hager (the capital of the recent Faro kingdom), Behbit Al-Hegaria and Tall Basta. These three archaeological sites were completely destroyed, with similarities in the damage patterns. For instance, in San El-Hager all obelisques and temple columns collapsed in the same direction (NNE-SSW), breaking into two or three segments showing a horizontal displacement of 1 meter (Fig. 2) and a rotation of

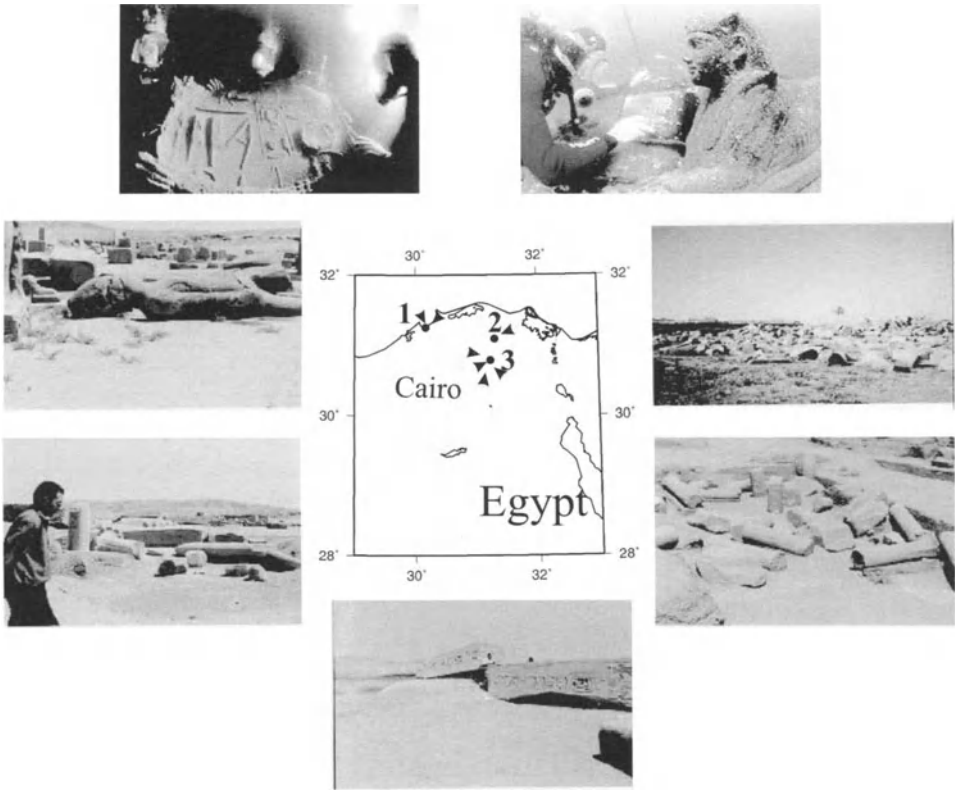

Figure 2
Examples of the damage to archaeological sites that are most probably caused by earthquakes. (1) Abu Kair Bay, at which part of old Alexandria was discovered under 8 meters of water, (2) San El-Hager, that include many destroyed obelisques, temples and statues covered by a few meters of alluvium and (3) Behbit Al-Hegaria, a completely destroyed city. The remains are of small size and are visible on the surface.

approximately 45 degrees. The general absence of explicit reports allows authors (e.g., SIEBERG, 1932; ANTONOPOULOS, 1980; AMBRASEYS *et al.*, 1994) to locate only very few earthquakes.

The Islamic period started in 622 AD. From the early date, the Muslims took a serious interest in history and paid considerable attention to "natural phenomena", especially to earthquakes which were considered as one of the portents of the Day of Resurrection "Qur'an, Sura 99 (the earthquake)". These religious and superstitious dimensions encouraged the Muslim society to report even minor shocks (AMBRASEYS *et al.*, 1994). However, it is not an easy task to use these reports to locate the earthquakes in time and space. This is mainly due to the potential shift between the Gregorian and Muslim calendars. This difference could be a source of much confusion (see AMBRASEYS *et al.*, 1994). Another source of confusion is the word "Miser", that could be related either with Cairo or with the whole country.

AMBRASEYS *et al.* (1994) made a major effort to review and relocate the earthquakes using the original reports. About 60 earthquakes are reported as felt and/or damaging in Cairo during this period (SIEBERG, 1932; MAAMOUN *et al.*, 1984; AMBRASEYS *et al.*, 1994). The most severe damage in this period is associated with the event of August 7, 1847. The instrumental period started in Egypt in 1899 when the first Milne seismograph was installed at Helwan (later in 1964 it became part of the WWSSN). By mid-1980s the number of working seismic stations started to increase. Currently the Egyptian National Seismological Network (ENSN) consists of the Cairo, Hurghada, Burg al Arab, Aswan and Toshka sub-networks that include more than 50-RF telemetry networks with vast communications between sub-arrays and the central sites. In addition to these seismograph stations, ENSN has 24 mobile seismograph stations and 24 strong motion accelerographs. By this dense network of instruments it is possible to record most of the ongoing seismic activity in Egypt. Generally, the majority of earthquakes reported in Egypt is concentrated in/around the Nile delta and the Nile valley. Luckily, most of these quakes register magnitude less than 5.

In 2001, the National Institute of Astronomy and Geophysics published a catalogue that covers the period 1997–2001. In this catalogue, fault plane solutions for selected events with a sizable amount of good records are given. As shown in Fig. 3, the normal faulting mechanism of WNW strike is the dominating mechanism along the Nile valley and its delta, while a strike-slip mechanism of ENE is more common around the Naser Lake (events 5 and 6 in Fig. 3). These mechanisms are in good agreement with the known tectonics along the Nile valley (SAID, 1981, WOODWARD CLYDE CONSULTANTS, 1985). However, we should emphasize that the tectonic setting under the highly-populated area is poorly understood. Judging from geological maps (EGYPTIAN GEOLOGICAL SURVEY, 1983), there are possible faults underneath the Metropolitan area of Cairo, however, their detailed characteristics are not known.

Based on both historical and recent seismicity, the Nile valley area is seismically active. This activity is usually reported as small to moderate. Nevertheless, some events caused considerable damage along the valley. The most severe damage is reported usually for the Cairo-Faiyoum area. The effects of the $M_L = 5.3$ event of 1992 are an example of severe damage caused by a moderate local earthquake. Despite the relatively small magnitude, at least 541 people were killed, 6,500 people were injured and 8,300 buildings were damaged or destroyed in the Cairo area alone. More than 1,000 Egyptian schools and many historical Egyptian constructions, e.g., mosques and temples, were damaged. The estimated losses are about $ one billion U.S. (JICA, 1993; NRIAG; 1993; EL-SAYED, 1996).

The Cairo-Faiyoum area was severely affected by large distant earthquakes too. Based on the damage reports given by AMBRASEYS *et al.* (1994), at least 80% of damage in the Cairo-Faiyoum area was caused by remote earthquakes that were located as far as the Hellenic Arc such as the event of 1926 ($M_s = 7.4$). This event

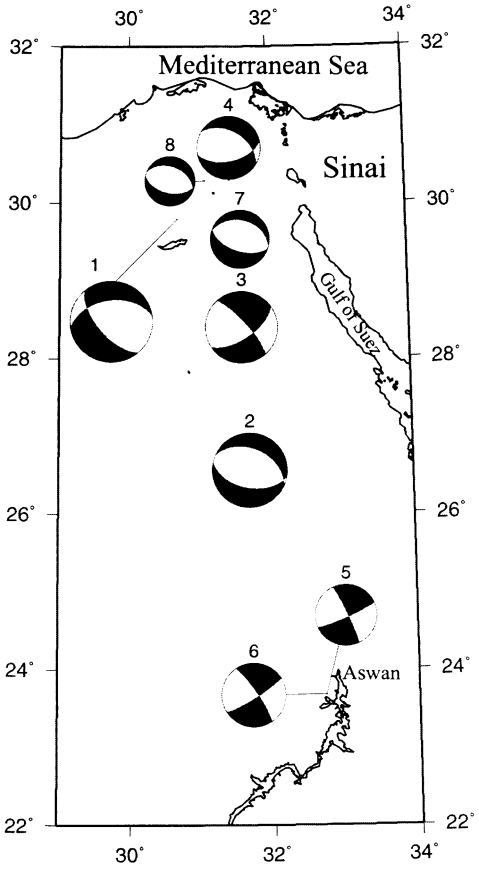

Figure 3
(a) Focal mechanism solutions available for the Nile valley and its delta in the time period 1992–2001 (NRIAG, 2001). The numbers in the figure are arranged in ascending order according to the date of the earthquake. The size of each beach ball is proportional to the magnitude of the earthquake (m_b = 3–5.3).

occurred close to Rhodes, 36.5N and 26.86E, at a distance of more than 700 km from Cairo (AMBRASEYS and ADAMS, 1998). The maximum reported intensity around the epicenter was VIII and it attenuated rapidly to V at about 100 km to the north. Nevertheless, in the Cairo-Faiyoum area the reported intensity was VII (see SHEBALIN *et al.*, 1974; MARGOTTINI, 1982) or V according to AMBRASEYS and ADAMS (1998). In Cairo, at that time a city with more than 200,000 houses, the shock caused considerable concern. In poorer districts, six adobe houses were ruined and about 450 suffered various degrees of damage. In the district of Faiyoum, a few adobe houses in farming settlements, two to three storeys high, collapsed, killing nine people (Fig. 4). From the damage distribution it seems that the Nile Canyon responded in an abnormal way to the propagated seismic waves, therefore, it is important to understand this phenomenon.

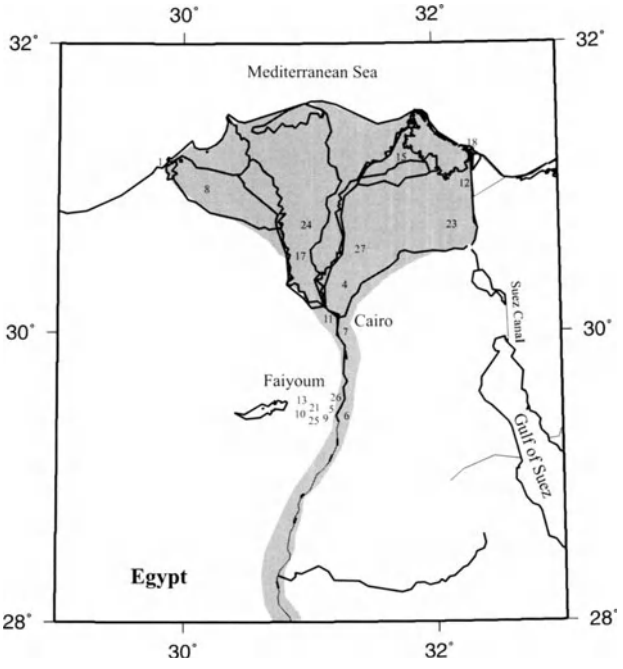

Figure 4
Distribution of the observed intensity during the event of 1926 in the Hellenic Arc, after AMBRASEYS *et al.* (1998). The shaded part shows the limits of the Eonile Canyon. 1: Alexandria [V], 4: Benha [IV], 5: Beni Salef [V], 6:Beni Suef [IV], 7: Cairo [V], 8: Damanhur [V], 9: El-Faiyoum [III], 10: Gebali [III], 11: El-Giza [IV], 12: Islmilia [IV]; 13: Kafr abud [III], 15: Mansoura [IV], 17: Minuf [IV], 18: Port Said [III], 23: Suez [II], 24: Tanta [IV], 26: El-Wasta [V], 27: Zagazig [III] (the numbers between square brackets are macroseismic intensities MSK scale).

Numerical Simulation

The subsoil condition is an important ingredient that controls the distribution of the observed damage. Tertiary formations are widely found in the highly populated area. Thick, unconsolidated Quaternary sediments overlie these rocks in the Faiyoum basin, the Nile delta, and all along the River Nile. The thickness of the alluvial sediments is estimated to be around 80 m in Metropolitan Cairo and 50 m in the vicinity of Giza. The ground water table also represents an important factor affecting the stability of the ground. It is estimated to lie 2 to 3 meters below the ground surface in Metropolitan Cairo and in the area of the River Nile. A very shallow water table is also observed in Faiyoum. The stress of such a condition reduces the value of $(\sigma_1 + \sigma_3)/2$, transporting the center of Mohr circle toward the origin (PRICE and COSGROVE, 1990), and consequently reduces the shear resistance capacity of the soils. Moreover, repacking of the soil particles during the earthquake may liberate the excess of pore space water and consequently lead to liquefaction underneath the foundation of the constructions (Makroum, personal communication).

The hybrid technique developed by FÄH *et al.* (1990, 1993, 1994) is used here to study the effect of the Nile graben sediments on the propagation of seismic waves. This technique combines the modal summation (PANZA, 1985; PANZA and SUHADOLC, 1987; FLORSCH *et al.*, 1991; PANZA *et al.*, 2000) and the finite-difference methods (VIRIEUX, 1984, 1986; LEVANDER, 1988). Each method is applied in that part of the structural model where it works most efficiently. The finite-difference method is applied in the laterally heterogeneous part of the local structural model, which contains the sedimentary basin, and the modal summation is applied to simulate wave propagation in the bedrock reference model, i.e., from the source position to the beginning of the local model of interest.

The seismic source used in this study represents the October 12, 1992 Cairo earthquake (Fig. 5a). The epicenter is localized about 75 km to the southeast of Cairo (22 km from the beginning of the 2-D model) at a depth of 23 km. In the

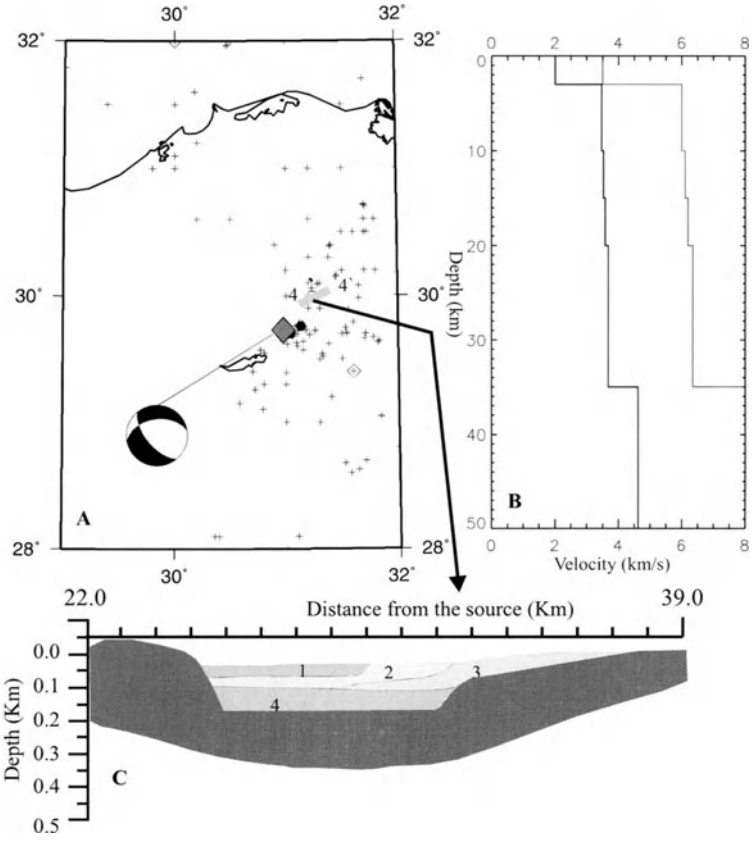

Figure 5
(a) Distribution of earthquake epicenters around the Cairo-Faiyoum area. The beach ball represents the focal mechanism of the October 12, 1992 earthquake. (b) Crustal model (V_p and V_s) adopted for the path from the source to the local model, and (c) the local model for the profile 4-4' (SAID, 1981).

numerical simulation, we use a double-couple point source with strike = 158°, dip = 67° and slip = 308° (EL-SAYED *et al.*, 1999). The strike of the fault coincides well with the geological lineaments of the area and with the distribution of the aftershock sequences (ABO-ELENEAN, 1993).

The reference bedrock model describing the path from the source to Cairo is shown in Figure 5b. The thickness, density and *P*-wave velocities of layers in this model are taken from the Bouguer anomaly and deep seismic sounding profiles published by the Egyptian General Petroleum Company. The *S*-wave velocity is assigned to be $V_p/1.73$. These data are stored in the Atlas of Geology at Cornell University, USA (BARAZANGI *et al.*, 1996). The quality factors are taken from XIE and MITCHELL (1990). For the upper mantle we have considered a standard continental model (DU *et al.*, 1998).

The local model considered in this study (Fig. 5c) is the profile (4-4') given by SAID (1981). This profile is located between Cairo and Faiyoum 22 km from the epicenter of the 1992 earthquake. The geotechnical parameters in/around this area have been investigated by many authors (e.g., MARZOUK, 1995; MOHAMMED, 1995; HELAL, 1998) and governmental building organizations (e.g., Educational Building Authority, EBA). These investigations were carried out by using shallow seismic techniques and drilling boreholes. We should emphasize that the velocities (V_p and V_s) given by different authors are in general agreement with laboratory measurements made by EBA. Table 1 summarizes the parameters used in our calculation for each layer.

To take into account the kind of buildings in the region, the high frequency limit for our numerical simulation has been chosen to be 5 Hz. *P-SV* (radial and vertical components) and *SH* (transverse component) synthetic seismograms are computed at 97 sites on the earth's surface along the 17-km long profile (Fig. 6). The reference seismic signals are calculated at the same positions but using the bedrock model. To investigate the effects due to the choice of the reference bedrock model adopted, the calculations carried out for the original reference model given in Figure 5b have been repeated assuming a 10% faster uppermost layer in the 1-D reference model. To account for the source magnitude, the signals' spectra are scaled using the scaling law of GUSEV (1983), as reported in AKI (1987). Response spectra with 5% damping (RS)

Table 1

Mechanical parameters for profile 4–4'. Numbers denote the layers composing the local model (Fig. 5c)

Layer	Density gm/cm^3	V_p km/sec	Q_p	V_s km/sec	Q_s
1	1.800	0.475	50.0	0.250	20.0
2	2.000	1.475	120.0	0.300	80.0
3	2.200	1.800	120.0	0.500	80.0
4	2.400	2.600	250.0	0.700	150.0
5	2.600	3.500	220.0	2.000	100.0

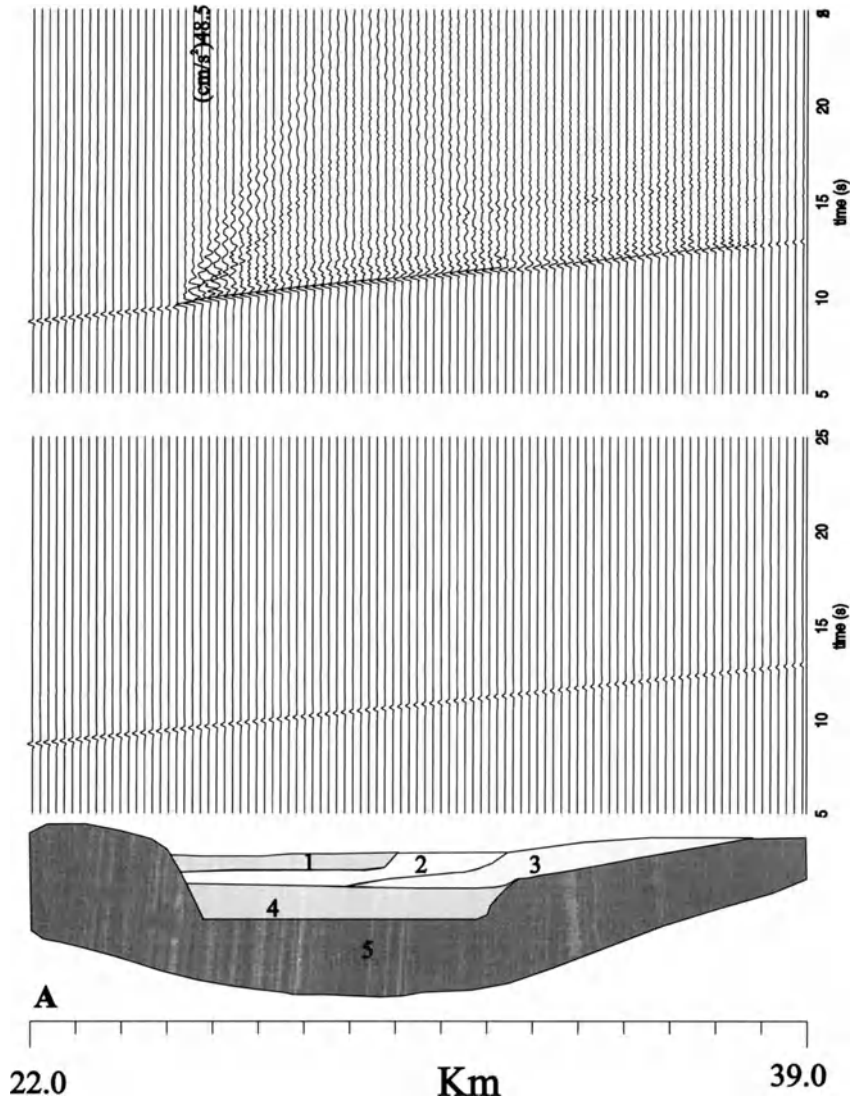

Figure 6
The cross section and the corresponding synthetic strong motion records calculated for the local model (top) and for the reference bedrock model (bottom) for the (a) transverse, (b) radial and (c) vertical components. For each component, the signals have been plotted normalized to the maximum one, for which the amplitude is indicated.

are computed at each site for the seismograms obtained for the 2–D model, and for the 1–D models (original and perturbed). The response spectra ratio RSR, computed as RS(2D)/RS(1D), is used as an estimate of the amplification due to the local soil conditions (Figs. 7 and 8).

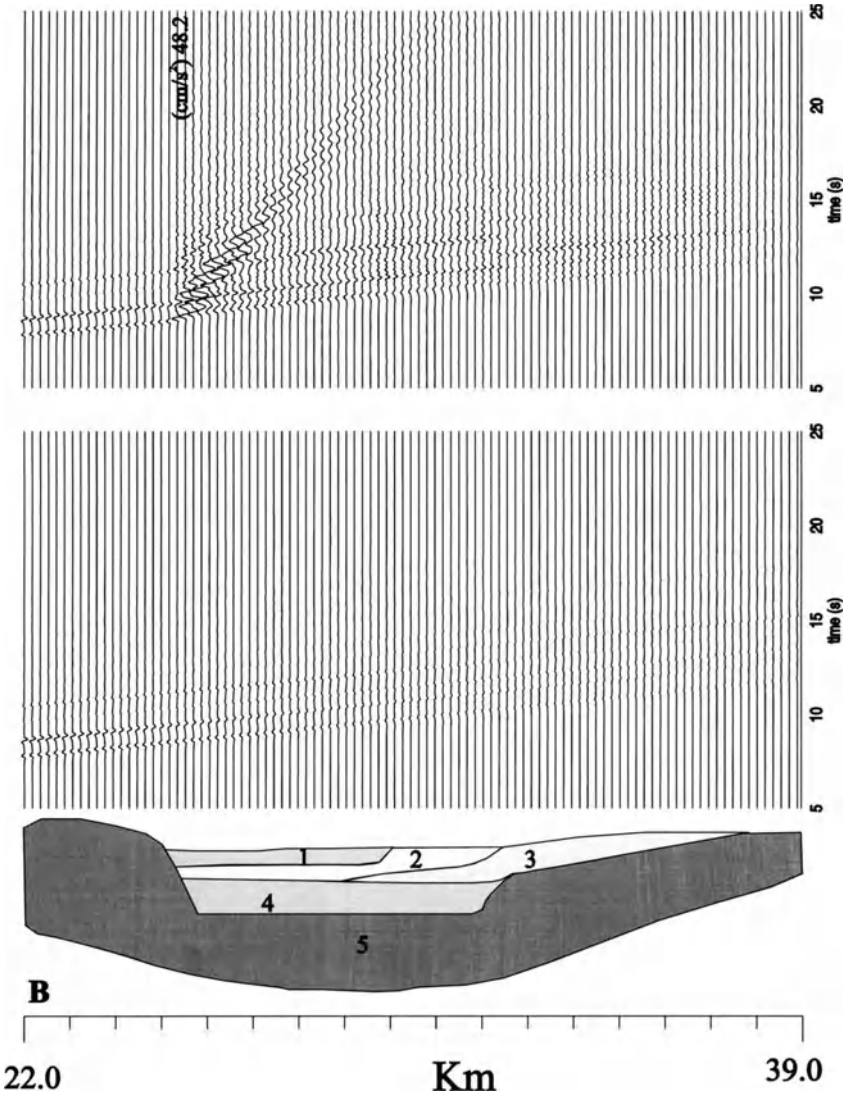

Figure 6 (Contd.)

To investigate the effect of distant earthquakes, another set of calculations was made assuming a source positioned at 150 km from the first site in 2-D (Fig. 10).

Results and Discussion

The transverse, radial and vertical components of synthetic accelerograms for the laterally varying (2-D) model have been compared with the corresponding ones

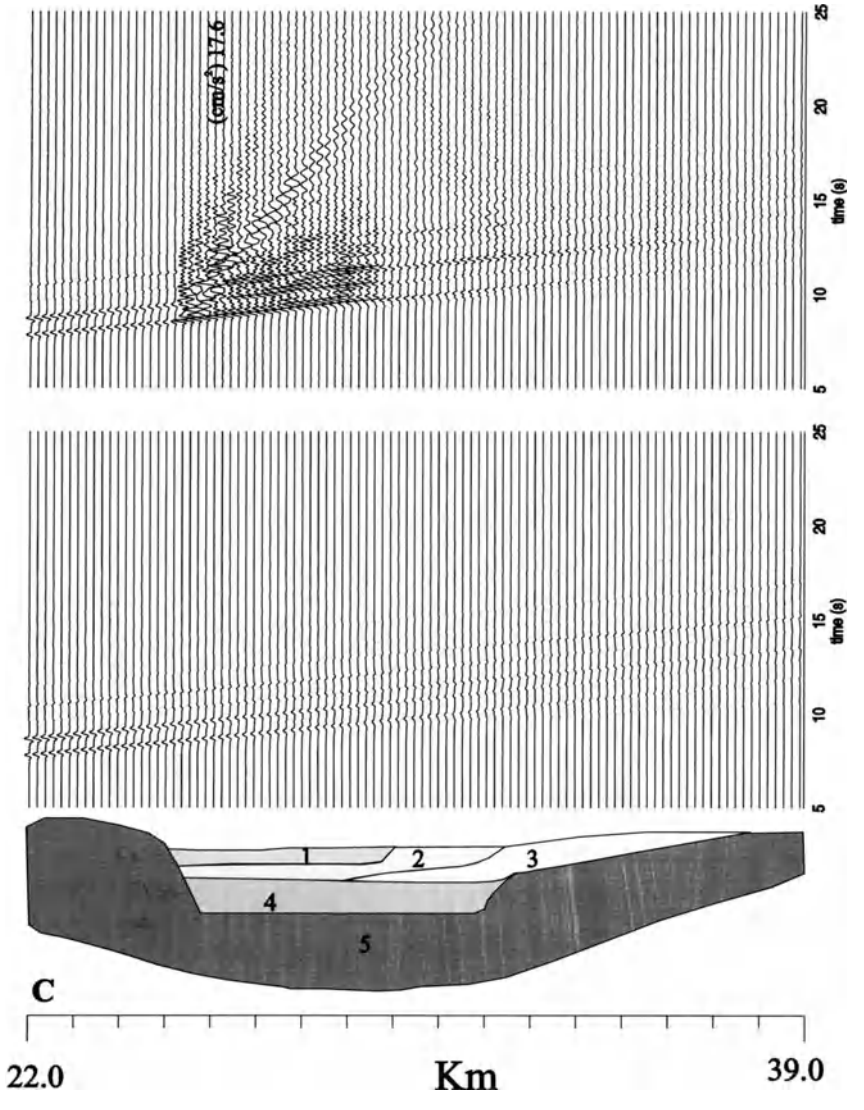

Figure 6 (Contd.)

Figure 7
The cross section and the Response Spectra Ratio (RSR) versus frequency for transverse (TRA), radial (RAD) and vertical (VER) components for: (1) the original model, and (2) the modified model, with the velocities of the uppermost layer increased by 10%.

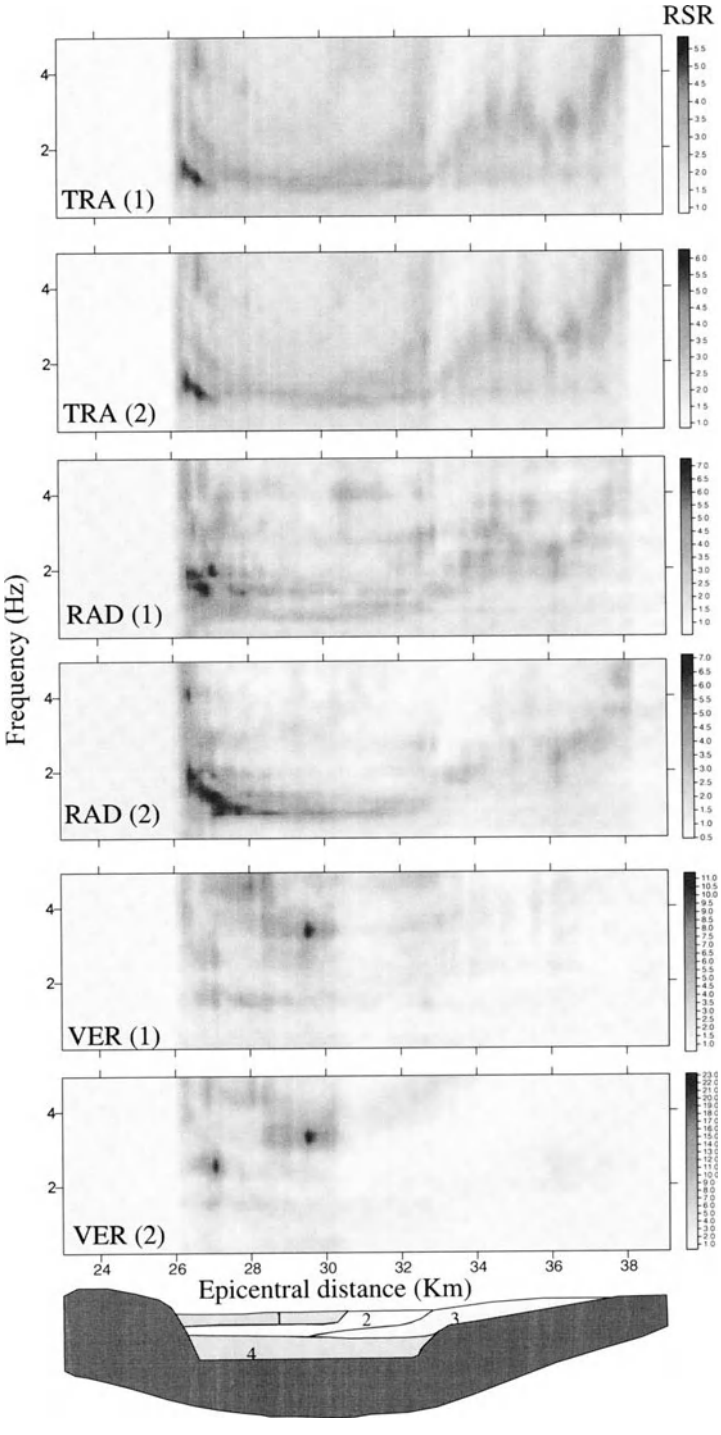
RSR
TRA (1)
TRA (2)
RAD (1)
RAD (2)
VER (1)
VER (2)
Frequency (Hz)
Epicentral distance (Km)
24
26
28
30
32
34
36
38
2
3
4

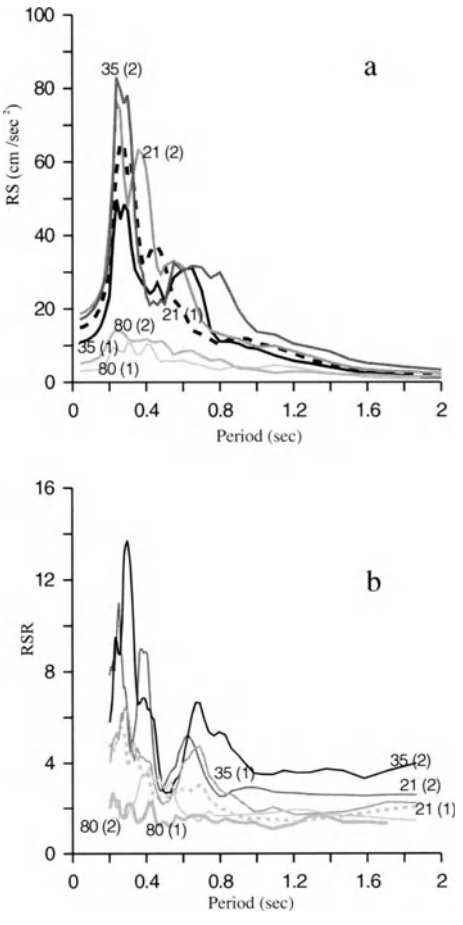

Figure 8
(a) Response Spectra (RS) and (b) Response Spectra Ratio (RSR) for some selected seismograms. (1) and (2) stand for original and modified reference models, respectively. Seismograms 21, 35 and 80 are located at distances of 26.36, 28.71 and 36.27 km from the source, respectively.

calculated using the bedrock model in order to assess the site-effects. As shown in Figure 6, the calculated accelerograms display a considerable difference in the peaks and shapes at the beginning of the local model.

The amplifications RSR are summarized in Fig. 7. For three selected sites the response spectra and the RSR are explicitly shown in Fig. 8, but are available at each site. For *SH* waves, the largest amplification (a factor of 6) occurs in the frequency band from 1—2 Hz. In some areas, e.g., at the edges of the local model, this band expands to higher frequencies. The pattern of the spectral amplification is quite different in the case of radial and vertical components of Rayleigh waves. In the vertical component, the amplification is stronger and occurs for frequencies between

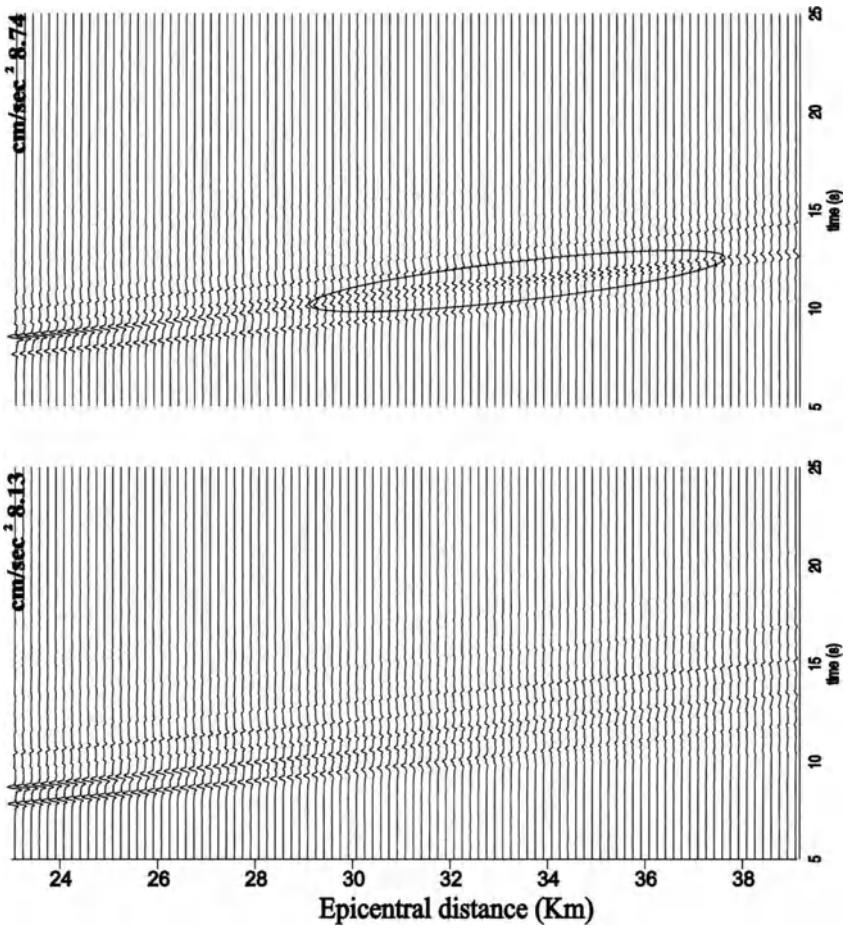

Figure 9
Synthetic strong motion records (vertical component) calculated for the original (bottom) and modified (top) reference bedrock models. The main difference between the two sets of seismograms is encircled by the elongated ellipse.

1.5 and 4.5 Hz. The studies by AMBRASEYS and SIMPSON (1996) and AMBRASEYS and DOUGLAS (2000) support this observation. These authors conclude that, at high frequencies and short distances, the vertical component response spectra may be larger and may exhibit stronger soil dependence than the horizontal ones. High amplification values for the vertical component at short periods also point out clearly the importance of considering vertical as well as horizontal components for engineering purposes. The most complicated pattern for the spectral amplification is observed in the case of the radial component of Rayleigh waves. As shown in Figure 7, the maximum amplification, about 7, is quite spread in space and frequency. For 10% changes in the uppermost layer of the bedrock reference model

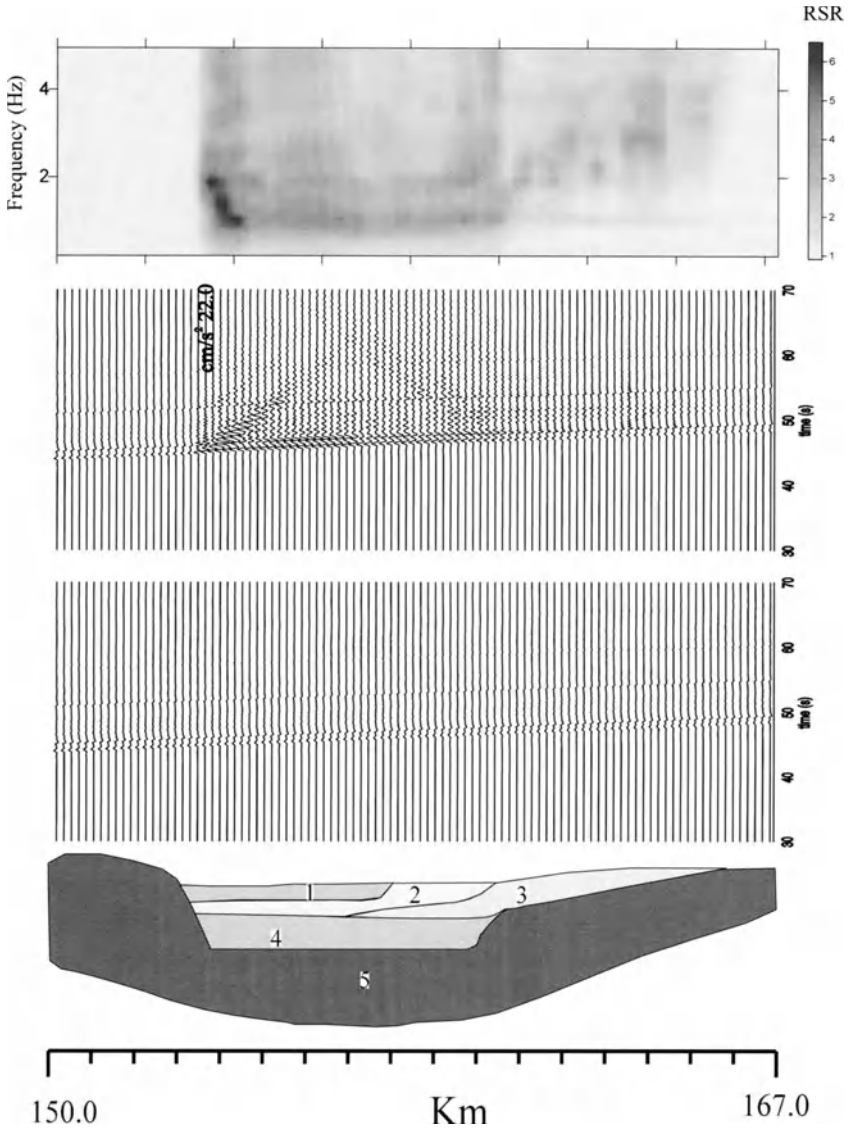

Figure 10
Example of synthetic strong motion records (transverse component) and response spectra ratio (RSR) versus frequency for a source located at 150 km from the left extreme of the cross section shown at the bottom of the figure.

the amplification pattern does not change significantly (Fig. 7), as far as the distribution in space and frequency is concerned. This stability is important, as it allows us to identify the areas along the profile where large amplifications might be expected independently on the reference model adopted. The absolute value of the

amplification varies ± 15% for the horizontal components, although for the vertical component the amplification changes by about 200%. It can be seen from Fig. 9 that for the perturbed reference model a phase with velocity around 3.1 km/sec is considerably more developed than in the case of the original reference model of Figure 5b. The interaction of this phase with the local model may reasonably explain the larger amplifications obtained. As our model is rather well constrained by the studies of several independent authors, we do not expect larger uncertainties in the absolute value of the amplifications.

By considering distant sources, the amplification becomes stronger at lower frequencies (Fig. 10). Comparing the seismograms and the spectral amplification in the case of distant and local sources we can see that, in the case of distant sources, different phases start to build up, adding more complexity to the waveforms. The amplification of seismic waves at low frequencies is certainly relevant to understand and interpret the damage caused by distant earthquakes, such as those of the Hellenic Arc (1994) and Aqaba (1995).

The October 12, 1992 and June 26, 1926 events are suitable events to verify our calculations for local and distant earthquakes, respectively. In the case of the 1992 local event, the most severe damage was reported for the regions (such as El-Aiyat, El-Beeadaa and Al-Akwan, Giza districts) where thick sediments are present and the water table is shallow (JICA, 1993). For example, at Berwash village (the area of maximum spectral amplification) 30% of houses collapsed, 50% suffered serious damage and 10% suffered light damage (JICA, 1993). On the other side of the valley, at Cairo city, the reported damage is relatively less than that reported at Giza (ELGAMAL *et al.*, 1993). In general, the areas of severe damage reported by JICA (1993) and ELGAMAL *et al.* (1993) correspond to the areas of maximum spectral amplification along our cross section.

The distribution of damage due to the 1926 distant event supports our calculations as well. The epicentral distance from Cairo is about 700 km, therefore energy peaks are observed at frequencies of 1–2 Hz (EL-SAYED *et al.*, 2000). Nevertheless, damage has been observed in a wide range of buildings in the Cairo-Faiyoum area, where the zones of maximum damage are the settlements located above the Nile Canyon filling sediments (Fig. 4). This behavior of the Nile Canyon sediments has been confirmed by observations following the events of 1996 (Cyprus) and the events of 1997 (Aqaba).

Conclusions

The main results of this study can be summarized as follows:

1. The soft sediments of the Nile valley can strongly amplify the seismic waves. Most of this amplification occurs at low frequencies and this may explain the severe effects caused by distant earthquakes in the Nile valley and its delta.

2. Maximum spectral amplifications are concentrated at the edges of the Nile basin.
3. Areas of thick sediments and shallow underground water table strongly amplify seismic waves.
4. Small variations in the definition of the reference model do not alter the general amplification pattern along the profile, but can lead to a considerable variation in the absolute value for the vertical component.

Acknowledgements

This work was carried out at the Department of Earth Sciences (DST), Trieste University, Italy. Financial support was provided by ICTP (TRIL Program and SAND Group), Italy and by the financial unit at Mansoura University. We express our sincere thanks to Profs. I. Korrat and M. El-Gamili for their critical comments and constructive suggestions. This research is a contribution to the IUGS-UNESCO-IGCP Project 414 "Realistic Modelling of Seismic Input for Megacities and Large Urban Areas", and to OEA, ICTP Net 40 "Seismic hazard in Northern-eastern Africa".

REFERENCES

ABO-ELENEAN, K. (1993), *Seismotectonics of the Mediterranean region north of Egypt and Libya.* M. Sc. Thesis, Faculty of Science, Mansoura University.

AKI, K. (1987), *Strong motion seismology. In Strong Motion Seismology*, NATO ASI Series, Series C: Mathematical and Physical Sciences (eds. Erdik, M. Ö. and Toksöz, M. N.) (D. Reidel Publishing Company, Dordrecht 1987), 204, pp. 3–39.

AMBRASEYS, N. N., MELVILLE, C. P., and ADAM, R. D., *The Seismicity of Egypt, Arabia and the Red Sea A Historical Review* (Cambridge University Press, UK, 1994).

AMBRASEYS, N. N. and ADAMS, R. D. (1998), *The Rhodes Earthquake of 26 June, 1926,* J Seismo *2*, 267–292.

AMBRASEYS, N. N., and SIMPSON, K. A. (1996), *Prediction of Vertical Response Spectra in Europe,* Earthquake Eng. Struct. Dyn. *25*, 401–412.

AMBRASEYS, N. N. and DOUGLAS, J. (2000), *Reappraisal of the Effect of Vertical Ground Motions on Response,* ESEE Report No. 00-4, Imperial College of Science, Technology and Medicine, Civil Engineering Department, London, 66 pp.

ANTONOPOULOS, J. (1980). *Data from Investigation on Seismic Sea Waves Events in the Eastern Mediterranean from 1000 to 1500 A.D.* Part 3, Annali di Geofisica *33*, 179–198.

BARAZANGI, M., FIELDING, E. J., ISACKS, B., and SEBER, D. (1996), *Geophysical and geological data bases and CTBT monitoring: A case study of the Middle East.* In *Monitoring a Comprehensive Test Ban Treaty* (eds. E. S. Husebye and A. M. Dainty) (Kluwer Academic Publishers, The Netherlands,1996) pp. 197–224.

BEADNELL, H. J. L. (1901), *Some Recent Geological Discoveries in the Nile Valley and Libyan Desert.* (an English translation of paper communicated to the inter. Geol. Congr. Paris, 1900). Stephen Austin and Son, London, 24 pp.

DU, Z. J., MICHELINI, A., and PANZA, G. F. (1998), *EurID: A Regionalized 3-D Seismological Model of Europe*, Phys. of Earth and Planet. Int., 105: 31–62.

EGYPTIAN GEOLOGICAL SURVEY (1983), *Geological Map of Greater Cairo Area 1:100,000.*

ELGAMAL, A. W., AMER, M., ADALIER, K., and ABDUL-FADL, A. (1993), *Engineering Aspect of the October 12, 1992 Egyptian Earthquake*. Technical report NCEER 91-7000B. National Center for Earthquake Engineering Research, State University of New at Buffalo, USA.

EL-GAMILI, M. (1982), *A Geophysical Interpretation of a Part of the Nile Valley, Egypt Based on Gravity Data,* J. Geol. Special Vol. Part 2, 101–120.

EL-SAYED, A. (1996), *Seismic Hazard of Egypt*. Ph.D. Thesis, Seismological Department Uppsala University, Sweden.

EL-SAYED, A., ARVIDSSON, R., and KULHANEK, O. (1999), *The 1992 Cairo Earthquake – A Case Study of Small Destructive Event*, J. Seismol. *2*, 1–10.

EL-SAYED, A., ROMANELLI, F., and PANZA, G. (2000), *Recent Seismicity and Realistic Waveforms Modeling to Reduce the Ambiguities about the 1303 Seismic Activity in Egypt*, Tectonophysics *328*, 341–357.

FÄH, D. (1992), *A Hybrid Technique for the Estimation of Strong Ground Motion in Sedimentary Basins*, Dissertation, Swiss Federal Institute of Technology, Zürich.

FÄH, D., SUHADOLC, P., and PANZA, G. F. (1990), *A New Method for the Realistic Estimation of Seismic Ground Motion in Megacities: The Case of Rome*, Earthquake Spectra *9*, 643–668

FÄH, D., IODICE, C., SUHADOLC, P., and PANZA, G. F. (1993), *Estimation of Strong Ground Motion in Laterally Heterogneous Media*: Modal summation-Finite Differences, Proceedings of the 9th European Conference of Earthquake Engineering, Sept. 11–16, 1990, Moscow 4A, 100–109.

FÄH, D., SUHADOLC, P., MUELLER, St., and PANZA, G. F (1994), *A hybrid Method for the Estimation of Ground Motion in Sedimentary Basins: Quantitative Modeling for Mexico City*, Bull. Seismol. Soc. Am. *84*, 383–399.

FAULKNER, R. O., *The ancient Egyptian Pyramids Texts* (Oxford, UK, 1969).

FLORSCH, N., FÄH, D., SUHADOLC, P., and PANZA, G. F. (1991), *Complete Synthetic Seismograms for High-frequency Multimodal SH Waves*, Pure Appl. Geophys. *136*, 529–560.

GUSEV, A. A. (1983), *Descriptive Statistical Model of Earthquake Source Radiation and its Application to an Estimation of Short-period Strong Motion*, Geophys. J. R. astr. Soc. *74*, 787–808.

HELAL, A. N. (1998), *Seismo-technical Characteristics of Foundation Beds at the Second Industrial Zone, Six of October City, Giza, Egypt,* Proc. 16th ann. meeting, 253–274.

HSU, K. J., RYAN, W. B. F., and CITA, M. B. (1973), *Late Miocene Desiccation of the Mediterranean,* Nature *242*, 239–243.

JICA, JAPAN INTERNATIONAL COOPERATION AGENCY (JICA) (1993), *Report of Japan Disaster Relief Team on the Earthquake in Arab Republic of Egypt of October 12, 1992*, 88 pp.

KEBEASY, R. M., *Seismicity*. In (R. Said, ed.), *The Geology of Egypt* (A. A. Balkema, Rotterdam, The Netherlands 1990), pp. 51–59.

KULHANEK, O., KORRAT, I., and EL-SAYED, A. (1993), *Connection between the Seismicity in Red Sea and Egypt*, Mans. Sci. Bull. Symp. Quaternary and Development in Egypt, Mansoura University, Egypt, 331–348.

LEVANDER, A. R. (1988), *Fourth-order Finite-difference P-SV Seismograms*, Geophys. *53*, 1425–1436.

MAAMOUN, M., MEGAHED, A., and ALLAM, A. (1984), *Seismicity of Egypt*, Bull of HIAG *4*, 109–160.

MARGOTTINI, G. (1982), *Osservazioni su alcuni grandi terremoti con epicentro in oriente. Campo macrosismico in Italia del terremoto greco del 1903*. Rep. CNEN-RT/AMB 982)3 Comit. Naz. Energ. Nucleare, Rome.

MARZOUK, I. (1995), *Engineering Seismological Studies for Foundation Rock for El-Giza Province*, NRIAG Bull. *11*, 265–296.

MESHERF, W. M., *Tectonic*. In (R. Said, ed.), *The Geology of Egypt* (A. A. Balkema, Rotterdam, The Netherlands 1990), pp. 113–155.

MOHAMMED, A. (1995), *Seismic Response Analysis of the Foundation Area of the 12 October 1992 Earthquake Determined from Seismic Refraction Technique*, NRIAG Bull. *11*, 297–328.

NRIAG, HELWAN INSTITUTE of ASTRONOMY and GEOPHYSICS (1993), *The Final Report on the Detailed Studies around Dahsour Earthquake October 12, 1992*, Seismological Department, Internal report.

NRIAG, HELWAN INSTITUTE of ASTRONOMY and GEOPHYSICS (2001), *Egyptian Seismological Bulletin*, Egyptian National Seismic Network ENSN, Internal report.

PANZA, G. F. (1985), *Synthetic Seismograms: The Rayleigh Waves Modal Summation*, J. Geophys. *58*, 125–145.

PANZA, G. F. and SUHADOLC, P., *Complete strong motion synthetics.* In (B. A. Bolt, ed), *Seismic Strong Motion Synthetics. Computational Techniques 4.* (Academic Press, Orlando (1987), pp. 153–204.

PANZA, G. F., ROMANELLI, F., and VACCARI, F. (2000), *Seismic Wave Propagation in Laterally Heterogeneous Anelastic Media: Theory and Applications to the Seismic Zonation*, Advances in Geophysics (Academic Press) *43*, 1–95.

PRICE, N. J. and COSGROVE, J. W., *Analysis of Geological Structure* (Cambridge University Press 1990).

ROSS D. and SCHLEE, J. (1973), *Shallow Structure and Geological Development of the Southern Red Sea*, Geol. Soc. Amer. Bull. *84*, 3827–3848.

SAID, R., *The River Nile* (Springer Verlag, New York, USA 1981).

SAID, R., *The Geology of Egypt* (A. A. Balkema Publishers, Rotterdam, The Netherlands 1990).

SANDFORD, K. S. (1934), *Paleolithic man and the Valley in Upper and Meddilk Egypt*, Chicago University Oriental Inst. Publ. *3*, 1–131.

SHEBALIN, N. V., KARNIK, V., and HADZIEVSKI, D. (1974), *Catalogue of Earthquakes 1901–1970 and Atlas of Isoseismal Maps*, 3 vols., UNDP/UNESCO Balkan Project Skopje.

SIEBERG, A. (1932), *Erdbebengeographie*, Handbuch der Geophysik, Band IV, Abschnitt VI, Berlin, Germany.

VIRIEUX, J. (1984), *SH-wave Propagation in Heterogenoues Media: Velocity-stress Finite Difference Method.* Geophysics *49*, 1933–1957.

VIRIEUX, J. (1986), *P-SV-wave Propagation in Heterogenoues Media: Velocity-stress Finite-Difference Method.* Geophysics *51*, 889–901.

WOODWARD-CLYDE CONSULTANTS (1985), *Earthquake Activity and Dam Stability Evaluations for the Aswan High Dam, Egypt*, Aswan High Dam authority, Ministry of Irrigation, Egypt.

XIE, J. and MITCHELL, B. J. (1990), *A Back-projection Method for Imaging Large-scale Lateral Variations of Lg coda Q with Application to Continental Africa*, Geophys. J. Int. *100*, 161–181.

(Received April 11, 2002, accepted December 2, 2002)

Pure appl. geophys. 161 (2004) 1003–1019
0033–4553/04/061003–17
DOI 10.1007/s00024-003-2488-8

Pure and Applied Geophysics

Seismicity and Seismic Hazard in Alexandria (Egypt) and its Surroundings

A. EL-SAYED[1], I. KORRAT[1] and H. M. HUSSEIN[2]

Abstract—Alexandria City has suffered great damage due to earthquakes from near and distant sources, both in historical and recent times. Sometimes the source of such damages is not well known. Seismogenic zones such as the Red Sea, Gulf of Aqaba-Dead Sea Hellenic Arc, Suez-Cairo-Alexandria, Eastern-Mediterranean-Cairo-Faiyoum and the Egyptian costal area are located in the vicinity of this city. The Egyptian coastal zone has the lowest seismicity, and therefore, its tectonic setting is not well known.

The 1998 Egyptian costal zone earthquake is a moderate complex source. It is composed of two subevents separated by 4 sec. The first subevent initiated at a depth of 28 km and caused a rupture of strike (347°), dip (29°) and slip (125°). The second subevent occurred at a shallower depth (24 km) and has a relatively different focal parameter (strike 334°, dip 60° and slip 60°). The available focal mechanisms strongly support the manifestation of a complex stress regime from the Hellenic Arc into the Alexandria offshore area.

In the present study a numerical modeling technique is applied to estimate quantitative seismic hazard in Alexandria. In terms of seismic hazard, both local and remote earthquakes have a tremendous affect on this city. A local earthquake with magnitude M_s = 6.7 at the offshore area gives peak ground acceleration up to 300 cm/sec^2. The total duration of shaking expected from such an earthquake is about three seconds. The Fourier amplitude spectra of the ground acceleration reveals that the maximum energy is carried by the low frequency (1–3 Hz), part of the seismic waves. The largest response spectra at Alexandria city is within this frequency band. The computed ground accelerations due to strong earthquakes in the Hellenic Arc, Red Sea and Gulf of Aqaba are very small (less than 10 cm/sec^2) although with long duration (up to 3 minutes).

Key words: Alexandria, Egypt, seismicity, modeling, seismic hazard.

Introduction

Alexandria represents the second largest city in Egypt. Historically, parts (Menouthis and Herakleion) of this city were completely destroyed and sunk in the Aboukir Bay under 6–8 meters of water (Fig. 1). The source and the date of destruction are not exactly known, however it most likely took place in the 7th or 8th century (as indicated by excavated coins and jewelries) by either land subsidence (GEOTIMES, 2000) or earthquakes (STANFORD REPORT, 2000).

[1] Department of Geology, Mansoura University, Mansoura, Egypt.
[2] National Research Institute of Astronomy and Geophysics, Seismology Department, Helwan, Egypt.

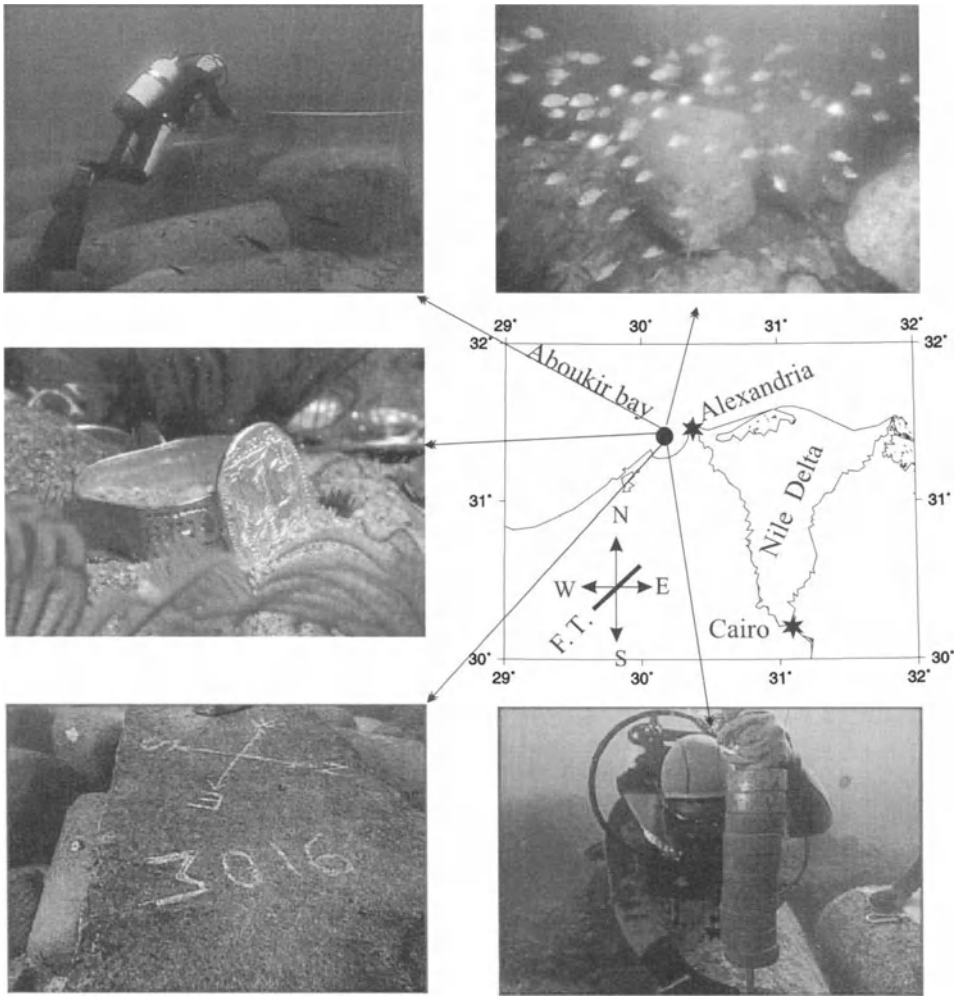

Figure 1
Examples of the archeological remain discovered in Aboukir Bay (solid circle) off Alexandria (solid star). All of the destroyed columns are collapsing (F.T) in the NE-SW direction.

The city was also shaken by five earthquakes in the last century. The most recent one occurred on May 28, 1998 (Fig. 2). This event had a moderate magnitude (m_b = 5.5 and $Mo = 2.0 \times 10^{24}$ dyne cm) and was located at about 250 km northwest of Alexandria (27.64°E and 31.45°N), It was felt with intensity II as far as Nicosia and Aqaba and injured one person in Cairo. Seismic stations in the surrounding areas recorded no activity before or after the mainshock.

Generally speaking, the Alexandria offshore area has low to moderate seismicity (Fig. 2(a & b)) however, regions like Hellenic Arc, Red Sea and Gulf of Aqaba which

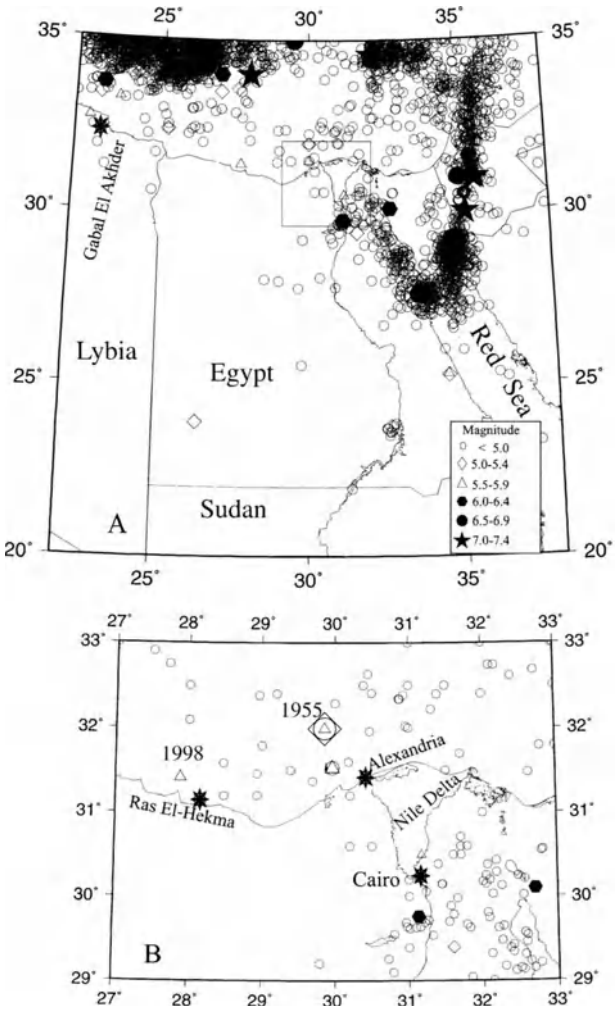

Figure 2
Distribution of earthquake epicenters in the vicinity of: (A) Egypt and (B) Alexandria (square area in A) within the time period 1900–2000. Star represents the destructive events. (★) denotes, the sites location.

are about 400–600 km from the city have high seismicity (Fig. 2a) and the impact on the city is sometime enormous (MAAMOUN *et al.*, 1984; KEBEASY, 1990; AMBRASEYS *et al.*, 1994).

The main objectives of this research work are to: (1) review the tectonic and seismic history in the site of Alexandria and its surrounding, (2) obtain the source parameters of the 1998 earthquake in an attempt to understand the tectonic behavior of the offshore area, and (3) estimate the level of seismic hazard expected from future strong earthquakes.

Tectonic Setting

The primary features of active plate tectonics in the vicinity of Egypt have been discussed in detail by many authors (McKENZIE, 1970, 1972; NEEV, 1975; BEN-MENAHEM *et al.*, 1976; GARFUNKEL and BARTOV, 1977; BEN-AVRAHAM, 1978; SESTINI, 1984; MESHERF, 1990). Egypt is located near three major plate boundaries, namely: the African-Eurasian margin (including the Hellenic Arc), Gulf of Aqaba-Dead Sea (the Levant transforms) fault and the Red Sea margin (Fig. 3a). The Sinai block or subplate is partially separated from the African plate by spread-apart or rifting along the Gulf of Suez (WOODWARD-CLYDE CONSULTANTS, 1985). In addition to these plate boundaries there is a megashear zone running from southern Turkey to Egypt (NEEV, 1975; KEBEASY, 1990) marked by relatively moderate and scattered seismicity.

The Alexandria offshore is located within the Afro-Arabic Platform block which is contiguous with southern Alpine overthrust belt (ORWIG, 1982). The contact between these blocks is traceable on seismic profiles from exposed areas in Syria and eastern Turkey into deep water south of the islands of Crete and Cyprus. This Afro-Arabic platform block is subdivided into four different units (ORWIG, 1982; SAID, 1990), which is also affected by a major fault known as the Suez-Cairo-Alexandria fault zone. This fault is characterized by a low to moderate seismic activity in Egypt. The event of October 1992 more likely occurred along one segment of this fault system.

On the other hand, the city of Alexandria itself is a part of the Nile Delta cone (Fig. 3b), which is considered as a large hinge zone that consists of several southward half-grabens. These grabens are deformed and bounded by east-west-oriented northward-dipping listric faults (HUSSEIN and ABD-ALLAH, 2001). Two mechanisms are suggested for the deformation of the Nile Delta hinge zone. The first one is related to the late Oligocene-Early Miocene compression cycle, in the direction NW-SE to NNW-SSE, that resulted from the Alpine Orogeny (end of the Eocene). This compression reactivated the E-W orientated deep-seated Mesozoic faults. The second mechanism is related to northward gravitational sliding of Oligocene-Pliocene shale and sandstone over the pre-Eocene carbonates rocks. Both mechanisms acted together during the deformation of the Nile Delta hinge zone (HUSSEIN and ABD-ALLAH, 2001). In general, these mechanisms create a complicated tectonic setting in the site of Alexandria and its vicinity (Fig. 3b).

Seismicity Review

Alexandria city has experienced about 25 damaging earthquakes spanning the time period 320 to 2000 (MAAMOUN *et al.*, 1984; AMBRASEYS *et al.*, 1994; EL-SAYED *et al.*, 2000). Nine of these earthquakes are located offshore of Alexandria. The magnitudes of these local earthquakes are moderate (M_s = 6.7), nonetheless they

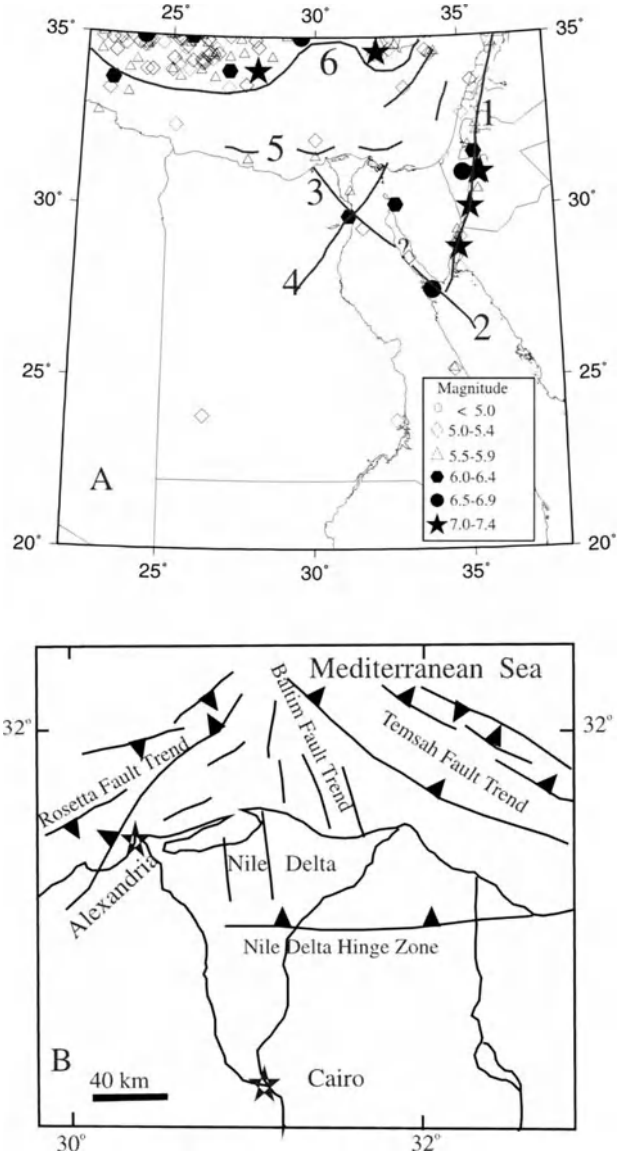

Figure 3

(A) The distribution of earthquake epicenters (with magnitude > 5.0 in time period 1900–2000) and the major tectonic elements in the vicinity of Egypt (modified from SESTINI, 1984; KEBEASY, 1990; MESHERF, 1990). (B) Local tectonic elements in the vicinity of Alexandria (modified from HUSSEIN and ABD-ALLAH, 2001). (1) Denote the Gulf of Aqaba-Dead Sea, (2) Red Sea, (3) Suez-Cairo-Alexandria fault zone, (4) Eastern-Mediterranean-Cairo-Faiyoum fault zone, (5) Egyptian Coastal zone and (6) Eastern-Mediterranean (Hellenic Arc).

were felt with intensities reaching IX, MSK (AMBRASEYS *et al.*, 1994). The event of 1955 (M_s = 6.7) is the most recent locally damaging earthquake. During this earthquake a few people were injured. A considerable number of adobe house were destroyed and a few of those with concrete construction suffered damage (MAAMOUN *et al.*, 1984; AMBRASEYS *et al.*, 1994). In general, the duration of shaking in Alexandria from such offshore earthquakes did not exceed a few (2–3) seconds (AMBRASEYS *et al.*, 1994).

The other 14 earthquakes were located mainly in the Eastern Mediterranean region (i.e., Hellenic Arc). These earthquakes have relatively large magnitudes, M_s = 7.8, (AMBRASEYS *et al.*, 1994). The observed intensity from such remote earthquakes in Alexandria extends to VI. According to AMBRASEYS *et al.* (1994), these remote earthquakes were generally felt in Alexandria for about 3 minutes or more. The most severe damage in Alexandria was related to events located in the Eastern Mediterranean (Ambraseys *et al.*, 1994). Some of these quakes (e.g., the event of 320) triggered a destructive tsunami that destroyed more than 50,000 houses (one third of the city) and killed 5,000 people in Alexandria.

Historical and recent reports indicated that the events which are located as far as the Red Sea and Gulf of Aqaba are felt in Alexandria but without damage. The recent examples of 1969 (M_s = 6.9) and 1995 (M_s = 7.3) in the northern Red Sea and Gulf of Aqaba, respectively, were felt in Alexandria with intensity (III–IV) but caused no damage. Unfortunately, the reported intensity data for Alexandria are insufficient to study their return periods.

The Effects of 1998 Earthquake

On May 28, 1998 a moderate (m_b = 5.5, Mo = 2.0×10^{24} dyne cm) earthquake occurred approximately 250 km northwest of Alexandria (27.64°E and 31.45°N). Immediately after the May 28, 1998 earthquake, 55 locations in the northern part of Egypt were surveyed to collect observations and reports of the shaking effects on buildings, ground and or people (HASSOUP and TEALAB, 2000). Based on this survey, maximum intensity (VII) was assigned at Ras El-Hekma village (~300 km west of Alexandria) on the Mediterranean Sea coast (Fig. 2b). The ground fissures trending NW-SE were observed along the beach. These fissures were observed only in those areas of unconsolidated sedimentary deposits. In terms of damage some cracks were observed in concrete buildings. On the other hand, in Alexandria there were no reports of damage. Some people left their houses; the windows rattled and hanging objects swung, but the direction of the ground motion was poorly identified. HASSOUP and TEALAB (2000) assigned an intensity V-VI in Alexandria city.

According to ISC reports, the event of 1998 was felt even as far as Nicosia (intensity = II) and Aqaba, causing one injury to a person in Cairo city. It is very important to mention that there was no seismic activity before or after the mainshock.

Modeling of 1998 Earthquake

The event of 1998 has triggered a considerable number of seismic stations worldwide. In modeling study, stations located within the distance range 30° – 90° were considered. For closer stations (< 30°) the upper mantle structure creates arrivals that do not belong to the source, while for distant stations (> 90°) the core arrivals started to influence the seismograms (CIPAR, 1980). To obtain the best data quality, only seismograms recorded by the digital network of Incorporated Research Institute for Seismology (IRIS) were used.

Altogether, twelve broadband body wave records (*P* and *SH*) were used. The choice of these records is mainly based on the signal-to-noise ratio. The available stations cover a relatively good azimuthal range, excepting the SW quarter of the sphere.

As the selected stations are located in different geological settings, a simplified average model proposed by Jeffreys-Bullen is adopted. According to this model the crust consists of two layers with thicknesses 15 and 18 km and *P*-wave velocities 5.6 and 6.5 km/sec, respectively. The two layers are underlined by a half-space layer with V_p 8.0 km/sec.

P-wave polarities of 14 seismograms were picked up and used to construct the starting focal mechanism in our inversion. This solution shows a reverse faulting mechanism with a constrained northwest nodal plane dipping northeast (Fig. 4).

The observed records were then inverted using the technique of KIKUCHI and KANAMORI (1991) for a single point source until the best fit (between observed and synthetics) was obtained (Fig. 4). The differences between the observed and synthetic records were calculated to obtain the residuals. Using these residual data, iterative inversion was carried out to determine the locations (in space and time) and seismic moments of the subsequent sources. In general, KIKUCHI and KANAMORI's (1991) technique used in the present study is developed to represent large complex sources, however, it is successfully extended to represent the complex events that have moderate magnitude (PINAR and TÜRKELLI, 1997; PINAR and KALAFAT, 1999).

In this study, the Green's functions for the six elementary tensors were calculated for a grid of 45 points separated by 4 km. These points represent a plane (9 in horizontal and 5 in depth) that includes the source area. The calculated Green's functions were convolved with the *Q* filter (1.0 and 4.0 seconds for *P* and *S* waves, respectively) and with source time function of a rise time $\tau_1 = 1.7$ and duration $\tau_2 = 3.4$ seconds. Using the above parameters, the first 60 seconds of the seismograms were simultaneously inverted, allowing the mechanism to change during the rupture to reduce the residuals.

It was not possible to model *SH* phases with a single source; on the other hand, two sources separated by 4 seconds give the best fit (Fig. 4). The suggested sources are located 8 km away from each other on a plane striking NNW-SSE with focal depths 28 and 24 km, respectively. As shown in Figure 4, for all stations, there is a

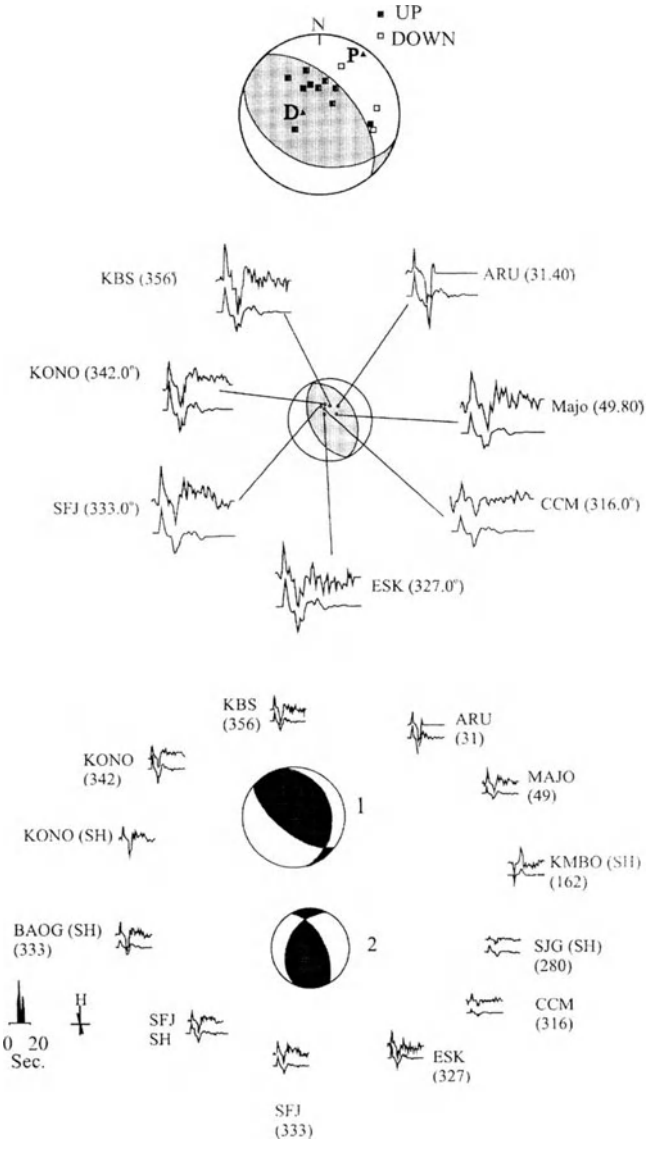

Figure 4
Focal mechanism obtained for the 1998 earthquake from (top) polarity data (middle) inversion of P waveforms and (lower) inversion of *P* and *SH* waveforms. Station name and azimuth (between brackets) are given beside the record. Beach balls 1 and 2 correspond to the first and second subevents, respectively.

relatively good agreement between observed and synthetics, except for the KMBO station which lies close to the nodal plane.

Based on modeling results, the rupture process started with the first subevent (strike = 347°, dip = 29°, slip = 125°) along a fault plane trending NNW-SSE of

low dip angle. Four seconds later, the second subevent (strike = 334°, dip = 60°, slip = 60°) coupled the motion to a shallower but steeper plane. The mechanism of the first subevent compares adequately with those of HUSSEIN *et al.* (2001) and the Centroid Moment Tensor (CMT) solution. Generally, the mechanism of the 1998 earthquake is similar to that of the 1955 and 1988 earthquakes (nearby offshore events, ABO-ELENEAN, 1993) in terms of fault type, reverse, but is relatively different in terms of fault trend and strike-slip component.

Seismic Hazard

The seismic hazard scenario for Alexandria and its environs was examined using the deterministic approach developed by COSTA *et al.* (1992, 1993). This method uses the information of earth's structure (crustal models) and level of seismicity (earthquake catalogue, seismogenic zones and focal mechanisms) to compute a synthetic seismogram that could be observed from an expected large earthquake.

The database of earthquake catalogue, seismogenic zones, and focal mechanisms of the identified seismogenic zones prepared by EL-SAYED *et al.* (2001) was used in this study. The obtained focal mechanism from body-wave inversion for the 1998 earthquake is used to describe the source complexity of the offshore area in better way, instead of the 1955 events derived from *P*-wave polarities (EL-SAYED *et al.*, 2001).

The structural models of the media beneath the considered area are represented by a number of flat layers (Fig. 5). The thickness, the density and the *P* and *S* waves of these layers are taken from deep seismic sounding and Bouguer anomaly profiles published by the Egyptian General Petroleum Company (GPC). These data are stored in the Atlas of Geology at Cornell University, USA (BARAZANGI *et al.*, 1996; MAKRIS *et al.*, 1988; EL-SAYED *et al.*, 2001). The *S*-wave velocity is taken as $V_P/1.73$. The quality factors are taken from XIE and MITCHELL (1990).

The geotechnical parameters (for the upper 300 m) in/and around this area have been investigated by many authors (e.g., MARZOUK, 1995; MOHAMMED, 1995; HELAL, 1998) and governmental building organizations (e.g., Educational Building Authority, EBA). These investigations were carried out by using shallow seismic techniques and drilling boreholes. It should be emphasized that the velocities (V_p and V_s) given by different authors are in a good agreement with laboratory measurements made by EBA. Figure 5 summarizes the crustal parameters used in this calculation. Due to a lack of specific models for the upper mantle, a standard continental model of HARKRIDER (1970) and DU *et al.* (1998) has been considered.

When the seismicity, the source mechanisms, the structural models and the observation points are defined, synthetic signals are computed using the modal summation technique (PANZA, 1985; PANZA and SUHADOLC 1987; FLORSCH *et al.*, 1991).

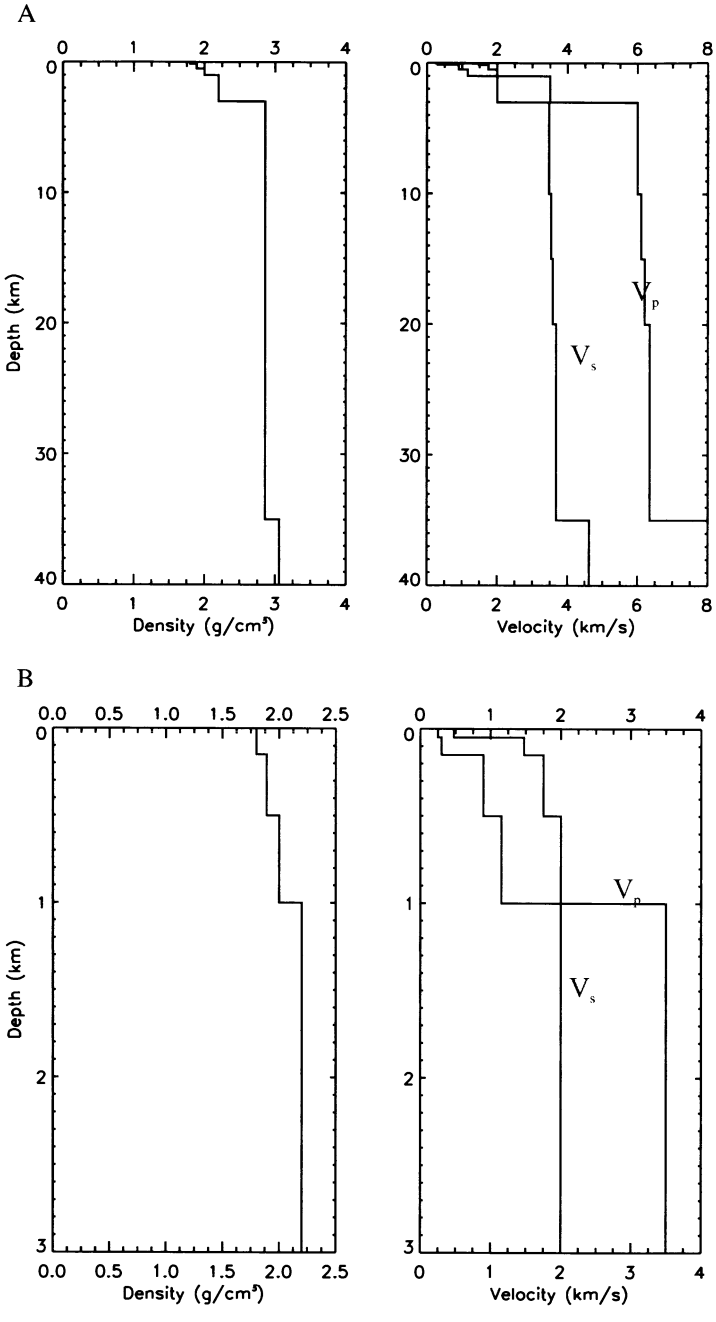

Figure 5
(A) Crustal model considered in this study and (B) zoom of the upper 3 km.

To study the ground motion in the vicinity of Alexandria, roundly 3000 earthquake were used (Fig. 2a). The horizontal *P-SV* (radial) and *SH* (transverse) components of motion were computed and rotated to the common reference system (N-S and E-W directions) after which their vector sum is calculated. The total number of seismograms expected for the above configuration would exceed 90,000. To reduce the computations, the source-receiver distance is kept below 100 km. At each observation point all seismograms generated by different sources are examined and the largest component of ground motion is selected for further analysis. The synthetic signals are computed to obtain the peak ground displacement (DMAX), velocity (VMAX) and acceleration (AMAX) reaching a maximum frequency of 10 Hz (Fig. 6).

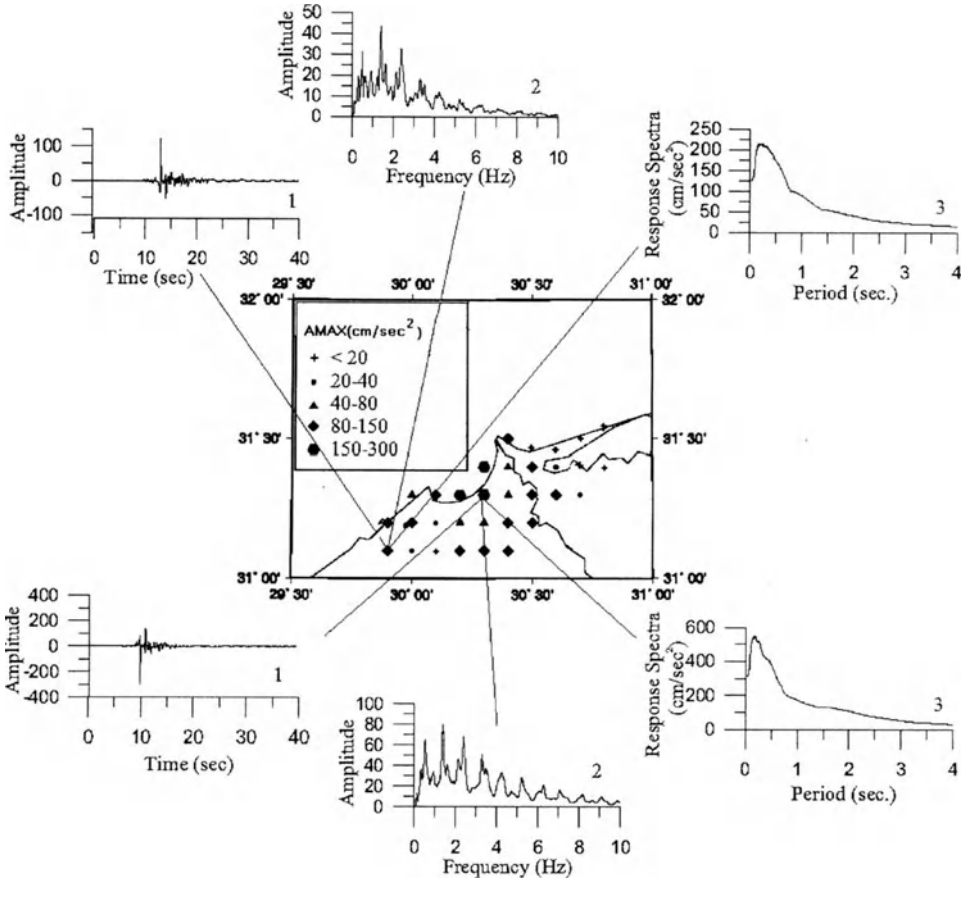

Figure 6

Distribution of the computed peak ground acceleration computed for earthquakes with epicenter distance = 100 km. 1, 2, 3 in the left of the traces refer to the calculated acclerograms, Fourier amplitude spectra and response spectra, respectively. AMAX stands for the maximum computed acceleration amplitude.

To investigate the effects of large, distant earthquakes, calculations were performed for the largest observed earthquakes in the most active zones, e.g., the Hellenic Arc, Gulf of Aqaba, Red Sea (Fig. 7).

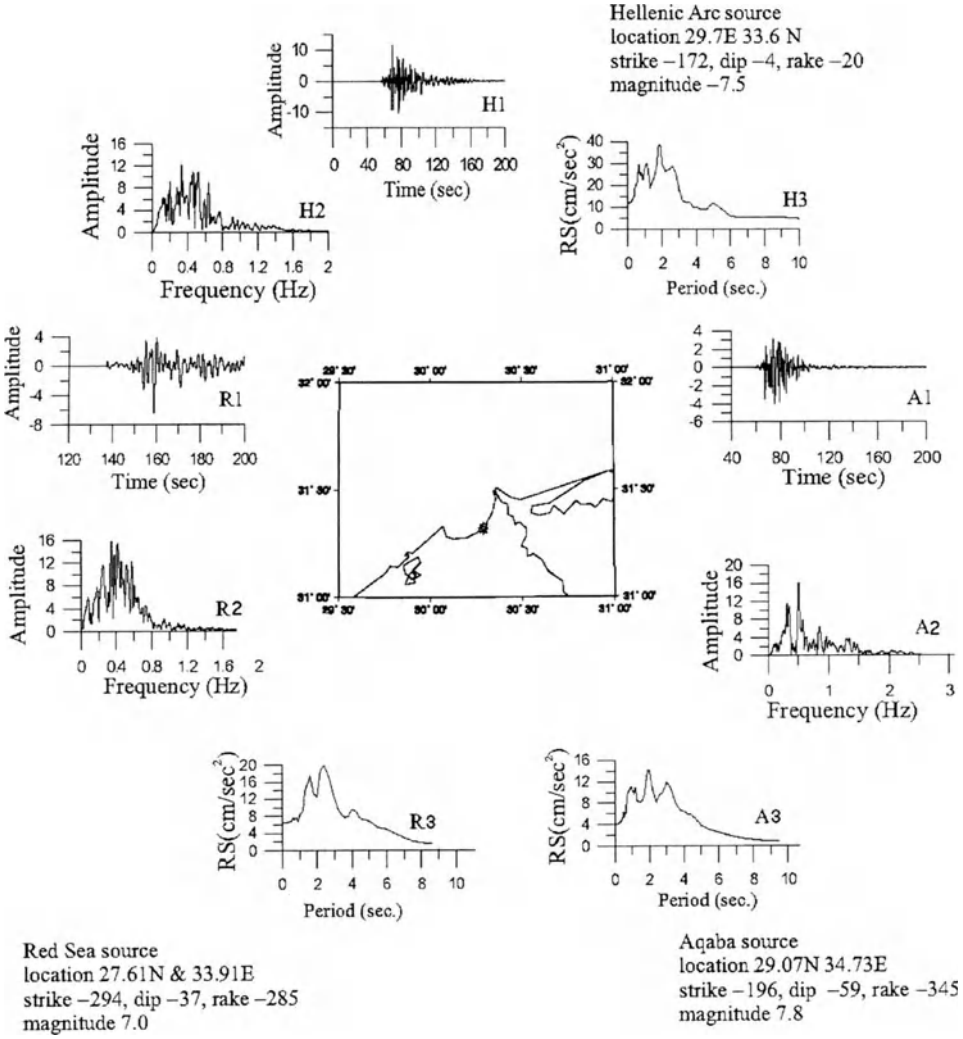

Figure 7
Computed peak ground acceleration at Alexandria using remote earthquakes. A, R, H corresponding to Aqaba, Red Sea and Hellenic Arc, respectively and 1, 2, 3 as in Figure 6. The parameters considered for each source are given in the top and bottom of the Figure. RS stands for response spectra.

Discussion

Alexandria is located approximately 300 to 600 km from three known active plate boundaries, namely: the Red-Sea, the Gulf of Aqaba and the Hellenic Arc (McKenzie 1970, 1972; Sestini, 1984; Mesherf, 1990). The interaction among these three plate boundaries created major fault zones in Egypt as: (1) Eastern-Mediterranean Cairo-Faiyoum fault zone (Neev, 1975; Sestini, 1984; Mesherf, 1990), (2) Suez-Cairo-Alexandria fault zone (Kebeasy, 1990). These fault zones are very close to the city of Alexandria (Fig. 3). Moreover, deep seismic sounding reveals that there are minor faults such as Rosetta fault which trend a few kilometers from Alexandria city (Fig. 3b, Hussein and Abd-allah, 2001).

As a result of this complex tectonic setting many earthquakes occurred in the vicinity of Alexandria, both in recent and historical time (Ambraseys *et al.*, 1994; Maamoun *et al.*, 1984). The spatial distribution of the earthquakes epicenters (Fig. 2) shows that there are areas of very intense (e.g., plate boundaries) and others of low (e.g., offshore area) activities. For those of intense seismicity, there are a considerable number of focal mechanisms that allow us to understand its geodynamic behaviors (McKenzie, 1970; and Rotstein and Kafka, 1982; Sestini, 1984; CMT database). Controversy, the number and quality of the focal mechanisms available for those of low seismic activity (like the Egyptian coastal zone) are not enough to have the clear understanding for the tectonic setting (Sestini, 1984; Kebeasy, 1990; Mesherf 1990).

The modeling of the 1998 earthquake (in the Egyptian coastal zone) reflected the complexity of the tectonic setting in this area. This complexity was generated originally by the interaction between the African and Euro-Asian plates and manifested towards the North African coast (Le Pichon and Sibuet, 1981). It is supported by the polarity mechanisms of the 1955, 1987 and 1988 earthquakes (Abo-Elenean, 1993). Other support is the recorded seismograms at Helwan station for the events of 1955, 1987, 1988 and 1998. *P* waves in these seismograms are not simple but rather complicated and usually include different phases of *P* waves (Hussain *et al.*, 2001).

As a result of this complex stress regime, damaging earthquakes had occurred in the vicinity of Alexandria (Ambraseys *et al.*, 1998; Kebeasy, 1990; Maamoun *et al.*, 1984). Some of these damaging earthquakes are apparently missing. As an example, the damage in Menouthis and Herakleion is more likely caused by an earthquake (which is not known yet). This is supported by: (1) the collapsed columns are falling down in the same direction NE-SW (Fig. 1), (2) the presence of coins and jewelry suggest a sudden collapse, (3) the sharp sand grains in the bottom of Aboukir Bay reflecting active tectonic environment, and (4) the Cairo-Alexandria fault system (NE-SW) is passing by the area and recently generated frequent moderate earthquakes (Geotimes, 2000). This does not exclude the possibilities of land subsidence as suggested in the Stanford Report (2000).

Such phenomena (liquefaction and land subsidence) were observed in the area after the event of 1926 (AMBRASEYS and ADAM, 1998).

As can be seen, the seismic hazard is relatively high in Alexandria. e.g., the area just in front of Alexandria represents a spot of activity that produces frequent moderate (M_s = 6.7) earthquakes (AMBRASEYS *et al.*, 1994). The computed ground motion (displacement DMAX, velocity VMAX and acceleration AMAX), at a distance less than 100 km, are 7.1 cm, 21 cm/sec and 300 cm/sec^2, respectively. These values are slightly higher than the computed values, at 1 Hz, by EL-SAYED *et al.* (2001). The Fourier amplitude spectra show that the energy of the peaks is of low frequencies that have the maximum response from the site (Fig. 6). The total duration of the computed ground motion traces are in the order of a few seconds. The concentration of damage to high buildings and construction that is generally of low frequencies response during the offshore events of 951 and 1955 support the obtained results. Other support is the duration of shaking. These earthquakes were strongly felt for 2–4 seconds (AMBRASEYS *et al.*, 1994), in agreement with the computed values. Unfortunately, there were no stations available in Alexandria to verify our calculation quantitatively but according to PANZA *et al.* (1999) conversion table the values of AMAX correspond to intensity VIII-IX which is in agreement with the one observed during the 1955 earthquake.

Remote events also could have their impact on Alexandria city. As an example, the ground motions due to an earthquakes with magnitude (M_s = 7.5) in the Hellenic, (M_s = 7.0) in the Red Sea or (M_s =7.8) in the Gulf of Aqaba have peaks of 4 cm, 5 cm/sec and 12 cm/sec^2, respectively. These peaks are reported around 1 Hz. Most of the remote earthquakes (e.g., the 320, 557, 1303, 1926 and 1996 events) were felt in Alexandria in the order of minutes (AMBRASEYS *et al.*, 1994; AMBRASEYS and ADAM, 1998; EL-SAYED *et al.*, 2001) as also predicated by our calculations. In general, the computed intensity for remote sources is smaller than the observed one by one-two units. This may be attributed to local site effects that are not taken into account in our model. The coupling between the long duration of shaking and the unconsolidated water-saturated soft sediments may cause liquefaction and thus increase the level of risk. It should be also emphasized that liquefaction phenomena were associated with the events of 1926 and 1998 (AMBRASEYS *et al.*, 1998; HASSOUP and TEALAB, 2001). In addition to the seismic risk, strong remote events had triggered a strong tsunami (e.g., the events of 320 and 1303) that caused severe damage to Alexandria (AMBRASEYS *et al.*, 1994; EL-SAYED *et al.*, 2001). The strongest tsunami is reported in 320. In Alexandria the sea water passed beyond its boundaries and flooded a vast amount of land, so that on retreat of the water the sea skiffs were found lodged on the roofs of many houses. In Alexandria, 50,000 houses were flooded and 5,000 people were drowned. Ships were carried by the waves over the city walls (AMBRASEYS *et al.*, 1994).

Conclusions

From this study we can draw the following conclusion:

1. Alexandria city is located in the vicinity of three plate boundaries that interact with each other generating a complex system of major and local faults close to Alexandria offshore. These faults are associated with small to moderate earthquakes. The focal mechanisms and the waveforms of the offshore events reflect the complexity of this tectonic zone. As a result of this complexity, it was very difficult to represent the moderate earthquake of 1998 by one source and fit both *P* and *SH* waves.

2. Some of the historical earthquakes information in the vicinity of Alexandria is probably missing. As the under-water archeological remains in Aboukir bay strongly support, the city was destroyed by either local or remote earthquakes.

3. Offshore events have strong and short duration of shaking at Alexandria city. The energies of the main peaks are of low frequencies (less that 4 Hz) that have the maximum response spectra from the site. While those in remote areas have a very long duration of shaking however their peaks are relatively weak. These peaks are also of a very low frequency, which is coherent with the response spectra.

4. Remote earthquakes in the Eastern Mediterranean may also cause liquefaction and/or trigger strong destructive tsunami in Alexandria.

Acknowledgements

This work was carried out at the Department of Geology, Mansoura University, Egypt. The first author is indebted to Professor Giuliano F. Panza, Trieste, Italy and Professor Ota Kulhanek, Uppsala University, Sweden for their continuous support. Our thanks also to Drs. Vaccari, Djallali, Parvez and Ayadi for their comments and technical assistance.

Part of this research is a contribution to the IUGS-UNESCO-IGCP Project 414 "Realistic Modelling of Seismic Input for Megacities and Large Urban Areas," to OEA, ICTP "Net 40 seismic hazard in the Northern-Eastern Africa" and to the project of Mansoura University "estimation of seismic hazard in DK, Egypt."

This manuscript was greatly improved by the careful reviews of Prof. A. Gusev and an anonymous reviewer.

References

ABO-ELENEAN, K. (1993), *Seismotectonics of the Mediterranean Region North of Egypt and Libya*, M.Sc. Thesis, Faculty of Science, Mansoura University, Egypt.

AMBRASEYS, N.N., MELVILLE, C.P., and ADAM, R. D. *The Seismicity of Egypt, Arabia and the Red Sea a Historical Review* (Cambridge University Press, UK 1994).

AMBRASEYS, N.N. and ADAMS, R.D. (1998), *The Rhodes Earthquake of 26 June (1926)*, J. Seismol. *2*, 267–292.

BARAZANGI, M., FIELDING, E.J., ISACKS, B., and SEBER, D. (1996), *Geophysical and geological databases and CTBT monitoring: A case study of the Middle East*, In *Monitoring a Comprehensive Test Ban Treaty* (Kluwer Academic Publishers, The Netherlands, E.S. Husebye and A.M. Dainty, eds.) 197–224.

BEN-AVRAHAM, Z. (1978), *The Structure and Tectonic Setting of the Levant Continental Margin, Eastern Mediterranean*, Tectonophysics *46*, 313–331.

BEN-MENAHEM, A., NUR, A., and Vered, M. (1976), *Tectonics, Seismcity, and Structure of the Afro-Eurasian Junction—The Breaking of an Incoherent Plate*, Physics of the Earth and Planetary Interiors *12*, 1–50.

COSTA, G., PANZA, G.F., SUHADOLC, P., and VACCARI, F. (1992), *Zoning of the Italian Region with Synthetic Seismograms Computed with Known Structural and Source Information*, Proceed. Tenth World Conference on Earthquake Engineering, Madrid, 435–438.

COSTA, G., PANZA, G.F., SUHADOLC, P., and VACCARI, F. (1993), *Zoning of the Italian Territory in Terms of Expected Peak Ground Acceleration Derived from Complete Synthetic Seismograms*, J. Appl. Geophys. *30*, 149–160.

CIPAR, J. (1980), *Teleseismic Observations of the 1976 Friuli, Italy Earthquake Sequence*, Bull. Seism. Soc. Am. *70*, 963–983.

DU, Z.J., MICHELINI, A., and PANZA, G.F. (1998), *EurID: A Regionalized 3-D Seismological Model of Europe*, Phys. of Earth and Planet. Int. *105*, 31–62.

EL-SAYED, A., ROMANELLI, F., and PANZA, G. (2000), *Recent Seismicity and Realistic Waveforms Modeling to Reduce the Ambiguities about the 1303 Seismic Activity in Egypt*, Tectonophysics *328*, 341–357.

EL-SAYED, A., VACCARI, F., and PANZA, G. (2001), *Deterministic Seismic Hazard in Egypt*, Geophys. J. Internat. *144*, 555–567.

FLORSCH, N., FÄH, D., SUHADOLC, P., and PANZA, G. F. (1991), *Complete Synthetic Seismograms for High-frequency Multimodal SH Waves*, Pure Appl. Geophys. *136*, 529–560.

GARFUNKEL, Z. and BARTOV, Y. (1977), *The Tectonics of the Suez Rift*. Bull. Geol. Surv. Israel *71*, 1–44.

GEOTIMES (December, 2000), Newsmagazine of the Earth Sciences the American Geological Institute.

HARKRIDER, D. (1970), *Surface Waves in Multilayered Elastic Media. Part II. Higher Mode Spectra and Spectral Ratios from Point Source in Plane Layered Earth Models*, Bull. Seismol. Soc. Am. *60*, 1937–1987.

HASSOUP, A. and TEALAB, A. (2000), *Attenuation of Intensity in the Northern Part of Egypt Associated with the May 28, 1998 Mediterranean*, Acta Geophy. Polonica *38*, 183–196.

HELAL, A. N. (1998), *Seismo-technical Characteristics of Foundation Beds at the Second Industrial Zone, Six of October City, Giza, Egypt*, Proc. 16th Annual Meeting, 253–274.

HUSSAIN, H., KORRAT, I., and EL-SAYED, A. (2001), *Seismicity in the Vicinity of Alexandria and its Implication to Seismic Hazard*, Proc. 2nd Internat. Symp on Geophys. Tanta. *2*, 57–64.

HUSSEIN, I.M. and ABD-ALLAH, A.M.A (2001), *Tectonic Evolution of the Northeastern Part of the African Continental Margin, Egypt*, J. African Earth Sci. *33*, 49–68.

KEBEASY, R.M., *Seismicity*. In *The Geology of Egypt* (R. Said ed.) (A.A. Balkema, Rotterdam, The Netherlands 1990) pp. 51–59.

KIKUCHI, M. and KANAMORI, H. (1991), *Inversion of Complex Body Waves – III*, Bull. Seismol. Soc. Am. *79*, 670–689.

LE PICHON, X. and SIBUET, J. C. (1981), *Passive Margins: A Model of Formation*, J. Geophys. Res. *86*, 3708–3720.

MAAMOUN, M., MEGAHED, A., and ALLAM, A. (1984), *Seismicity of Egypt*, HIAG Bull. *4*, 109–160.

MAKRIS, J., RIHM, R., and ALLAM, A. (1988), *Some Geophysical aspects of the evluation and the structure of the crust in Egypt*. In *The Pan African Belt of Northeastern Africa and Adjacent Areas* (S. El-Gaby and R.O. Greiling, eds.) pp. 345–369.

MARZOUK, I. (1995), *Engineering Seismological Studies for Foundation Rock for El-Giza Province*, NRIAG Bull. *11*, 265–296.

MCKENZIE, D. (1970), *Plate Tectonics of the Mediterranean Region*, Nature *326*, 239–243.

MCKENZIE, D. (1972), *Active Tectonic of the Mediterranean Region*, Geophys. J. R. Astr. Soc. *30*, 109–185.

MESHERF, W. M., *Tectonic framework of the northern Egypt and the eastern Mediterranean region*. In *The Geology of Egypt* (R. Said, ed.) (A.A. Balkema, Rotterdam, The Netherlands 1990).

MOHAMMED, A. (1995), *Seismic Response Analysis of the Foundation Area of the 12 October 1992 Earthquake Determined from Seismic Refraction Technique*, NRIAG Bull. *11*, 297–328.

NEEV, D. (1975), *Tectonic Evolution of the Middle East and Levantine Basin (Eastern Most Mediterranean)*, Geology *3*, 683–686.

ORWIG, E. R. (1982), *Tectonic Framework of Northern Egypt and the Eastern Mediterranean Region*, 6th Petrol. Explor. Seminar, EGPC, Cairo, Egypt.

PANZA, G.F. (1985), *Synthetic Seismograms: The Rayleigh Waves Model Summation*, J. Geophys. *58*, 125–145.

PANZA, G.F. and SUHADOLC, P., *Complete strong motion synthetics.* In *Seismic Strong Motion Synthetics. Computational Tecniques 4* (B.A. Bolt ed.) (Academic Press, Orlando 1987) pp. 153–204.

PANZA, G.F., VACCARI, F., and CAZZARO, R., *Deterministic Seismic Hazard Assessment. Vrancea Earthquakes: Tectonic and Risk Mitigation* (F. Wenzel *et al.*, eds.) (Kluwer Academic Publishers, The Netherlands 1999) pp. 269–286.

PANZA, G.F., VACCARI, F., COSTA, G., SUHADOLC, P., and FÄH, D. (1996), *Seismic Input Modelling for Zoning and Microzoning*, Earthquake Spectra *12*, 529–566.

PINAR, A. and TÜRKELLI, N. (1997), *Source Inversion of the 1993 and 1995 Gulf of Aqaba Earthquakes 283*, 279–288.

PINAR, A. and KALAFAT, D. (1999), *Source Processes and Seismotectonic Implications of the 1995 and 1996 Cyprus, Eastern Mediterranean Region, Earthquakes 301*, 217–230.

ROTSTEIN, Y. and KAFKA, A. L. (1982), *Seismotectonics of the Southern Boundary of Anatolia, Eastern Mediterranean Region: Subduction, Collision and Arc Jumping*, J. Geophys. Res. *87*, 7694–7706.

SAID, R. *The Geology of Egypt* (A.A. Balkema Publishers, Rotterdam, The Netherlands 1990).

SESTINI, G. *Tectonic and sedimentary history of NE African margin (Egypt/Libya).* In *The Geological Evaluation of the Eastern Mediterranean* (J. E. Dixon and A. F. Robertson eds.) (Blackwell Scientific Publishers, Oxford, UK 1984) pp. 161–175.

STANFORD REPORT (December, 2000), *Scientists, Archaeologists and Historians Unravel the Mystery of Egypt's Sunken Cities.*

WOODWARD-CLYDE CONSULTANTS (1985), *Earthquake Activity and Dam Stability Evaluations for the Aswan High Dam, Egypt*, Aswan High Dam Authority, Ministry of Irrigation, Egypt.

XIE, J. and MITCHELL, B.J. (1990), *A Back-projection Method for Imaging Large-Scale Lateral Variations of Lg Coda Q with Application to Continental Africa*, Geophys. J. Int. *100*, 161.

(Received April 11, 2002, accepted November 15, 2002)

Pure appl. geophys. 161 (2004) 1021–1040
0033–4553/04/061021–20
DOI 10.1007/s00024-003-2486-x

Pure and Applied Geophysics

Linear Amplification of Horizontal Strong Ground Motion in Zagreb (Croatia) for a Realistic Range of Scaled Point Sources

MARIJAN HERAK[1], IVAN LOKMER[1], FRANCO VACCARI[2,3] and GIULIANO F. PANZA[2]

Abstract—The linear amplification of the larger horizontal component of strong ground motion along a selected profile in the city of Zagreb is estimated by examining the synthetic waveforms corresponding to a suite of 16 realistically chosen scaled point sources. The accelerograms, computed for the average bedrock model by modal summation, are propagated through local laterally heterogeneous anelastic models by the finite-difference algorithm. The ratio of peak ground acceleration (PGA) and of the response spectra (RS), obtained by using local and bedrock models, define the PGA and RS amplification AMP(PGA) and AMP(RS), respectively. Even variations of the order of commonly observed uncertainties of only dip and rake angles of the causative fault show that both AMP(PGA) and AMP(RS) vary at some sites by more than a factor of two. It follows that, especially for strongly laterally heterogeneous structures, local effects must be determined for each of the relevant sources considering all associated uncertainties as completely as possible. Such a conclusion certainly holds for the case of the microzonation of Zagreb, where the local geology is quite complex, and the seismicity is not confined to a single seismic source zone.

Key words: Amplification of strong motion, source mechanism, Zagreb, microzonation.

Introduction

On November 9, 1880 at half-past seven a.m. the citizens of Zagreb were awakened by a devastating earthquake, the strongest known event which occurred in the Zagreb epicentral area. Its intensity in the epicenter, near the village of Kašina, about 15 km from the center of Zagreb is today estimated to have been VIII °MSK. A detailed survey of earthquake effects conducted in Zagreb after the earthquake revealed that a total of 1,754 (45.8%) buildings were damaged, and 485 (12.6%) of them suffered heavy damage (Fig. 1). At the time Zagreb had about 30,000 inhabitants. Today the

[1] Department of Geophysics, Faculty of Science, University of Zagreb, Horvatovac bb, 10000 Zagreb, Croatia.

[2] Department of Earth Sciences, University of Trieste, Via E. Weiss 1, 34127 Trieste, Italy.

[3] INGV - Osservatorio Vesuviano, via Diocleziano 328, 80124 Napoli, Italy.

*Corresponding author: Prof. Marijan Herak, Department of Geophysics, Faculty of Science, University of Zagreb, Horvatovac bb, 10000 Zagreb, Croatia. E-mail: herak@rudjer.irb.hr

Figure 1
Photographs of the damage to the interiors of the church in Kašina and the Zagreb cathedral caused by the great Zagreb earthquake of 1880. The damage to the 14th century cathedral was so severe that it had to be completely rebuilt.

number of people living in Zagreb and its vicinity is close to 1 million, and an earthquake comparable to the one of 1880 would have enormous impact not only on the citizens of Zagreb, but also on the entire Croatian economy. The return period for an $M = 6$ event (corresponding to epicentral intensity of VIII–IX °MSK according to Herak, 1989) is estimated for the Zagreb region by MARKUŠIĆ and HERAK (1999) to be about 150 years. Zagreb is located on a terrain where soil conditions vary from shallow soil at the foothills of the Medvednica Mt., to rather deep soft soil deposits in the Sava River valley. All this clearly indicates that Zagreb is in urgent need of seismic zonation. Some attempts were made, but no study was ever concluded and officially accepted. Ever since 1930, no event exceeding magnitude 5 has occurred in the area, which is why there are no strong-motion records available, and deterministic modeling remains the only way to undertake the zonation of the city.

The first step in this direction was taken by LOKMER *et al.* (2002), who analyzed the linear amplification of strong ground motion along a profile which runs from Kašina through the center of the city and ends on the banks of the Sava River (Fig. 2). They noticed that amplification properties for the three wave types differ from each other and attributed this to source-specific radiation patterns of *P*, *SV*, and *SH* waves. The fact that amplification may significantly depend on source geometry was also recently reported by PANZA *et al.* (2000) for the Catania (Italy) area. If this is true and the variation of amplification is significant for a realistic range

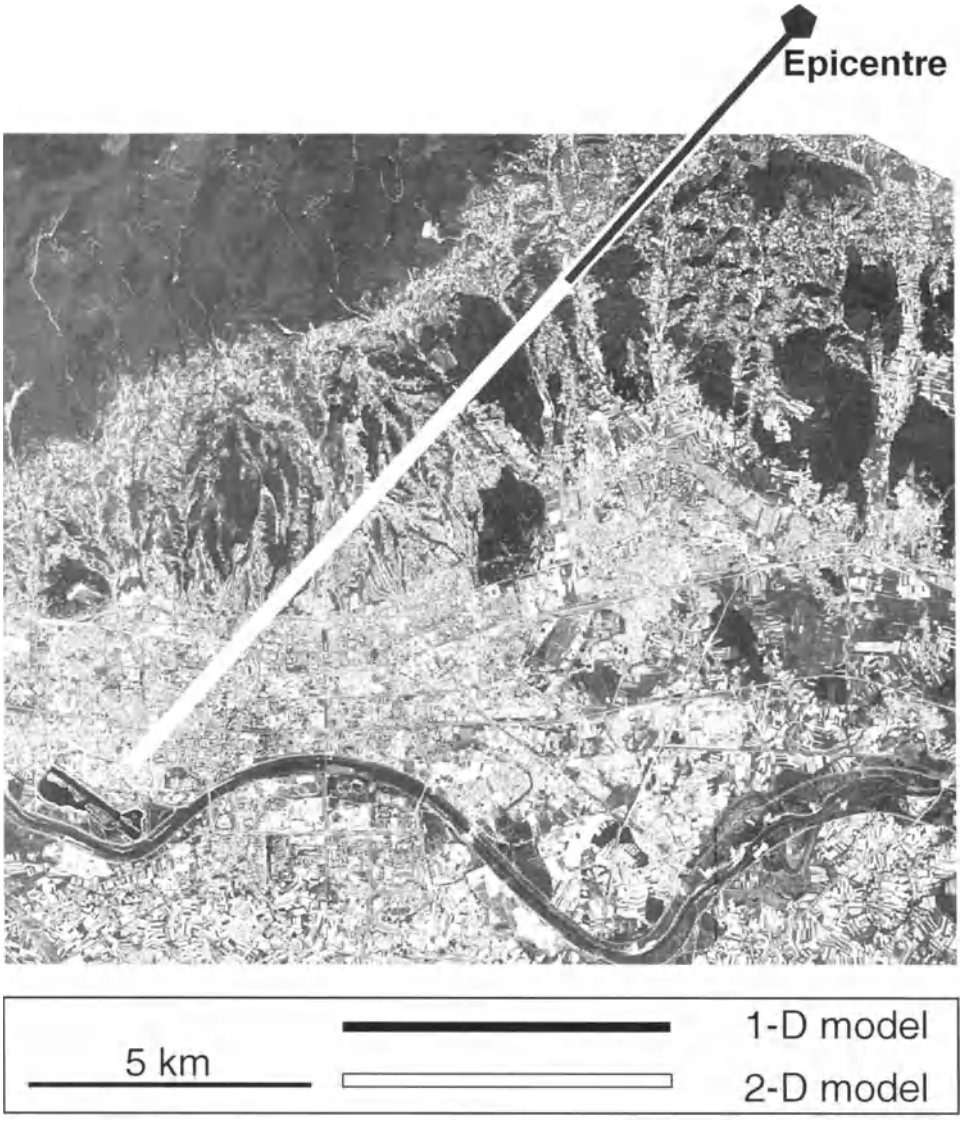

Figure 2
Satellite image of the Zagreb area, with the profile superimposed (from LOKMER *et al.*, 2002).

of source properties, considering only one reference source model can lead to amplification estimates that might not be representative of a future earthquake.

The goal of this study is to estimate linear amplification properties of soil along the same profile as used by LOKMER *et al.* (2002) (Fig. 2) for a suite of sources that may realistically be expected in the vicinity of the epicenter of the great Zagreb earthquake of 1880. In particular, we shall examine the influence that the uncertainty

of the assumed faulting geometry has on the evaluated parameters related to the larger component of the horizontal ground motion. Throughout this paper we shall consider linear amplification effects only, and the term amplification is used to mean the ratio of ground motion parameters on the surface of the soil profile and those that would be observed if only bedrock was present. The attempt to model nonlinear amplification which is dependent on the seismic load is beyond the scope of this study. The consequence of this is that results are directly applicable only to small-to-medium ground acceleration levels of approximately up to 200 cm/s^2 (BERESNEV *et al.*, 1998). Such accelerations are expected in epicentral regions of moderate magnitude events (up to a magnitude of about 6) or during aftershock sequences of large events. However, because the nonlinear effects tend to reduce the amplification levels, the linear models yield more conservative results and are therefore suited for general purpose seismic zoning projects. Furthermore, we assume the scaled point-source of seismic waves. This is a limiting factor for close events of large magnitude because synthetic seismograms will not reflect the source size, its complexity and duration, but only average amplitude spectral properties, as empirically determined globally (*e.g.*, GUSEV, 1983). The adoption of a spectral scaling law corresponds to averaging on the directivity function and on the regional variations due to different tectonic regimes, although it ensures to obtain reliable spectral scenarios. This limitation is therefore much less severe if spectral or PGA amplification is the main topic of interest instead of actual time-histories, and small- to medium-magnitude events are considered, as it is the case here.

Methods

The computation of complete synthetic seismograms has been carried out by the hybrid method, originally due to FÄH *et al.* (1990), FÄH (1992) and FÄH *et al.* (1993). The method has been used to simulate observed strong ground motion in cities such as Mexico City (FÄH *et al.*, 1994), Bucharest (CIOFLAN *et al.*, 2002), and Russe (KOUTEVA *et al.*, 2001). A detailed review of recent realistic modeling of seismic input for 13 megacities and large urban areas in Europe, Central America, Africa and Asia using the same methodology is presented by PANZA *et al.* (2002). The flowchart of the algorithm is given in Figure 3. Synthetic signals are first computed by the modal summation (PANZA, 1985; PANZA and SUHADOLC, 1987; FLORSCH *et al.*, 1991; PANZA *et al.*, 2000) along the bedrock (1-D) model that represents the average path between the assumed source and the local, laterally heterogeneous (2-D) structure beneath the local area of interest. A double-couple point source of seismic waves is assumed, described by the strike (φ) and dip (δ) of the causative fault, its rake (λ) and the depth (h) of focus.

The bedrock model is defined as a stack of horizontal layers, each characterized by its thickness, longitudinal and transversal wave velocity, density, and Q-factor, controlling the anelastic attenuation. The seismograms were

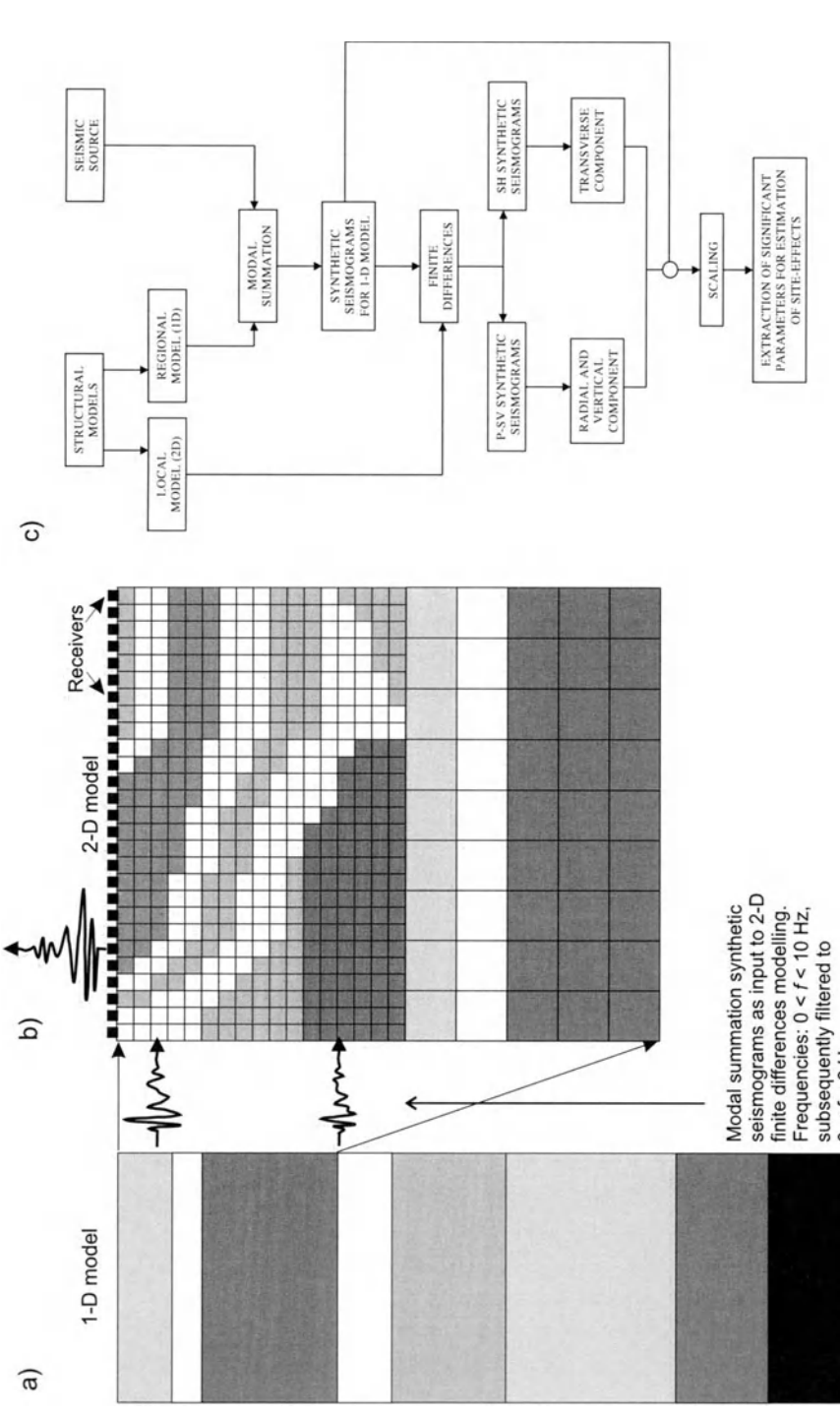

Figure 3
Schematic representation of the hybrid technique. The modal summation is applied considering the regional bedrock model (a) to compute the input signals for the laterally varying local part (b) where signals are propagated by finite-difference numerical modeling to a set of sites on the surface. (c) Flowchart of the algorithm. (modified from LOKMER *et al.*, 2002).

computed for frequencies reaching 10 Hz, and were subsequently filtered to $f \leq 6$ Hz. These signals are numerically propagated through the laterally varying local structure by the finite-difference method (VIRIEUX, 1984; 1986; LEVANDER, 1988). The finite-difference grid (2500 × 544 nodes) is formed first, approximating the laterally varying model. A grid-step of 5 m is chosen, obeying the empirical condition that at least 10 points per minimum wavelength (about 50 m in our case, corresponding to 6 Hz waves with a velocity of 300 m/s) are required. In the vertical direction, after the first 360 points (1.8 km), the grid-step is increased to 45 m, so that the laterally varying model extends to depths exceeding twice the assumed hypocentral depth of 5 km (see below), which is enough for the procedure to yield reliable results. This increase in grid, step is justified by the results of tests conducted prior to computations which indicate that the wavelengths that reach these depths (> 1.8 km) are much longer and thus even a reduced grid resolution is still satisfactory for our modeling. In this way we constructed a discretized local model extending to a depth of 13 km. The reflections from the artificial boundaries of the model are suppressed by applying the techniques considered by FÄH (1992). Synthetic seismograms of the vertical, transversal and radial components of ground motion were computed at a predefined set of equidistant points (125 m apart) at the surface. After scaling the signals' spectra to the assumed seismic moment by using the curves proposed by GUSEV (1983) as reported in AKI (1987), peak ground acceleration (PGA) and the ratios of PGA and response spectra for local and bedrock models were extracted from the computed seismograms.

Data

The input data consist of: *a*) *the regional* (*bedrock*) *model parameters* describing the average properties of the Earth's interior along the path between the source and the beginning of the local, laterally heterogeneous, part of the profile; *b*) *the local model parameters*, and *c*) *the source parameters*. The structural models are the same ones used by LOKMER *et al.* (2002) and are given in Figure 4. The hypocenter of the $M = 6$ earthquake, located 15 km to the NE from the center of Zagreb, is assumed to be associated with the Zagreb fault system running WSW–ENE on the southern side of the Medvednica Mt. (Fig. 5), and not with the nearby Kašina fault. This choice has been made on the basis of the elongation of the isoseismal lines (from the isoseismal map stored in the Macroseismic archives of the Geophysical Department, Zagreb), which is approximately parallel to the strike of the Zagreb fault system. LOKMER *et al.* (2002) used $\varphi = 60°$, $\delta = 80°$, $\lambda = 120°$, $h = 5$ km to describe the source. We now examine the uncertainty of this set of parameters. The strike of 60° is probably the most certain of all, and there is ample evidence in the geological literature (*e.g.*, PRELOGOVIĆ *et al.*, 1998)

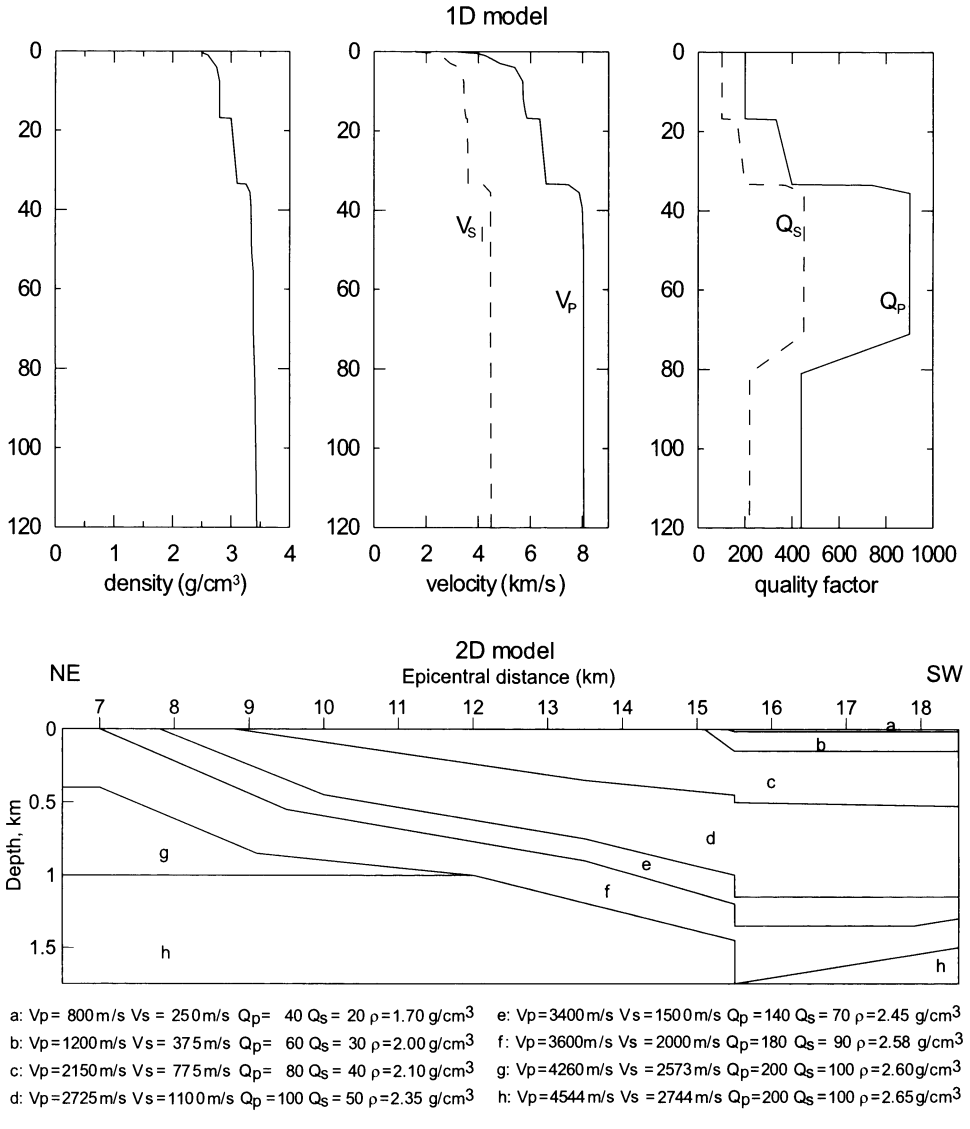

Figure 4
Regional bedrock model and a representation of the local laterally heterogeneous model. V_P, Vs, Q_P, Q_S and ρ are velocities of the longitudinal and transversal waves, the corresponding Q-factors and density, respectively. Only the first 1.8 km of the 2-D model are shown, below it is the same as the 1-D model.

to back it up. However, the strike of Zagreb faults is the only well-known parameter, and the system is marked as the one of unknown sense of displacement by PRELOGOVIĆ *et al.* (1998). The cross section and distribution of hypocenters which they published suggest that the fault is nearly vertical, with a small dip to the NW near the surface, which turns to a small southeastward dip as the

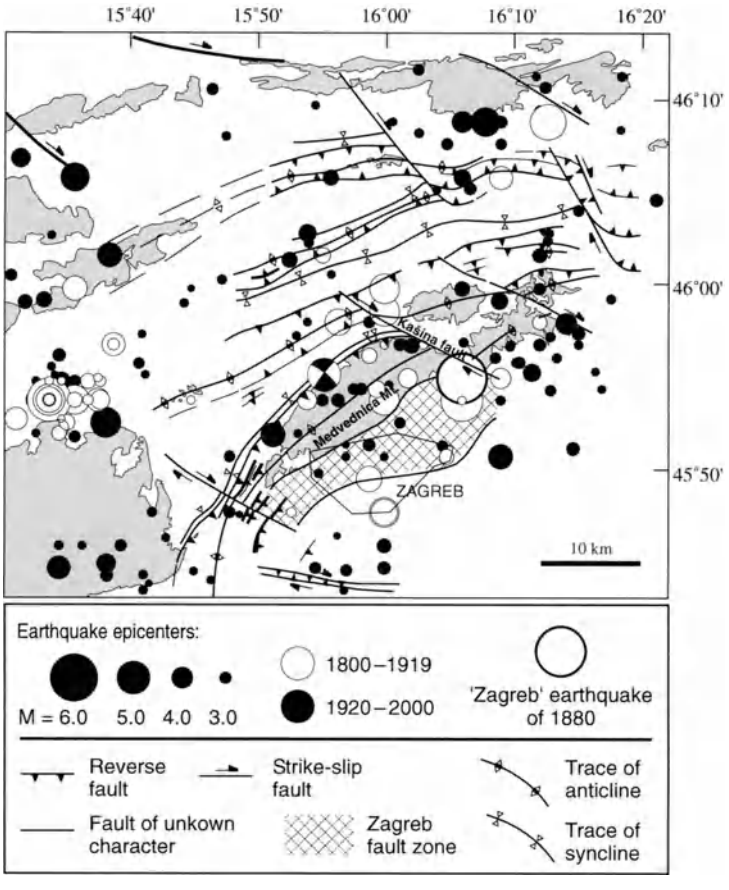

Figure 5
Map of the main geological features and of the seismicity in the Zagreb area (after TOMLJENOVIĆ *et al.*, 2001 and PRELOGOVIĆ *et al.*, 1998). Epicenters are from the updated version of the earthquake catalog published by HERAK *et al.* (1996).

seismogenic depths are reached. Although LOKMER *et al.* (2002) assumed it to be a right-lateral fault, today it seems more probable that left-lateral, mostly strike-slip motions prevail. Such a conclusion is based on results of a study dealing with Neogen-Quaternary structures and recent seismicity of NW Croatia presented by TOMLJENOVIĆ *et al.* (2001) (Fig. 5, see also PRELOGOVIĆ *et al.*, 1998). As the earthquake of 1880 occurred at a place where the Zagreb fault zone intersects the NW–SE trending right-lateral strike-slip Kašina fault, under the mostly N–S oriented regional stress (HERAK *et al.*, 1995; PRELOGOVIĆ *et al.*, 1998), the only possible sense of motion on the Zagreb fault is then left-lateral. Therefore we decided to adopt the reference source at a depth of 5 km, with the orientation described by the triplet $(\varphi, \delta, \lambda) = (60°, 80°, 20°)$. We will assume that φ is nearly

Table 1

Parameters of 16 faulting mechanisms considered. The reference one is the mechanism number 6 (bold print).

	Faulting mechanism number															
	1	2	3	4	5	**6**	7	8	9	10	11	12	13	14	15	16
φ	60	60	60	60	60	**60**	60	60	60	60	60	60	240	240	240	240
δ	60	60	60	60	80	**80**	80	80	90	90	90	90	80	80	80	80
λ	0	20	40	60	0	**20**	40	60	0	20	40	60	0	20	40	60

perfectly known, and will allow variation in the dip and rake thus defining 16 realistic source geometries to investigate, as shown in Table 1. The dip varies so that the fault is always rather steep, while the most uncertain parameter, λ, changes between 0° and 60° from pure strike-slip to predominantly dip-slip motion. To keep the convention of the dip to the right-hand side with respect to the strike direction for faults 13–16 (which dip to the NW), their strike is increased by 180 degrees.

In order to reduce the amount of computations, we decided to focus on the larger of the two horizontal components, this being the most conservative approach. The decision of which of the two components to keep (transversal or the radial one) was made on the basis of the PGA of the signals computed for the bedrock model by modal summation. It turned out that for most of the assumed mechanisms, with the exception of mechanisms 4, 8 and 12 from Table 1, Love and *SH* waves clearly dominate over *P-SV* and Rayleigh waves (Fig. 6). Because in cases 4, 8 and 12 (with $\lambda = 60°$) the two wave types are of comparable amplitudes, they were both kept, and the larger component was selected for each of the distances only after the finite-difference part of the modeling.

Results

Synthetic accelerograms for all three components of motion computed assuming the reference mechanism are given in Figure 7. The wavetrains clearly reflect the complexity of the underlying terrain. PGA and its linear amplification factor AMP(PGA) (defined as the ratio of the PGA values for each of the sites on top of the bedrock (1D) and the laterally varying (2-D) part of the model, AMP(PGA) = PGA(2D)/PGA(1D)) for the reference mechanism are shown in Figure 8. For the three components, the distribution of AMP(PGA) with distance is rather different, although a sudden increase is always present as the waves reach the fault at the epicentral distance of 15.5 km. Frequency-space plots of the amplification of response spectra (RS) for the reference case (AMP(RS) = RS(2-D)/RS(1-D)) are presented in Figure 9. For all other source mechanisms,

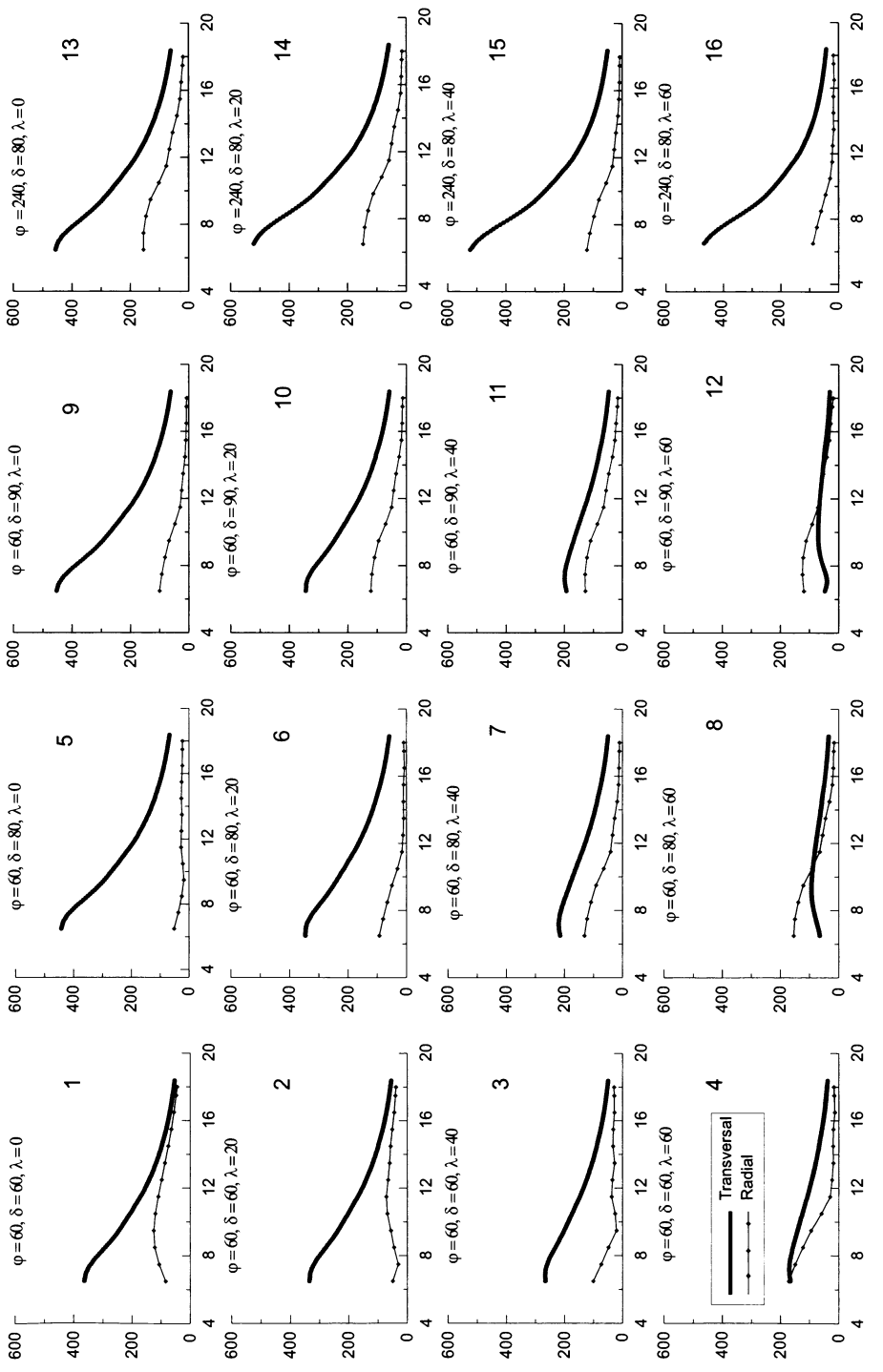
φ=60, δ=60, λ=0
φ=60, δ=60, λ=20
φ=60, δ=60, λ=40
φ=60, δ=60, λ=60
φ=60, δ=80, λ=0
φ=60, δ=80, λ=20
φ=60, δ=80, λ=40
φ=60, δ=80, λ=60
φ=60, δ=90, λ=0
φ=60, δ=90, λ=20
φ=60, δ=90, λ=40
φ=60, δ=90, λ=60
φ=240, δ=80, λ=0
φ=240, δ=80, λ=20
φ=240, δ=80, λ=40
φ=240, δ=80, λ=60
1
2
3
4
5
6
7
8
9
10
11
12
13
14
15
16
Transversal
Radial
0
200
400
600
4
8
12
16
20

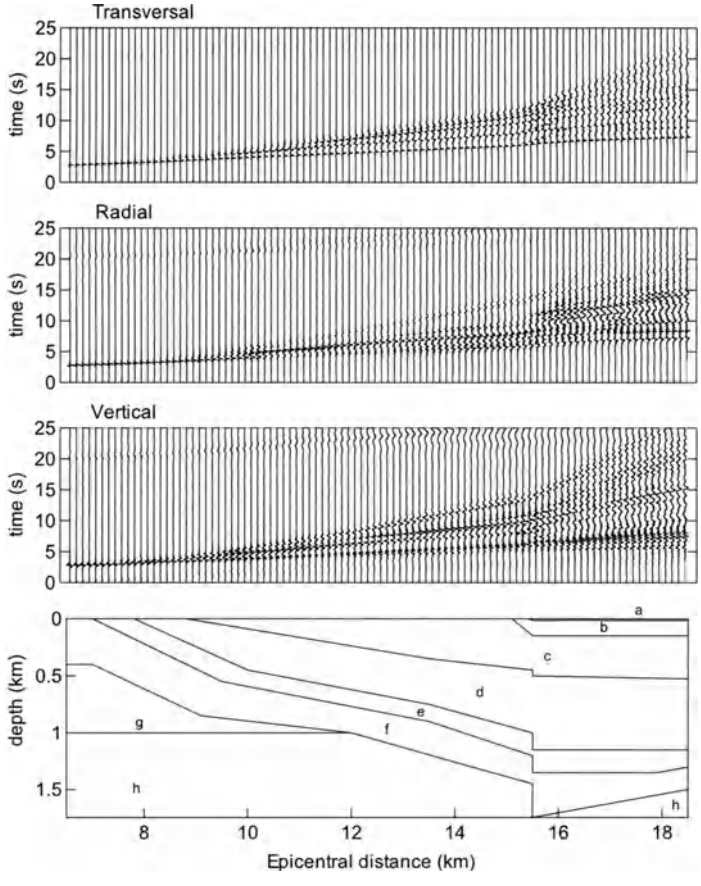

Figure 7
Synthetic accelerograms at selected receivers for the reference source mechanism (No. 6 in Table 1). The amplitudes are normalized to the maximum for each trace (see Fig. 8 for actual PGA values). The local model is shown at the bottom (see Fig 4).

only the results pertaining to the larger horizontal component were considered. Examples for four selected cases are given in Figures 10 and 11. They show that all quantities studied clearly depend on the parameters which define the faulting geometry. PGA *vs.* distance for all cases is given in Figure 12 together with the empirical horizontal PGA attenuation function proposed by HERAK *et al.* (2001).

◀

Figure 6
PGA of the transversal (thick line) and of the radial component (thin dotted line) computed by modal summation and assuming the bedrock model *vs.* epicentral distance (km), for the 16 focal mechanisms given in Table 1. The radial component is of comparable amplitude to the transversal one only for the mechanisms 4, 8, and 12.

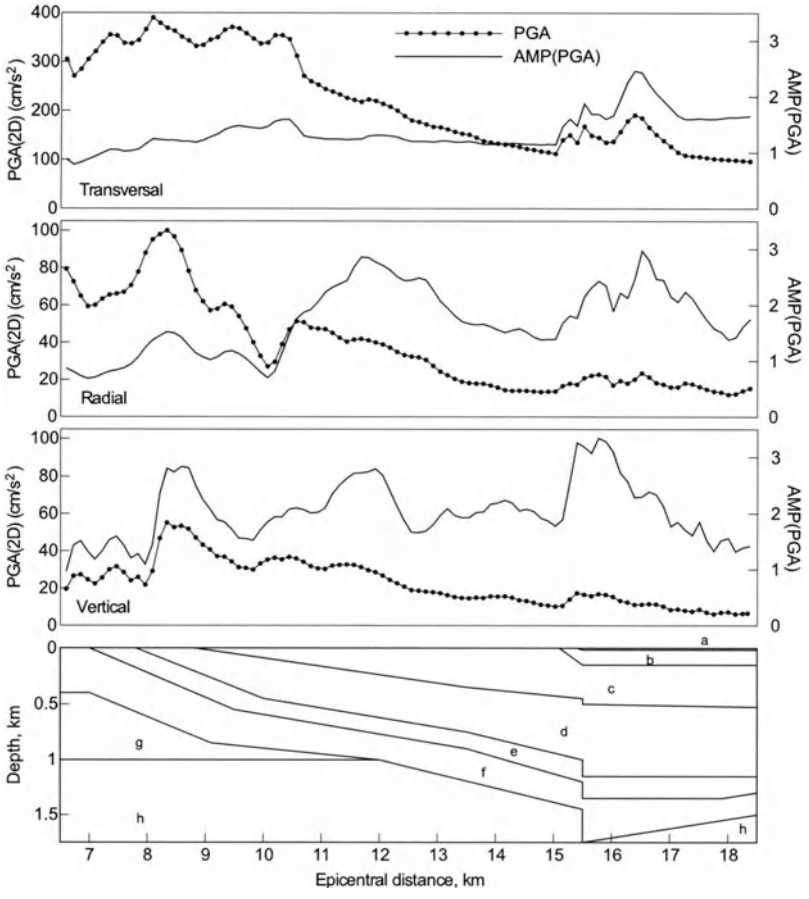

Figure 8
PGA and PGA amplification, AMP(PGA), profiles for the reference source mechanism.

This attenuation relation, even though derived using data from the Dinarides area, is used in Croatia as the best guess for other parts of the country (including Zagreb) in which only a few strong motion records have been obtained to date. Although, especially for epicentral distances longer than 10 km, synthetic PGA decays with distance more rapidly than the empirical values would suggest, most synthetic values fall within the $\pm 2\sigma$ range of the empirical relationship, which suggests that the scaling to the assumed magnitude ($M_L = 6$) is properly done. Figure 13a presents the envelopes of all obtained AMP(PGA) values (maximal and minimal values at each of the virtual receivers), together with the curve of the reference mechanism. Except for the first 3 km of the local profile, the variability of AMP(PGA) with the assumed faulting parameters is of considerable magnitude, exceeding at some distances a factor of 2. Similar behavior is seen if the

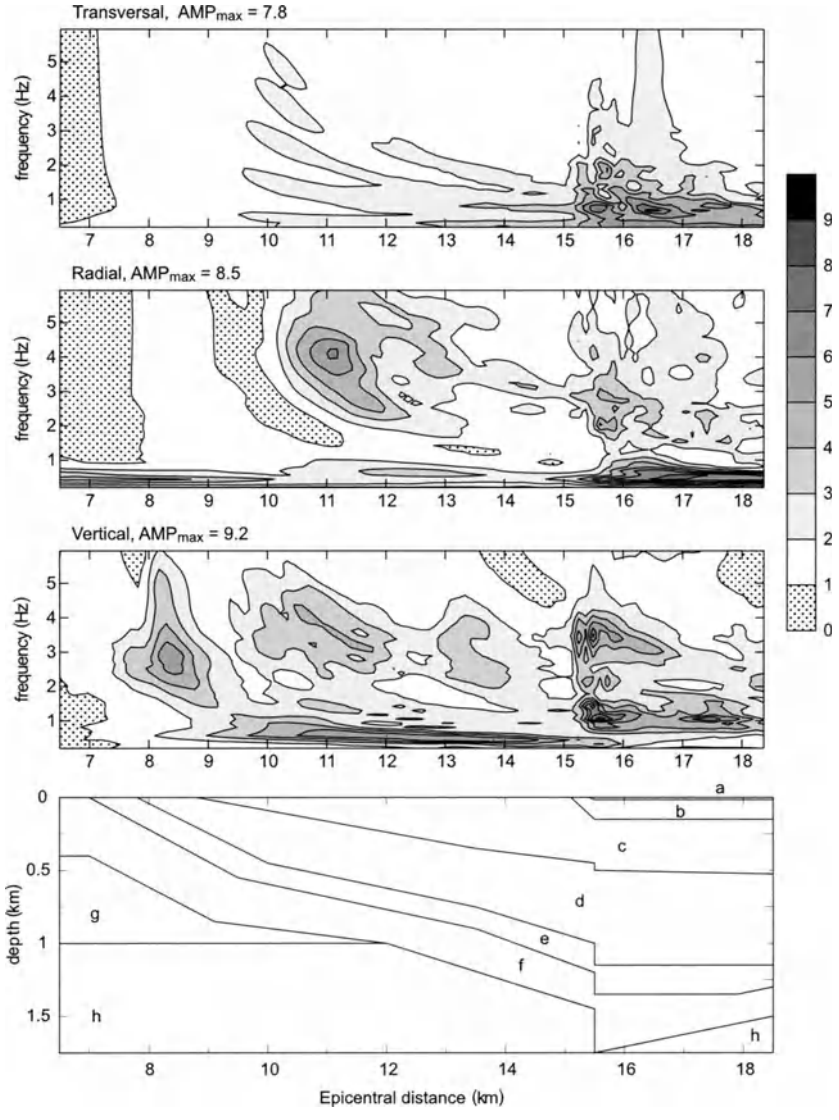

Figure 9
Frequency-space plots of amplification of response spectra, AMP(RS), for the reference focal mechanism. Amplification factors are presented by different levels of gray as given by the vertical bar on the right.

amplification spectra for the transversal component of the reference mechanism (Fig. 9, maximum amplification of 7.8 for frequencies below 1 Hz at the distance of 16.5 km) are compared with the upper envelope of all computed amplification spectra for the larger horizontal component (maximum values for each frequency

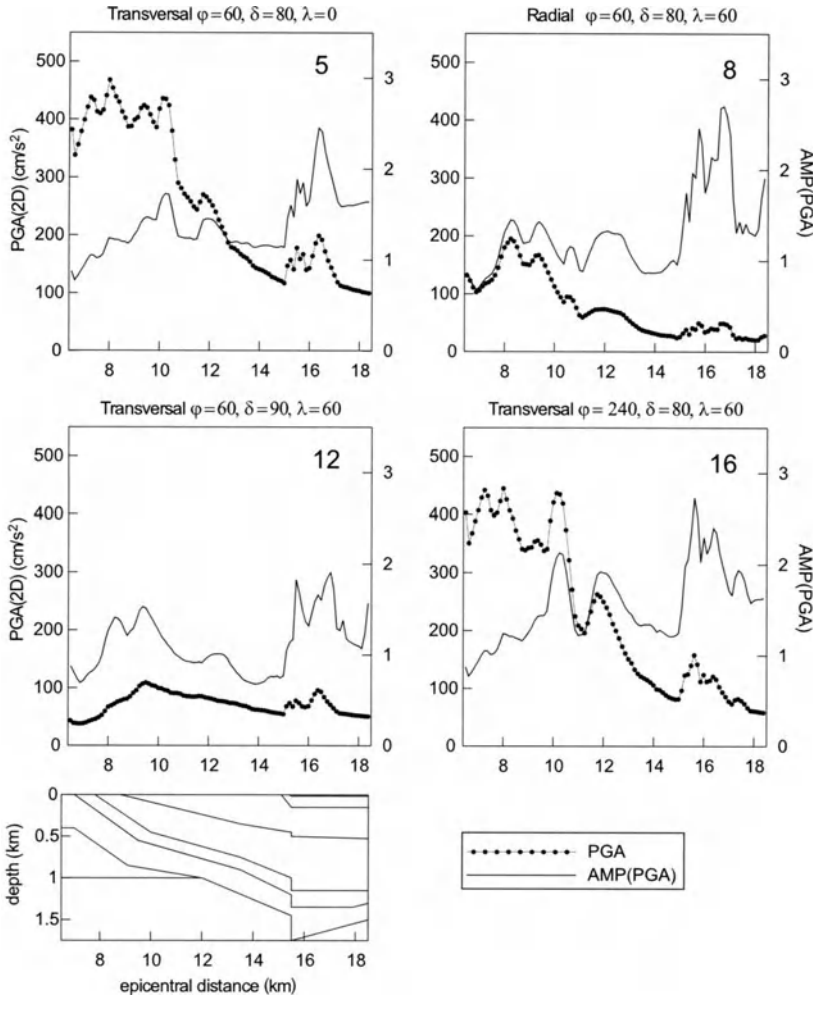

Figure 10
PGA and AMP(PGA) for the four selected cases (5, 8, 12 and 16 from Table 1).

and distance) as given in Figure 13b. The latter exhibits a similar shape but an overall larger amplification with a maximum of 9.9 for frequencies below 2 Hz.

Discussion and Conclusions

Figures 8–13 clearly show that none of the three strong-motion related quantities considered (PGA, AMP(PGA), AMP(RS)) should be regarded as independent of faulting geometry. While this is to some extent expected for PGA (strike-slip and thrust faulting events, for instance, have been statistically shown by *e.g.*, BOORE *et al.*

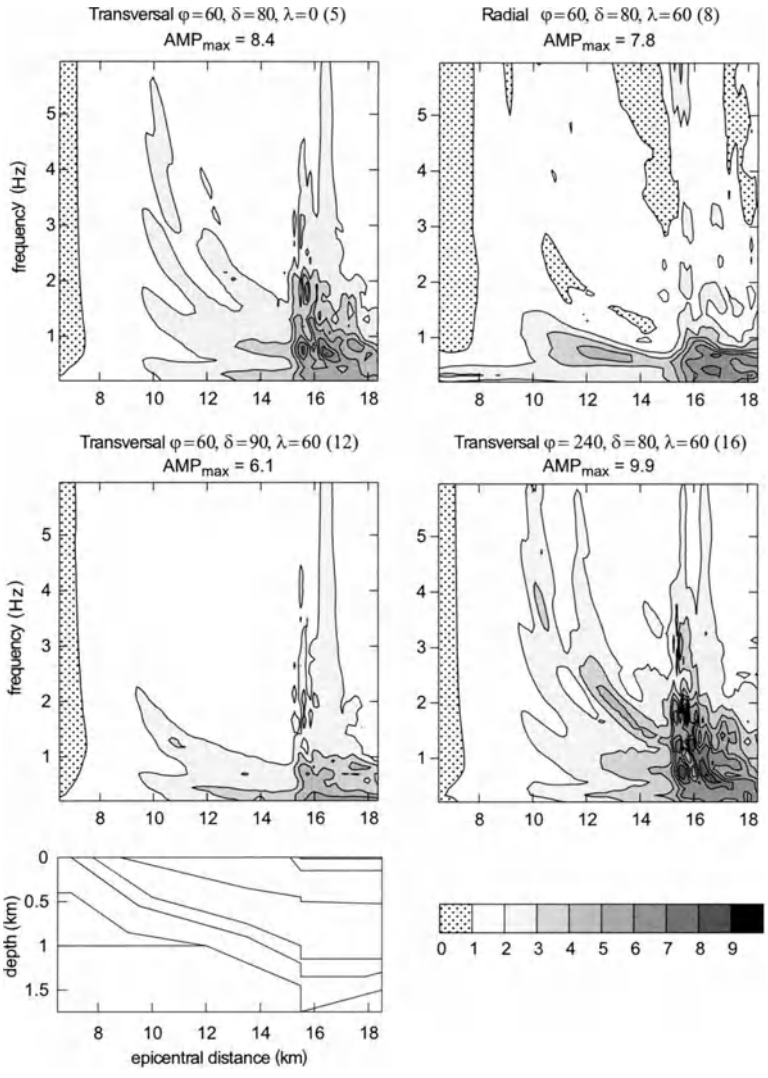

Figure 11
Amplification of the response spectra, AMP(RS), for the four selected cases (5, 8, 12 and 16 from Table 1).

(1997) to produce different PGA for the same magnitudes, distances and soil types) it is not the case with AMP(PGA) and AMP(RS) which are usually considered to be only site-dependent. Our results suggest that even the variation of only dip and rake, within the range generally measured during an aftershock sequence, may produce amplification profiles that significantly differ from one another. This occurs if the wavetrains that reach a given epicentral distance follow very different paths in the bedrock and in the local models. In such a case the depth variation of amplitudes at

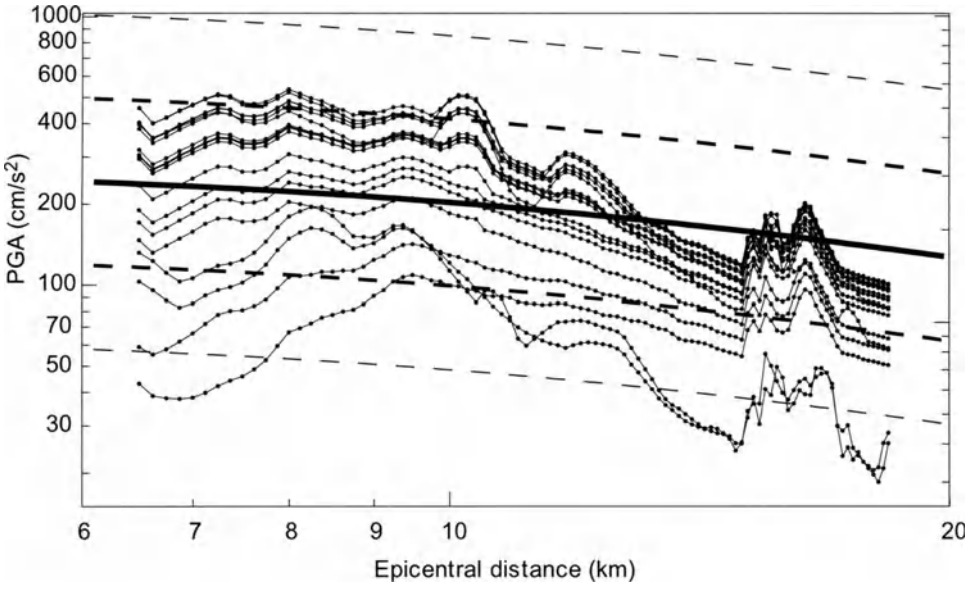

Figure 12
All 16 PGA profiles. The thick line is the attenuation of PGA predicted by the empirical relationship (HERAK *et al.*, 2001) for a $M = 6$ earthquake. Thick and thin dashed lines denote 1σ- and 2σ-confidence intervals for the HERAK *et al.* (2001) relation, respectively.

the very entrance into the local model has a strong influence on the amplifications/deamplifications observed at the free surface. The depth variation of wavefield generated by the source may be rather strong and rapidly changing as a function of the source orientation. Therefore, it may easily happen that, at some distance, the ray in the local model has a larger (or smaller) amplitude than in the bedrock (1-D) model, not only because of soil induced amplification (or deamplification), but also because it corresponds to a different take-off angle from the source, thus carrying a larger (smaller) amount of energy radiated by the source. The range of simulated PGA values presented in Figure 12 is large enough to mostly explain the scatter of observed data used to derive empirical attenuation relations. In realistic 3-D finite-source geometries, where rays reach the nearby site from various depths and azimuths, such arguments gain even more importance.

Although our conclusions follow from the numerical analyses of a specific case of the city of Zagreb, they are valid wherever the subterrain is complex enough to produce significantly different raypaths when the local soil is considered instead of the bedrock.

Here we have only dealt with the effects that uncertainties in dip and rake have on the parameters which characterize strong motions at a site. There are, of course, uncertainties related with all other input parameters, of which those associated with the model parameterization probably play the most important role. Estimation of

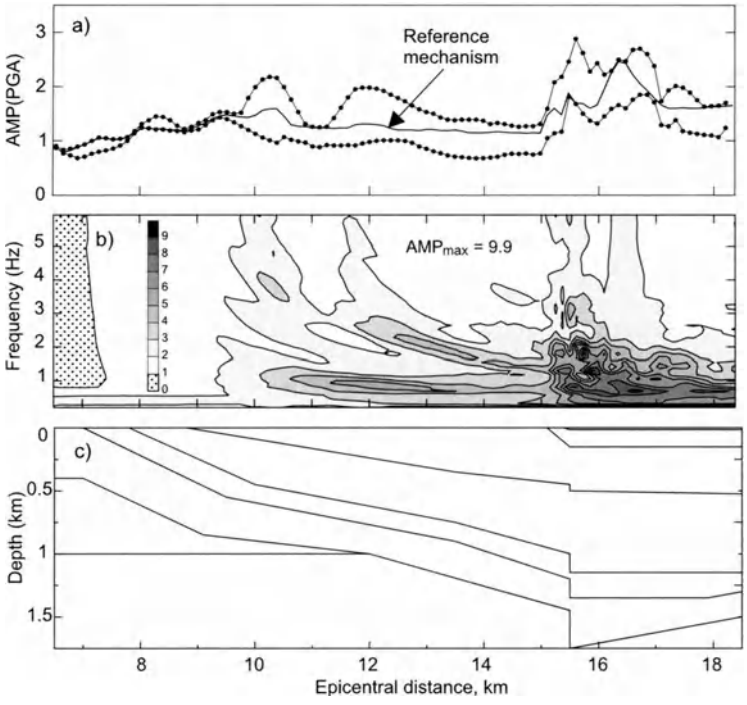

Figure 13
a) Upper and lower envelopes of AMP(PGA) (maximum and minimum of the 16 values computed for each epicentral distance, dotted solid lines), and the AMP(PGA) for the reference source mechanism (solid line); b) maximum values of AMP(RS) versus frequency and epicentral distance; c) local model (see Fig. 4).

their effects by the variational method similar to the one used here would require an enormous amount of computation time and is at present possible only for the simplest of models. The remaining source parameters, that were here assumed constant (epicentral distance, depth, strike), as well as those considered only indirectly (seismic moment) or not at all (rupture duration, source function, source dimensions, factors contributing to nonlinear soil behavior...) are never perfectly known. Just to demonstrate what effect the distance uncertainty may have, we have computed AMP(PGA) profiles for the reference source geometry considering two additional distances from the beginning of the laterally heterogeneous part of the model, as illustrated in Figure 14. Again, AMP(PGA) clearly depends on the source position, and varies by almost a factor of two in the last half of the local model.

Everything said above raises the question of the very meaning and interpretation of amplification itself. Sometimes very large amplification corresponds to a faulting mechanism, which produces small absolute PGA (and *vice versa*, see examples in Fig. 10), so that the actual damage may be uncorrelated with the *a priori* determined amplification profiles like the ones in Figures 10 and 13a.

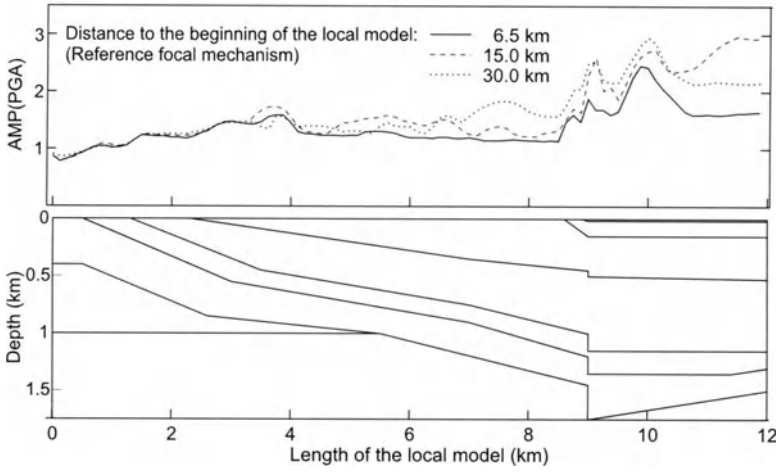

Figure 14
AMP(PGA) profiles for the reference source mechanism (6.5 km) and for the same source (No. 6 from Table 1) placed at different distances (15 and 30 km) from the beginning of the local model.

Furthermore, localities with very similar soil stratification at equal distance but at different azimuths from the source, may actually experience considerably disparate effects, solely due to differences in the geometry of the raypaths. From this it follows that the local effects, needed to properly assess the earthquake hazard at any site, must be determined for each of the relevant sources considering all associated uncertainties as completely as possible, so that envelope curves like those shown in Figure 13a could be considered representative of the possible ground motion scenario. Such a conclusion is especially important for the microzonation of cities like Zagreb, where the local geology is quite complex, and seismicity is not confined to a single seismic source zone.

Acknowledgements

We thank two anonymous referees whose constructive criticism aided us in improving the early version of the manuscript. We benefited from discussions with Prof. E. Prelogović and Mr. B. Tomljenović related to the local geology. This study has been done within the framework of the UNESCO-IUGS-IGCP project "Realistic Modelling of Seismic Input for Megacities and Large Urban Areas," and the Project No. 0119333 (Seismicity of Croatia) funded by the Ministry of Science and Technology of the Republic of Croatia. All funding is gratefully acknowledged.

References

AKI, K., *Strong Motion Seismology*. In *Strong Motion Seismology*, NATO ASI Series, Series C: *Mathematical and Physical Sciences* (eds. Erdik, M. Ö., and Toksöz, M. N.) (D. Reidel Publishing Company, Dordrecht 1987) *204*, 3–39.

BERESNEV, I. A., ATKINSON, G. M., JOHNSON, P. A., and FIELD, E. H. (1998), *Stochastic Finite-Fault Modeling of Ground Motions from the 1994 Northridge, California Earthquake. II. Widespread Nonlinear Response at Soil Sites*, Bull. Seismol. Soc. Am. *88*, 1402–1410.

BOORE, D. M., JOYNER, W. B., and FUMAL, T. E. (1997), *Equations for Estimating Horizontal Spectra and Peak Acceleration from Western North American Earthquakes: A Summary of Recent Work*, Seism. Res. Lett. *68*, 128–153.

CIOFLAN, C. O., APOSTOL, B. F., MOLDOVEANU, C. L., PANZA, G. F., and MARMUREANU, G. H. (2002), *Deterministic Modeling for Microzonation of Bucharest: Case Study for August 30, 1986 and May 30–31, 1990 Vrancea Earthquakes*, ICTP Preprint IC/2002/25.The Abdus Salam International Centre for Theoretical Physics, Trieste, Italy.

FÄH, D., *A Hybrid Technique for the Estimation of Strong Ground Motion in Sedimentary Basins*, Dissertation, Swiss Federal Institute of Technology, Zürich 1992.

FÄH, D., IODICE, C., SUHADOLC, P., and PANZA, G. F. (1993), *A New Method for the Realistic Estimation of Seismic Ground Motion in Megacities: The Case of Rome*, Earthquake Spectra *9*, 643–668.

FÄH, D., SUHADOLC, P., MUELLER, ST., and PANZA, G. F. (1994), *A Hybrid Method for the Estimation of Ground Motion in Sedimentary Basins: Quantitative Modeling for Mexico City*, Bull. Seismol. Soc. Am. *84*, 383–399.

FÄH, D., SUHADOLC, P., and PANZA, G. F. (1990), *Estimation of Strong Ground Motion in Laterally Heterogeneous Media: Modal Summation–Finite Differences*, Proceedings of the 9th European Conference of Earthquake Engineering, Sept. 11–16, 1990, Moscow *4A*, 100–109.

FLORSCH, N., FÄH, D., SUHADOLC, P., and PANZA, G. F. (1991), *Complete Synthetic Seismograms for High-frequency Multimode SH-Waves*, Pure Appl. Geophys. *136*, 529–560.

GUSEV, A. A. (1983), *Descriptive Statistical Model of Earthquake Source Radiation and its Application to an Estimation of Short-period Strong Motion*, Geophys. J. R. Astr. Soc. *74*, 787–808.

HERAK, M. (1989), *The Magnitude-intensity-focal Depth Relation for the Earthquakes in the Wider Dinara Region*, Geofizika *6*, 13–21.

HERAK, M., HERAK, D., and MARKUŠIĆ, S. (1995), *Fault Plane Solutions for Earthquakes (1956–1995) in Croatia and Neighbouring Regions*, Geofizika *12*, 43–56.

HERAK, M., HERAK, D., and MARKUŠIĆ, S. (1996), *Revision of the Earthquake Catalogue and Seismicity of Croatia, 1908–1992*, Terra Nova *8*, 86–94.

HERAK, M., MARKUŠIĆ, S., and IVANČIĆ, I. (2001), *Attenuation of Peak Horizontal and Vertical Acceleration in the Dinarides Area*, Studia Geophysica et Geodaetica *45*, 383–394.

KOUTEVA, M., PANZA, G. F., PASKALEVA, I., and ROMANELLI, F. (2001), *Modelling of the Ground Motion at Russe site (NE Bulgaria) due to the Vrancea Earthquakes*, ICTP Preprint IC/2001/145, The Abdus Salam International Centre for Theoretical Physics, Trieste, Italy.

LEVANDER, A. R. (1988), *Fourth-order Finite-difference P-SV Seismograms*, Geophysics *53*, 1425–1436.

LOKMER, I., HERAK, M., PANZA, G. F., and VACCARI, F. (2002), *Amplification of Strong Ground Motion in the City of Zagreb, Croatia, Estimated by Computation of Synthetic Seismograms*, Soil Dynamics and Earthquake Engineering *22*, 105–113.

MARKUŠIĆ S. and HERAK, M. (1999), *Seismic Zoning of Croatia*, Natural Hazards *18*, 269–285.

PANZA, G. F. (1985), *Synthetic Seismograms: The Rayleigh Waves Modal Summation*, J. Geophys. *58*, 125–145.

PANZA, G. F. and SUHADOLC, P. (1987), *Complete strong motion synthetics*. In *Seismic Strong Motion Synthetics, Computational Techniques* 4, (ed. B. A. Bolt) (Academic Press, Orlando 1987) pp. 153–204.

PANZA, G. F., ROMANELLI, F., and VACCARI, F. (2000), *Seismic Wave Propagation in Laterally Heterogeneous Anelastic Media: Theory and Applications to the Seismic Zonation*, Advances in Geophysics, Academic Press, *43*, 1–95.

PANZA, G. F., ALVAREZ, L., AOUDIA A., AYADI, A., BENHALLOU, H., BENOUAR, D., CHEN YUN-TAI, CIOFLAN, C., DING ZHIFENG, EL-SAYED, A., GARCIA, J., GAROFALO, B., GORSHKOV, A., GRIBOVSZKI,

K., HARBI, A., HATZIDIMITRIOU, P., HERAK, M., KOUTEVA, M., KUZNETZOV, I., LOKMER, I., MAOUCHE, S., MARMUREANU, G., MATOVA, M., NATALE, M., NUNZIATA, C., PARVEZ, I., PASKALEVA, I., PICO, R., RADULIAN, M., ROMANELLI, F., SOLOVIEV, A., SUHADOLC, P., TRIANTAFYLLIDIS, P., and VACCARI, F. (2002), *Realistic Modeling of Seismic Input for Megacities and Large Urban Areas (the UNESCO/IUGS/IGCP project 414)*, Episodes *25*, 3, 160–184.

PRELOGOVIĆ, E., SAFTIĆ, B., KUK, V., VELIĆ, J., DRAGAŠ, M., and LUČIĆ, D. (1998), *Tectonic Activity in the Croatian Part of the Pannonian Basin*, Tectonophysics *297*, 283–293.

TOMLJENOVIĆ, B., CSONTOS, L., HERAK, M., and HERAK, D. (2001), *Neogene-quaternary structures and recent seismicity in NW Croatia (Hrvatsko Zagorje and Karlovac Basins)*, The Stephan Mueller Topical Conference of the European Geophysical Society, *Quantitative Neotectonics and Seismic Hazard Assessment: New Integrated Approaches for Environmental Management*, Balatonfured, September 22–26, 2001, Hungary, Abstract book, 63–64.

VIRIEUX, J. (1984), *SH-wave Propagation in Heterogenoues Media: Velocity-stress Finite-difference Method*, Geophysics *49*, 1933–1957.

VIRIEUX, J. (1986), *P-SV Wave Propagation in Heterogenoues Media: Velocity-stress Finite-difference Method*, Geophysics *51*, 889–901.

(Received April 4, 2002, accepted December 2, 2002)

Pure appl. geophys. 161 (2004) 1041–1059
0033–4553/04/061041–19
DOI 10.1007/s00024-003-2500-3

Pure and Applied Geophysics

Ground Motion Zoning of Santiago de Cuba: An Approach by SH Waves Modelling

LEONARDO ALVAREZ[1,2], JULIO GARCÍA[1], FRANCO VACCARI[3,4], GIULIANO F. PANZA[2,4], BERTHA GONZÁLEZ[1], CARMEN REYES[1], BÁRBARA FERNÁNDEZ[1], RAMÓN PICO[5], JOSÉ A. ZAPATA[1], and ENRIQUE ARANGO[1]

Abstract—The expected ground motion in Santiago de Cuba basin from earthquakes which occurred in the Oriente fault zone is studied. Synthetic *SH*-waves seismograms have been calculated along four profiles in the basin by the hybrid approach (modal summation for the path source-profile and finite differences for the profile) for a maximum frequency of 1 Hz. The response spectra ratio (RSR) has been determined in 49 sites, distributed along all considered profiles with a spacing of 900 m. The corresponding RSR versus frequency curves have been classified using a logical-combinatorial algorithm. The results of the classification, in combination with the uppermost geological setting (geotechnical information and geological geometry of the subsoil) are used for the seismic zoning of the city. Three different main zones are identified, and a small sector characterized by major resonance effects, due to the particular structural conditions. Each zone is characterized in terms of its expected ground motion parameters for the most probable strong earthquake ($M_S = 7$), and for the maximum possible ($M_S = 8$).

Key words: Synthetic seismograms, surface waves, zoning, Santiago de Cuba.

Introduction

In a previous paper, the realistic modelling of *P-SV* and *SH* waves for a frequency up to 1 Hz was done for two profiles in Santiago de Cuba city (ALVAREZ *et al.*, 2001a). Those results show the influence of the basin structure on the ground motion, and indicate the limits and possibilities of using the modelling of waves propagation for microzoning purposes. Within the framework of UNESCO/IUGS/IGCP Project 414 "Realistic modelling of seismic input for megacities and large urban areas", it has been decided to refine those results by using more detailed information about the shallow geology (geotechnical information, and geological

[1] Centro Nacional de Investigaciones Sismológicas, Cuba (CENAIS).
[2] The Abdus Salam International Centre for Theoretical Physics, Italia (ICTP).
[3] Istituto Nazionale di Geofisica e Vulcanologia - Osservatorio Vesuviano, Naples, Italy (INGV-OV).
[4] Dipartimento di Scienze della Terra, Università di Trieste, Italia (DST).
[5] Instituto de Cibernética, Matemática y Física, Cuba (ICIMAF).

geometry of the subsoil) and regional deep structure, and to extend them to all the present and perspective areas of the city. Santiago de Cuba is the second most populated city of Cuba. Located close to the boundary between the Caribbean and North American plates, it is exposed to a relatively high level of seismic hazard (ALVAREZ *et al.*, 1999; RODRÍGUEZ *et al.*, 1997). Earthquakes felt in the city with I = VIII degrees on the MSK scale, have a recurrence period of about 80 years and there exists a high probability of occurrence of a $M_S = 7$ earthquake in the near future (RUBIO, 1985) close to the city, in the Oriente transform fault system. This hypothetical earthquake is used as "scenario" for calculating synthetic seismograms along four profiles in the city by the hybrid technique (FÄH, 1992; FÄH *et al.*, 1993, FÄH and PANZA, 1994) based on modal summation and finite differences. The procedure computes wavetrains generated by a seismic source buried in a regional crust-upper mantle structure (bedrock), and uses this motion as input to the local structure. The signals in the bedrock anelastic structure are generated by the modal summation approach (PANZA, 1985; PANZA and SUHADOLC, 1987; FLORSCH *et al.*, 1991; PANZA *et al.*, 2000); the waveforms along the local, laterally varying anelastic structure are then computed using a finite-difference scheme (VIRIEUX, 1984, 1986; LEVANDER, 1988) applied to the local structure. The results of the modelling are used to make the seismic zoning of the local structure, using as zoning criteria the "response spectra ratio" (RSR), i.e., the spectral amplification defined by:

$$\mathrm{RSR} = [\mathrm{Sa(2D)}/\mathrm{Sa(1D)}]$$

where Sa(2D) is the response spectrum (at 5% of damping) for the signals calculated in the laterally varying structure, and Sa(1D) is the one calculated for the signals in the bedrock regional reference structure.

Geological Setting of the Santiago de Cuba Basin

Santiago de Cuba is characterized, from the geological point of view, by rocks, and stiff and unconsolidated sediments of different age, origin and lithological composition. The study region of the present work covers an area of approximately 250 km^2. Recently, the analysis of new borehole data, as well as detailed field surveys, have supplied a more detailed geological map of Santiago de Cuba basin (MEDINA *et al.*, 1999). Following those authors, three kinds of geological formations are present in the basin:

- *Formations of the Paleogene Volcanic Arc.* El Cobre Group is made up of several formations with a great complexity from the lithological point of view. It mainly consists of conglomerates and sandstones with tuffaceous composition, gravelites, tuffs, tuffites and limestones with lava flows of intermediate composition. They outcrop at the west and at the north of the study region and are presumed to be

the bedrock foundation of the basin. This zone is not included in our study, because the development of the city is not oriented in that direction, due to its topographic characteristics.

- *Neogene rocks.* La Cruz formation comprises three members: Quintero, Tejar and Santiago. It is composed of polimitic conglomerates, calcarenites, argilites, calcareous sandstones, marls and reef sandstones, as well as of calcareous silts and sandy argilites. All members are represented in Santiago de Cuba city and its surroundings.
- *Quaternary formations.* They are of several kinds. The first one mainly comprises gravelly alluvium (gravels, sands and clays with calcareous composition). We can find these soils mostly filling river basins, such as the San Juan River basin in the eastern part of the city. The second kind can be identified bounding the Santiago de Cuba and Cabañas bays, and is composed of sandy clays and peat, as well as man-made ground and bay mud. Additionally present are the formations Camaroncito, Jaimanitas and Rio Maya, characterized by different kinds of limestone.

Three faults cross the basin (ARANGO, 1996; PÉREZ and GARCÍA 1997). They are denominated El Cristo (present in the northwestern part of the study region), Bahía (along the eastern board of Santiago de Cuba Bay) and Sardinero (in the southeast corner of the study region).

A compilation of the structural parameters, geotechnical information, and geological geometry of the subsoil in Santiago de Cuba was constructed in the form of a database containing more than 600 boreholes' data. The quality of these data is variable consisting, in the main, of visual description and classification of strata. The depth of penetration of boreholes varies: the majority reaches less than 25 m, there are 83 between 25 and 50 m, 31 between 50 and 120 m and only 3 reach approximately 200 m of depth.

Using these data, the generalized geological zoning has been performed, compiling a set of maps representing the setting at different depths (5 m intervals close to the surface, 10–20 m intervals from 80 to 200 m). In the compilation of these maps, the real, very detailed lithological composition has been considered. The analysis of these maps, together with the consideration of the intervals of variation of the physical-mechanical properties of the rocks present in the geological maps, permitted us to simplify and generalize the map of MEDINA *et al.* (1999). The result of this generalization is shown in Figure 1. As can be seen from the figure, only six kinds of soils are present, corresponding to sands and sandstones of Quaternary formations, clays, sands and magmatic intrusions from Neogene formations, calcareous rocks and limestones from Neogene and Quaternary formations, as well as volcano-clastic rocks, tuffs, tuffites and agglomerates of El Cobre formation of the Paleogene Volcanic Arc. Additionally, significant lenses of gravelly alluvium (gravels, sands and clays with calcareous composition) are present at depth in different parts of the basin.

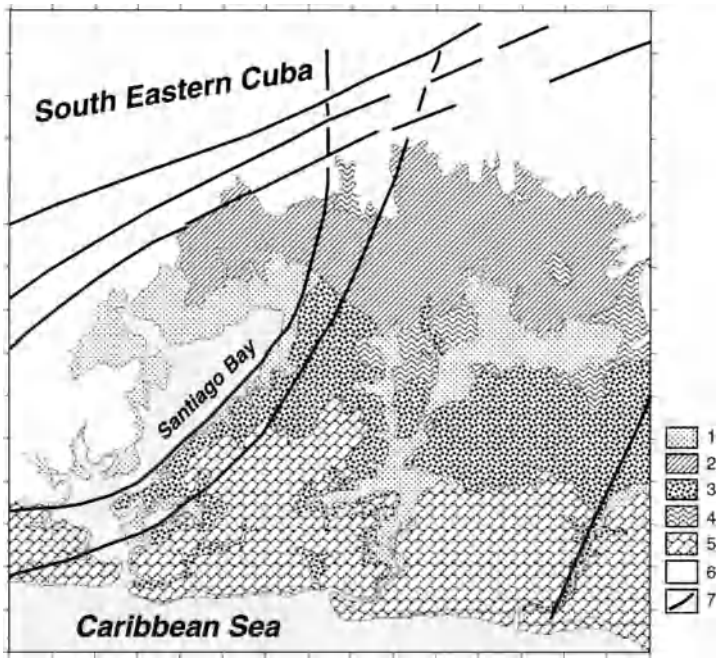

Figure 1
Simplified geological scheme of Santiago de Cuba basin (modified from MEDINA *et al.*, 1999), 1—sand and sandstones (Quaternary formations), 2—clays (Neogene), 3—marls (Neogene), 4—magmatic intrusions, 5—calcareous rocks and limestones (Neogene and Quaternary formations), 6 — rocks from El Cobre formation (Paleogene Volcanic Arc), 7—faults; the ticks on the frame of the figure are 1 km apart, the left-low corner has coordinates 19.954°N and 75.897°W.

Regional Structural Model

The crust structure in the region is very complicated, as can be seen in ALVAREZ *et al.* (2001b) and we will use only a simplified regional model, consisting of a slight modification of the anelastic parameters of structure *L* of the cited paper (Figure 2). This was constructed, for a depth less than 30 km, using the contribution of ARRIAZA (1998), who reinterpreted the results of BOBENKO *et al.* (1980), while for depths ranging from 30 to 150 km the results of the *P*-wave tomography study of VAN DER HILST (1990) and of the gravimetric study of ORIHUELA and CUEVAS (1993) have been considered. For depths greater than 150 km, the standard oceanic model of HARKRIDER (1970) is used.

The upper frequency limit for the numerical simulation has been fixed at 1 Hz. Although approximate, it is accepted that such results are pertinent for buildings of ten storys and more, lifelines, etc. This kind of building exists in Santiago de Cuba city since approximately 15 years ago, when a program of construction of typical 12-, 15- and 18-story buildings began. A recent study of the microseisms spectral content,

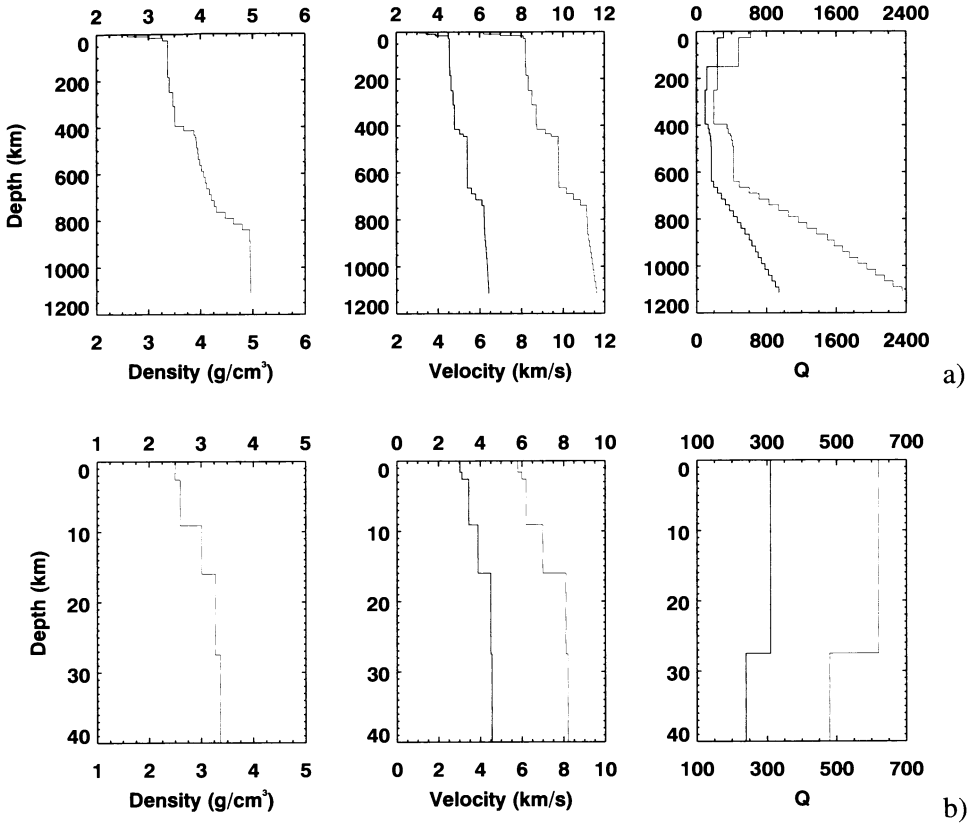

Figure 2
a) Regional structural model; b) detail of the first 40 km.

based on *in situ* measurements at the base and at the last floor of the buildings indicates that free oscillation periods of 18-story buildings range from 0.8–1.2 seconds (GONZÁLEZ, 1998; SEO *et al.*, 1998), and it is known that these periods tend to increase with the ageing of the building. Consequently, our results will be useful for future city planning and for mitigation of the seismic risk to existing buildings.

Two Dimensional Structural Profiles in the Basin

For studying the influence of the sedimentary basin structure on the seismic input, four profiles were selected across the basin. They follow the conditions that all the zones present in the simplified geological scheme of Figure 1 are sampled (only the small bodies of magmatic intrusions were not included) and that the traces pass

close to the places where the deeper boreholes of our database are located. The corresponding cross sections have been prepared using, for depth < 50 m, mainly boreholes' data from a band 0.25 km wide at both sides of each profile trace. More distant boreholes have been used for larger depths, reaching 210 m. The cross sections show smooth transitions through the different zones and sharp ones when crossing the fault present in the study area. The data pertaining to the mechanical properties (*P*- and *S*-wave velocities and quality factors) of the strata (see Table 1) were taken from the literature (PAVLOV, 1984; ISHIHARA, 1993; BERGE-THIERRY *et al.*, 1999), as no direct measurements were available. Nevertheless, the selected values are in correspondence with other measurements made on similar soils elsewhere in Cuba. The density is supported by laboratory measurements data, present in our database. The grid used in the finite-difference calculations was selected with dimension, at the surface, $\Delta x = \Delta z = 0.015$ km, in agreement with the details given in the sections.

The sources are placed on the Oriente transform fault system at 30 km of depth and at a distance of 25 km from the coast, in the main seismogenetic zone that affects the region, where the expected strong earthquakes are likely to be located. In Figure 3 the locations of sources and the profiles's traces are shown.

Results

a) Synthetic Seismograms

Synthetic seismograms for *SH* waves have been calculated along the selected profiles in the city by the hybrid approach (FÄH, 1992, FÄH *et al.*, 1993). The sites are placed on the surface with a fixed spacing of 900 m. For each site we calculate displacement, velocity and acceleration seismograms for a point source with seismic moment $Mo = 1.0 \times 10^{13}$ N-m, focal depth $h = 30$ km, and focal mechanism: dip $= 21°$, azimuth $= 302°$ and rake $= 21°$. This mechanism corresponds to the

Table 1

Physical properties of the different layers present in the selected profiles

No.	Brief Description	V_P (Km/s)	V_S (Km/s)	ρ (g/cm^3)	Q_P	Q_S
1	Sands	1.2	0.35	1.8	100	50
2	Clays	0.8	0.3	1.6	100	50
3	Marls	1.3	0.6	2.0	150	50
4	Calcareous soils	0.9	0.5	1.8	150	50
5	Calcareous rocks	2.5	1.4	2.3	200	100
6	Igneous rocks	2.4	0.8	2.1	350	150

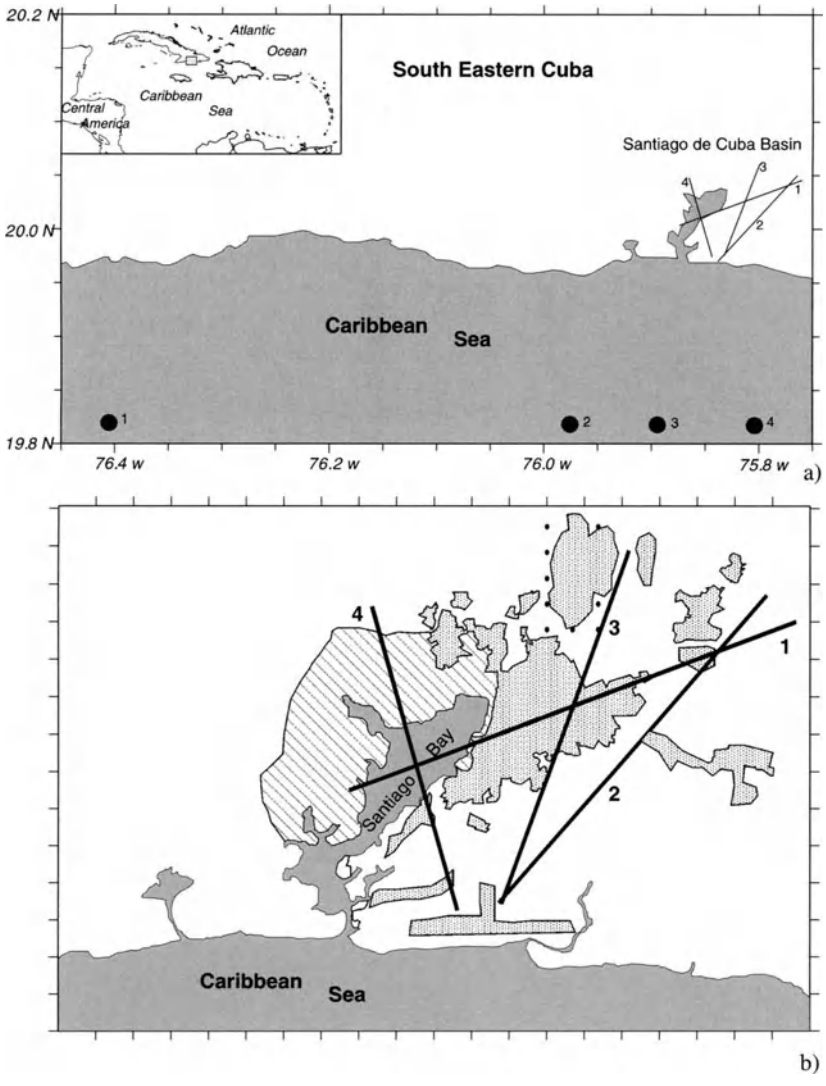

Figure 3
a) Position of the sources and profiles; b) detail of profile traces in the basin and city plan (dotted areas correspond to human settlements, hatched areas correspond to industrial areas). The ticks on the frame of the figure are 1 km apart, the left-low corner has coordinates 19.945°N and 75.945°W.

Harvard University determination of one local earthquake that can be considered representative of the seismic sources in this sector of the Oriente fault zone. These seismograms then have been scaled in the frequency domain (PANZA *et al.*, 1996) for possible earthquakes of different magnitudes by using the scaling law of GUSEV (1983), as reported by AKI (1987).

The "response spectra ratio" (RSR), as has been expressed before, is used as the basis of the zoning of the city. The plots of RSR, as functions of frequency and position along the profiles, are shown together with the corresponding cross sections in Figure 4. The RSR is larger and more variable for frequencies greater than 0.4 Hz. At the end of profile 2 a clear resonance effect, characterized by very high values that correspond in the time domain to long wave trains is present. Additionally, the occurrence of two kinds of patterns is clear. Those corresponding to profiles 2 and 3

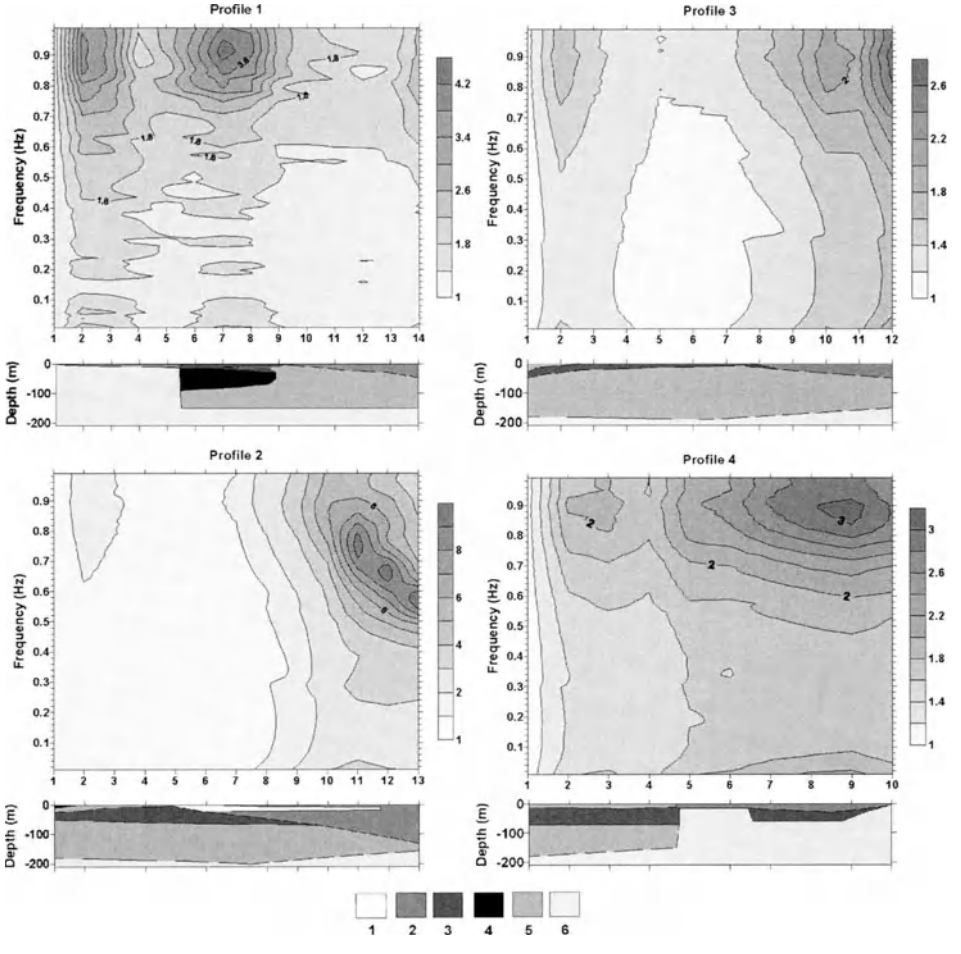

Figure 4
Relative response spectra (RSR) of SH waves as a function of frequency along each profile. The models of each profile are plotted below each panel. The numbers along the x axes correspond to the ordinal site position. The epicentral distances of the first site in profiles 1, 2, 3 and 4 are 103.9 km, 43.5 km, 34.5 km and 33.6 km, respectively. Along each profile, the distance between two adjacent sites is 900 m. The numbering in the legend corresponds to the different layers, whose parameters are given in Table 1.

are relatively smooth, in accordance with the smooth variation of the layering, while the ones corresponding to profiles 1 and 4 present rapid variations that are well correlated with the sharp lateral boundaries in the layers, due to the presence of a fault.

b) RSR Curves Classification

The RSR vs. frequency curves have been analyzed in order to make the zoning of the basin. The RSR data for each site are sampled at 0.05 Hz from 0.39 to 0.99 Hz for a total of 13 points at each site. The obtained 49 curves are shown in Figure 5. These data are processed, for the classification in compact sets, with a non-supervised logical-combinatorial algorithm included in *PROGNOSIS system* (RUIZ *et al.*, 1992). To perform this analysis the curves are numbered continuously from the first (profile 1) to the last (profile 4), and in each profile from the beginning to the end. The main features of the algorithm are:

- Let the curve number "j" be the object "O_j", and the value of the RSR at frequency number "i" be the variable "x_i". Then, the value of RSR at the frequency number "i" in the curve number "j" will be "$x_i(O_j)$".

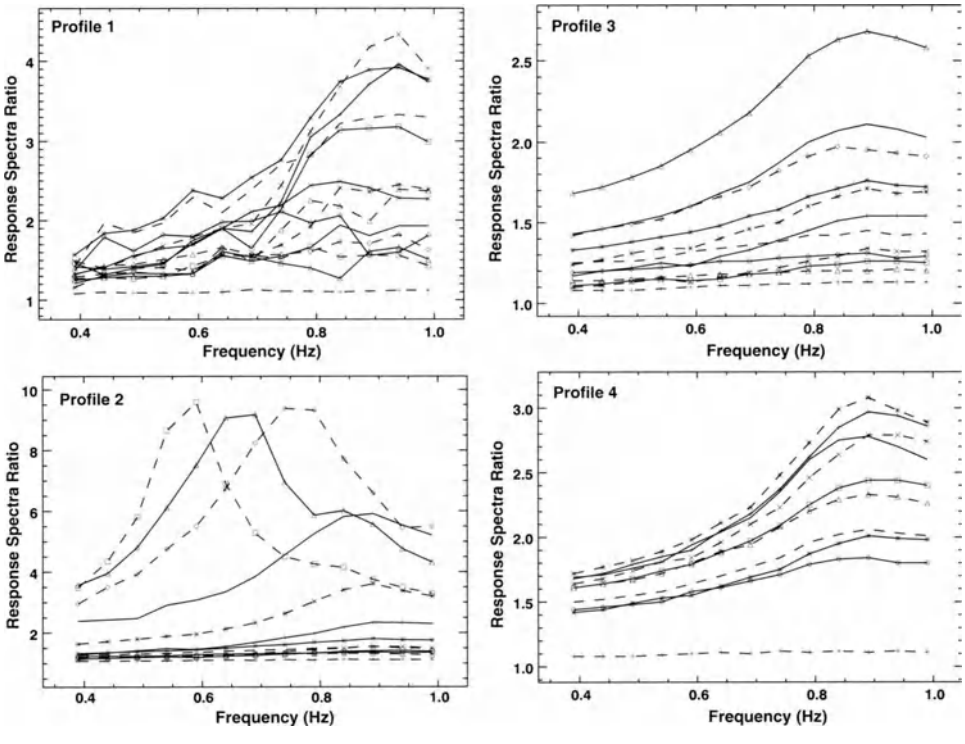

Figure 5
Response spectra curves for all profiles from 0.39 to 0.99 Hz, sampled at 0.05 Hz.

- Let $\max(x_i)$ and $\min(x_i)$ be the extremes of the variable x_i over all the objects. The similarity between objects is calculated by the formula

$$S(O_l, O_k) = \frac{1}{n} \sum_{i=1}^{n} \frac{|x_i(O_l) - x_i(O_k)|}{\max(x_i) - \min(x_i)} .$$

- Two objects O_i and O_j are β_o-*similar*, if and only if $S(O_i,O_j) \geq \beta_o$, where β_o, the level of the classification, is between 0 and 1. An object belongs to a compact set if the most similar to it is into this set too, or if it is the most similar to other objects belonging to the set.
- The compact sets are graphically represented in a dendrogram, where the different β_o levels in which they are grouped can be seen. Selecting interactively over this scheme the level β_o, a particular partition in β_o-compact sets can be determined (PICO, 1999).
- The procedure starts determining the main β_o-compact sets; then, some of the sets can be subdivided using additional criteria, and the average curve for each final set is calculated.

Initially, for a level of similarity $\beta_o = 0.25$, nine sets have been obtained. The first one, which comprised many curves with the smaller RSR values present in the data set that form a wide sector in RSR vs. frequency graph, was subdivided in four subgroups attending to the range of variation, in average, of RSR. As a result twelve groups have been identified and their average curves are shown in Figures 6a,b. In the following they will be referred as "typical" curves of the groups.

In this set, 5 limit groups can be isolated. The curves 3, 6, 7 and 8 correspond to the last four sites in profile 2, where the surface waves resonance effect was identified, while curve 10 corresponds to the first sites in each profile, where no RSR increments can be expected. In Figure 7 the results of classification are compared with the geological scheme of the basin. For the seismic zoning, a sort of correspondence between surface geology and RSR level was sought. For mapping our results, a generalization of the 12 typical RSR curves was done. It consists in a grouping of close curves into a common one, considering also the geological characteristics along the profiles. As a result, three such groups were identified: high—(2,5,9), intermediate—(4,12), low—(1,10,11). Consequently, the zoning of the basin was made in terms of these three groups. The boundaries between zones follow, whenever possible, the boundaries between the different elements of the geological map (slightly smoothed). For the zones not crossed by the profiles we took into account the results obtained in similar (by structure in depth) zones crossed by them. The zoning scheme is shown in Figure 8, where the small subzone, corresponding to the sites where the resonance effect has been identified, is delimited by a thick dashed line. The average RSR curves for each zone are shown in Figure 9.

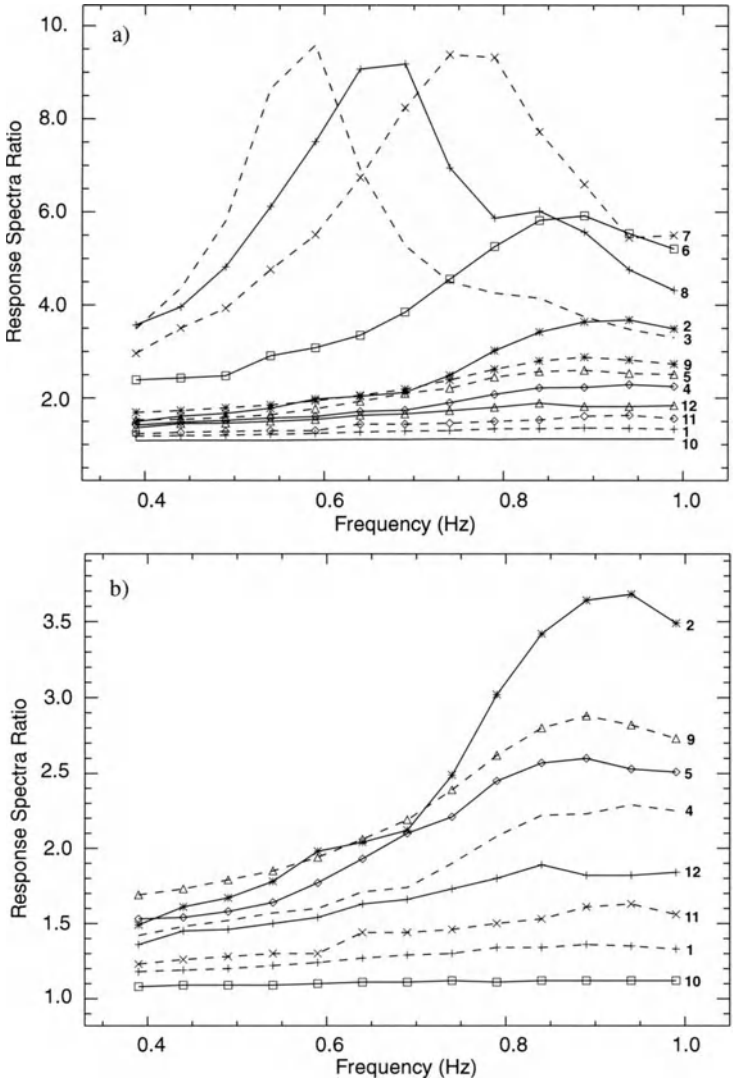

Figure 6
Typical RSR curves versus frequency obtained as a result of the classification procedure. a) All groups; b) detail after removing the four curves that present anomalous higher values.

c) Expected Ground Motions

For obtaining information about the expected ground motions in the Santiago de Cuba basin, the obtained synthetic signals have been scaled to $M_S = 7$, the most probable strong earthquake, and to $M_S = 8$, the maximum possible earthquake, as estimated from seismotectonic considerations (COTILLA and

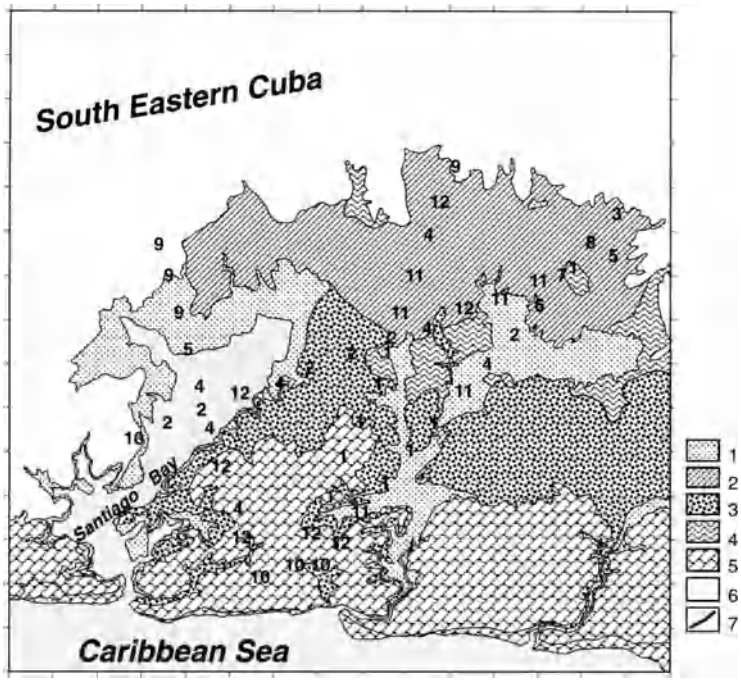

Figure 7
Representation of the results of the classification of all curves over the geological map. The numbers correspond to the typical curves shown in Figure 6, while the legend is equivalent to the one of Figure 1. The ticks on the frame of the figure are 1 km apart, the left-low corner has coordinates 19.954°N and 75.897°W.

ALVAREZ, 1991). From these scaled signals the maximum ground motion displacement (d_{max}), velocity (v_{max}) and acceleration (a_{max}) have been determined. As the frequency content of our signals is out of the range in which the maximum peak values of acceleration are commonly observed, the values of the design ground acceleration (DGA) are obtained by scaling acceleration seismograms with the design response spectra for the soils S1, S2 and S3 of the Cuban building code (NORMA CUBANA, 1999). A rough estimation of the real peak ground acceleration can be obtained from the maximum spectral value MSV, through MSV = 2.5 * DGA. A discussion of this procedure can be found in PANZA *et al.* (1996) and ALVAREZ *et al.* (1999). In Tables 2 and 3 the results for $M_S = 7$ and $M_S = 8$ earthquakes are reported, respectively. Finally, recalling that the Effective Peak Acceleration (EPA) is defined as the average spectral acceleration in the period interval from 0.1 s to 0.5 s divided by 2.5 (APPLIED TECHNOLOGY COUNCIL, 1978), we see that EPA is equivalent to the DGA, calculated using design response spectra.

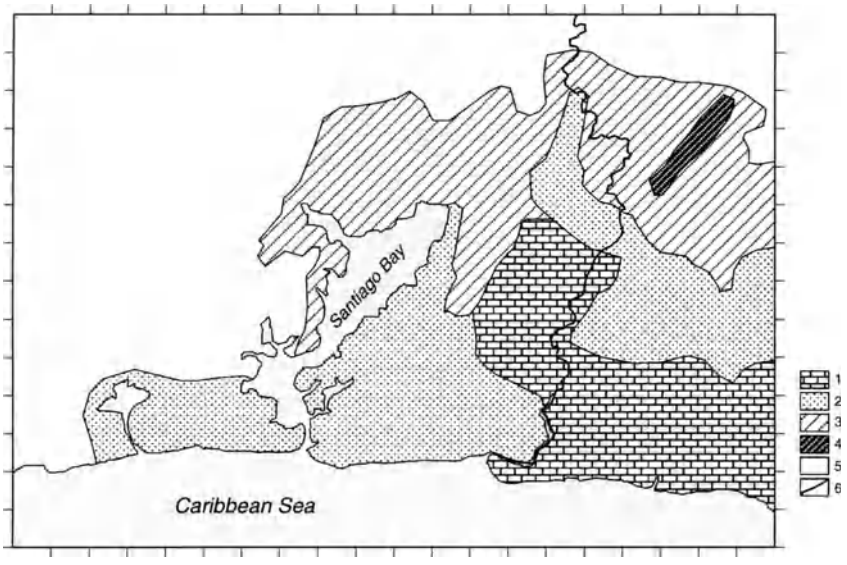

Figure 8
Zoning of Santiago de Cuba basin: 1—low RSR level, 2—intermediate RSR level, 3—high RSR level, 4—subzone, of the previous one, where resonance effect was identified, 5—zone of El Cobre formation, not included in our analysis, 6—San Juan River. The ticks on the frame of the figure are 1 km apart, the left-low corner has coordinates 19.945°N and 75.945°W.

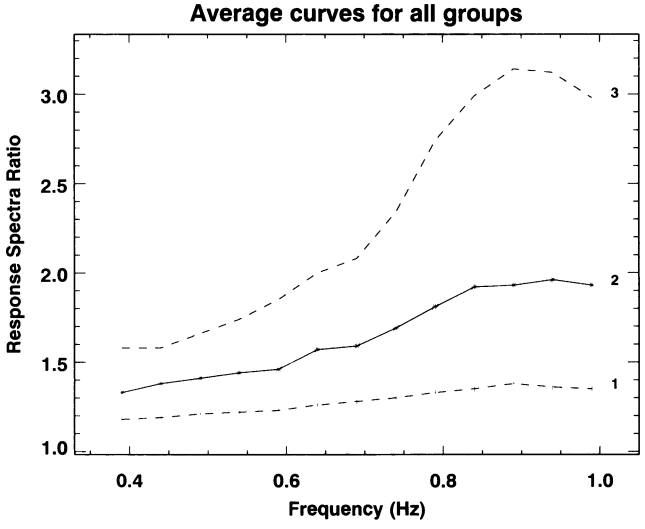

Figure 9
Average RSR curves versus frequency for each zone of the zoning scheme: 1—low RSR level, 2—intermediate RSR level, 3—high RSR level.

Table 2

Ground motion parameters for an earthquake of $M_S = 7$ in the sites located along all the profiles

No.	d_{max} (cm)	v_{max} (cm/s)	a_{max} (cm/s^2)	DGA_{S1} (cm/s^2)	DGA_{S2} (cm/s^2)	DGA_{S3} (cm/s^2)
		Profile 1, $\Delta = 103.9$ km to the beginning of profile				
1	0.23	0.09	0.22	0.74	0.43	0.36
2	0.24	0.13	0.41	1.65	1.12	0.97
3	0.24	0.12	0.39	1.36	0.92	0.80
4	0.24	0.10	0.30	0.99	0.66	0.55
5	0.24	0.11	0.25	0.82	0.55	0.48
6	0.24	0.11	0.28	1.18	0.80	0.70
7	0.24	0.11	0.34	1.46	0.99	0.86
8	0.24	0.10	0.34	1.23	0.83	0.72
9	0.24	0.09	0.28	0.77	0.53	0.46
10	0.23	0.09	0.25	0.76	0.45	0.36
11	0.23	0.09	0.24	0.76	0.45	0.36
12	0.23	0.09	0.22	0.74	0.46	0.39
13	0.23	0.09	0.21	0.74	0.49	0.42
14	0.24	0.10	0.27	0.96	0.64	0.54
		Profile 2, $\Delta = 43.5$ km to the beginning of profile				
15	2.48	3.26	9.89	30.14	19.93	16.86
16	2.63	3.89	12.91	41.41	27.71	23.59
17	2.55	3.60	11.65	36.59	24.30	20.61
18	2.48	3.40	10.63	32.90	21.85	18.48
19	2.43	3.32	10.06	31.31	20.66	17.44
20	2.37	3.27	9.64	29.48	19.58	16.56
21	2.32	3.26	9.56	29.26	19.43	16.51
22	2.37	3.60	11.55	36.75	24.79	21.28
23	2.49	4.00	14.48	51.52	34.75	29.83
24	2.74	4.37	18.96	82.81	55.85	47.94
25	2.92	5.06	22.55	149.45	99.24	83.93
26	2.98	5.14	18.93	163.39	107.82	90.49
27	2.96	4.71	16.61	165.08	107.54	89.13
		Profile 3, $\Delta = 34.5$ km to the beginning of profile				
28	3.12	3.76	11.94	36.29	24.10	20.38
29	3.31	4.54	15.78	50.88	34.28	29.43
30	3.21	4.23	14.48	44.54	29.81	25.38
31	3.14	4.14	13.73	41.67	27.67	23.55
32	3.07	4.07	12.88	39.27	26.08	22.06
33	3.01	4.12	12.76	38.97	25.97	22.11
34	2.96	4.15	12.71	39.46	26.41	22.48
35	2.97	4.32	13.87	44.58	29.83	25.52
36	2.98	4.47	14.78	47.74	31.95	27.35
37	3.08	4.91	17.47	57.49	38.47	32.83
38	3.02	4.79	16.66	54.92	36.75	31.29
39	3.18	5.48	20.30	70.65	47.28	40.25
		Profile 4, $\Delta = 33.6$ km to the beginning of profile				
40	1.87	2.46	7.55	22.77	15.12	12.79
41	2.03	3.16	11.01	36.06	24.32	20.87
42	2.04	3.21	11.43	37.25	25.12	21.56

Table 2
(contd.)

No.	d_{max} (cm)	v_{max} (cm/s)	a_{max} (cm/s^2)	DGA_{S1} (cm/s^2)	DGA_{S2} (cm/s^2)	DGA_{S3} (cm/s^2)
43	1.99	3.10	10.68	34.81	23.30	19.96
44	2.04	3.45	12.31	42.50	28.66	24.60
45	2.02	3.47	12.51	43.47	29.32	25.16
46	2.01	3.60	13.32	47.12	31.78	27.28
47	1.98	3.68	13.82	49.87	33.64	28.87
48	1.96	3.70	13.91	51.18	34.52	29.63
49	1.89	3.49	12.88	46.97	31.68	27.19

Discussion

The RSR patterns show the influence of the different geological features. There is a "regular" behavior, characterized by very small RSR values, at small frequencies, followed by a smooth monotonous RSR increment from about 0.4 Hz, until 0.9 Hz, where the relative maximum is reached, and a small decrease until 1 Hz. There are two exceptions to this relatively simple pattern. The first is at the end of profile 2, where the RSR pattern shows the appearance of very large amplitudes in the range 0.6–0.8 Hz, in the form of a narrow peak, followed by a sharp decrease towards 1 Hz. In this part there is a thick clay layer, however before reaching it the waves travel through a structure in which a relatively big lens of sand of the small San Juan River basin is embedded into the clays. It results in a cumulative increase of waves amplitude and duration, which remain after the sand lens is passed. This effect is similar to what has been obtained by ALVAREZ *et al.* (2001), where the largest RSR values for *SH* waves, along the San Juan River, were obtained at the sites where the thickness of Quaternary sediments was bigger. The second exception is represented by the oscillating RSR patterns in the entire analyzed frequency range for the profiles 1 and 4, due to the presence of Bahía fault.

Our zoning results are a scheme, not a map, because the density of RSR calculations is not sufficient to construct a map. Figure 8 has been obtained extending our local results to the whole study area. Surface geology alone cannot explain the different RSR patterns found and it is necessary to consider the data of the deeper structure. For example, the limestones in the south of the study region are classified in two different levels: to the west of San Juan River in the intermediate level, while to the east in the low level. This difference is due to the structure at depth; limestones in the west lie over marls, while in the east this layer of marls does not appear.

Table 3

Ground motion parameters for an earthquake of $M_S = 8$ in the sites located along all the profiles

No.	d_{max} (cm)	v_{max} (cm/s)	a_{max} (cm/s^2)	DGA_{S1} (cm/s^2)	DGA_{S2} (cm/s^2)	DGA_{S3} (cm/s^2)
		Profile 1, $\Delta = 103.9$ km to the beginning of profile				
1	1.62	0.55	0.94	3.20	1.88	1.58
2	1.62	0.71	1.86	7.56	5.14	4.45
3	1.62	0.66	1.79	6.24	4.24	3.67
4	1.60	0.59	1.29	4.48	2.96	2.48
5	1.58	0.61	1.15	3.69	2.51	2.17
6	1.58	0.62	1.28	5.41	3.68	3.19
7	1.58	0.60	1.51	6.63	4.51	3.91
8	1.58	0.57	1.55	5.62	3.82	3.31
9	1.57	0.51	1.29	3.55	2.42	2.09
10	1.57	0.50	1.13	3.14	1.96	1.62
11	1.56	0.50	1.06	3.19	1.97	1.61
12	1.56	0.50	0.99	3.12	2.05	1.73
13	1.56	0.48	0.96	3.33	2.21	1.87
14	1.57	0.49	1.20	4.31	2.86	2.42
		Profile 2, $\Delta = 43.5$ km to the beginning of profile				
15	15.92	14.84	44.33	135.40	89.91	76.14
16	16.50	17.64	58.11	188.10	125.88	107.17
17	16.08	16.28	52.36	165.11	109.93	93.59
18	15.67	15.39	47.52	148.42	98.55	83.36
19	15.39	15.00	44.77	140.42	93.24	78.86
20	15.05	14.88	42.91	133.23	88.47	74.99
21	14.80	14.83	42.97	131.95	88.04	74.96
22	14.97	16.29	52.27	167.51	112.98	96.97
23	15.48	18.04	65.33	237.10	159.92	137.26
24	16.55	19.87	85.05	381.56	257.35	220.89
25	17.25	22.34	1.60	673.84	447.48	380.98
26	17.59	21.59	85.68	720.94	475.74	399.28
27	17.19	21.31	76.39	726.95	473.54	392.50
		Profile 3, $\Delta = 34.5$ km to the beginning of profile				
28	16.49	16.92	53.16	164.03	108.92	92.58
29	17.26	20.39	70.54	232.10	156.54	134.37
30	16.78	19.04	65.10	202.42	135.46	115.33
31	16.40	18.66	61.83	188.02	125.57	106.91
32	16.00	18.38	57.89	177.08	117.59	100.01
33	15.68	18.61	57.27	176.34	118.01	100.47
34	15.37	18.72	56.81	179.56	120.17	102.31
35	15.33	19.45	61.94	203.08	135.90	116.61
36	15.32	20.09	66.17	217.45	145.58	124.95
37	15.71	22.11	78.71	262.27	175.51	150.25
38	15.38	21.57	74.95	250.37	167.55	142.65
39	16.00	24.71	91.45	322.09	215.55	183.51
		Profile 4, $\Delta = 33.6$ km to the beginning of profile				
40	9.84	11.09	33.72	102.82	68.27	58.06
41	10.49	14.26	49.85	164.17	110.72	95.04
42	10.48	14.54	51.72	170.12	114.40	98.20

Table 3

(contd.)

No.	d_{max} (cm)	v_{max} (cm/s)	a_{max} (cm/s^2)	DGA_{S1} (cm/s^2)	DGA_{S2} (cm/s^2)	DGA_{S3} (cm/s^2)
43	10.17	14.02	47.76	158.69	106.23	91.18
44	10.36	15.63	54.62	194.82	131.40	112.79
45	10.20	15.62	55.95	198.92	134.16	115.16
46	10.12	16.09	59.97	215.44	145.31	124.72
47	9.99	16.63	62.95	229.12	154.53	132.64
48	9.82	16.82	63.29	234.00	157.82	135.46
49	9.46	15.87	57.98	214.77	144.86	124.34

Conclusions

We study, along four profiles crossing Santiago de Cuba basin, the influence of the local soil conditions on seismic ground motion (*SH*-waves) due to earthquakes which occurred in the Oriente fault zone. A seismic zoning of the city has been done considering (1) the synthetic response spectra ratios (RSR) computed at sites along these profiles, (2) the surface geology and (3) the deeper structure of the basin. With the exception of four sites, where a big resonance effect, due to particular structural conditions, is present, all the RSR curves versus frequency have a common shape and differ only by their absolute value. Three different zones are identified. Each zone is characterized in terms of its expected ground motion parameters for two scenario earthquakes: the most probable ($M_S = 7$), and the maximum possible ($M_S = 8$). Where comparable, our results follow the general trend evidenced by previous investigations.

Acknowledgements

We acknowledge the support by MURST Cofin 2000 Project (Active Deformation at the Northern Boundary of Adria), CNR-C007F8_008, PNRA-Projects 1B and 3A and by the Associateship Program of the Abdus Salam International Centre for Theoretical Physics. This work is a contribution to the UNESCO-IUGS-IGCP Project 414 "Realistic Modeling of Seismic Input for Megacities and Large Urban Areas."

References

ALVAREZ, L., ROMANELLI, F., and PANZA, G. F. (2001a), *Synthetic Seismograms in Laterally Heterogeneous Anelastic Media: Modal Summation for the Case of Offshore Seismic Sources (Deep-sea Trough)*, The Abdus Salam ICTP Preprint IC/2001/169, 24 pp.

ALVAREZ, L., VACCARI, F., PANZA, G. F., and GONZÁLEZ, B. E. (2001b) *Modelling of Ground Motion in Santiago de Cuba City from Earthquakes in Oriente Fault Seismic Zone*, Pure Appl. Geophys. *158*, pp. 1763–1782.

ALVAREZ, L., VACCARI, F., and PANZA, G. F. (1999), *Deterministic Seismic Zoning of Eastern Cuba*, Pure Appl. Geophys. *156*, 469–486.

APPLIED TECHNOLOGY COUNCIL (1978), *Tentative Provisions for the Development of Seismic Regulations for Buildings*, U.S. National Bureau of Standards, Special Publication 510.

ARANGO, E. (1996), *Geodinámica de la región de Santiago de Cuba en el límite de las Placas de Norteamérica y el Caribe*, Tesis en opción al Grado de Master en Ciencias. Instituto Politécnico Nacional, México, D.F., 111 pp.

ARRIAZA, G. (1998), *Nuevos enfoques en la interpretación y procesamiento de las ondas refractadas para el estudio del basamento de Cuba*, Tesis presentada en opción al grado científico de Doctor en Ciencias Geológicas, La Habana, 179 pp.

AKI, K, *Strong motion seismology*. In *Strong Ground Motion Seismology*, NATO ASI Series, Series C: Mathematical and Physical Sciences, vol. 204 (eds. Erdik, M. Ö and Toksöz, M. N.) (D. Reidel Publishing Company, Dordrecht, 1987) pp. 3–41.

BERGE-THIERRY, C., LUSSOU, P., HERNÁNDEZ, B., COTTON, E., and GARIEL, J. C. (1999), *Computation of the strong motions during the 1995 Hyogoken-Nambu earthquake, combining the k-square spectral source model and the discrete wavenumber technique*. In *Proceedings of the Second International Symposium on the Effects of Surface Geology on Seismic Motion*, Yokohama, Japan, 1–3 December, 1998; Volume 3, The Effects of Surface Geology on Seismic Motion, Recent Progress and New Horizon on ESG Study, pp. 1414–1424.

BOVENKO, V. G., SHCHERBAKOVA, B. Ye., and HERNÁNDEZ, G. (1980), *New Geophysical Data on the Deep Structure of Eastern Cuba (in Russian)*, Sov. Geol. *9*, 101–109.

COTILLA, M. and ALVAREZ, L. (1991), *Principios del mapa sismotectónico de Cuba*. Revista Geofísica del Instituto Panamericano de Geografía e Historia *35*, 113–124.

FÄH, D. (1992), *A Hybrid Technique for the Estimation of Strong Ground Motion in Sedimentary Basins*, Ph.D. Thesis, Nr. 9767, Swiss Fed. Inst. Technology, Zürich, 161 pp.

FÄH, D., IODICE, C., SUHADOLC, P., and PANZA, G. F. (1993), *A New Method for the Realistic Estimation of Seismic Ground Motion in Megacities, the Case of Rome*, Earthquake Spectra *9*, 643–668.

FÄH, D. and PANZA, G. F. (1994), *Realistic Modelling of Observed Seismic Motion in Complex Sedimentary Basins*, Ann. Geofis. *37*, 1771–1797.

FLORSCH, N., FÄH, D., SUHADOLC, P., and PANZA, G. F. (1991), *Complete Synthetic Seismograms for High-frequency Multimode SH-waves*, Pure Appl. Geophys. *136*, 529–560.

GONZÁLEZ, B. E. (1998), *El método de los microsismos en la solución de tarea de la sismología ingenieril*, Memorias del III Congreso cubano de Geología y Minería (GEOMIN98), Vol. I, pp. 284–286, Editorial Palcograf, ISSN 939-7117-01-0.

GUSEV, A. A. (1983), *Descriptive Statistical Model of Earthquake Source Radiation and its Application to an Estimation of Short-period Strong Motion*, Geophys. J. Roy. Astron. Soc. *74*, 787–800.

HARKRIDER, D. G. (1970), *Surface Waves in Multilayered Elastic Media. Part II. Higher Mode Spectra and Spectral Ratios from Point Sources in Plane Layered Earth Models*, Bull. Seismol. Soc. Am. *60*(6), 1937–1987.

ISHIHARA, K., Chairman (1993), *The Technical Committee for earthquake Geotechnical Engineering (TC-4) of the International Society for Soil Mechanics and Foundation Engineering, Manual for Zonation on Seismic Geotechnical Hazards*, The Japanese Society of Soil Mechanics and Foundation Engineering, 145 pp.

LEVANDER, A. R. (1988), *Fourth-order Finite-difference P-SV Seismograms*, Geophys. *53*, 1425–1436.

MEDINA, A., ESCOBAR, E., ORTÍZ, G. RAMÍREZ, M., DÍAZ, L., MÓNDELO, F., MONTEJO, N., DIÉGUEZ, H., GUEVARA, T., and ACOSTA, J. (1999), *Reconocimiento geólogo-geofísico de la cuenca de Santiago de Cuba, con fines de riesgo sísmico*, Empresa Geominera de Oriente, Santiago de Cuba, 32 pp., graphic annexes.

NORMA CUBANA (1999), *Propuesta de nueva norma cubana sismorresistente*, 110 pp. (draft).

ORIHUELA, N. and CUEVAS, J. L. (1993), *Modelaje sismogravimétrico de perfiles regionales del Caribe central*, Revista Ingeniería, Universidad Central de Venezuela *8*, 55–73.

PANZA, G. F. (1985), *Synthetic Seismograms: The Rayleigh Waves Modal Summation*, J. Geophys. Res. *58*, 125–145.

PANZA, G. F. and SUHADOLC, P. (1987), *Complete strong motion synthetics*. In (B. A. Bolt, ed.) *Seismic Strong Motion Synthetics, Computational Techniques* 4 (Academic Press, Orlando, 1987), pp. 153–204.

PANZA, G. F., VACCARI, F., COSTA, G., SUHADOLC, P., and FÄH, D. (1996), *Seismic Input Modelling for Zoning and Microzoning*, Earthquake Spectra, *12*, 529–566.

PANZA, G. F., ROMANELLI, F., and VACCARI, F. (2000), *Seismic Wave Propagation in Laterally Heterogeneous Anelastic Media: Theory and Applications to the Seismic Zonation, Advances in Geophysics*, Academic Press 43, 1–95.

PAVLOV, O. Y. (1984), *Seismic Microzoning* (in Russian), Moscow, Nauka.

PÉREZ, C. and GARCÍA, D., *Tectónica de la Sierra Maestra (Sureste de Cuba)*. In *Estudios sobre Geología de Cuba* (eds Furrazola, G. and Núñez, K.) (Centro Nacional de Información Geológica, Instituto de Geología y Paleontología, La Habana, 1997) pp. 462–473.

PICO, R. (1999), *Determinación del umbral de semejanza β_0 para los algoritmos de agrupamiento lógico-combinatorios, mediante el dendrograma de un algoritmo jerárquico*. SIARP'99, IV Simposio Iberoamericano de Reconocimiento de Patrones. Memorias, pp. 259–265

RODRÍGUEZ, M., ALVAREZ, L., and GARCÍA, J. (1997), *Estimaciones probabilísticas de la peligrosidad sísmica en Cuba*, Revista Geofísica del Instituto Panamericano de Geografía e Historia, No. 47, pp. 46–77.

RUBIO, M. (1985), *The Assessment of Seismic Hazard for the Republic of Cuba*, Ph.D. Thesis, Institute of Geophysics, Science Academy of Czechoslovakia, Prague.

RUIZ, J., PICO, R., LÓPEZ, R., ALAMINOS, C., LAZO, M., BAGGIANO, M., BARRETO, E., SANTANA, A., ALVAREZ, L., and CHUY, T. (1992), *PROGNOSIS y sus aplicaciones a las geociencias*. In IBERAMIA-92, III Congreso Iberoamericano de Inteligencia Artificial, MEMORIAS. México, LIMUSA, pp. 561–586.

SEO, K., GONZÁLEZ, B. E., ARANGO, E., *et al.* (1998), *Past, Present and Perspective Research on Seismic Microzoning in the Cities of Santiago de Cuba and Havana*, Proceedings of the workshop to exchange research information in the international scientific research project "Joints Studies on Seismic Microzonation in Earthquake Countries," Tokyo Institute of Technology, Japan, 17 pp.

VAN DER HILST, R. D. (1990), *Tomography with P, PP and pP Delay-time Data and the Three-dimensional Mantle Structure below the Caribbean Region*, Ph.D. Thesis, University of Utrecht.

VIRIEUX, J. (1984), *SH-wave Propagation in Heterogeneous Media: Velocity-stress Finite-difference Method*, Geophysics *49*, 1933–1957.

VIRIEUX, J. (1986), *P-SV Wave Propagation in Heterogeneous Media: Velocity-stress Finite-difference Method*, Geophysics *51*, 889–901.

(Received April 23, 2002, accepted December 16, 2002)

Pure appl. geophys. 161 (2004) 1061–1080
0033–4553/04/061061–20
DOI 10.1007/s00024-003-2497-7

Pure and Applied Geophysics

Duration Magnitude Scale and Site Residuals for Northern Morocco

ISSAM MOUAYN[1,2], BEN AISSA TADILI[3], LAHSEN AÏT BRAHIM[1], MOHAMED RAMDANI[3], MOHAMED LIMOURI[4], and NACER JABOUR[5]

Abstract—The first empirical duration magnitude (M_D) formula is developed and tested for the Northern Morocco Seismic Network (NMSNET). This relationship is obtained by relating the IGN (Instituto Geografico National, Madrid) body-waves $mbLg^{IGN}$ to the duration (τ), and the epicentral distance (Δ), at 25 analogue stations of the NMSNET for 479 earthquakes with $2.5 \leq mb \leq 5.4$, from March 1992 to February 2001. M_D estimates are significantly more precise while introducing a correction term for each of these stations, $cSta_j$. The magnitude for the i^{th} event $(M_D)_i$ is the mean value of individual $M_{D_{ij}} = -0.14 + 1.63\log_{10}(\tau_{ij}) + 0.031(\Delta_{ij}) + cSta_j$.

The $cSta_j$ corrections reduce considerably the local site effects which influence the recorded durations and cause stations to either overestimate, or underestimate M_D up to 0.5 magnitude units. Average station M_D residuals ($-cSta_j$) are found to be independent of the distance from the epicenter to at least 10 degrees. It seems evident that regional geological features in the immediate behavior of stations have a systematic effect on the corresponding obtained residuals: older well-consolidated Precambrian crystalline rocks produce high negative residuals (shorter durations), younger unconsolidated sediments produce high positive residuals (longer durations), whereas, intermediate M_D site residuals appear to be the result of the effect of various factors, principally age and state of consolidation of the bedrock, combined with the local tectonic.

Key words: Northern Morocco, duration, site residuals, short period, magnitude, tectonics.

Introduction

The frequency distribution of radiated seismic energy changes with earthquake size (AKI, 1967). Local or near-regional large events cause magnitude scales to suffer serious limitations, such as saturation (KANAMORI, 1977; HANKS and KANAMORI, 1979), and discrepancies between scales (GUTENBERG and RICHTER, 1956). In the case when the seismic signal saturates the seismograms, only duration

[1] Faculté des Sciences, Département de Géologie, Laboratoire de GEORISK Rabat – R.P.1014, Maroc.

[2] Personnel Postal Address: B.P. 9149, Rabat-Océan, Rabat, Maroc. E-mail: issamouayn@yahoo.fr

[3] Institut Scientifiques, Département de Physique du Globe, Agdal, Rabat, Maroc.

[4] Faculté des Sciences, Département de Physique, Rabat – R.P.1014, Maroc.

[5] Centre National de la Coordination et de Planification de la Recherche Scientifique et Technique, Laboratoire de Géophysique, Agdal, Rabat, Maroc.

can be measured. The usefulness of the coda duration as an estimate of earthquake size has been proved by many authors in the past (LEE and STEWART, 1981). They developed formulas relating the duration of the signal (τ) to the local magnitude for various areas. TSUMURA (1967) established a formula for Japan of the shape: $M_D = -2.53 + 2.85\log(\tau) + 0.0014(\Delta)$, where ($\Delta$) is the epicentral distance in kilometers, with $3 < M < 5$. LEE *et al.*'s (1972) empirical equation for the central California is: $M_D = 0.87 + 2.00\log(\tau) + 0.0035(\Delta)$, where $0.5 < M < 6$. BAKUN (1984), also for central California, proposed a relationship of the form: $M_D = 0.92 + 0.607\log^2(\tau) + 0.00268(\Delta)(1.5 < M < 5.3)$. For northern California, HIRSHORN *et al.*'s (1987) formula is of the form: $M_D = -0.72 + 2.95\log(\tau) + 0.001(\Delta)$, with $3 < M < 6$. The preferred equation of MICHAELSON (1990) for central California is without term in distance (Δ), but she included two terms of corrections, one for sensitivity and the other for the station site, respectively α and δ such as : $M'_D = -1.03 + 2.1\log(\tau) + 0.0026(\tau) + \alpha + \delta$, with $1.1 < M < 5.6$. EATON (1992) developed for northern California a dependent duration formula for computing magnitudes of the form: $M_D = -0.81 + 2.22\log(\tau) + 0.011(\Delta) + \log(\text{CAL15/CAL}) + D' + HF(h)$. The majority of these authors developed formulas relating the local magnitude M_L to (τ) and (Δ), where (τ) is the average recorded duration and (Δ) the corresponding average epicentral distance. Following BAKUN (1984), we adopted $m_b\text{Lg}^{IGN}$ magnitude values presented in the IGN Bulletins and considered the individual values of (τ) and (Δ) rather than their averages. The choice of $m_b\text{Lg}^{IGN}$ magnitude to calibrate the Moroccan network for duration-magnitude has been made on the basis of two important reasons. Firstly, the Digital Spanish Seismic Network is the nearest network to the Northern Morocco Seismic Network, and the majority of events occurring in Morocco or neighbouring regions are recorded by both networks. Secondly, the number of these events published in the IGN Bulletins is very important when compared to those published in the ISC (International Seismological Centre) Bulletins. Data from ISC present serious distortions arising from source radiation, distribution of reporting stations, amplitude saturation (KUGE, 1992), and data (concerning Morocco) reported in the NEIC (National Earthquake Information Centre) Bulletins are simply the m_bLg (MDD: Madrid) IGN values. Finally, the use of m_b values based on the Lg phase seems suitable for near-regional distances at which these phases (Lg) dominate the records and are followed by a long and slowly decaying coda (SINGH and HERRMANN, 1983; XIE and NUTTLI, 1988). The study of direct Lg recorded at regional distances has recently gained considerable interest for estimating the magnitude-yield relationships (PATTON, 1988).

During the period 1990–1993, duration magnitudes determined by the Geophysics Laboratory (LAG) of the "Centre National de Coordination et Planification de la Recherche Scientifique et Technique" (CNCPRST) of Rabat were obtained using an empirical formula of the form $M_d = a\log_{10}(\tau) - b$. The resulting magnitudes presented serious differences with those published in the

Bulletins of the International Seismological Centre (ISC), the NEIC, or in the IGN Bulletins for the same events. Since March 1994 the LAG adopted duration magnitude formulas for computing magnitudes at individual stations. These individual empirical equations were of the form $M_D = a + b\log_{10}(\tau) + c(\Delta)$, where a, b, and c are constants calculated for each station (MOUAYN, 1994). Stations used in this study are composed of 21 telemetered stations by the LAG, while 4 other non-telemetered stations are run by the Scientific Institute Department of the Physics of the Globe (DPG) of Rabat. These 25 selected stations constitute only a part of the Moroccan Seismic Network. The NMSNET currently covers 95 stations comprising several types of stations: A set of telemetered stations, a set of portable stations, and recently installed broadband seismic stations. For computing the coda-duration magnitude at individual stations, empirical equations have been obtained on the basis of a few durations reported in the 1991–1993 LAG catalogues (less than 15 duration per station). Therefore, the magnitudes calculated suffered severe imprecision. Considering the availability of more numerous and better quality data, establishing a good duration-dependent magnitude formulation was in order.

Data

A set of 479 earthquakes (Fig. 1) was selected as the common events published in the Moroccan LAG and DPG seismological bulletins, and the Spanish IGN seismological bulletins. These events were divided into two subsets: 395 events from January 1993 to December 1998 with a total of 1,934 durations measured from seismograms available at the 25 NMSNET analogue stations (Fig. 1 and Table 1). These data are used to derive the relationship between (τ), (Δ) and M_D and are referred to as the *independent set*. The obtained equation was then applied to an additional 84 events (511 durations) which have known $m_b\mathrm{Lg}^{IGN}$ magnitudes to evaluate how well the new M_D predicted $m_b\mathrm{Lg}^{IGN}$. This second set of earthquakes is referred to as the *test set*, and it is composed of 4 events recorded between March 1992 and December 1992, with magnitude $4.4 \leq m_b\mathrm{Lg}^{IGN} \leq 5.3$, provided from the yearly seismological bulletin of the I.G.N. The other 80 events were recorded in the period time from January 1999 to February 2001. For both sets, durations were read on the seismograms by using the prescription of REAL and TENG (1973). The duration (τ) is defined as the time in seconds, on a vertical component short-period seismogram, from the P arrivals until the coda falls beneath some absolute amplitude level for the last time. In our case, this level corresponds to the background noise initial signal. Signals abnormally short, abnormally long, or for which the end could not be isolated from the background noise, were not included in this study. Epicentral distances (Δ) in degrees were calculated by using revised Hypo71 (LEE and LAHR, 1975). Origin times, locations, and magnitudes were taken from IGN Bulletins.

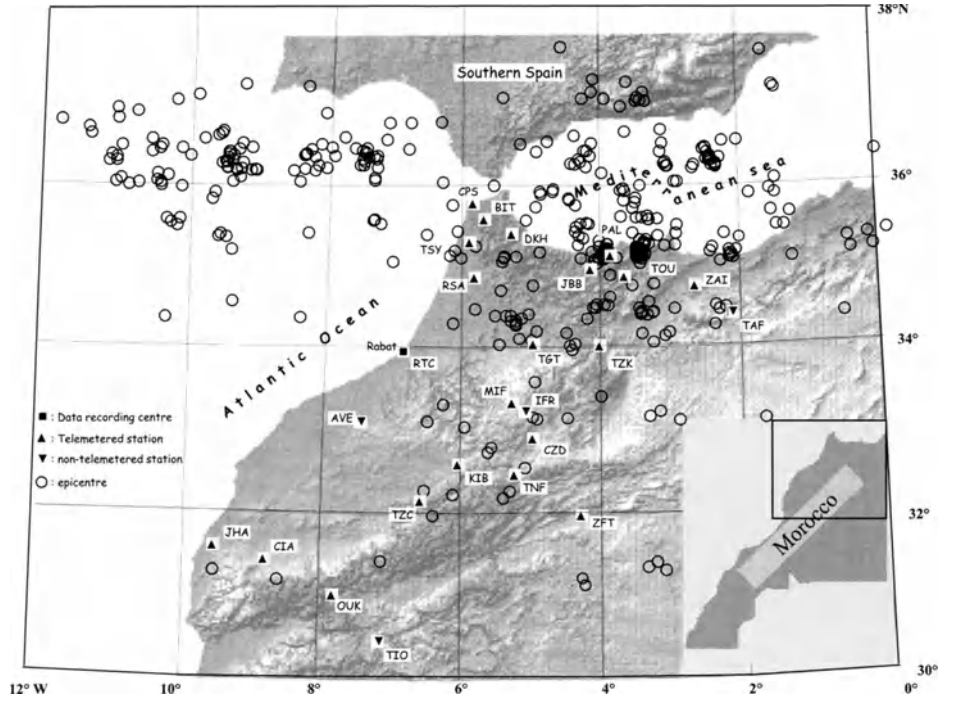

Figure 1
Epicenters and NMSNET station locations used in this study for the entire data set. Background image is a colored shaded topographic relief map of Northern Morocco and Southern Spain.

Data Analysis

Derivation of the M_D Equation

It is now proven that, if the envelope of the coda follows a t^{-q} relationship with increasing time, the duration magnitude, M_D can be computed from a relationship of the form $M_D = q\log_{10}(\tau) + r$ with $q = 1.5$ (HERRMANN, 1975). The observed relationship between magnitude and duration is shown to be a result of the particular shape of the signal coda as a function of time. The correlation between $m_b\mathrm{Lg}^{IGN}$ and the signal duration recorded by the NMSNET stations for the entire data *sets* is illustrated in Figure 2. The best fit between $m_b\mathrm{Lg}^{IGN}$ and the common logarithm of (τ) is represented by a linear function: $m_b\mathrm{Lg}^{IGN} = 1.54\log_{10}(\tau) + 0.12$ where 1.54 is the value of the coefficient q proposed when the envelope of the coda can be well approximated by t^{-q} power law (HERRMANN, 1975). This argues clearly the necessity of adopting a magnitude-$\log_{10}(\tau)$ relationship. The goal here is to quantify $m_b\mathrm{Lg}^{IGN}$, in terms of duration of the coda. The employed technique is a complete linear least-square regression analysis (JOBSON, 1991), with independent

Table 1

Station Corrections $cSta_j$.

No.	Code	Name	Sub-Network/ NT	Location		$cSta_j$	AMSR	Number of data
				Lat. (N)	Long. (W)			
1	TIO	Tiouine	Non-Telemetered	30.550	−7.150	***0.29***	*−0.29*	77
2	OUK	Oukaimden	Chichaoua	31.209	−7.868	***0.24***	*−0.24*	24
3	TZK	Tazeka	Ifrane	34.089	−4.184	***0.17***	*−0.17*	151
4	TAF	Tafouralt	Non-Telemetered	34.480	−2.240	***0.16***	*−0.16*	101
5	MIF	Mishlifen	Ifrane	33.409	−5.229	***0.16***	*−0.16*	48
6	ZAI	Zaio	Zaio	34.803	−2.746	***0.15***	*−0.15*	114
7	ZFT	Ezzeft	Midelt	32.034	−4.352	***0.15***	*−0.15*	29
8	KIB	El Ksiba	Beni Mellal	32.576	−6.039	***0.13***	*−0.13*	81
9	IFR	Ifrane	Non-Telemetered	33.310	−5.070	***0.12***	*−0.12*	125
10	CZD	Col de Zad	Midelt	33.033	−5.043	***0.08***	*−0.08*	127
11	TNF	Tounfite	Midelt	32.530	−5.319	***0.07***	*−0.07*	26
12	TZC	Tazercounte	Beni Mellal	32.148	−6.490	***0.06***	*−0.06*	50
13	PAL	Palemas	Zaio	35.225	−3.942	***−0.04***	*0.04*	109
14	JBB	Jbel Babet	Zaio	35.013	−4.198	***−0.06***	*0.06*	49
15	DKH	Dar Kharkour	Tanger	35.490	−5.360	***−0.08***	*0.08*	51
16	TOU	Touzarine	Zaio	34.962	−3.754	***−0.08***	*0.08*	122
17	CPS	Cap Spartel	Tanger	35.791	−5.910	***−0.11***	*0.11*	87
18	TGT	Taghat	Ifrane	34.070	−5.055	***−0.11***	*0.11*	95
19	RSA	Sarsar	Tanger	34.877	−5.828	***−0.12***	*0.12*	74
20	BIT	Ibn Batouta	Tanger	35.648	−5.729	***−0.13***	*0.13*	63
21	TSY	Tnine Sidi l'Yamani	Tanger	35.373	−5.970	***−0.14***	*0.14*	97
22	JHA	Jbel Lahdid	Chichaoua	31.736	−9.454	***−0.23***	*0.23*	23
23	CIA	Chichaoua	Chichaoua	31.565	−8.759	***−0.25***	*0.25*	58
24	RTC	Rabat Centre	Data Reception Centre	33.990	−6.858	***−0.32***	*0.32*	44
25	AVE	Averoes	Non-Telemetered	33.170	−7.240	***−0.32***	*0.32*	109

NT : Non-Telemetered Station
Number of data : number of duration measurements per station
Magnitude formula used: $Mp_{ij} = -0.14 + 1.63\log_{10}(\tau)_{ij} + 0.031(\Delta)_{ij} + 0.031(\Delta)_{ij} + cSta_j$
AMSR = Average magnitude station residual = $-cSta_j$

variables $\log_{10}(\tau)$ and (Δ). The quantity $m_b\mathrm{Lg}^{IGN}$ is assumed to be the chosen reference magnitude, to which the variables $\log_{10}(\tau)$ and (Δ) are related, with errors ε, as: $m_b\mathrm{Lg}^{IGN} = c_0 + c_1\log_{10}(\tau) + c_2(\Delta) + \varepsilon$, where c_0, c_1 and c_2 are the constants to be determined. We solve for the model the constants, and then use these to calculate M_D. In this case, both the errors due to measurement and the lack of fit of the model are contained in ε. If errors are small and randomly distributed, then the model is considered satisfactory for these work data. We adopt for M_D the model represented by the following equation (1) in which $cSta_j$ is added as station correction, considered also as the *site correction:*

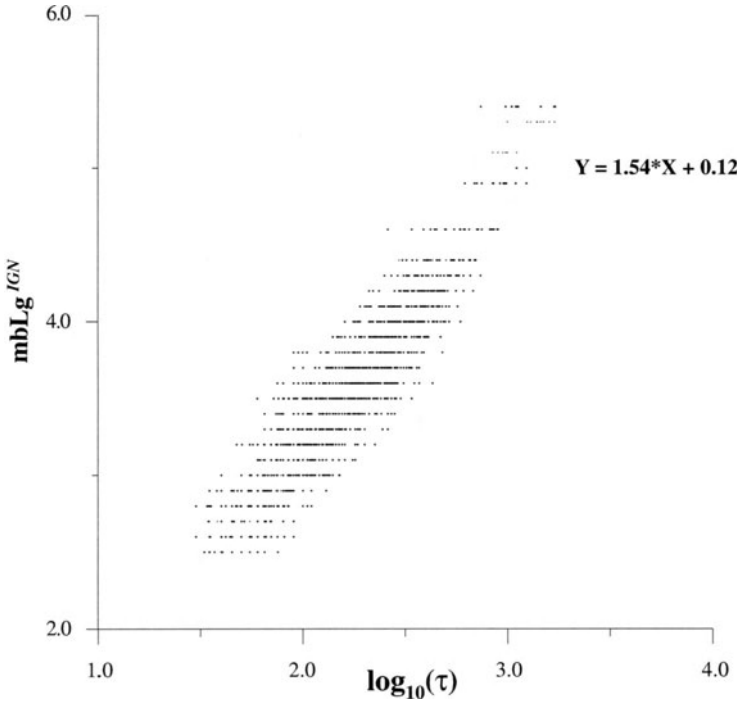

Figure 2
$m_b\mathrm{Lg}^{IGN}$ magnitude per earthquake versus individual observations of $\log_{10}(\tau)$ for the entire data of this study (2,445 durations). The straight line represents the best fit between $m_b\mathrm{Lg}^{IGN}$ and $\log_{10}(\tau)$.

$$M_{D_{ij}} = c_0 + c_1 \log_{10}(\tau_{ij}) + c_2(\Delta_{ij}) + cSta_j \ , \tag{1}$$

where a double subscript ij denotes an observation of event i at instrument j; a subscript i denotes a unique event, and a subscript j denotes a unique instrument.

Iterative Procedure

To adjust M_D against the data of this paper (*independent set*) we used a two-stage iterative procedure. In the first stage we solve for the constants c_{01}, c_{11}, and c_{21} by regressing initially, τ and Δ against $m_b\mathrm{Lg}^{IGN}$ with the station corrections $cSta_j$ being reset to zero. The quantities c_{01}, c_{11}, and c_{21} are the resultant coefficients of the first iteration of the regression. In the second stage the c_{i1} were substituted into equation (1) and $cSta_{j1}$ estimated. The first station corrections $cSta_{j1}$ are included in the next iteration of the regression, and the process repeated until the variance and standard errors converged to a stable minimum, with station corrections being updated between iterations. The adopted final coefficients c_0, c_1, and c_2 are those obtained from the last iteration of the regression as: $c_{0k} = c_0$, $c_{1k} = c_1$, $c_{2k} = c_2$, and

$cSta_j = \sum cSta_{jk}$, k being the number of iterations. The resultant magnitude estimate formulation is:

$$M_{D_{ij}} = -0.14 + 1.63 \log_{10}(\tau_{ij}) + 0.031(\Delta_{ij}) + cSta_j \quad (2)$$

with $c_0 = -0.14$, $c_1 = 1.63$ and $c_2 = 0.031$. The values of $cSta_j$ are listed in Table 1.

The magnitude of the ith event is the mean of individual station estimates $M_{D_{ij}}$, and M_D uncertainty is the standard deviation of the mean. The duration magnitude $M_{D_{ij}}$ estimated by equation (2) is plotted versus $\log_{10}(\tau)$ to illustrate the strong correlation between these parameters (Fig. 3a.). $M_{D_{ij}}$ estimated by equation (2) accounts for 95 percent of the variance pertaining to the regression, predicting $m_b\mathrm{Lg}^{IGN}$ reasonably well (Fig. 3b), while introducing station corrections assumed to be the site corrections, and the opposite of the average station magnitude residuals. This assumption is made on the basis that the sensitivity and the class component (low gain, vertical) had no error leaked into the site corrections, and therefore the instrument corrections were set equal to zero. To ensure that instruments had no direct effect on the durations, we have used in this study only stations with the same instrument response curves (1-Hz natural frequency), and for which attenuation setting does not change during the survey period. It is known that there is no obvious change in the residuals/site corrections when amplification changes at station (BAKUN, 1984). This remains according to the assumption that (τ) does not depend critically on station amplification (LEE *et al.*, 1972).

Testing the Magnitude Equation M_D

One way of investigating whether the newly computed M_D values agree with the $m_b\mathrm{Lg}^{IGN}$ observations was to apply first the new duration-dependent magnitude relationship to the *test set* events. 511 durations for 84 events with epicentral distances ranging between 10 and about 1,000 km (1 to 10°) are used to plot M_D estimated by the model (2) with the appropriate station corrections versus the $m_b\mathrm{Lg}^{IGN}$. Figure 4 is a good illustration of the strong correlation between the two magnitudes scales. M_D estimates are obtained accounting for 91 percent of the data variance (Table 2). The residuals ($M_D - m_b\mathrm{Lg}^{IGN}$) range between -0.16 to 0.4 magnitude units, with 80% of these residuals near zero, proving that the estimated values of magnitude using our formula are mostly equal to those given by the IGN. In the second time the M_D formula is applied to the entire data sets (all events in this study) to determine whether the new computing procedure with the M_D equation is well satisfied (Fig. 5). We effectively found that the best fit between the $m_b\mathrm{Lg}^{IGN}$ and M_D values is a linear function of the form $Y = 0.91X + 0.32$, with a coefficient of determination R-squared of about 0.94. The obtained result confirms the strong evidence that the model used in this study conformed with the data of this paper. Individual residuals ($M_D - m_b\mathrm{Lg}^{IGN}$) calculated for 479 events (2,445 durations) range between -0.54 magnitude units underestimating $m_b\mathrm{Lg}^{IGN}$ and 0.47 magnitude units

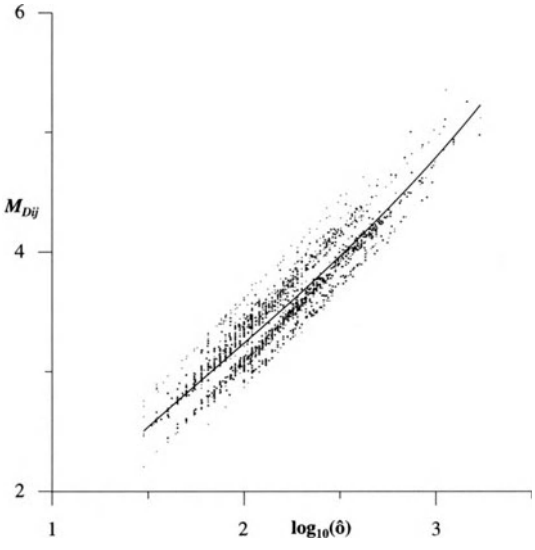

Figure 3a
$M_{D_{ij}}$ estimated and adjusted (independent set) for station corrections. The curved line is the best fit between $M_{D_{ij}}$ (corrected for site effect) and $\log_{10}(\tau)$.

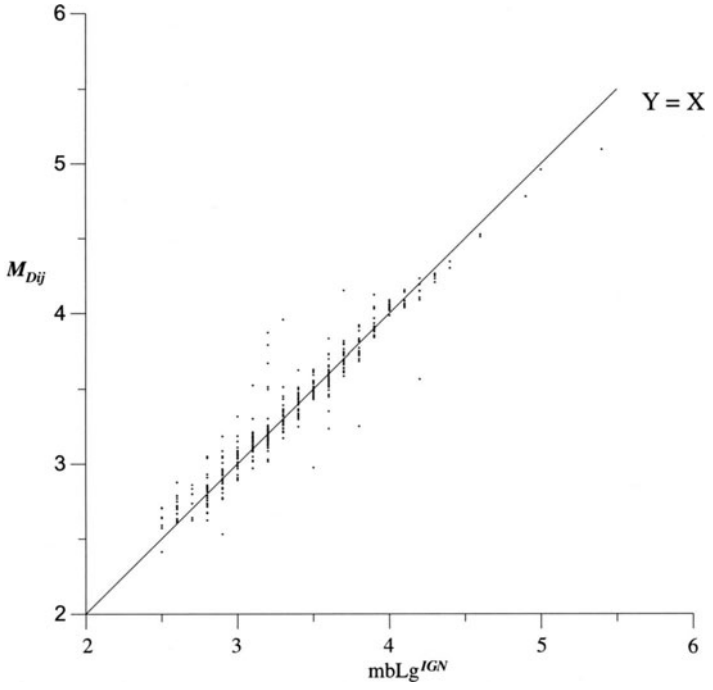

Figure 3b
$M_{D_{ij}}$ estimated versus $m_b\text{Lg}^{IGN}$ for each event of the independent set. The straight line has a slope of 1.

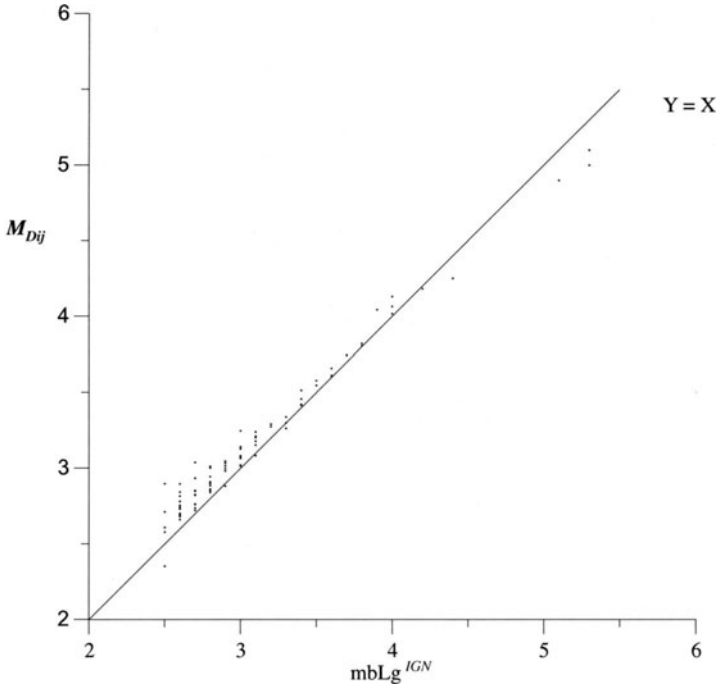

Figure 4
$M_{D_{ij}}$ estimated versus $m_b\text{Lg}^{IGN}$ for each event of the test set. The straight line has a slope of 1.

Table 2

Variance Analysis

	Variables		Standard Error	R^2	*F* Test	Number of degrees of freedom
	$\log_{10}(\tau)$	Δ (km)				
Independent Set						
no $Csta_j$	(+)	(+)	1.08	0.84	5248	1931
with $cSta_j$	(+)	(+)	0.87	0.95	17190	1931
Test set						
with $cSta_j$	(+)	(+)	0.97	0.91	2346	508

(+): variables included in this model
R^2: Correlation coefficient
F Test: *F* test compared to the *F* of the model

overestimating $m_b\text{Lg}^{IGN}$. To check for probable correlation between individual station magnitude residual values and their corresponding M_D estimated magnitudes, durations common logarithm ($\log_{10}(\tau)$), or epicentral distances Δ, we have plotted these residuals (for each event of the entire data) versus M_D, versus $\log_{10}(\tau)$ and

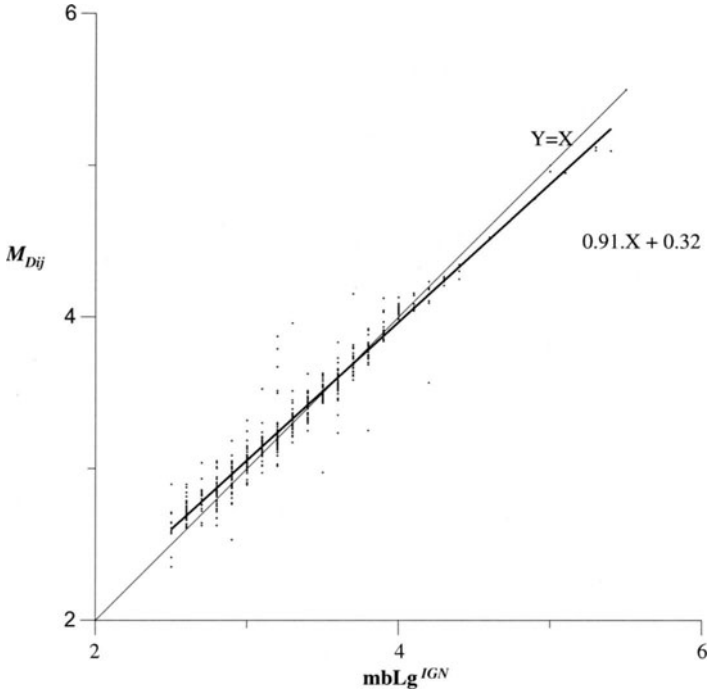

Figure 5
$M_{D_{ij}}$ estimated versus $m_b\mathrm{Lg}^{IGN}$ for the entire data set events. The dashed grey line ($Y = 0.91X + 0.3$) represents the best fit between $M_{D_{ij}}$ corrected for the site effect, and $m_b\mathrm{Lg}^{IGN}$. The straight has a slope of 1.

versus Δ, respectively, (Figs. 6a, b and 6c). It has been found that M_D estimates which are obtained by applying equation (2) show a good agreement for $2.5 \leq m_b\mathrm{Lg}^{IGN} \leq 4.5$ (Fig. 6a.). M_D has a negative bias in the range from 4.5 to 5.4 (Fig. 6a.). This may be due to the insufficiency of data with $m_b\mathrm{Lg}^{IGN} > 4.5$ (Table 3, Fig. 7) but it cannot affect the adequacy of the model, considering the overall character of the data used in this study. This is because the majority of the earthquakes felt in Morocco have magnitudes ranging between 3.5 and 4.5, as underlined in other seismology studies in Morocco (Aït Brahim *et al*, 2002). It is clear and expected that for large events ($M > 4.5$) uncertainties in M_D will be important. For small events ($M \leq 4.5$), however, uncertainties in M_D calculations will be minor. We also found that there is no apparent systematic error in M_D with (τ) (Fig. 6b.), or with Δ (Fig. 6c.), and therefore residuals are uncorrelated as a function of $\log_{10}(\tau)$, or Δ to at least 10°.

Station Corrections (*Site Corrections*)

In this study, station corrections are computed using the model in equation (2) and introduced to reduce the particular effect of local geological heterogeneity at the

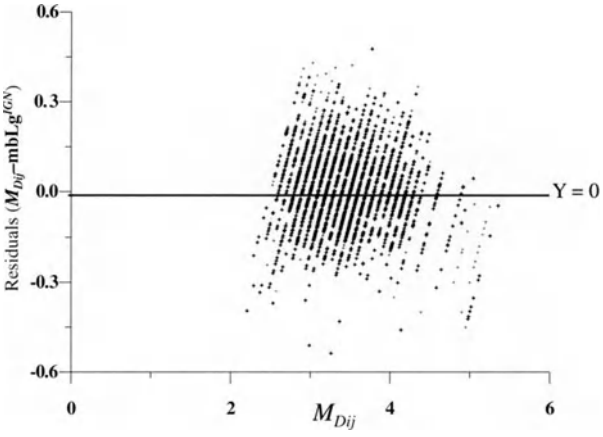

Figure 6a
Residuals ($M_{D_{ij}} - m_b\text{Lg}^{IGN}$) versus $M_{D_{ij}}$ for the entire data sets (2,445 durations).

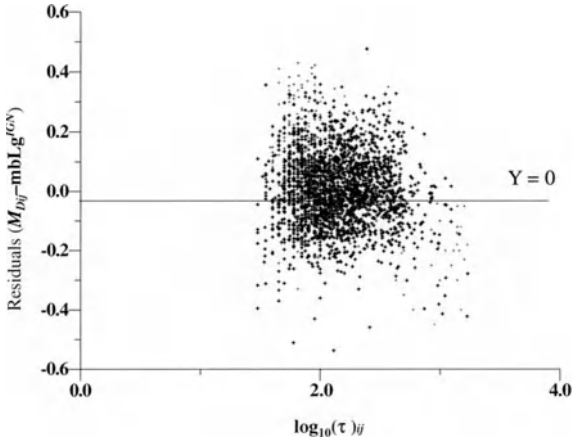

Figure 6b
Residuals ($M_{D_{ij}} - m_b\text{Lg}^{IGN}$) versus $\log_{10}(\tau)_{ij}$ for all the data sets (2,445 durations).

site of the stations, and therefore can be viewed as the resultant errors in the prediction of the coda length assuming a simple description of the physical parameters of a seismic event. The seismic source is in general represented only by a single variable which is the magnitude (or the seismic moment) of an earthquake, and the volume of the medium between the hypocenter and the station is simply represented by the epicentral distance Δ. This single variable Δ cannot explain all the propagation-path effects which influence the durations and result in either overestimating or underestimating the magnitude at a station. It is implicit that station

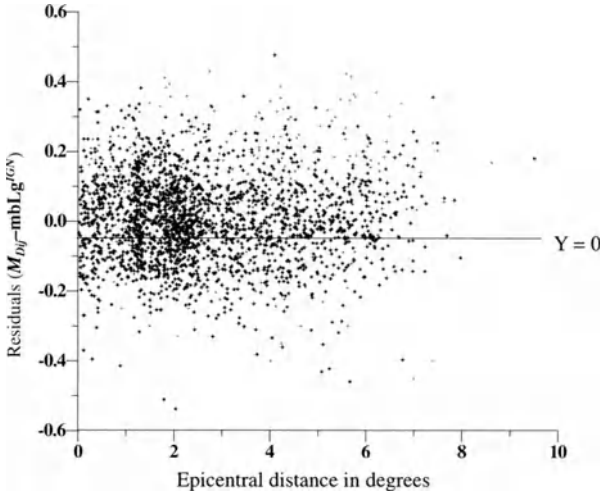

Figure 6c
Residuals ($M_{D_{ij}} - m_b\text{Lg}^{IGN}$) versus Δ_{ij} (in degrees) for the entire data sets (2,445 durations).

Table 3

Distribution by magnitude of Events of this Study

Magnitude	2.5–3	3–3.5	3.5–4	4–4.5	4.5–5	5–5.5
Events	160	181	105	24	5	3

corrections are not resulting from a bad representation of the seismic source properties, since a source can be viewed as a point (as well as it can be considered as a volume) from which the seismic energy is radiated in all directions. This energy is quantified by an intrinsic parameter such as the magnitude (or the seismic moment). Clearly, although durations can be influenced by amplification or attenuation properties in a volume from the hypocenter to the receiver, we can easily consider that only an averaged influence is generated by a backscattering phenomenon in all directions of this volume, especially, backscattering heterogeneity in a volume surrounding the source and receiver (TSUJIURA, 1978; AKI, 1980). The coda-wave energy is observed homogeneously distributed in the crust (AKI, 1969; MAYEDA *et al.*, 1992). This influence may not be evaluated because it may not be isolated—as a known value—from the total correction attributed to each station. Nonetheless it is clear that an implicit error in magnitude estimation due to the path-propagation properties in this volume, and resulting from a particular regions geological properties, can be represented by a characteristic supplementary additive mean value correction for this region, and therefore can be leaked into the station correction for physical attenuation properties of local geology in the immediate vicinity of stations. This is due to the fact that surface geology exerts significant influence on the site

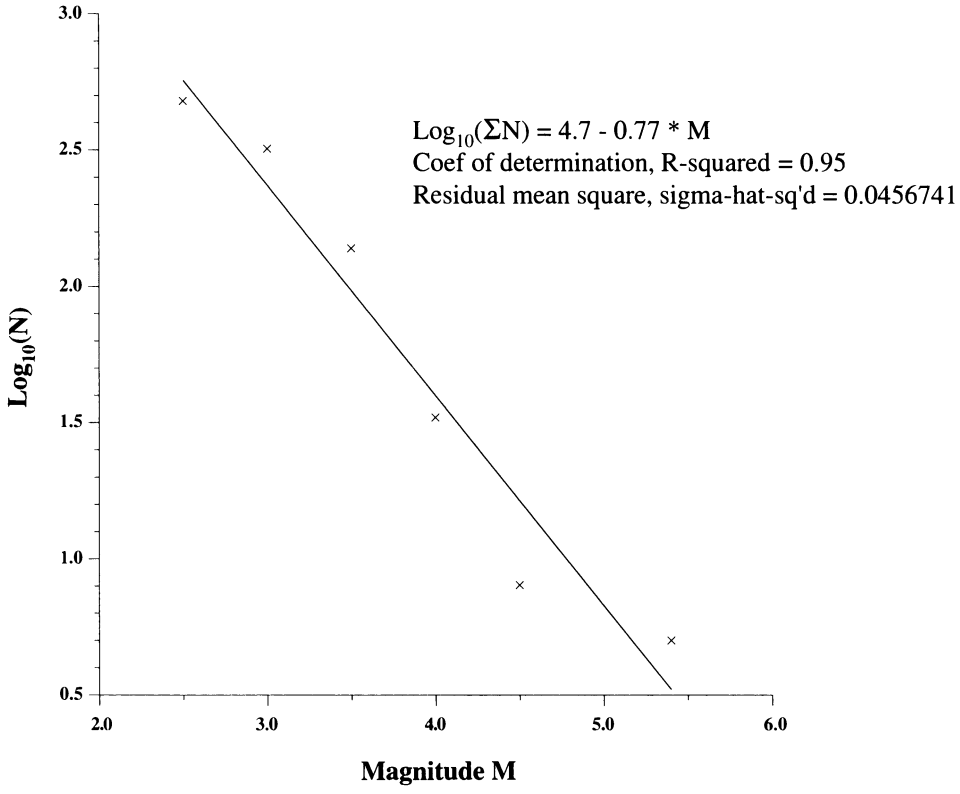

Figure 7
Magnitude-frequency relations for the 479 events used in this study.

amplification (BORCHERDT, 1970; BORCHERDT and GIBBS, 1976; ROGERS *et al.*, 1979; MICHAELSON, 1990; SU *et al.*, 1992). In this study, site corrections (station corrections) $cSta_j$ are obtained in the range between -0.29 to 0.32 magnitude unit (see Table 2). In an attempt to check for the eventual correlation between these corrections and the geology underlying the stations we prefer the use of the average station magnitude residuals $ASMR$ term which are the site residuals (Table 2) rather than using station corrections $cSta_j$ ($AMSR = -cSta_j$).

M_D Site Residuals and their Dependence on Lithology and Tectonics

Site residuals $AMSR$ ranging between -0.29 and $+0.32$ (Table 2) are plotted at station locations on a simplified schematic structural map with major tectonic features of northern Morocco (Fig. 8). Negative (positive) site residual means that corresponding stations tend to underestimate (overestimate) the M_D magnitude, and consequently have shorter (longer) durations than expected coda duration. The geological properties of the individual sites were read from the $1{:}10^6$ scaled geological

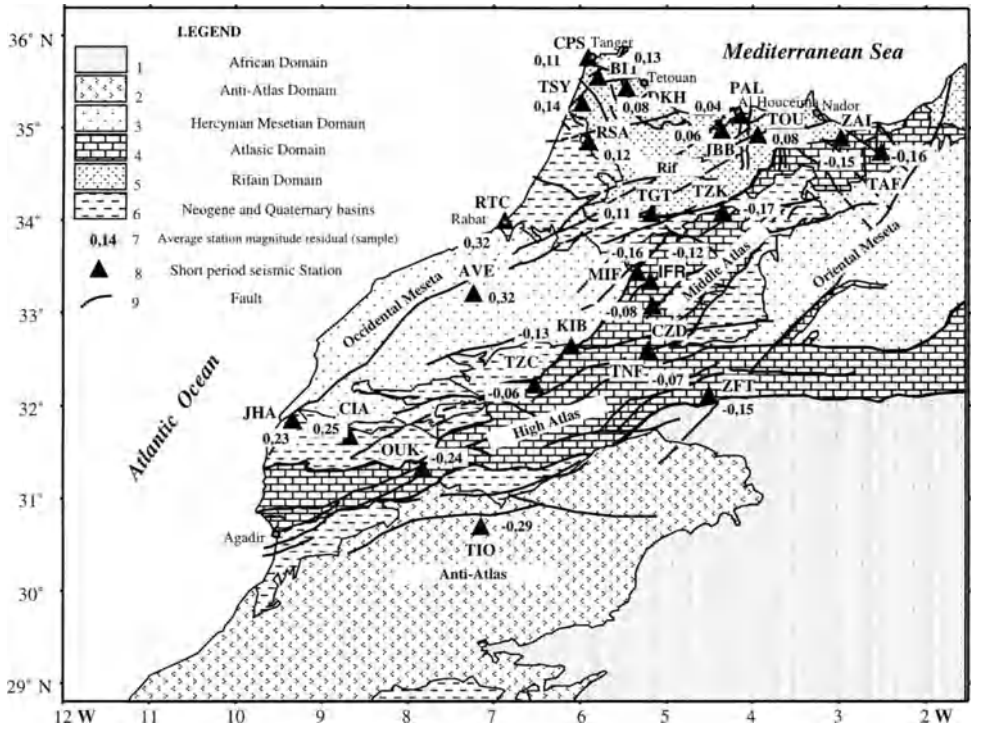

Figure 8
Simplified schematic structural map of northern Morocco.

map of Morocco (editions service géologique du Maroc, 1985), and tectonic map of northern Morocco (AÏT BRAHIM, 1991).

We found that stations AVE, RTC, CIA, and JHA which have the highest positive site residuals (0.23 to 0.32) are installed on a stable competent block corresponding to the occidental Meseta. This domain of the Hercynian chain is composed mainly of Palaeozoic formations deformed during Hercynian orogeny (PIQUÉ, 1979). Since then, this domain is a homogeneous stable and competent block with an isostatically compensated crust (BENSARI, 1987; SEBER *et al.* 1996), and it is characterized by poor seismic activity and a particular amplification of the seismic signals. The amplification effect observed at these stations can be attributed to the low impedance of younger, less consolidated quaternary sediments (BEAUDET, 1961; SU *et al.*, 1992) at station sites, or it can be viewed as a systematic result of the presence of a probable zone which causes the signal to be amplified before being acceded by the Mesetian domain (SEBER *et al.*, 1993). Thickness of sedimentary layers at these sites is not important compared to the thickness of the Palaeozoic substratum. In this case, we note no contradiction with the Kappa effect (ANDERSON and HOUGH, 1984) which predicts the dominance of

attenuation due to high absorption for younger sediments since these are not well represented.

The second group of stations with positive residuals ranging between 0.04 and 0.14 is represented by CPS, BIT, TSY, RSA, TGT, DKH, JBB, PAL and TOU. These stations are situated in the Rifain domain. CPS, BIT, TSY, RSA, and TGT are installed along the Rifain external domain with residuals between 0.11 and 0.14. This domain deformed during the middle and upper Miocene tectonic phase (ANDRIEUX, 1971; AÏT BRAHIM, 1991) is characterized by the presence of NW-SE to E-W trending crustal thrust faults. This zone is characterized by an important negative gravity anomaly (−150 m gal) along 300 km (VAN DEN BOSCH, 1974), caused by a tectonic crustal thickening due to the thrusting of the external Rifain domain over the internal domain and the thrusting of this last one over the Mesetian and Atlasic foreland (AÏT BRAHIM *et al.*, 1990). In this area the recent faulting and the absence of younger unconsolidated sediments appear to be the cause of the moderate amplification observed in these sites. Stations JBB, DKH, PAL, and TOU with positive near zero residuals (0.04 to 0.08) are disposed along the thrust front of the Rifain internal domain characterized by the ascension of ultramafic material situated at depth of 23 to 29 km (BELLOT, 1985). This domain comprises napes with a slim continental crust (gneiss and micaschist) and their ultrabasic basement constituting peridotite and Kinzigite over which lay the Palaeozoic and the limestone dorsal (1800 m) at Tetouan (Haouz Chain) and at Al Houceima (Boukkouya chain). In this domain no attenuation or amplification is noted. This is because the majority of events of this study are located in the homogeneous and competent block of the Alboran crust which represents either the source or the receiver areas.

In the Atlasic domain, residuals are negative and range from −0.06 to −0.17 for stations TZC, KIB, ZFT, TNF, CZD, IFR, MIF, TZK, ZAI, and TAF. This domain is affected by the upper Miocene deformation (LAVILLE, 1985; PIQUÉ *et al.*, 1998; MOREL *et al.*, 2000). In this tectonic phase, the competent Precambrian and Palaeozoic substratum were intensively fractured and the Jurassic limestone cover plied and detached at the Triassic argillites level (LAVILLE, 1985; PIQUÉ *et al.* 2000). This intracontinental mountain chain (more than 4 km altitude) with no crustal "root" (WIGGER *et al.*, 1992; GOMEZ *et al.*, 1998) is considered to have a relatively important seismic activity with focal depths up to 150 km (HATZFELD, 1978). This area which absorbs the maximum deformation resulting from the Africa-Europe convergence shows a notable seismic wave decay (low amplification) due, initially, to the dominance of Precambrian and Palaeozoic rigid blocks over which Jurassic limestone formations lay, and secondly, to the absence of younger sediments at station sites. The negative, near zero residuals for TNF, CZD, and TZC (−0.06 to −0.08) may be explained by the location of all these stations on active crustal faults which limit the middle and high Atlas (AÏT BRAHIM, 1991; MOREL *et al.*, 2000).

Lastly, OUK and TIO stations with the highest negative residuals of −0.24 and −0.29 respectively, are located in two different domains; the OUK station in the high Atlas and the TIO station in the anti-Atlas domains, however they are both installed on 2000 M year-old Precambrian crystalline rocks (gneiss, migmatite, granitoid) representing the rigid and stable West African basement (2000 to 4000 M years). This clearly explains the important decay both in duration and amplitude of seismic waves observed in these geological units (old and well-consolidated rocks), and as established by many authors (BOORE and ATKINSON, 1992; EATON, 1992; SU *et al.*, 1992) for different regions of the earth.

Conclusion

The first coda-duration magnitude (M_D) formula is presented and tested for the northern Morocco seismic network (NMSNET). This formula is obtained using 479 earthquakes with $2.5 \leq m_b \leq 5.4$ from March 92 to February 2001. The magnitude for the i^{th} event $(M_D)_i$ is the mean value of individual station estimates: $M_{D_{ij}} = -0.14 + 1.63\log_{10}(\tau_{ij}) + 0.031(\Delta_{ij}) + cSta_j$ where (τ_{ij}) is the duration of the recorded signal, (Δ_{ij}) the epicentral distance, $cSta_j$ the site correction and subscripts i and j denote an event i recorded at a station j. Instrument gain settings infrequently change during the survey period. Special care was taken to ensure that the corresponding records were not included in this study. Thus no corrections were considered for the sensitivity of the used instruments (low-gain, analogue, short-period vertical component). In this empirical approach we noted the following points: (1) M_D site residuals $(-cSta_j)$ are the results of the local site effects which influence the recorded durations and make stations overestimating or underestimating M_D up to 0.5 magnitude units; (2) M_D site residuals are found to be independent of the distance from the epicenter to at least 10°; (3) particular values of M_D site residuals may be systematically related to geologically underlying stations, such as bedrock lithology, structural domain, and tectonic features. It has been found that higher negative residuals (−0.29 and −0.24) have been obtained for the high and anti-Atlas old Precambrian crystalline rocks (gneiss, migmatite, granitoid,..) which constitute a part of the rigid and stable West African basement. In these units we note an important attenuation (low amplification) of the seismic waves. Intermediate negative residual values (−0.17 to −0.12) have been observed at stations in the middle and high Atlas Palaeozoic deformed rocks, beside a moderate attenuation of the seismic energy. Near zero negative residuals (−0.06 to −0.08) are also obtained for stations located in the areas. These residuals may be explained by the location of the corresponding stations on the active Mesozoic and Quaternary crustal faults limiting the middle and high Atlas belts. Near zero positive residuals (0.04 to 0.08) have been obtained for stations disposed on the thrust front of the Rifain internal domain which is on the Alboran crust.

Intermediate positive residuals (0.11 to 0.14) have been observed at stations located on the thrust front of the external Rifain domain over the Mesetian and Atlasic forelands. The moderate amplification noted here may be caused by the absence of younger sediments and the recent tectonic activity. Concludingly, the higher positive residuals (0.23 to 0.32) correspond to the stations set in the occidental Meseta domain which is a homogeneous block with quaternary younger deposits. In this area we have noted an important amplification of seismic waves mainly due to the low impedance for younger, less consolidated sediments. In general our results have shown that older competent rocks produce higher negative residuals (shorter durations), while younger less consolidated sediments produce higher positive residuals (longer durations). The interpretations given to explain the correlation between geological properties in the immediate vicinity of station sites and intermediate positive or negative residuals, are an unusual result requiring more study, and therefore, may not be fully justified.

Acknowledgements

We are grateful to two anonymous reviewers for their constructive comments. The first author expresses his sincere thanks to Mohamed Fathi and Mohamed Niinia, from the "Direction Generale de l'Hydraulique" DGH, Rabat-Agdal; without their collaboration this paper would not have been written. Moussa Maadadi from the CNCPRST (Rabat), and Mohamed Ikharrazen from the IS (Rabat), for their contribution in selecting the necessary data for this work. Discussions with Zouhair Mouayn regarding the statistical approach are much appreciated. Special thanks are due to Mounir Lemghari from Audiotel, Agdal, Rabat, for his precious technical assistance providing the necessary software, and computing equipments to accomplish this work. Conclusively the first author extends his gratitude to Concettina Nunziata for her assistance during the reviewing process.

References

Aït Brahim, L., Chotin, P., Ramdani, M., and Tadili, B. (1990), *Failles Actives dans le Rif Central et Oriental (Maroc)* - C.R. Acad. Sci. Paris, *t. 310, série II*, 1123–1129.

Aït Brahim, L. (1991), *Tectonique Cassante et Etat de Contraintes Récentes du Maroc Nord. Résultat de la Cinématique des Plaques Afrique-Europe et du Bloc d'Alboran*, Thèse Doct. d'état, Departement de Geologie, Université Med.V, Rabat, 233 pp.

Aït Brahim, L., Tadili, B., Nakhcha, C., Mouayn, I., Ramdani, M., Limouri, M., El Qadi, A., Sossey Alaoui, F., and Benhalima, M. (2002), *Using Active Faults and Seismicity for the Strong Motion Modelling in the Eastern Rif (Northern Morocco)*, Pure Appl. Geophys., *Special Issue* (Seismic ground Motion in Large Urban Areas), accepted.

Aki, K. (1967), *Scaling Law of Seismic Spectrum*, J. Geophys. Res. *72*, 1217–1231.

AKI, K. (1969), *Analysis of the Seismic Coda of Local Earthquakes as Scattered Waves*, J. Geophys. Res. *74*, 615–631.

AKI, K. (1980), *Attenuation of Shear Waves in the Lithosphere for Frequencies 0.005 to 25 Hz*, Phys. Earth Planet. Interiors. *21*, 50–60.

ALSAKEN, A., KVAMME, L. B., HANSEN, R. A., DAHLE, A., and BUNGUN, H. (1992), *The ML Scale in Norway*, Bull. Seismol. Soc. Am., *81(2)*, 379–398.

ANDERSON, J. and HOUGH, S. E. (1984), *Model of the Shape of Fourier Amplitude Spectrum of Acceleration at High Frequencies*, Bull. Seismol. Soc. Am. *74*, 1969–1993.

ANDRIEUX, J. (1971), *La structure du Rif Central, Etude des Relations entre la Tectonique de Compression et les Nappes de Glissement dans un Tronçon de la Chaine Alpine*, Notes et Mém. Serv. Géol. Maroc, Rabat, *235*, 450 pp.

BAKUN, W. H. and LINDH, G. (1977), *Local Magnitude, Seismic Moment, and Coda Duration for Earthquakes Near Oroville, California*, Bull. Seismol. Soc. Am. *67(63)*, 615–629.

BAKUN, W. H. (1984), *Magnitudes and Moments of Duration*, Bull. Seismol. Soc. Am. *74(6)*, 2335–2356.

BAKUN, W. H. (1984), *Seismic Moments, Local Magnitudes, and Coda-Duration Magnitudes for Earthquakes in Central California*, Bull. Seismol. Soc. Am. *74*, 439–458.

BAKUN, W. H. and JOYNER W. B. (1984), *The M_L Scale in Central California*, Bull. Seismol. Soc. Am. *74*, 1827–1843.

BEAUDET, A. (1969), *Le plateau Central Marocain et ses Bordures: Etudes Géomorphologiques*, Thèse lettres, Paris, 473 pp.

BELLOT, A. (1985), *Etude Gravimétrique du Rif Paléozo: la Forme du Massif des Beni Bousera*, Thèse, USTL, Montpellier, 120 pp.

BENSARI, D., *Connaissance Géophysique du Maroc* (ed. CNCPRST, Rabat-Maroc, 1987).

BOORE, M. D. and ATKINSON, G. M. (1992), *Source Spectra for the 1988 Sauguenay, Quebec, Earthquakes*, Bull. Seismol. Soc. Am. *82(2)*, 683–719.

BORCHERDT, R. D. (1970), *Effect of Local Geology on Ground Motion Near San Francisco Bay*, Bull. Seismol. Soc. Am. *60*, 29–61

BORCHERDT, R. D. and GIBBS, J. F. (1976), *Effect of Local Geological Conditions in the San Francisco Bay Region on Ground Motion and the Intensities of 1906 Earthquake*, Bull. Seismol. Soc. Am. *66*, 467–500.

EATON, J. P. (1992), *Determination of Amplitude and Duration Magnitude and Site Residuals from Short-period Seismographs in Northern California*, Bull. Seismol. Soc. Am. *82(2)*, 533–579.

FRANKEL, A. and WENNENBERG, L. (1987), *Energy-flux Model of Seismic Coda: Separation of Scattering and Intrinsic Attenuation*, Bull. Seismol. Soc. Am. *77*, 1223–1251.

GUTENBERG, B. and RICHTER, C. F. (1956), *Magnitude and Energy of Earthquakes*, Ann. Geofis. *9*, 1–15.

HANKS, T. C. and KANAMORI, H. (1979), *A Moment Magnitude Scale*, J. Geophys. Res. *84*, 2348–2350.

HATZFELD, D. (1978), *Etude Sismotectonique de la Zone de Collision Ibéro-maghrébine*, Thèse Univ. Grenoble 1, 281 pp.

HERTMANN, R. B. (1975), *The Use of Duration as Measure of Seismic Moment and Magnitude*, Bull. Seismol. Soc. Am. *65*, 899–913.

HIRSHORN, B., LINDH, A., and ALLEN, R. (1987), *Real Time Signal Duration Magnitudes from Low-gain Short Period Seismometers*, U.S. Geol. Surv., *Open-File Rep.* 87–630.

JOBSON, J. D., *Applied Multivariate Data Analysis, Volume I: Regression and Experimental Design* (Springer-Verlag, New York, 1991).

KANAMORI, H. (1977), *The Energy Release in Great Earthquakes*, J. Geophys. Res. *82*, 2348–2350.

KUGE, K. (1992), *Systematic Difference in the ISC Body-wave Magnitude-seismic Moment Relationship Between Intermediate and Deep Earthquakes*, Bull. Seismol. Soc. Am. *82(2)*, 819–835.

LAVILLE, E. (1985), *Evolution Sédimentaire Tectonique et Magmatique du Bassin Jurassique du Haut Atlas (Maroc)*, Thèse d'Etat, Univ. Montpellier, 166 pp.

LEE, W. H. K., BENNET, R., and MEAGHER, K. (1972), *A Method of Estimating Magnitude of Local Earthquakes from Signal Duration*, U.S. Geol. Surv., *Open File Report*, 28 pp.

LEE, W. H. K. and STEWART, S. W., *Principles and Applications of Microearthquake Networks*, Adv. Geophys. 2 (Academ. Press, New York (1981)), 293 pp.

LEE, W. H. K. and LAHR, J. C. (1975), *HYPO71 (revised): A Computer Program for Determining Hypocenter, Magnitude, and First Motion Pattern of Local Earthquakes*, U.S. Geol. Surv., *Open-File Report*, 75–311.

MEYEDA, KOYANAGI, K. S., HOSHIBA, M., AKI, K., and ZENG, Y. (1992), *A Comparative Study of Scattering Intrinsic, and Coda Q^{-1} for Hawaii, Long Valley, and Central California between 1.5 and 15.0 Hz*, J. Geophys. Res. *97*, 6643–6659.

MICHAELSON, C. A. (1990), *Coda Duration Magnitudes in Central California: An Empirical Approach*, Bull. Seismol. Soc. Am. *80(5)*, 1190–1204.

MOREL J. L., ZOUINE E. M., and POISSON, A. (2000), *Relation Entre la Subsidence des Bassins Moulouyens et la Création des Reliefs Atlasiques (Maroc): un Exemple d'Inversion Tectonique depuis le Néogène*, Bull. Soc. Géol. Fr. *t. 164*, 79–91.

MOUAYN, I. (1994), *Magnitudes de Seismes: Determination et Interpretation Géologique des Coefficients de Calibration des Stations du Réseau Sismique National*, Mémoire de CEA, Departement de Geologie, Univ. Med. V, Rabat, 107 pp.

PATTON, H. J. (1988), *Application of Nuttli's Method to Estimate Yield of Nevada Test Site Explosions Recorded on Lawrence Livermore Laboratory's Digital Seismic System*, Bull. Seismol. Soc. Am. *78*, 1759–1772.

PIQUÉ, A. (1979), *Evolution structurale d'un segment de la chaîne hercynienne: la Meseta marocaine nord-occidentale*, Sci. géol. Mém. Strasbourg *56*, 243 pp.

PIQUÉ, A., AÏT BRAHIM, L., AÏT OUALI, R., AMRHAR, M., CHARROUD, M., GOURMELEN, C., LAVILLE, E., REKHISS, F., and TRICART, P. (1998), *Evolution Structurale des Domaines Atlasiques du Maghreb au Méso-Cénozo; le Rôle des Structures Héritées dans la Déformation du Domaine Atlasique de l'Afrique du Nord*, Bull. Soc. géol. France, 1998, *t.169(6)*, 797–810.

PIQUÉ, A., CHARROUD, M., LAVILLE, E., AÏT BRAHIM, L., and AMRHAR, M. (2000), *The Tethys Southern Margin in Morocco and Cenozoic Evolution of the Atlas Domain, Peri-tethys*, Memoir5: New data on Peri-tethys Basins, Mém. Mus. natn. Hist. nat. *182*, 93–106, Paris ISBN: 2-85653-524-0.

REAL, C. R. and TENG, T. (1973), *Local Richter Magnitude and Total Signal Duration in Southern California*, Bull. Seismol. Soc. Am. *63*, 1809–1827.

ROGERS, A. M., TINSLEY, J. C., HAYS, W. W., and KING, K. W. (1979), *Evaluation of the Relation between Near-Surface Geologic Units and Ground Response in the Vicinity of Long Beach, California*, Bull. Seismol. Soc. Am. *69*, 1603–1622.

SEBER, D., BARAZANGI, M., TADILI, B., RAMDANI, M., BENBRAHIM, A., and BENSARI, D. (1996), *Three-dimensional Upper Mantle Structure Beneath the Intraplate Atlas and Interplate Rif Moutains of Morocco*, J. Geophys. Res. *101, B2*, 3125–3138.

SEBER, D., BARAZANGI, M., TADILI, B., RAMDANI, M., BENBRAHIM, A., BENSARI, D., and EL ALAMI, S. O. (1993), *Sn TO Sg Conversion and Focusing Along the Atlantic Margin, Morocco: Implications for Earthquake Hazard Evaluation*, Geophys. Res. Lett. *20(14)*, 1503–1506.

SINGH, S. and HERMANN, R. B. (1983), *Rationalisation of Crustal Coda Q in the Continental United States*, J. Geophys. Res. *88*, 527–538.

SU F., AKI, K., TENG, T., ZENG, Y., KOYANAGY, S., and MEYDA, K. (1992), *The Relation Between Site Amplification Factor and Surficial Geology in Central California*, Bull. Seismol. Soc. Am. *82(2)*, 580–602.

SUTEAU, A. M. and WHITCOMB, J. H. (1979), *A Local Earthquake Coda Magnitude and its Relation to Duration, Moment M_o, and Local Richter Magnitude M_L*, Bull. Seismol. Soc. Am. *69(2)*, 353–358.

SWERYN, D. J. and NUTTLI O. W. (1974), *Earthquake Magnitude Scales*, Geophys. Surveys, *1*, 429–458.

TSUJIURA, M. (1978), *Spectral Analysis of the Coda Waves from Local Earthquakes*, Bull. Earthq. Res. Inst. *53*, 1–48.

TSUMURA, K. (1967), *Determination of Earthquake Magnitude from Total Duration of Oscillation*, Bull. Earthquake Res. Inst., Tokyo Univ. *15*, 7–18.

VAN DEN BOSH, J. W. (1974), *Quelques Principes Généraux de l'Interprétation Gravimétrique Illustrés par des Exemples Empruntés à la Carte Gravimétrique du Maroc (Structure du Rif et Intrusions Granitiques au Maroc Central)*, Notes et Mém. Serv. Géol. Maroc *255*, 117–136.

WIGGER P., ASCH, G., GIESE, P., HEINSOHN, W., EL ALAMI, S. O., and RAMDANI, F. (1992), *Crustal Structure Along a Traverse Across the Middel and High Atlas Mountains Derived from Seismic Refraction Studies*, Geologische Rundschau *81*, 237–248.

XIE, J. and NUTTLI, O. W. (1988), *Interpretation of High-frequency Coda at Large Distances: Stochastic Modelling and Method of Inversion*, Geophys. J. *95*, 579–595.

(Received December 12, 2001, accepted December 20, 2002)

Pure appl. geophys. 161 (2004) 1081–1091
0033–4553/04/061081–11
DOI 10.1007/s00024-003-2487-9

Pure and Applied Geophysics

Using Active Faults and Seismicity for the Strong Motion Modeling in the Eastern Rif (Northern Morocco)

L. Aït Brahim[1], B. Tadili[2], C. Nakhcha[1], I. Mouayn[1], M. Ramdani[2], M. Limouri[3], A. El Qadi[3], F. Sossey Alaoui[1], and M. Benhalima[1]

Abstract—The aim of this study is to conduct a probabilistic seismic hazard analysis for the eastern Rif area in northern Morocco. The source zones were established on the basis of the seismicity database, the fracturing analysis deduced from Landsat7 ETM digital enhancement and marine seismic reflection profiles. By the use of this information together with the selected attenuation relationship, the peak ground acceleration contour maps are produced for specific return periods. The map has been divided into intervals of 0.1 degrees in both latitude and longitude to calculate the values at each grid point and draw the seismic hazard curves. The results of seismic hazard assessment are displayed as iso-acceleration contours expected to be exceeded during typical economic life times of structures.

Key words: Seismicity, seismic zones, seismic hazard assessment, eastern Rif, Morocco.

1. Introduction

The Rif belt represents the southernmost part of the Betic-Rif orocline and belongs to the alpine peri-Mediterranean chain (Durand Delga and Fontbote, 1980). It results from the superposition of several tectonic, compressive and distensive phases of alpine age, which succeeded one another from the Eocene age until the current one (Mourier, 1982). The study area constitutes an eastern part of the Rif chain being in contact with the southwestern end of the Alboran ridge. It is worth mentioning, from north to south, the Bokkoya chain (internal domain), the Tisirene flyschs unit (internal domain), the Ketama unit (external domain), the Temsamane unit and the external Rif units (Andrieux, 1971).

The eastern Rif is acknowledged to be the most seismically active region in Morocco (Aït Brahim *et al.*, 1990; Cherkaoui, 1991; El Alami *et al.*, 1998; Vaccari

[1] Faculté des Sciences de Rabat, Département de Géologie, Laboratoire GEORISK, B.P. 1014 Agdal Rabat Maroc. E-mail: aitbrahi@challa.fsr.ac.ma

[2] Institut Scientifique, Département de Physique du Globe, Agdal Rabat Maroc. E-mail: Tadili@israbat.ac.ma

[3] Laboratoire Conception et Systèmes, Département de Physique, Université Mohammed V, Faculté des Sciences, Avenue Ibn Batouta B.P. 1014 Agdal Rabat Maroc. E-mail: limouri@fsr.ac.ma

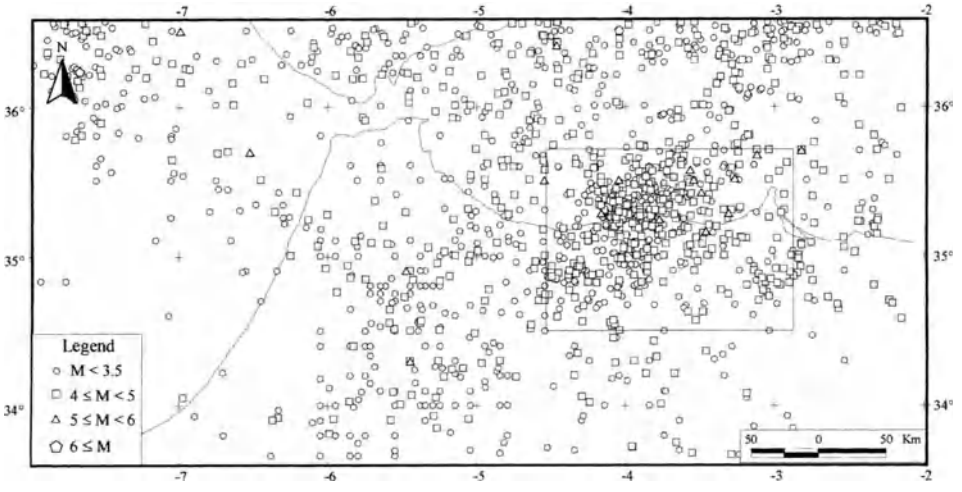

Figure 1
Seismicity of the North of Morocco (1900–1999).

et al., 2001) (Fig. 1). This study is aimed to: 1. Establish a fracturing map started from the use of space imagery associated with ground control and the seismic reflection data originating studies from (CHALOUAN *et al.*, 1997; CALVERT *et al.*, 1997). 2. Possible relationship between the fracturing deduced from this analysis and the seismicity. 3. Defining seismotectonic zones in order to calculate the seismic hazard by the use of the Gutenberg-Richter relation ($\log_{10}N = a - bM$). 4. Using the attenuation relationship of JOYNER and BOORE (1981) to relate the expected ground motion at each site during an earthquake with its magnitude and distance from the site.

2. Methodology

To evaluate seismic hazard, we have identified seismic source zones; which are characterized by active faults network and homogeneous seismicity (frequency and magnitude distribution). In order to establish a neotectonical map, we used a Landsat7 ETM image (path 200, row 036 acquired on the 25th of April 2000 at 10h 43min 18s) and a set of 1/20000 scaled aerial photographs followed by a ground control. The general methodology in calculating seismic hazard is well established in the literature (CORNELL, 1968). The method involves two separate models: a seismicity model describing geographical distribution event sources and the distribution of magnitudes, and an attenuation model describing the effect at any site given as a function of magnitude and source to site distance. The seismicity model may comprise a number of source regions, the seismicity of which should be expressed in terms of a recurrence relationship of events with magnitudes greater or equal to a certain value. For forecasting seismic occurrences numerous models have

been developed. The simplest stochastic model for earthquake occurrences is the homogeneous Poisson model, which is used in this study. Although not specifically required in the SEISRISK III program utilized, the recurrence relationship of the events is expressed with the help of the empirical relationship first defined by Gutenberg-Richter: $\log_{10}N = a - bM$, where N is the number of shocks with magnitude greater or equal to M per unit time and unit area, (a) is a rate parameter, and (b) represents the decrease with magnitude. This is related with the ratio of earthquake magnitude expected in the region. Using an application of the total probability theorem, the probability per unit time, that ground motion amplitude (a^*) is exceeded, can be expressed as follows (McGuire, 1993; McGuire and Arabasz, 2000):

$$P[A > a^* \text{in time } t]/t = \sum_i v_i \int \int [1 - F_A(a/m, r)] f_M(m) f_R(r/m) dm\, dr,$$

where [1 - $F_A(a/m,r)$] is the probability that an earthquake of magnitude (m) at a distance (r) produces a ground motion amplitude at the site which is greater than (a). Given (m) and (r), $f_M(m)$ is the probability density function for magnitude and $f_R(r/m)$ is the probability distribution function for distance.

3. *Fracturing Analysis*

The fracturing analysis deduced from digital enhancement of Landsat7 ETM imagery (Fig. 2) and followed by a ground control enabled us to show that the eastern Rif is affected by a series of faults oriented NE-SW, N-S and NW-SE (Fig. 3). These faults networks complete the studies carried out by Biju Duval *et al.*, (1976); Aït Brahim (1991); Deffontaines *et al.* (1992) and Chotin *et al.* (1997).

The NE-SW oriented faults (N020°E to N050°E) correspond to the left lateral strike-slip system such as the Nekor fault, the Boussekour fault and those which cross the entire Bokkoya and the Tisirne flyschs units. The faults of N-S direction (N170°E to N020°E) are composed of normal faults with left-lateral strike-slip components such as that of bas-Nekor fault. The latter, also observed by Chotin *et al.* (1997) on Radar SAR ERS-1 imagery, starts from the Mediterranean Sea crossing the South to the foreland. To the west of Al-Hoceima other faults of the same direction cross the Tisirene and Ketama units; the most important of these are the Rouadi and Al-Hammam faults in N170°E direction, which are active during the recent quaternary since they affect the sedimentary series of the ancient quaternary (Aït Brahim, 1991). The faults of NW-SE direction (N120°E to N140°E), with right-lateral strike-slip movement, appear mainly in the Bokkoya unit and in east RasTarf, namely the Boudinar and Oued-ourdane fault.

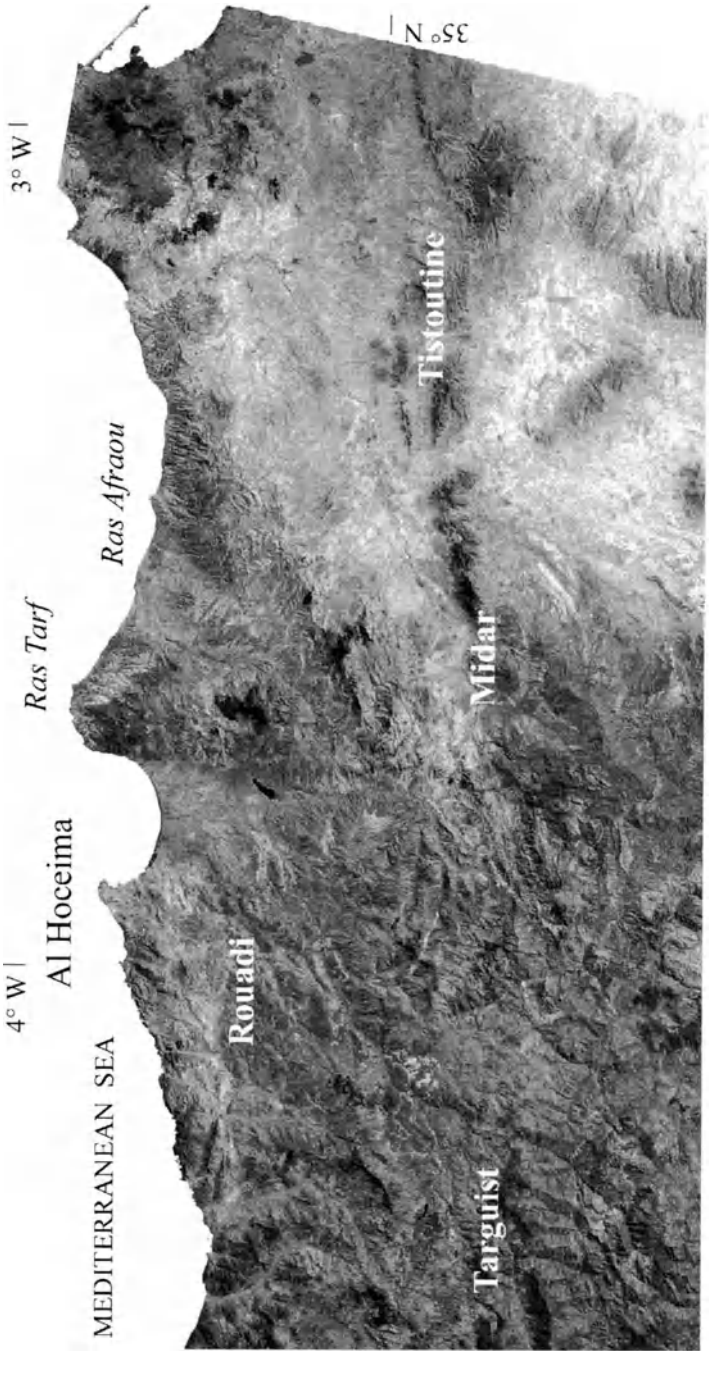

Figure 2
Eastern Rif Landsat7 ETM imagery.

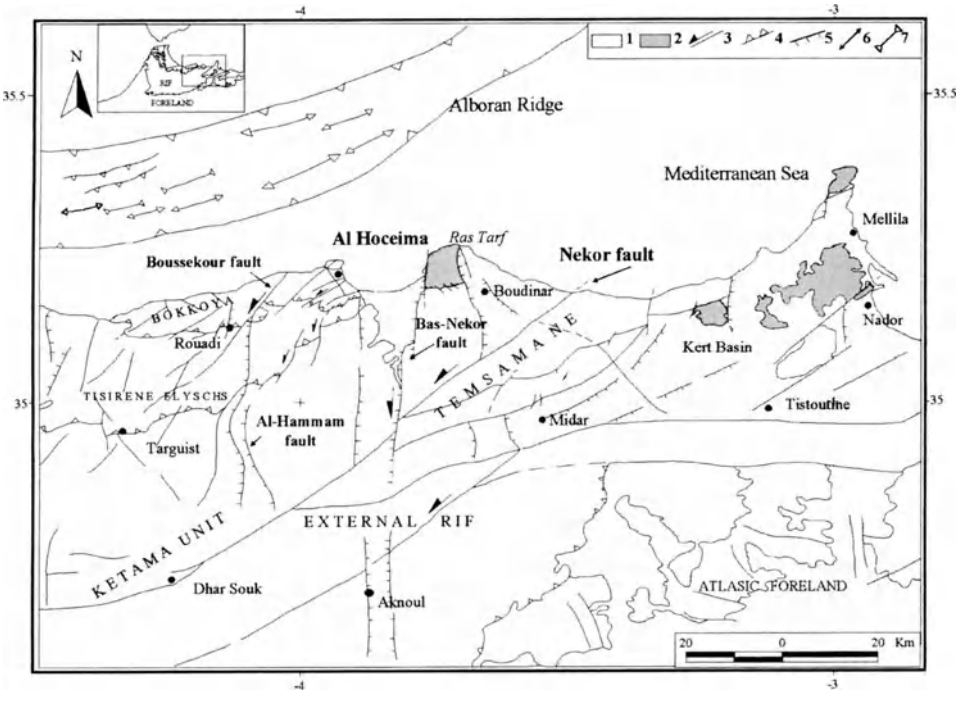

Figure 3
Neotectonic map of the eastern Rif. 1—Neogene and Quaternary. 2—Neogene volcanics. 3—Lateral strike-slip fault. 4—Reverse fault. 5—Normal fault. 6—Anticline. 7—Sincline.

In the marine domain, the seismic reflection study oriented by CHALOUAN *et al.* (1997) and CALVERT *et al.* (1997) shows reverse faults and folds NE-SW to E-W oriented in the Alboran ridge (Fig. 3).

4. Seismicity

Several Moroccan and foreign sources (CHERKAOUI, 1991; TADILI, 1991; UDAIS *et al.*, 1986) announced that Morocco for several centuries has been exposed to many destructive earthquakes of which the most significant and catastrophic is that of 1 November 1755 (magnitude estimated at 9), called the earthquake of Lisbon, and which was felt throughout Morocco where it claimed several thousand victims.

In eastern Rif the seismic activity is important (Figs. 1 and 4); strong earthquakes have occurred and some of them caused many losses and considerable destruction in the area (CHERKAOUI, 1991; TADILI, 1991; AÏT BRAHIM, 2001). The last one is the event of May 26th, 1994 of magnitude 5.6 which caused extensive damage in the city of Al Hoceima and its surroundings (EL ALAMI *et al.* 1998; NAKHCHA, 1994).

The basic seismicity data used in the present work and located between latitudes 34.4°–35.60°N, and longitudes 2.8°–4.6°W; came from the catalogue of earthquakes established by RAMDANI, (1991) and TADILI (1991); then, completed for the period from 1900 to 1999 with the data collected by the seismic network of Morocco.

5. *Seismic Zones*

We define a seismic source zone as a seismically homogeneous area in which every point within the source zone is assumed to have the same probability of being the epicenter of a future earthquake. The delineation of seismic source zones required a complete utilization of the geology, fracturing map started from the use of space imagery associated with ground control, and seismicity data (Fig. 4).

We regarded 3.5 as the magnitude threshold for our study. This is with the fact that on the one hand, the majority of the earthquakes felt in Morocco have

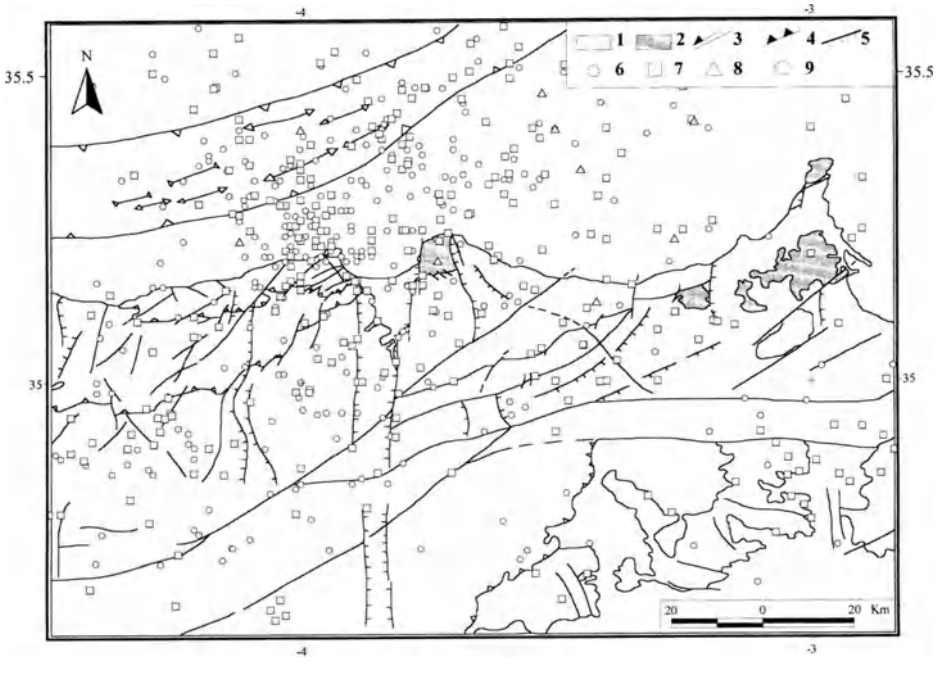

Figure 4
Seismotectonic map showing the recorded earthquakes that occurred in the region during the period 1900–1999. 1—Neogene and Quaternary. 2—Neogene volcanism. 3—Lateral strike-slip fault. 4—Reverse fault. 5—Normal fault. 6—Anticline. 7—Syncline. 8—($0 \leq M < 3.5$). 9- ($3.5 \leq M < 5$). 10—($5 \leq M < 6$). 11—($5 \leq M < 6$).

magnitudes ranging between 3.5 and 4.5 and on the other hand, all the events higher than this value formed part of this analysis.

Seismic source zones used in this study are defined according to the principles that:

— Seismotectonic zone of the Alboran ridge (Z1) is located in the Mediterranean Sea. The seismic activity is probably related to the reverse faults movement of NE-SW direction of the Alboran ridge.

— Seismotectonic zone of bas-Nekor basin (Z2) is characterized by an important concentration of epicenters. The latter are located along the normal faults with left-lateral strike-slip components which limits the bas-Nekor basin and Ras-Tarf high overhanging.

— Seismotectonic zone of the Bokkoya and Tisirene units, including the Boussekkour fault (Z3). The epicenters in this zone are aligned along the NE-SW direction. The left lateral strike-slip of the Boussekkour fault as well as other faults of the same direction are responsible for this seismicity.

— Seismotectonic zone of Jbel Al-Hamam (Z4) is characterized by a weak seismicity along faults of N170-N010°E direction.

— Seismotectonic zone to the south of the Nekor fault (Z5) is also characterized by weak seismic activity.

The result of this zoning is shown in Figure 5.

6. *Attenuation Relationship*

Assessment of the seismic hazard requires an appropriate strong-motion attenuation relationship which depicts the propagation and modification of strong ground motion as a function of earthquake size (magnitude) and the distance between the source and the site of interest. The relationship proposed by JOYNER and BOORE (1981) was chosen for calculations. This function was used by MARIA-JOSÉ JIMÉNEZ *et al.* (1999) in the Ibero-Maghreb region.

$$\log A = -1.02 + 0.25M - 0.00255(R^2 + 7.32)^{1/2} - \log(R^2 + 7.32)^{1/2},$$

where A is the maximum PGA (g), and R is the hypocentral distance (km).

7. *Seismic Hazard Computation*

Earthquake hazard analysis requires the assessment of earthquake hazard parameters such as the maximum magnitude, $M_{\max}$, the activity rate λ, and the b value of the Gutenberg-Richter relation. The parameters of the frequency-magnitude

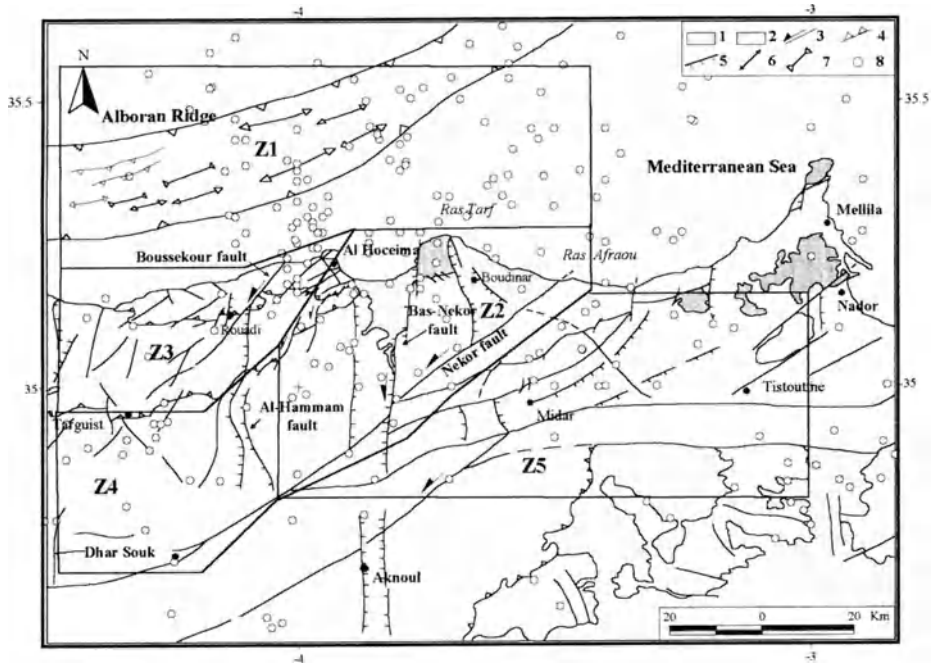

Figure 5
Seismic zoning established in the region. 1—Neogene and Quaternary. 2—Neogene volcanism. 3—Lateral strike-slip fault. 4—Reverse fault. 5—Normal fault. 6—Anticline. 7—Syncline. 8—Magnitude higher or equal to 3.5.

relationship were determined for each source by a least-squares fit. Table 1 shows the seismic hazard parameters for the magnitude $M \geq 3.5$ in each zone.

In order to calculate the probabilistic seismic hazard in the region, we used the SEISRISK III code designed by BENDER and PERKINS (1987). The attenuation function is input as a table of values of the chosen ground motion parameter as a function of magnitude and distance. The program is based on the assumption that the site acceleration has a Poisson distribution with a mean annual rate, and generates a cumulative distribution of the acceleration for each specified site. Using

Table 1

Seismic hazard parameters in the eastern Rif.

Zone source	N	M_{max}	a	b	β	$\lambda \times 10^{-4}$
Z1	183	5.1	5.989	1.220	2.810	0.251
Z2	133	5.5	4.117	0.796	1.834	0.352
Z3	329	6.4	3.210	0.558	1.285	0.293
Z4	36	4.9	5.044	1.175	2.706	0.581
Z5	39	4.9	5.411	1.215	2.798	0.091

the accelerations and the exceedance rate of accelerations and linear interpolation, the program determines the ground acceleration value corresponding to the level of non-exceedance chosen at a grid of sites. The hazard calculations were performed for a grid of points with spacing of 0.1° in latitude, and 0.1° in longitude.

8. Results and Conclusion

Figure 6 shows the contours of horizontal acceleration calculated to have a 90% probability of not being exceeded during exposure times of 50 years at a grid of sites in the eastern Rif. The map indicates that the highest values of the peak ground acceleration (PGA) are presented in the Al Hoceima city and the surrounding area (Z1, Z2, and Z3). The seismic activity in these zones is moderate; it has the strong-recorded earthquake in the past. The acceleration value 13% g for 50 years lifetime in the Al Hoceima city has a 90% probability of not being exceeded. The smallest accelerations are expected southeast of Nekor fault (Z5), the PGA values are less than 12% g in this region. Consequently, the seismic hazard map in eastern Rif presented in Figure 5 shows that the contour levels of the accelerations range from 6% to 15% g. The results we obtained, in general, are in good agreement with recently published regional studies (JIMÉNEZ *et al.*, 1999) in the Ibero-Maghreb region. Figure 7 displays the map obtained, when considering of the effect of the

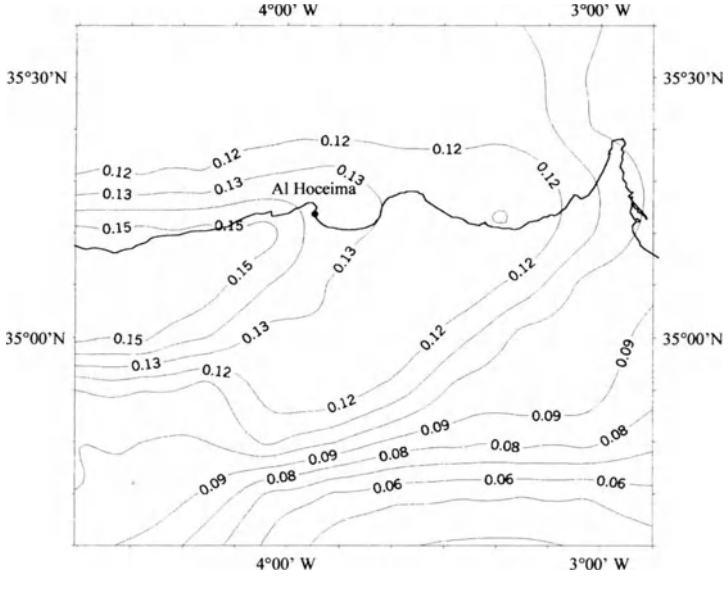

Figure 6
Peak ground acceleration (*g*) values with 90% probability of not being exceeded during a period of 50 years.

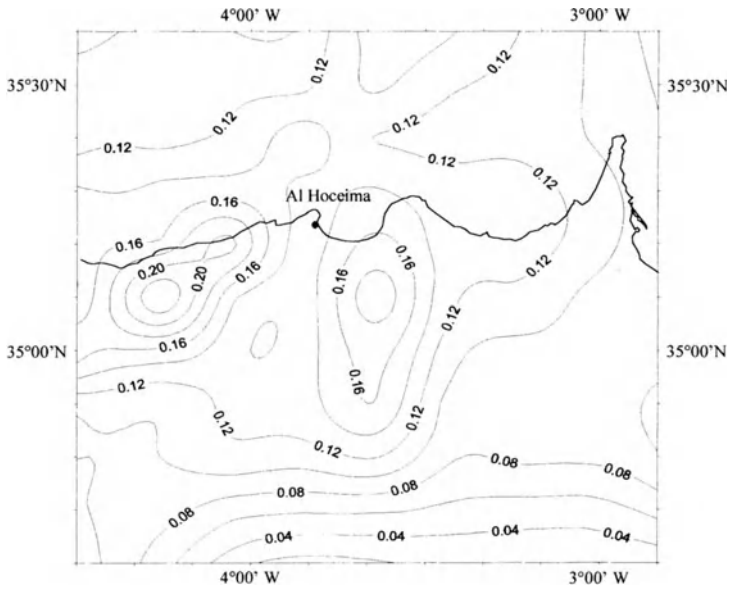

Figure 7
Peak ground acceleration (g) values with 90% probability of not being exceeded for a period of 50 years, by taking account of the effect of the principal active faults in the area.

principal active faults in the area. While comparing it with the map corresponding to the same period (Fig. 5), we notice that the contribution of these faults increases the values of accelerations in certain areas. The zone of Bas-Nekor shows a slight increase in limiting acceleration (16% g), and the zone of Boussekour (21% g). South of the area, with latitudes lower than 34.90°N, accelerations always remain weak between 4% g and 12% g. According to these results, we can say that the traced maps indicate the zones clearly presenting a high risk in the area. These zones have maximum values of 15% g, or 21% g if we take account of the eastern Rif principal active tectonic faults for one period of 50 years recurrence.

References

Aït Brahim L. (1991), *Tectonique cassante et états de contraintes récents au nord du Maroc; contribution à l'étude du risque sismotectonique*, Thèse d'Etat, Rabat, 360 pp.

Aït Brahim, L. (2001), *Contexte géodynamique de l'activité sismique au Maroc*, Revue Essentiel *3*, August 2001, 51–55.

Aït Brahim, L., Chotin, P., Ramdani, M., and Tadili, B. (1990), *Failles actives dans le Rif central et oriental (Maroc)*, C. R. Acad. Sci. Paris *310*, série II, 1123–1129.

Andrieux, J. (1971), *La structure du Rif central. Etude des relations entre la tectonique de compression et les nappes de glissement dans un tronçon de la chaîne alpine*, Notes et Mém. Serv. Géol. Maroc, Rabat *235*, 450.

BENDER, B. and PERKINS, D.M. (1987), *SEISRISK III : A Computer Program for Seismic Hazard Estimation*, U.S. Geol. Surv. Bull. *1772*, 48.

BIJU DUVAL, B., RIVEREAU, J.C., LAMPERIEN, C., and LOPEZ, N. (1976), *Commentaire de l'esquisse photogéologique du domaine méditerranéen. Grands traits structuraux à partir des images Landsat*, Rev. Inst. Fr. Pétr. *XXXI*, 365–400.

CALVERT, A., GOMEZ, F., SEBER, D., BARAZANGI, M., JABOUR, N., IBENBRAHIM, A., and DEMNATI, A. (1997), *An Integrated Geophysical Investigation of Recent Seismicity in the Al-Hoceima Region of North Morocco*, Bull. Seismol. Soc. Am. *87*, 637–651.

CHALOUAN, A., SAJI, R., MICHARD, A., and BALLY, A. W. (1997), *Neogene Tectonic Evolution of the Southwestern Alboran Basin as Inferred from Seismic Data off Morocco*, AAPG Bulletin *81*, *7*, 1161–1184.

CHERKAOUI, T. (1991), *Contribution à l'étude de l'aléa sismique au Maroc*, Université Joseph Fourier, Grenoble, France, Thèse, 21 June 1991, 247 pp.

CHOTIN, P., AÏT BRAHIM, L., DEFFONTAINES, B., and NAKHCHA, C. (1997), *La faille du Bas-Nekor : Témoin de la dynamique actuelle d'échappement du Maroc septentrional vers l'ouest*, Photo-Interprétation *3–4*, 159–170.

CORNELL, C.A. (1968), *Engineering Seismic Risk Analysis*, Bull. Seismol. Soc. Am. *58*, 1583–1606.

DEFFONTAINES, B., AÏT BRAHIM, L., CHOTIN, P., and ROSANOV, M. (1992), *Investigation of Active Faults in Morocco Using Morphometric Methods and Drainage Pattern Analysis*, Geologische Rundschau *81/1*, 199–210.

DURAND DELGA, M. and FONTBOTE, J.M. (1980), *Le cadre structural de la Méditerranée Occidentale*, 26^{e} congrès Geol. Intern. Colloque C5, Paris, *Mém. Bur. Rech. Géol. Min 115*, 67–85.

EL ALAMI, S.O., TADILI, B., CHERKAOUI, T., MEDINA, F., RAMDANI, M., AÏT BRAHIM, L., and HARNAFI, M. (1998), *The Al Hoceima Earthquake of May 26, 1994 and its Aftershocks : A Seismotectonic Study*, Annali Di Geofisica *41*, 519–537.

JIMÉNEZ, M., GARICA-FERNANDEZ, M. and the GSHAP Ibero-Maghreb Working Group (1999), *Seismic Hazard Assessment in the Ibero-Maghreb Region*, Annali Di Geofisica *42*, 1057–1065.

JOYNER, W.B. and BOORE, D.M. (1981), *Peak Horizontal Acceleration and Velocity from Strong-motion Records Including Records from the 1979 Imperial Valley, California Earthquake*, Bull. Seismol. Soc. Am. *71*, 2011–2038.

MCGUIRE, R. K. and ARABASZ, W.J. (2000), *An Introduction to Probabilistic Seismic Hazard Analysis*, Geotechnical and Environmental Geophysics *I* : Review and Tutorial.

MCGUIRE, R. K. (1993), *Computations of Seismic Hazard*, Annali Di Geofisica *XXXVI*, 3–4.

MOURIER, T. (1982), *Etude géologique et structurale du massif des Bokoyas (Rif oriental, Maroc*, Thèse de troisième cycle, Université de Paris XI, Orsay 6, 267.

NAKHCHA, C. (1994), *Etude sismotectonique de la région d'Al Hoceima*, Mémoire DEA, Faculté des Sciences de Rabat, 150 pp.

RAMDANI, M. (1991), *Etude sismotectonique du Nord du Maroc*, Thèse, Université Mohammed I, Faculté des Sciences d'Oujda, 250 pp.

TADILI, B. (1991), *Etude du risque sismique dans le Maroc Nord*, Doctorat d'Etat Faculté Sciences, Oujda, 250 pp.

UDAIS, A., ESPINOSA, A.F., MEZCUA, J., BUFOIN, E., VEGAS, H., NISHENKO, P., MARTINEZ-SOLARES, J.M., and LOPEZ-ARROYO, A. (1986), *Seismicity and Tectonic Map of the North Eurasian Plate Boundary (Azores-Iberia-Tunisia)*, U.S. Geological Survey OFSS Denver,CO, *80225*.

VACCARI, F., TADILI, B., EL QADI, A., RAMDANI, M., AIT BRAHIM, L., LIMOURI, M. (2001), *Deterministic Seismic Hazard Assessment for North Morocco*, JSEE, summer 2001, Vol. 3, *1*, 1–12.

(Received April 11, 2002, accepted October 14, 2002)

Pure appl. geophys. 161 (2004) 1093–1106
0033–4553/04/061093–14
DOI 10.1007/s00024-003-2498-6

Pure and Applied Geophysics

Realistic Modeling of Seismic Wave Ground Motion in Beijing City

Z. DING[1], F. ROMANELLI[2], Y. T. CHEN[1], and G. F. PANZA[2,3]

Abstract—Algorithms for the calculation of synthetic seismograms in laterally heterogeneous anelastic media have been applied to model the ground motion in Beijing City. The synthetic signals are compared with the few available seismic recordings (1998, Zhangbei earthquake) and with the distribution of observed macroseismic intensity (1976, Tangshan earthquake). The synthetic three-component seismograms have been computed for the Xiji area and Beijing City. The numerical results show that the thick Tertiary and Quaternary sediments are responsible for the severe amplification of the seismic ground motion. Such a result is well correlated with the abnormally high macroseismic intensity zone in the Xiji area associated with the 1976 Tangshan earthquake as well as with the ground motion recorded in Beijing city in the wake of the 1998 Zhangbei earthquake.

Key words: Synthetic seismograms, seismic ground motion, Beijing City.

1. Introduction

Beijing City is situated in an active seismic zone, oriented in the NW–SE direction, stretching from Bohai Sea to the city of Zhangjiakou along the northern margin of the North China Plain. Historically, Beijing City has been rocked by destructive earthquakes in the past (see Fig. 1). The last great event was the 1697 Sanhe-Pinggu earthquake (M = 8), which occurred approximately 50 km from the city. The maximum observed macroseismic intensity in Beijing, caused by that earthquake, was XI, on the China Seismic Intensity Table (XIE, 1957), which is close to the MSK scale. The 1976 Tangshan earthquake (M = 7.8) caused a maximum intensity of VIII in Beijing City. The latest strong event felt in Beijing was in 1998 caused by the M_s 6.2 Zhangbei earthquake.

Estimation of the expected seismic ground motion is a key issue in the design of rational measures for mitigation impact of seismic hazard. For a given study area, a possible solution to the seismic microzonation problem is to assemble a comprehensive set of recorded strong ground motions and to group those seismograms that

[1] Institute of Geophysics, China Seismological Bureau, Beijing, 100081, China.
E-mail: ding@cdsn.org.cn
[2] Dipartimento di Scienza della Terra, Via Weiss 4, 34127 Trieste, Italy.
[3] SAND Group, ICTP, Strada Costiera 11, I-34100 Trieste, Italy.

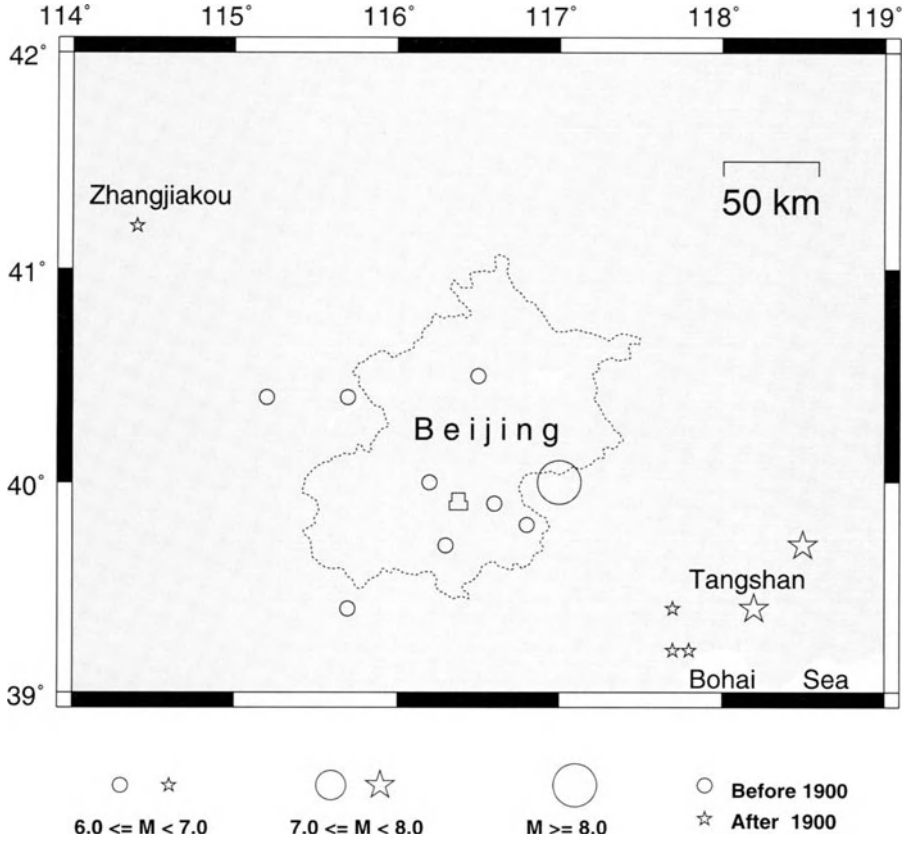

Figure 1
Epicenters in and around the Beijing area (stars represent the events after 1900; circles represent the events before 1900).

represent similar source, path and site effects. However, such a database is ordinarily not available in practice. An alternative and complementary way is based on the use of computer codes, which take into account the seismic waves propagation in anelastic laterally heterogeneous media, the complexity of seismic sources and the site effects. Realistic models thus formulated are expected to simulate ground motions at a given site arising from a given earthquake scenario.

In the present paper, we use the modal summation method (PANZA, 1985; PANZA and SUHADOLC, 1987; FLORSCH *et al.*, 1991; PANZA *et al.*, 2000) to compute the synthetic broadband seismogram in the reference bedrock model, using two different approaches to calculate the synthetic seismograms in laterally heterogeneous anelastic structures. The analytical coupling coefficient algorithm (LEVSHIN, 1985; VACCARI *et al.*, 1989; ROMANELLI, *et al.*, 1996, 1997) uses several contiguous 1-D models with vertical discontinuities in welded contact to mimic a 2-D model. The hybrid method uses the results of the modal summation as the input signal,

and calculates the seismograms in the local laterally heterogeneous structures by using a finite-difference algorithm (FÄH *et al.*, 1993, 1994; FÄH and SUHADOLC, 1995).

In this work, we compute seismic ground motions in Beijing in respect of two strong earthquakes at epicentral distances in the range 110–160 km (the 1976 M_s 7.8 Tangshan earthquake) and 200–235 km (the 1998 M_s 6.2 Zhangbei earthquake), and compare these with the observed records and macroseismic intensities.

2. Structures and Modeling Method

Beijing City is situated in the Beijing Tertiary Depression Zone, the thickness of the Tertiary sediments reaching 2 km in the southwestern part of the city (Figs. 2, 3). Quaternary sediments whose thickness increases from the mountain-plain boundary to the southeastern direction cover all of the plain area. Whilst most of the city is covered by Quaternary sediments which average about 0.1 km in thickness (Fig. 4), there are two abnormally thick Quaternary sediment zones near the city, one in the northwest, and the other in the northeast suburbs reaching a maximum thickness of about 0.8 km.

The seismic ground motion in Beijing City is computed in accordance with two great earthquakes, the 1976 Tangshan earthquake and the 1998 Zhangbei

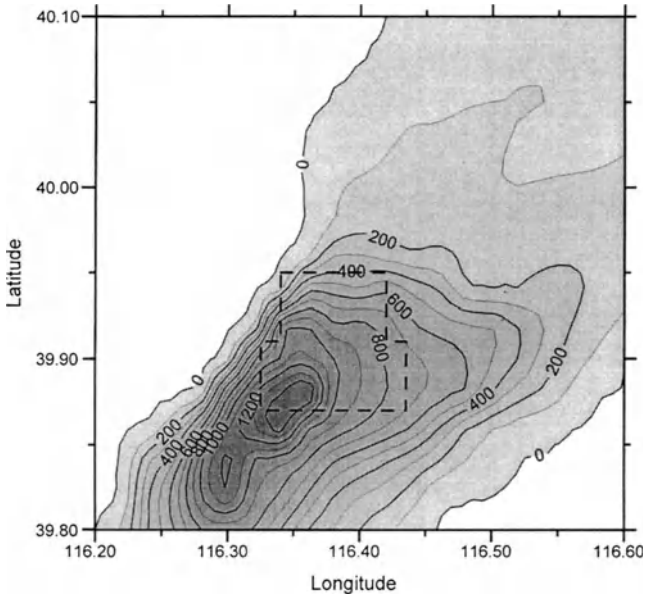

Figure 2
Thickness (in meters) of the Early Tertiary Sediment Layer in Beijing City (dashed polygon).

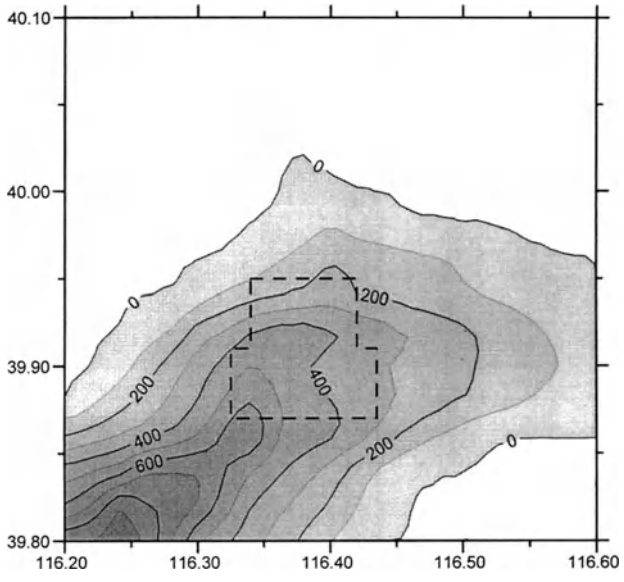

Figure 3
Thickness (in meters) of the Late Tertiary Sediment Layer in Beijing City (dashed polygon).

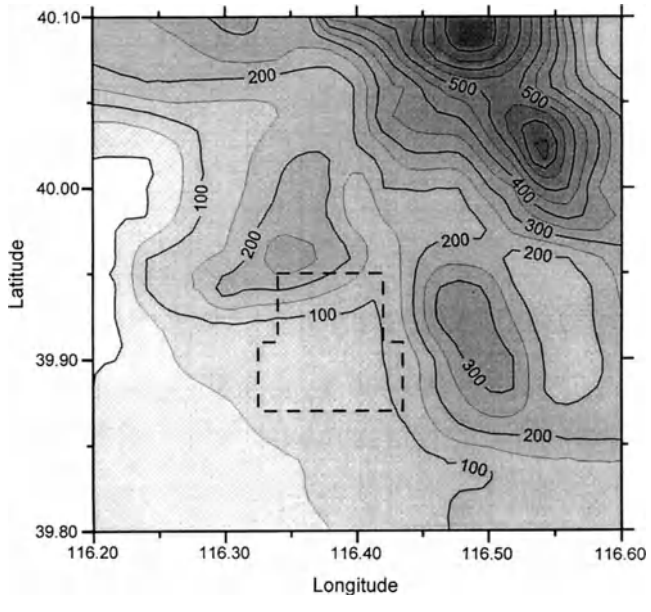

Figure 4
Thickness (in meters) of the Quaternary Sediment Layer in Beijing City (dashed polygon).

earthquake. The hybrid algorithm is applied to model the seismic ground motion in the Beijing City area, while the coupling coefficient algorithm is applied in the Xiji area, on the eastern border of Beijing City. In both cases, the effects of source, path and site have been taken into account.

To provide for the source finiteness for different magnitudes, we use the scaling laws of GUSEV (1983) by properly weighting the source spectrum in the frequency domain, as reported in AKI (1987).

Comparison of the observed data with the synthetic results represents the quality check of our modeling.

3. *Modeling for the Tangshan Earthquake*

The July 28, 1976 Tangshan earthquake claimed at least 230,000 victims and greatly disrupted the political and economic life of China. The earthquake, located about 160 km east of Beijing City, had a magnitude M_s = 7.8 (Chinese Seismic Network Report). According to the general trend of isoseismals, Beijing City lies in the zone of macroseismic intensity VI, but abnormally high intensities are reported as well. More specifically, in the northwest, the observed macroseismic intensity is VII, and in the Xiji area, on the eastern border of Beijing City, as high as VIII (Fig. 5).

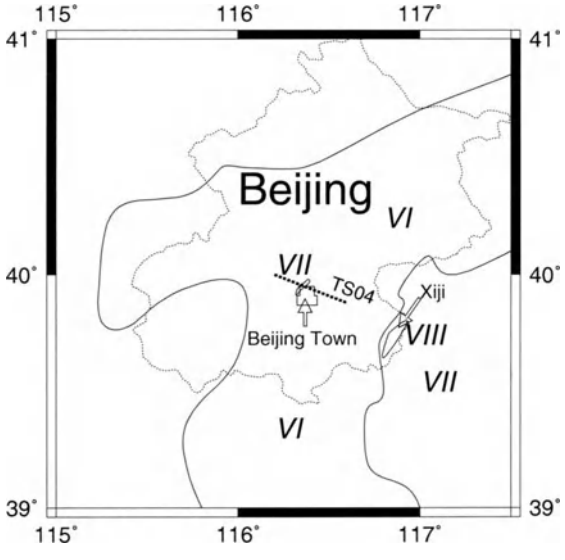

Figure 5
Intensities of the 1976 Tangshan Earthquake reported in the Beijing Area. The intensity in most areas of Beijing City is VI. While intensities in Xiji (VIII) and the northwestern part of Beijing City (VII) are characterized by anomalously high intensity values.

Based on previous studies (ZHANG *et al.*, 1980), the parameters of the Tangshan earthquake adopted in this study are:

Location: 39.4°N, 118.2°E

Depth = 11 km

M_0 = 1.8 * 10^{27} dyn * cm

Source Mechanism: Strike = 30°, Dip = 90°, Rake = 180°.

The Xiji area, located over the Dachang Tertiary depression zone, has a specially shallow structure. The thickness of the Quaternary sediment is about 0.4 km and the depth of the Tertiary sediments in the Xiji area reach 3.0 km. The Tertiary sediments in Xiji are substantially thicker compared with that in the neighboring areas. SUN *et al.* (1998) simulated the seismic ground motion for *SH* waves in the Xiji area, using the hybrid method. Here we extend their work using the coupling coefficient algorithm (LEVSHIN, 1985; VACCARI *et al.*, 1989; ROMANELLI *et al.*, 1996, 1997) to compute the synthetic seismograms for *SH* and *P-SV* waves.

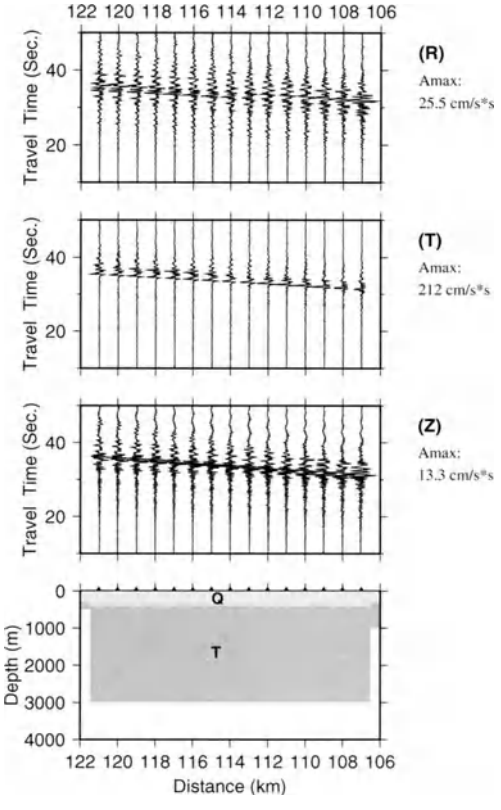

Figure 6

Synthetic Seismograms in Xiji Area for the 1976 Tangshan Earthquake. Q and T represent the Quaternary and Tertiary sediments, which cover the bedrock. The geophysical properties of the sediments are given in Table 1 of DING *et al.* (this issue).

Figure 6 shows the local structure and the synthetic three-component ground accelerations in the Xiji area in respect of the event parameters representing the 1976 Tangshan earthquake, the largest amplitudes being obtained in the transverse component of motion (*SH* waves).

To estimate site effects, we use as reference signals the synthetic seismograms computed for the average one dimension (1-D) bedrock model defined by SUN *et al.* (1998), which includes the crust and upper mantle structures and has no sediments at the surface. Figure 7 shows the comparison between the peak values obtained with the bedrock (1-D) and the realistic laterally varying (2-D) structures. There are abnormally large amplitudes at epicentral distances in the range between 109 and 112 km. At approximately 110 km, the maximum amplitude is larger than 200 (cm/s*s), quite compatible with the observed anomalous intensity (VIII). The ratios of maximum amplitude and Arias intensity (ARIAS, 1970), AMAX(2D)/AMAX(1D)

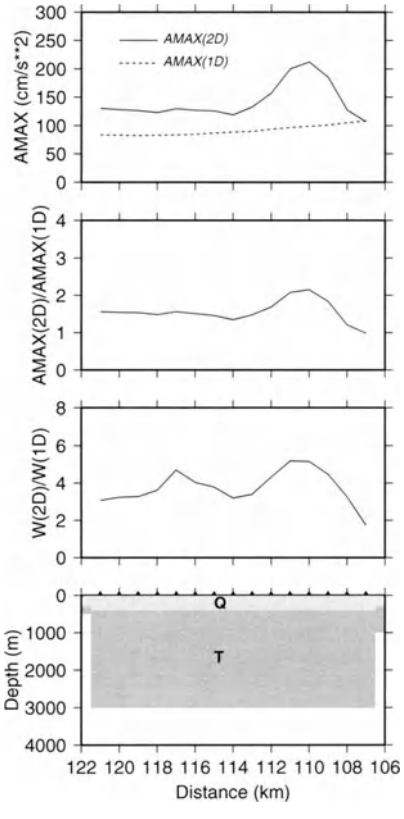

Figure 7
AMAX(2D)/AMAX(1D) and W(2D)/W(1D) along the profile adopted to model the seismic ground motion in the Xiji Area. Q and T represent the Quaternary and Tertiary sediments, which cover the bedrock.

and W(2D)/W(1D), reach the highest values in the Xiji area. There are two peaks in the Arias intensity ratio W(2D)/W(1D): more than 5 at a distance close to 110 km, due to the large peak values of the seismograms in the laterally varying model, and over 4 at a distance close to 117 km, mainly due to the long duration of the ground motion in the laterally varying model. These results explain quite naturally how the local mechanical properties amplify the seismic ground motion and cause the abnormally high intensity value, observed in the Xiji area during the 1976 Tangshan earthquake. Our results confirm the results obtained by SUN *et al.* (1998) who used the 2-D finite-difference algorithm.

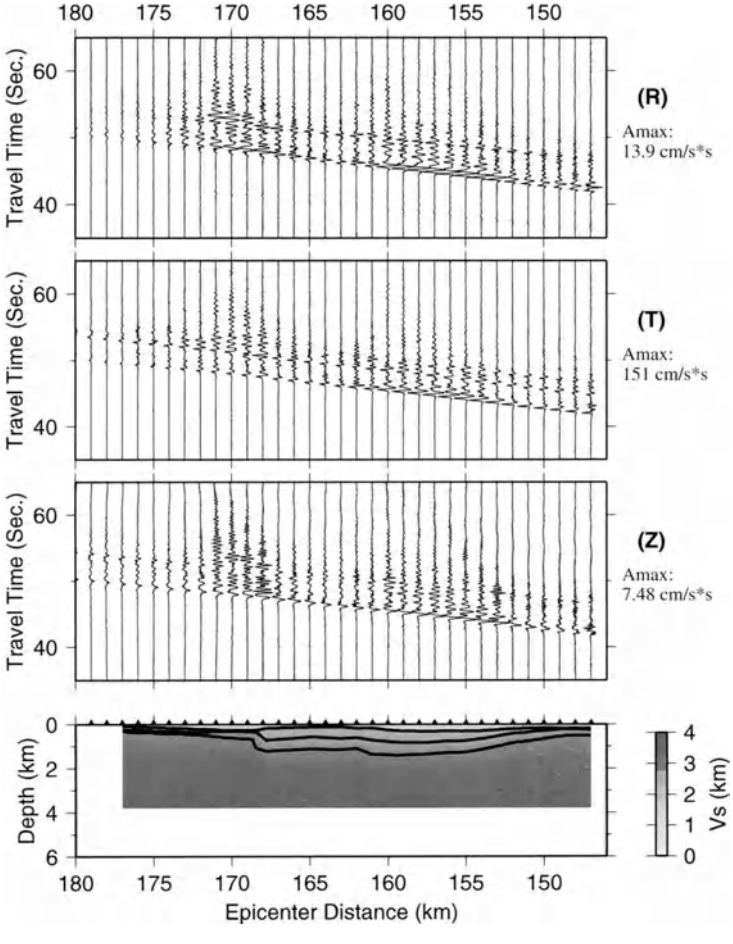

Figure 8
Cross section and the synthetic acceleration (radial, R; transverse, T, and vertical, Z) along the profile TS04. The contour lines shown in the model represent the boundaries of the three sedimentary layers, which cover the bedrock.

An abnormally high intensity (VII) area is observed in the northern part of Beijing town as well. To study this phenomenon we consider a profile TS04 (see Fig. 5) that points from the epicenter of the 1976 Tangshan earthquake towards Beijing . The profile penetrates the northern part of Beijing town, and crosses the abnormally high intensity (VII) area. The distance along the profile is measured from the epicenter of the 1976 Tangshan earthquake.

Along this profile, two thick Quaternary sediment areas are encountered at distance of 153–163 km and 170 km. The synthetic three-component acceleration seismograms along the profile TS04 were obtained (Fig. 8) by using the hybrid method (FÄH *et al.*, 1993, 1994; FÄH and SUHADOLC, 1995). In the simulated seismograms, the amplitude of the transverse component is found to be about 10

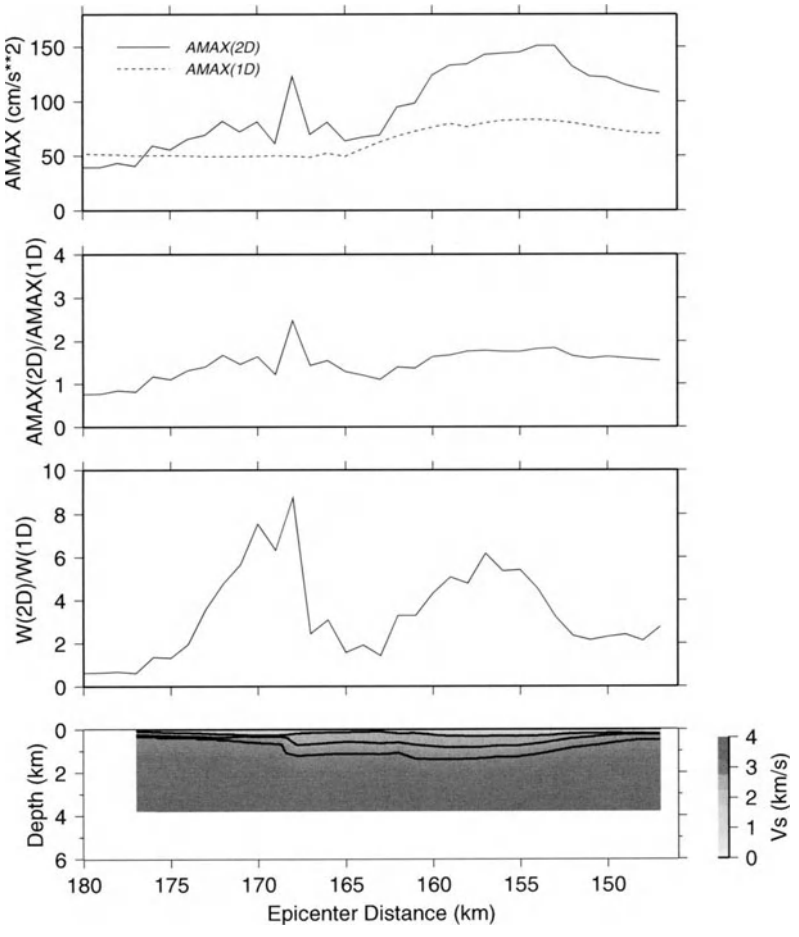

Figure 9
AMAX, AMAX(2D)/AMAX(1D) and W(2D)/W(1D) along profile TS04.

times the radial and vertical components, as in the Xiji area. The waveform variations of all three components along the profile are strongly correlated to the thickness of the Quaternary sediments. At distances of 153–160 km and 168–171 km, the amplitudes and the durations of the seismograms are enhanced. The values of AMAX around 150 cm/s*s are quite compatible with intensity VII. The ratios AMAX(2D)/AMAX(1D) and W(2D)/W(1D), obtained using the bedrock model of SUN *et al.* (1998) reach their peaks over the two thick Quaternary sediment areas (Fig. 9). In the northwestern part of Beijing town (about 170 km in TS04), the ratios AMAX(2D)/AMAX(1D) and W(2D)/W(1D) can be as large as 2.5 and 8.0, respectively. This site coincides with the narrow, abnormal (one-degree higher) intensity zone, observed during the 1976 Tangshan earthquake.

4. *Modeling for the Zhangbei Earthquake*

Next, the source parameters of the 1998 Zhangbei earthquake (Havard CMT solution), given below were used to computer ground accelerations in Beijing.

Date: January 10, 1998

Location: (41.2°N, 114.4°E)

Depth = 15 km

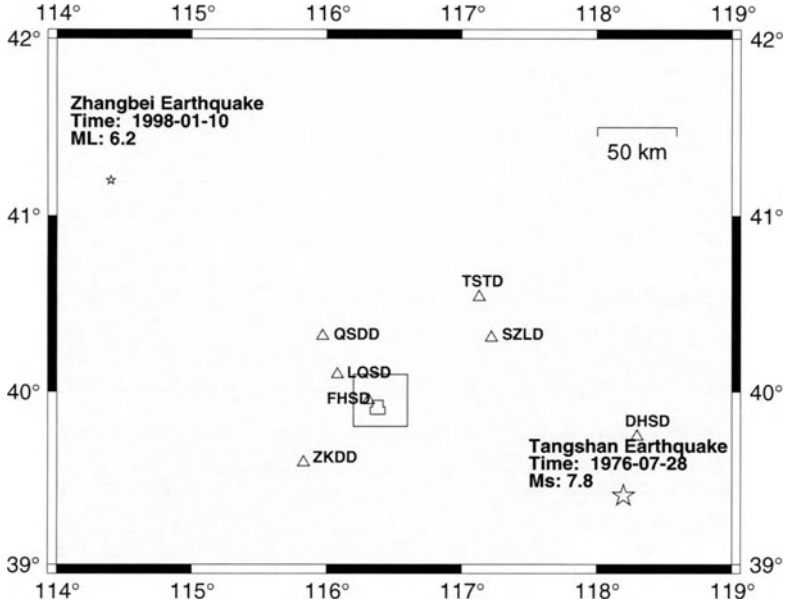

Figure 10

Beijing Seismic Network Stations; triangles represent the location of seismic stations and stars the epicenters of the 1976 Tangshan and the 1998 Zhangbei earthquakes.

M_0 = 6.1 * 10^{24} dyn*cm
NP1: Strike = 200°; Dip = 44°; Slip = 136°
NP2: Strike = 324°; Dip = 61°; Slip = 55°

Because of the NE orientation of the distribution of aftershocks, we selected NP1 as the preferred fault plane solution, and Rake = 180°.

The Zhangbei earthquake was the latest strong earthquake that occurred near Beijing City. Since several digital seismic stations had been deployed in the Beijing area before the earthquake (Fig. 10), we had an opportunity to compare our synthetic seismograms computed in this area with real seismic records.

For the main shock, only one station, FHSD, recorded a good seismograms, others being saturated. Some aftershocks with magnitude $M_L > 4$ were well recorded by most of these stations. Figure 11 shows the records (transverse component—the largest one) for the aftershock that occurred on January 17, with magnitude M_L = 4.6. The four stations, QSDD, LQSD, FHSD, and ZKDD are almost from the same azimuth with respect to the epicenter. In the records of QSDD, LQSD, and ZKDD, located in the mountain area, the amplitude of the seismic waves decreases with increasing epicentral distance. The station FHSD, located over thick sediments, does not follow the rule showing relatively large amplitudes (comparable to the ones of QSDD).

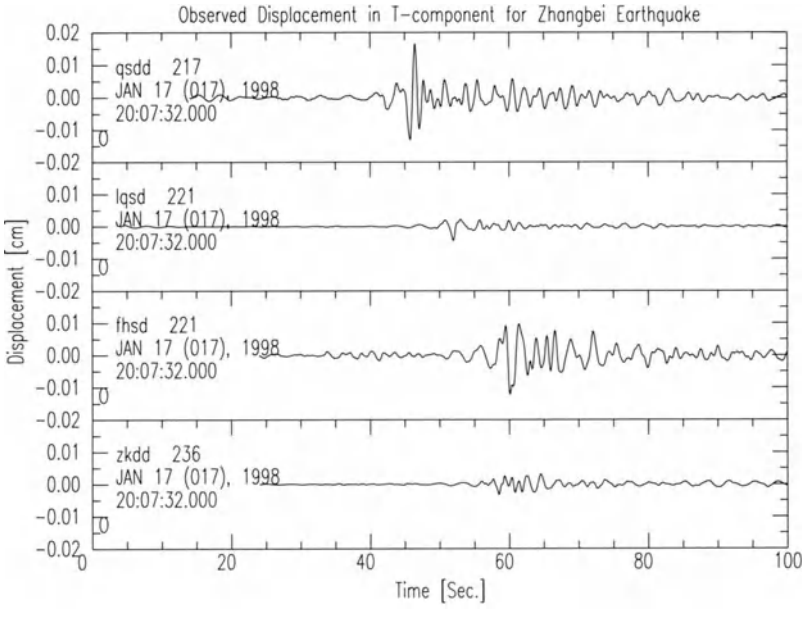

Figure 11
Observed Seismograms for the aftershock, with magnitude M_L = 4.6, occurred on Jan. 17, 1998, of the 1998 Zhangbei earthquake. The epicenter distances of the recording stations, QSDD, LQSD, FHSD, and ZKDD, are 164, 187, 213 and 216 km, respectively. Station FHSD is located in the thick sediments area, while the other three stations lie on bedrock . The signals, after deconvolution for the instrument response, are low-pass filtered with a cut-off frequency of 1 Hz.

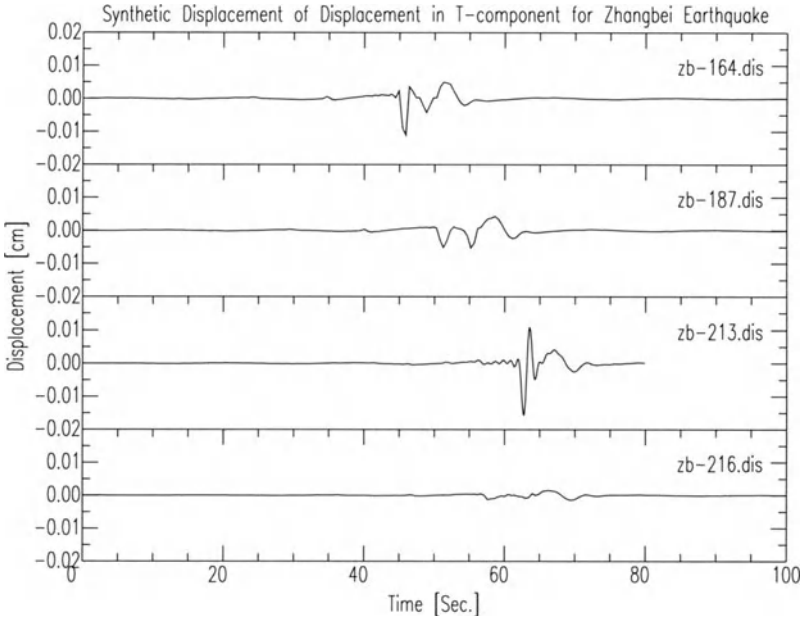

Figure 12
Synthetic seismograms for the aftershock, with magnitude $M_L = 4.6$, occurred on Jan. 17, 1998, of the 1998 Zhangbei earthquake. The synthetic seismograms are calculated at stations QSDD, LQSD, FHSD and ZKDD. The 1st, 2nd and 4th seismograms are calculated using the modal summation method applied to the bedrock model. The 3rd seismogram is the result of the finite-difference method applied to the model shown in Figure 8. The maximum frequency in the calculation is 1 Hz.

Seismograms at stations QSDD, LQSD, FHSD, and ZKDD were also simulated (Fig. 12), at QSDD, LQSD, and ZKDD, using the bedrock model and the modal summation method. At FHSD, we used hybrid method with the laterally heterogeneous model, shown in Figure 8. The synthetic signals show that the thick sediments beneath FHSD amplify the peak values of seismic ground motion, as seen in the actual records.

5. *Conclusions*

Three-component broadband synthetic accelerograms have been calculated for sites in Beijing City in respect of the 1976 Tangshan and the 1998 Zhangbei earthquake, to be regarded as calibration events.

Both the synthetic seismograms and observed data show that the thick Quaternary sediment in the northwest of Beijing town and in Xiji area amplify the seismic wave ground motion.

This satisfactory comparison between observed and synthetic waveforms represents a sound justification for extending ground motion modeling to sites

where observations are not available. Thus, it would be possible to study expected seismic ground motions at close sites covering all of Beijing City, thereby generating a seismic microzonation map as a basic map for land-use planning and specification of building codes and practices by local authorities, city planners, land-use specialists and civil engineers.

Acknowledgements

This work is a contribution to the UNESCO-IUGS-IGCP Project 414 "Realistic Modeling of Seismic Input for Megacities and Large Urban Areas." This research has been carried on in the framework of the bilateral project "Geophysical Studies for the Deterministic Evaluation of Seismic Risk," with the contribution of the Italian Ministry of Foreign Affairs (MAE), Directorate General for Cultural Promotion and Cooperation. The research received support from the Chinese National Key Basic Research and Development Program (973 Program) No. 2002CB412709, MOST of China and China Seismological Bureau. We acknowledge Dr. Franco Vaccari and Dr. Francesco Marrara for their kind help in the calculations. Dr. Zhang Wenbo supplied some seismic recordings. This is the contribution No. 02A10001, Institute of Geophysics, China Seismological Bureau. We have used the public domain graphics software (WESSEL and SMITH, 1995a, 1995b).

REFERENCES

AKI, K., *Strong Motion Seismology*. In *Strong Ground Motion Seismology* (eds. Erdik, M. Ö. and Toksöz, M. N.) (NATO Advanced Study Institute Series, Series C: Mathematical and Physical Sciences, D. Reidel Publishing Company. The Netherlands 1987), *204*, pp. 3–39.

ARIAS, A. (1970), *A measure of earthquake intensity*. In *Seismic Design for Nuclear Power Plants* (ed. R. Hansen), Cambridge, Massachusets.

DING, Z., CHEN, Y. T., and PANZA, G. F. (2004), *Estimation of Site Effects in Beijing City*, Pure Appl. Geophys. *161*(5/6), 1107–1123.

FÄH, D., IODICE, C., SUHADOLC, P., and PANZA, G. F. (1993), *A New Method for the Realistic Estimation of Seismic Ground Motion in Megacities: The Case of Rome*, Earthquake Spectra *9*(4), 643–668.

FÄH, D., SUHADOLC, P., MUELLER, St., and PANZA, G. F. (1994), *A Hybrid Method for the Estimation of Ground Motion in Sedimentary Basin: Quantitative Modelling for Mexico City*, Bull. Seismoc. Soc. Am. *84*, 383–399.

FÄH, D., and SUHADOLC, P. (1995), *Application of Numerical Wave-propagation Techniques to Study Local Soil Effects: The Case of Benevento (Italy)*, Pure Appl. Geophys. *143*, 513–536.

FLORSCH, N., FÄH, D., SUHADOLC, P., and PANZA, G. F. (1991), *Complete Synthetic Seismograms for High-frequency Multimode SH-waves*, Pure Appl. Geophys. *136*, 529–560.

GUSEV, A. A. (1983), *Descriptive Statistical Model of Earthquake Source Radiation and its Application to an Estimation of Short-period Strong Motion*, Geophys. J. R. Astr. Soc. *74*, 787–800.

PANZA, G. F., SCHWAB, F. A., and KNOPOFF, L. (1973), *Multimode Surface Waves for Selected Focal Mechanisms, I. Dip-slip Sources on a Vertical Fault Plane*, Geophys. J. R. Astr. Soc. *34*, 265–278.

PANZA, G. F. (1985), *Synthetic Seismograms: The Rayleigh Waves Modal Summation*, J. Geophysics *58*, 125–145.

PANZA, G. F. and SUHADOLC, P., *Complete strong motion synthetics.* In *Seismic Strong Motion Synthetics* (ed. B. A. Bolt) (Academic Press, Orlando, 1987), *Computational Techniques 4*, 153–204.

PANZA, G. F., ROMANELLI, F., and VACCARI, F. (2000), *Seismic Wave Propagation in Iaterally Heterogeneous Anelastic Media: Theory and Applications to Seismic Zonation*, Advances in Geophysics *43*, 1–95.

ROMANELLI, F., ZHOU, B., VACCARI, F., and PANZA, G. F. (1996), *Analytical Computation of Reflection and Transmission Coupling Coefficients for Love Waves*, Geophys. J. Int. *125*, 132–138.

ROMANELLI, F., BEKKEVOLD, J., and PANZA, G. F. (1997), *Analytical Computation of Coupling Coefficients in Non-Poissonian Media*, Geophys. J. Int. *129*, 205–208.

SUN, R., VACCARI, F., MARRARA, F., and PANZA, G. F. (1998), *The Main Features of the Local Geological Conditions Can Explain the Macroseismic Intensity Caused in Xiji-Langfu (Beijing) by the Tangshan 1976 Earthquake*, Pure Appl. Geophys. *152*, 507–522.

VACCARI, F., GREGERSEN, S., FURLAN, M., and PANZA, G. F. (1989), *Synthetic Seismograms in Laterally Heterogeneous, Anelastic Media by Modal Summation of P-SV waves*, Geophys. J. Int. *99*, 285–295.

WESSEL, P. and SMITH, W. H. F. (1995), *New Version of the Generic Mapping Tools Released*, EOS Trans. AGU *76*, 329.

WESSEL, P., and SMITH, W. H. F. (1995), *The Generic Mapping Tools (GMT) Version 3.0 Technical Reference and Cookbook*, SOEST/NOAA.

XIE, Y. (1957), *A New Scale of Seismic Intensity Adapted to the Conditions in Chinese Territories*, Acta Geophysica Sinica *6*, 35–48.

ZHANG, Z., LI Q., GU, J., JIN, Y., YANG, M., and LIU, W. (1980), *The Fracture Processes of the Tangshan Earthquake and Analyses of Mechanics*, ACTA Seismologica Sinica *1*, 111–129.

(Received May 7, 2002, accepted September 3, 2002)

Pure appl. geophys. 161 (2004) 1107–1123
0033–4553/04/061107–17
DOI 10.1007/s00024-003-2495-9

Pure and Applied Geophysics

Estimation of Site Effects in Beijing City

Z. DING[1], Y. T. CHEN[1], and G. F. PANZA[2,3]

Abstract—For the realistic modeling of the seismic ground motion in lateral heterogeneous anelastic media, the database of 3-D geophysical structures for Beijing City has been built up to model the seismic ground motion in the City, caused by the 1976 Tangshan and the 1998 Zhangbei earthquakes. The hybrid method, which combines the modal summation and the finite-difference algorithms, is used in the simulation. The modeling of the seismic ground motion, for both the Tangshan and the Zhangbei earthquakes, shows that the thick Quaternary sedimentary cover amplifies the peak values and increases the duration of the seismic ground motion in the northwestern part of the City. Therefore the thickness of the Quaternary sediments in Beijing City is the key factor controling the local ground effects. Four zones are defined on the base of the different thickness of the Quaternary sediments. The response spectra for each zone are computed, indicating that peak spectral values as high as 0.1 g are compatible with past seismicity and can be well exceeded if an event similar to the 1697 Sanhe-Pinggu occurs.

Key words: Site effects, synthetic seismograms, Beijing City.

1. Introduction

China is one of the countries exposed to the largest seismic hazard in the world. Death caused by seismic activity exceeds the sum of victims caused by other natural hazards. Most provinces in China have historical records of destructive earthquakes.

China is located at the intersection of the Pacific Ocean seismic belt with the Euro-Asian seismic belt, and it is affected by the strongest continental seismic activity in the world. The historical records contain thousands of destructive earthquakes which occurred in China. They include eight earthquakes with magnitude greater than or equal to 8 before 1900. The 1556 ShanXi earthquake (M=8) claimed 830,000 victims. Past 1900, there were nine earthquakes with magnitude greater than or equal to 8, seven of which occurred in the continental area. The most immense was the 1950 Tibet earthquake with a magnitude of 8.6. The 1976 Tangshan earthquake (M=7.8) claimed at least 230,000 victims and destroyed a modern city in a few seconds. Based on the high level of seismic activity in China, the loss of human life and property due

[1] Institute of Geophysics, China Seismological Bureau, Beijing, 100081, China.
E-mail: ding@cdsn.org.cn
[2] Dipartimento di Scienza della Terra, Via Weiss 4, 34127 Trieste, Italy.
[3] SAND Group, ICTP, Strada Costiera 11, I-34100 Trieste, Italy.

to seismic hazard is important and urgent to mitigate, especially in the megacities and large urban areas.

Beijing, the capital city of China, has a large population (about 12 million) and hosts many important economic and political centers. The city recurrently suffered from earthquakes. The latest great event was the 1697 Sanhe-Pinggu earthquake (M=8), sited 50 km from the city. The maximum observed macroseismic intensity in Beijing was XI. The intensity was scaled on the China Seismic Intensity Table (XIE, 1957). The 1976 Tangshan earthquake (M=7.8) registered in Beijing a maximum intensity of VIII. The 1998 Zhangbei earthquake (M=6.2) was the latest strong event felt in Beijing. The spatial distribution and the physical properties of the local structures are often correlated to the seismic damage distribution.

The estimation of the seismic ground motion produced by possible strong earthquakes (earthquake scenarios) is useful to reduce the seismic damage. In a companion paper DING *et al.* (2004) have modeled digital recordings of the 1998 Zhangbei earthquake. One of the stations, FHSD, is located on the thick Quaternary sediment area, approximately 200 km from the epicenter. The observed seismograms show that the seismic waves are substantially stronger at the station FHSD than at other stations located in the mountain area, at similar epicentral distances. The modeling of DING *et al.* (2004) explains quite naturally the observations, i.e. that the Quaternary sediments enlarge the peak values and the duration of the seismic waves at the station FHSD. Using the same modeling technique validated by DING *et al.* (2004) we can immediately compute the ground motion due to any scenario earthquake. In this manner, we obtain the seismic response at any place for any potential strong earthquake, and can estimate the distribution of future earthquakes, effects and damage in the research area.

For such a purpose, we built the data set of the physical properties of the local 3-D underground structure in Beijing City. With this data set, the geophysical structure along an arbitrary cross section can be obtained, and the latest computer codes developed at the Department of Earth Science, University of Trieste, Italy are used for the calculation of realistic ground motion (PANZA, 1985; PANZA and SUHADOLC, 1987; FLORSCH *et al.*, 1991; FÄH *et al.*, 1993, 1994; PANZA *et al.* 2000).

2. The Structures Database

The research area for Beijing City is defined latitudinally 39.8°N to 40.1°N and longitudinally 116.2°E to 116.6°E. The data from local dense drilling wells and geological survey results (GAO and MA, 1993) are employed to define the distribution of the Quaternary and Tertiary sediment properties and thickness. In the research area there is no sedimentary cover in the mountain area, while the Quaternary sediments cover the entire plain district where the thickness increases from the northwestern mountain-plain boundary to the southeast. There are two abnormally

thick Quaternary sediment zones near the city; one at the northwest margin of the city, the other within the northeast suburbs. In the latter the thickness reaches 800 meters.

The parameters in the database constructed to study the seismic ground motion in Beijing City include the density, the seismic velocities of P and S waves, and the attenuation parameter Q values for the different sedimentary units (Quaternary, Late Tertiary and Early Tertiary). The density values are obtained from local geophysical surveys and gravity inversion results (GROUP OF RESULTS OF DEEP GEOPHYSICAL PROSPECTING, 1986). The S wave velocity is derived from shallow seismic exploration and drilling well data.

Table 1 lists the available ranges of the considered parameters of the sediments. In the local geophysical data set the thickness of the three sedimentary layers is specified on a $0.02° \times 0.02°$ horizontal grid. At any point in the volume, the density, the P and S-wave velocity and the Q value can be obtained from the data set. These parameters are then used to build-up the input structural model for the calculation of the synthetic seismograms in the laterally heterogeneous anelastic media.

The synthetic seismograms are calculated along the profiles by using the hybrid method, which combines the modal summation (1-D) and the finite-difference (2-D) algorithms (PANZA, 1985; PANZA and SUHADOLC, 1987; FLORSCH *et al.*, 1991; FÄH *et al.*, 1993, 1994; PANZA *et al.* 2000). In the calculation, the seismic source, the travel path from the source to the research area and the site structure are all taken into account. The bedrock reference 1-D structure is taken from SUN *et al.* (1998).

In the hybrid calculation the finite-difference method requires that there are at least ten grid points inside the shortest wavelength (FÄH, *et al.*, 1994). In our model the minimum S-wave velocity is 0.4 km/s. If we consider an upper frequency limit of 4 Hz, the minimum wavelength is 100 meters, thus a grid size of 10 meters is appropriate to describe the structural model. The dimensions of the local laterally heterogeneous models used in Beijing City are 4 km (depth) by about 40 km (horizontal).

To provide for the source finiteness we use the scaling laws of GUSEV (1983) by properly weighting the source spectrum in the frequency domain, as reported in AKI (1987). By using the scaled signals in the frequency domain, the response spectral ratio (RSR) corresponding to the laterally varying model and to the bedrock model, versus frequency and distance along the profiles, have been calculated to estimate the local response.

Table 1

Geophysical Properties of the Sediments

	Density (g/cm^3)	V_P (km/s)	V_S (km/s)	Q_S
Quaternary	1.8–2.2	1.0–3.5	0.4–2.0	40–60
Later Tertiary	2.4–2.5	4.0–4.6	2.35–2.65	100–130
Early Tertiary	2.6–2.8	5.0–5.6	2.9–3.3	150–175
Bedrock	2.85	5.9–6.1	3.44–3.54	200

The seismic ground motion in Beijing City is simulated for two selected large earthquakes: the 1976 Tangshan and the 1998 Zhangbei earthquakes, which lie to the southeast and the northwest of the City, respectively. These events can be considered representative of the most dangerous seismogenic areas around Beijing. The three-component broadband synthetic seismograms along five profiles crossing the city area have been calculated, with the maximum frequency of 4 Hz. The ground motion in this frequency band is effective for various buildings existing inside the research area. Three profiles, TS02, TS03, TS04, point towards the epicenter of the 1976 Tangshan earthquake, two profiles, ZB05 and ZB06, point towards the epicenter of the 1998 Zhangbei earthquake.

3. Synthetic results

The 1976 Tangshan earthquake produced damage in Beijing City. The observed macroseismic intensity was VI in most of Beijing City. However an abnormal intensity was observed in the northwestern part of the city with a value of VII. The source parameters of the earthquake can be referred to DING *et al.* (2004). The

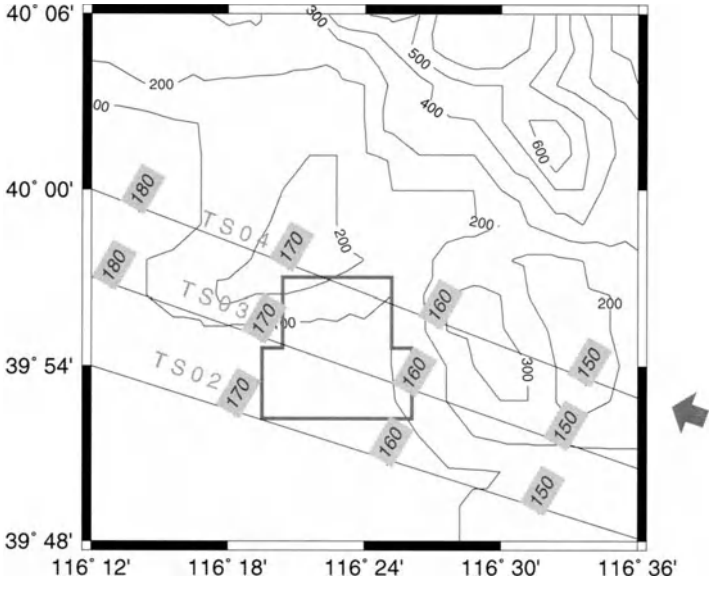

Figure 1
Profiles for the 1976 Tangshan Earthquake. The background contours represent the Quaternary sediment depth in meters. The polygon represents the city of Beijing. Three profiles, TS02, TS03 and TS04 are shown in the figure. The profiles point towards the epicenter of the 1976 Tangshan earthquake, which is located in the southeast. The numbers along the profiles are the distances from the epicenter, in km.

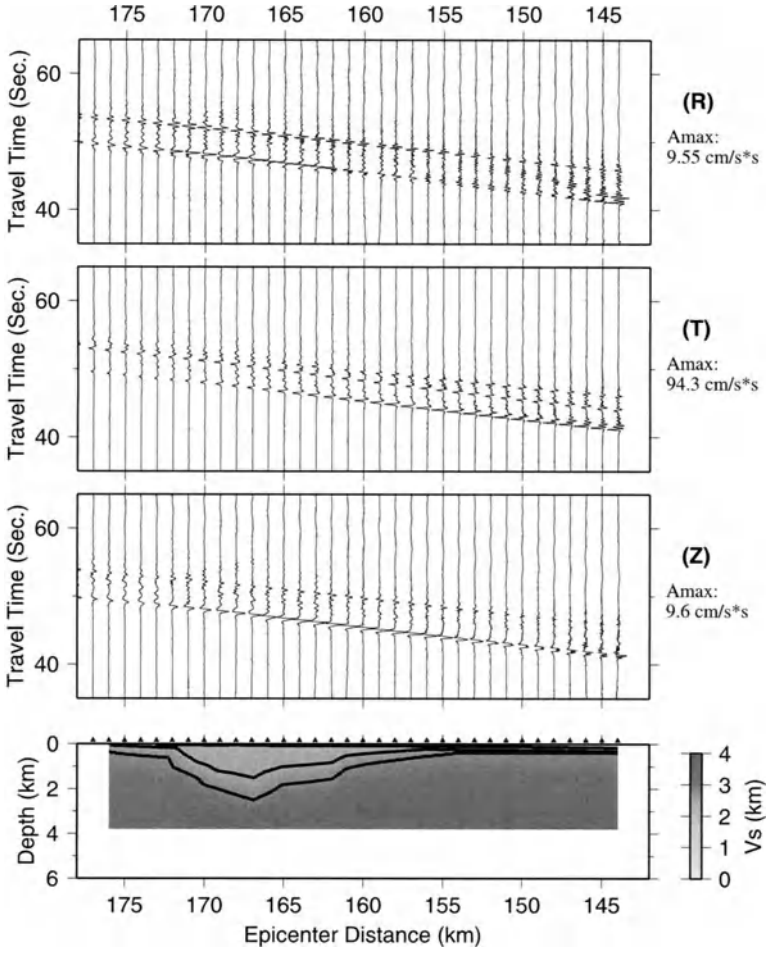

Figure 2
The local structural model and the synthetic seismograms along the profile TS02. The lines in the bottom figure outline the three sediment layers. Radial, transverse and vertical components of the synthetic ground acceleration.

seismic ground motion for the 1976 Tangshan earthquake is modeled along the three profiles, TS02, TS03 and TS04, and shown in Figure 1. The distance along the profile is measured from the epicenter of the 1976 Tangshan earthquake.

The profile TS02 passes south of the city. The Quaternary sediment is thinner westward (toward the mountain area) with increasing epicenter distance. The Tertiary Beijing depression is located between the distance of 160 and 172 km (Fig. 2). The synthetic seismograms reveal that the thick Tertiary sediments amplify only the seismic ground motion of Rayleigh and *P-SV* waves. The Love and *SH* waves which, due to the source orientation with respect to the considered profiles in

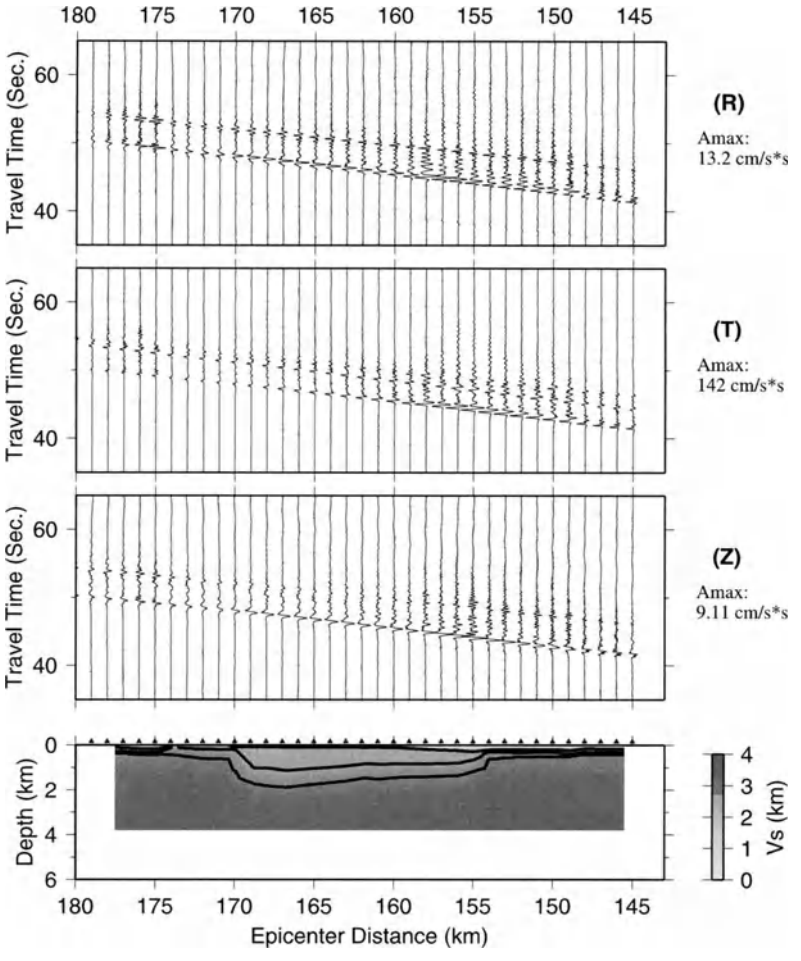

Figure 3
The local structural model and the synthetic seismograms along the profile TS03. The lines in the bottom figure outline the three sediment layers. Radial, transverse and vertical components of the synthetic ground acceleration.

the city are the strongest waves in this case, do not show significant unusual phenomena.

The profile TS03 passes through the center of the city. The seismic waves are mainly controlled by the thickness of the Quaternary sediments (Fig. 3). The acceleration amplitudes are enlarged at the distance of 148–160 km and 175 km, where thicker Quaternary sediments exist.

The profile TS04 passes through the northern part of the City. The cross section cuts across the Tertiary depression zone between the distance of 157 and 168 km, and the thickness of the Tertiary sediments along TS04 is not as large as along TS02 and

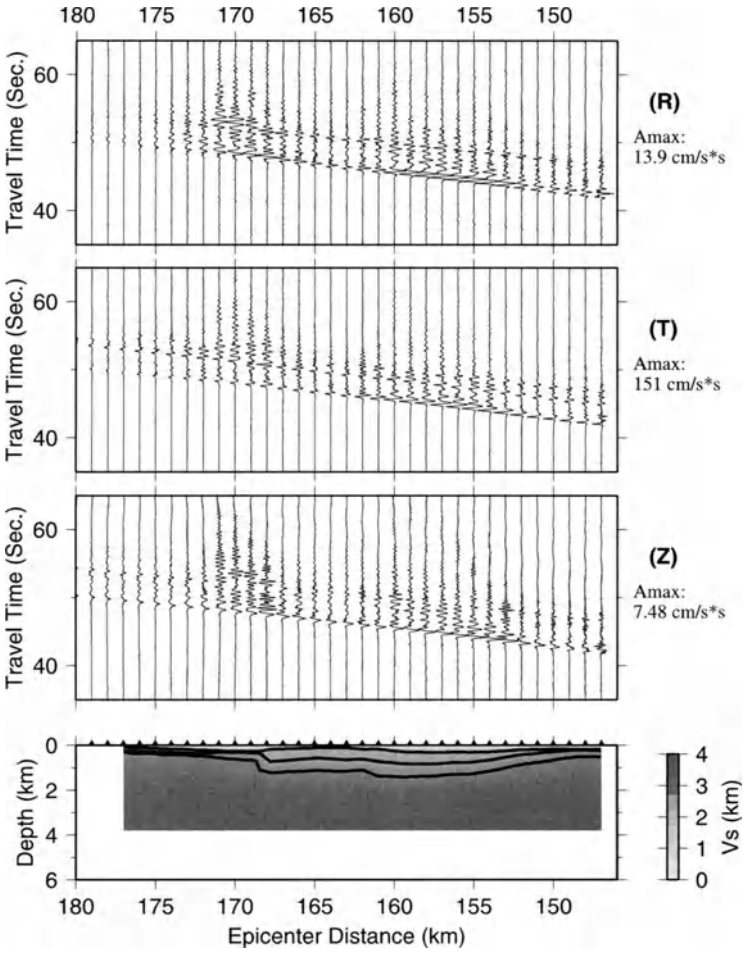

Figure 4
The local structural model and the synthetic seismograms along the profile TS04. The lines in the bottom figure outline the three sediment layers. Radial, transverse and vertical components of the synthetic ground acceleration.

TS03. Two thick Quaternary sediment areas are situated around 153–163 km and 170 km (see Fig. 4). The synthetic acceleration time history of profile TS04 is shown in Figure 4. The amplitude of the transverse component is 10 times larger than the radial and vertical components, and the waveforms of all three components along the profile are mainly controlled by the thickness of the Quaternary sediment. Enlarged amplitudes and longer durations of seismic ground motion characterize the northwestern part of the city, at the distance of 170 km. This is the district of Beijing where, during the 1976 Tangshan earthquake, abnormally high — one degree

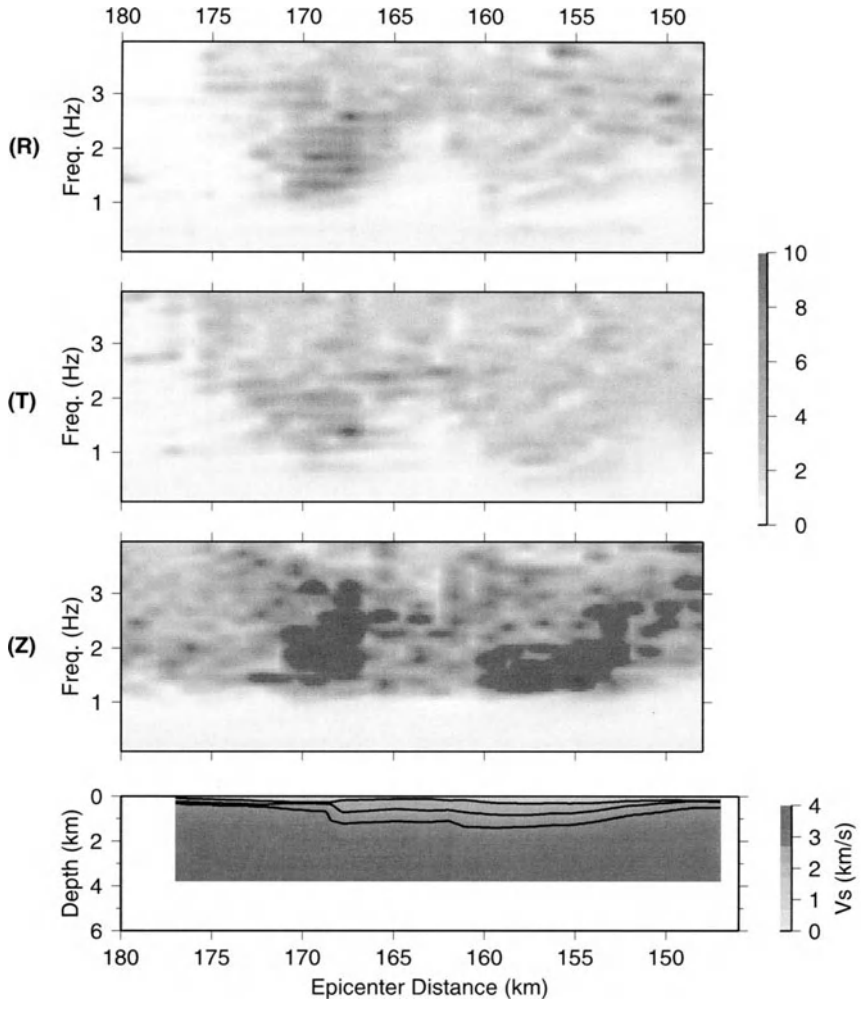

Figure 5
RSR versus frequency and distance along profile TS04.

higher than the value in the surrounding area — macroseismic intensity has been observed.

In Figure 5 the RSR versus epicentral distance and frequency reaches the large values corresponding to of the thick Quaternary sediment at about 170 km and at the frequency of 1–2 Hz, which is the fundamental resonant frequency of the Quaternary sediment layer there. For the transverse component, which is the dominant one, the RSR for a set of selected sites is shown in Figure 6, to illustrate the variation of the dominant frequency along the profile.

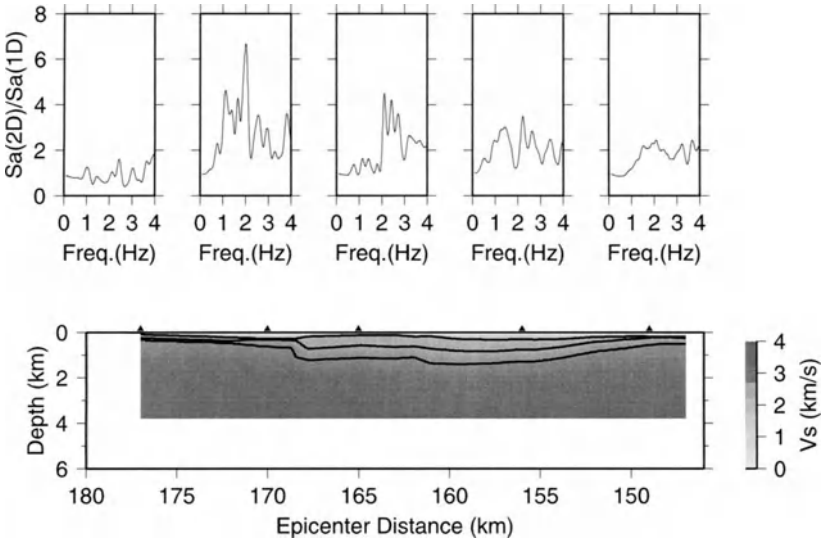

Figure 6
RSR of *SH* waves at selected sites along profile TS04.

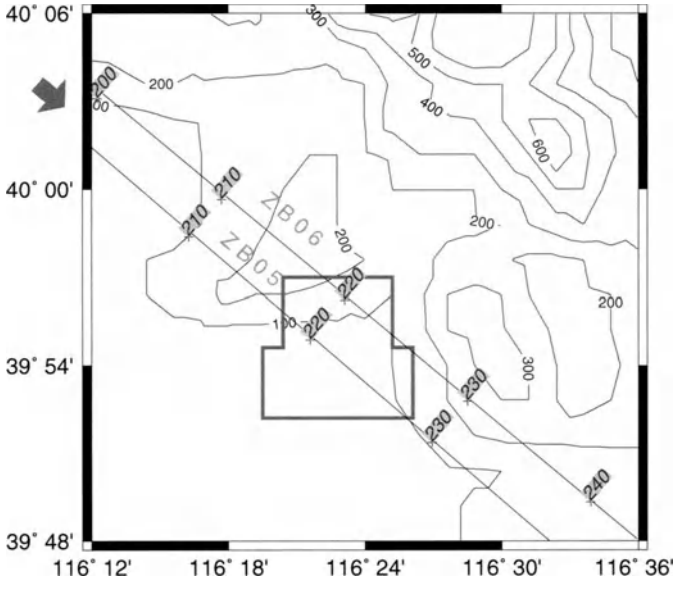

Figure 7
Profiles for Zhangbei Earthquake. The background contours represent the Quaternary sediment depth in meters. The polygon represents the city of Beijing. Two profiles, ZB05 and ZB06 are shown in the figure. The profiles point towards the epicenter of the 1998 Zhangbei earthquake, which is located in the northwest. The numbers along the profiles are the distances from the epicenter, in km.

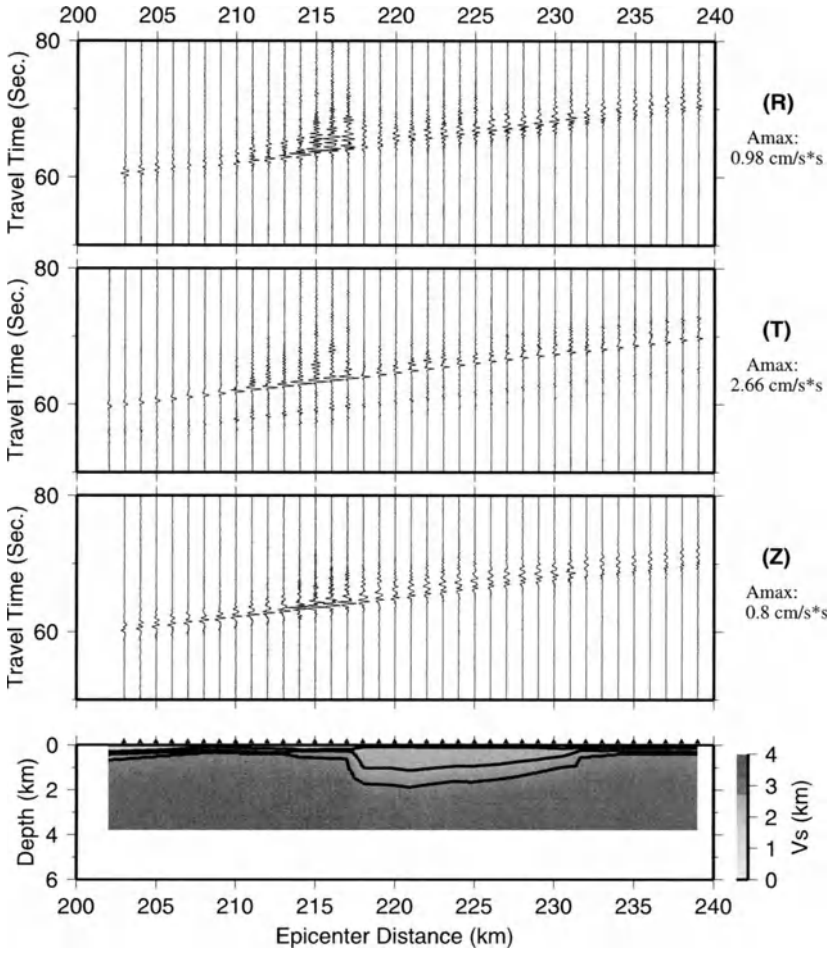

Figure 8
The local structural model and the synthetic seismograms along the profile ZB05. The lines in the bottom figure outline the three sediment layers. Radial, transverse and vertical components of the synthetic ground acceleration.

On January 10, 1998 an earthquake occurred in Zhangbei County, which is located to the northwest of Beijing City at a distance of about 200 km. The source parameters of the earthquake can be referred to DING *et al.* (2004). The scale of the profiles is the distance from the epicenter.

The profile ZB05 passes through the northwest and southeast corners of the City. There are thick Quaternary sediments between 212 km and 217 km, while the Tertiary depression zone is located between 217 km and 231 km. Figure 8 shows the local structure and the synthetic seismograms along the profile. The seismic waves are obviously amplified at about 215 km, where the thick Quaternary sediments are located.

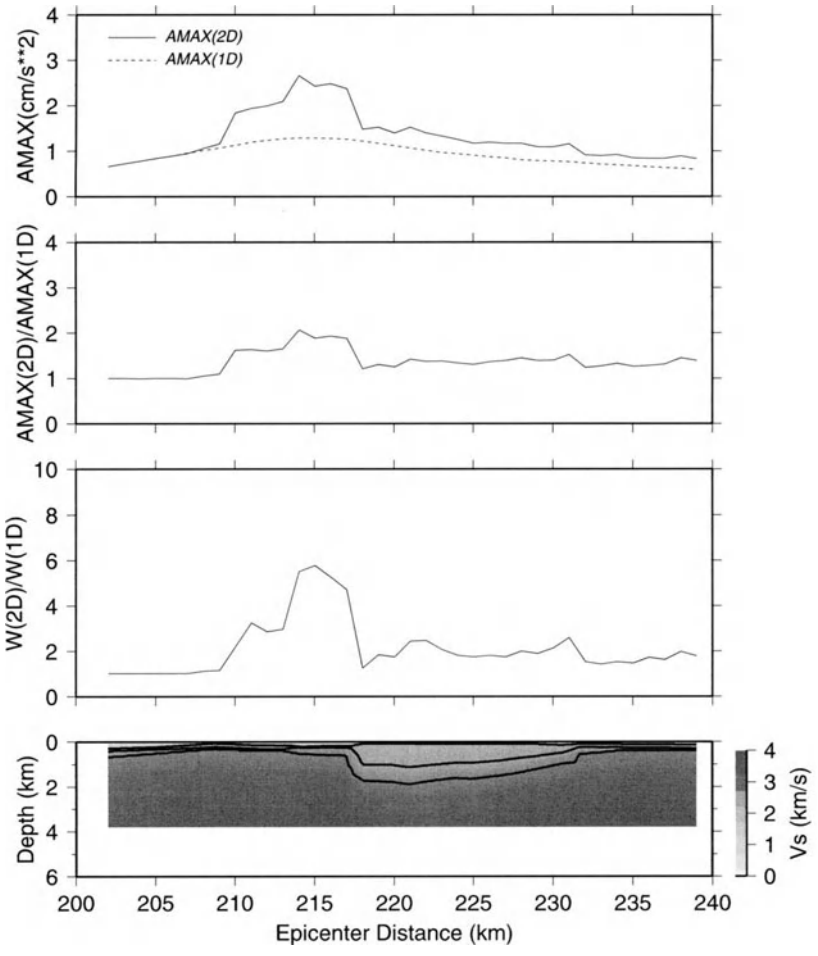

Figure 9
AMAX, AMAX(2D)/AMAX(1D) and W(2D)/W(1D) along the profile ZB05.

Figure 9 shows the maximum acceleration (AMAX) and the ratios AMAX(2D)/AMAX(1D) and W(2D)/W(1D) versus epicenter distance. Here (2D) represents the local lateral 2-D inhomogeneous structure, (1D) the reference 1-D bedrock structure and W is the so-called relative Arias intensity (ARIAS, 1970) defined as:

$$W = \frac{\pi}{2g} \int_0^\infty [\ddot{x}(\tau)]^2 d\tau \ ,$$

where x is the ground displacement and g is the gravity acceleration. These parameters reach peak values at an epicenter distance of approximately 215 km, where the thick Quaternary sediments are located.

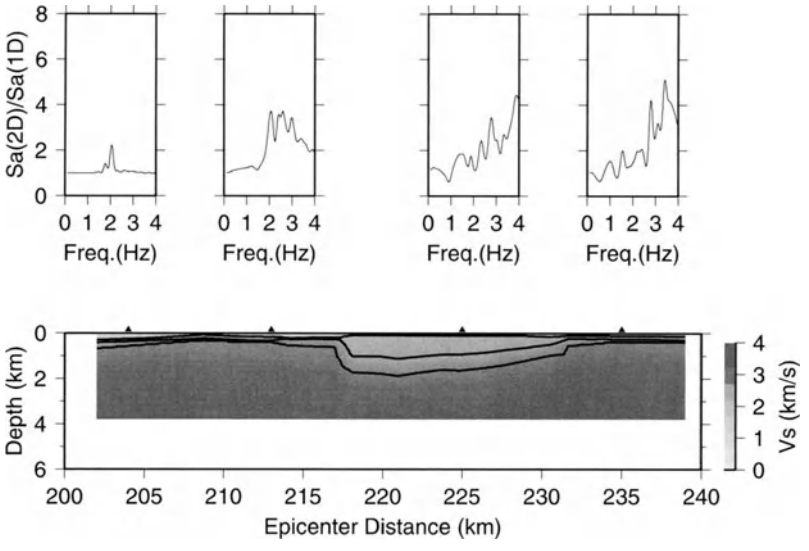

Figure 10
RSR of *SH* waves at selected sites along the profile ZB05.

From the RSR versus frequency and distance along this profile (Fig. 10) the dominant part at 213 km is mainly at high frequency, from 1.7 to 3 Hz. This is the fundamental resonant frequency for the thick Quaternary sediment. For other places with thinner Quaternary sediments the dominant frequency is higher, exceeding 2.5 Hz.

Profile ZB06 crosses the north and east suburbs and the northeastern part of the City. Two thick Quaternary sediment zones lie on the profile at about 215 km and 232 km. Figure 11 presents the synthetic three-component acceleration time histories along the profile: the amplification of the seismic waves is controlled by the thickness of the Quaternary sediments.

4. Site Effects in Beijing City

From the synthetic acceleration time histories used to model the ground motion arising from the 1976 Tangshan and the 1998 Zhangbei earthquakes, it can be concluded that mainly the thickness of the Quaternary sediments controls the seismic ground motion variations in Beijing City. The two earthquakes are at different azimuths, therefore it is reasonable to extend such a conclusion to the entire research area (PANZA *et al.*, 2000). Four zones can be defined accordingly to the thickness of the Quaternary sediments: Zone 1 includes the areas with a thickness of Quaternary sediments less than 50 m, Zone 2 between 50 m and 100 m, Zone 3 between 100 m

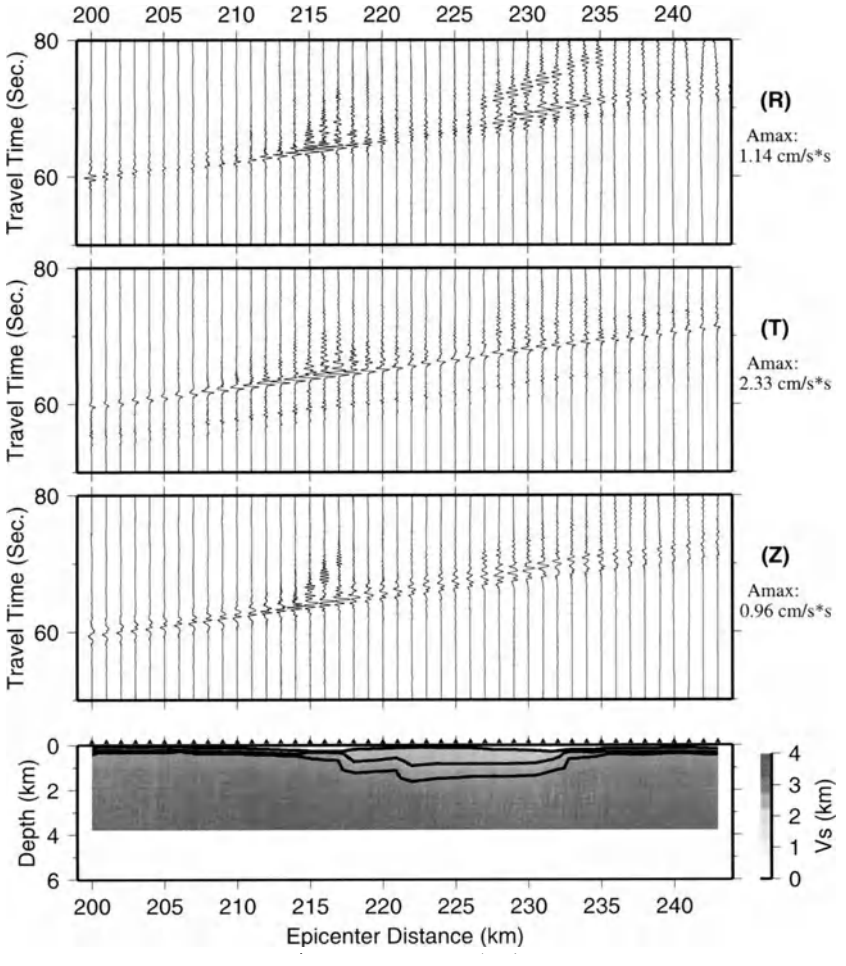

Figure 11
The structural model and the synthetic seismograms along the profile ZB06.

and 200 m, and Zone 4 greater than 200 m. The distribution of the four zones is shown in Figure 12.

For the Tangshan earthquake the RSR have been computed for all sites located in each of the four zones along the profiles TS02, TS03 and TS04. From these values the average and the maximum RSR for 0% and 5% damping of the oscillator are determined and shown in Figure 13. Such spectral properties can be considered representative of the four zones shown in Figure 12.

Figure 14 displays the absolute response spectra for each zone. As in the case for the EC8 design spectrum, the DGA can be obtained by dividing the largest spectral value by 2.5 in each zone. Therefore the DGA in Beijing City for the 1976 Tangshan

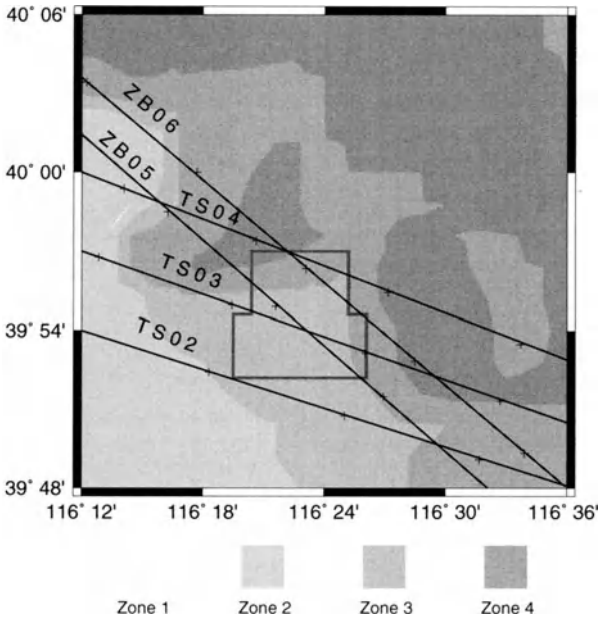

Figure 12
Different site effect zones in Beijing City.

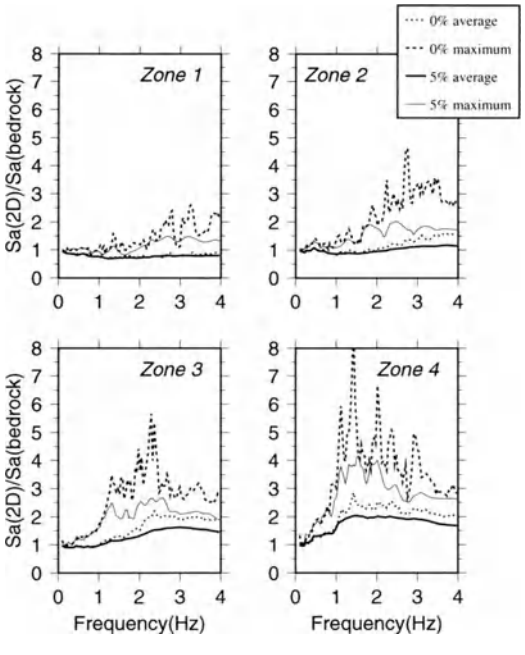

Figure 13
Maximum and average RSR for the four zones (for 0% and 5% damping).

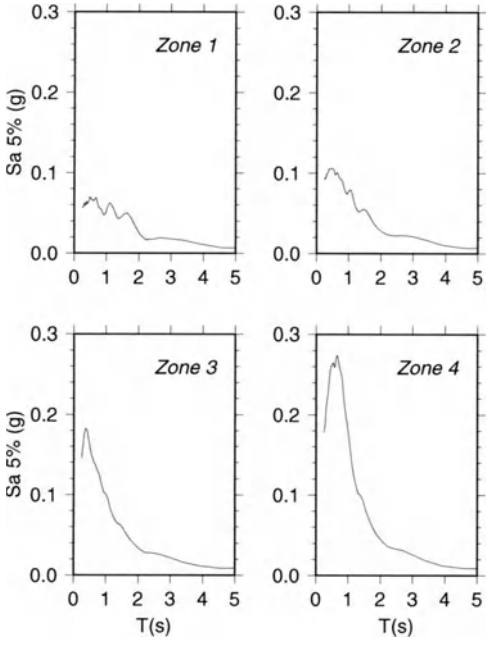

Figure 14
Absolute spectral acceleration (5% damping) for the four zones.

earthquake could be obtained as 0.03 g, 0.04 g, 0.07 g and 0.1 g for Zone 1, Zone 2, Zone 3 and Zone 4, respectively.

5. *Conclusions*

3-D geological and geophysical models have been built for Beijing City. With this database realistic three-component broadband synthetic seismograms have been calculated with a cutoff frequency of 4 Hz. The synthetic acceleration time histories are computed along five selected profiles.

Along all profiles the thick Quaternary sediments effect a large amplitude and long duration of the ground motion due to resonance effects and to the excitation of local surface waves.

Four zones are defined in accordance with the thickness of the Quaternary sediments in the area of Beijing City; each characterized by different spectral responses. The response spectra indicate that peak spectral values as high as 0.1 g are compatible with the past seismicity and can be well exceeded if an event similar to the 1697 Sanhe-Pinggu occurs.

Acknowledgements

This work is a contribution to the UNESCO-IUGS-IGCP Project 414 "Realistic Modeling of Seismic Input for Megacities and Large Urban Areas." This research has been carried on within the framework of the bilateral project "Geophysical Studies for the Deterministic Evaluation of Seismic Risk," with the contribution of the Italian Ministry of Foreign Affairs (MAE), Directorate General for Cultural Promotion and Cooperation. The research received support from the Chinese National Key Basic Research and Development Program (973 Program) No. 2002CB412709, MOST of China and China Seismological Bureau. We acknowledge Drs. Fabio Romanelli, Franco Vaccari and Francesco Marrara for their kind assistance in the calculation. This is contribution No. 02A10002, Institute of Geophysics, China Seismological Bureau. We have used public domain graphics software (WESSEL and SMITH, 1995a, 1995b).

REFERENCES

AKI, K., *Strong motion seismology*. In *Strong Ground Motion Seismology* (eds. Erdik, M. Ö. and Toksöz, M. N.) (NATO Advanced Study Institute Series, Series C: Mathematical and Physical Sciences, D. Reidel Publishing Company. The Netherlands 1987), *204*, pp. 3–39.

ARIAS, A. (1970), *A measure of earthquake intensity*. In *Seismic Design for Nuclear Power Plants* (ed. R. Hansen), Cambridge, Massachusets.

DING, Z., ROMANELLI, F., CHEN, Y., and PANZA, G. F. (2004), *Realistic Modeling of Seismic Strong Ground Motion in Beijing Area*, Pure Appl. Geophys. *161*, 1093–1106.

FÄH, D., IODICE, C., SUHADOLC, P., and PANZA, G. F. (1993), *A New Method for the Realistic Estimation of Seismic Ground Motion in Megacities: The Case of Rome*, Earthquake Spectra *9*(4), 643–668.

FÄH, D., SUHADOLC, P., MUELLER, St., and PANZA, G. F. (1994), *A Hybrid Method for the Estimation of Ground Motion in Sedimentary Basin: Quantitative Modelling for Mexico City*, Bull. Seismol. Soc. Am. *84*, 383–399.

FLORSCH, N., FÄH, D., SUHADOLC, P., and PANZA, G. F. (1991), *Complete Synthetic Seismograms for High-frequency Multimode SH Waves*, Pure Appl. Geophys. *136*, 529–560.

GAO, W., MA, J., *Seismo-geological Surroundings and Seismic Hazards in Capital Area* (Seismological Press, Beijing, 1993).

GROUP OF RESULTS OF DEEP GEOPHYSICAL PROSPECTING, State Seismological Bureau, Results of Deep Exploration of the Crust and Upper Mantle of China (Seismological Press, Beijing, 1986).

GUSEV, A. A. (1983), *Descriptive Statistical Model of Earthquake Source Radiation and its Application to an Estimation of Short-period Strong Motion*, Geophys. J. R. Astr. Soc. *74*, 787–800.

PANZA, G. F. (1985), *Synthetic Seismograms: The Rayleigh Waves Modal Summation*, J. Geophysics *58*, 125–145.

PANZA, G. F. and SUHADOLC, P., *Complete strong motion synthetics*. In *Seismic Strong Motion Synthetics*, (ed. B. A. Bolt) (Academic Press, Orlando, 1987), *Computational Techniques 4*, 153–204.

PANZA, G. F., ROMANELLI, F., and VACCARI, F. (2000), *Seismic Wave Propagation in Laterally Heterogeneous Anelastic Media: Theory and Applications to Seismic Zonation*, Advances in Geophysics *43*, 1–95.

SUN, R., VACCARI, F., MARRARA, F., and PANZA, G. F. (1998), *The Main Features of the Local Geological Conditions can Explain the Macroseismic Intensity Caused in Xiji-Langfu (Beijing) by the Tangshan 1976 Earthquake*, Pure Appl. Geophys. *152*, 507–522.

WESSEL, P. and SMITH, W. H. F. (1995a), *New Version of the Generic Mapping Tools Released*, EOS Trans. AGU *76*, 329.

WESSEL, P. and SMITH, W. H. F. (1995b), *The Generic Mapping Tools (GMT) Version 3.0 Technical Reference and Cookbook*, SOEST/NOAA.

XIE, Y. (1957), *A New Scale of Seismic Intensity Adapted to the Conditions in Chinese Territories*, Acta Geophysica Sinica *6*, 35–48.

(Received May 7, 2002, accepted September 3, 2002)

Pure appl. geophys. 161 (2004) 1125–1147
0033–4553/04/061125–23
DOI 10.1007/s00024-003-2499-5

Pure and Applied Geophysics

Microzonation of Bucharest: State-of-the-Art

C. L. MOLDOVEANU[1,2], M. RADULIAN[1], GH. MARMUREANU[1], and G. F. PANZA[3,4]

Abstract—The 1940 ($M_w = 7.7$) and 1977 ($M_w = 7.4$) Vrancea earthquakes (Romania) inflicted heavy damage and casualties in Bucharest and the statistics indicate a recurrence interval of 25 years for $M_w \geq 7.0$ events. Under these circumstances, the seismic microzonation represents important information for detailed urban planning that establishes an appropriate level of preparedness to the earthquake threat. This paper reviews the main studies concerning the seismicity of the Vrancea region, the site conditions of the city, the characterization of the building stock, and the codes of practice that regulate the antiseismic design. The first-order microzonation of Bucharest was performed starting from the existing database of structural and geotechnical parameters. New insights originating from direct instrumental observation and interpretation of the local effects as well as realistic numerical modeling that update and improve the input data necessary for a detailed microzoning map of the city are also discussed.

Key words: Bucharest, Vrancea earthquake, damage, microzonation, antiseismic code.

1. Introduction

The strong intermediate-depth earthquakes of the Vrancea region have caused a high toll of casualties and extensive damage over the last several centuries in the Romanian territory. The occurrence of these earthquakes is irregular, but they are not infrequent. Statistics based on historical records (ONCESCU *et al.*, 1999) indicate that about three destructive subcrustal earthquakes per century occur in Vrancea. They can produce peak ground displacement of about 30 cm and peak acceleration on the order of about 30% of the gravity acceleration, 0.3 g (RADULIAN *et al.*, 2000a).

Bucharest is the most populated and most important city of Romania (Fig. 1), the principal political, administrative, economic, financial, banking, educational,

[1]National Institute for Earth Physics, Calugareni 12, P.O.Box: MG 2, 76900 Bucharest-Magurele, Romania. E-mails: cmold@ipruniv.cce.unipr.it; mircea@infp.ro; marmur@infp.ro

[2]Dipartimento di Scienze della Terra, Universita' degli Studi di Parma, Parco Area delle Scienze, 157/A - 43100, Parma, Italy.

[3]Dipartimento di Scienze della Terra, Universita' degli Studi di Trieste, Via E. Weiss 4, 34127 Trieste, Italy. E-mail: panza@dst.units.it

[4]The Abdus Salam International Center for Theoretical Physics, SAND Group, Trieste, Italy.

Figure 1
Geographical map of Romania. Topography, main rivers, provinces and some towns for reference are shown.

scientific and cultural center of the country. The city is located in S-SE Romania, at an altitude of 60–90 m, at 44°25′50″ latitude north and 26°06′50″ longitude west.

Romania's capital is the major city in the Balcanic area exposed to the significant hazard produced by strong Vrancea earthquakes. The metropolitan area is characterized by the presence of 2 million inhabitants (on 01.01.1998), accounting for 9% of the total population of the country and for 15% of the urban total. In terms of population size, Bucharest ranks third in the region after Athens and Istanbul. The downtown area is about 230 km^2 and among its main features are the presence of a considerable number of high-risk structures and infrastructures, and geological settings consisting of deep sedimentary deposits.

Historical data show that during past centuries Bucharest suffered repeatedly important damage due to strong Vrancea earthquakes (RADU, 1979; PURCARU, 1979). Within the last 28 years the city was threatened by two events with moment magnitudes $M_w > 7.0$ (1977 and 1986). The strongest one, recorded in 1977 ($M_w = 7.4$), claimed more than 1,500 lives, the majority of them in the capital where the inflicted destruction was the heaviest observed in modern times. The studies

published to date indicate that the alluvium/sedimentary layer in Bucharest amplifies, to a varying extent, the site response to seismic waves in the period range 0.1 to 1.2 s, a critical period range for many elements of the built environment (e.g., LUNGU *et al.*, 1994). Under these circumstances it is urgent that the decision-makers (e.g., city planners, civil engineers, and civil defense) should establish an appropriate level of preparedness for the earthquake threat. To accomplish this complex target, the information regarding the local seismic hazard evaluation of the Bucharest area represents a key element to be taken into account. The modifications of the ground motion parameters, due to the influence of the near-surface layers (seismic microzonation), must be integrated with the design parameters for the soil-structure interaction (aseismic design). The first seismic microzonation of Bucharest was performed after the strong 1940 Vrancea event ($M_w = 7.7$) by GHICA (1953), and since then this problem has become a permanent topic of geological and engineering investigations, through various approaches and methods. Due to the complex character of the subject, on one hand, and to the new numerical/modeling methods and computational/information progress, on the other hand, the study of the seismic site effects in Bucharest develops and improves continuously.

This paper presents the state-of-the-art of the microzonation study of Bucharest together with the seismicity of the Vrancea region and the legislation addressing antiseismic codes.

2. *Vrancea Region Seismicity*

The seismic regime of the national territory is characterized by a moderate to high earthquake activity with both shallow and intermediate-depth events (Fig. 2). The Romanian catalogue covers a relatively extended time interval and its completeness thresholds are: from 1411 to 1800 for $M_w \geq 7.0$, from 1801 to 1900 for $M_w \geq 6.5$, from 1901 to 1935 for $M_w \geq 5.5$, from 1936 to 1977 for $M_w \geq 4.5$, and from 1978 up to the present for $M_w \geq 3.0$ (ONCESCU *et al.*, 1999). Vrancea is the main seismogenic zone of Romania and exhibits the following remarkable features:

(a) highly restricted hypocentral area within 45°–46°N latitude and 26°–27°E longitude, at the SE corner of the strongly bent Carpathian arc;

(b) shallow seismic activity — located mainly in the lower crust ($h > 15$ km) with small to moderate magnitudes; $M_L = 5.3$ (1914) is the strongest crustal event ever recorded;

(c) subcrustal seismicity, very well clustered in a focal volume confined between 60 and 180 km of depth, represents the major feature of Vrancea region; the persistent rate of occurrence amounts to 12–15 events monthly ($M_L \geq 3$); the corresponding epicentral area is limited to a rectangle of about 30×70 km^2 NE-SW oriented that partly overlaps the epicentral area of the crustal events (RADULIAN *et al.*, 2000b); maximum ground displacements up to 30 cm and peak

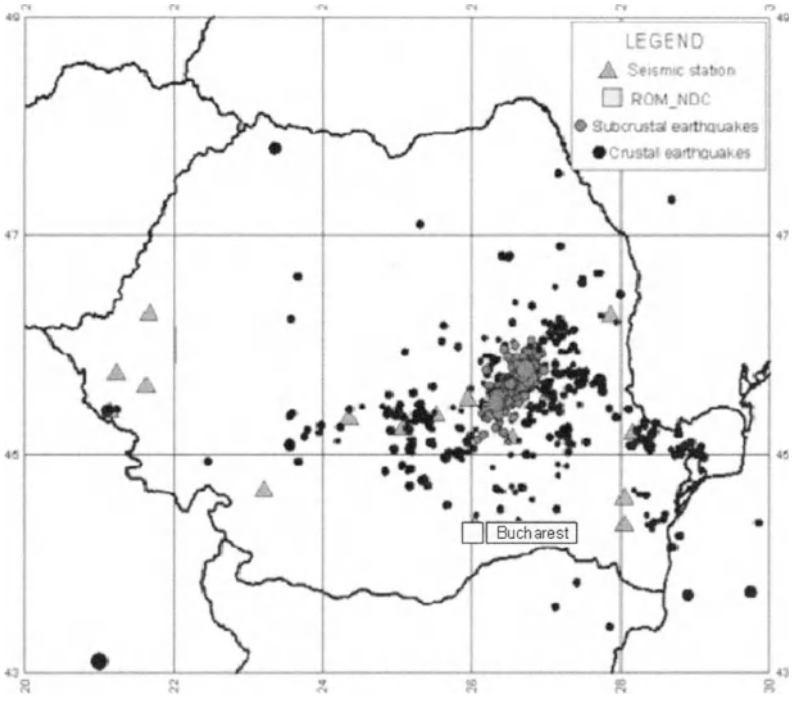

Figure 2
Romanian seismicity map. Crustal and subcrustal earthquakes are shown for the time interval 1995–2000.

accelerations on the order of 0.3 g were recorded in the area situated eastward and southward of the Carpathians arc (RADULIAN *et al.*, 2000a);

(d) the recurrence times estimated from the available catalogues are: 10 years for $M_w \geq 6.5$, 25 years for $M_w \geq 7.0$ and 50 years for $M_w \geq 7.4$ (WENZEL *et al.*, 1999);

(e) the large earthquakes (instrumentally recorded) show a remarkably similar fault plane solution that typically has strike SW-NE (220°), dip 60° to 70° to the NW, and slip roughly 80° to 90° (RADULIAN *et al.*, 2000b, WENZEL *et al.*, 1999); the stress regime is clearly compressive; despite the similarity of the fault plane solutions, significant variations of the radiation pattern are noticeable, which reflect the dynamics of the rupture process (ONCESCU and BONJER, 1997);

(f) the total seismic moment released by the last four strong events (1940, 1977, 1986 and 1990) is similar to a maximum possible Vrancea source of magnitude $M_w = 8.0$ which means an average amount of seismic moment released of 8×10^{20} Nm/yr (WENZEL *et al.*, 1999); according to ONCESCU and BONJER (1997) the sum amounts to 7.5×10^{20} Nm for a period of about 100 years;

(g) the depth interval between 110 and 130 km is considered to be a candidate for the next strong Vrancea event since this remained unruptured during at least the last 150 years (ONCESCU and BONJER, 1997).

Several geophysical models based either on subduction processes or on slide break-off and necking have been proposed to explain the amazingly confined Vrancea subcrustal seismicity (e.g., FUCHS *et al.*, 1978; ONCESCU, 1984; TAVERA, 1991; GIRBACEA, and FRISH, 1998). Additional physical insight originates from estimates of the deformation rate in the source volume, recent tomographic results and models of stress distribution within a passive slab (WENZEL *et al.*, 1999).

3. Bucharest Local Site Conditions

The synthesis of the geological data available was first presented by LITEANU (1951) and then by others, e.g., MANDRESCU and RADULIAN (1999), LUNGU *et al.* (1999a).

Bucharest city (Fig. 3) is situated in the Romanian Plain, along the roughly parallel valleys of the Dambovita and Colentina rivers. Structurally the downtown is located in the central part of the Moesian Platform, at an average epicentral distance of 160 km from the Vrancea region. Topographically the city is built on a plane slightly dipping southeast, following the direction of the Dambovita and Colentina rivers, which divide the city into several morphological units: Bucharest Plain (Dambovita – Colentina interstream), Baneasa-Pantelimon Plain, Cotroceni-Vacaresti Plain, and the meadows along the abovementioned rivers. The hydrostatic level ranges between 1 and 5 m in Dambovita and Colentina meadows, between 5 and 10 m in the Dambovita – Colentina interstream, and below 10 m in the Cotroceni – Vacaresti and Baneasa – Pantelimon plains.

The foundation ground in Bucharest is represented exclusively by Quaternary deposits. The large amount of geological, geotechnical and hydrological data (the geotechnical bore-holes alone exceed 10,000) provided by Proiect Bucuresti Institute, the S.C. Prospectiuni S.A., Metrou S.A., and others, allow us to separate different Quaternary deposits according to their genesis and lithological composition. In this framework more than 2,000 boreholes were analyzed, and the seismic wave velocity was measured by seismic refraction in about 200 points. These data have been synthesized by MANDRESCU and RADULIAN (1999) and are shown in Figure 4. Four main classes of deposits are identified:

(1) *alluvial-proluvial deposits* (*loesslike deposits*) which contain clay and sandy yellow dust, with loess dolls; the structure of these deposits is macroporous and very compressible in a saturated state and their thickness ranges between 10 to 16 m in the Cotroceni-Vacaresti Plain and between 3 to 6 m in the Dambovita — Colentina interstream, respectively;

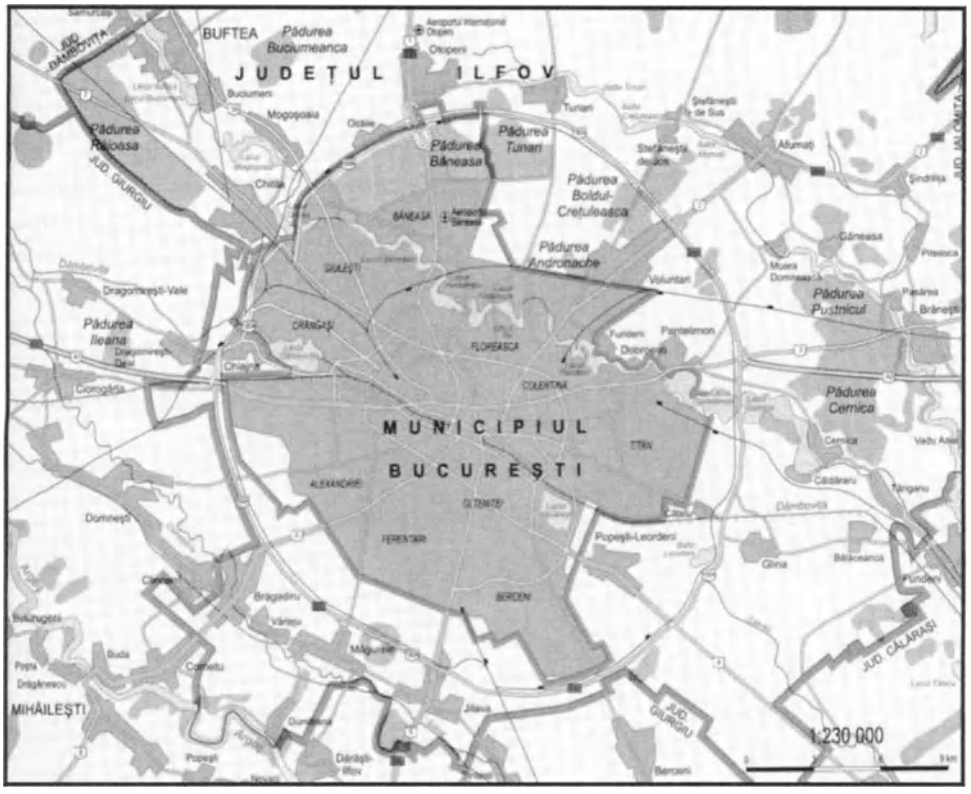

Figure 3
Bucharest city (Municipiul Bucuresti) map.

(2) *diluvial deposits* represented by loesslike and clay deposits with slightly macroporous structure; they overlay a most of the Dambovita terraces; an increase of the clay content is noticed as compared with the loesslike deposits in the plains;
(3) *alluvial deposits* consisting of clays, dusty and sandy clays and mud; the predominant clay character at surface changes in depth, the clay content diminishes in comparison with sand; these deposits are found in Dambovita and Colentina meadows;
(4) *artificial fills* that largely stand in the Dambovita – Colentina interstream.

4. Seismic Damage Inflicted on Bucharest by Strong Vrancea Earthquakes

The city dates from the 14th century and is recorded for the first time in 1459 as the residence of Prince Vlad Tepes. It was the capital of Wallachia in the 17–19th centuries, subsequently of Romania since 1862. The effects of the strong Vrancea

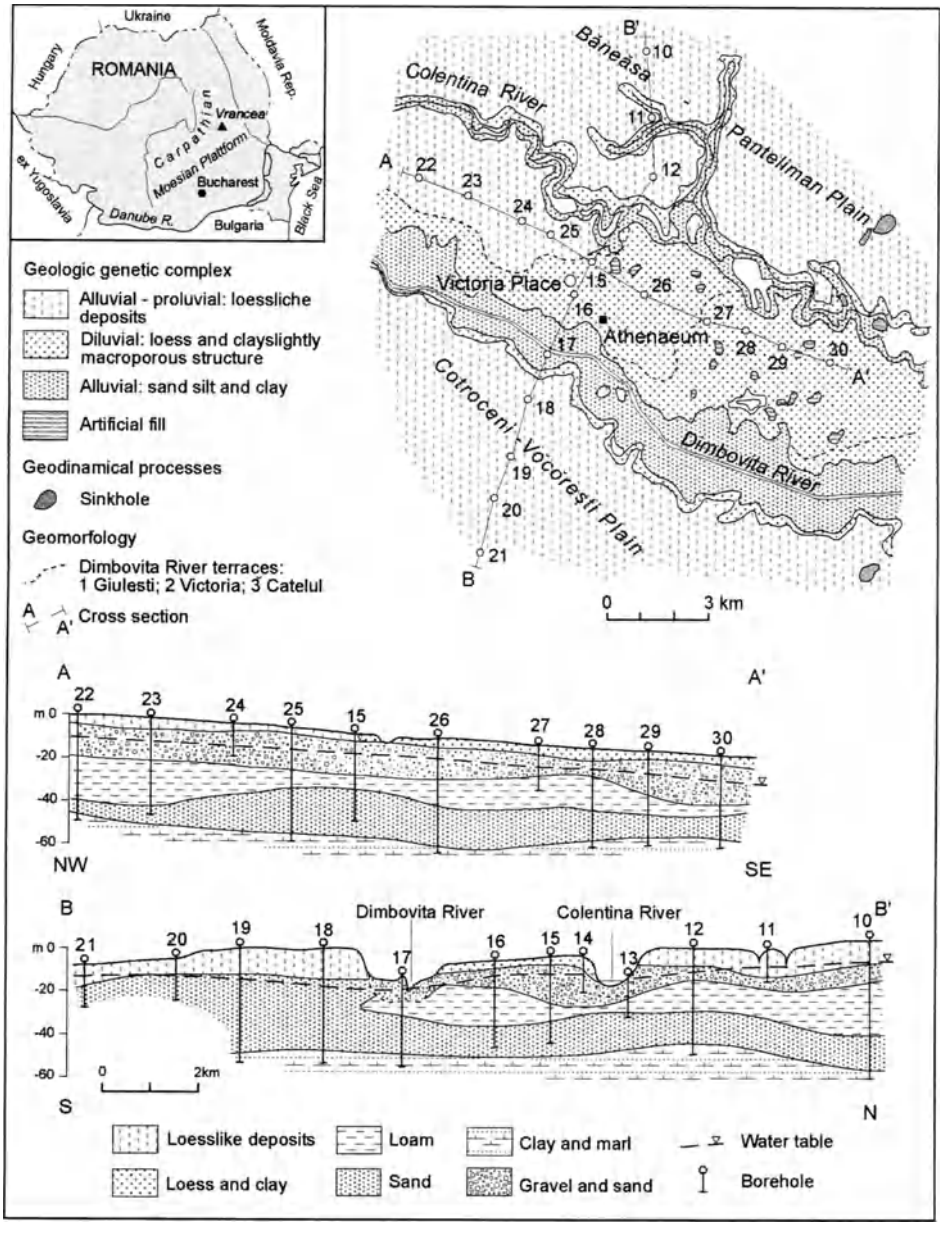

Figure 4
Engineering geological map of Bucharest (MANDRESCU and RADULIAN, 1999).

earthquakes in Bucharest were first documented in the 17th century. The first report describes the $M_w = 7.1$ Vrancea event that occurred on August 19, 1681 (STEFANESCU, 1901). According to the contemporary account, "the Earth shook so

strongly that nobody had ever related." The next strong event hit the town on June 11, 1738 ($M_w = 7.7$) and destroyed the walls and the tower of the Prince's Court in Bucharest; many houses and churches were damaged, and a "deep fracture" opened near the town. The strongest historically recorded event ($M_w = 7.9$) occurred on October 26, 1802, and accordingly was described by contemporaries as the "big earthquake". During this earthquake all the church towers in Bucharest cawed in, and many churches and houses collapsed. Another major earthquake occurred on January 11, 1838 ($M_w = 7.5$) and caused the collapse of five churches and extensive damage to fifty other churches and several hundred houses.

During the last century the city was affected by two highly destructive earthquakes: November 10, 1940 ($M_w = 7.7$, $h = 150$ km), and March 4, 1977 ($M_w = 7.4$, $h = 94$ km). The seismic effects inflicted on Bucharest by the 1940 earthquake are summarized as follows: 167 people lost their lives; many buildings, some of them with reinforced-concrete frames, suffered severe damage; a new 13-storey reinforced concrete structure (Carlton Hotel), sited in the central zone of the city, collapsed. The damage was scattered both in terms of district distribution and damage degree (MANDRESCU and RADULIAN, 1999). Consequently, the Romanian authorities decided for the first time to introduce rules for antiseismic building design. These recommendations were mostly ignored and buildings were cosmetically repaired. The consequences were catastrophic during the next major earthquake in 1977, which produced the most destructive effects ever recorded in modern times in Bucharest. 1,424 people were killed, 32 buildings of 8-12 storeys collapsed, 150 long-standing buildings of 6-9 storeys were heavily damaged (many of them were subsequently demolished). These buildings were located in the central part of the city and had old, flexible, reinforced concrete frame structures. Their fundamental period ranged from 0.7 to 1.6 s. This range corresponds to the maximum in the acceleration response spectrum obtained for the only reliable accelerogram recorded in Bucharest during that earthquake (AMBRASEYS, 1977; MANDRESCU, 1978). The rigid structures of similar height (e.g., large panel precast concrete structures, cast-in-place reinforced concrete shear wall structures, as well as masonry dwellings of 1–3 storeys) have fundamental periods from 0.2 to 0.7 s, and therefore suffered relatively slight seismic damage. The evaluation of the damage distribution in Bucharest was performed by analyzing the status of the building stock. By direct inspection 2,429 buildings were grouped into three classes: A — 1,293 masonry buildings, B — 739 reinforced concrete frame structures, and C — 397 large panel precast concrete structures and cast-in-place reinforced concrete shear-wall structures (MANDRESCU, 1978). The building response to the seismic input was evaluated in a scale from 0 to 5. Figure 5 presents the territorial damage distribution for the buildings of A and B classes, expressed in terms of MSK-64 intensity (MANDRESCU and RADULIAN, 1999). The largest values of the damage degree were concentrated in the central zone of the city. The C class buildings, mainly sited in the new residential districts, did not suffer significant damage. The damage degree of a sample of about 18,000 buildings was

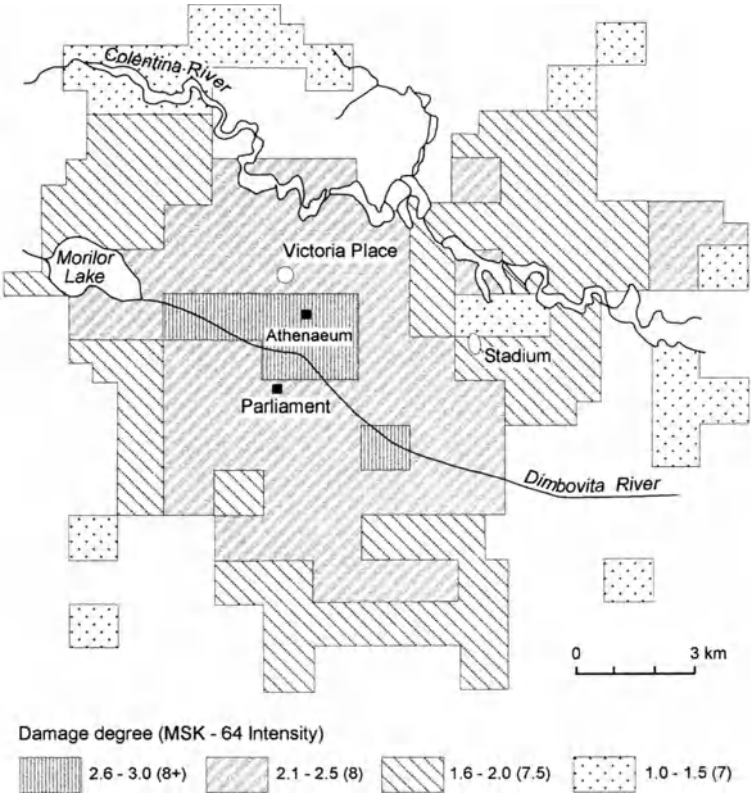

Figure 5
The 1977 earthquake: damage distribution in Bucharest corresponding to masonry buildings and reinforced concrete frame structures (MANDRESCU and RADULIAN, 1999).

evaluated in terms of MSK-64 intensity. According to their fundamental period (empirically estimated) these structures can be grouped into three classes: 0.00–0.15 s, 0.15–0.25 s, and 0.70–1.00 s. The results are shown in Figure 6 (MANDRESCU and RADULIAN, 1999), and reveal the concentration of the maximum effects in the central part of the city and the tendency of the damage degree to increase with the increase of the fundamental period of the structure (SANDI and PELEA, 1982).

5. Dominant Periods of the Site Effects in Bucharest from Noise Measurements

The spectral method demonstrates a clear peak in the H/V- ratios (horizontal and vertical amplitudes of the seismic recordings) that correlates with the fundamental resonance period of the site, in particular in a soft soil environment (e.g., BARD, 1995). The thickness of the alluvial sediments in Bucharest supposedly varies between

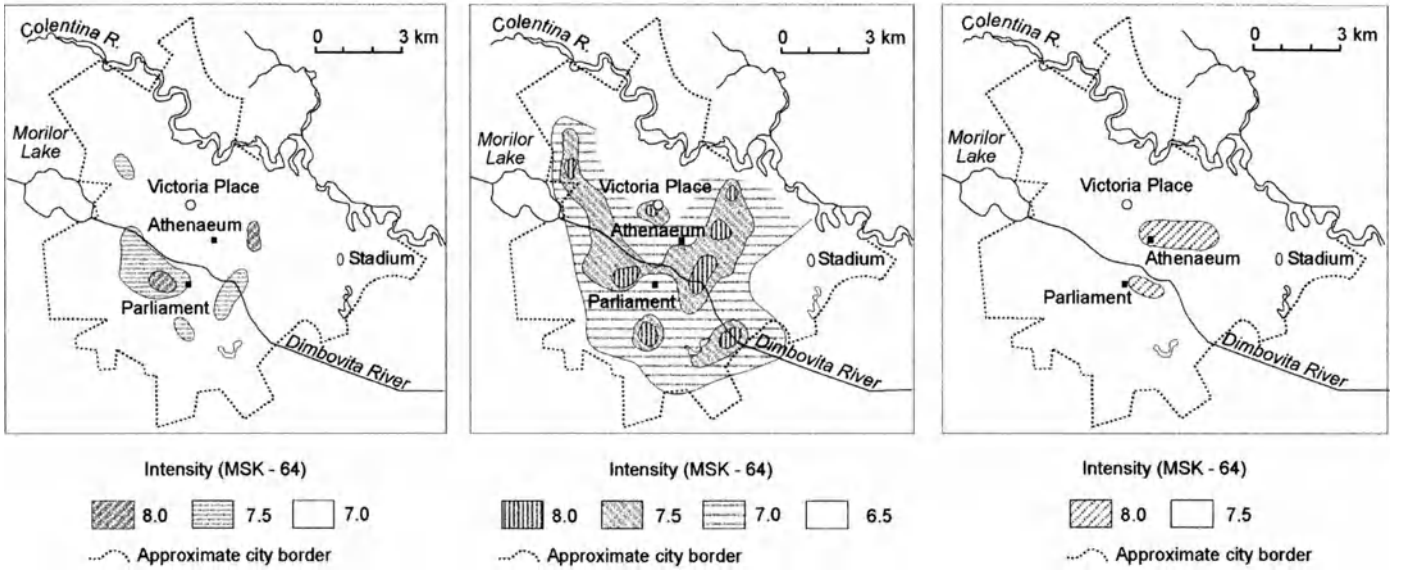

Figure 6
The macro-intensity MSK-64 distribution in Bucharest for the March 4, 1977 earthquake for the following different period ranges: (a) 0.00–0.15 s, (b) 0.15–0.25 s, 0.25–1.00 s (MANDRESCU and RADULIAN, 1999).

100 and 200 m. In order to examine the local soil resonance several experimental studies were carried out in the Romanian capital.

SANDI and PELEA (1982) performed the first systematic measurements of ambient seismic noise in the central part of Bucharest, on a local profile EW-oriented. In the sampled area the spectral amplification factor is almost constant for periods below 0.15 s, and it increases by about 35% for periods from 0.35 to 0.7 s, mostly in the western sites of the city, close to the Dambovita River.

Another site response experiment was performed by BONJER *et al.* (1999) using the noise ambient measurements as well as the records of small earthquakes. The ambient noise ratios were determined along two profiles that cross each other in downtown Bucharest (a wide city area). This experiment documented the existence of a broad and stable soil resonance in the range of 1 to 2 seconds. The resonance peaks around 1.4 s would correspond to a 120-m thick layer of unconsolidated sediments, with a shear-wave velocity $Vs = 0.35$ km/s (simple horizontal layer resonance interpretation). This is a very important observation since flexible reinforced-concrete frame 6–12-storey buildings are expected to experience a shift of their fundamental resonance towards the range of the strongest site resonance (e.g., AMBRASEYS, 1977; ROJAHN, 1984). This observation is also valid for those buildings that already have been weakened by the 1940 and 1977 earthquakes, as well as by the bombing during World War II, and might have been further weakened by the 1986 and 1990 earthquakes. Under these circumstances, an earthquake similar to the one of 1977, with the same spectral content, would be an enormous threat to the Romanian capital (BONJER *et al.*, 1999).

6. *Seismic Microzonation Maps of Bucharest*

The first seismic zonation of Romanian territory was performed in 1941 (one year after the devastating $Mw = 7.7$ earthquake). Practically no map was prepared, however the country was divided into two regions: a seismic one was represented by the provinces of Moldova (eastern part of the country), Walachia (southern part of the country), and Brasov area (southeastern part of the Transylvania province, inside the Carpathian arc), and a non-seismic one, represented by the rest of the national territory. The evolution of the macroseismic zonation maps of Romania may be inferred from the following documents: (1) *STAS 2923-52* and *STAS 2923-63*, macrozonation of the territory of R.S. Romania, *State Office for Standardization, OSS*, Bucharest, 1952 and 1963, (2) *Decree 66/1977*, Romanian Government, 1977, (3) *STAS 11100/1-77*, macrozonation of the territory of R.S. Romania, *Romanian Institute for Standardization, IRS*, Bucharest, 1978, (4) *STAS 11100/1-91 and SR 11100/1-93* Macrozonation of the territory of Romania, *Romanian Institute for*

Standardization, IRS, Bucharest, 1991 and 1994. The main features of these maps can be summarized as follows (LUNGU *et al.*, 1999b):

(1) absence of the 9^{th} degree intensity zone (Mercalli-Cancani scale) in the epicentral Vrancea region; the 8^{th} degree intensity in Bucharest is surrounded by a 7^{th} degree intensity zone; low seismicity (i.e., the 6^{th} degree intensity) in southeastern Romania (including Cernavoda and half of Dobrogea province, between the Danube River and the Black Sea) (1952 map);

(2) a very small 9^{th} degree intensity zone is identified in the epicentral region; the 8^{th} and 7^{th} degree intensity zones have the same borders like as in the 1952 map; a 7^{th} degree intensity is assigned to the provinces of Transylvania and Dobrogea (1963 map);

(3) the 7^{th} degree intensity zone from the 1963 zonation map is extended towards the SW of Romania (Craiova); inside the 7^{th} degree intensity zone some cities are settled at higher local intensity as follows: Bucharest – 8.0, Iasi – 7.5, Zimnicea – 7.5, Craiova – 7.5; the northeastern part of the Dobrogea province receives the 6^{th} degree intensity (1977 map);

(4) Iasi city is assigned to an 8^{th} degree intensity; the Dobrogea province and the southeastern of the Transylvania province are declared zones of 7^{th} degree intensity (1991 and 1993 maps).

We can observe that all these seismic zoning maps assign to Bucharest city an 8^{th} degree seismic intensity that, on the MSK-64 scale, corresponds to a peak ground acceleration (PGA) of 0.20–0.25 g (LUNGU *et al.*, 1999b).

The seismic microzonation studies of the Romanian capital can be separated into two groups: before and after the strong 1977 Vrancea earthquake. The first studies were carried out by GHICA (1953), CIOCIRDEL *et al.* (1964), and MANDRESCU (1972, 1978). The seismic microzoning maps of Bucharest elaborated before 1977 were based on MEDVEDEV'S method (1962) which considers the influence of the surficial soil and water table level on the building behavior. The city area was divided into three microzones following the main geomorphological units. Even if not identical, these microzones are similar for all the authors. The associated macroseismic intensities were: the 8^{th} degree for Dambovita and Colentina meadows, the 7^{th} – 8^{th} degree for the central part of the city, and the 7^{th} degree for the plains of Cotroceni–Vacaresti, Baneasa–Pantelimon and the largest part of the Dambovita–Colentina interstream. The damage distribution inflicted by the 1977 earthquake is in disagreement with the microzoning maps of Bucharest existing at that time. The criteria based on the acoustic impedance of the foundation ground proved inadequate. This might be because: (a) MEDVEDEV'S method (1962) is defined for source and local conditions (small epicentral distances, shallow earthquakes and thin sedimentary deposits) very different from those that characterize Vrancea events and the Bucharest site (large epicentral distances, intermediate-depth events, and thick sedimentary deposits), (b) the 1977 earthquake had peculiar spectral characteristics,

and (c) the vulnerability of the building stock cannot be ignored when drawing the microzoning maps (MANDRESCU and RADULIAN, 1999).

In 1977, after evaluating the earthquake effects, the NCST (Commission for the seismic microzonation of Bucharest) proposed a preliminary microzoning map of Bucharest (Fig. 7). The distribution of the maximum acceleration is concentric with the maximum expected values (0.4 g) in the central part of the city. This pattern is not sustained either by the surficial soil distribution, or by the subsurface geological conditions, and does not fit the PGA values and spectral content of the records in Bucharest and in its environs for the 1986 and 1990 earthquakes (MANDRESCU and RADULIAN, 1999).

The urbanization process in the central part of the city took place mainly in two periods: at the beginning of the last century and between the two World Wars. Simultaneously the number of inhabitants nearly trebled. The buildings constructed in these periods had no earthquake design provisions, and suffered damage during

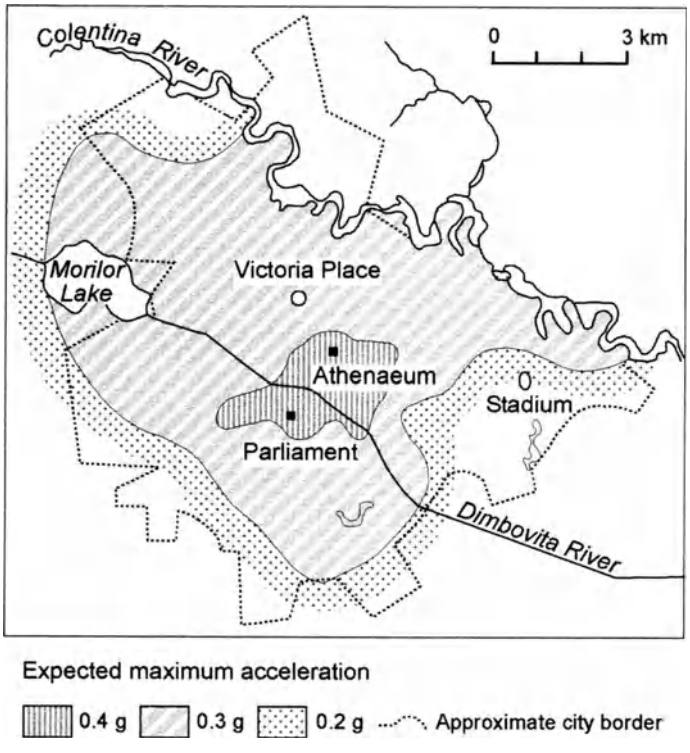

Figure 7
Preliminary seismic microzoning map of Bucharest (NCST REPORT, 1977). The distribution of the maximum acceleration is concentric, with the maximum expected value (0.4 g) in the central part of the city.

the 1940 earthquake and World War II. Moreover, part of these civil constructions successively changed their vocation, which imposed important structural alterations that ignored the original design. For these reasons, MANDRESCU and RADULIAN (1999) stress the importance of mapping the vulnerability distribution for each type of building. Only by comparing these maps with the seismic microzonation and the damage distribution maps, can we better understand the real cause of the earthquake effect pattern.

7. Ground Motion Modeling

In microzoning studies, the mapping of the strong ground motion can rely on either recorded or theoretically computed seismic signals, or both. To use recorded data requires a dense set of instruments to be triggered when a strong earthquake occurs. The preparation of a sufficiently large database of recorded strong motion signals represents a difficult, if not practically impossible task in the near future. While waiting for the increment of the strong ground motion data set, the theoretical computation of the seismic signals (by exploiting the available information concerning the tectonic and geological/geotechnical properties of the propagation medium, the theoretical knowledge of the physics of the source and of the wave propagation) represents a very useful approach to perform immediate mapping of the seismic ground motion for microzonation purposes. Obviously, whenever possible modeling has to be calibrated with the available recordings.

Strong motion recorded accelerograms for the Bucharest area are very scarce and correspond to the last three strong Vrancea events (1977, 1986 and 1990). Nonetheless they represent a database that, integrated by modeling, may permit a realistic estimate of the seismic input, for a given set of earthquake scenarios.

The first studies devoted to the mapping of the seismic ground motion in Bucharest due to the strong Vrancea earthquakes by means of synthetic signals have been carried out by MOLDOVEANU and PANZA (1999, 2001) and MOLDOVEANU *et al.* (2000). The numerical method implied is a complex hybrid waveform modeling (FÄH *et al.*, 1994; PANZA *et al.*, 2001) that combines modal summation (PANZA, 1985; VACCARI *et al.*, 1989; FLORSCH *et al.*, 1991; ROMANELLI *et al.*, 1996) with finite-difference techniques (ALTERMAN and KARAL, 1968; BOORE, 1972; KELLY *et al.*, 1976), and allows us easy parametric tests. The input information necessary for the modeling consists of the source mechanism, the average regional structural model, and the laterally heterogeneous anelastic local structure.

MOLDOVEANU and PANZA (1999) and MOLDOVEANU *et al.* (2000) succeeded in modeling the ground motion in Bucharest for the May 30, 1990, Vrancea event with good accuracy for microzonation purposes. The frequency window considered in the computations extends up to 1 Hz and allows us the modeling of the seismic input

appropriate for 10-storey and higher buildings. This is in agreement with the observed predominant period, 1.0–1.5 s, of the ground motion induced by the major Vrancea subcrustal earthquakes in Bucharest. Even if a relatively simple local structure and seismic source have been considered, the matching between records and the computed signals is at a satisfactory level for seismic engineering. The comparison observed-synthetic signals accounts for the shape, peak ground acceleration (PGA), duration, frequency content, and response spectra (Sa) (computed with 5% and 10% of critical damping). By considering the two dominant scenario earthquakes for Vrancea, MOLDOVEANU and PANZA (2001) analyzed the source influence on the local response in order to define generally valid ground motion parameters to be used in the seismic hazard estimations. This was done along an array of equally spaced sites on a profile, NE-SW oriented, which crosses the central part of the city. The source has its own (detectable) contribution to the ground motion and its effects on the local response in Bucharest are quite stable on the transversal component (T), while the radial (R) and vertical (V) components are sensitive to the scenario earthquake. Although the strongest local effects affect the T component, both observed and synthetic, a complete determination of the seismic input for the built environment requires the knowledge of all three components of motion (R, V, T).

The numerical modeling performed to date demonstrates that standard convolutive approaches are not reliable and that detailed numerical schemes are required to obtain realistic estimates of the seismic amplification/response due to site effects. These kinds of computations applied for the Bucharest site supply synthetic results consistent with the observations (e.g., MOLDOVEANU *et al.*, 2000; MOLDOVEANU and PANZA, 2001; CIOFLAN *et al.*, this issue).

8. Characterization of Bucharest Building Stock

The evolution of the building stock (construction rate) in Bucharest and in Romania can be divided into three time intervals that are correlated to the economic and political changes at the national level: (a) before 1970 (moderate), (b) from 1970 to 1990 (very high), and (c) after 1990 (low, both for civil and industrial purposes). The building stock in Bucharest was constructed according to the Romanian ruling seismic code that was subjected to modifications (updated) in 1941, 1964, 1971, 1978, 1992 and 1996. Obviously, the seismic risk of a structure strongly depends on its height, design and site location. Table 1 presents the distribution of the tall buildings in Bucharest by period of construction and number of stories, as defined by the data supplied by the 1992 census (LUNGU *et al.*, 1999b).

The dynamic response of a structure is characterized by its fundamental period of vibration. During recent decades the building construction in Romania was generally based on standard projects. Table 2 presents the fixed-base period (i.e., the period of the structure without the fill-in walls) of the various types of standard structures in

Table 1

Distribution of tall buildings censored in 1992 in Bucharest, grouped by period of construction and number of stories (LUNGU et al., 1999)

Stories	< 1945	1945 – 1963	1964 – 1970	1971 – 1977	1978 – 1990	1990 – 1992
9	89	104	45	88	1550	21
10	17	77	137	51	177	4
11	63	70	447	830	1063	5
> 11	9	34	7	87	72	1
Total	486	434	657	1091	2970	36

Table 2

Fixed-base period (structure without in-fill walls) and the relative frequency of various building structures in Bucharest reported by the Typified Building Design Institute (IPCT) (LUNGU and CORNEA, 1988)

IPB-code of the structure	Number of stories	Structure type (1)	Period T, s		Estimated number of:	
			Transverse	Longitudinal	Staircases	Apartments
D3g	5	Shear-wall	0.17	0.23	30	600
D3f	5		0.19	0.31	5	100
P4m	5	Prefabricated	0.14	0.16	106	2120
P4r	5	shear-wall	0.14	0.15	18	360
P4o	5		0.13	0.15	78	1560
P6b	9		0.30	0.39	225	7000
P11f	9	Shear-wall	0.36	0.44	66	2400
P11e	9		0.44	0.50	99	3200
D13b	9		0.51	0.60	22	800
D13b	11		0.65	0.83	27	1200
D11d	11		0.37	0.58	21	660
G	9	Shear-wall	0.36		–	4000

[1] Including the ground floor Total: 24000 apt.

Bucharest, according to the data of the Romanian Institute for Building Design (IPCT) (LUNGU and CORNEA, 1988). The fixed-base period is larger than the actual period of the building and the post-earthquake period exceed the pre-earthquake period.

The main structural types of buildings used in Romania are designed for a peak ground acceleration (PGA) that corresponds to the 7^{th} or the 8^{th} degree on the MSK-64 macroseismic intensity scale. Table 3 presents the fundamental period, both longitudinal and transversal, of the main structural types used in Romania, constructed before 1990. The maximum MSK design intensity considered and the number of structure storeys are also indicated. The buildings are grouped according to the IPCT code of the structure (LUNGU and CORNEA, 1988).

Table 3

Fundamental period (longitudinal and transversal) of the main structural types used in Romania, according to the data of the Typified Building Design Institute (IPCT). The maximum MSK intensity considered, the number of stories and the IPCT code of the structure are also reported. (LUNGU and CORNEA, 1988)

IPCT – code of structure	MSK seismic Intensity	Number of stories (1)	Type of structure	Period T, s	
				Longit.	Transv.
No. 770	7	5	Prefabricated shear-wall	0.13	0.15
No. 1402	8	9	(dense walls)	0.38	0.33
				0.44	0.37
				0.44	0.30
No.1340	7	5	Prefabricated shear-wall (rare walls)	0.15	0.15
No.1403	7	5	Shear-wall,	0.22	0.20
			With prefabricated slabs	0.19	0.20
No.1406	7	9		0.67	0.62
No.1421	7	5	Dual structure	0.26	0.23
No.1422	8	5	(frame and shear-wall)	0.21	0.21
No.1426	8	9		0.56	0.38
No.1377/a	8	5	Frame	0.54	0.46
				0.53	0.47
				0.50	0.49
No.1410	7	9	Frame	0.90	0.82
No.1378/a	7	9	Frame	0.86	0.75
				0.92	0.90
				0.90	0.88
No. –	7.5	5	Frame,	0.47	0.45
			With shear-walled columns	0.45	0.45
				0.44	0.43
				0.42	0.46
No. –	7.5	9	Frame,	0.68	0.70
			With shear-wall columns	0.72	0.70
				0.70	0.69
				0.65	0.63
No.1376	7	3	Columns and	0.57	0.55
No.1376	7	4	flat slabs	0.47	0.48

[1] Including ground floor.

9. Romanian Code of Practice and Eurocode

The national code for the antiseismic design of the buildings is represented by the Romanian Code of Practice (P100). This code was revised in 1992 and 1996 and it includes the latest experience and concepts in seismic design. The European prestandard in the field is represented by Eurocode 8 (EC8) which was published in 1998. Both P100 and EC8 are based on the capacity design procedure. They provide the rules for the modification of seismic action effects in order to direct the potential

plastic hinge at the base of the walls and to avoid brittle fracture in shear. The elastic response spectra considered in the framework of the two distinctive codes are presented in Figure 8.

The regulations of the codes EC8 and P100 are similar, still in practice they imply different design requirements for the same structure. For illustrating them, PASCU and MUNTEANU (1999a) considered the case of a regular multistory frame structure and accomplished a comparison of the structural design and detailing provisions included in EC8 and P100, respectively. The major differences between the two structures are: (1) the base shear force value is 20% larger in P100 than in EC8; (2) the interstorey drift limit is 230% more restrictive for the P100 designed frames in comparison to those of the EC8; (3) the more severe interstorey drift limitation and the larger base shear force value require the cross-sectional area of the members of the P100 structure to be up to 200% larger than the homologue EC8-designed; (4) the P100-designed beams require larger (by about 10–25%) flexural reinforcing ratios than EC8-designed ones; (5) the EC8 shear reinforcing ratios are larger by 10–30% than those of the P100; (6) the EC8-designed columns have larger (by 20–40%) reinforcing ratios than the homologue P100-designed; (7) the EC8 shear reinforcement ratios of the columns become up to 300% larger than those of the corresponding P100.

According to the regulations from *STAS 11100/1-91* and *SR 11100/1-93*, the present zonation map of the Romanian territory assigns to Bucharest area an 8^{th} degree of intensity (MSK). The past seismic design practice required the increase by at least one degree of intensity for any essential facility in the city, i.e., buildings and

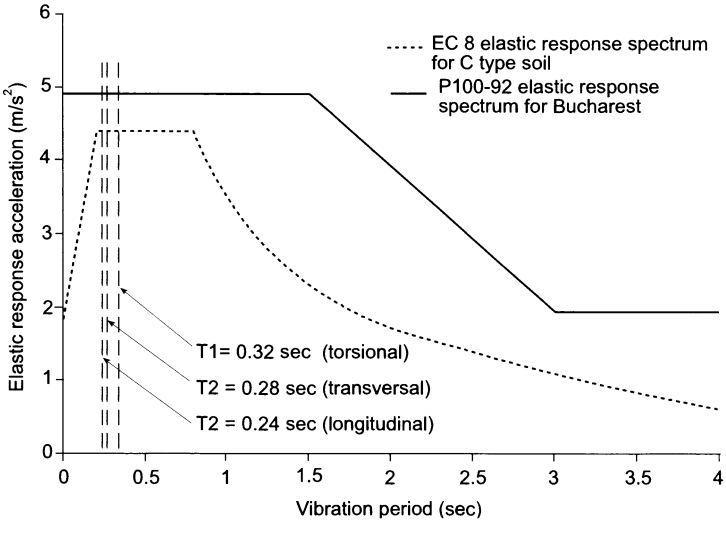

Figure 8
Elastic design spectra considered by EC8 and P100.

structures that are intended to remain operational in case of an extreme intensity earthquake (LUNGU *et al.*, 1999b). The requirement of a 9th degree intensity in Bucharest corresponds to a PGA of 0.32 g (MSK-64 macroseismic intensity converted into PGA).

10. Conclusion

The important destruction and the large number of victims experienced in Bucharest during the extreme 1940 and 1977 Vrancea earthquakes require vigorous investigations to reduce life and economic losses. The assessment and mitigation of earthquake risk are particularly important in the Romanian capital since major investments and vital lifeline systems are concentrated in this seismically dangerous area. Therefore, the next large Vrancea earthquake will inflict serious economic and social consequences, unless comprehensive action is timely taken.

The earthquake effects on the ground surface are defined by the seismic zoning and microzoning, and by the antiseismic design parameters, respectively. Generally speaking, a detailed urban planning rests on the proper knowledge of: (1) regional geology and tectonics, (2) regional seismicity and earthquake catalogues, (3) seismic ground motion and zoning, (4) faulting and permanent ground deformations, and (5) engineering aspects of disastrous earthquakes. The investigations of the major previous events supply the information regarding (a) the damage distribution on different structural types, and (b) the social and economic implications of earthquakes in the region. This allows us the evaluation of the adequacy between the existing building codes and regulations, on one side, and the geological regional and local site conditions, on the other side.

The seismic zonation of Romania and a first-order microzonation of Bucharest have been performed using the existing database on structural and geotechnical parameters. The available information is still not satisfactory for a detailed assessment of the site effects in the entire Romanian territory. The new studies concerning direct instrumental observation and interpretation of the local effects on the soft soil environment in the city, on one hand, and the realistic numerical modeling which considers the contribution of the source, travel path and local site condition, tested against the recorded seismograms, on the other hand, update and improve the database necessary for a detailed microzoning map of Bucharest. The microzoning map proposed by NCST after the evaluation of the effects inflicted on Bucharest by the March 4, 1977 ($M_w = 7.4$) Vrancea event, and expressed in terms of expected accelerations, displays a concentric distribution with the maximum value of 0.4 g localized in the central part of the metropolitan area (Fig. 7). The geological subsoil condition and the instrumental observations of the 1986 ($M_w = 7.2$) and 1990 ($M_w = 6.9$) Vrancea earthquakes do not correlate with this distribution. CIOFLAN *et al.* (this issue) propose an improvement of the microzoning map of the capital. The

city area is divided into five zones (Fig. 9) on the basis of: (a) the local lithological data, (b) the epicentral distance variations not larger than 3 km, and (c) the recorded seismograms available for both 1986 and 1990 events. No zone is indicated for the northwestern part of the city since no instrumental recorded signals are available here. The numerical simulations (in the frequency range 0.05–1.0 Hz) have been extended to all regions of the city where similar geological structures are present. Each zone is assigned the representative response spectra that, together with the recorded and/or simulated seismograms, give a more adequate evaluation of the seismic site response than those expressed exclusively in terms of expected PGA. Even if the NCST (1977) and the CIOFLAN *et al.* (this issue) maps are expressed in terms of different parameters used by civil engineering, the main observation is that the concentric distribution of

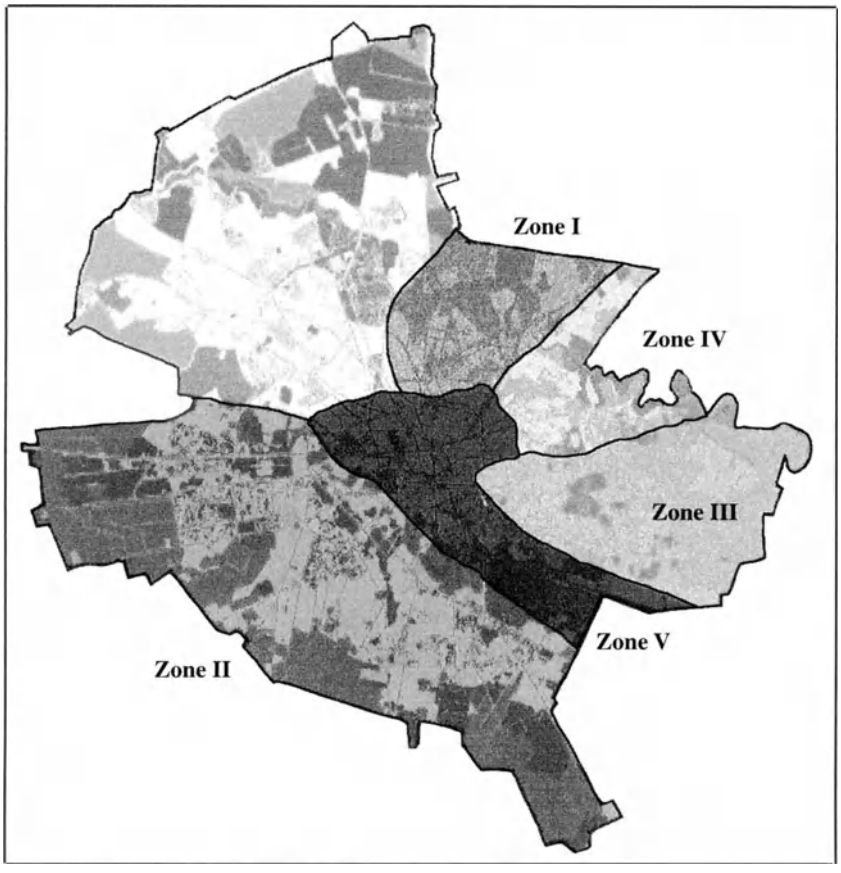

Figure 9
Preliminary zoning map of Bucharest (CIOFLAN *et al.*, this issue). The five zones have been defined on the basis of: (a) the local lithological data, (b) the epicentral distance variations no larger than 3 km, and (c) the recorded seismograms available for both the 1986 and 1990 events.

the expected local effects visible in the NCST (1977) map and not consistent with the available observations is not present on the map shown in Figure 9.

The Romanian P100 seismic code includes the latest experience and concepts in seismic design and its regulations have important similarities to the EC8. Damage to the built environment caused by earthquakes is known to depend both on the ground motion characteristics (amplitude, frequency distribution and shaking duration) and on the characteristics of engineering structures (resonance period of the structures in relation to subsoil local transfer function). Of course, the existing building infrastructure must be retrofitted with advanced knowledge, materials, and technologies related to the peculiarities of the Romanian building stock.

Future efforts in Romania, as elsewhere, must be focused on developing increasingly reliable microzonation maps for earthquake ground shaking in all urban areas where the seismic risk is moderate and high. These studies should be focused on: (a) the compilation of the available topographical, geological, geotechnical data in the form of maps (1:10,000 – 1:25,000 scale) and a GIS database, (b) the collection of seismic records (e.g., strong motion and seismic noise) using a dense network of instruments deployed in the target area, (c) the application of the numerical techniques for the modeling of the seismic ground motion, and (d) the evaluation of the building stock vulnerability taking into account the advanced knowledge, materials, technologies and peculiarities of the Romanian conditions.

The optimal exploitation of the realistic estimation of the site effects, based on the scenario-like modeling approaches used to predict the seismic strong motion and limited to technical problems is certainly not a simple task. In fact, the results of the microzoning are used by end users, such as local authorities, city planners, land-use specialists and civil engineers, whose background is very different and for whom the recommendations must be clear and sound.

Acknowledgements

The authors have been supported by the UNESCO-IUGS-IGCP project 414 "Realistic Modelling of Seismic Input for Megacities and Large Urban Areas" and NATO Science for Peace Project 972266 "Impact of Vrancea earthquakes on the security of Bucharest and other adjacent urban areas" (Ground motion modeling and intermediate-term prediction), with the contribution of the Italian Ministry of Foreign Affairs (MAE), Directorate General for Cultural Promotion and Cooperation.

References

ALTERMAN, Z. S. and Karal, F. C. (1968), *Propagation of Elastic Waves in Layered Media by Finite Difference Methods*, Bull. Seismol. Soc. Am. *58*, 367–398.

AMBRASEYS, N. N. (1977), *Long-period Effects in the Romanian Earthquake of March 1977*, Nature *268*, 324–325.

BARD, P. Y., *Effects of Surface Geology on Ground Motion: Recent Results and Remaining Issues.* In *Proc. 10th European Conf. Earthquake Engineering* (ed. Duma, G.) (A.A.Balkema, Rotterdam 1995) pp. 305–323.

BONJER, K-P., ONCESCU, M.-C., DRIAD, L., and RIZESCU, M., *A Note on Empirical Site Response in Bucharest, Romania.* In *Vrancea Earthquakes: Tectonics, Hazard, and Risk Mitigation*, (eds. Wenzel, F., Lungu, D., and Novak, O.) (Kluwer Academic Publ. 1999) pp. 149–162.

BOORE, D. M., *Finite-difference Methods for Seismic Waves Propagation in Heterogeneous Materials.* In *Methods in Computational Physics*, Vol. 11 (ed. Bolt, B.A.) (New York, Academic Press 1972) pp. 1–37.

CIOCIRDEL, R., TITARU, E., and CISMIGIU, A. (1964), *Seismic Microzoning of Bucharest City*, Arh. IGP, Bucharest (in Romanian).

CIOFLAN, C. O., APOSTOL, B., MOLDOVEANU, C. L., PANZA, G. F., and MARMUREANU, G. (2004), *Deterministic Approach for the Seismic Microzonation of Bucharest*, Pure Appl. Geophys. 161, Nos. 5/6, 2004.

FÄH, D., SUHADOLC, P., MUELLER, St., and PANZA, G. F. (1994), *A Hybrid Method for the Estimation of the Ground Motion in Sedimentary Basins: Quantitative Modelling for Mexico City*, Bull. Seismol. Soc. Am. *84* (2), 383–399.

FLORSCH, N., FÄH, D., SUHADOLC, P., and Panza, G. F. (1991), *Complete Synthetic Seismograms for High-frequency Multimode SH Waves*, Pure Appl. Geophys. *136*, 529–560.

FUCHS, K., BONJER, K. P., BOCK, G., RADU, C., ENESCU, D., JIANU, D., NOURESCU, A., MERKLER, G., MOLDOVEANU, T., and Tudorache, G. (1978), *The Romanian Earthquake of March 4, 1977. II. Aftershocks and Migration of Seismic Activity*, Tectonophysics *53*, 225–247.

GHICA, S. (1953), *Geologic Microzonation of Bucharest City*, Arh. Deo. Geol., MMPG, Bucharest (in Romanian).

GIRBACEA, R. and FRISH, W. (1998), *Slab in the Wrong Place: Lower Lithospheric Mantle Delamination in the Last Stage of the Eastern Carpathian Subduction Retreat*, Geology *26*, 611–614.

KELLY, K. R., WARD, R. W., TREITEL, S., and ALFORD, R. M., (1976), *Synthetic Seismograms: A Finite-difference Approach*, Geophysics *41*, 2–27.

LITEANU, G. (1951), *Geology of the City of Bucharest*, Technical Studies, Serie E, Hydrogeology *1* (in Romanian).

LUNGU, D. and CORNEA, T. (1988), *Ground Motion Parameters for the Design of Earthquake Resistent Structures in the City of Bucharest*, Institute Proiect-Bucharest (in Romanian).

LUNGU, D. M., SCHERER, R. J., ZSOHAR, M., and COMAN, O. (1994) *On the Phenomenon of Long Periods of Ground Vibration During the 1990, 1986 and 1977 Earthquake Records from Vrancea Source.* In *Earthquake Resistance Construction and Design* 1 (eds. Savidis, S. A., Balkema, A. A.) (Rotterdam 1994) pp. 51–59.

LUNGU, D., ALDEA, A., MOLDOVEANU, T.,CIUGUDEAN, V., and STEFANICA, M. (1999a), *Near-surface Geology and Dynamic Properties of Soil Layers in Bucharest.* In *Vrancea Earthquakes: Tectonics, Hazard, and Risk Mitigation* (eds. Wenzel, F., Lungu, D., Novak, O.) (Kluwer Academic Publ. 1999a) pp. 137–148.

LUNGU, D., DEMETRIU, S., and ARION, C. (1999b), *Seismic Vulnerability of Buildings Exposed to Vrancea Earthquakes in Romania.* In *Vrancea Earthquakes: Tectonics, Hazard, and Risk Mitigation* (eds. Wenzel, F., Lungu, D., Novak, O.) (Kluwer Academic Publ. 1999) pp. 215–224.

MANDRESCU, N. (1972), *Experimental Researchs on Seismic Microzoning*, St. Cerc. Geol. Geogr. Geofiz. *10*(2), 103–116 (in Romanian).

MANDRESCU, N. (1978), *The Vrancea Earthquake of March 4, 1977 and the Seismic Microzoning of Bucharest.* In *Proc. Int. Conf. Microzonation*, vol. 1 (San Francisco 1978), pp. 339–411.

MANDRESCU, N., and RADULIAN, M. (1999), *Seismic Microzoning of Bucharest (Romania): A Critical Review.* In *Vrancea Earthquakes: Tectonics, Hazard, and Risk Mitigation* (eds. Wenzel, F., Lungu, D., Novak, O.) (Kluwer Academic Publ. 1999) pp. 109–122.

MEDVEDEV, S. V. (1962), *Seismic Engineering*, Moscow.

MOLDOVEANU, C. L. and PANZA, G. F. (1999), *Modelling for Microzonation Purposes of the Seismic Ground Motion in Bucharest, Due to the Vrancea Earthquake of May 30, 1990.* In *Vrancea Earthquakes: Tectonics, Hazard, and Risk Mitigation* (eds. Wenzel, F., Lungu, D., Novak, O.) (Kluwer Academic Publ. 1999) pp. 85–97.

MOLDOVEANU, C. L., and MARMUREANU, G., PANZA, G. F., and Vaccari, F. (2000), *Estimation of Site Effects in Bucharest Caused by the May 30–31, 1990, Vrancea seismic Events*, Pure Appl. Geophys. *157*, 249–267.

MOLDOVEANU, C. L., and PANZA, G. F. (2001), *Vrancea Source Influence on Local Seismic Response in Bucharest*, Pure Appl. Geophys. *158*, 2407–2429.

ONCESCU, M. C. (1984), *Deep Structure of Vrancea Region, Romania, Inferred from the Simultaneous Inversion for Hypocenters and 3-D Velocity Structure*, Ann. Geophys. *2*, 23–28.

ONCESCU, M. C. and BONJER, K. P. (1997), *A Note on the Depth Recurrence and Strain Release of Large Vrancea Earthquakes*, Tectonophysics *272*, 291–302.

ONCESCU, M. C., MARZA, V. I., RIZESCU, M., and POPA, M. (1999), *The Romanian Earthquake Catalogue Between 984–1996*. In *Vrancea Earthquakes: Tectonics, Hazard, and Risk Mitigation* (eds. Wenzel, F., Lungu, D., Novak, O.) (Kluwer Academic Publ. 1999) pp. 43–48.

PANZA, G. F. (1985), *Synthetic Seismograms: The Rayleigh Waves Modal Summation*, J. Geophys. *58*, 125–145.

PANZA, G. F., ROMANELLI, F., and Vaccari, F. (2001). *Seismic Wave Propagation in Laterally Heterogeneous Anelastic Eedia: Theory and Applications to Seismic Zonation*, Advanced in Geophysics *43*, 1–95.

PASCU, P. and MUNTEANU, M. (1999a), *Eurocode versus Romanian Seismic Practice. Case Study of an Eight-storey RC Frame Building*, In *Vrancea Earthquakes: Tectonics, Hazard, and Risk Mitigation* (eds. Wenzel, F., Lungu, D., Novak, O.) (Kluwer Academic Publ. 1999) pp. 233–240.

PURCARU, G. (1979), *The Vrancea, Romania, Earthquake of March 4, 1977 – A Quite Successful Prediction*, Phys. Earth. Planet. Inter. *18*, 274–287.

RADU, C. (1979), *Catalogul cutremurelor puternice produse pe teritoriul Romaniei. Partea I: inainte de 1901; Partea II – 1901 – 1979*, In *Cercetari Seismologice aspra Cutremurului din 4 Martie 1977* (eds. Cornea, I., Radu, C.) (CSEN Centrul de Fisica Pamantului si Seismologie, Bucuresti) pp. 723–752 (in Romanian).

RADULIAN, M., VACCARI, F., MANDRESCU, N., PANZA, G. F., and MOLDOVEANU, C. L. (2000a), *Seismic Hazard for Romania: Deterministic Approach*, Pure Appl. Geophys. *157*, 221–247.

RADULIAN, M., MANDRESCU, N., PANZA, G. F., POPESCU, E, and UTALE, A. (2000b), *Characterization of Seismogenic Zones of Romania*, Pure Appl. Geophys. *157*, 57–77.

ROJAHN, N. N. (1984), *The Interrelationship Between the Ground Motion Spectra, Building Period, Number of Storeys and Maximum Interstory Drift: A Basis for Evaluating Earthquake Damage Potential*, In *Critical Aspects of Earthquake Ground Motion and Building Damage Potential* (eds. Rojahn, C., Sharpe, R. L.) (Redwood City 1984) pp. 89–94.

ROMANELLI, F., BING, Z., VACCARI, F., and PANZA, G. F., (1996), *Analytical Computations of Reflection and Transmission Coupling Coefficients for Love Waves*, Geophys. J. Int. *125*, 132–138.

SANDI, H., and PELEA, V. (1982), *Engineering Study on Ground Motion*, In *Romanian Earthquake of March 4, 1977* (ed. Balan, St.) (Acad. Publ. Houses Bucharest) pp. 137–221 (in Romanian).

STEFANESCU, G. (1901), *Earthquakes in Romania in 1391 Time Interval, from 455 until 1878*, An. Acad. Rom. *II*, XXIV (in Romanian).

TAVERA, I. (1991), *Etude des mecanismes focaux de gros seismes at seismicite' dans la region de Vrancea-Romania* (*Raport stage DEA de geophysique interne*) (Institut de Physique du Globe, Universite' de Paris).

VACCARI, F., GREGERSEN, S., FURLAN, M., and PANZA, G. F. (1989), *Synthetics Seismograms in Laterally Heterogeneous, Aanelastic Media by Modal Summation of the P-SV Waves*, Geophys. J. Int. *99*, 285–295.

WENZEL, F., LORENZ, F. P., SPERNER, B., and ONCESCU, M. C. (1999) *Seismotectonics of the Romanian Vrancea area*. In *Vrancea Earthquakes: Tectonics, Hazard, and Risk Mitigation* (eds. Wenzel, F., Lungu, D., Novak, O.) (Kluwer Academic Publ. 1999) pp. 15–25.

(Received February 18, 2002, accepted January 15, 2003)

Pure appl. geophys. 161 (2004) 1149–1164
0033–4553/04/061149–16
DOI 10.1007/s00024-003-2496-8

Pure and Applied Geophysics

Deterministic Approach for the Seismic Microzonation of Bucharest

C. O. CIOFLAN[1], B. F. APOSTOL[1], C. L. MOLDOVEANU[1,2], G. F. PANZA[3,4], and GH. MARMUREANU[1]

Abstract—The mapping of the seismic ground motion in Bucharest, due to the strong Vrancea earthquakes is carried out using a complex hybrid waveform modeling method which combines the modal summation technique, valid for laterally homogeneous anelastic media, with finite-differences technique, and optimizes the advantages of both methods. For recent earthquakes, it is possible to validate the modeling by comparing the synthetic seismograms with the records. We consider for our computations the frequency range from 0.05 to 1.0 Hz and control the synthetic signals against the accelerograms of the Magurele station, low-pass filtered with a cut-off frequency of 1.0 Hz of the 3 last major strong ($M_w > 6$) Vrancea earthquakes. Using the hybrid method with a double-couple seismic source approximation, scaled for the source dimensions and relatively simple regional (bedrock) and local structure models, we succeeded in reproducing the recorded ground motion in Bucharest at a satisfactory level for seismic engineering. Extending the modeling to the entire territory of the Bucharest area, we construct a new seismic microzonation map, where five different zones are identified by their characteristic response spectra.

Key words: Microzonation, synthetic seismograms, Bucharest, Vrancea.

1. Introduction

The historical seismic activity of the Romanian territory is known since the Roman times (the 1st century b.c.). All major events originate at intermediate depth in the Vrancea region which is localized at the arched bending of the Carpathian Mountains. In Romania, the first instrumental records became available after 1934 when the first seismographic stations started to operate in the country. Bucharest City is located on a relatively stable platform with a single minor fault (Tg. Fierbinti-Urziceni) at about 40 km N from Bucharest. The seismicity of the region is relatively

[1] National Institute for Earth Physics, 12, Calugareni Str, P.O. Box MG-2, 769191 Magurele, Bucharest, Romania. E-mails: cioflan@infp.ro; apostol@infp.ro; marmur@infp.ro

[2] Department of Earth Sciences, Univ. of Parma, Parco Area delle Scienze 157 A, 43100, Parma, Italy. E-mail: cmold@ipruniv.cce.unipr.it

[3] Department of Earth Sciences, Univ. of Trieste, 4, Via Weiss, I-34127 Trieste, Italy.

[4] The Abdus Salam International Center for Theoretical Physics (ICTP), SAND Group, Trieste, Italy. E-mail: panza@dst.units.it

low: about 50 events in the last century, with a medium magnitude $M_w \approx 2.7$. For the event with maximum magnitude in the area ($M_w = 5.0$, depth of the source ≈ 42 km (Romplus catalog) there is no damage reported. Bucharest is the largest cultural and economic center of Romania exposed to seismic risk due to the strong Vrancea earthquakes. It has an urbanized area of 228 km^2 and 2.53 millions inhabitants that represent about 10% of the country's population. During the last century the City was affected by three Vrancea earthquakes with moment magnitude $M_w > 7$ which occurred in 1940, 1977 and 1986. The most severe effects on the national territory were inflicted by the March 4, 1977 event, $M_w = 7.4$. Victims of this event totalled 1,574, out of which 1,424 were registered in Bucharest, where 32 tall buildings collapsed. The World Bank's loss estimation due to the 1977 earthquake (Report No.P.-2240-RO, 1978) indicates a total loss of 2.05 Billion US dollars of which more than 2/3 were in Bucharest, where half of the total loss was accumulated from building damage. The most controversial question in the definition of the standards to be used in the evaluation of the regional or local seismic hazard regards the criteria and methods to be employed should they be of a probabilistic or deterministic method? For solving this dilemma studies carried out for some of the most recent strong earthquakes (e.g. the 1977 Vrancea and 1985 Mihoacan earthquakes) have proved to be important sources of basic knowledge and have acted as a catalyst in the use of zoning in seismic risk management. The post-earthquakes studies (e.g., PANZA *et al.*, 1996) have shown that earthquake destruction is the result of the interaction of three complex systems: 1) the solid earth system made up of a) the seismic source, b) the propagation of the seismic waves, c) the geometry and physical conditions of the local geology; 2) the anthropised system, whose most important feature in this context is the quality of construction (buildings, bridges, dams, pipelines etc.); 3) the social, economic and political system which governs the use and development of a settlement before it is struck by an earthquake.

The seismic hazard at regional and local scale for Bucharest has been the object of many studies, based mainly on probabilistic and/or traditional deterministic methods that make use of the large quantity of macroseismic information available, since the strong motion records are rather scarce. This study is a deterministic approach based on the computation of realistic synthetic seismograms using the hybrid method (FÄH *et al.*, 1990, 1993; FÄH, 1992). The method allows us to estimate the parameters of the seismic motion at any site of interest for given seismic sources and geological/geotechnical properties of the propagation media.

2. *Characteristics of Vrancea Region*

Bucharest City is exposed to the seismic hazard generated by the intermediate-depth events originating in the Vrancea region which is located at the intersection of four tectonic structures: East-European Plate, Moesian, Black Sea and Intra-Alpine

(Pannonian-Carpathian) subplates (SOLOVIEV *et al.*, 2000). The statistics show that in this seismic region up to five shocks with $M_w \geq 6.5$ occur each century (RADULIAN *et al.*, 2000 B). Their effects are felt over a large territory, from Central Europe to Moscow and from Greece to Scandinavia.

The focal volume in which the intermediate-depth events occur is restricted to a parallelepiped 100-km long, 40-km wide, with a vertical extension from 70 km to 180 km depth (MOLDOVEANU *et al.*, 2000). The crustal events are also present in the Vrancea region and the epicentral depths do not exceed 40 km. The seismic activity is concentrated within an epicentral area of about 3000 km^2, NE-SW oriented and delimited by the rectangle of coordinates: 45.5°–45.9° N, and 26.4°–26.9° E.

Several models have been proposed to explain the main tectonic aspects in Vrancea that consider a paleo- (MCKENZIE 1972; ONCESCU and TRIFU, 1987) or an active subduction (ENESCU and ENESCU 1993), a pure shear faulting or tensile faulting, etc. (ISMAIL-ZADEH *et al.*, 2000).

The strong earthquakes originating in the Vrancea region during the last century caused important economic damage and loss of human lives in Romania and in the neighboring countries. These events are: November 10, 1940 ($M_w = 7.7$; $M_0 = 5.1 \cdot 10^{20}$ Nm); March 4, 1977 ($M_w = 7.4$; $M_0 = 1.5 \cdot 10^{20}$ Nm) August 30, 1986 ($M_w = 7.1$; $M_0 = 6 \cdot 10^{19}$ Nm); May 30 and 31 ($M_w = 6.9$; $M_0 = 3.8 \cdot 10^{19}$ Nm, respectively $M_w = 6.4$; $M_0 = 3.8 \cdot 10^{18}$ Nm).

The typical focal mechanism of strong Vrancea earthquakes ($M_w > 6$) is a reverse faulting, with principal T axes almost vertical and P axes horizontal (RADULIAN *et al.*, 2000a). The fault plane orientation can be grouped in two main types:

— fault plane NE-SW oriented and P axes perpendicular to the mountain arc (class A);

— fault plane NW-SE oriented with P axes parallel to the mountain arc (class B).

3. Soil Characteristics in the Bucharest Area

Bucharest City is located in the central part of the Moesian subplate (age: Precambrian and Paleozoic) in the Romanian Plain. After a Cretaceous and a Miocene deposit (with the top at roundly 1000 m of depth) a Pliocene shallow water deposit (~ 700-m thick) was settled. The surface geology consists mainly of Quaternary alluvial deposits. Later loess covered these deposits, and rivers carved the present landscape. From the surface: —seven lithological formations are identified (MANDRESCU, 1972): (i)—Backfill (thickness h up to 3 m); (ii)—Sandy-clay superior deposits (loess and sand, $h = 3$–16 m) from Holocene, and the others from Pleistocene; (iii)—"Colentina" gravel (gravel and sand, $h = 2$–20 m); (iv)—Intermediate cohesive deposits of lacustral origin (80% clay and some sand, $h = 0$–25 m); (v)—"Mostistea" banks of sands (mainly sand, sometimes lenses of clay included, $h = 10$–15 m); (vi)—Lacustral deposits from clay and sands ($h = 10$–

60 m) and (vii)—"Fratesti" gravel (gravel and sands separated by clay, $h = 100$–180 m).

Strong lateral variations in depth and thickness of these 7 layers can be observed throughout Bucharest. A considerable number of geotechnical drillings are available for the central part of the city. The majority of these holes penetrate the upper 30–40 m, and some of them extend to depths between 70 m and 180 m (WENZEL *et al.*, 2000). An important role in the evaluation of the site effects in Bucharest must be associated with the numerous aquifers underground in the city. There are three main aquifer systems: (i) "Colentina" located about 8 m deep, (ii) "Mostistea" situated at about 25–30 m depth, and (iii) "Fratesti"—the deepest aquifer consisting of three layers located between 120 and 200 m deep.

The available soil data indicate that the surface geology on the eastern side of Bucharest comprises a succession of clay and sand layers. The corresponding average shear-wave velocity has values lower than 380 m/s in the uppermost 200 m of depth. Due to this velocity structure dangerous amplifications in the long-period range could be expected in this city area in case of strong Vrancea earthquakes.

The eastern, southern, and center of the city are covered by predominantly clayey soil profiles and exhibit large control periods of the response spectra, with the corner period T_c ranging from 1.1–1.5 s. The northern part of Bucharest is covered by predominantly sandy soil profiles. Here the medium control period of the response spectra spans the interval $T_c = 0.6$–1.0 s. The geometry, NE-SW oriented, of the T_c isolines corresponding to the 1986 and 1990 Vrancea earthquakes is quite similar, even if the T_c values for 1986 Vrancea event, $M_w = 7.1$ are about 1.5 times larger than the T_c values for the 1990 Vrancea event, $M_w = 6.9$ (LUNGU *et al.*, 2000).

4. Deterministic Seismic Microzonation of Bucharest

The simulation of the seismic strong motion is performed using a hybrid method that combines the modal summation technique (PANZA, 1985, 1993; VACCARI *et al.*; 1989; ROMANELLI *et al.*, 1996; PANZA *et al.*, 2001) and the finite-difference technique (VIRIEUX, 1984, 1986). The modal summation allows a description of the seismic waves propagation through an anelastic, horizontally-layered structure containing the seismic source and the path Vrancea-Bucharest (bedrock structure). Further, the finite-difference technique is used to describe the seismic ground motion of Bucharest sedimentary cover, described as a stack of anelastic layers with lateral heterogeneities (local structure). The input data are the earthquake scenario and the geological structures through which the seismic waves propagate from the source to the sites of interest. The earthquake scenario is described as a point double-couple source and the relevant fault plane solution is taken from CMT catalogue (Harvard University and/or ROMPLUS catalogue). The source parameters we consider in the modeling are given in Table 1.

Table 1

Seismic source parameters used for the numerical simulations

Quake	Hypocenters			Mechanism solutions			M_w	M_0
M/D/Y	Lat.	Long.	Depth	Strike	Dip	Rake		
5/30/90	26.89	45.83	74 km	236	63	101	6.9	$3.0 \cdot 10^{19}$ Nm
5/31/90	26.91	45.85	87 km	308	71	97	6.4	$3.8 \cdot 10^{18}$ Nm
8/30/86	26.49	45.52	131 km	227	65	104	7.1	$6.0 \cdot 10^{19}$ Nm

The bedrock structure represents an averaged regional model, modified from RADULIAN *et al.* (2000-b) to take into account recent tomographic results (MARTIN *et al.*, 2002). Figure 1 displays the variations with depth of density, phase velocities and quality factors for *P* and *S* waves in the upper 300 km of the bedrock model, below this depth an average continental model is used. The local structures considered are representative of the profiles whose position is shown in Figure 2.

The S_1 and S_2 cross sections are modeled with horizontal layers of sediments; the minimum shear-wave velocities are 367 m/s for S_1, 420 m/s for S_2 while the corresponding quality factor is 30. The S_1 structure has a low velocity channel (for both *P* and *S* waves) between 1.75 km and 3.25 km of depth. The structure S_2 has two channels (for both *P* and *S* waves) in the depth intervals 1.82–2.02 km and 2.2–2.6 km. For the S_3 cross section a more detailed structural model is used. Nine tilted (by about 4%) layers form it. Inside the first three, water–bearing layers of sediments and the velocity varies laterally within the limits given in Figure 3. The smallest shear-wave velocity in this model is 163 m/s and Q_s is 11. The unconsolidated sediments consist of loess-like deposits, dusty clays, sand with gravel (Mostistea sands, Colentina gravel), sand, clayey marls, gravel and sands with thin lignite lenses

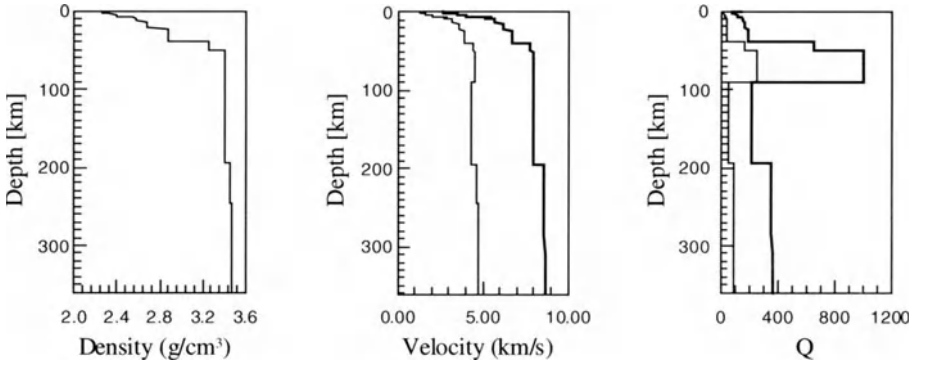

Figure 1

The bedrock structure: variation with depth of the density, V_s and V_p and the corresponding quality factors.

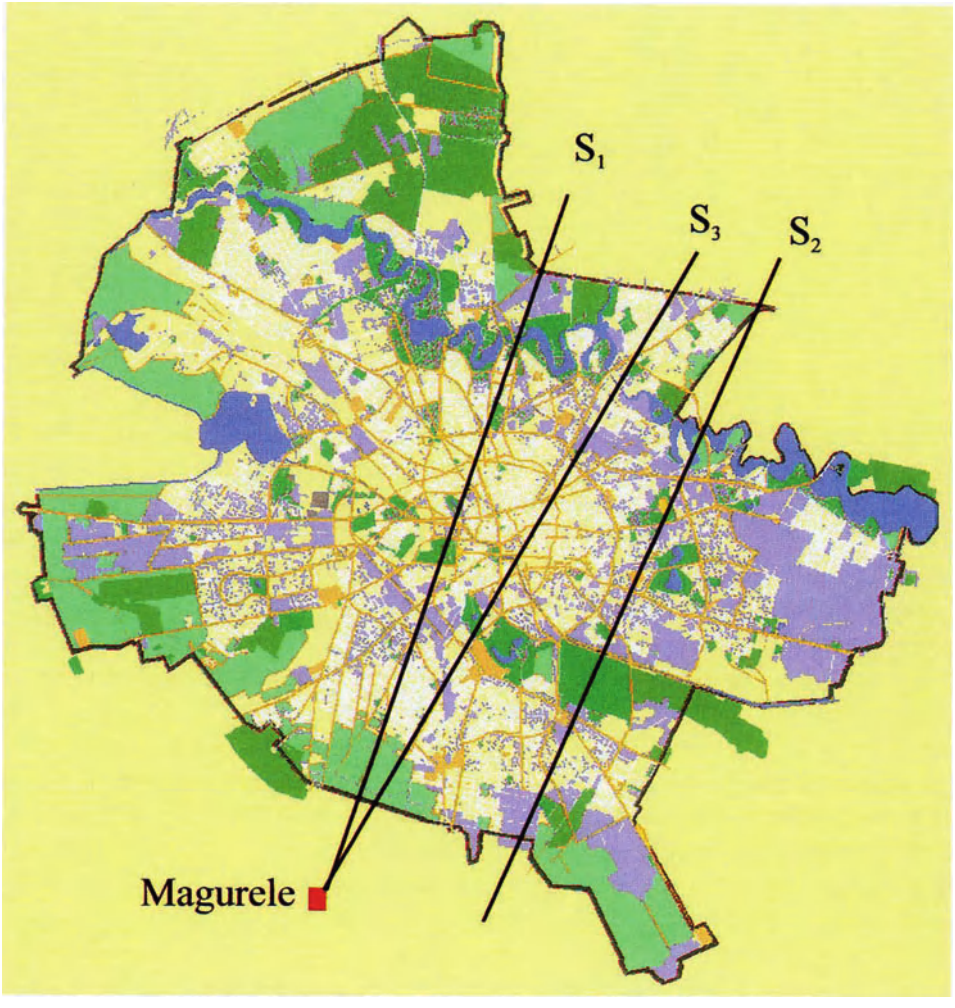

Figure 2
City sketch with the location of the profiles used in the numerical simulations; S_1 and S_2 are parallel and are about 3.5 km apart.

interbedded. The seismic wave velocities have been measured by seismic refraction (MANDRESCU, 1972) and Q_P and Q_S values are evaluated from empirical correlation with the geology.

In the case of the May 30, 1990 earthquake the epicentral distance for all the cross sections ranges from 165 to 185 km.

With these input data, complete signals (displacement, velocity and acceleration) have been computed by using the hybrid method. The frequency range considered in the simulations is the interval 0.05–1.0 Hz, appropriate for 10-story or higher buildings. The real seismic signal considered for the validation of the synthetic

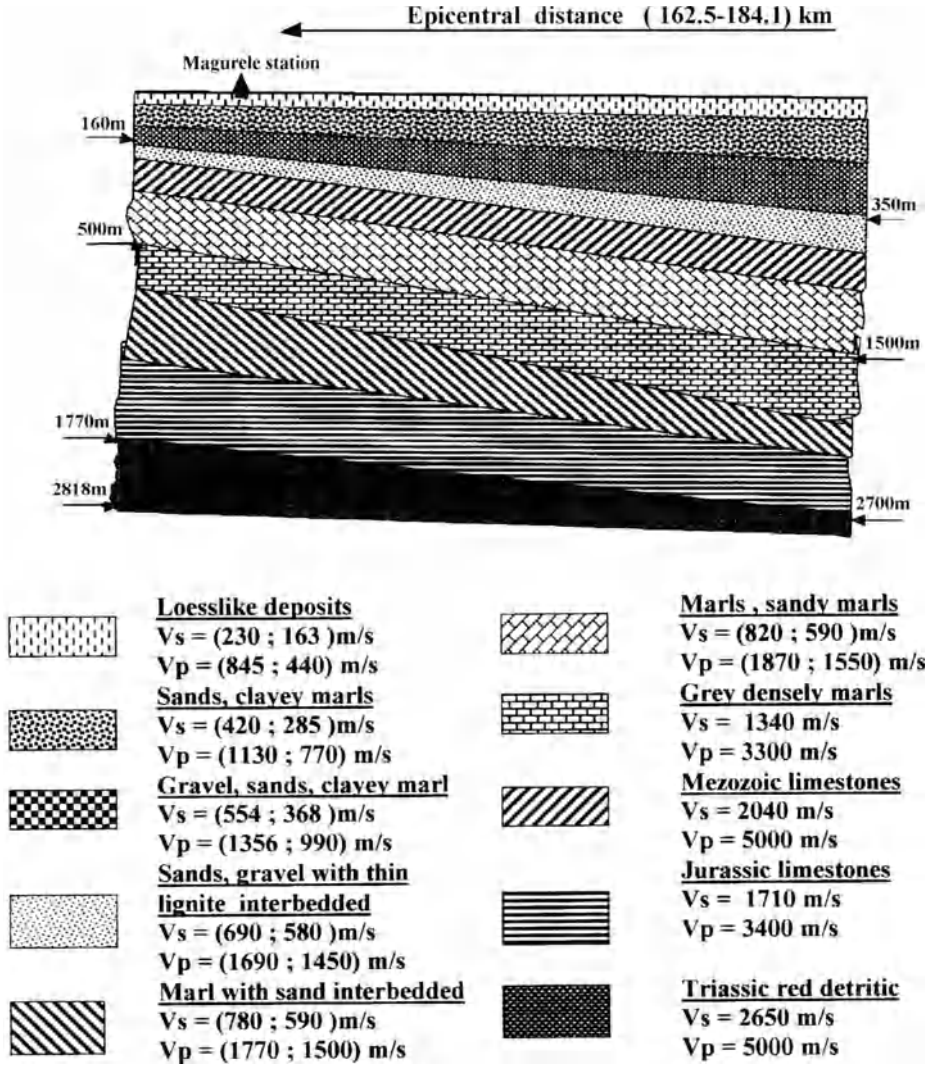

Figure 3
Local structure S_3 used for the ground motion modelling induced in Bucharest by the May 30, 1990, Vrancea earthquake.

seismograms is represented by the three-component record at Magurele seismic station, located at the southwestern part of the city, which was triggered by the May 30, 1990 Vrancea earthquake. The recorded signals, band-pass Butterworth filtered from 0.1 Hz to 1 Hz, are presented in Figure 4. The corresponding synthetic seismograms are shown in Figure 5. The synthetic seismograms reproduce well the shape of the recorded ones and the amplitudes for the vertical (VER) and the transverse (TRA) components (the origin time in Figs. 4 and 5 is not the same).

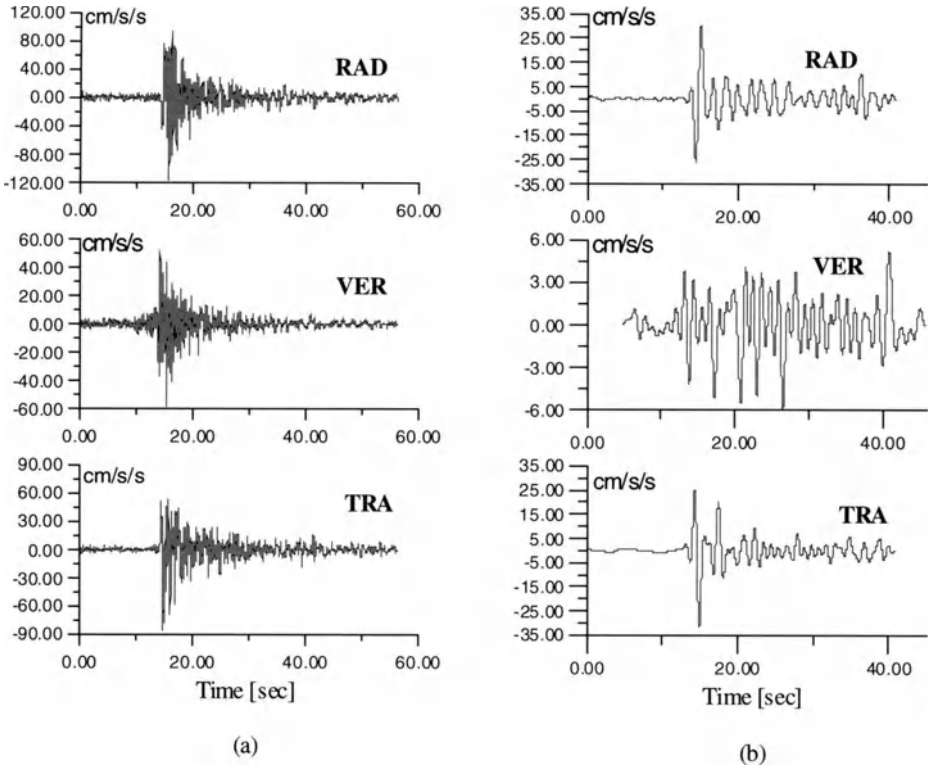

Figure 4
The three-component accelerogram recorded at Magurele seismic station during the May 30, 1990 Vrancea earthquake (a), and the low-pass filtered (0.05–1 Hz) one (b).

Obviously our synthetic time series computed for both bedrock (1-D) and local structure (2-D) can be processed in the same way as the real seismograms in order to obtain the response spectra and the spectral ratio. These quantities, together with PGA (the maximum value of the synthetic accelerograms) are of main importance for seismic engineering purposes.

Figure 6 displays the distribution of the peak ground acceleration (PGA) values along each studied profile, simulated for the case of the May 30, 1990 earthquake. Both the shape and the amplitudes of the spatial distribution of the synthetic PGA are quite similar along S_1 and S_2 profiles, while they are remarkably different along S_3. This is due to the specific geometry and to the lateral variations of the seismic waves velocity in the tilted layers of profile S_3.

To discuss the site effects it is convenient to consider the spatial distribution of the relative peak ground acceleration PGA (2-D)/PGA(1-D), where 2-D indicates the computations for the laterally varying model and 1-D indicates the computations for the bedrock model. Figure 7 shows the relative PGA vs. epicentral distance along the

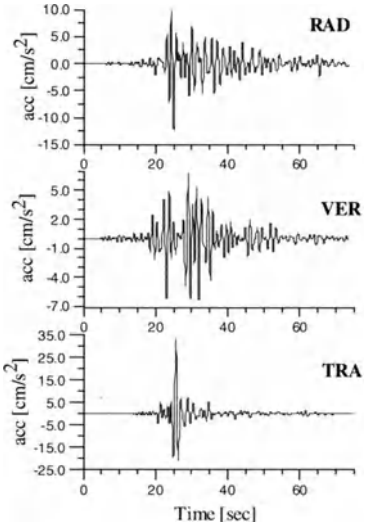

Figure 5
The synthetic seismogram simulated for the Magurele site in the case of the May 30, 1990 earthquake.

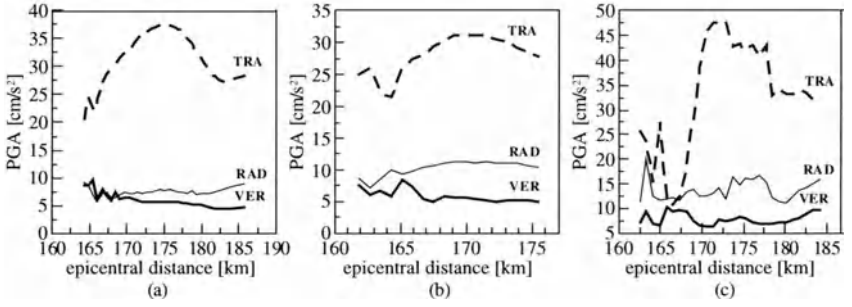

Figure 6
The spatial distribution of the synthetic peak ground acceleration (radial component RAD—thin line, vertical component VER—thick line and the transverse one TRA—dashed line) along profile S_1 (a), S_2 (b) and S_3 (c) for the case of the May 30, 1990 earthquake.

S_1 and S_2 profiles as regards the Aug. 30, 1986 (a,b) and May 31, 1990 (c,d) earthquakes.

The synthetic signals computed using the hybrid method along the local profiles show that the local effects, in terms of PGA, affect mainly the vertical (VER) and the transverse (TRA) components. For these components the local amplification of PGA ranges from 1.2 to 2.9. The radial (RAD) component is less affected, the maximum amplification being 2 .The relative PGA shows different site effects along S_1 and S_2 (Fig. 7). The strong amplification of the TRA and RAD components along the S_1 profile can be due to the differences in the thickness of the same

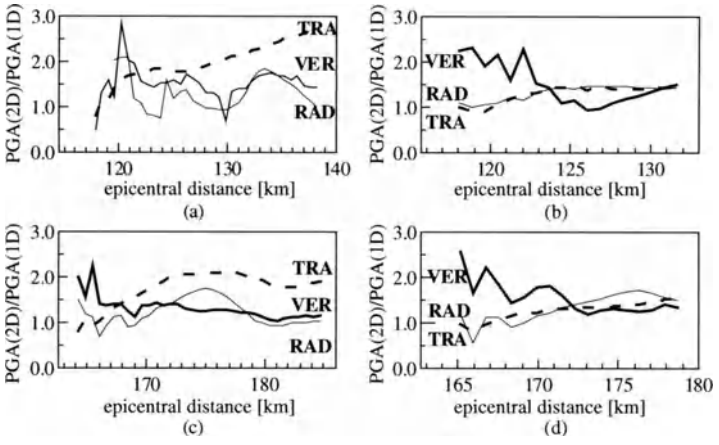

Figure 7
The spatial distribution of relative peak ground accelerations (radial component RAD—thin line, vertical component VER—thick line and the transverse one TRA—dashed line) along profiles S_1 and S_2 in the case of the August 31, 1986 (a and c) and May 31, 1990 (b, d) events.

sedimentary layers and to the presence of a 127-m thick layer, composed of weak consolidated Quaternary sediments. This layer extends to 400 m of depth and has a shear-wave velocity of about 800 m/s and a corresponding quality factor $Q_s = 30$.

The synthetic response spectra ratios (RSR), i.e., the ratio between the response spectra for the laterally varying model, Sa(2-D), and the one for the bedrock model, Sa(1-D), computed with 5% critical damping, are shown in Figures 8–10. Figure 8 shows a different response of the local structures S_1 and S_2 in the case of the May 30, 1990 event (class A event, $M_w = 6.9$). Figure 9 represents the Sa (2-D)/ Sa (1-D) along profile S_3 computed for 2 variants: (a) with horizontal layers, and (b) with 4% tilt layers to mimic the geological local structure. We see that the tilting of the layers induces an amplification of the seismic response, especially for the RAD and TRA components. Important site effects are induced in a confined area located at about 170–178 km epicentral distance, which corresponds to the central part of the city. This effect of the seismic waves propagation explains the abnormal high intensity, VIII+ degree MSK-76, reported in the center of Bucharest after the March 4, 1977 earthquake $M_w = 7.4$ (MANDRESCU and RADULIAN, 2000).

In Figure 10, the peak response in the RAD component along S_2 in the case of August 30, 1986 event (class A event, $M_w = 7.1$) is 1.8 at about 0.3–0.4 Hz. This peak can correspond to the first 360 m of weak Quaternary and Tertiary deposits. The same peak is again present in the case of the May 31, 1990 (class B, $M_w = 6.4$) event, but the maximum RSR (2.2) in the RAD component along S_2, appears at about 0.8–0.9 Hz. For the VER component the maximum RSR (4) along S_2 corresponds to the

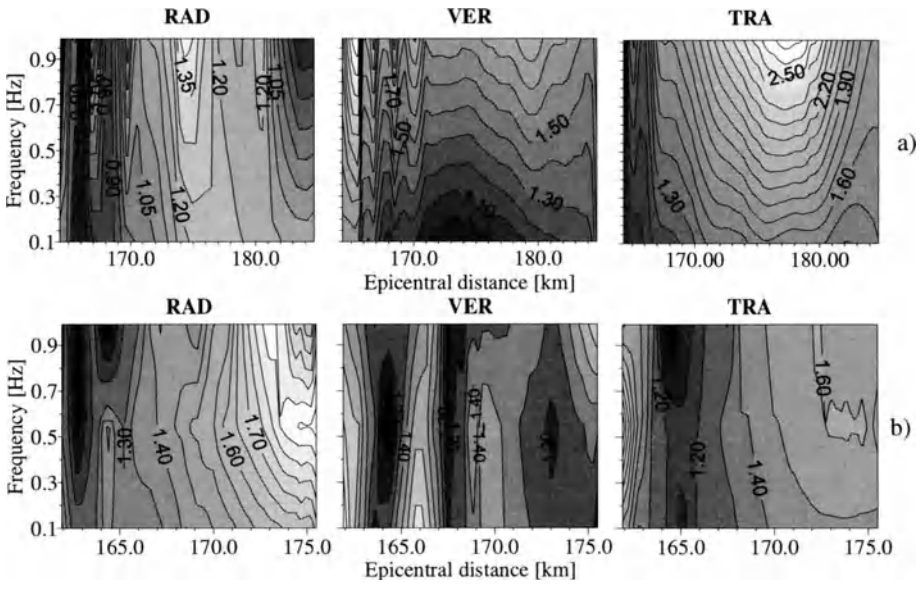

Figure 8
The Relative Spectra Response (RSR), i.e., Sa(2D)/Sa(1D), versus frequency and epicentral distance for S_1 and S_2 profiles (a, b) in the case of the May 30, 1990 earthquake displayed separately for the radial component (RAD), for the vertical component (VER) and the transverse one (TRA).

frequency interval 0.6–0.65 Hz in the case of the August 30, 1986 earthquake. For the May 31, 1990 event the RSR value in the 0.6–0.65 Hz interval is just 2.2, and the maximum value (3.5) is reached at about 0.85–0.9 Hz, i.e., at the uppermost frequency limit used in our modeling. The RAD and VER components are very sensitive to the change of the focal mechanism from class A to class B, while the site effects in the TRA component are relatively stable as shown also by the parametric tests performed by MOLDOVEANU and PANZA (2001). The shift of the maximum RSR values from 0.4 to 0.9 Hz (RAD) or from 0.6 to 0.9 Hz (VER) shows that the frequency content of the seismic ground motion changes with earthquake magnitude. From the modeling one may expect that in Bucharest the large magnitude Vrancea earthquakes induce seismic ground motion that peaks in the low frequency band (<1 Hz), since they are able to significantly excite soil layers with low modal frequency. On the other side, the $M_w < 7$ intermediate-depth events have no such capability and therefore induce seismic ground motion that maximizes in a higher frequency band (>1 Hz). Observations of past strong earthquakes (1977, 1986 and both 1990 events) indicate that the modeling is in agreement within the considered frequency limits, with the real soil response in Bucharest. The dominant recorded period decreases from 1.7 seconds for the strongest event (March 4, 1977, $M_w = 7.4$) to about 1 second (the absolute maximum is actually reached at about 0.4 seconds,

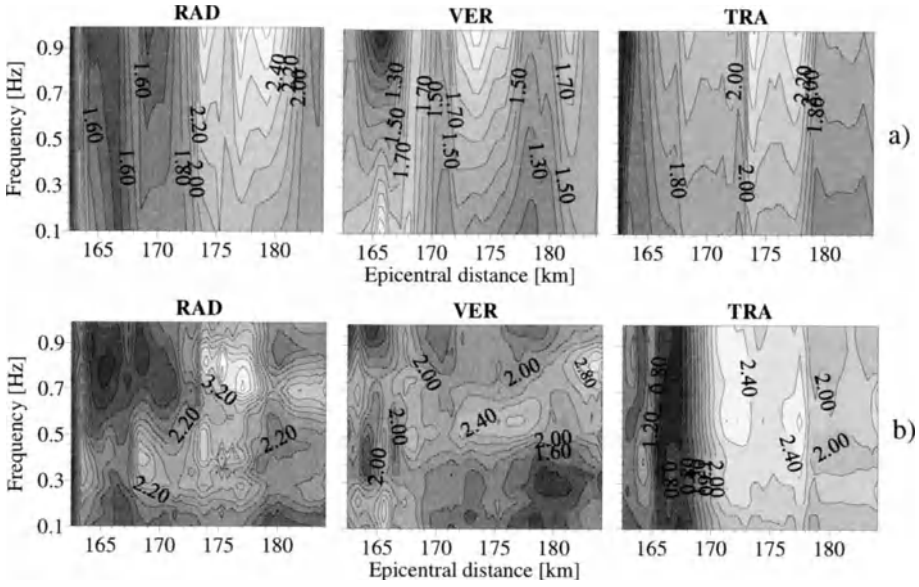

Figure 9
The RSR along S_3 vs. frequency and epicentral distance simulated for the May 30, 1990 earthquake in the case of a structure with horizontal layers (a) and the case of the more realistic structure with tilted layers (b).

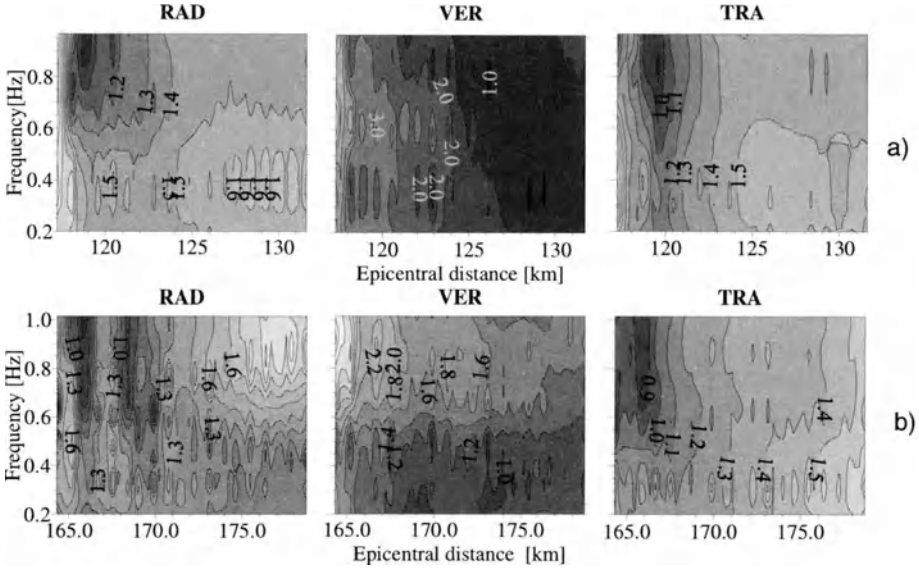

Figure 10
The RSR along S_2, simulated for the August 30, 1986 (a) and May 31, 1990 (b) events.

i.e., outside our modeling frequency band) for the smallest one (May 31, 1990, $M_w = 6.4$).

5. Conclusions

The hybrid technique that we have used makes possible the study of the local soil effects even at long distances from the source, as in the case of Bucharest, taking into account the characteristics of the seismic source, and the effects of the seismic waves propagation. Applied in microzonation studies, this technique provides realistic estimates of spectral amplifications and can supply, when necessary, the lack of strong motion recordings for the "target" site.

The synthetic time series computed by the hybrid method using S_1 and S_1 profiles have been successfully compared with the damage distribution caused in Bucharest by the March 4, 1977 earthquake (MOLDOVEANU and PANZA, 1999).

From the RSR of the synthetic seismograms, computed for the 1986 and 1990 Vrancea earthquakes in the 0.05–1.0 Hz frequency range, it can be concluded that the thickness of the Quaternary and Tertiary sediments strongly affects the seismic ground motion in Bucharest.

On the basis of the results reached and considering the high seismic hazard, it is reasonable for preparedness purposes to extend the results of the numerical simulations to all city zones where the geological conditions are similar to those represented in the studied profiles. The regionalization following these criteria is shown in Figure 11. The variation of the epicentral distances for these regions is less than 3 km. To each of the five zones we assign a representative site, chosen along the virtual arrays used in the numerical simulations. The corresponding response spectra computed for 0% and 5% critical damping are shown in Figure 12, for the case of the May 30, 1990 Vrancea event.

Further computations regarding the simulation of the seismic ground motion excited by other strong Vrancea events (such as the March 4, 1977, $M_w = 7.4$ or November 10, 1940, $M_w = 7.7$ events), and for the "maximum expected earthquake" will substantially improve the reliability of this first deterministic zonation for Bucharest. The ongoing activity regards the extension of the frequency interval of the simulations in order to include the resonance of the masonry buildings.

The numerical simulations of Vrancea strong earthquakes performed by means of the used method makes it possible to obtain at low cost and exploiting large quantities of existing data (e.g. geotechnical parameters, surface geology data, seismological data), the definition of the realistic seismic input to build structures of interest. The synthetic data set, including those corresponding to the "maximum expected" Vrancea event, tighter with the recorded ones can be fruitfully used by civil engineers in design of new seismo-resistant constructions and in the reinforcement of the existing ones.

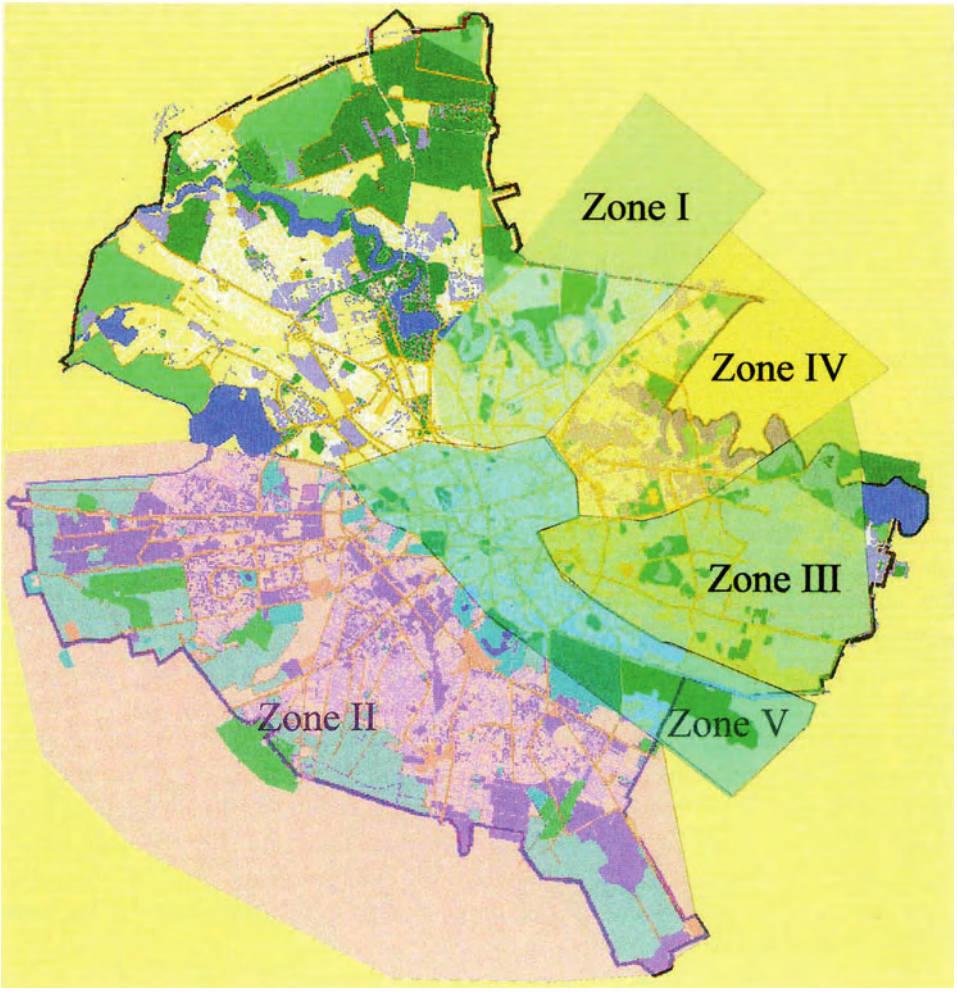

Figure 11
Preliminary seismic zonation map of the city.

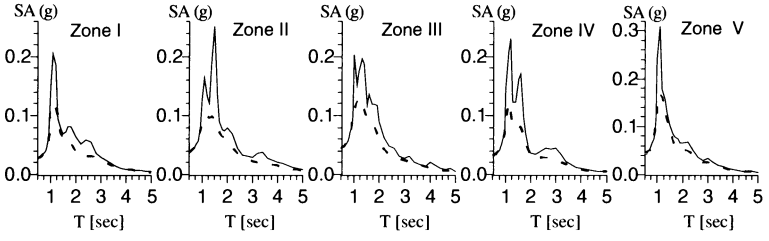

Figure 12
Acceleration response spectra (0% damping—solid line; 5% damping—dashed line) representative of the five zones shown in Figure 11.

Acknowledgements

This paper is a contribution to the UNESCO-IUGS-IGCP project 414 "Realistic Modelling of Seismic Input for Megacities and Large Urban Areas." With the contribution of the Italian Ministry of Foreign Affairs (MAE), Directorate General for Cultural Promotion and Cooperation.

References

ENESCU, D. and ENESCU, B. D. (1993), *A New Model Regarding the Subduction Process in the Vrancea Zone*, Rom. J. Phys. *38*, 321–328.

FÄH, D. (1992), *A Hybrid Technique for the Estimation of Strong Ground Motion in Sedimentary Basins*, Ph.D. Thesis, Swiss Federal Institute of Technology, Zürich.

FÄH, D., JODICE, C., SUHADOLC, P., and PANZA G. F. (1993), *A New Method for the Realistic Estimation of Seismic Ground Motion in Megacities: The Case of Rome*, Earthquake Spectra *9*, 643–668.

FÄH, D., SUHADOLC, P., and PANZA G. F., *Estimation of Strong Ground Motion in Laterally Heterogeneous Media: Modal Summation-Finite Difference*, Proc. Of the 9th European Conference of Earthquake Engineering, *4A*, 100–109, Moscow, 11–16 Sept, 1990.

FÄH, D., SUHADOLC, P., and PANZA G. F. (1993), *Variability of seismic ground motion in complex media: the Friuli area (Italy)*. In *Geophysical Exploration in Area of Complex Geology*, II (eds. Cassinis, R., Helbig, K., and Panza, G. F.), J. Appl. Geophys. *30*, 131–148.

ISMAIL-ZADEH, A. T., PANZA, G. F., and NAIMARK, B. M. (2000), *Stress in the Descending Relic Slab beneath Vrancea, Romania*, Pure Appl. Geophys. *157*, 111–130.

LUNGU, D., ARION, C., ALDEA, A., and CORNEA, T. (2000), *City of Bucharest Seismic Profile: From Hazard Estimation to Risk Mitigation*, Earthquake Hazard and Countermeasures for Existing Fragile Buildings (eds. Lungu, D. and Saito, T.), 43–67, Independent Film, Bucharest.

MCKENZIE, D. P. (1972), *Active Tectonics of the Mediterranean Region*, Geophys. J. R. Astr. Soc. *39*, 109–185.

MANDRESCU, N., *Cercetari experimentale de microzonare seismica*, Revue Roumaine de Geologie, Geophysique et Geographie, serie de GEOPHYSIQUE *10*, 103–116, Acad.Roumaine, Bucharest, 1972 (in Romanian).

MANDRESCU, N. and RADUALIAN, M., *Seismic microzoning of Bucharest*, In (eds. Wenzel, F., Lungu, D., and Novak, O.) *Vrancea Earthquakes: Tectonics, Hazard and Risk Mitigation* (Netherlands: Kluwer Academic Publ.: 2000) pp. 109–122.

MARTIN, M., WENZEL, F., ACHAUER, U., KISSLING, E., MOCANU, V., MUSACCHIO, G., RADULIAN, M., and the CALIXTO Working Group (2002), *High-resolution Images of a Slab Detachment Process*, Seismol. Res. Lett.

MOLDOVEANU, C. L. and PANZA, G. F., *Modelling for microzonation purposes of the seismic ground motion in Bucharest, due to the Vrancea earthquake of May 30, 1990*, In *Vrancea Earthquakes: Tectonics, Hazard, and Risk Mitigation* (eds. Wenzel, F. and Lungu, D.) (Kluwer Academic Publ., 1999) pp. 85–97.

MOLDOVEANU, C. L. and PANZA, G. F. (2001), *Vrancea Source Influence on Local Seismic Response in Bucharest*, Pure Appl. Geophys. *158*, 2407–2429.

MOLDOVEANU, C. L. MARMUREANU, G., PANZA, G. F., and VACCARI, F. (2000), *Estimation of Site Effects in Bucharest Caused by the May 30–31, 1990, Vrancea Seismic Events*, Pure Appl.Geophys. *157*, 249–267.

ONCESCU, M. C. and TRIFU, C. -I. (1987), *Depth Variation of the Moment Tensor Principal Axes in Vrancea (Romania) Seismic Region*, Ann. Geophysicae *5B*, 149–154.

PANZA, G. F. (1985), *Synthetic Seismograms: The Rayleigh Modal Summation*, J. Geophys. *58*, 125–145.

PANZA, G. F. (1993), *Synthetic Seismograms from Multimode Summation Theory and Computational Aspects*, Acad. Geod. Geoph. Mont. Hung. *28*, 1–2, 197–247.

PANZA, G. F., VACCARI, F., COSTA, G., SUHADOLC, P., and FÄH, D. (1996), *Seismic Input Modelling for Zoning and Microzoning*, Earthquake Spectra *12*, 3, 529–566.

PANZA, G. F., ROMANELLI, F., and VACCARI, F. (2001), *Seismic Wave Propagation in Laterally Heterogeneous Anelastic Media: Theory and Applications to seismic Zonation*, Advanced in Geophys. *43*, 1–95.

RADULIAN, M., MANDRESCU, N., and PANZA, G. F. (2000a), *Characterization of Seismogenic Zones of Romania*, Pure Appl. Geophys. *157*, 57–78.

RADULIAN, M., VACCARI, F., MANDRESCU, N., PANZA, G. F., and MOLDOVEANU, C. L. (2000b), *Seismic Hazard of Romania: Deterministic Approach*, Pure Appl. Geophys. *157*, 221–248.

ROMANELLI, F., BING, Z., VACCARI, F., and PANZA, G. F. (1996), *Analytical Computations of Reflection and Transmission Coupling Coefficients for Love Waves*, Geophys. J. Int. *125*, 132–138.

ROMPLUS CATALOG accessible via Internet at wwww.infp.ro/Labs/catal.html

SOLOVIEV, A. A., VOROBIEVA, I. A., and PANZA, G. F. (2000), *Modelling of Block Structure Dynamics for the Vrancea Region: Source Mechanism of the Synthetic Earthquakes*, Pure Appl. Geophys. *157*, 97–110.

VACCARI, F., GREGERSEN, S., FURLAN, M., and PANZA, G. F. (1989), *Synthetics Seismograms in Laterally Heterogeneous, Anelastic Media by Modal Summation of the P-SV Waves*, Geophys. J. Inter. *99*, 285–295.

VIRIEUX, J. (1984), *SH-wave Propagation in Heterogeneous Media: Velocity-stress Finite-differences Method*, Geophysics *49*, 11, 1993–1957.

VIRIEUX, J. (1986), *P-SV -wave Propagation in Heterogeneous Media: Velocity-stress Finite-differences Method*, Geophysics *51*, 4, 889–991.

WENZEL, F., CIUGUDEAN, V., WIRTH, W., KIENZLE, A., HANNICH, D., BONJER, K. -P., MOLDOVEANU, T., and Sokolov, V., *Options for Rapid Ground Motion Assessment in Bucharest*, Earthquake Hazard and *Countermeasures for Existing Fragile Buildings* (eds. Lungu, D. and Saito, T.) 81–91, Independent Film, Bucharest, 2000.

(Received March 18, 2002, accepted October 14, 2002)

Pure appl. geophys. 161 (2004) 1165–1184
0033–4553/04/061165–20
DOI 10.1007/s00024-003-2501-2

Pure and Applied Geophysics

Site-specific Microzonation Study in Delhi Metropolitan City by 2-D Modelling of SH and P-SV Waves

IMTIYAZ A. PARVEZ[1], F. VACCARI[2,4], and G. F. PANZA[2,3]

Abstract— Delhi – the capital of India lies on a severe earthquake hazard threat not only from local earthquakes but also from Himalayan events just 200–250 km apart. The seismic ground motion in a part of Delhi City is computed with a hybrid technique based on the modal summation and the finite-difference scheme for site-specific strong ground motion modelling. Complete realistic *SH* and *P-SV* wave seismograms are computed along two geological cross sections, (1) north-south, from Inter State Bus Terminal (ISBT) to Sewanagar and (2) east-west, from Tilak Bridge to Punjabi Bagh. Two real earthquake sources of July 15, 1720 (MMI = IX, $M = 7.4$) and August 27, 1960 ($M = 6.0$) have been used in modelling. The response spectra ratio (RSR), i.e. the response spectra computed from the signals synthesized along the laterally varying section and normalized by the response spectra computed from the corresponding signals, synthesized for the bedrock reference regional model, have been determined. As expected, the sedimentary cover causes an increase of the signal amplitude, particularly in the radial and transverse components. To further check the site-effects, we reversed the source location to the other side of the cross section and recomputed the site amplifications. There are only a few sites where a large amplification is invariant with respect to the two source locations considered. The RSR ranges between 5 to 10 in the frequency range from 2.8 to 3.7 Hz for the radial and transverse components of motion along the NS cross section. Along the EW cross section RSR varies between 3.5 to 7.5 in the frequency range from 3.5 to 4.1 Hz. The amplification of the vertical component is considerable at high frequency (>4 Hz.) whereas it is negligible in lower frequency range.

Key words: Seismic Microzonation, synthetic seismograms, response spectra ratio, Delhi.

Introduction

The recent Bhuj earthquake of January 26, 2001 left thousands dead, hundreds of thousands injured and a considerably large number destitute. Damage to property apparently reached billions of Rupees. This was a shocking event that generated untold misery and captured media attention world wide. Several megacities in India, such as Delhi, Mumbai, Kolkata and Guwahati, face a severe earthquake hazard. A

[1] CSIR Centre for Mathematical Modelling and Computer Simulation (C-MMACS), NAL Belur Campus, Bangalore – 560 037, India.
[2] Department of Earth Sciences, University of Trieste, Via E. Weiss 4, 34127 Trieste, Italy.
[3] The Abdus Salam International Centre for Theoretical Physics, SAND Group, Trieste, Italy.
[4] Istituto Nazionale di Geofisica e Vulcanologia - Osservatorio Vesuviano, Naples, Italy.

growing number of large industrial settlements are also located in earthquake-prone areas.

Delhi is a fast growing megacity that influences the economic and industrial development of most of the country. The estimated population of urban Delhi is now around 12.2 million. An example of the study of site effects and microzonation of a part of Metropolitan Delhi city is presented here, based on a detailed modelling along two cross sections: North-south from ISBT to Sewanagar and east-west from Tilak Bridge to Punjabi Bagh. Full synthetic strong motion waveforms have been computed using the hybrid method developed by FÄH *et al.* (1993a, b). The earthquake source of the July 15, 1720 (MMI = IX, $M = 7.4$) event is considered for the NS cross section, while the source of the August 27, 1960 ($M = 6.0$) earthquake is adopted for the modelling along the EW cross section. The site amplification, in terms of response spectra ratio (RSR), has been determined. The computations have been repeated placing the source at both sides of each profile, in order to analyze the variation in the obtained amplification patterns.

Site-specific Strong Ground Motion Modelling

One of the basic problems associated with the study of seismic zonation/microzonation is to determine the seismic ground motion, at a given site, due to an earthquake with a given magnitude (or moment) and epicentral distance. The ideal solution for such a problem could be to use a wide database of recorded strong motions and to group those accelerograms that have similar source, path and site effects. In practice however, such a database is not available. Actually, the number of recorded signals is relatively low and the installation of local arrays in each zone with a high level of seismicity is too expensive an operation that requires a lengthy interval to gather statistically significant data sets.

While waiting for data accumulation, a preventive tool is supplied by the realistic modelling, based on computer codes developed from the knowledge of the seismic source and of the propagation of seismic waves associated with the given earthquake scenario. Both the properties and the geometrical configuration of near surface soft soil materials, due to their low density, high compressibility and low strength can influence the amplitude of ground motion. These characteristics can amplify the earthquake-induced ground motion, causing, even for relatively low magnitudes, damage (up to collapse) also to structures which are located far from the epicenter.

With the available geological, geophysical, seismological and seismotectonic data, we can compute realistic seismograms from the first principals of physics (e.g., PANZA *et.al.* 2000; Field, E.H. and the SCEC Phase III Working Group, 2000). FÄH *et al.* (1993a, b) developed a hybrid method that combines the modal summation technique (PANZA, 1985; PANZA and SUHADOLC, 1987; FLORSCH *et al.*,

1991; PANZA *et al.*, 2001) with finite differences (VIRIEUX, 1984, 1986; LEVANDER, 1988), exploiting both methods to their best. In the framework of the UNESCO-IUGS-IGCP Project 414 "Realistic Modelling of Seismic Input for Megacities and Large Urban Areas" (PANZA *et al.*, 1999a), this hybrid approach has been successfully applied for the purpose of the deterministic seismic microzoning in several urban areas: Beijing (SUN *et al.*, 1998), Benevento (FÄH and SUHADOLC, 1995; MARRARA and SUHADOLC, 1998), Bucharest (MOLDOVEANU and PANZA, 1999; MOLDOVEANU *et al.*, 2000), Catania (ROMANELLI *et al.*, 1998a, b), Mexico City (FÄH *et al.*, 1994), Rome (FÄH *et al.*, 1993b; FÄH and PANZA, 1994), Naples (NUNZIATA *et al.*, 1995, 2000), Santiago de Cuba (ALVAREZ *et al.*, 2001) and Delhi (PARVEZ *et al.*, 2002).

With this approach, source, path and site effects are all taken into account and a detailed study of the wavefield that propagates at long distances from the epicenter is possible. Several techniques have been proposed to empirically estimate the site effects using observations. As pointed out by PANZA *et al.* (2001), those techniques supply reliable information about the site response to non-interfering seismic phases, but they are not adequate in most real cases when the seismic sequel is formed by several interfering waves. ROMANELLI and VACCARI (1999) and LOKMER *et al.* (2002) demonstrated that the focal mechanism can play an important role in the local amplification of seismic ground motion, sometimes masking the effects of the local structure itself. Given the complexity of the problem of site response estimation, the realistic modelling of ground motion can be considered the primary path to take in the assessment of the hazard. This can be done considering several scenario earthquakes and taking envelopes of averages and of upper extremes of the parameters describing the hazard itself, extracted from the synthetic signals, that can be calibrated against the available records, if any.

Geological Background and Seismicity of Delhi

Delhi is located at the northern end of the Aravalli Mountains and it is mostly surrounded by Gangetic alluvium. An extension of the Aravalli Hills enters the Delhi region from the south, spreads out into a rocky table-land and traverses in a north-easterly direction across the Delhi State (SETT, 1964). The conspicuous longitudinal ridge, trending NNE-SSW runs from the west of the capital city and terminates at the right bank of the Yamuna in the north (Fig. 1). The largest part of Delhi lies in the alluvium, but the small hills and ridges in and around New Delhi consist of Alwar quartzites. Delhi area is occupied by quartzites interbedded with mica schist belonging to the Delhi Super Group, unconformably overlain by unconsolidated Quaternary to recent sediments. The quartzites are gray to brownish gray, massive to thinly bedded and structurally form a coaxially refolded

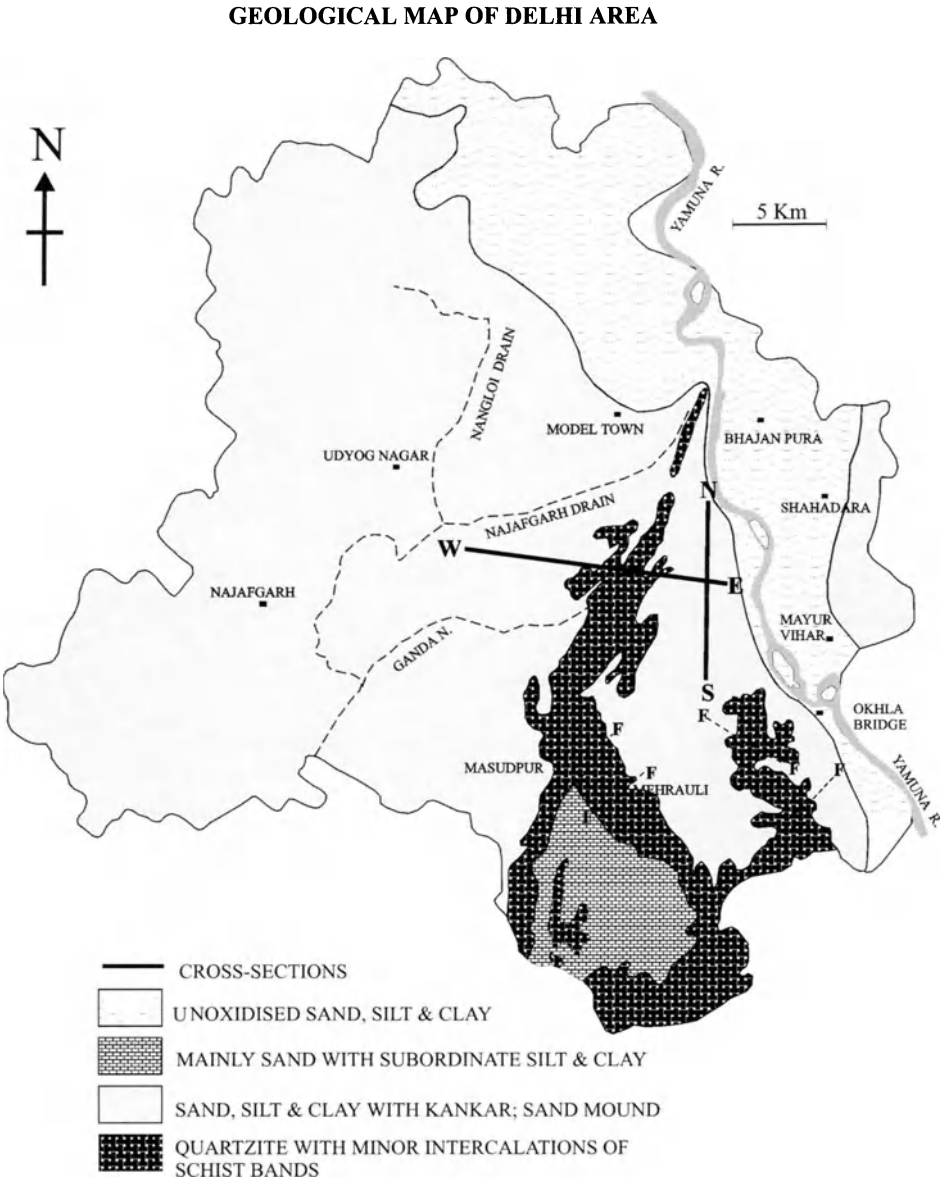

Figure 1
Generalized geological map of the Delhi area and the locations of the cross sections used in the present study for the numerical modelling (modified after GSI, 1997).

regional antiform plunging southwest. The major planar structure strikes NE-SW with steep southeasterly dips. These quartzites occur in the central and southern parts of the area while the Quaternary sediments comprising older and newer

alluvium cover the rest of the area (Fig. 1). The older alluvium comprises silt, clay with minor lenticular fine sand and kankar beds. The newer alluvium mainly consists of unoxidised sands, silt and clay occurring in the older and active flood plains of the Yamuna River. The thickness of the alluvium, both on the eastern and western sides of the ridge, is variable, although it is generally larger to the west of the ridge (GSI, 1997).

Delhi and its environs are seismically active. Earthquakes of magnitudes 3 to 7.4 have been observed in and around Delhi during the past three centuries. Figure 2 shows the epicenters of some moderate and large earthquakes which occurred in Delhi region, as well as the events which occurred in the Himalayan region, along the Main Boundary Thrusts (MBT) and Main Central Thrusts (MCT), that have been felt in Delhi. The Himalayan thrust zone, just 200–250 km north of the megacity, has been identified as a significant seismic gap in the Central Himalayas (KHATTRI, 1987; BILHAM *et al.*, 2001), thus it can presently be considered as one of the most hazardous areas of the world. Delhi is therefore quite vulnerable to Himalayan earthquakes and its burgeoning population and industrial works face increasing risk from seismic hazard.

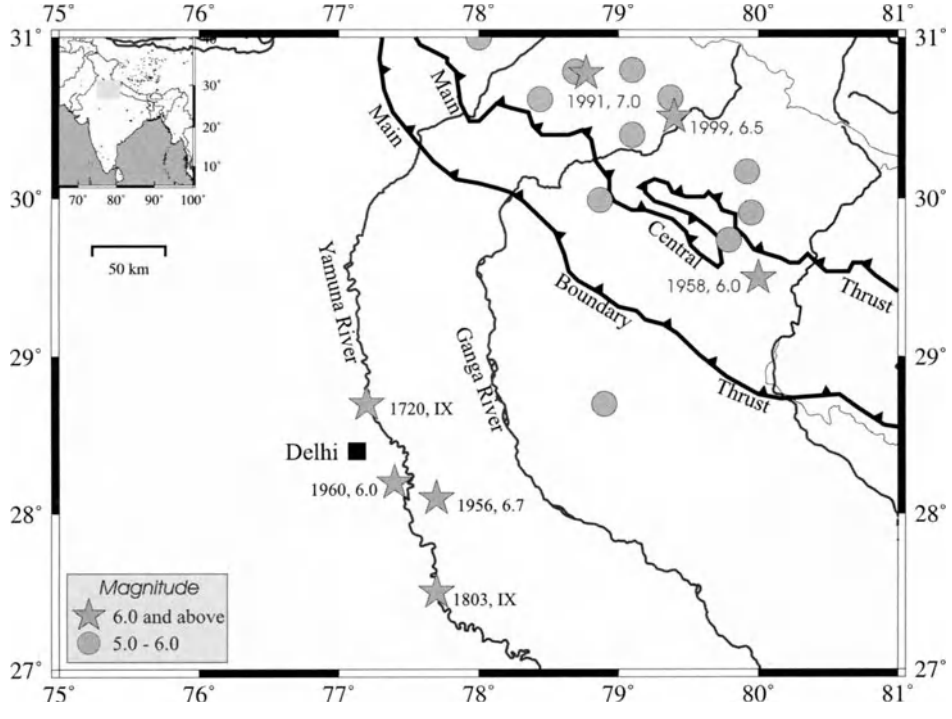

Figure 2
The regional map of Delhi and its surrounding areas with the epicenters of the earthquakes which occurred in the region.

Input Parameters

The input data, necessary for the ground motion simulation with the hybrid approach, consist of the laterally heterogeneous local model, the regional bedrock model and the earthquake source model.

2-D Cross sections

As discussed earlier, the aim of the present study is to define the site effects due to the presence of sub surface material above the bedrock. Figure 3 shows the local soft soil above the bedrock for two representative geological cross sections in Delhi City (IYENGAR, 2000). The NS cross section runs from ISBT to Sewanagar and the EW cross section from Tilak Bridge to Punjabi Bagh. These profiles, initially available up to 30–35 m of depth, have been further extended below, to approximate the bedrock depth level, using IYENGAR (2000) data. The details of the material properties of these cross sections are also shown in Fig. 3. The *S*-wave velocity (V_s) and density (ρ) are adopted from the range given by IYENGAR (2000) and, to be conservative, we have assumed *P*-wave velocity, $V_p = 2V_s$. The quality factor (Q_p and Q_s) values for the different soils are taken from standard compilations. The regional bedrock structure (Fig. 3) is taken from the structural polygon no. 3 of PARVEZ *et al.* (2003).

Earthquake Source

Many earthquakes have occurred in and around Delhi city since ancient time. For the modelling, we chose the events of July 15, 1720 (MMI = IX, $M = 7.4$) and August 27, 1960 (MMI = VII, $M = 6.0$). The 1720 event was used as a seismic source in the modelling for the NS cross section, with an epicentral distance of 10 kms from the nearest site in the local model. The epicenter (28.7°N, 77.20°E) and magnitude ($M = 7.4$) of this event are taken from the Global Seismic Hazard Assessment Program (GSHAP) catalogue. This event was very devastating and damaging. IYENGAR (2000) reports that people were frightened by the noise below the ground, the shaking of the walls, and the cracking of the roofs of buildings, and that nine or ten strong aftershocks occurred during the day and the following night. Most of the damage occurred within a relatively narrow area running in the north-south direction. There were reports describing that the market road from the Kabuli gate, to the north, up to Lal Darvaza, to the south, had eroded at several places, and buildings were razed to ground.

During recent times, the most significant event was the shock of August 27, 1960, with its epicentral tracts about 45 km from Delhi, towards Gurgaon. The probable cause of this event was a slip fracture in the weak brittle zone beneath the alluvium or along the contact of the alluvium with the Aravalli Mountains. NATH *et al.* (1968) report that 100 people were injured and 2 died during this quake. The area over which the shock was felt extended up to Kanpur to the

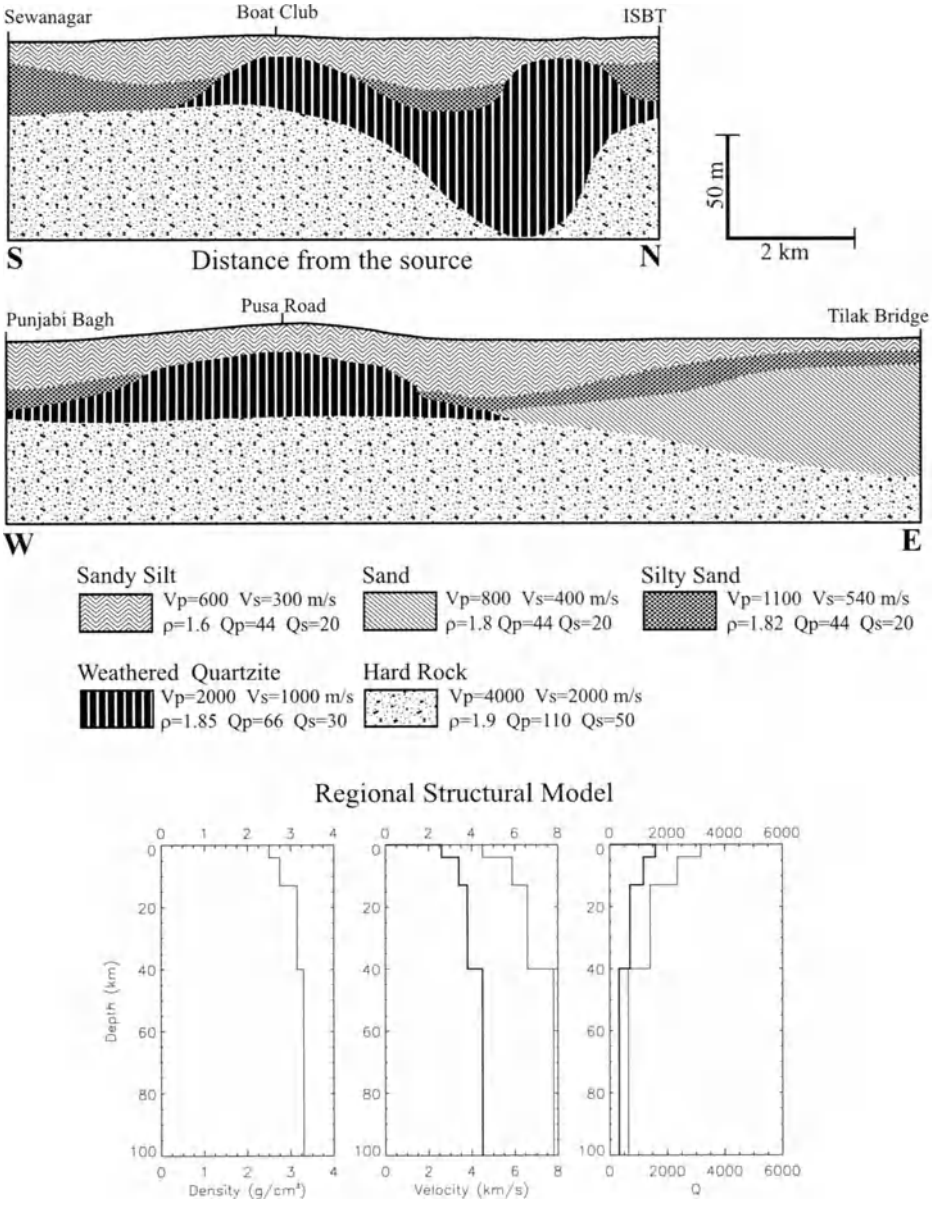

Figure 3

The soil properties of the NS cross section from ISBT to Sewanagar and the EW cross section from Tilak Bridge to Punjabi Bagh. The original model (IYENGAR, 2000) gives *S*-wave velocity (V_s) density (ρ); to be conservative we have assumed $V_p = 2V_s$. The Q values for the different soils are taken from standard compilations. The regional bedrock model is also shown.

southeast and to Jaipur to the southwest. However, the damage was confined to parts of Delhi and Gurgaon cities. This event is assumed in our modelling along the EW cross section.

For the definition of the focal mechanisms to be adopted in the simulations, given that no fault plane solution is available in the literature for both events, we considered the earthquake of October 10, 1956 which took place near Moradabad about 150 km east of Delhi. The focal mechanism of this event was obtained by MOLNAR *et al.* (1973) and shows a normal faulting. The depth of the source is assumed to be 8 km for both events.

Numerical Modelling of Seismic Ground Motion

The hybrid method used couples two computational techniques that permit the solution of the equation of motion in a laterally varying anelastic medium with no limitations for the source-receiver distance.

The seismic wavefield is computed in the 1-D part of the structural model ("regional" bedrock model, where the source is located) with the modal summation method and it is introduced in the laterally heterogeneous local model and numerically propagated in it with the finite-difference method. Preliminary to any computation, the soundness of the boundary conditions applied to the borders of the local model and the correct specification of the anelasticity has to be tested. The testing procedure is based on the comparison between the synthetic seismograms computed at the same sites of the "regional" bedrock model, both using the hybrid and the modal summation methods. The choice of the input parameters describing the boundary conditions and the anelasticity of the model is considered acceptable if the peak amplitudes of the numerically computed signals do not differ by more than 5% from those computed by mode summation.

Results along the NS Cross Section

The synthetic seismograms (*SH* and *P-SV* waves) have been computed with the hybrid method for an array of 100 sites regularly spaced, every 100 meters, along the NS cross section. For the source modelling of the event of July 15, 1720, we consider two possible locations; one 10 km to the north (original location of the event) and the other 10 km to the south of the profile, in order to analyze the ground motion amplifications obtained for waves travelling in the two opposite directions. Figure 4 shows the three-component synthetic strong motion accelerograms computed for the "northern source," whereas the similar accelerograms, computed for the "southern source," are shown in Figure 5. These figures clearly define the trend of the amplification effects and reflect well the geometry of

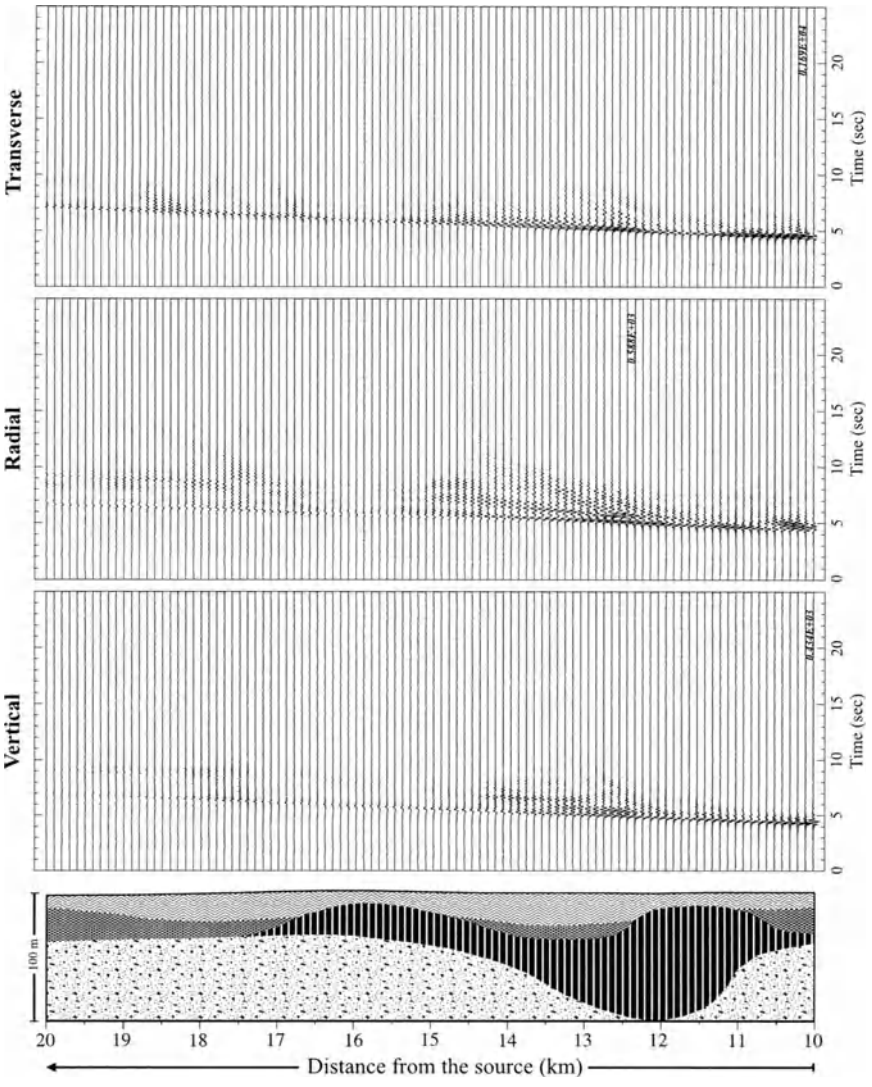

Figure 4
The NS cross section and corresponding synthetic strong motion records computed when the source is to the North of the cross section. The maximum amplitude value in cm/sec^2 is also indicated.

the cross section models used in the computations. Peak acceleration (AMAX) of 1.6 g is estimated in the transverse component at 10.2 km of epicentral distance from the source in Figure 4, whereas a similar value is seen in Figure 5 at a distance of 11 km from the source. This is a rather large value and represents a severe seismic hazard, as can be expected in the epicentral area of an event of magnitude 7.4. We believe that the peak values within 10 km of epicentral

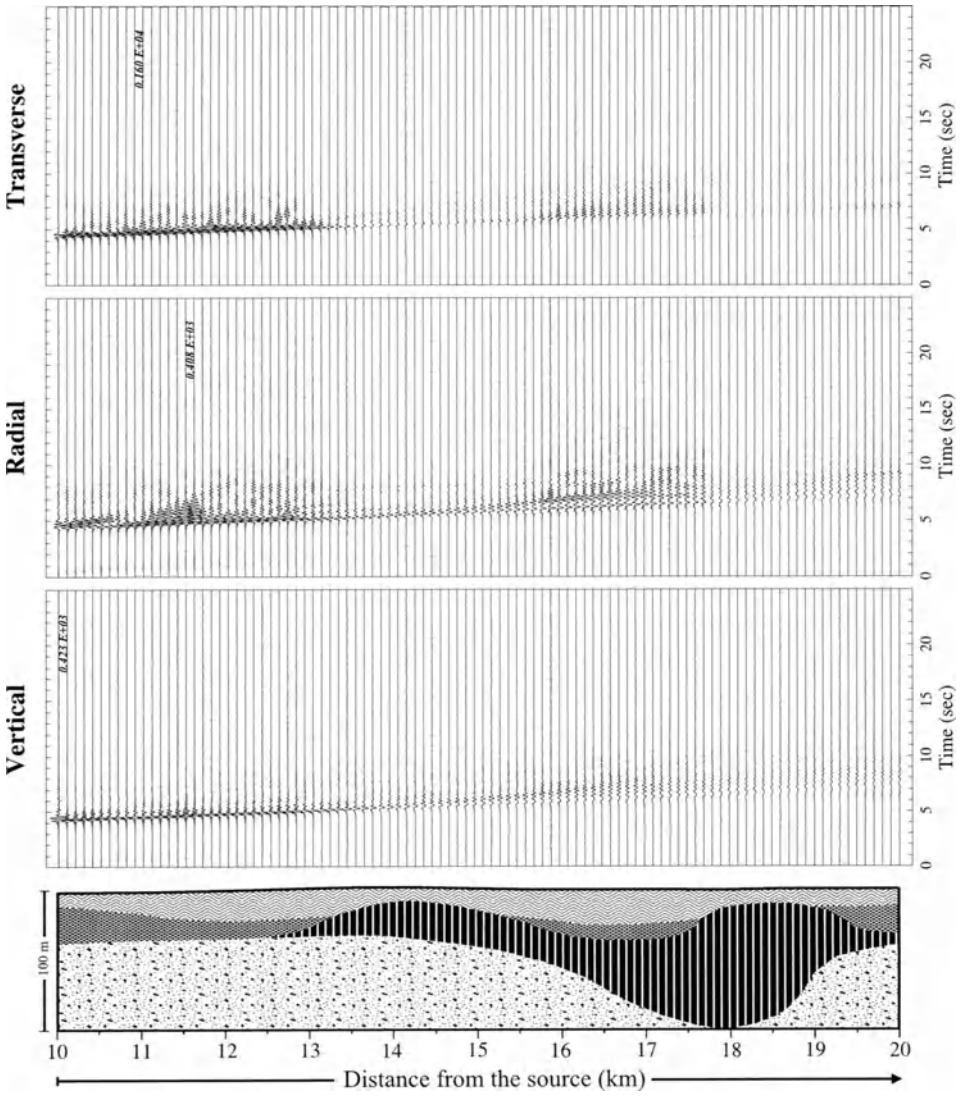

Figure 5
Same as Figure 4 but for the source to the south of the cross section.

distance are saturated for a large event in terms of damage/ground motion like that observed at the epicenter. Such high values of AMAX are in agreement with the reports of the damage caused by the 1720 earthquake (IYENGAR, 2000). The radial components of ground motion exhibit peak values ranging from 0.41 to 0.59 g, and the vertical components reach similar peak amplitudes, ranging from 0.42 to 0.43 g.

The response spectra ratio (RSR), i.e., the response spectra computed from the signals synthesized along the local model normalized by the response spectra computed from the corresponding (same epicentral distance) signals synthesized for the regional bedrock model, is another parameter relevant for earthquake engineering purposes. The distribution of RSR as a function of frequency and epicentral distance along the profile, up to a maximum frequency of 5 Hz is shown

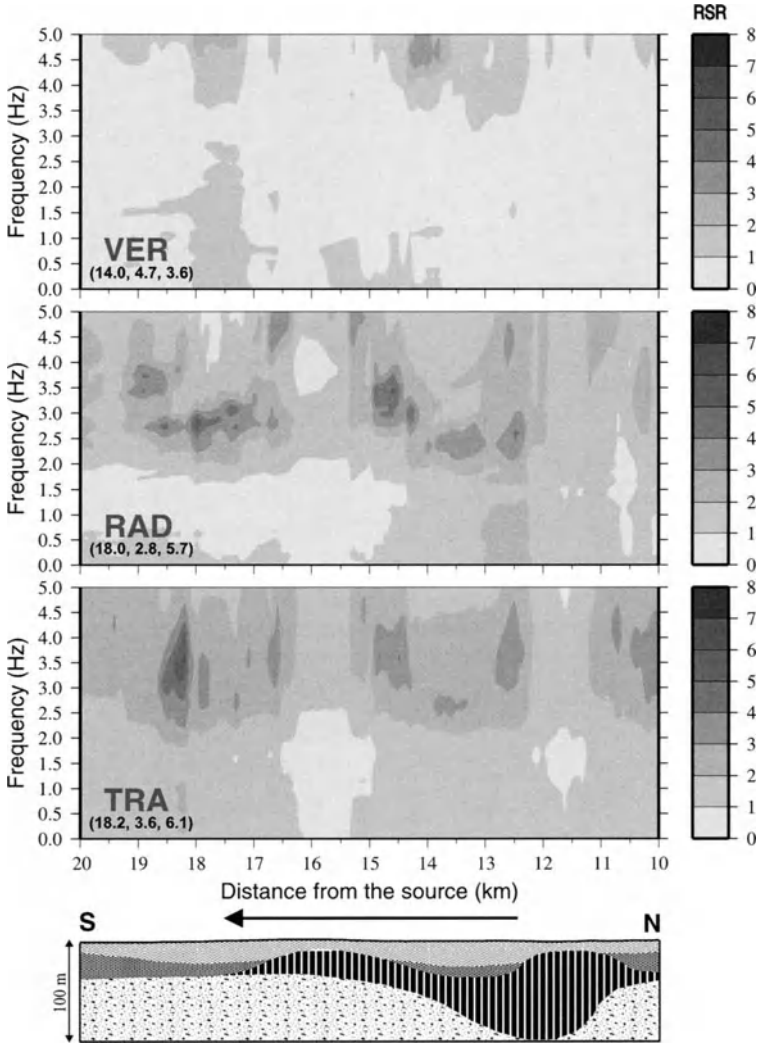

Figure 6

The NS cross section and the corresponding plot of response spectra ratio (RSR) versus frequency, when the source is to the north of the cross section. The numbers in parentheses represent in order the distance in km, frequency in Hz and value of the peak RSR, where maximum amplification is found.

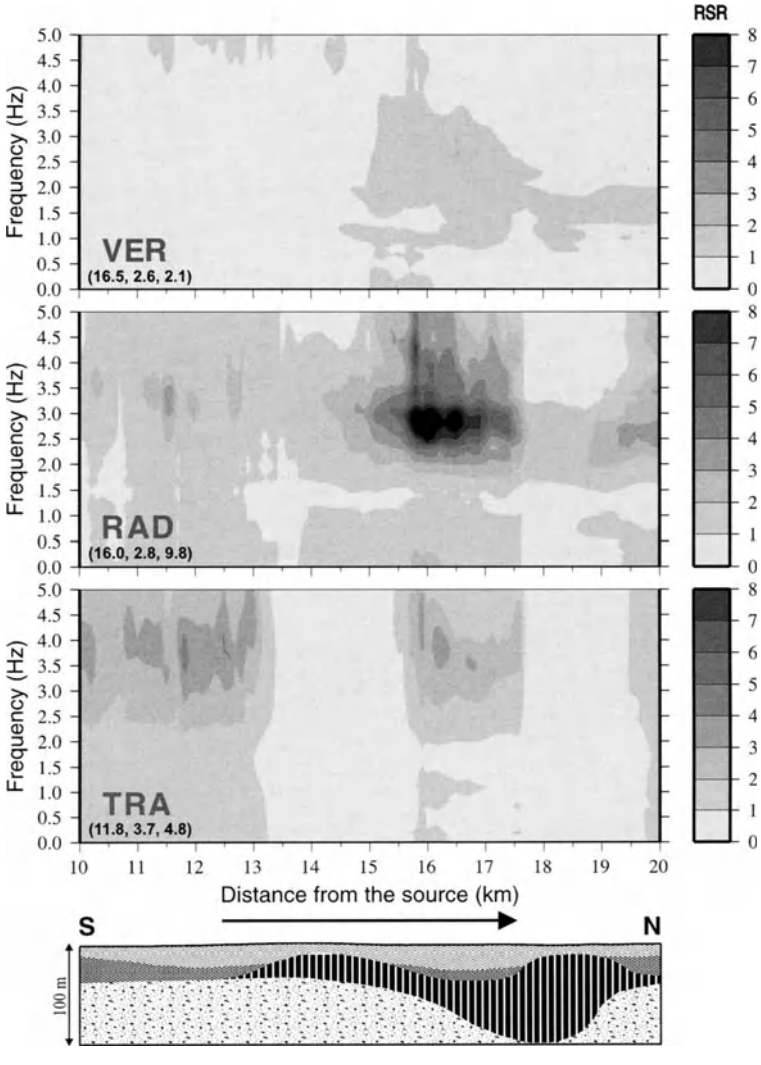

Figure 7
Same as Figure 6 but for the source to the south of the cross section. The maximum RSR, of about 10, is obtained in the radial component and it is shown by the black contour (this is the only component where RSR exceeds the upper limit of the legend of RSR).

for the three components in Figure 6 (northern source) and in Figure 7 (southern source). For each component of motion, the numbers in parentheses identify the maximum amplification. In order, the distance from the source in km, the frequency in Hz and the value of RSR are given. A 5% damping of the response spectra is considered since reinforced concrete buildings are already or will be built in the area. There are sites where the amplifications are relevant in all the three

components, even if the maximum amplifications are always found in the horizontal components. If we compare Figures 6 and 7, we see that the direction of propagation of the waves influences the pattern of amplification significantly. We can notice a shift both in the frequency and the location of the peaks. For instance, if we look at the position of the absolute maximum, found in the radial component for the southern source, we see that for the northern source we have an amplification around 3 instead of 10. Substantial differences can be seen in the patterns of the vertical component as well. Almost no amplification is observed for the southern source in the region where the highest amplification of almost 4 is obtained with the northern source. Such differences could not be predicted by the widely used convolutive approaches, most of which are based on the treatment of vertically propagating wavefields.

Results along EW Cross Section

Synthetic seismograms (*SH* and *P-SV* waves) have been computed for an array of 100 receivers regularly spaced every 140 meters using the source model corresponding to the event of August 27, 1960. At first we placed the source to the east of the cross section, where the 1960 event actually occurred. Then we moved the source to the west of the cross section and recomputed the synthetic seismograms to discern if and how the amplification pattern changes. Figure 8 shows the three-component synthetic seismograms when the source is to the east of the cross section whereas the similar seismograms are shown in Figure 9 for the source placed to the west of the cross section. As in the case of the NS profile, the geometry of the cross section clearly influences the waveforms for both propagation directions. Here the largest acceleration (AMAX) is seen in the vertical component rather than in the horizontal components. For instance, 0.06 g is seen at 48.7 km from the source in Figure 8, and 0.07 g is seen in Figure 9 at the distance of 45.5 km from the source. The peak acceleration in the radial component is around 0.05 g and the transverse component is less than 0.025 g.

The distribution of RSR versus frequency and epicentral distance along the profile, up to a maximum frequency of 5 Hz is shown for the three components in Figures 10 (eastern source) and 11 (western source). The maximum amplification is obtained for the transverse components: less than 8 in Figure 10 and almost 6 in Figure 11 at a frequency of 3.9 and 3.7 Hz, respectively. The radial components have nearly the same amplification in both cases whereas the vertical component shows amplification around 4 at frequencies higher than 4.5 and 4.9 Hz, respectively. If we compare Figures 10 and 11, there is hardly any difference. Contrary to the case of the NS profile, even if we reverse the propagation direction, the response spectra ratio along several parts of the EW profile is practically the same for all three components. Part of the explanation could be found in the larger epicentral distance adopted for the EW profile (45 km instead of 10 km). The local

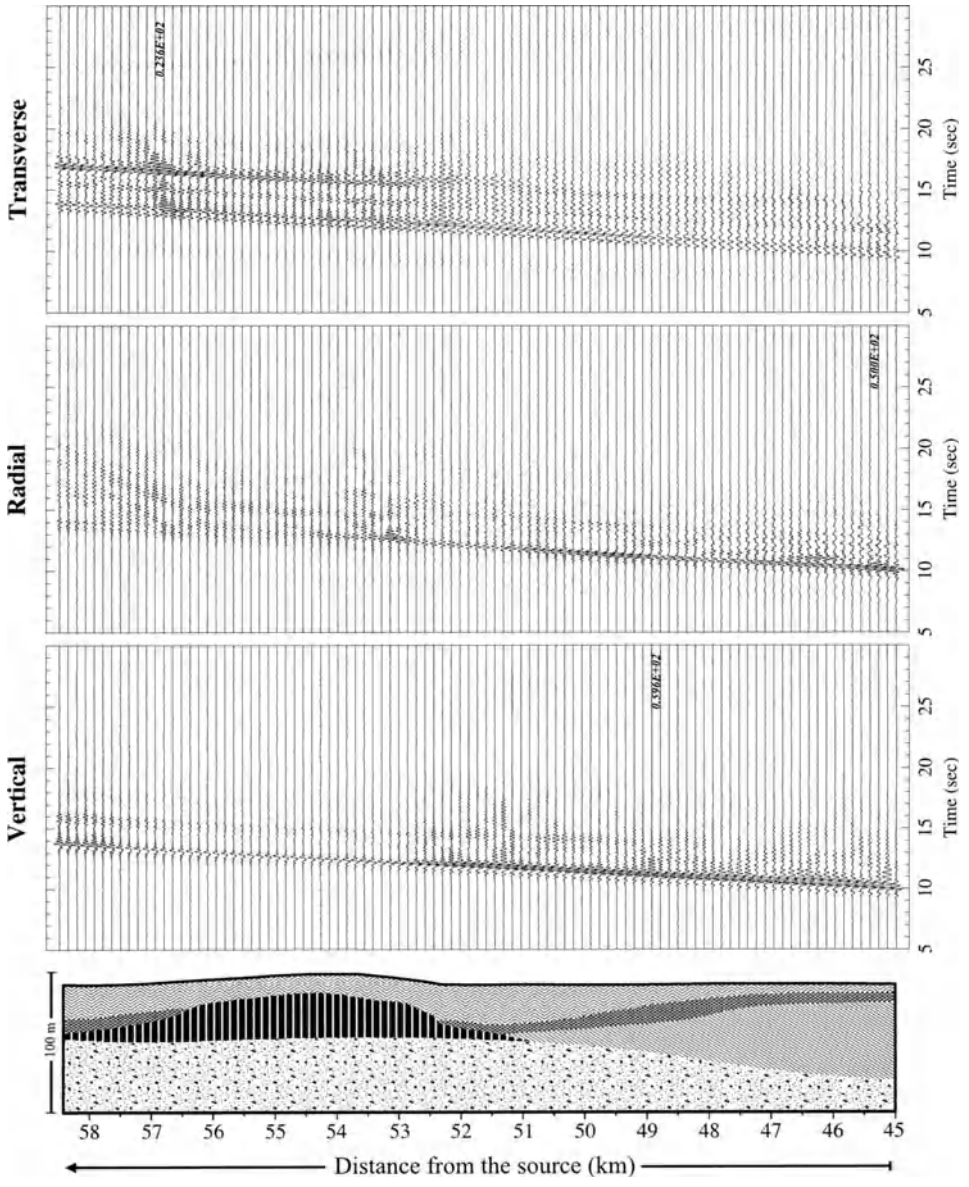

Figure 8.
The EW cross section and corresponding synthetic strong motion records computed when the source is to the east of the cross section.

amplifications, seen along the two profiles, show that in general the local intensity (MCS) increments can be as large as two units, with respect to the average value observed in the entire urban area (PANZA *et al.*, 1999b).

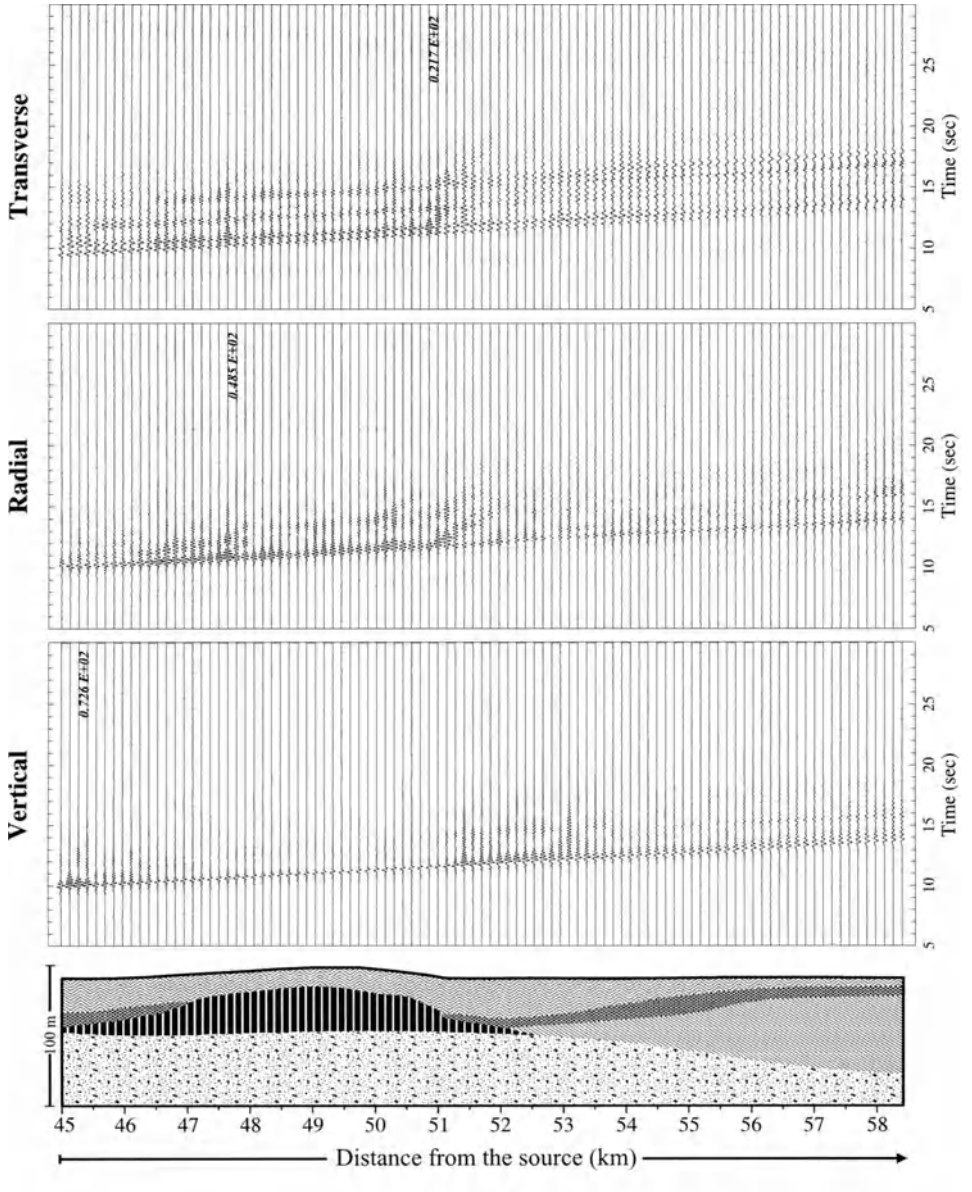

Figure 9
Same as Figure 8 but for the source to the west of the cross section.

Discussion and Conclusions

Delhi represents a typical example of a megacity, which is under severe seismic threats not only from local earthquakes but also from Himalayan earthquakes, located just 200–250 km from the city. The city has already suffered serious damages

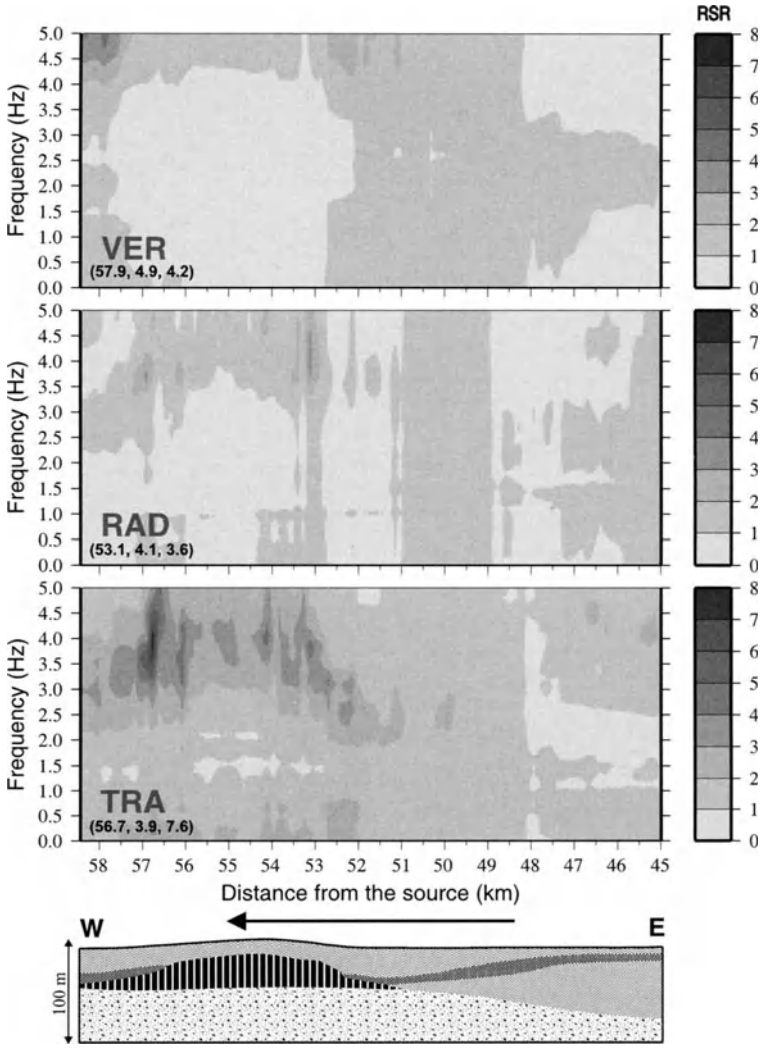

Figure 10
Same as Figure 6 for EW cross section when the source is to the east of the cross section.

in the past because of the degraded conditions of the historical built environment, and the severe local site amplification. In the present scenario, the high population density and the nature of built environment increase the vulnerability of many parts of this megacity. Such vulnerability may be reduced through the retrofitting of ancient buildings and monuments and through the design of reinforced concrete structures that are able to better resist the high amplitudes of the seismic ground motion. Sound anti-seismic construction requires the knowledge of seismic site response, both in terms of peak ground acceleration and response spectral ratio.

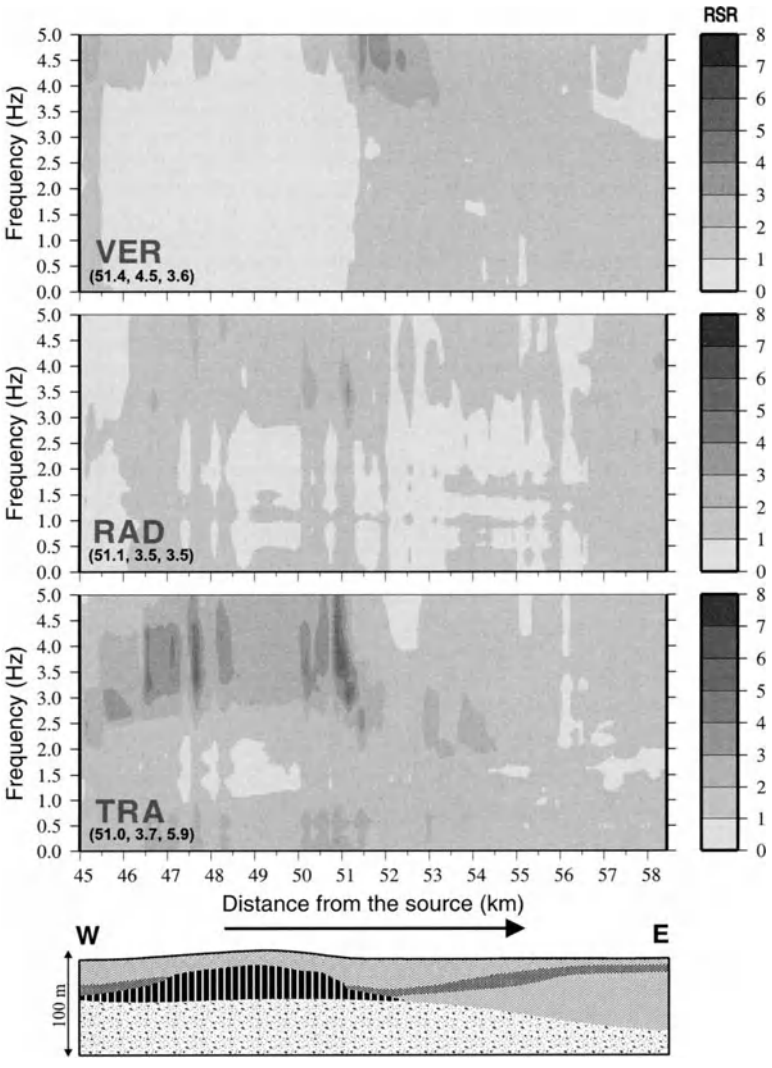

Figure 11
Same as Figure 6 for EW cross section when the source is to the west of the cross section.

The present paper illustrates the simulation of the ground motion along two cross sections located in Delhi City. Realistic *SH*- and *P-SV*-wave seismograms are computed twice: (i) placing the source at a given distance from one side of the profile and (ii) placing the same source to the other side of the profile, keeping the distance unchanged. The ground motion modelling of complete *SH* and *P-SV*-waves and the response spectra ratio (RSR) indicate that the laterally heterogeneous shallow soil deposits, composed of sandy silt and silty sand materials, are responsible for a large increase in site amplification of the horizontal components of motion. These

amplification effects of the sediments peak in the frequency range from 2.8–3.7 Hz (NS cross section) or from 3.5–4.1 Hz (EW cross section) for the horizontal components, while the vertical component is amplified at higher frequencies (up to 4.7 Hz in the case of NS cross-section, and 4.9 Hz for the EW cross section). The peak spectral amplifications, for the transverse and radial components, reach similar values and, in general, they are larger than those for the vertical component of motion. In our opinion, a correct definition of the response spectrum of the studied area should be based on the average or, better, on the maximum spectral amplifications computed along the profiles. Maximum spectral amplifications of the transverse and radial components, computed with a 5% response spectral damping, range between more than 3 to about 10 in the frequency range from 2.8 to 4.1 Hz.

Given a certain earthquake scenario, and an appropriate structural model, based on detailed geological, geophysical and geotechnical data, it is possible to realistically evaluate the local amplification in the frequency range of interest for civil engineering, and to obtain valuable parameters for the realistic microzonation. This is possible by applying numerical modelling that takes into account source, propagation and local site effects, without having to resort to convolutive methods. PARVEZ *et al.*, (2003) have compared the PGA with distance, of the Uttarkashi (1991, $M_w = 6.8$) event and two more events of north east India with the results obtained by the synthetic signals and found in good agreement. However, the strong motion records of the Chamoli event (1999, $M_w = 6.5$) available at few sites of Delhi City can be used for calibration in future studies of the microzonation of Delhi City. This is the first detailed study undertaken for Delhi City based on ground motion modelling, in terms of both the peak ground acceleration and the spectral amplification carried out along two profiles. PARVEZ *et al.* (2002) have shown just one example computed along the NS cross section. The results of this study can readily be applied to site-specific design spectra based on average or maximum amplification and should strictly be followed in revising the building codes. Such building codes must not only allow but encourage on demand the use of such site-specific design procedures on soft-soils, in order to protect buildings during earthquakes comparable to those we have considered in the modelling.

This is a good starting point for the microzonation of Delhi City. Many more 2-D cross sections have been collected for the city. Generation of the ground motion histories for the entire city is currently attempted. One of the important aspects of future studies will be to model the site-effects, due to the subsurface soil of Delhi City, as brought about by an expected great earthquake in the Central Himalayas.

Acknowledgements

Part of this study started when IAP availed the fellowship under the framework of Training and Research in Italian Laboratory (TRIL) and Associateship program

of ICTP, Trieste, Italy. This study has been conducted within the framework of the UNESCO-IUGS-IGCP project "Realistic Modelling of Seismic Input for Megacities and Large Urban Areas". Dr. Gangan Prathap, Scientist-in-Charge, C-MMACS has provided the facilities to IAP and given permission to publish this work. We are grateful to Prof. V.K. Gaur for his valuable suggestion and constant encouragement. We also thank Prof. R.N. Iyengar for providing important data and literature.

References

ALVAREZ, L., PANZA, G. F., VACCARI, F., and GONZALEZ, B. (2001), *Modelling of Seismic Ground Motion in Santiago de Cuba City from Earthquakes in the Oriente Fault Seismic Zone*, Pure. Appl. Geophys. *158*, 1763–1782.

BILHAM, R., GAUR, V. K., and MOLNAR, P. (2001), *Himalayan Seismic Hazard*, Science *293*, 1442–1444.

FÄH, D., SUHADOLC, P., and PANZA, G. F. (1993a), *Variability of seismic ground motion in complex media: The Friuli area (Italy)*. In *Geophysical Exploration in Areas of Complex Geology, II* (eds. Cassinis, R., Helbig, K. and Panza, G. F.) J. Appl. Geophys. *30*, 131–148.

FÄH, D., IODICE, C., SUHADOLC, P., and PANZA, G. F. (1993b), *A New Method for the Realistic Estimation of Seismic Ground Motion in Megacities: The Case of Rome*, Earthquake Spectra *9*, 643–668.

FÄH, D. and PANZA, G. F. (1994), *Realistic Modelling of Observed Seismic Motion in Complex Sedimentary Basins*, Annali di Geofisica *37*(6), 1771–1797.

FÄH, D., SUHADOLC, P., MUELLER, St., and PANZA, G. F. (1994) *A Hybrid Method for the Estimation of Ground Motion in Sedimentary Basins: Quantitative Modelling for Mexico City*, Bull. Seism. Soc. Am. *84*, 383–399.

FÄH, D. and SUHADOLC, P. (1995), *Application of Numerical Wave-propagation Techniques to Study Local Soil Effects: The Case of Benevento (Italy)*, Pure Appl. Geophys. *143*, 513–536.

FIELD, E. H. and the SCEC PHASE III WORKING GROUP (2000), *Accounting for Site Effects in Probabilistic Seismic Hazard Analyses of Southern California: Overview of the SCEC Phase III Report*, Bull. Seism. Soc. Am. *90*, S1–S31.

FLORSCH, N., FÄH, D., SUHADOLC, P., and PANZA, G. F. (1991), *Complete Synthetic Seismograms for High-frequency Multimode SH Waves*, Pure Appl. Geophys. *136*, 529–560.

G.S.I. (1997), *Contribution of Geological Survey of India in Delhi Area – A Resume*, 1–41.

IYENGAR, R. N. (2000), *Seismic Status of Delhi Megacity*, Current Science *78*(5), 568–574.

KHATTRI, K. N. (1987), *Great Earthquakes, Seismicity Gaps and Potential for Earthquakes Disaster along the Himalayan Plate Boundary*, Tectonophysics *138*, 79–92.

LEVANDER, A. R. (1988), *Fourth-order Finite-difference P-SV Seismograms*, Geophysics *53*, 1425–1436.

LOKMER, I., HERAK, M., PANZA, G. F., and VACCARI, F. (2002), *Amplification of Strong Ground Motion in the City of Zagreb, Croatia, Estimated by Computation of Synthetic Seismograms*, Soil Dynamics and Earthquake Engineering *22*, 105–113.

MARRARA, F. and SUHADOLC, P. (1998), *Observation and Modelling of Site Effects in the Volvi basin, Greece*. In: (K. Irikura, K. Kudo, H. Okada and T. Sasatani, eds.), *The Effects of Surface Geology on Seismic Motion* (Balkema, Rotterdam, The Netherlands, 1998), pp. 973–980.

MOLDOVEANU, C. L. and PANZA, G. F. (1999), *Modelling for Micronization Purposes, of the Seismic Ground Motion in Bucharest, due to Vrancrea Earthquake of May 30, 1990*. In *Vrancea Earthquakes: Tectonics, Hazard and Risk Mitigation* (F. Wenzel et al., eds.), 85–97 (Kluwer Academy Publ. 1999).

MOLDOVEANU, C. L., MARMUREANU, G., PANZA, G. F., and VACCARI F. (2000), *Estimation of Site Effects in Bucharest, Caused by the May 30–31, 1990, Vrancrea Seismic Events*, Pure Appl. Geophys. *157*, 249–267.

MOLNAR, P., FITCH, T. J., and WU, F. T. (1973), *Fault Plane Solutions of Shallow Earthquakes and Contemporary Tectonics of Asia*, Earth Planet. Sci. Lett. *16*, 101–112.

NATH, M., NARAIN, K., and SRIVASTAVA, J. P. (1968), *The Delhi Earthquake of 27th August, 1960*, Rec. Geol. Surv. India *98*, 367–382.

NUNZIATA, C., FÄH, D., and PANZA, G. F. (1995), *Mitigation of Seismic Hazard of a Megacity: The Case of Naples*, Annali di Geofisica *38*, 649–661.

NUNZIATA, C., COSTA, G., MARRARA, F., and PANZA, G. F. (2000), *Validated Estimation of Response Spectra for the 1980 Irpinia Earthquake in the Eastern Area of Naples*, Earthquake Spectra *16*, 643–660.

PANZA, G. F. (1985), *Synthetic Seismograms: The Rayleigh Waves Modal Summation*, J. Geophys. *58*, 125–145.

PANZA, G. F. and SUHADOLC, P. (1987), *Complete strong motion synthetics.* In (B. A. Bolt, ed.), *Seismic Strong Motion Synthetics, Computational Techniques 4*, (Academic Press, Orlando, 1987), pp. 153–204.

PANZA, G. F., ROMANELLI, F., and VACCARI, F. (1999a), *The IUGS-UNESCO IGCP Project 414: Realistic Modelling of Seismic Input for Megacities and Large Urban Areas*, Episodes *22*, 26–32.

PANZA, G. F., VACCARI, F., and CAZZARO, R. (1999b), *Deterministic Seismic hazard assessment.* In *Vrancea Earthquakes: Tectonics, Hazard and Risk Mitigation* (F. Wenzel *et al.* eds.), 269–286 (Kluwer Academy Publ. 1999b)

PANZA, G. F., RADULIAN, M., and TRIFU, C.-I. (eds) (2000), *Seismic Hazard of the Circum-Pannonian Region*, Pure Appl. Geophys. *157* (2000), No. 1/2. (Birkhäuser Verlag, Basel, Switzerland 2000).

PANZA, G. F., ROMANELLI, F., and VACCARI, F. (2001), *Seismic Wave Propagation in Laterally Heterogeneous Anelastic Media: Theory and Application to Seismic Zonation.* (R. Dmowska and B. Saltzman eds.), Advances in Geophysics, (Academic Press, San Diego, USA *43*, 1–95).

PARVEZ, I. A., VACCARI, F., and PANZA, G. F. (2003), *A Deterministic Seismic Hazard Map of India and Adjacent Areas*, Geophys. Jr. Int. *155*, 489–508.

PARVEZ, I. A., PANZA, G. F., GUSEV, A. A. and VACCARI, F. (2002), *Strong-motion Amplitude in Himalayas and a Pilot Study for the Deterministic First-order Microzonation in a Part of Delhi City*, Current Science *82*, 158–166.

ROMANELLI, F., VACCARI, F., and PANZA, G. F. (1998a), *Realistic Modelling of Ground Motion: Techniques for site response estimation.* In *Proc. of 6th U.S. National Conf. Earthquake Engin.* Seattle, U.S.A. 31 May–4 June, 1998, CD-ROM: paper 433.

ROMANELLI, F., NUNZIATA, C., NATALE, M., and PANZA G. F. (1998b), *Site response estimation in the Catania area.* In (K. Irikura, K. Kudo, H. Okada and T. Sasatani, eds.) *The Effects of Surface Geology on Seismic Motion* (Balkema, Rotterdam, The Netherlands, 1998b, pp. 1093–1100.

ROMANELLI, F. and VACCARI, F. (1999) *Site Response Estimation and Ground Motion Spectrum Scenario in the Catania Area*, Jr. of Seismology *3*, 311–326.

SETT, D. N. (1964), *Groundwater Geology of the Delhi Region.* Bull. Geol. Surv. India, Series B, No. 16.

SUN, R., VACCARI, F., MARRARA, F., and PANZA, G. F. (1998), *The Main Features of the Local Geological Conditions Can Explain the Macroseismic Intensity Caused in Xiji-Langfu (Beijing) by the MS = 7.7* TANGSHAN 1976 earthquake, Pure Appl. Geophys. *152*, 507–521.

VIRIEUX, J. (1984), *SH-wave Propagation in Heterogeneous Media: Velocity-stress Finite-difference Method*, Geophysics *49*, 1933–1957.

VIRIEUX, J. (1986) *P-SV Wave Propagation in Heterogenoues Media: Velocity-stress Finite-Difference Method*, Geophysics *51*, 889–901.

(Received April 2002, accepted October 14, 2002)

Pure appl. geophys. 161 (2004) 1185–1203
0033–4553/04/061185–19
DOI 10.1007/s00024-003-2493-y

Pure and Applied Geophysics

PART I: Theoretical Site Response Estimation for Microzoning Purposes

P. TRIANTAFYLLIDIS[1], P. SUHADOLC[2], P. M. HATZIDIMITRIOU[1], A. ANASTASIADIS[3], and N. THEODULIDIS[3]

Abstract—We estimate the theoretical site response along seven cross sections located in the city of Thessaloniki (Greece). For this purpose the 2-D structural models used are based on the known geometry and the dynamic soil properties derived from borehole measurements and other geophysical techniques. Several double-couple sources have been employed to generate the seismic wavefield, and a hybrid method that combines the modal summation with finite differences, has been deployed to produce synthetic accelerograms to a maximum frequency of 6 Hz for all components of motion. The ratios between the response spectra of signals derived for the 2-D local model and the corresponding spectra of signals derived for the 1-D bedrock reference model at the same site, allow us to estimate the site response due to lateral heterogeneities. We interpret the results in terms of both geological and geometrical features of the models and of the characteristics of the wave propagation. The cases discussed confirm that the geometry and depth of the rock basement, along with the impedance contrast, are responsible for ground amplification phenomena such as edge effects and generation and entrapment of local surface waves. Our analysis also confirms that the peak ground acceleration is not well correlated with damage and that a substantially better estimator for possible damage is the spectral amplification.

Key words: Site response, 2-D finite-differences modeling, hybrid method, spectral ratios, Thessaloniki, Greece.

Introduction

The destructive effects of the large earthquakes that occurred during recent years (e.g. KOBE 1995, CHI-CHI 1999, IZMIT 1999), which mostly impacted urban areas with a heavy casualty toll, have fostered numerous studies on the estimation of seismic ground motion in a given urban area before the occurrence of a damaging earthquake. This task requires the detailed knowledge of both the subsurface structure within the city and of the probable location and characteristics of seismic sources around it. On the other hand, one needs theoretical methods and related computer codes that allow the simulation of the expected seismic ground motion. Detailed numerical simulations play an important role in

[1] Aristotle University, Geophysical Laboratory, P.O.Box 111, GR-54124 Thessaloniki, Greece.
[2] University of Trieste, Department of Earth Sciences, V. Weiss 1, I-34127 Trieste, Italy.
[3] Institute of Eng. Seismology and Earthq. Engineering (ITSAK), GR-55102 Thessaloniki, Greece.

the computation of ground motion, especially in areas of complex geology, because they can provide realistic synthetic waveforms at places where no recordings are available. Synthetics are compared with observations wherever instrumental data are available, in order to validate and, if needed, to further improve the theoretical techniques. Consequently, during recent years several methods have been proposed for the theoretical estimation of seismic response at a specific site (e.g., FÄH and SUHADOLC, 1994; FURUMURA and TAKENAKA, 1996; WALD and GRAVES, 1998; FIELD *et al.*, 2000).

The theoretical methods that study the wave equation can be classified (e.g., FÄH *et al.*, 1993; SUHADOLC, 1997) into two sizable categories: numerical and analytical methods. Numerical methods make use of grid techniques, i.e., the discretization of the medium and the derivatives (in time and space) of the wave equation and subsequent solution of the derived system of linear equations. In analytical methods, differential equations and boundary conditions are translated into integral equations that are discretized and solved by using various mathematical techniques. Analytical methods usually require as input data models with simple geometries, as opposed to numerical methods which are more suitable to process relatively complex structures, even if restricted by the size of the model due to limitations of computer memory.

In this study we extend the work of TRIANTAFYLLIDIS *et al.* (1998), who applied the hybrid method and derived preliminary results for two of the cross sections, to a total of seven cross sections located within the city of Thessaloniki.

Method

The hybrid method employed in this work for the construction of synthetics is throughly described in other papers (FÄH, 1992; FÄH and SUHADOLC, 1994; FÄH *et al.* 1994; PANZA *et al.*, 2000). It combines two techniques: finite differences (FD) and modal summation (MS). The structural model used in the computations consists of two parts: A simple 1-D "bedrock" or "regional" structure and a 2-D lateral heterogeneous structure. The source is located in the 1-D structure and the calculations are performed in two stages. The seismic wavefield is propagated from the source to the boundaries of the laterally heterogeneous area applying the MS method. The time series that result from this technique are used to excite the wave propagation in the laterally heterogeneous medium and the seismic wavefield is propagated with the FD technique. The hybrid approach thus allows the calculation of the local seismic wavefield for short (few kilometers) as well as for long (several hundred kilometers) epicentral distances. The use of the MS method also permits the study of extended sources which can be modeled as a sum of point sources properly distributed in time and space, allowing the simulation of a realistic rupture process at the causative fault (e.g., SARAÒ *et al.*, 1998; BAJC *et al.*, 2001).

Even if currently relatively powerful computers with considerable memory are available, there will always be memory limitations in the use of the FD method. The need to study wave propagation either for spatially very extended areas or at high frequencies ($f > 5$ Hz) is becoming in fact increasingly greater. To ascertain that spurious reflections from the artificial boundaries of the FD grid in space have been properly treated, we initially compare the results from the MS computation with those from FD for the simple case of the 1-D regional velocity model. The 2-D simulations are only performed if the differences between the above results vary within 2–5%.

Data and Process

Our 2-D simulations are based on detailed geotechnical information originating from a series of tests and extended geophysical prospects (cross-hole and down-hole measurements, surface-wave inversions) carried out within the entire urban area of Thessaloniki by the Laboratory of Soil Mechanics and Foundation Engineering of Aristotle University of Thessaloniki. The known geometry and the dynamic properties of the soil (density, body-wave velocities and quality factors) that were used resulted from various studies of this area (PITILAKIS *et al.*, 1992; ANASTASIADIS, 1994; RAPTAKIS, 1995).

All information has been elaborated in order to construct seven 2-D cross sections, each one along a profile with different orientation (Fig. 1), covering most of the city area.

After the selection of the location of each profile, all available information on subsurface layer properties derived from existing bore-holes in the surroundings (RAPTAKIS *et al.*, 1994; PITILAKIS and ANASTASIADIS, 1998) were projected on the related section. In such a way, also by stratigraphically correlating between the adjacent bore-holes, 2-D cross sections have been constructed. Apart from the geometry of the layering, which was rather well constrained by data, all dynamic layer properties (densities, body wave velocities, quality factors) were estimated by RAPTAKIS (1995). The 2-D local velocity models along each of the seven profiles were thus constructed, their thickness varying according to the depth of the solid bedrock. Each such local velocity model is underlain by a common "regional" velocity model derived from the studies of the wider area of the Serbomacedonian geological zone (LIGDAS and LEES, 1993; PAPAZACHOS, 1998) to which the city area belongs. Consequently, the local 2-D velocity model overlies the regional 1-D model, consisting of homogeneous, horizontal and anelastic layers. The layering of the seven cross sections, as well as each layer dynamic properties, are shown in detail by TRIANTAFYLLIDIS *et al.* (2004) (PART-II, this volume).

The focal mechanisms of the double-couple point sources that were used to excite the seismic wavefield impingent on the cross sections and allowing the construction of the 2-D synthetic accelerograms, are shown in Table 1. The fault

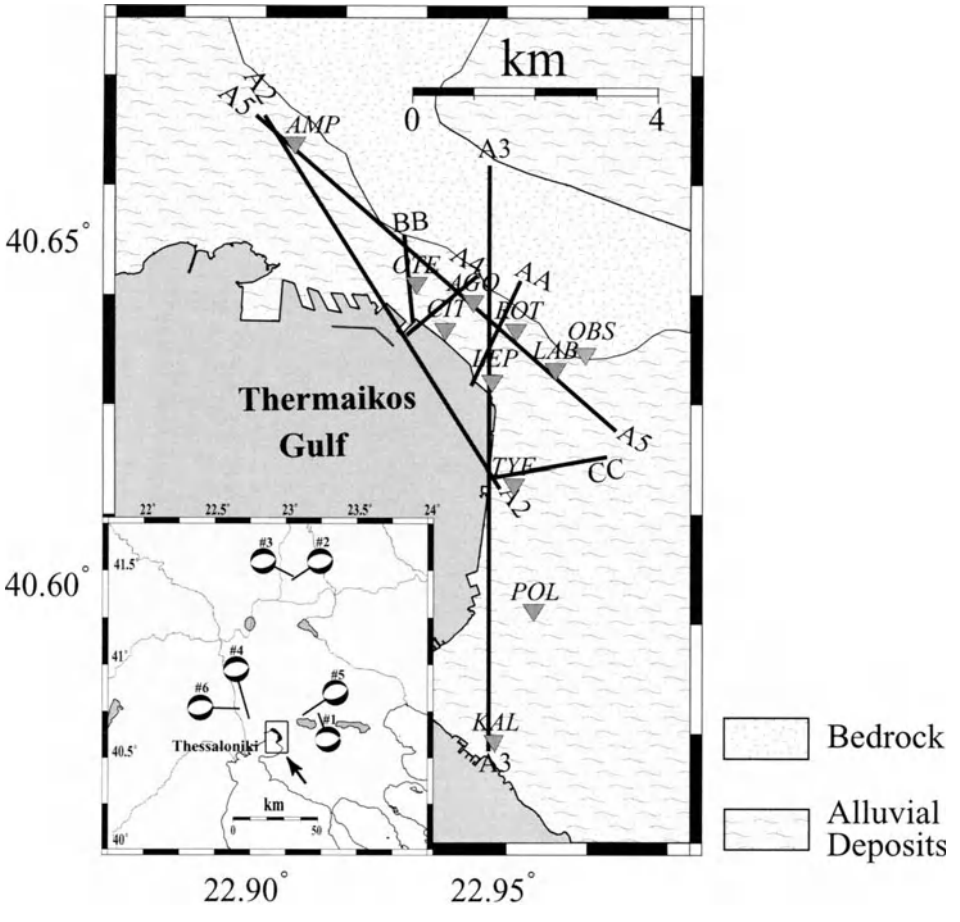

Figure 1
Map of Thessaloniki and the cross sections along which the seismic response (site effects) is estimated through the hybrid method (see text). In the inset, the focal mechanisms of the simulated events are shown, while the arrow denotes the area under investigation.

Table 1

Parameters of earthquakes used for the construction of synthetic accelerograms.

No.	Date	Long.°	Lat.°	M_S	Depth (km)	Strike	Dip	Rake
1.	780620	40.740°	23.230°	6.5	6.0	278°	46°	−70°
2.	931222	41.450°	23.040°	3.3	7.0	76°	45°	−94°
3.	931216	41.470°	23.050°	4.7	7.0	76°	45°	−94°
4.	940108	40.712°	22.742°	2.5	6.0	76°	45°	−94°
5.	780704	40.730°	23.120°	5.1	6.0	252°	37°	−88°
6.	940216	40.764°	22.676°	2.0	5.0	76°	45°	−94°

plane solution of source #1 (Table 1) corresponds to that of the destructive earthquake ($M_s = 6.5$) of June 20, 1978, whereas source #5 corresponds to its largest aftershock ($M_s = 5.1$) of July 4. The fault plane solutions used for sources #2, #3, #4 and #6 (Table 1), are representative of the active stress field in the area of northern Greece according to PAPAZACHOS and KIRATZI (1996).

In Table 2 we report some parameters of the seven sections that were used: the first column shows the section's code name, whereas the second one gives the event number (see Table 1). The third column gives the distance between the source and the first virtual receiver in the 2-D grid; the fourth column gives the interval between the receivers along the section. The fifth and sixth columns show the length of the FD grid in the horizontal and vertical dimensions, respectively.

In order to estimate the seismic motion allowing for the lateral heterogeneities, the hybrid method (FÄH, 1992) was applied for the construction of two sets of synthetic accelerograms along each section. The first set was calculated by assuming that the receivers are placed on the 1-D regional velocity model, whereas the second set is obtained by placing the receivers on top of the local 2-D velocity model. The two simulations were performed for all components of motion for a maximum calculation frequency of 6 Hz. In order to check the accuracy of the 2-D computations, the synthetics that resulted from the hybrid method when using the 1-D regional velocity model were compared with the ones that came out from the application of the purely analytical MS method for the same model. The amplitude differences were always less than 5%, an acceptable value (FÄH, 1992), and a confirmation of the validity of the boundary conditions applied in the hybrid method. The site response (or site effects) along the profiles is (are) estimated through spectral ratios. For each receiver along the section, the spectrum of the synthetic accelerogram calculated using the local 2-D model is divided by the respective synthetic spectrum obtained at the same receiver with computations performed using the 1-D regional model.

Table 2

Technical characteristics of the seven sections used as input to the application of hybrid method.

Section	Source used	Source distance (km)	Receivers interval (m)	FD grid dimensions (m)	
				Horizontal	Vertical
AA	#2	90.60	35	1300	5075
BB	#3	91.43	30	1300	6120
CC	#1	26.46	30	1500	6318
A2	#4	15.45	81	7100	6480
A3	#2	89.67	81	7700	6375
A4	#5	17.22	30	1400	8970
A5	#6	23.70	90	7000	10230

Results

In Figure 2 we show an example of the hybrid method results: the synthetic accelerograms obtained along the 2-D local velocity model of section A5. The time origin of the accelerograms is the instant in which the seismic waves enter the FD grid. The waveforms have been normalized per component to the amplitude of the waveform with the maximum Peak Ground Acceleration (PGA).

From the synthetics it is possible to extract the variation of some ground motion related quantities along the 2-D local velocity section, such as peak ground acceleration, PGA(2D), and Arias intensity, W(2D). Arias intensity is defined as

$$W = \frac{\pi}{2g} \int_0^\infty [\ddot{x}(T)]^2 \, dt \ ,$$

where, x, is the ground displacement, g, the gravity acceleration, t, the time and, T, the motion duration (Arias, 1970). Dots indicate differentiation in time.

In order to eliminate as much as possible the effects of source and regional propagation, the two quantities PGA(2D) and W(2D) are normalized to the quantities PGA(1D) and W(1D), respectively. The latter are calculated for the regional 1-D velocity model and the normalization performed for each receiver. In this way, the calculation of the relative peak ground acceleration, PGA(2D)/PGA(1D), and the relative Arias intensity, W(2D)/W(1D), allows the estimation of 2-D site response as compared with the site response obtained from the 1-D laterally homogeneous regional velocity model. Figures 3a and 3b show the variation of the above quantities along all sections for the radial (up), transverse (middle) and vertical (bottom) components. The variation of PGA(2D)/PGA(1D) is shown with a dashed line and is measured on the left vertical axis, whereas W(2D)/W(1D) is given as a continuous line and is measured on the right vertical axis. As can be expected from the definition of W, this quantity presents high values at those points along the models where the synthetic waveforms have high amplitudes and long durations.

Along section AA, the relative PGA and Arias intensity have their highest values (2.5 to 5), especially for the radial component, at a distance of 91 km from the seismic source at the transition from bedrock to alluvium. An analogous observation was made by FÄH and SUHADOLC (1994) as well as MARRARA and SUHADOLC (1998) for the city of Benevento, and the explanation was sought in the lateral high impedance between the superficial layers and rocky bedrock (edge effect), giving rise to the excitation of local surface waves. Something similar occurs for section BB, the

►

Figure 2
An example of the hybrid method results: the three component synthetic accelerograms computed for the local 2-D model along section A5 (Table 2) with a maximum calculation frequency of 6 Hz.

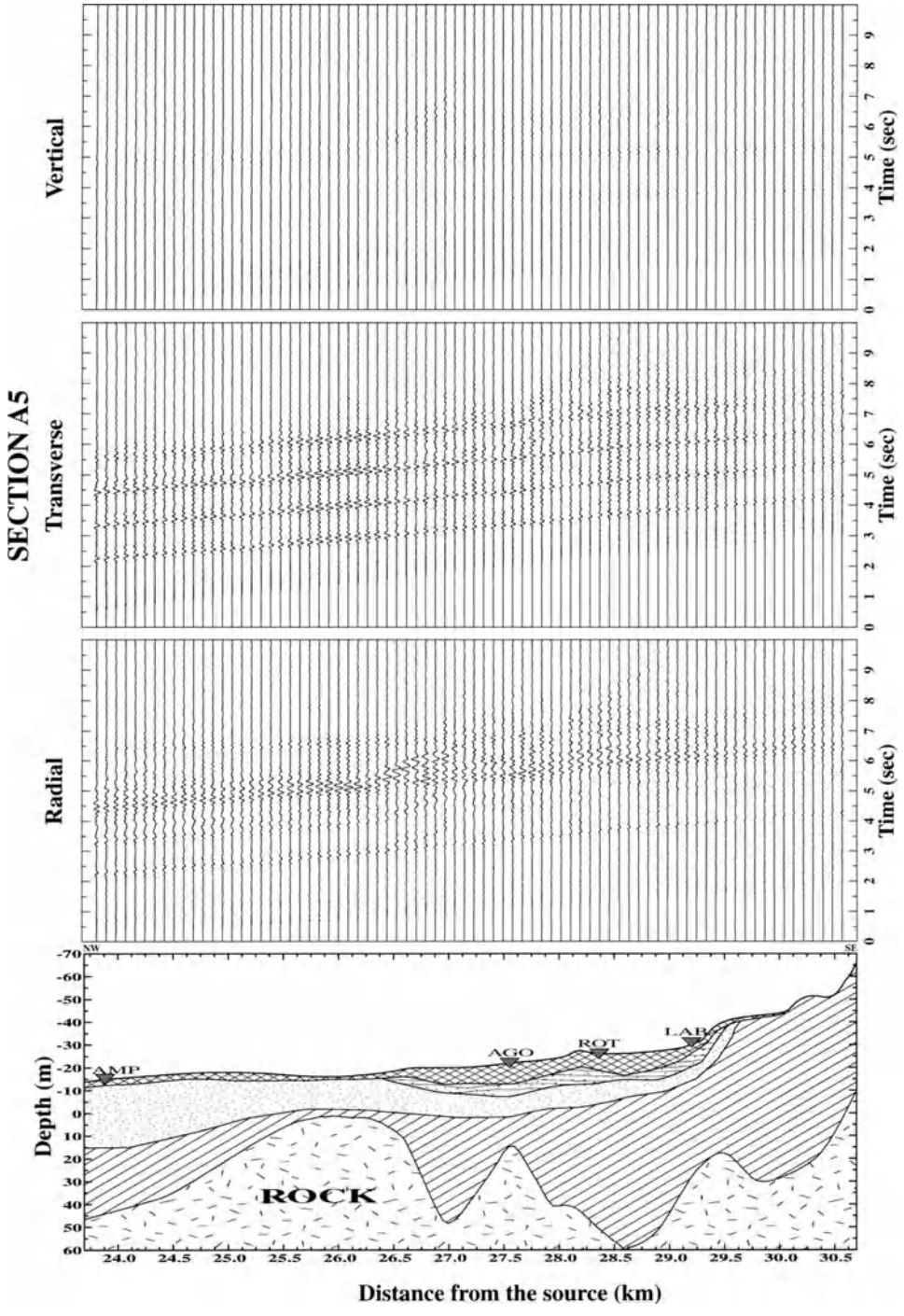
SECTION A5
Vertical
Transverse
Radial
Time (sec)
NW
SE
AMP
AGO
ROT
LAB
ROCK
Depth (m)
Distance from the source (km)

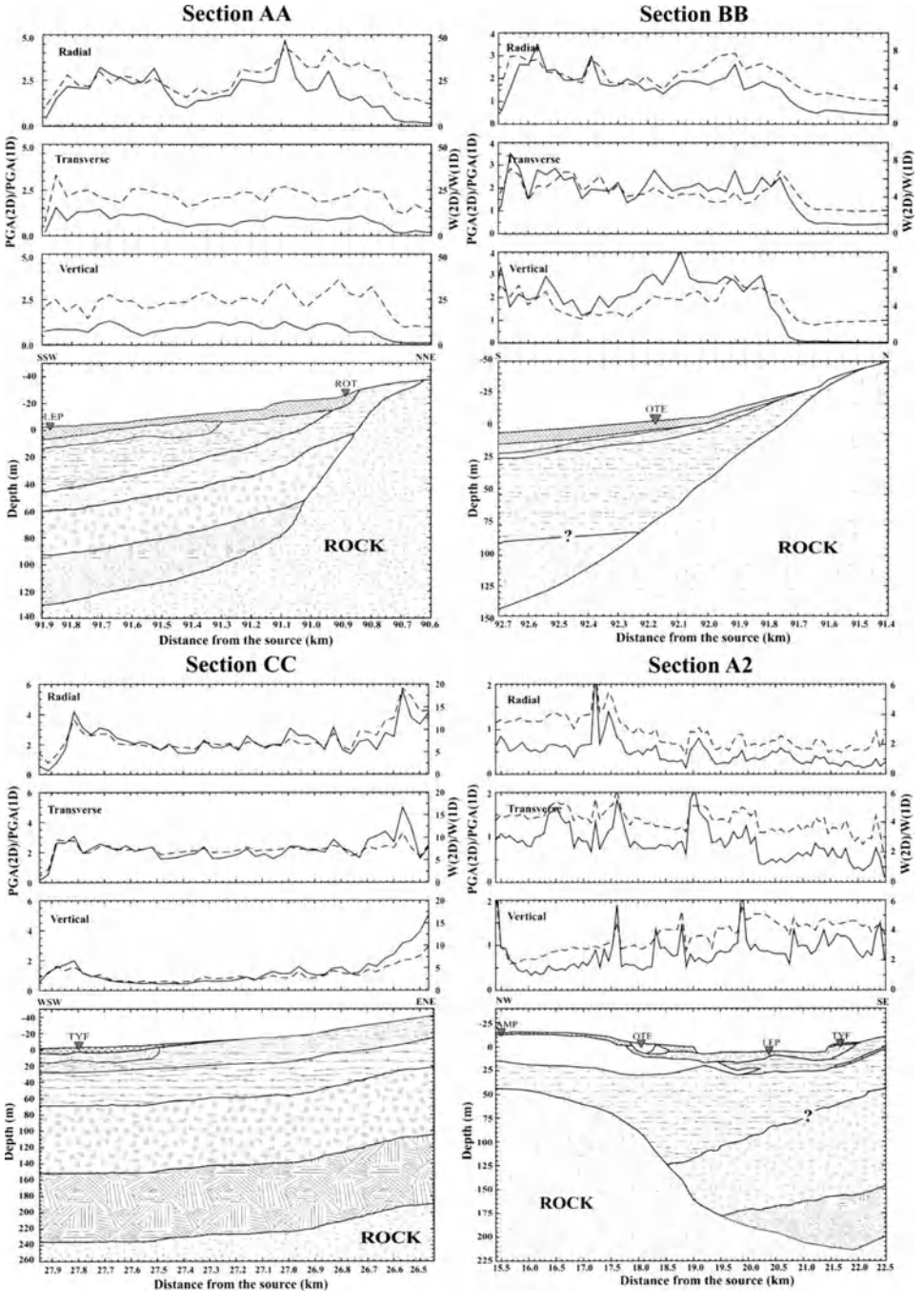
Section AA
Radial
Transverse
Vertical
PGA(2D)/PGA(1D)
W(2D)/W(1D)
SSW
NNE
ROT
LEP
Depth (m)
ROCK
Distance from the source (km)
Section BB
Radial
Transverse
Vertical
PGA(2D)/PGA(1D)
W(2D)/W(1D)
OTE
?
Depth (m)
ROCK
Distance from the source (km)
Section CC
Radial
Transverse
Vertical
PGA(2D)/PGA(1D)
W(2D)/W(1D)
WSW
ENE
TYF
Depth (m)
ROCK
Distance from the source (km)
Section A2
Radial
Transverse
Vertical
PGA(2D)/PGA(1D)
W(2D)/W(1D)
NW
SE
SMP
OTE
LEP
TYF
?
Depth (m)
ROCK
Distance from the source (km)

maximum of relative PGA and Arias intensity appearing close to the position of station OTE (Fig. 3a). Low values of these quantities are characteristic, especially for the vertical component, for the part of the model where the bedrock approaches the surface. At the other edge of the basin, slightly increased values of PGA(2D)/PGA(1D) and W(2D)/W(1D) are observed, which are probably due to the boundary conditions that delimit the artificial basin boundaries. Similar boundary effects are also seen on the ENE side of section CC (Fig. 3a), despite the simple geometry of the profile giving rise to stable values of PGA and W. Sections A2 (Fig. 3a) and A3 (Fig. 3b) have a relatively complex subsurface structure giving rise to high values of PGA(2D)/PGA(1D) and W(2D)/W(1D) at distances of 17.5 km and 90.5 km from the seismic source, respectively. Especially for the case of section A3 (Fig. 3b), the edge effect is very intense, causing high ground accelerations particularly for the vertical component, as denoted by the values of relative PGA (Fig. 3b) that exceed 4. Very strong edge effect at the discontinuity between the basin and the solid bedrock is noticed close to the area of station AGO on section A4. Conversely, in the part of the model which is closer to the seismic source (17.2 to 17.5 km), as well as in the deeper parts of the basin (18.2 to 18.6 km), the acceleration amplitudes for the 2-D model are relatively low (Fig. 3b), giving values of PGA(2D)/PGA(1D) below 1 for the three components. It is worth noting that at CIT the values of PGA(2D)/PGA(1D) and W(2D)/W(1D) are relatively low, despite the position of this site located only about half a kilometer away towards the center of the basin. At the site CIT, located over a thick package of sediments, strong damage had been observed during the earthquake of June 20, 1978. This only confirms that quantities such as PGA or duration of motion provide only a crude estimation of seismic motion and that they are not very good indicators of damage potential (e.g., FÄH and SUHADOLC, 1994).

The synthetic accelerograms of section A5 (Fig. 2) are very characteristic and the observed waveforms reflect the complex geometry of the 2-D model and particularly the bedrock surface anomalies. The waveforms over the small basin part of the model with the thick sedimentary layers (distances between 28 km and 29.5 km from the source) show high durations due to the trapped energy both within the superficial layers and in the basin with local surface waves generated. On the other end, the already mentioned edge effect might be responsible for the high values of PGA(2D)/PGA(1D) and W(2D)/W(1D) in the area where the bedrock rises to very shallow depths (25.5 km to 26.5 km from the seismic source), especially for the transverse component (Fig. 3b).

Other ground motion related quantities, which also can be extracted from the synthetics that were estimated with the numerical simulation for the 2-D local

◀

Figure 3a
Variation of quantities PGA(2D)/PGA(1D) (thin line) and W(2D)/W(1D) (thick line) along sections AA, BB, CC and A2 for all components of motion. The ratio PGA(2D)/PGA(1D) is measured on the left and W(2D)/W(1D) is measured on the right axis.

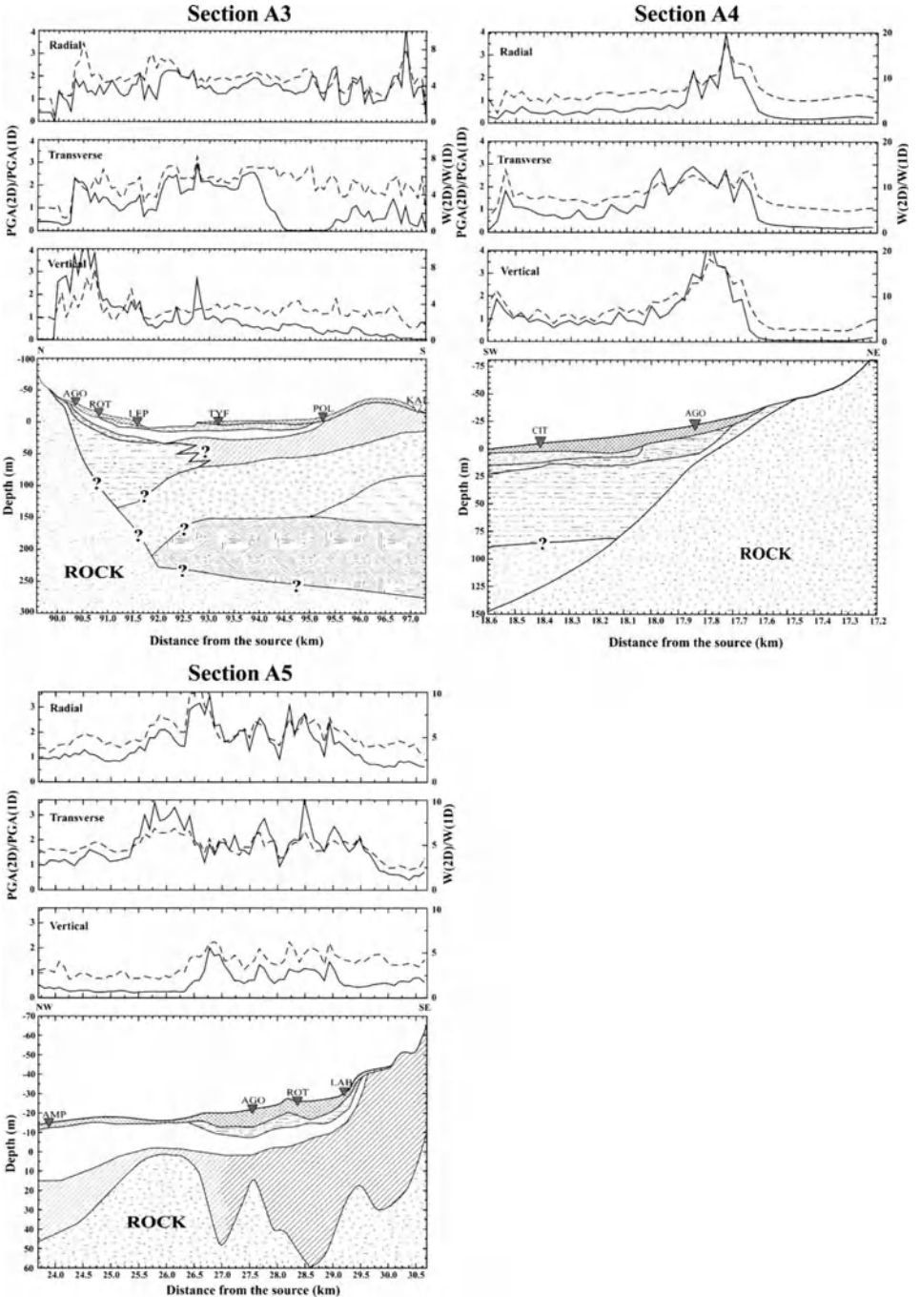

Figure 3b
The same as Figure 3a but for sections A3, A4 and A5.

velocity model, are the Fourier Amplitude Spectrum, FAS(2D), and the Spectral acceleration, Sa(2D), or response spectrum. In order to estimate the above quantities that are due only to the heterogeneities of the local velocity model, we normalized them to the respective quantities FAS(1D) and Sa(1D), as they were calculated for the 1-D regional velocity model with the hybrid method for the given source-receiver distance. By this normalization, the effects of the radiation pattern and propagation in the regional model were reduced and the results obtained reflect the effect of the 2-D local model on the seismic motion. In Figure 4 the variation with frequency of the ratio FAS(2D)/FAS(1D) is shown, indicatively only for section BB and Figure 5 (a and b) displays the ratios Sa(2D)/Sa(1D) between spectra with 5% damping for all components of motion along all the profiles.

The quantity FAS(2D)/FAS(1D) is estimated at ten selected sites on the surface of each section. The selection of these sites has been made based on the geometry and the layer parameters of each profile. In other words we proceeded to check all those points where the local soil profile has interesting features. Wherever along the profile a seismometer [RefTek station] was placed that recorded some event (LACHET *et al.*, 1996), the ratio FAS(2D)/FAS(1D) was computed also at those locations.

The variation with frequency of the ratio Sa(2D)/Sa(1D) between spectra with 5% damping is presented in color for all three components of motion along each section. The white spots that appear at some profiles indicate amplifications that are slightly higher than the maximum value specified on the color scale of each section. For section AA (Fig. 5a) the radial component is generally more amplified than the other two for all frequencies, and the highest values of amplification are observed for frequencies below 3 Hz. Moreover, low amplifications are observed in the middle of the basin at frequencies smaller than 4.5 Hz for all components. This indicates that the spectral amplification obtained from the 2-D local model is only a few times higher than the 1-D regional model amplification for these specific epicentral distances and azimuthal positions.

In the same figure, the simple geometry of section's BB bedrock interface is outlined. At distances from 91.75 km to 92.2 km from the seismic source, the amplification of the vertical component is high for frequencies above 3 Hz. Moving over the center to the basin edge (92.5–92.8 km from source), all components' spectral amplifications become high. This increase of spectral amplification for the horizontal components appears at frequencies 1 to 3 Hz, whereas for the vertical component it is less intense and appears at higher frequencies (3 to 5 Hz).

In the next graph of Figure 5a the horizontal layering and the relatively simple geometry of section CC produce, as expected, rather simple results. The radial component presents slightly higher amplifications than the other two. Actually, there are no important differences observed between the spectral amplification due to 2-D local and 1-D regional velocity models in the entire basin area. Close to site TYF (27.65 km, approximately) the vertical component amplification is low enough, while for the horizontal one it is significantly higher.

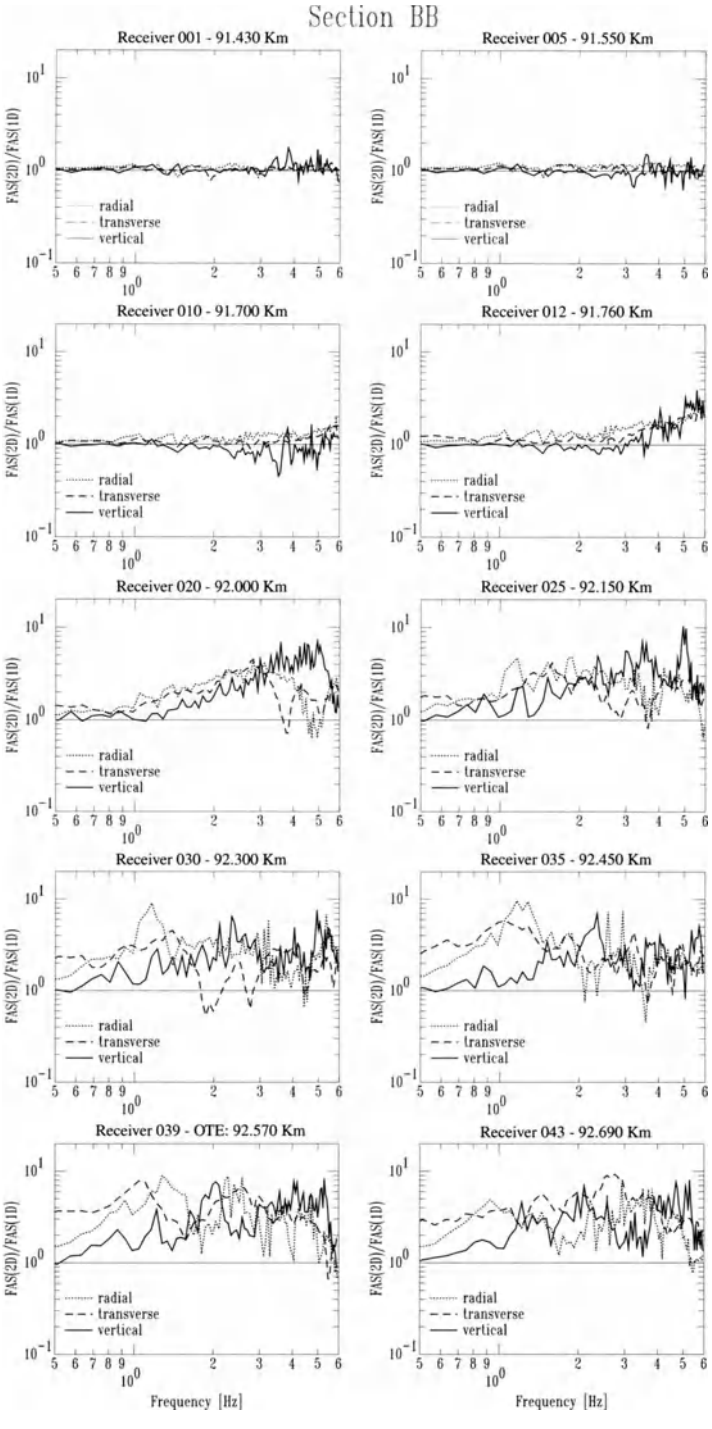
Section BB
Receiver 001 - 91.430 Km
Receiver 005 - 91.550 Km
Receiver 010 - 91.700 Km
Receiver 012 - 91.760 Km
Receiver 020 - 92.000 Km
Receiver 025 - 92.150 Km
Receiver 030 - 92.300 Km
Receiver 035 - 92.450 Km
Receiver 039 - OTE: 92.570 Km
Receiver 043 - 92.690 Km
FAS(2D)/FAS(1D)
radial
transverse
vertical
Frequency [Hz]

In the final graph of Figure 5a, where the variation of Sa(2D)/Sa(1D) along section A2 is presented, it seems that at distances approaching 18.5 km from the seismic source, where the layer geometry is horizontal, the amplification for all components, in particularly the vertical one, is quite low. The only exception is the radial component for frequencies ranging 1 to 1.5 Hz. For distances ($>$ 18.6 km) farther from the seismic source, where the geology is more complex, the amplification appears at higher frequencies, and this is probably due to the effect of the thin superficial layers.

In the first graph of Figure 5b, the high amplification zones (up to 92 km) outline the interface between bedrock and basin boundaries of section A3, especially for the horizontal components. At the basin's center, between sites TYF and POL (93 to 95 km) a zone of increased amplification appears at different frequencies for each component. For the radial component the maximum amplification is recognized between 0.5 Hz and 2.5 Hz, whereas for the transverse component the maximum is seen between 1.5 Hz and 4 Hz. The vertical component has high amplifications at the same distances from the source, but for much higher frequencies (5 to 6 Hz) and are unevenly distributed. These high amplifications at high frequencies can be attributed to local surface waves which are trapped in the layers close to the surface. The spectral amplifications along section A4 have a very similar frequency variation in space and the level is approximately the same for all three components (Fig. 5b). At site AGO (about 17.9 km from the source) the values of amplification are relatively low for frequencies less than 3 Hz, but reach values ranging from 4 to 6 for higher frequencies. Very high values of amplification, especially for horizontal components, appear close to the area of CIT (around 18.4 km from the source) and exceed the value of 9 at frequencies mainly below 3 Hz. The low amplitude of the ratio PGA(2D)/PGA(1D) computed at the same site (Fig. 3b) contrasts with the above results. As mentioned earlier this can be explained by the fact that PGA(2D)/PGA(1D) is a frequency-independent quantity. Therefore, it is evident from the figure that the amplification of spectral acceleration occurs at different frequencies for the sites CIT and AGO. Combining this observation with the extent of damage in the area around CIT during the earthquake of June 20, 1978, the importance of estimating spectral amplifications for earthquake engineering purposes is evident. The knowledge of site response in relation to the complete frequency content of a specific design earthquake is therefore the only reliable image of seismic hazard useful for engineers.

The last graph of Figure 5b shows the variation of Sa(2D)/Sa(1D) along section A5. The bedrock configuration is clearly evidenced at distances 25.5 to

◀

Figure 4
Variation of ratio FAS(2D)/FAS(1D) at selected sites indicatively along section BB for radial (dotted), transverse (dashed) and vertical component (continuous line).

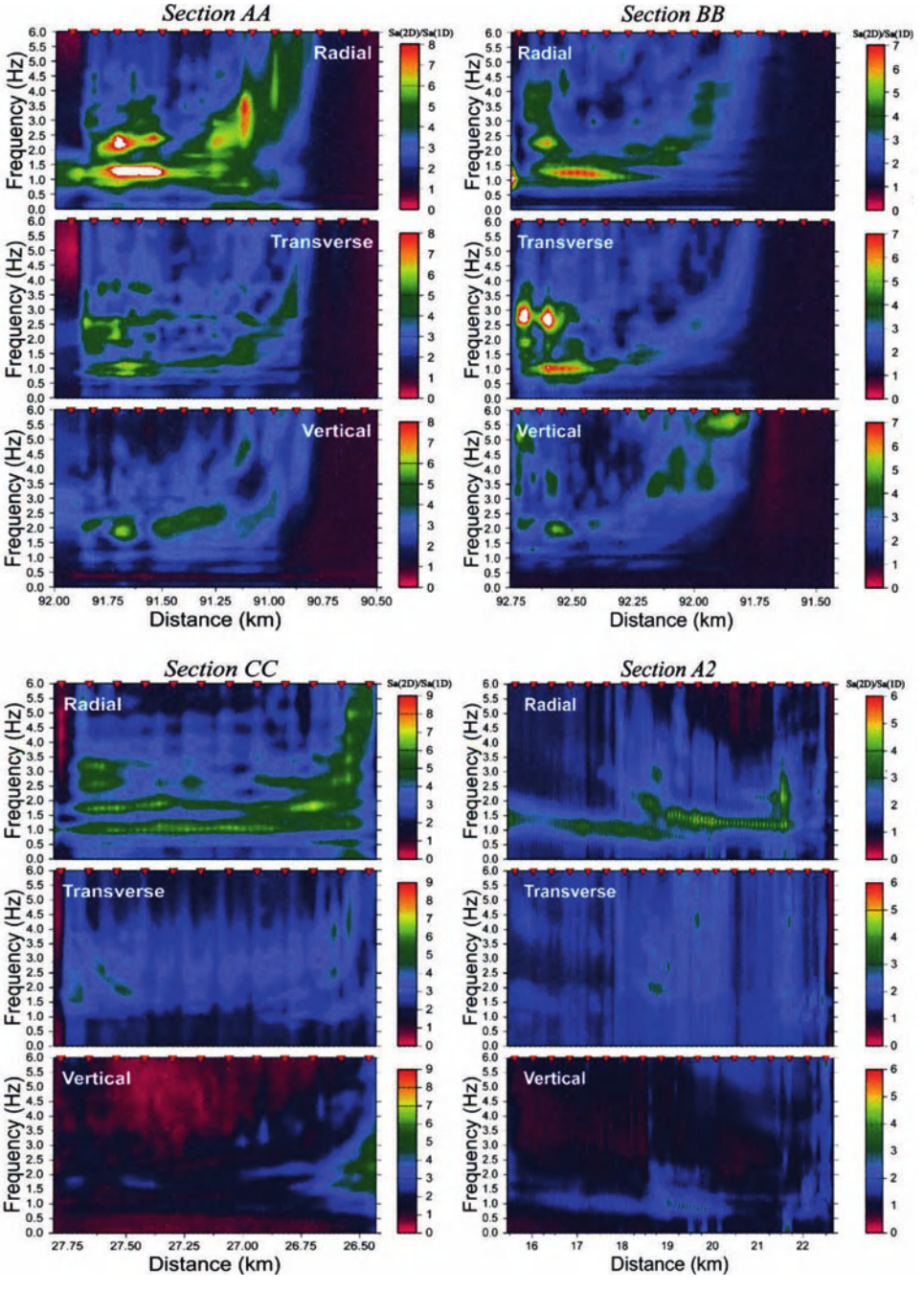

Figure 5a
Colored presentation of the Sa(2D)/Sa(1D) ratio with frequency, along sections AA, BB, CC and A2 (spectra computed with 5% dumping) for all three components.

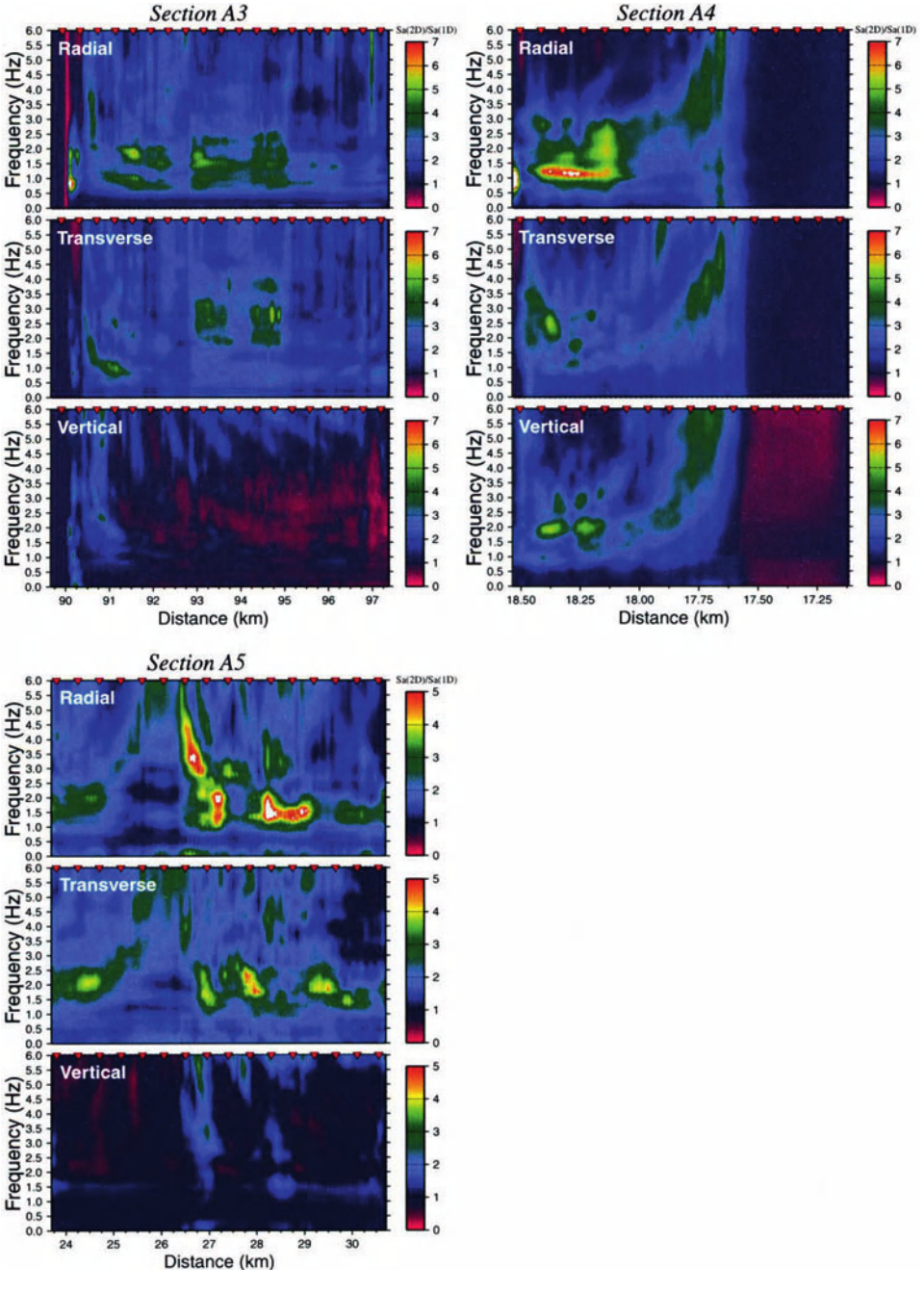

Figure 5b
The same as Figure 5a, but for sections A3, A4 and A5.

26.5 km from the source by low values of amplification at low frequencies for both horizontal components, with essentially no amplification on the vertical component. Along the points where the total width of the sedimentary layers increases (from 26.5 km on), the horizontal components appear to be strongly amplified between 1 and 2 Hz. On the contrary, the vertical component generally shows low amplifications that vanish at higher frequencies. This is probably due to the presence of the clay layer below the superficial alluvial deposits, which amplifies the vertical component of the surface waves producing high amplifications only at frequencies exceeding 4.5 Hz.

Conclusions

We have used the seismic waves propagation in non-homogeneous media to estimate the maximum expected seismic amplification at selected points within the city of Thessaloniki. The hybrid method proposed by FÄH (1992) has been used, taking into account the 2-D geometry and the variation of dynamic parameters along different cross sections crossing the city area with different orientations. The conclusions are compendiously presented in the following paragraphs.

Generally, the very low cost and the high computational speed make the 1-D methods for site response estimation useful in geologically simple regions with low seismicity, where usually no experimental data exists. However, in places where the subsurface geology pattern is complicated, this simple approach is not sufficient, as demonstrated by, e.g., TRIANTAFYLLIDIS *et al.* (1998) and MARRARA and SUHADOLC (2001). Thus, the use of at least a 2-D numerical simulation is required to acquire reliable estimations of seismic motion amplification. In the event strong motion observations are available, it is of course possible to have discordances between theoretical and experimental estimations of site effects. This is mainly due to two reasons: a) unavailability of a sufficiently detailed knowledge of the large number of parameters that characterize the input model and b) the neglecting of possible 3-D effects.

The cases we have discussed in this paper confirm that the geometry and depth of the rock basement are important factors that can significantly affect the seismic amplification of a certain site (see section A5 in Fig. 5b). In cases where the rock basement is located at shallow depths under the surface, the major differences of impedance between the surface layers and the basement generate edge effects (see section A3 in Fig. 5b). It has also been observed that the thin low-velocity surface layers generate resonance and entrap local surface waves, thereby creating increased amplifications (generally between 1 and 4 Hz) for the horizontal components, whereas the vertical component is only amplified at higher (over 5 Hz) frequencies. This phenomenon is particularly evident in sections BB, A3 and A5 (Figs. 5a and 5b).

We have also demonstrated that, in some cases, the value of the PGA alone does not constitute a reliable measure of seismic motion amplification. For instance, at site AGO of section A4 the relative PGA values are higher than those at site CIT, although the latter is located in the center of the basin where the thickness of the underlying sediments is higher. However, the spectral amplification (Sa) values at these two sites are significantly different from each other, thus explaining the different levels of damage caused by the 1978 earthquake at these two sites.

The proposed 2-D models based on the geotechnical and geophysical investigations explain quite well the main amplification features at the area of interest. Such detail in the knowledge of the subsurface structure can be, therefore, considered as sufficient, within the related frequency range, to reliably estimate for engineering purposes the ground motion shaking effects within a city, given a scenario earthquake.

Purposeful to making the results applicable for antiseismic planning and the mitigation of seismic hazard, with emphasis on large urban areas such as the city of Thessaloniki, the next step (e.g. FÄH *et al.*, 1993; PANZA *et al.*, 2001) is to employ such results to construct microzoning maps for each scenario earthquake.

Acknowledgements

This work has been financially supported and performed within the framework of the following projects: "Progetto Finalizzato Beni Culturali, CNR, Italy," UNESCO-IUGS-IGCP project 414 and EU project "EVG1-CT-2001-00040."

REFERENCES

ANASTASIADIS, A. (1994), *Contribution to the Study and the Determination of Dynamic Properties of Typical Greek Soils*, Ph.D. Thesis (in Greek), Dept. of Civil Eng., Aristotle Univ. of Thessaloniki, pp. 1–389.

ARIAS, A., *A measure of earthquake intensity*. In (R. J. Hansen, ed.) *Seismic Design for Nuclear Power Plants*, (MIT Press, Cambridge, Massachusetts 1970), pp. 438–483.

BAJC, J., AOUDIA, A., SARAÒ, A., and SUHADOLC, P. (2001), *The 1998 Bovec-Krn Mountain (Slovenia) Earthquake Sequence*, Geophys. Res. Lett. *28*, 1839–1842.

FÄH, D. (1992), *A Hybrid Technique for the Estimation of Strong Ground Motion in Sedimentary Basins*, Ph.D. Thesis, Nr 9767, Swiss Federal Institute of Technology, Zürich.

FÄH, D., IODICE, C., SUHADOLC, P., and PANZA, G. F. (1993), *A New Method for the Realistic Estimation of Seismic Ground Motion in Megacities: The Case of Rome*, Earthquake Spectra *9*, 643–668.

FÄH, D., and SUHADOLC, P. (1994), *Application of Numerical Wave-propagation Techniques to Study Local Soil Effects: The Case of Benevento (Italy)*, Pure Appl. Geophys. *143*, 513–536.

FÄH, D., SUHADOLC, P., MUELLER, St., and PANZA, G. F. (1994), *A Hybrid Method for the Estimation of Ground Motion in Sedimentary Basin: Quantitative Modeling for Mexico City*, Bull. Seismol. Soc. Am. *84*, 383–399.

FIELD, E. H., and the SCEC PHASE III WORKING GROUP (2000), *Accounting for Site Effects in Probabilistic Seismic Hazard Analyses of Southern California: Overview of the SCEC Phase III Report*, Bull. Seismol. Soc. Am. *90*, 6B, S1–S31.

FURUMURA, T., and TAKENAKA, H. (1996), *2.5-D Modeling of Elastic Waves Using the Pseudospectral Method*, Geophys. Res. Lett. *25*, 785–788.

LACHET, C., HATZFELD, D., BARD, P. Y., THEODULIDIS, N., PAPAIOANNOU, C., and SAVVAIDIS, A. (1996), *Site Effects in the City of Thessaloniki (Greece). Comparison of Different Approaches*, Bull. Seismol. Soc. Am. *86*, 1692–1703.

LIGDAS, C. N., and LEES, J. M. (1993), *Seismic Velocity Constraints in the Thessaloniki and Chalkidiki Areas (Northern Greece) from a 3-D Tomographic Study*, Tectonophysics *228*, 97–121.

MARRARA, F., and SUHADOLC, P. (1998), *Site Amplifications in the City of Benevento (Italy): Comparison of Observed and Estimated Ground Motion from Explosive Source*, J. of Seismol. *2*, 125–143.

MARRARA, F., and SUHADOLC P. (2001), *2-D Modeling of Site Effects along the "EURO-SEISTEST" Array (Volvi Graben, Greece)*, Pure Appl. Geophys. *158*, 12, 2369–2388.

PANZA, G. F., and SUHADOLC, P., *Complete strong motion synthetics.* In *Seismic Strong Motion Synthetics*, Computational Techniques *4* (B. A. Bolt, eds.), (Orlando, Academic Press (1987)), pp. 153–204.

PANZA, G. F., ROMANELLI, F., and VACCARI, F. (2000), *Seismic Wave Propagation in Laterally Heterogeneous Anelastic Media: Theory and Applications to Seismic Zonation.* Advances in Geophysics *43*, 1–95.

PANZA, G. F., VACCARI, F., and ROMANELLI, F. (2001), *Realistic Modeling of Seismic Input in Urban Areas: A UNESCO-IUGS-IGCP Project*, Pure Appl. Geophys. *158*, 12, 2389–2406.

PAPAZACHOS, C. B. (1998), *Crustal P- and S-velocity Structure of the Serbomacedonian Massif (Northern Greece) Obtained by Non-linear Inversion of Travel Times*, Geophys. J. Int. *134*, 25–39.

PAPAZACHOS, C. B., and KIRATZI, A. A. (1996), *A Detailed Study of the Active Crustal Deformation in the Aegean and Surrounding Area*, Tectonophysics *253*, 129–153.

PITILAKIS, K., MARGARIS, B., LEKIDIS, V., THEODOULIDIS, N., and ANASTASIADIS, A. (1992), *The Griva, Northern Greece, Earthquake of December 21, 1990, Seismological, Structural and Geotechnical Aspects*, J. of Eur. Earthq. Eng. *2*, 20–35.

PITILAKIS, K., and ANASTASIADIS, A. (1998), *Soil and Site Characterization for Seismic Response Analysis*, Proc. 11th ECEE, 65–90, Paris 6–11 September, France.

RAPTAKIS, D. (1995), *Contribution to the Determination of the Geometry and the Dynamic Properties of Soil Formations and their Seismic Response*, Ph.D. Thesis (in Greek), Dept. of Civil Eng., Aristotle Univ. of Thessaloniki.

RAPTAKIS, D., KARAOLANI, E., PITILAKIS, K., and THEODULIDIS, N. (1994), *Horizontal to Vertical Spectral Ratio and Geological Conditions: The Case of a Downhole Array in Thessaloniki (Greece)*, Proc. XXIV Gen. Ass. ESC, Athens, Greece 3, 1570–1578.

SARAÒ, A., DAS, S., and SUHADOLC, P. (1998), *Effect of Non-uniform Station Coverage on the Inversion for Earthquake Rupture History for a Haskell-type Source Model*, J. Seismol. *2*, 1–25.

SUHADOLC, P. (1997), *Local Effects on Strong Ground Motion: Basic Physical Phenomena and Estimation Methods for Microzoning Studies*, Proc. of the Advanced Study Course on Seismic Risk "SERINA", 21–27 Sept., 1997, Thessaloniki, Greece, 229–299.

TRIANTAFYLLIDIS, P., HATZIDIMITRIOU, P. M., SUHADOLC, P., THEODULIDIS, N., and PITILAKIS, K. (1998), *Comparison between 1-D and 2-D Site Effects Modeling in Thessaloniki*, Proc. 2nd International Symposium on: *The Effects of Surface Geology on Seismic Motion*, 1–3 Dec., 1998, Yokohama, Japan, 2, 981–986.

TRIANTAFYLLIDIS, P., HATZIDIMITRIOU, P. M., THEODULIDIS, N., SUHADOLC, P., PAPAZACHOS, C., RAPTAKIS, D., and LONTZETIDIS, K. (1999), *Site Effects in the City of Thessaloniki (Greece) Estimated from Acceleration Data and 1-D Local Soil Profiles*, Bull. Seismol. Soc. Am. *89*, 521–537.

TRIANTAFYLLIDIS, P. A., HATZIDIMITRIOU, P. M., and SUHADOLC, P. (2001), *1-D Theoretical Modelling for Site Effect Estimations in Thessaloniki - Comparison with Observations*, Pure Appl. Geophys. *158*, 12, 2333–2347.

TRIANTAFYLLIDIS, P., HATZIDIMITRIOU, P. M., SUHADOLC, P., THEODULIDIS, N., and ANASTASIADIS, A. (2004), *PART-II: Comparison of Theoretical and Experimental Site Effect Estimation Results*, Pure Appl. Geophys. *161*, 1205–1219.

WALD, D. J., and GRAVES, R. W. (1998), *The Seismic Response of the Los Angeles Basin, California*, Bull. Seismol. Soc. Am. *88*, 337–356.

(Received February 25, 2002, accepted November 18, 2002)

Pure appl. geophys. 161 (2004) 1205–1219
0033–4553/04/061205–15
DOI 10.1007/s00024-003-2494-x

Pure and Applied Geophysics

PART II: Comparison of Theoretical and Experimental Estimations of Site Effects

P. TRIANTAFYLLIDIS[1], P. M. HATZIDIMITRIOU[1], P. SUHADOLC[2], N. THEODULIDIS[3], and A. ANASTASIADIS[3]

Abstract—To check the reliability and the quality of the theoretically estimated ground responses obtained from the 2-D simulation by the application of the hybrid method in PART-I, we compare some of them with those obtained at the same sites from observed data using the Standard Spectral Ratio (SSR). The comparison validates our synthetic modeling and shows that in cases of complex geometries, the use of at least 2-D numerical simulations is required in order to reliably evaluate site effects and thus facilitate the microzonation of the city of Thessaloniki.

Key words: Experimental records, Standard Spectral Ratio, numerical modeling.

Introduction

The unequal distribution of damage from earthquakes that occurred during the last two decades both worldwide (e.g., MEXICO 1985, LOMA PRIETA 1989, NORTHRIDGE 1994, KOBE 1995, ISMIT 1999) and in Greece (e.g., THESSALONIKI 1978, KALAMATA 1986, KOZANI 1995, ATHENS 1999) is still a challenge to seismologists and earthquake engineers. In the last decade the causes for this differentiation in seismic motion have been looked for in the characteristics of the source, the properties of the propagation path as well as the geological features of the recording site (e.g., AKI, 1988, 1993; KUDO, 1995; BARD, 1997). Many researchers have worked on the estimation of local site effects with experimental methods, as well as on the improvements of existing or development of new experimental techniques (e.g., BORCHERDT, 1970; NOGOSHI and IGARASHI, 1971; LANGSTON, 1979; NAKAMURA, 1989).

Even if this intense research has led to an understanding of the broad reasons of the spatial variation of ground response, many details of it remain unexplained. This is due to the fact that there is a variety of parameters that can affect the final

[1] Aristotle University, Geophysical Laboratory, P.O.Box 111, GR-54124 Thessaloniki, Greece.
[2] University of Trieste, Department of Earth Sciences, V. Weiss 1, I-34127 Trieste, Italy.
[3] Institute of Eng. Seismology and Earthq. Engineering (ITSAK), GR-55102 Thessaloniki, Greece.

result, making the modeling of site effects rather challenging. The parameters of the seismic source (e.g., seismic moment, stress drop, mechanism, fracture characteristics and the spectral content of the released energy) can have a non-negligible influence on site effects (e.g., TRIANTAFYLLIDIS *et al.*, 2002). In fact, they control the generation of the wavefield which is propagated in the numerical simulations (e.g., CRANSWICK, 1985). The effect of the propagation path is related to the amplitude of seismic waves, to the type of waves and angle of incidence of the seismic wavefield on the analyzed site. Only at the end we have to account for the influence of the geometrical and dynamical parameters of the layers under the investigated site.

Thus, to understand and explain the observations we need theoretical modeling of the wavefield generation and propagation. Theoretical methods are especially useful in seismic design, since the recordings from major earthquakes at areas with dense networks of instruments are relatively rare. We also need efficient methods to estimate the ground response before the occurrence of the next earthquake and the sole means of achieving this is again through detailed numerical modeling.

Such theoretical estimates need, however, always to be thoroughly checked against observations, wherever possible. This is a rather difficult task, since methods to estimate ground response from observations are not unique and can be subject to strong criticism (e.g., the so-called Nakamura's method). It is also sometimes impossible (e.g., when the source is not known) to numerically model the experimentally derived estimates.

In this paper we compare the theoretical ground response estimates obtained from the application of the hybrid method (TRIANTAFYLLIDIS *et al.*, 2004) with the ones obtained from the experimental method of SSR (TRIANTAFYLLIDIS *et al.*, 1999).

Experimental and Theoretical Spectral Ratios

The experimental ratios used in the comparison were acquired by applying the Standard Spectral Ratio (SSR) method to a set of accelerograms recorded by RefTek stations equipped with CMG-5 accelerometers during a four-months period (November 1993-February 1994) at different sites within Thessaloniki (TRIANTAFYLLIDIS *et al.*, 1999). In this technique, also known as reference station technique, first introduced by BORCHERDT (1970) and still widely used, the records at each site are compared to the records for the same events at a nearby bedrock site (reference site) through spectral ratios. In the application of this method we will use the station OBS as a reference station, because it is located on bedrock (Fig. 1).

As discussed in TRIANTAFYLLIDIS *et al.*, (2004, this volume) we used all available geotechnical and geological information to construct seven 2-D profiles with different orientations within the city. In Figure 1, the geometry of each section is throughly

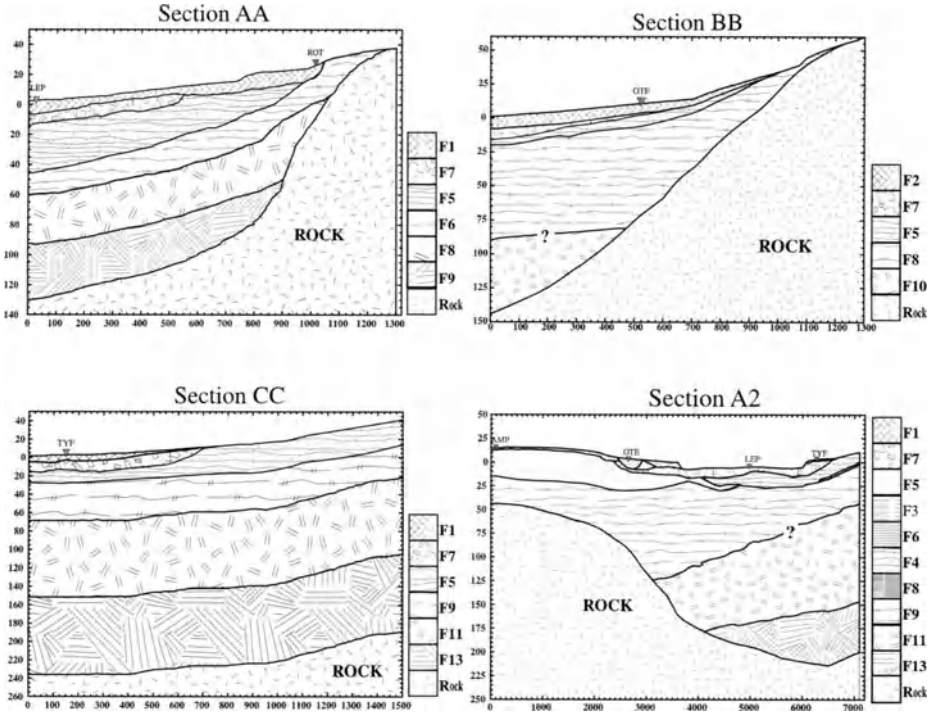

Figure 1a
Geometry of profiles AA, BB, CC and A2.

presented, as well as their position at the wide area in comparison with the other sections. The dynamic parameters that characterize the formations of each section (density, velocities and quality factors) are shown in Table 1. The question marks in sections BB, A2, A3 and A4 denote uncertainties in the formation boundaries.

The comparison between the experimental and 2-D theoretical spectral ratios has been performed for all of the events of Table 1 of PART-I at those sites of the city where the RefTek stations had been installed. Moreover, for each of the previous events the above results were also compared with the ones obtained from 1-D simulations by applying the modal summation method (PANZA, 1985; PANZA and SUHADOLC, 1987; FLORSCH *et al.*, 1991). We must note that the comparison with the results from the 1-D simulation differs from the one in the work of TRIANTAFYLLIDIS *et al.*, (1999). In that paper there is a comparison between the mean theoretical amplification of four events and the mean experimental amplification which resulted from 34 recorded events. In this paper, wherever a comparison between the seismic responses that resulted from the SSR method and the 1-D simulations takes place, we have calculated the spectral ratios between the synthetic accelerograms resulting from the local 2-D velocity model over the ones calculated at station OBS (local/

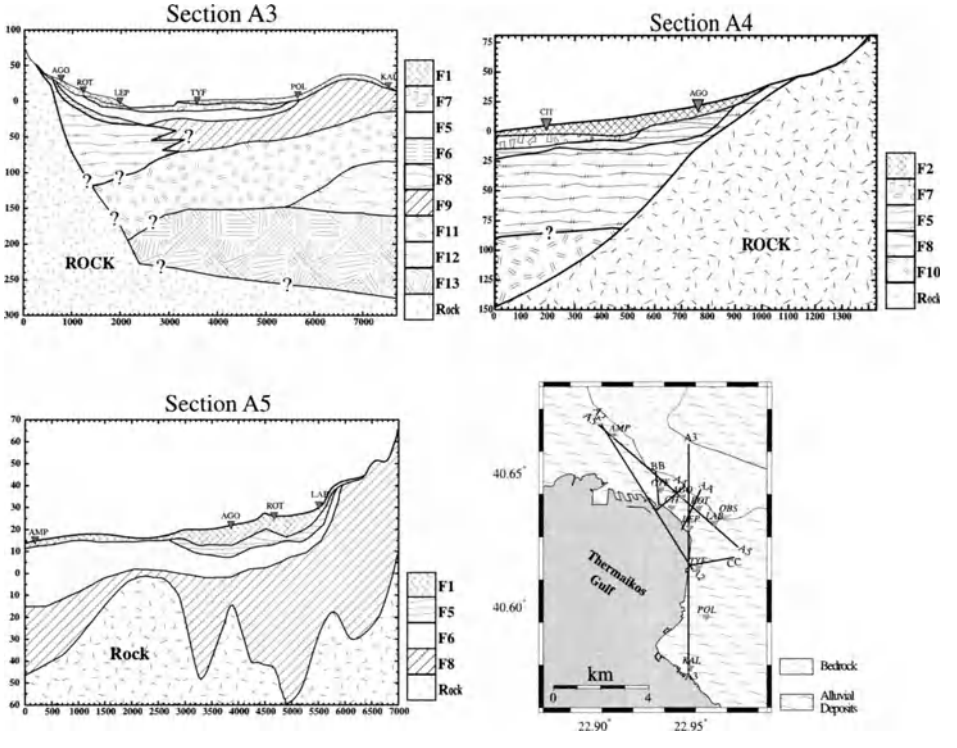

Figure 1b
The same as Figure 1a but for profiles A3, A4, A5 and their position in the wider area.

Table 1

Averaged values of densities, body wave velocities (V_P, V_S) and quality factors (Q_P, Q_S) used in the 2-D computations. The geometry of each formation is outlined in Figure 1.

Formation	Density ($g \cdot cm^{-3}$)	V_P ($m \cdot sec^{-1}$)	V_S ($m \cdot sec^{-1}$)	Q_P	Q_S
F1	1.85	450	225	60	20
F2	1.9	1750	225	60	20
F3	2.0	1600	280	100	20
F4	1.9	1700	280	50	15
F5	2.0	1700	350	60	20
F6	1.9	1800	370	50	15
F7	1.7	1600	180	70	25
F8	2.0	1900	450	50	15
F9	2.0	1600	500	70	25
F10	2.0	2000	700	60	20
F11	2.1	2500	650	100	50
F12	2.2	2800	750	120	60
F13	2.2	3200	850	150	80

OBS). Station OBS is located on bedrock (gneiss) and its local 1-D velocity model coincides with the regional velocity model.

Comparison between Experimental and Theoretical Results

The comparison of the results (obtained by modal summation, hybrid and SSR) is performed through spectral ratios computed at the sites with earthquake recordings from RefTek stations during the field experiment (TRIANTAFYLLIDIS *et al.*, 1999). We will call such sites "instrumented sites." The spectra of the synthetic accelerograms obtained at the instrumented sites from 1-D and 2-D local velocity models are divided by the spectrum of the accelerograms computed with the modal summation method for the same source and the 1-D local velocity model at site OBS. We shall denote such spectral ratios as "local/OBS." This is done to make the comparisons possible. In fact, the application of the SSR method requires that the spectra of the horizontal components at each instrumented site are divided by the respective spectra of the same earthquake at site OBS. Along section A5 no comparison between theoretical and experimental amplifications is possible, because of the lack of records at the stations along this profile for earthquake #6 of Table 1 (PART-I). Before dividing their spectra, the horizontal synthetic waveforms were rotated in order to obtain the same orientation as that of the experimental ones (i.e., North-South and East-West). In this way the local/OBS spectral ratios are compatible with the SSR ratios and therefore the comparison with the experimental data is possible.

In Figures 2 (a, b, c and d) the comparison of the amplification obtained from SSR (continuous line) with the theoretical amplifications from the 2-D (dashed line) and 1-D simulation (dotted line) is shown for each component. At site ROT on section AA (Fig. 2a), there is a good agreement between the experimental and the 2-D amplification for all components within the whole frequency range. Contrastingly, the 1-D amplification differs completely from the other two for the vertical component and remains at the same amplitude level for the horizontal components, also the shape of the spectral amplification is different. At site LEP, on the same section, the theoretical 2-D is very similar with the experimental one for both horizontal components, while the 1-D estimate has approximately a three times lower amplitude in the E-W component. For the vertical component at site LEP, only the theoretical estimation of the amplification is given because there were no recordings available.

Similar results are also obtained at site OTE on section BB (Fig. 2a). The ratios of the N-S component vary at the same amplitude level up to approximately 4 Hz, whereas for higher frequencies the amplitude of the experimental amplification is definitely higher. In the E-W component the 2-D theoretical and the experimental amplifications almost coincide for frequencies higher than 1.5 Hz, whereas the 1-D

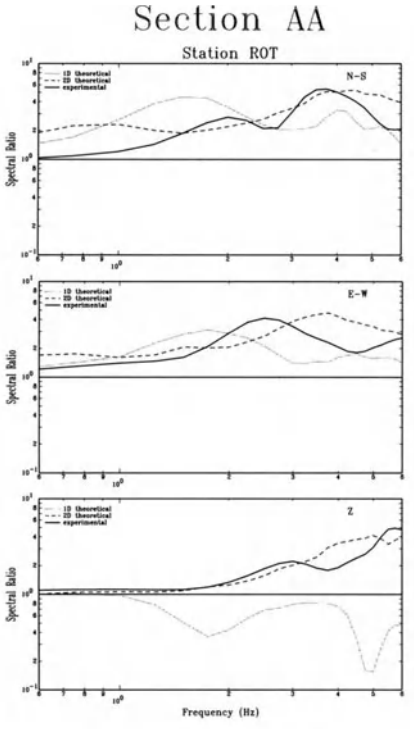
Section AA
Station ROT
1D theoretical
2D theoretical
experimental
N-S
E-W
Z
Spectral Ratio
Frequency (Hz)

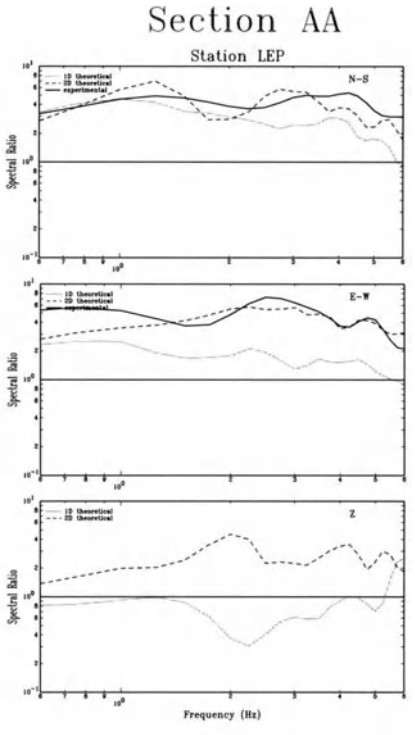
Section AA
Station LEP
1D theoretical
2D theoretical
experimental
N-S
E-W
Z
Spectral Ratio
Frequency (Hz)

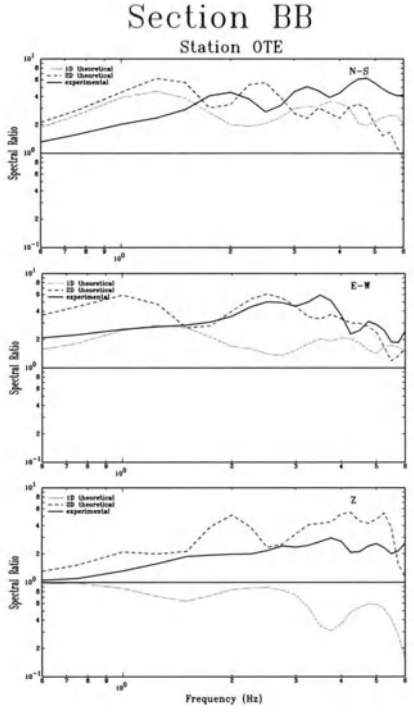
Section BB
Station OTE
1D theoretical
2D theoretical
experimental
N-S
E-W
Z
Spectral Ratio
Frequency (Hz)

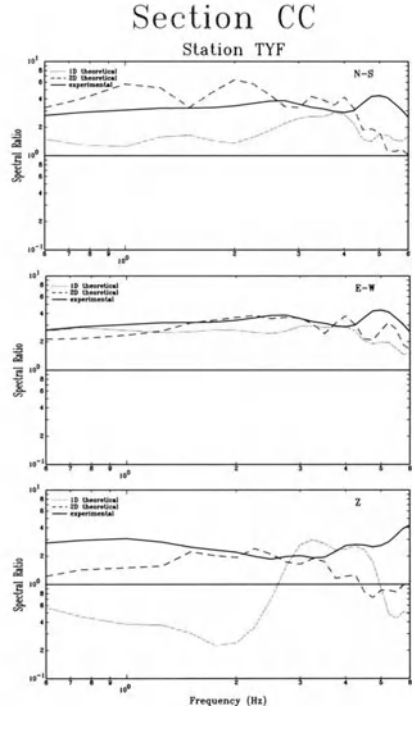
Section CC
Station TYF
1D theoretical
2D theoretical
experimental
N-S
E-W
Z
Spectral Ratio
Frequency (Hz)

amplification is underestimated especially for frequencies between 2 and 4 Hz. Finally, for the vertical component there is sufficient agreement between theoretical 2-D and experimental amplifications, with a slight overestimation for the amplitudes of the theoretical ones in all the considered frequency range. On the contrary, the 1-D amplification shows discrepancies with the other two both in amplitudes as well as in the spectral shape.

At site TYF on section CC (Fig. 2a), the three ratios coincide for the E-W component and a very good agreement of the theoretical 2-D and experimental amplification for the N-S component is seen up to approximately 4.5 Hz. The ratios manifest a sufficient agreement for the vertical component up to 3.5 Hz, with a clear underestimation of the experimental amplification for higher frequencies, whereas the 1-D ratio remains totally different. At the sites located along section A2 (Fig. 2b) the primary discrepancies among the three ratios are seen for all components. At site AMP there is a relative agreement between the experimental and the 2-D ratio for all components and frequencies higher than 2 Hz, whereas for lower frequencies all horizontal component ratios differ significantly in shape as well as in amplitudes. Moreover, differences in the ratios appear at site OTE (Fig. 2b), except for the E-W component at frequencies above 2 Hz.

For site LEP (Fig. 2b) there are no experimental data available and therefore only the theoretical estimation of the amplification is given, with only slight differences between 1-D and 2-D ratios. At site TYF (Fig. 2b) the image is like the one at OTE, i.e., good agreement of the three ratios for the E-W component for frequencies higher than 2 Hz, whereas for other components the experimental ratio is obviously overestimated when compared to the theoretical one. It is quite probable that the disagreements observed at most sites of section A2 are due to a non-realistic 2-D design profile, as well as to the simulated event (#4, Table 1, PART-I), which is located at an epicentral distance less than 16 km. Such short epicentral distances can be critical for the application of the hybrid method, because they do not leave enough space for an efficient absorbing zone (FÄH, 1992) leading to the generation of fake reflections at the distant boundary of the 2-D local model, which partly distort the calculated seismograms.

Section A3 has the largest number of comparable instrumented sites and therefore the results at these sites lead to a reliable control of the theoretical methods, as well as of the parameters selected for the simulations. Generally, the three ratios present the same spectral shape and vary at similar amplification levels. Exceptions are the 1-D ratios of E-W components (for frequencies lower than 2.5 Hz) at sites

◀

Figure 2a

Comparison of seismic motion amplification obtained from experimental SSR (continuous line) with the theoretical amplifications which resulted from 2-D theoretical (dashed line) and the 1-D simulation (dotted line) at recording sites along sections AA, BB and CC. The comparison is made for the N-S (up), E-W (middle) and vertical (bottom) components.

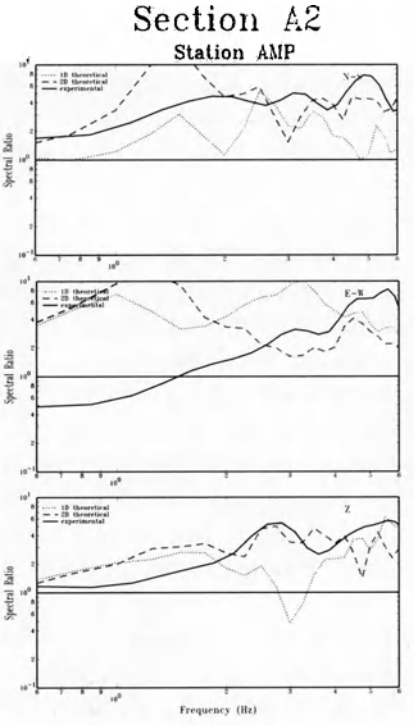
Section A2
Station AMP
Spectral Ratio
N-S
E-W
Z
Frequency (Hz)

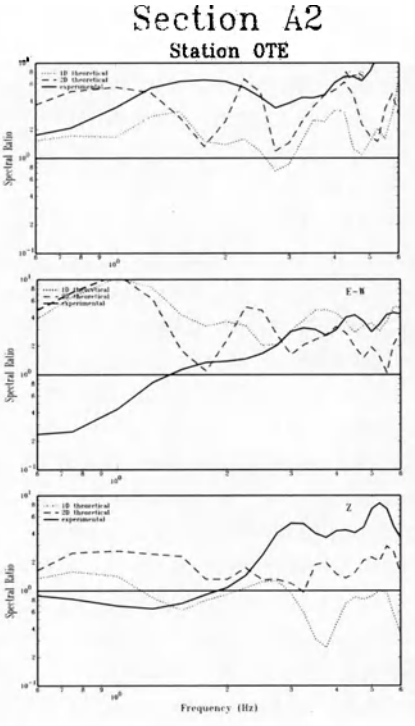
Section A2
Station OTE
Spectral Ratio
E-W
Z
Frequency (Hz)

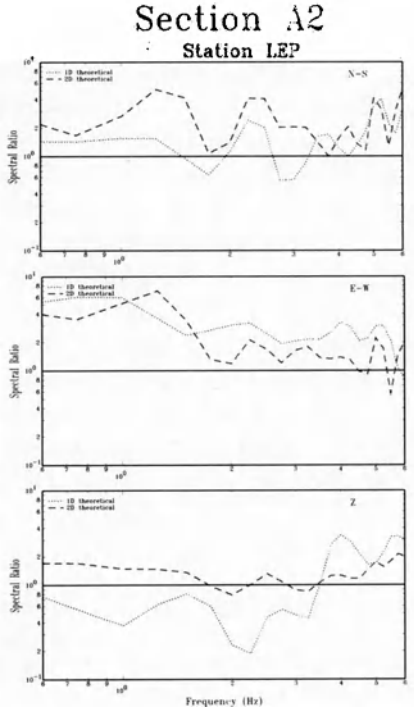
Section A2
Station LEP
Spectral Ratio
N-S
E-W
Z
Frequency (Hz)

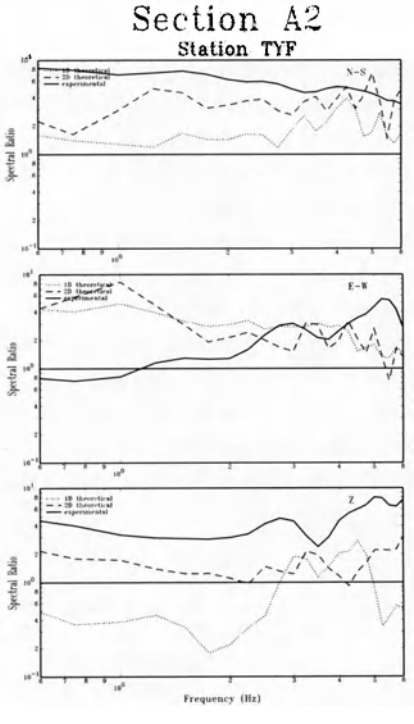
Section A2
Station TYF
Spectral Ratio
N-S
E-W
Z
Frequency (Hz)

ROT (Fig. 2c), POL and KAL (Fig. 2d). At the other sites, AGO, TYF, LEP (Fig. 2c) and POL, the amplification for the 2-D velocity model is in good agreement with the experimental one, while the 1-D amplification is also most often in good agreement with the other two.

Comparison between the Theoretical and Experimental Strong Motion Amplifications due to the 1978, July 4th Earthquake ($M_s = 5.1$)

At site CIT on section A4, digitized signals obtained by an analogue SMA-1 accelerograph are available (CARYDIS *et al.*, 1983). The instrument was triggered by the biggest aftershock (July 4th, $M_s = 5.1$) of the seismic sequence initiated by the strong earthquake, which hit the city of Thessaloniki in 1978 (June 21st, $M_s = 6.5$). The same earthquake also triggered the instrument at site OBS (PETROVSKI and NAUMOVSKI, 1979). This allowed the estimation of the amplification at site CIT by the SSR method with respect to station OBS. Figure 3 displays the recordings of the strong aftershock of July 4th, 1978 at site CIT (left) and site OBS (right), which were used in the computation of the experimental amplification through the application of SSR. For each component the value of PGA is given in cm · sec^{-2}. In the last graph of Figure 2d the experimental amplification obtained from the simulation of this earthquake by applying the SSR method is compared to the theoretical one obtained from the hybrid and modal summation methods in local 2-D and 1-D models, respectively, of site OBS. The very good agreement in amplification of the experimental data and the theoretical 2-D model is obvious for the two horizontal components over the entire frequency range. The 1-D amplification differs from the previous two for frequencies above 4 Hz, yielding relatively higher values. The similarity of the experimental ratio with the theoretical 2-D one refers not only to the same amplitude level, but also to the spectral shape of amplification with a matching of troughs and basins within the complete frequency band. This is not observed for the vertical component, for which we observe a shifting of troughs of 0.5–1 Hz, whereas the amplitude of the two curves lies at the similar level. At site AGO only the theoretical estimation of the amplification can be made, due to lack of experimental records from the simulated earthquake.

From the above Figures 2 and 3, the success of the theoretical 2-D simulations to estimate the amplification of each site, giving with sufficient detail its expected amplitude and in most cases the fundamental frequency, is quite obvious. Moreover, the amplifications obtained from theoretical 1-D simulations, may contribute only to

◀

Figure 2b
The same as Figure 2a but for section A2.

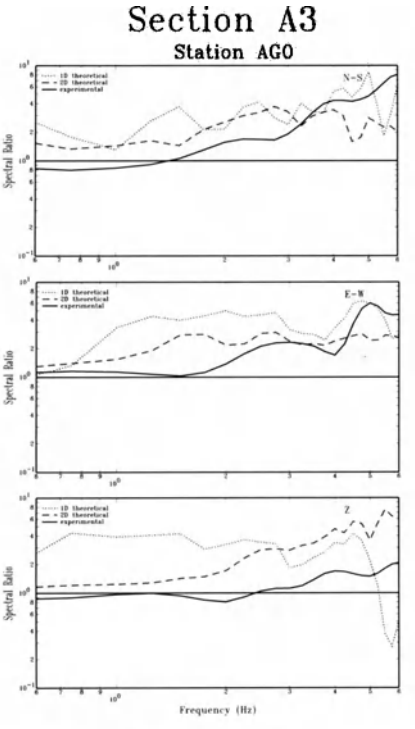
Section A3
Station AGO
1D theoretical
2D theoretical
experimental
N-S
E-W
Z
Spectral Ratio
Frequency (Hz)

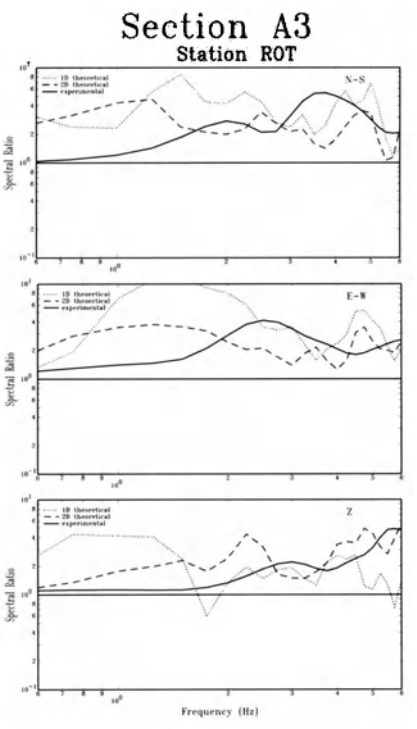
Section A3
Station ROT
1D theoretical
2D theoretical
experimental
N-S
E-W
Z
Spectral Ratio
Frequency (Hz)

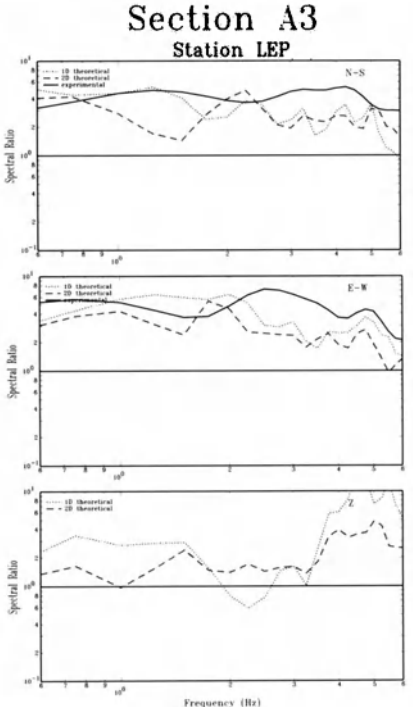
Section A3
Station LEP
1D theoretical
2D theoretical
experimental
N-S
E-W
Z
Spectral Ratio
Frequency (Hz)

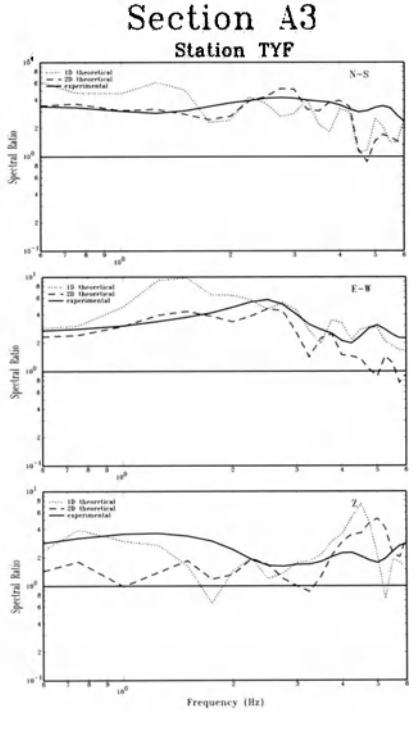
Section A3
Station TYF
1D theoretical
2D theoretical
experimental
N-S
E-W
Z
Spectral Ratio
Frequency (Hz)

a first-order estimation of amplitudes and fundamental frequencies, particularly for the horizontal components.

Discussion

Although the comparison between the amplifications emanating the experimental techniques and those estimated theoretically with the hybrid method is very satisfactory, in some sites certain discordances have been observed, concerning the amplification amplitudes and the spectral ratio shape. This misfit between the theoretical and experimental curves is particularly evident for frequencies above 4 Hz and makes the theoretical results meaningful only for lower frequencies. Possible reasons for such discordances are the scattering effect and the influence of the 3-D geometry for a specific frequency window. This is quite evident when the level of the estimated amplification is different for each (horizontal) component.

Another reason could be the fact that the receivers of the experimental measurements were not located exactly over the examined section and only their vertical structure was projected on it. That is why the positions of the real and synthetic receivers are not always coincident and the geological-geotechnical conditions may differ from those which were initially used as input data.

The differences between the focal mechanisms of the simulated earthquakes and the earthquake recorded during the experiment may also be a cause of disagreement. Apart from the 1978 earthquakes of Thessaloniki (#1, #5, Table 1, PART-I), which were simulated using the 2-D approach, the other focal mechanisms represent the average stress field of the area. Although the use of the average focal mechanism would be essential for a microzonation study, for the case of a future design earthquake in this area, the comparison with the experimental recordings of an earthquake with a different focal mechanism may present certain differences, as already noted by MOLDOVEANU and PANZA (2001).

For this reason and because of the sensitivity of the numerical methods to the variations of source parameters (focal mechanism, depth, source-receiver distance and azimuth) the simulation must always be conducted with the same limitations as those of the observations. More specifically, the calculation of the synthetic waveforms must be made at the same stations (examined site and reference station) where the instrumental observations were recorded. Additionally, the comparison should always be made at the same components (N-S, E-W and vertical) considering the same spectral ratios (synthetic waveforms of the local model to these of the reference station).

◀

Figure 2c
The same as Figure 2a but for section A3.

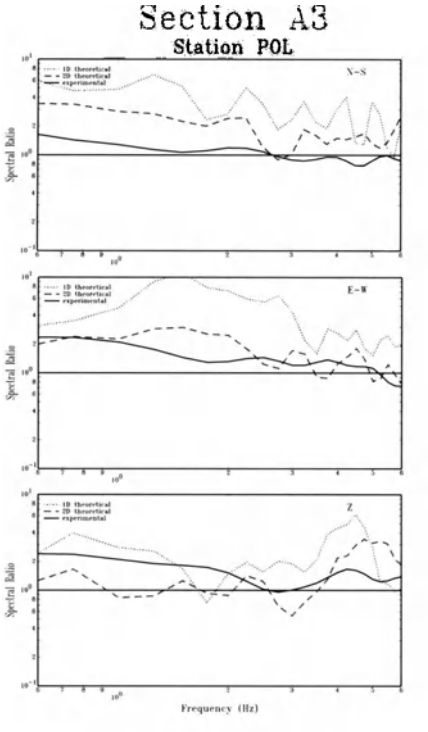
Section A3
Station POL
N-S
E-W
Z
Spectral Ratio
Frequency (Hz)

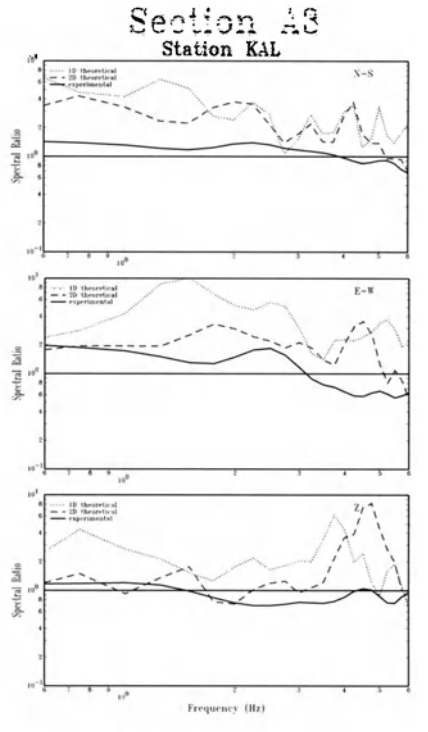
Section A3
Station KAL
N-S
E-W
Z
Spectral Ratio
Frequency (Hz)

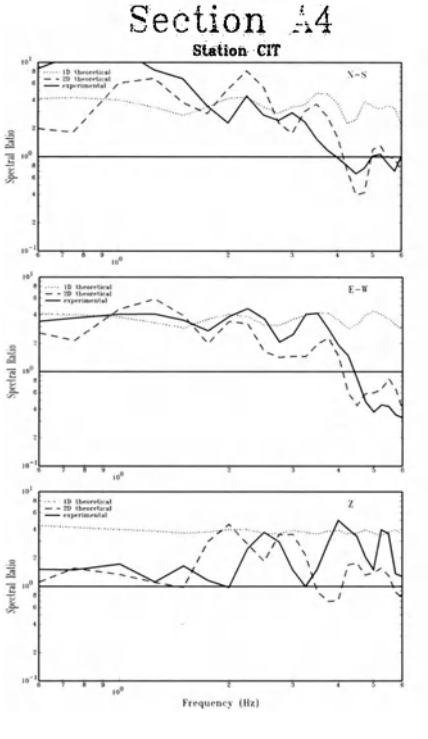
Section A4
Station CIT
N-S
E-W
Z
Spectral Ratio
Frequency (Hz)

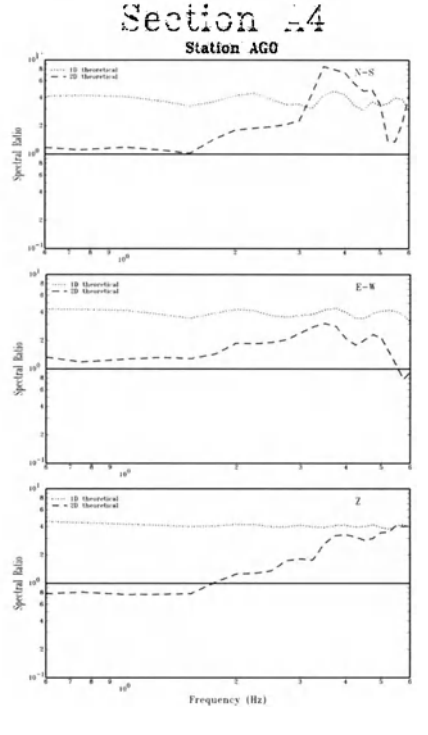
Section A4
Station AGO
N-S
E-W
Z
Spectral Ratio
Frequency (Hz)

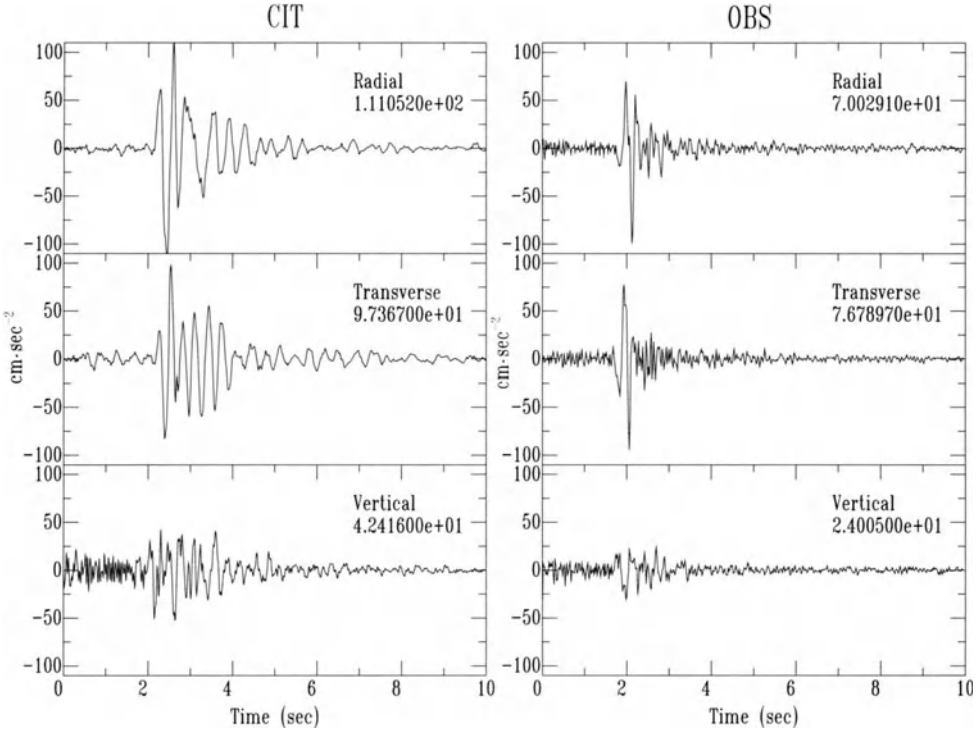

Figure 3
Digitized waveforms of the radial (up), transverse (middle) and vertical (bottom) components of the largest aftershock of the 1978 seismic sequence (July 4, 1978, $M_S = 5.1$) at sites CIT (left) and OBS (right).

For future references or microzonation studies, the site effects could be more accurately estimated (taking the spectral ratios of the corresponding components at the same site) by simulating first the local one- or two-dimensional geometry of the layers at the specific site and the regional one-dimensional afterwards (reference model). In this way, the differences due to the propagation path in the regional bedrock model are eliminated. In the case of contiguous earthquakes, i.e., when the source-station distance is comparable to the distance between the stations, these dissimilarities are particularly intense. They are the result of the difference in distance between the analyzed site and the reference station, as well as of the different azimuth between the source and the two stations.

The hybrid method constitutes a very useful tool which can offer applicative and practical results for regions where the theoretical estimation of the seismic motion

◀

Figure 2d
The same as Figure 2a but for sections A3 and A4.

amplification is required and detailed geotechnical data are available, especially at regions with no significant seismic activity or densely populated urban areas. The methodology followed in this study provided us with results which could be easily and effectively used in microzonation and seismic hazard reduction studies of the city.

Acknowledgements

This work has been financially supported and performed within the framework of the following projects: "Progetto Finalizzato Beni Culturali, CNR, Italy," UNESCO-IUGS-IGCP project 414 and EU project "EVG1-CT-2001-00040."

References

AKI, K. (1988), *Local site effects on strong ground motion.* In *Earthquake Engineering and Soil Dynamics II-Recent Advances in Ground Motion Evaluation*, 27–30 June, Park City, Utah.

AKI, K. (1993), *Local Site Effects on Weak and Strong Ground Motion.* Tectonophysics *218*, 93–111.

BARD, P. Y. (1997), *Local Effects on Strong Ground Motion: Basic Physical Phenomena and Estimation Methods for Microzoning Studies*, Proc. of the Advanced Study Course on Seismic Risk "SERINA", 21–27 Sept., 1997, Thessaloniki, Greece, 229–299.

BORCHERDT, R. D. (1970), *Effects of Local Geology on Ground Motion near San Francisco Bay*, Bull. Seismol. Soc. Am. *60*, 29–61.

CARYDIS, P. G., DRAKOPOULOS, J. C., PANTAZOPOULOS, S., and TAFLAMBAS J. (1983), *Evaluation of the June 20 and July 5, 1978, Thessaloniki Strong Motion Records, The Thessaloniki, Northern Greece, Earthquake of June 20, 1978 and its Seismic Sequence*, Tech. Chamber of Greece, Sect. of Centr. Macedonia, 231–256.

CRANSWICK, E. (1988), *The Information Content of High-Frequency Seismograms and the Near-Surface Geologic Structure of "hard rock" Recording Sites*, Pure Appl. Geophys. *128*, 333–363.

FÄH, D. (1992), *A Hybrid Technique for the Estimation of Strong Ground Motion in Sedimentary Basins*, Ph.D. Thesis, Nr. 9767, Swiss Federal Institute of Technology, Zürich.

FLORSCH, N., FÄH, D., SUHADOLC, P., and PANZA, G. F. (1991), *Complete Synthetic Seismograms for High-Frequency Multimode SH Waves*, Pure Appl. Geophys. *136*, 529–560.

KUDO, K. (1995), *Practical Estimates of Site Response — State-of-art Report*, 5th Conf. on Seismic Zonation, III, Nice, France.

LANGSTON, A. C. (1979), *Structure under Mount Rainier, Washington, Inferred by Body Waves*, J. Geophys. Res. *84*, B9, 4749–4762.

MOLDOVEANU, C. L. and PANZA, G. F. (2001), *Vrancea Source Influence on Local Seismic Response in Bucharest*, Pure Appl. Geophys. *158*, 2407–2429.

NAKAMURA, Y. (1989), *A Method for Dynamic Characteristics Estimation of Subsurface Using Microtremor on the Ground Surface*, QR Railway Tech. Res. Inst. *30*, 1.

NOGOSHI, M. and IGARASHI, T. (1970), *On the Propagation Characteristics of Microtremor*, J. Seismol. Soc. Japan *23*, 264–280 (in Japanese with English abstract).

NOGOSHI, M. and IGARASHI, T. (1971), *On the amplitude characteristics of microtremor (Part 2)*, J. Seismol Soc. Japan *24* (in Japanese with English abstract).

PANZA, G. F. (1985), *Synthetic Seismograms: The Rayleigh Waves Modal Summation*, J. Geophys. *58*, 125–145.

PANZA, G. F. and SUHADOLC, P. (1987), *Complete strong motion synthetics.* In *Seismic Strong Motion Synthetics*, Computational Techniques *4*, (B.A. Bolt, ed.), Orlando, (Academic Press) pp. 153–204.

PETROVSKI, D. and NAUMOVSKI, N. (1979), Processing of Strong Motion Accelerograms, *Part I – Analytical Methods 66*, Skopje.

TRIANTAFYLLIDIS, P., HATZIDIMITRIOU, P. M., THEODULIDIS, N., SUHADOLC, P., PAPAZACHOS, C., RAPTAKIS, D., and LONTZETIDIS, K. (1999), *Site Effects in the City of Thessaloniki (Greece) Estimated from Acceleration Data and 1-D Local Soil Profiles*, Bull. Seismol. Soc. Am. *89*, 521–537.

TRIANTAFYLLIDIS, P., SUHADOLC, P., HATZIDIMITRIOU, P. M., ANASTASIADIS, A., and THEODULIDIS, N. (2004), *PART-I: Theoretical Site Response Estimation for Microzoning Purposes*, Pure Appl. Geophys. *161*, 1185–1203

TRIANTAFYLLIDIS, P., SUHADOLC, P., and HATZIDIMITRIOU, P. M. (2002), *Influence of Source on 2–D Site Effects*, Geophys. Res. Lett., *29*, 6.

(Received February 25, 2002, accepted November 18, 2002)

Pure appl. geophys. 161 (2004) 1221–1237
0033–4553/04/061221–17
DOI 10.1007/s00024-003-2491-0

Pure and Applied Geophysics

Deterministic Earthquake Scenarios for the City of Sofia

S. SLAVOV[1], I. PASKALEVA[2], M. KOUTEVA[3],
F. VACCARI[4] and G. F. PANZA[5]

Abstract—The city of Sofia is exposed to a high seismic risk. Macroseismic intensities in the range of VIII – X (MSK) can be expected in the city. The earthquakes that can influence the hazard in Sofia originate either beneath the city or are caused by seismic sources located within a radius of 40 km. The city of Sofia is also prone to the remote Vrancea seismic zone in Romania, and particularly vulnerable are the long-period elements of the built environment. The high seismic risk and the lack of instrumental recordings of the regional seismicity make the use of appropriate credible earthquake scenarios and ground-motion modelling approaches for defining the seismic input for the city of Sofia necessary. Complete synthetic seismic signals, due to several earthquake scenarios, were computed along chosen geological profiles crossing the city, applying a hybrid technique, which combines the modal summation technique and finite differences. The modelling takes into account simultaneously the geotechnical properties of the site, the position and geometry of the seismic source and the mechanical properties of the propagation medium. Acceleration, velocity and displacement time histories and related quantities of earthquake engineering interest (e.g., response spectra, ground-motion amplification along the profiles) have been supplied. The approach applied in this study allows us to obtain the definition of the seismic input at low cost, exploiting large quantities of existing data (e.g. geotechnical, geological, seismological). It may be efficiently used to estimate the ground motion for the purposes of microzonation, urban planning, retrofitting or insurance of the built environment, etc.

Key words: Seismic hazard, ground-motion modelling, hybrid approach, Sofia.

Introduction

The city of Sofia is the main administrative center in Bulgaria, with the densest population. Large industrial zones are located in its vicinity. If a strong earthquake should occur in the Sofia area it could produce disastrous damage in a large region,

[1] Department of Physics, University of Sofia, Bulgaria.
[2] Central Laboratory for Seismic Mechanics and Earthquake Engineering, Bulgarian Academy of Sciences, Sofia, Bulgaria.
[3] Central Laboratory for Seismic Mechanics and Earthquake Engineering, Bulgarian Academy of Sciences, Acad. G. Bonchev str. bl. 3, 1113 Sofia, Bulgaria. E-mail: mihaela@dst.univ.trieste.it
[4] Department of Earth' Sciences, University of Trieste, Italy,INGV - Osservatorio Vesuviano, Naples, Italy.
[5] Department of Earth' Sciences, University of Trieste, Italy, SAND Group - The Abdus Salam International Centre for Theoretical Physics, Trieste, Italy.

followed by numerous heavy consequences for the entire country (communications, lifelines). Therefore the purpose of our study is to:

(1) contribute to the earthquake hazard assessment of Sofia, providing earthquake scenarios with respect to specific earthquakes that can affect the city, as suggested by the geological outline, the regional earthquake hazard and the seismicity records at Sofia;
(2) supply synthetic seismic signals computed using source and structural models available in the literature and to validate these theoretical results on the base of the available reports on earthquake damage;
(3) provide site response estimates at Sofia due to the chosen earthquake scenarios.

In general there are two main classes of methods used to generate synthetic ground motion: numerical and analytical methods. In this study, the synthetic ground motion was generated applying a hybrid approach (FäH *et al.*, 1993; 1994a,b). It combines the modal summation technique (PANZA, 1985; PANZA and SUHADOLC, 1987; PANZA *et al.*, 2000), used to describe the seismic wave propagation in the anelastic bedrock structure with the finite-difference method (VIRIEUX, 1984, 1986; LEVANDER, 1988) used to model wave propagation in the anelastic, laterally inhomogeneous sedimentary media. The computations were performed separately for the SH and P-SV waves. This hybrid procedure has been proved successfully for several major cities: Mexico (FÄH *et al.*, 1994b), Rome and Naples, Italy (FÄH *et al.*, 1994a; VACCARI *et al.*, 1995), Bucharest (PANZA *et al.*, 2002), Thessaloniki (TRIANTAFYLLIDIS *et al.*, 1998), Beijing (SUN *et al.*, 1998), Naples (NUNZIATA *et al.*, 2000), Zagreb (LOKMER *et al.*, 2001).

Geological Outline

Sofia valley is situated in the northernmost part of the Central-Balkan neotectonic region. It coincides with the Sofia graben, a structure set in the downlift regions of the western part of the Sredna Gora tectonic zone. In the south the graben is limited by a fault belt which extends along the northern edge of the Vitosha and Lozen mountains and in the north by the Negushevo fault zone (CHRISTOSKOV *et al.*, 1989; JARANOFF, 1960). Recent neotectonic studies (TZANKOV and NIKOLOV, 1996) consider that the graben had been developed under the leading part of the listric faulting along the two sides of the corresponding segment of the first-rate neotectonic Maritza protofracture. This protofracture passes through the axial part of the Sofia field and marks the initial zone of the extension opening of the fault basin. The seismicity of the zone is related mainly to the marginal neotectonic faults of Sofia graben (SOLAKOV *et al.*, 2001). There are two main fault structures in the southeast-northwest direction present in the region. Other cross-faults as well as a number of disjunctive disturbances, e.g., the Lozen terrace, the central Sofia terrace, Slatina uplift, contribute to the regional seismicity.

The Sofia Kettle extends from east to west 75 km long and 26 km wide in its western part. The average altitude at Sofia Kettle is about 550 m. The Kettle is relatively flat with a relief gradually rising towards the surrounding mountains. The city of Sofia is situated in the central part of the Kettle, near the foot of the Vitosha and Ljulin mountains. The Quaternary cover, building up the uppermost part of the Sofia Kettle, is from 3 m to 100 m thick and higher. It is covered by Pliocene and Quaternary sediments from 200 m to 700 m thick, in some places reaching 1200 m. The Quaternary sediments, rather different in their composition and properties, are widespread and lie over older rock and soil. The permeability of these sediments predetermines the shallow water table in the region and the possibility for suffusion or liquefaction of the fine water-saturated sands. Neogene sediments with various grain size distributions and a high content of silt fraction (42–82 %), take part to depths of 25–30 m below the surface (FRANGOV, 1995; IVANOV, 1997; IVANOV *et al.*, 1998). The "cultural" layer is composed of old structures, technogenic soils, industrial and household waste. The first layer of old structure remnants is the thickest in the central part of the town (up to 10 m). The distribution of the technogenic soil, composed of reworked rocks and soil and industrial waste, is in proximity to the opened pits, the big city residential buildings and the power stations. Recently a detailed geological map of the surface soil conditions at Sofia (23.30 E, 42.60 N – 23.50 E, 42.80 N) has been constructed (PASKALEVA and KOUTEVA, 2001a). It covers a grid 1 x 1 km, following a four—degree scale, where soil is distinguished as rocks (soil parameter s = 3), intermediate soils (s = 1, 2) and weak soil (s = 0). Among all these soil types present at Sofia, the intermediate weak soil takes a predominant part in the area of interest.

Local Seismicity

Strong earthquakes with magnitude, M, up to 7 shook Sofia in the past centuries (BONCHEV *et al.*, 1982; Shebalin *et al.*, 1999; SOLAKOV *et al.*, 2001). During the last two centuries three destructive earthquakes occurred: in 1818, $M_s \sim 6.0$), in 1858, $M_s \sim 6.5$ (near the town of Sofia, macroseismic intensity I = IX–X, MSK–64) and in 1905, $M_s \sim 6.5$ (in the western marginal part of the Sofia Kettle). In the same period several weaker events with I = VI–VII (MSK–64) were also reported. In 1907 (M = 4.6), 1909 (M = 4.6) and 1910 (M = 4.8) earthquakes with I up to V–VI (MSK) were felt in Sofia. On October 18, 1917, a strong earthquake (M = 5.3) with its epicenter in the vicinity of Sofia occurred and the maximum observed macroseismic intensity was I = VII–VIII (MSK) (KIROV, 1952; PETKOV and CHRISTOSKOV, 1965; CHRISTOSKOV, 1992). In the recently compiled earthquake catalogue (SHEBALIN *et al.*, 1999), for the region of Sofia, limited by the rectangle 42.25 N, 22.75 E–43.25 N, 24.00 E, 79 events within the magnitude interval M = 4–7 have been reported for the time period 1687–1990. In fact, since 1900 four earthquakes with magnitude 5 and

higher occurred in the valley: 1904, Apr. 11, M = 5.2, 1912, Sept. 16, M = 5.3, 1928, Apr. 18, M = 5.0, and 1934, June 7, M = 5.3. No strong events have been reported, nonetheless the tectonic processes generating the earthquakes are obviously still active (PASKALEVA *et al.*, 2004). During the period 1977–2000, 147 events occurred in the Sofia seismic zone, the strongest one (1980, Sept. 03) was with a magnitude of M = 4.3 [NEIC]. In 1983 epicentral macroseismic intensity Io $\sim$ V and I = III–V were reported for Sofia and vicinity due to the earthquake of Dec. 22, M = 3.6, which struck just beneath the city (GLAVCHEVA, 1993).

An epicenter map of all reported seismic events with magnitude M = 4.0–7.0 is shown in Figure 1 (MATOVA, 2001). The weak earthquake epicenters are located along the faults as well as in the horsts to the north, east and south of the Sofia graben. The strong and moderate earthquake epicenters are concentrated along the faults, and also in the fault crossing joints, mainly in the central and the southern parts of the Sofia graben. The earthquakes with focal depths of 11–30 km are concentrated near the Vitosha fault and in the vicinity of its crossings with the Chepintsi and the Vladaya faults (Fig. 1).

Earthquake Hazard Estimates

Several studies treating the seismic hazard in Bulgaria (BONCHEV *et al.*, 1982; OROZOVA–STANISHKOVA *et al.* 1994, 1996) and particularly for Sofia (PETKOV and CHRISTOSKOV, 1965; CHRISTOSKOV *et al.*, 1989; STANISHKOVA and SLEJKO, 1991; RANGUELOV and TOTEVA, 1996, 1998; SOLAKOV *et al.*, 2001), based on different approaches, have shown the high seismic hazard at Sofia and the surrounding area. Maximum macroseismic intensity at Sofia, I = IX (MSK), already observed in 1858 (BONCHEV *et al.*, 1982), can be expected to occur within a period of 150 years (CHRISTOSKOV *et al.*, 1989). The recently constructed seismic hazard maps of the Circum-Panonian Region (PANZA and VACCARI, 2000) reveal that Sofia could suffer macroseismic intensity reaching VIII–X (MSK—76) (MEDVEDEV, 1977). The first seismic microzonation map for Sofia was constructed in 1964 in terms of macroseismic intensity (PETKOV and CHRISTOSKOV, 1965). In this map three zones can be distinguished: zone "A", which encompasses covers the south-eastern central part of the town with maximum expected intensity (MSK) I = IX and some small "spots" out of this part; zone "B" with I = I–1 that covers mainly the northern part of the center of the town, and zone "C" with intensity I = I–1 up to I–2, that covers most of the city area, at that time. This seismic microzonation map has been extended to a larger area of the city. The macroseismic intensity at Sofia varies within 2 degrees (MSK). The intensity variation along the considered profiles is used to control the validity of the obtained theoretical results (Figs. 4, 5). If coseismic effects are considered (e.g., landsliding, liquefaction) the intensity still varies within the same interval ΔI = 2. In this case its distribution within the investigated territory changes

Figure 1

Seismic events with magnitude M = 4.00–7.00 in the blocks of the Sofia graben and the adjacent horsts: 1—faults: a—block boundary, b—sector of the Vitosha fault zone activated during the 1858 Sofia earthquake (M = 6.5–7.0); 2—the block of the Sofia graben, 3—the block of the adjacent horsts, 4—epicenters of earthquakes with magnitude: a—M = 6.0–7.0; b—M = 5.0–5.9, c—M = 4.0–4.9; 5—depths of earthquake hypocentres: a—up to 10 km, b—11–20 km, c—21–30 km; 6—blocks of considerable seismic mobility: a—of the graben, b—of the horsts; 7—blocks of moderate seismic mobility: a—of the graben, b—of the horsts; 8—seismic active sector of Vitosha fault during the Sofia earthquake in 1858.

visibly, particularly in the southwestern part of the region, however the maximum intensity remains at the southern part of the city center.

Several papers have been published addressing the seismic hazard in Bulgaria (e.g., BONCHEV *et al.*, 1982; OROZOVA-STANISHKOVA and SLEJKO, 1994). Different authors consider different seismic zones that can influence the seismic hazard at Sofia (e.g., PASKALEVA and KOUTEVA, 2001; SOLAKOV *et al.*, 2001). Kresna, Plovdiv, Negotinska Krayna and Gorna Orjahovitza are considered to be the main seismic zones in Bulgaria capable of influencing the seismic hazard of Sofia. Sofia is also prone to the remote Vrancea seismic zone (Romania), the long-period elements of the built environment being particularly vulnerable to these events. The available data

are rather limited and the statistical determination of the coefficients of the Frequency—Magnitude Relationships (FMR) for these zones is affected by major uncertainties (MOLCHAN *et al.*, 1997). Preliminary computations were carried out applying a maximum likelihood based procedure (MOLCHAN *et al.*, 1997). Two schematic tectonic models (TODOROVSKA *et al.*, 1995; PASKALEVA and KOUTEVA, 2001) were considered with respect to the Earthquake Catalogue for east and southeast Europe (SHEBALIN *et al.*, 1999) for the Bulgarian territory and the Romanian earthquake catalogue for Vrancea zone in Romania, ROMPLUS (www.infp.infp.ro). The preliminary estimates of these coefficients, which are given in Table 1, show quite large confidence intervals for the b—values.

The probabilistic seismic hazard analysis (PSHA) for the Sofia area, carried out by SOLAKOV *et al.* (2001) provides a sensitivity analysis of the PGA, keeping the same seismic source model and the same seismicity characteristics, and varying the standard deviations in the PGA attenuation mode. A difference up to 200% in the PGA value for 1000-years period was obtained and this result has been related to the fact, that regional, but not local attenuation functions were used. A doubt springs from the fact that in general the regional data sets are statistically not significant to represent the very different seismotectonic styles that are not mixable, and usually attenuation functions are derived with the assumption of the same propagation model for all events considered (DECANINI *et al.*, 2001). In this study an attempt to avoid such uncertainties, when particularly accounting for site response in the seismic hazard analyses, is performed. In our computations a deterministic procedure for ground motion modelling, capable of synthesizing the seismic ground motion from a basic understanding of fault mechanism and seismic wave propagation, has been applied (FÄH *et al.*, 1993; 1994a, b).

Parameterization of the Earthquake Scenarios and the Models Adopted

The seismicity of the Sofia region involves the upper 20–30 km of the lithosphere. Maximum macroseismic intensity I = VIII –IX can be expected at Sofia

Table 1

Estimates of the b coefficient of the FMR

Seismic zone	b Tectonic model 1	b Tectonic model 2
Sofia	0.50 ± 0.30	0.55 ± 0.33
Negotinska Krayna		1.01 ± 0.50
Kresna	0.69 ± 0.08	0.72 ± 0.08
Plovdiv	0.73 ± 0.08	0.76 ± 0.10
Gorna Orjahovitza	0.80 ± 0.20	0.76 ± 0.23
Vrancea	0.65 ± 0.15	0.70 ± 0.15

(GLAVCHEVA, 1990), if an earthquake with maximum magnitude M_{max} = 7 (BONCHEV *et al.*, 1982) occurs at a depth close to 20 km. Maximum macroseismic intensity IX (and higher) can be provoked by events with M_{max} = 6.5 and focal depth around 7 km. In the computations carried out in this study, on the basis of the earthquake history at Sofia and on the available seismic hazard assessments provided in the literature, three shallow earthquake scenarios (Table 2) were considered. They correspond to seismic sources located at different distances and azimuths (up to 30 km distant from Sofia) (SLAVOV, 2000). Preliminary computations were carried out with respect to a local seismic source that can strike just beneath the city. The earthquake epicenters correspond to real seismic event, which struck Sofia: March 9, 1980; December 22, 1983; December 14, 1995 and April 20, 1996. The complete scenarios are constructed considering the conservative combinations of information available in the literature (e.g., NEIC, SHANOV *et al.*, 1992; GLAVCHEVA *et al.*, 1996).

A generalized scheme of the model adopted for the numerical experiments is shown in Figure 2. The seismic waves propagation path consists of the travelled path between the source and the target site (the "bedrock structure") and the target local cross sections. The data used to build-up the local structural models, to 1000 m below the surface, are obtained from a large set of boreholes and geological cross sections (PETROV and ILIEV, 1970; KAMENOV and KOJUMDIEVA, 1983; FRANGOV, 1995; IVANOV, 1997; IVANOV *et al.*, 1998). The lower part of the local model describing the structure below this 1 km, coincides with the bedrock velocity model available in the literature and assumed to be the same for the Sofia Kettle (STANISHKOVA and SLEJKO, 1991). A summary of the geophysical properties of the geological strata beneath the city of Sofia considered in this study is shown in Table 3. The models' grids used in the computations are summarized in Table 4. This study deals with the two-dimensional problem of wave propagation and ground motion modelling.

Table 2

Earthquake scenarios studied by the numerical experiments

Profile identification as shown in Fig. 3	Earthquake date, location, latitude (La) Longitude (Lo) magnitude (M)			Seismic source moment tensor considered in the computations				
				Strike angle	Dip angle	Rake angle	Focal depth	Epicentral distance to the nearest profile considered
	La.[^{0}]	Lo.[^{0}]	M	[^{0}]	[^{0}]	[^{0}]	[km]	[km]
AB	42.95	23.36	4.4	135	43	111	10	25.0
	42.76	23.39	3.6	A Ricker impulse introduced at 2 km beneath the city				
CD	42.54	23.52	3.3	21	44	309	2	8.6
EF	42.79	23.49	6.5	340	77.6	285	8	15.0

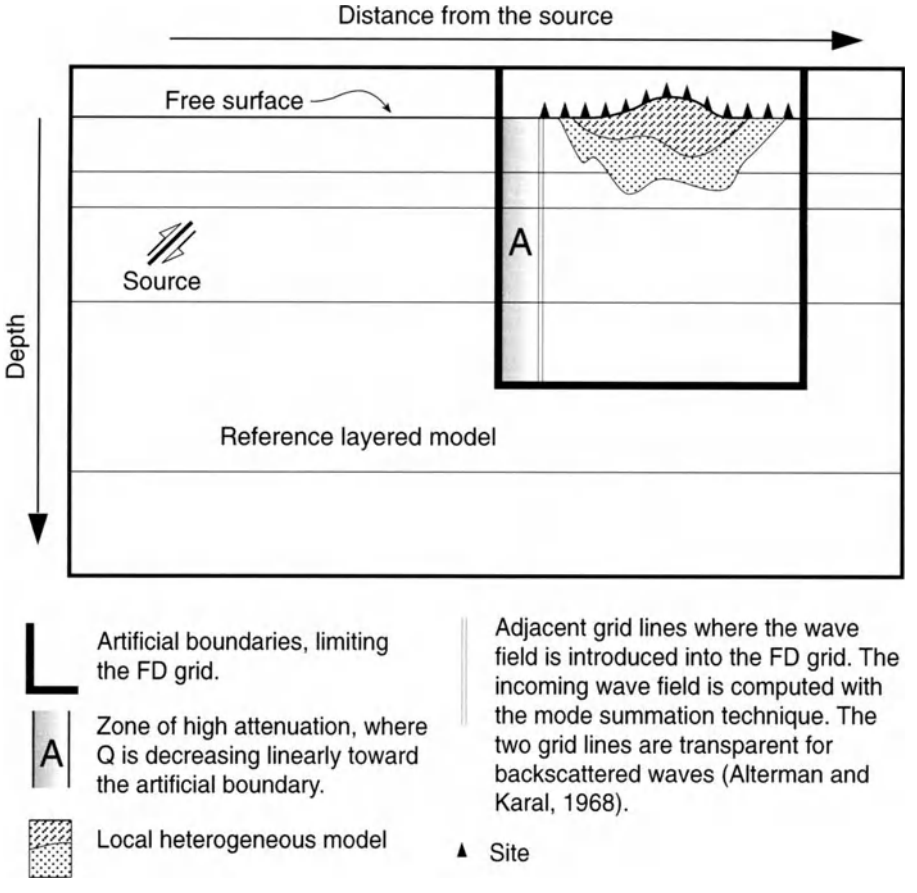

Figure 2
A generalized scheme of the model adopted for the numerical experiments.

Table 3

Geophysical properties of the geological strata used to model the Sofia kettle

Layer	Density	Seismic wave propagation velocities		Attenuation factor, Q	
	ρ [kg/m^3]	Vp [m/s]	Vs [m/s]	Qp	Qs
Soil Layer	1800	310	180	40	15
Quaternary cover	1970	950	550	50	20
Tertiary sediments	1920	1400	800	75	30
Senonian marls	2000	1900	1100	100	40
Triassic limestones	2020	2100	1200	120	50
Senonian andesites	2540	3600	2100	200	80

Table 4

Mesh and model size considered in the FD computations

Profile	Mesh size		Model size	
	X, grid points	Z, grid points	X, km	Z, km
AB	2082	577	10.41	19.80
CD	2939	310	11.76	3.95
EF	2978	474	11.91	10.00

Considering the regional topography of the studied area, it is advisable to perform investigations, implementing a three-dimensional model as well. This can be done as soon as significant records become available and that will allow the assessment of possible 3-D effects.

Numerical Experiments and Discussion of the Results

Complete synthetic seismic signals have been generated for all sites of interest along the profiles investigated, (Fig. 3 $\sim$ 100 sites per profiles), following the earthquake scenarios given in Table 2. Two groups of experiments have been performed: (A) ground-motion modelling, applying an algorithm based on the modal summation method (PANZA, 1985; PANZA and SUHADOLC, 1987), 1-D, and (B) modelling, making use of the hybrid technique (FäH *et al.* 1993; 1994 a,b), 2-D. The distant seismic sources were considered as buried double-couple point sources. The local seismic source was modelled by introducing a single Ricker impulse at the bottom of the model.

The chosen frequency interval (up to 5 Hz) covers practically the entire range of elements of the built environment present at Sofia. Synthetic seismic signals along the profiles investigated (Fig. 3, Table 2) are computed and acceleration, velocity and displacement time histories are obtained for all ground-motion components, transverse (TRA), radial (RAD) and vertical (VER). Different quantities of earthquake engineering interest, such as peak ground accelerations (PGA), peak ground velocities (PGV), peak ground displacements (PGD), response spectra amplitudes (SA) and PGA / PGV ratios, are derived from the computed seismic signals. The site response along the investigated profiles is defined as Response Spectra Ratio (RSR). These RSR are the ratios between the amplitudes of the response spectra, for 5% damping (SA), computed taking into account the local heterogeneous media (SA2), and the corresponding values obtained considering only the bedrock structure (SA1), RSR = SA2 / SA1. The distributions of RSR versus frequency and epicentral distance for all studied scenarios have been mapped.

Comparisons between the seismic signals simulated by the modal summation method and those, obtained applying the hybrid technique for the simple bedrock

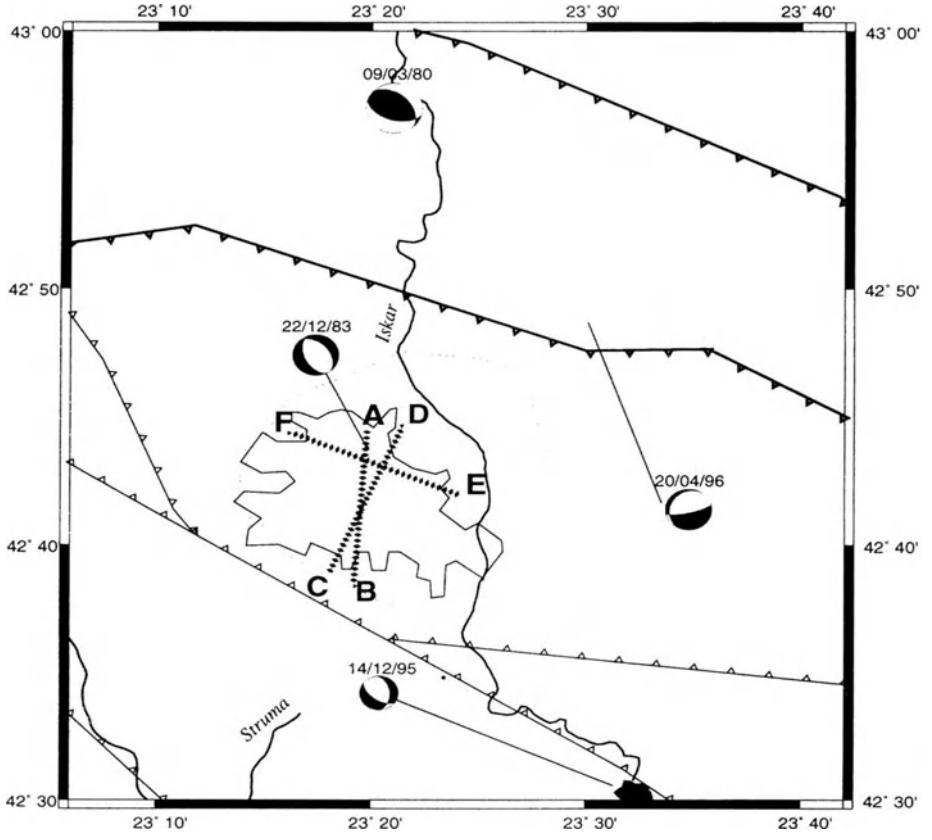

Figure 3
A generalized tectonic scheme of the Sofia region, investigated profiles (AB, CD and EF), location and focal mechanisms of the considered earthquakes.

layered structural model have been carried out. These tests are always necessary when the hybrid approach is applied in a new region. The differences between both the modal summation method and the hybrid technique are negligible (less than 3–5 %). It means that the control of the accuracy of the FD part of the computations, depending upon the efficiency of the absorbing boundaries, the correct discretization of the structural model, the presence of all phases in the seismograms and the treatment of anelasticity, has been successfully achieved.

To validate the theoretical computations, the observed macroseismic information was used. No instrumental data are available for the considered events since the digital seismological station (VTS—Sofia) began operation in May 1996. The macroseismic maps for the earthquakes in 1907, 1909, 1910, 1917, 1941, 1947 and 1952 (PETKOV and CHRISTOSKOV, 1965; GLAVCHEVA, 1990; CHRISTOSKOV *et al.*, 1989) are too general with respect to the microzonation purposes and no information is available on the fault plane solution of the mapped earthquakes. The few published

maps of seismic microzonation for Sofia (PETKOV and CHRISTOSKOV, 1964; SOLAKOV, 2001) show maximum variations within two degrees of macroseismic intensity. Macroseismic intensity variation $\Delta I = 2$ is also reported for the earthquake of December 22 (GLAVCHEVA, 1990), that has been considered for the computations of the ground motion along the AB profile. The existing relation between PGA and the macroseismic intensity, I (MEDVEDEV 1977), and between PGA/PGV and I (SEED and IDRISS, 1982) have been used to provide theoretical estimates of the macroseismic intensity of each site. The theoretically estimated macroseismic intensity varies within two degrees in the investigated region, which is in agreement with the available observation. The synthetic signals obtained considering an earthquake scenario with magnitude $M = 6.5$ and focal depth H = 8 km show 200 cm/s^2 < PGA < 400 cm/s^2, I = VIII–IX (MEDVEDEV 1977). This result is consistent with the parameterization of the isoseimals from Bulgarian earthquakes (GLAVCHEVA, 1990).

The maximum SA(2D) values, computed for 5% damping were normalized to the corresponding SA(1D) values for each site along the profiles investigated. The results for all components TRA, RAD and VER are shown in Figures 4.1–4.3. Along profile AB, Figure 4.1, the theoretical curves for TRA, RAD and VER justify the one-degree intensity increment, although they fail to explain larger intensity increments. Regarding the scenario, dealing with earthquakes beneath the city, the TRA–SA ratio variation matches the reference intensity graph within epicentral distances 25–26 km, 28–30 km and 31–33 km. Most impressive are the results we obtained along profile CD (Fig. 4.2). The peaks in the SA(2D)/SA(1D) for all components TRA, RAD and VER follow the lateral variation of the structural model. The variation of SA(2D)/SA(1D) explains well local intensity increments as large as 3, and in general are in agreement with the variation of I along the profile. For both profiles AB and CD the VER component seems uncorrelated with the intensity variation. The possible correlation of the computed amplification of the VER component to the observed damage has been reported (e.g., LOKMER *et al.*, 2001; PANZA *et al.*, 2002). Along the EF profile (Fig. 4.3) the RSR for the horizontal components varies within 2 and 4, in agreement with the reported one-degree local intensity increment. The comparison between the intensity, theoretically estimated on the base of the PGA(2D)/PGA(1D) or PGV/PGA ratios and the reported intensity, leads to similar conclusions. The observed mismatch between the synthetic signals and the reported intensity is not surprising. It may warrant refinement and renovation of the seismic microzonation intensity maps, however it can be due to inadequacies in the assumed parameters describing the source and the medium.

A successful test for the numerical modelling of the ground motions at Sofia stems from most of the PGV/PGA ratios. The computed ratios agree with the values suggested by SEED and IDRISS (1982) and DECANINI (pers. com., 1998) for intermediate soil (V_s < 0.3 km/s) and rocks and deep stiff soil (0.6 km > V_s > 0.3 km/s), Figures 5.1–5.3.

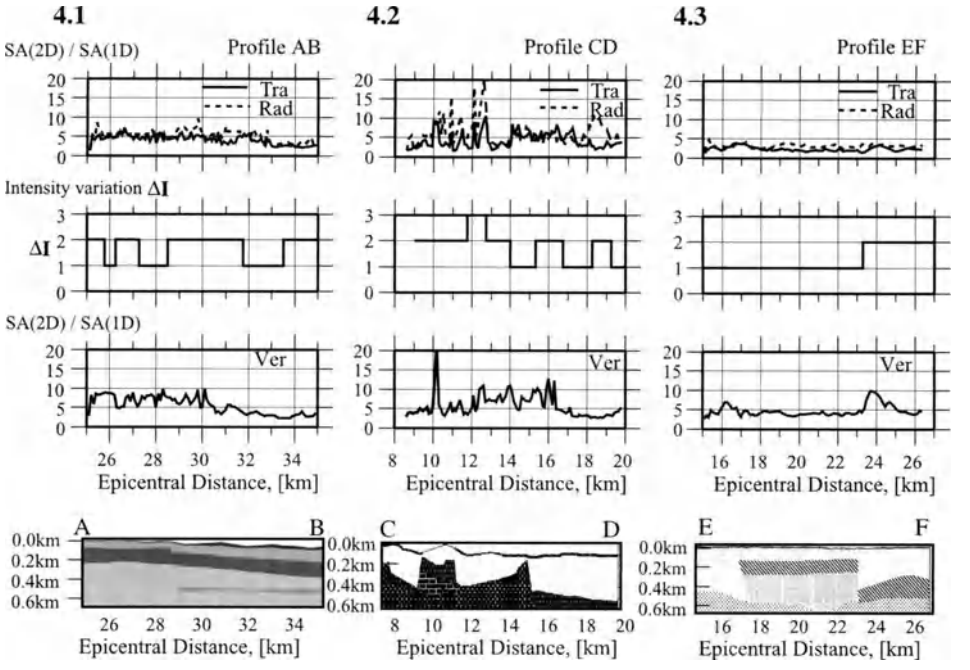

Figure 4
Spectral ratio Sa(2D)/SA(1D) for 5% damping, along the profile investigated (as shown in Fig. 3). Comparison with the macroseismic intensity I [MSK] variation graph along the same profiles (a fragment of map of seismic microzonation of Sofia). Transverse (TRA—solid line), radial (RAD—dashed line) and Vertical (Ver) components are shown). Figure 4.1: Profile AB; Figure 4.2: Profile CD; Figure 4.2: Profile EF.

Site amplification is estimated in terms of RSR distributions versus frequency and epicentral distance (Figs. 6.1–6.3). In Figure 6.1 the site amplification along the AB profile, which is exposed to a distant earthquake, is shown. One can see that the TRA component is amplified up to 4.6 (1.5–2.0 Hz), the RAD amplification reaches 3.6 (1.0–1.75 Hz) and the VER RSR increases to 7.5 within the frequency interval 1.25–3.00 Hz. If an earthquake strikes just beneath the profile AB (Table 3) then the ground motion at the site can be amplified by 10–11 times within the frequency interval 1.25–2 Hz (not shown in the figures). Along the CD profile (Fig. 6.2) the highest amplification is observed for the RAD component compared to the other two components. The maximum amplifications for all ground motion components (TRA, RAD and VER) are observed at frequencies higher than 3.5 Hz. For the RAD RSR reaches 7–8.5 (at 2.5–5 Hz), due to the VER RSR being to 3.5–5.0 (3.5–5.0 Hz) and for the TRA, the largest RSR is about 6 (3.5–4.5 Hz). The amplification along the profile EF is shown in Figure 6.3. TRA shows rather consistent amplification (less than 3) within the entire frequency

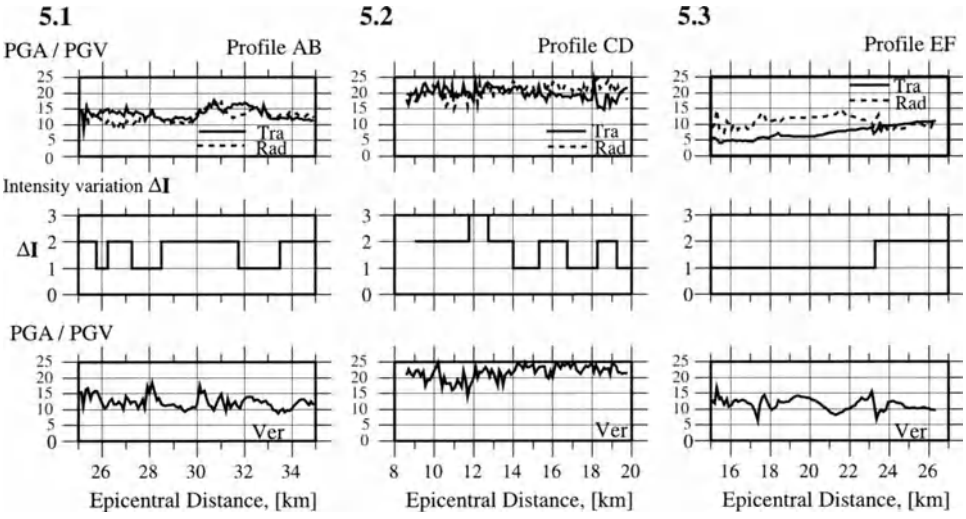

Figure 5
Scheme of the ratio of the peak ground velocity PGV to the peak ground acceleration PGA along the investigated profiles (as shown in Fig. 3), related to the macroseismic intensity *I* [MSK] variation along the same profiles (a fragment of map of seismic microzonation of Sofia). Transverse (TRA—solid line), radial (RAD—dashed line) and Vertical (Ver) components are shown). Figure 5.1: Profile AB; Figure 5.2: Profile CD; Figure 5.2: Profile EF.

interval considered, RAD has its maximum amplification (2.5–3.0) at 3.5–4.5 Hz and VER amplifies to 3.5–4.0 at frequencies 0.5 Hz and 1.3–1.8 Hz. For all scenarios the maximum amplifications along the profiles correspond to the weak or intermediate soil conditions as shown in the map of engineering geological conditions at Sofia (PASKALEVA and KOUTEVA, 2001).

In all scenarios the presence of thick sediments leads to an increase of the ground-motion amplitudes and of the amplification, due to multiple reflections. The maximum PGA values correspond to both the thickest sediments and the thickest parts of the surface low velocity layer. A comparative study of the spectral amplification of the different ground-motion components reveals that TRA, RAD and VER significantly contribute to the seismic input, where as the RAD component exerts the prime influence on the site amplification, reaching values up to 7–8 whereas for TRA and VER components, the maximum amplification is 5–6. This result differs from the widely accepted idea that the transverse component predominantly contributes to the seismic input definition.

Four earthquake scenarios were chosen and complete synthetic seismic signals were generated along three geological profiles crossing the city of Sofia. A hybrid procedure that accounts simultaneously, into the ground-motion estimate, the seismic source moment tensor and the mechanical characteristics of the propagating media was used. The results obtained through the theoretical modelling

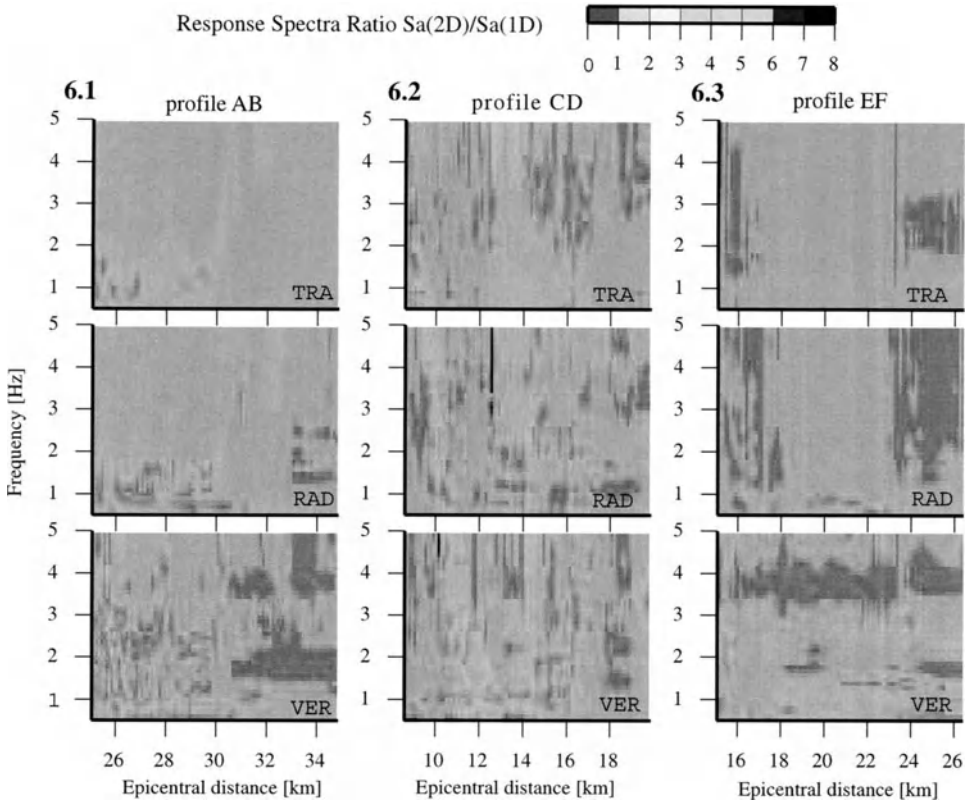

Figure 6
Site amplification defined as Response Spectra Ratio, (RSR), mapped versus frequency and epicentral distance along the profiles investigated (as shown in Fig. 3). Transverse (TRA), radial (RAD) and vertical (VER) components are shown.

have been successfully compared with the macroseismic field information available.

The approach used to model the ground motion at Sofia capably provides realistic acceleration, velocity, displacement time histories and related quantities of earthquake engineering interest. The most important result concerns the site response behavior. The comparative study of the spectral amplification of the different ground-motion components shows that TRA, RAD and VER significantly contribute to the seismic input. RAD exerts the major influence on the site amplification—this fact differs from the widely accepted idea that the transverse component predominantly affects the seismic input definition. The obtained results can be used for different engineering purposes, urban planning, retrofitting of the built environment, insurance industry, earthquake preparedness, earthquake risk reduction and earthquake risk management.

Acknowledgements

This research is a contribution to the UNESCO–IUGS–IGCP 414 Project "Realistic Modelling of Seismic Input for Mega cities and Large Urban Areas." It has also been supported by the NATO: SfP IVESB 972266 and 65/219.33/01/12/2000, by the Marie-Curie Training site grant EVK2-CT-2000-57002 and Scientific BG Fund NZ 10031.

References

ALTERMAN, Z. S., and KARAL, F. C. (1968), *Propagation of Elastic waves in Layered Media by Finite Difference Methods*, Bull. Seismol. Soc. Am. *58*, 367–398.

BONCHEV, E., BUNE V., CHRISTOSKOV, L., KARAGYULEVA, J., KOSTADINOV, V., REISNER, G., RIZIKOVA, S., SHEBALIN, N., SHOLPO, V., and SOKEROVA, D. (1982), *A Method for Compilation of Seismic Zoning Prognostic Maps for the Territory of Bulgaria*, Geologica Balkanica *12/2*, 3–48.

CHRISTOSKOV, L., GEORGIEV, TZV., DENEVA, D., and BABACHKOVA, B. (1989), *On the Seismicity and Seismic Hazard of Sofia Valley*, Proc. Of the 4th Int. Symposium on the *Analysis of Seismicity and Seismic Risk*, Bechyne Castle, CSSR, IX, 1989, pp. 448–454.

CHRISTOSKOV, L. (1992), *100 Years Seismology in Bulgaria*, Bulg. Geoph. J. *XVIII/1*, 3–21.

DECANINI, L., MOLLAIOLI, F., PANZA, G. F., ROMANELLI, F. and VACCARI, F. (2001), *Probabilistic vs. deterministic evaluation of seismic hazard and damage earthquake scenarios: A general problem, particularly relevant for seismic isolation*, Proc. 7th International Seminar on *Seismic Isolation, Passive Energy Dissipation and Active Control of Vibrations of Structures*, Assisi, Italy, October 2–5, 2001.

FÄH, D., IODICE, C., SUHADOLC, P., and PANZA, G. F. (1993), *A New Method for the Realistic Estimation of Seismic Ground Motion in Megacities: The Case of Rome*, Earthquake Spectra *9*, 643–668.

FÄH, D., IODICE, C., SUHADOLC, P., and PANZA, G. F. (1994a), *Application of Numerical Simulations for a Tentative Seismic Microzonation of the City of Rome*, Annali di geofisica *XXXVIII, 5–6*, 607–615.

FÄH, D., SUHADOLC, P., MUELLER, S. T., and PANZA, G. F. (1994b), A Hybrid Method for the Estimation of Ground Motion in Sedimentary Basins; Quantative Modelling for Mexico city, BSSA *84*, 383–399.

FRANGOV, G. (1995), Assessment of the Conditions and Factors, Determining the Geological Hazards at the Sofia Kettle, Rep. to CGMR (in Bulgarian).

GLAVCHEVA, R. (1990), *Parametrization of the Isoseismal from Bulgarian Earthquakes*, Bulg. Geoph. J. *XVI, 4*, 38–44 (in Bulgarian).

GLAVCHEVA, R. (1993), *Atlas of Isoseismal Maps, Bulgaria 1981–1990*, Geoph. Inst., BAS.

GLAVCHEVA, R., GEORGIEV, T. Z., BOTEV, E., BABACHKOVA, B. L., and TOTEVA, T. (1996), *Sofia Graben and the Earthquake of December 14, 1995*, Bulgarian Geophys. J. *XXII, 3*, 44–50.

IVANOV, P. (1997), *Assessment of the Geological Conditions in the Sofia Kettle under Seismic Impact*, Proc. International IAEG Conference, Athens, 1997, Balkema, Rotterdam, 1265–1270.

IVANOV, PL., FRANGOV, G., and YANEVA, M. (1998), Engineering Geological Characteristics of Quaternary Sediments in the Sofia Graben, Proc. 3rd WG Meeting, 2–5, 12, 1998, Sofia, 33–37.

JARANOFF, D., *Tectonics of Bulgaria* (Technika, Sofia 1960).

KAMENOV, B. and KOJUMDJIEVA, N. (1983), *Stratigraphy of the Neogene in Sofia Basin*, Paleontology, Stratigraphy and Lithology *18*, 69–85.

KIROV, K. (1952), *A Contribution to Studying of the Earthquakes in Sofia Valley*, An. of Main Direction for Geological and Mine Researches *5*, 407–417 (in Bulgarian).

LEVANDER, A. R. (1988), *Fourth-order Finite-difference P-SV Seismograms*, Geophysics *53*, 1425–1436.

LOKMER, I., HERAK, M., PANZA, G. F., and VACCARI, F. (2001), *Amplification of Strong Ground Motion in the City of Zagreb, Croatia, Estimated by Computations of Synthetic Seismograms*, ICTP Preprints, *IC/2001/26*.

MATOVA, M. (2001), *Recent manifestations of seismotectonic activity in Sofia region and their land subsidence potential*, Proc. Final Conf. of UNESCO-BAS Project on Land Subsidence, June 27–30, 2001, Sofia, 93–98.

MEDVEDEV, S. V. (1977), *Seismic Intensity Scale MSK–76*, Publ. Inst. Geophys. Pol. Acad. Sc. *117*, 95–102.

MOLCHAN, G., KRONROD, T., and PANZA, G. F. (1997), *Multi–scale Seismicity Model for Seismic Risk*, BSSA *87*, *5*, 1220–1229.

NEIC, National Earthquake Information Center, http://wwwneic.cr.usgs.gov/neis/epic/epic_global.html

NUNZIATA, C., COSTA G., MARRARA, F., and PANZA, G. F. (2000), *Validated Estimation of Response Spectra for the 1980 Irpinia Earthquake in the Eastern Area of Naples*, Earthquake Spectra *16*, *3*, 643–661.

OROZOVA-STANISHKOVA I., and SLEJKO, D. (1994), *Seismic Hazard of Bulgaria* , Natural Hazards *9*, 247–271.

OROZOVA-STANISHKOVA I., COSTA, G., VACCARI, F., and SUHADOLC, P. (1996), *Estimates of 1 Hz Maximum Accelerations in Bulgaria for Seismic Risk Reduction Purposes*, Tectonophysics *258*, 263–274.

PANZA, G. F. (1985), *Synthetic Seismograms: The Rayleigh Waves Modal Summation*, J. Geophysics *58*, 125–145.

PANZA, G. F. and SUHADOLC, P. (1987). *Complete strong motion synthetics.* In *Seismic Strong Motion Synthetics* (ed. Bolt B.A.) (Academic Press, Orlando) pp. 153–204.

PANZA, G. F., ROMANELLI, F., and VACCARI F. (2000), *Seismic wave propagation in Laterally Heterogeneous Anelastic Media: Theory and Applications to Seismic Zonation*, In *Advances in Geophysics 43*, pp.1–95.

PANZA, G. F. and VACCARI, F. (2000), *Introduction.* In *Seismic Hazard of the Circum-Pannonian Region* (eds. Panza, G. F., Radualian, M., and Trifu, C.) (Pure Appl. Geophys. Topical Volume, Birkhäuser Verlag, Basel, Switzerland, 2000) pp.5–10.

PANZA, G. F., CIOFLAN, C. O., KOUTEVA, M., PASKALEVA, I., and ROMANELLI, F. (2002), *An Innovative Assessment of the Seismic Hazard from Vrancea Intermediate-depth Earthquakes: Case Studies in Romania and Bulgaria* (submitted to the 12 E CEE, Ref. No. 230).

PASKALEVA, I. and KOUTEVA, M. (2001a), *A Contribution to the Seismic Risk Assessment of Sofia Region and the Town of Russe from Deterministic Modelling*, Report on Bilateral Project "Engineering Seismic Hazard and Risk Assessment of Selected Cities in the Balkan region," CLSMEE-BAS—DST-UNIVTS, May-June 2001.

PASKALEVA, I. and KOUTEVA M. (2001), *An Approach for Microzonation of the Town of Russe in Connection with Recent Vrancea Earthquakes and Shabla Zone*, Report on Bilateral Project Engineering Seismic hazard and Risk Assessment of Selected Cities in the Balkan Region, "CLSMEE-BAS—DST-UNIVTS, May-June 2000.

PASKALEVA, I., MATOVA, M., and FRANGOV, G. (2002), *Expert Assessment of the Displacements Provoked by Seismic Events: Case Study for the Sofia Metropolitan Area* (Pure Appl. Geophy. Topical Volumes, Birkhäuser Verlag, Basel, Switzerland, 2004)

PETKOV, I. and CHRISTOSKOV, L. (1965), *On Seismicity in the Region of the Town of Sofia Concerning the Macroseismic Zoning*, Ann. Sofia Univ. *58*, 163–179.

PETROV, P. and ILIEV, I. (1970), *The Effect of Engineering Geological Conditions on Seismic Microzoning in Sofia*, Proc. 3rd Eur. Symposium on EE, Sofia, 79–86.

RANGUELOV, B. (1996), *Seismicity and Site Effects on the Sofia Valley District*, Proc. 1st WG meeting, Oct. 31–Nov. 3, Sofia, 28 -31.

RANGUELOV, B. and TOTEVA, T. (1998), *Recent Seismicity Observed Around Sofia City*, Proc. 3rd WG Meeting, Dec. 2–5, Sofia, 7–9.

ROMPLUS Earthquake Catalogue, Romanian Catalogue on line, Computer File, www.infp.infp.ro.

SEED, H. B. and IDRISS, I. M. (1982), *Ground Motions and Soil Liquefaction during Earthquakes*, EERI, 1–134.

SHANOV, S., SPASSOV, E., and GEORGIEV, T. (1992), *Evidence for the Existence of a Paleosubduction Zone Beneath the Rhodopean Massif (Central Balkan)*, Tectonophysics *206*, 307–314.

SHEBALIN, N., LEYDECKER, G., MOKRUSHINA, N. TATEVOSSIAN, R., ERTELEVA, O., and VASSILIEV, V., *Earthquake Catalogue for Central and Southeastern Europe 342 BC–1990 AD* (European Commission, Report No. ETNU CT 93 - 0087) (1999).

SLAVOV, S. L., *Ground Motion Modelling in the City of Sofia* (TRIL—ICTP Visitors report) (2000).

SOLAKOV, D., SIMEONOVA, S. T., and CHRISTOSKOV, L. (2001), *Seismic Hazard Assessment for the Sofia Area*, Annali di Geofisica *44*, *3*. 541–555.

STANISHKOVA, I. and SLEJKO, D. (1991), *Seismic Hazard of the Main Bulgarian Cities*, In *Atti del 10° Convegno Annuale del Gruppo Nazionale di geologica della terra solida*; Roma, 6–8 Novembre, 1991, 123–134.

SUN, R., VACCARI, F., MARRARA, F., and PANZA, G. F. (1998), *The Main Features of the Local Geological Conditions can Explain the Macroseismic Intensity Caused in Xiji-langfu (Beijing) by the M_S = 7.7 Tangshan 196 Earthquake*, Pure Appl. And Geophys. *152*, 507–521.

TODOROVSKA,M., PASKALEVA, I., and GLAVCHEVA, R. (1995), *Earthquake Source Parameters for Seismic Hazard Assessment: Examples of Bulgaria*, Proc.10th ECEE, Vienna, Austria.

TRIANTAFYLLIDIS, P., HATZIDIMITRIOU, P. M., SUHADOLC, P., THEODULIDIS, N., and PITILAKIS, K., *Comparison between 1-D and 2-D site effects modelling*. In *The Effests of the Surface Geology on Seismic Motion*, (eds. Irikura, K., Kudo, K., Okada H., and Sasatani , T.) (Balkema, Rotterdam, 2, 1998) pp. 981–986.

TZANKOV, TZ., and NIKOLOV G. (1996), *Recent Bilateral Listric Destruction in Western Stara Planina Mountain and Western Fore Balkan, Bulgaria*, C.R.Bulg. Acad. Sci. *49*, *4*, 53–55.

VACCARI, F., GREGERSEN, S., FURLAN, M., and PANZA, G. F. (1989), *Synthetic Seismograms in Laterally Heterogeneous, Anelsatic Media by Modal Summation of P-SV Waves*, Geoph.. J. Int. *99*, 285–295.

VACCARI, F., NUNZIATA C., FäH, D., and PANZA, G. F. (1995), *Reduction of Seismic Vulnerability of Megacities: The Cases of Rome and Naple*s, Proc. 5th Int. Conf. on *Seismic Zonation*, EERI, Oct., 1995, Nice, France, 1392–1399.

VIRIEUX, J. (1984), *SH—Velocity-stress Finite-difference Method: Velocity-stress Finite-Difference Method*, Geophysics *49*, 1933–1957.

VIRIEUX, J. (1986), *P-SV Wave Propagation in Heterogenoues Media: Velocity-stress Finite-difference Method*, Geophysics *51*, 889–901.

(Received April 30, 2002, accepted July 10, 2002)

Pure appl. geophys. 161 (2004) 1239–1264
0033–4553/04/061239–26
DOI 10.1007/s00024-003-2489-7

Pure and Applied Geophysics

Seismic Ground Motion in Napoli for the 1980 Irpinia Earthquake

C. NUNZIATA[1]

Abstract—The seismic ground motion in the urban area of Napoli has been computed for the 1980 earthquake (M_S = 6.9) with a hybrid technique based on the mode summation and the finite difference methods. The detailed geological setting of each quarter has been reconstructed from several stratigraphies and six geological zones have been recognized. Shear-wave velocity profiles have been assigned, based on hole tests and inversion of Rayleigh group velocities artificially generated.

Realistic *SH* and *P-SV* wave seismograms have been computed along the representative cross sections of each zone, by assuming selected velocity profiles. Spectral amplifications of 2–4 have been computed at frequencies roughly corresponding to the eigenfrequencies of the most damaged buildings. Moreover, following the intensity-PGA correlations found for the Italian territory, the predicted peak ground accelerations, 0.04–0.10 g correspond to the intensity range VII-VIII on the MCS scale, in agreement with the observed data.

Key words: Napoli, Irpinia earthquake 1980, synthetic seismograms, spectral amplification.

1. Introduction

Napoli is a good example of a large Mediterranean city with high seismic risk, mostly because of the high vulnerability due to the high density of population and the nature of the built environment. On the other hand, the seismic hazard is strictly dependent on the seismic amplification of the complex geological setting, with volcanic products erupted by different vents, and altered by weathering and rill-wash processes. In addition, during recent centuries the streams from the surrounding hills have been drained and filled with heterogeneous materials; often waste, and cavities have been artificially generated to extract tuff, extensively used as building stone.

Vulnerability may be reduced through the adequate retrofitting of ancient buildings and monuments as well as through the design of new reinforced structures which better resist the earthquake loads. Sound anti-seismic construction requires the knowledge of a correct seismic site response, both in terms of peak ground acceleration and response spectral content, based on methods which take into account source, travel path and local, well-defined soil conditions.

[1] Dipartimento di Geofisica e Vulcanologia, Univ. Napoli "Federico II"
E-mail: Conunzia@unina.it

Based on the historical records, the largest experienced intensity in Napoli is VIII on the MCS scale (ESPOSITO *et al.*, 1992). The 1980, Irpinia earthquake (M_S = 6.9, M_L = 6.5) is representative of a strong shaking in Napoli since it caused intensity VII on the MSK scale (POSTPISCHL *et al.*, 1985), roughly equivalent to intensity VIII (MCS). The damage was concentrated in the historical center and in the eastern area, and was verified through more than 20,000 stability essays on buildings (Fig. 1).

A lower level of damage was expected in Napoli since moderate peak ground accelerations of 0.06 g and 0.04 g, with dominant frequencies 2.5 and 3 Hz, were recorded along the north-south and east-west directions at the seismic station Torre del Greco, about 10 km east of Napoli located on a lava flow on the flanks of Vesuvius (Fig. 2). The recorded seismograms at Torre del Greco, the only instrumental recording of ground acceleration close to Napoli, have been reasonably

Legend

Very high Damage	High Damage	Medium damage	Low damage	Available data unreliable
11. Montecalvario	4. Chiaia	2. Bagnoli	1. Arenella	9. Miano
19. Poggioreale	5. S. Ferdinando	7. Chiaiano	3. Barra	14. Pendino
20. S. Lorenzo	10. Avvocata	16. Pianura	6. Posillipo	15. Mercato
21. Vicaria	12. S. Giuseppe	22. S. Pietro	8. Fuorigrotta	17. Piscinola
29. Zona Industriale	13. Porto		18. Ponticelli	24. Secondigliano
	26. Stella		23. S. Giovanni	30. Scampia
	27. S. Carlo		25. Soccavo	
			28. Vomero	

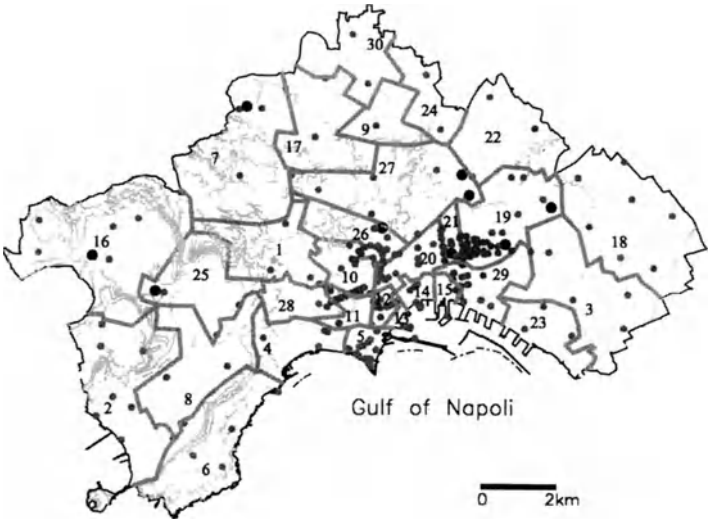

Figure 1
Urban map with quarter limits of Napoli (arabic numbers) and damage caused by the 1980 Irpinia earthquake. Location of drillings (grey dots) and FTAN measurement sites (black dots) is also shown.

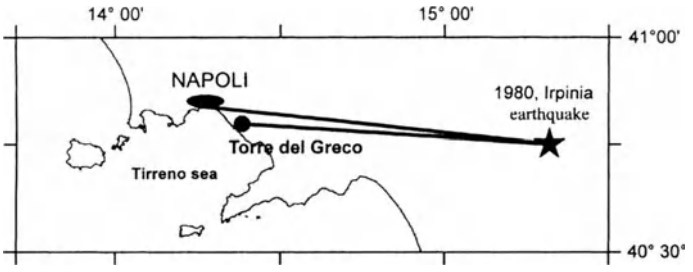

Figure 2
Location of epicenter of Irpinia 1980 earthquake, Torre del Greco (seismic station) and Napoli.

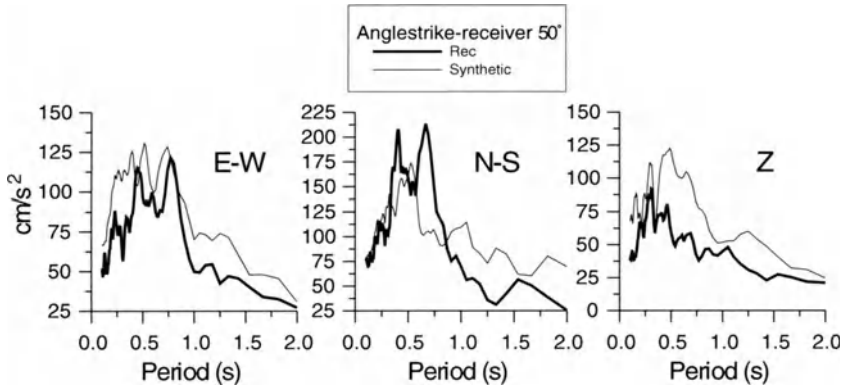

Figure 3
Comparison between synthetic and recorded response spectra, computed for a source-receiver backazimuth of 50°, at Torre del Greco accelerometer station (from NUNZIATA *et al.*, 2000).

fitted by synthetic seismograms (NUNZIATA *et al.*, 2000) computed with the mode summation technique (PANZA, 1985; FLORSCH *et al.*, 1991) (Fig. 3).

This validation and the availability of detailed geotechnical information pertaining to the local soil conditions allowed us to compute quite realistic ground motion at two areas of Napoli (Fig. 1): S. Lorenzo quarter, representative of the historical center (NUNZIATA *et al.*, 2002) and Centro Direzionale, within the quarter of Poggioreale, a newly developed area with skyscrapers of important social use (NUNZIATA *et al.*, 2000). Synthetic seismograms were computed by using the hybrid approach developed by FÄH (1992) which is based on the mode summation and the finite difference methods.

The aim of this paper is to estimate the seismic ground motion in Napoli for the 1980 Irpinia earthquake, based on the reconstruction, quarter by quarter of the geological, geotechnical and geophysical setting. Realistic *SH* and *P-SV* wave seismograms with complete body and surface waves are computed with the hybrid method developed by FÄH (1992) along representative geological cross sections, by assuming selected velocity profiles to test the sensitivity of the spectral amplification.

Then, average and maximum spectral amplifications and acceleration response spectra are considered for seismic risk mitigation.

2. Numerical Modelling of Seismic Ground Motion

The 1980 Irpinia earthquake (M_S = 6.9, M_L = 6.5) is the first strong event recorded close to Napoli at the seismic station Torre del Greco (Fig. 2).

The recorded seismograms at Torre del Greco have been used to calibrate synthetic seismograms computed with the mode summation technique (PANZA, 1985; FLORSCH *et al.*, 1991). The average reference model given by VACCARI *et al.* (1990) has been assumed for the propagation of the wavefield from the epicenter to Torre del Greco station and the source mechanism has been chosen accordingly with the main shock (0 s subevent) of the 1980 Irpinia earthquake: dip 65°, rake 270°, strike 315° (PANTOSTI and VALENSISE, 1993). Synthetic seismograms have been properly scaled to a finite dimension source according to the magnitude M_s = 6.9 of the Irpinia earthquake, by using the moment-magnitude relation given by KANAMORI (1977) (from which a seismic moment of 2.5×10^{19} Nm is computed) and the spectral scaling law proposed by GUSEV (1983) as reported in AKI (1987). Reasonable agreement between synthetic and observed response spectra (Fig. 3) has been obtained for a source-receiver back azimuth of 50° and a source depth of 7.0 km (NUNZIATA *et al.*, 2000).

This validation at hand and the availability of detailed geotechnical information concerning the local soil conditions has allowed us to compute quite realistic ground motion in Napoli by using the hybrid approach developed by FÄH (1992). The propagation of the waves from the source to the complex laterally varying structure is computed with the mode summation technique (PANZA, 1985; FLORSCH *et al.*, 1991), and in the laterally heterogeneous structure it is computed with the finite-difference method. A schematic representation of the hybrid method is shown in Figure 15. The path from the source to the laterally varying region is represented by a layered anelastic structure. The causative fault of the main shock of the 1980 earthquake is located approximately 90–100 km from Napoli. The angle between the strike of the fault and the epicenter cross section lines is 50°.

3. Geological Setting of Napoli

The geological setting of Napoli has been reconstructed from numerous geotechnical and stratigraphic data (AA.VV., 1967; Comune di Napoli, 1994) (Fig. 1). It is mainly characterized by pyroclastic materials, soil (pozzolana) and rock (tuff), from Campi Flegrei different eruptive centers and Vesuvius, that often underwent morphological changes due to the influence of the meteoric and marine agents and the urban settlement. The original material that forms the tuffs and the

volcanic soil is in general the same, with the volcaniclastic rocks being the result of the hardening of the volcaniclastic soil by post-depositional hydrothermal alteration. Such hardening is not homogeneous so that welded facies may vanish and the tufaceous formation becomes incoherent, especially at the borders or where such bodies taper. Neapolitan soil includes sand along the coast, and alternations of volcanic soil, alluvial soil and organic materials.

Laboratory measurements of physical properties of several specimens extracted from drillings and quarries (AA.VV., 1967; VINALE, 1988; COMUNE DI NAPOLI, 1994; NUNZIATA *et al.*, 1999), show that Neapolitan soil generally ranges from silty sand to sandy silt.

The most widespread products belong to the Neapolitan Yellow Tuff (NYT) eruption (12,000 years), pozzolana and tuff, and the recent eruptions ($< 12{,}000$ years), essentially pozzolana. The tuff horizon also consists of ancient tuffs (Ignimbrite, Campi Flegrei and Vesuvius tuffs older than 15,000 years) in the northern and eastern part of Napoli. The tuff horizon is on average at 10–30 m of depth, but deepens to more than 90 m in the western area and more than 40 m in the southeastern area of Napoli. The compact tuff horizon represents the Neapolitan seismic bedrock with $V_s > 750$ m/s (NUNZIATA *et al.*, this issue).

Taking into account the stratigraphies, six geologically homogeneous zones can be recognized in Napoli (Fig. 4).

Zone 1—Zone 1 is comprehensive of the quarters of Fuorigrotta, Bagnoli, Soccavo and Pianura, in the western part of Napoli (Fig. 1). The analysis of many

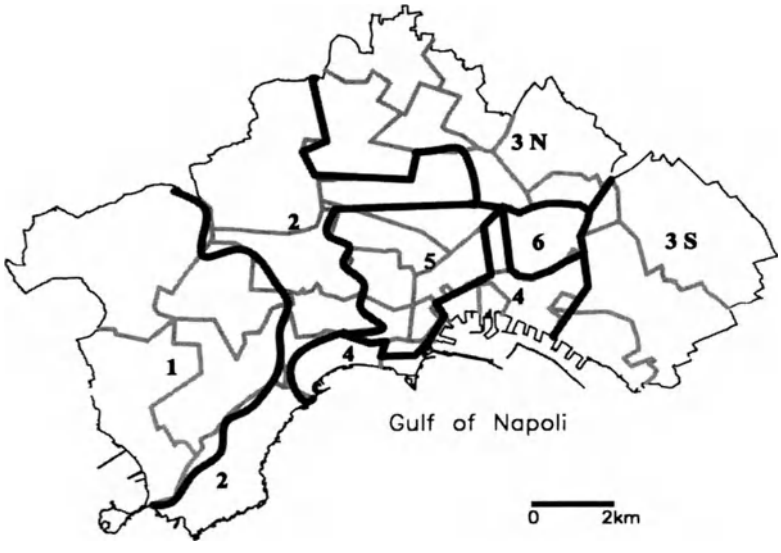

Figure 4
Map of the homogeneous geological zones of Napoli (black lines). The limits of the quarters are also shown (grey lines).

stratigraphies points out that the area is quite homogeneous, being characterized by a thick cover (more than one hundred meters) of recent pyroclastic products (< 12,000 years) on marine sand or occasionally, Neapolitan Yellow Tuff formation.

Zone 2—Zone 2 is comprehensive of the quarters of Chiaiano, S. Carlo, Arenella, Vomero and Posillipo (Fig. 1). It is characterized by the presence of recent pyroclastic products and man-made materials on Neapolitan Yellow Tuff (NYT) formation, both soil and lithoid facies. The NYT tuff horizon is generally 15 m deep from the ground surface, and sporadically very shallow (< 5 m) or deeper than 20 m.

Zone 3—Zone 3 is located on the eastern side of Napoli and has been divided into a northern part, zone 3N, and a southern part, zone 3S. Zone 3N includes the quarters of Piscinola, Miano, Secondigliano, Scampia, S. Pietro, part of Poggioreale, while Ponticelli, Barra, and S. Giovanni belong to zone 3S (Fig. 1). It is characterized by the presence of ancient tuff horizon at about 40 m of depth. A cover of NYT pozzolana and Campanian Ignimbrite products characterizes zone 3N, and of Vesuvius tuff, both soil and lithoid facies, zone 3S.

Zone 4—In the recent past this area was under sea level. As a consequence, the representative stratigraphic soil column consists of marine sand on NYT formation, both soil and lithoid facies. NYT tuff horizon is generally at 30 m of depth, and deepens on the southeastern side of Napoli. It comprehends the quarters of Chiaia, the southern part of S. Ferdinando, the southern part of Porto, Mercato, Pendino, Vicaria, and Zona Industriale (Fig. 1).

Zone 5—This zone includes the historical center of Napoli, that is the quarters of S. Lorenzo, Avvocata, Montecalvario, S. Giuseppe, Stella, and the southern part of S. Carlo (Fig. 1). The main peculiarity is the presence of several cavities in the tuff formation. The first excavations were tuff quarries and aqueducts and are dated VIII century B. C. Tuff was extracted to be used as a building stone and, preferably, in the same place. Thus it commonly happened that a building was built with tuff stones extracted below it. The shallow geological setting has been complicated by huge, natural and artificial, morphological changes, as for example the filling of river beds and hollows with alluvial materials and bricks. Hence the historical center of Napoli is characterized by a cover of man-made ground, up to 20 m of thickness, and pyroclastic soil (pozzolana) overlying a NYT tuff horizon with several cavities.

Zone 6—This zone comprehends the southern part of Poggioreale quarter (Fig. 1). Considerable geological, geotechnical and geophysical information is available for this area since Centro Direzionale with many skyscrapers has been built here after the 1980 earthquake. The area was a marsh recently drained both for urban development and for the reduction of the water supply. Water channels were later filled with bricks and waste materials. The sub-soil, affected by significant lateral variations, is mainly formed by man-made ground, alluvial soil (ash, sand, peat), loose and slightly cemented pozzolanas, NYT tuff and marine sand. It is a flat area about 10 m above sea level with the water table a few meters deep (NUNZIATA *et al.*, 2000).

4. Spectral Amplification

Sophisticated computing techniques such as finite difference can be applied if detailed geometries and seismic parameters, mostly shear-wave velocities V_s, are available. Several measurements of V_s have been made in Napoli by down- and cross-hole tests (COMUNE DI NAPOLI, 1994; VINALE, 1988). The analysis of such measurements, together with the geological and geotechnical characteristics of the investigated soils, has evidenced a wide scattering of V_s velocities, even for the same formation, mostly due to the textural characteristics and the different hardening degrees, and to the influence of the vertical pressure, for the incoherent deposits (NUNZIATA *et al.*, 1999; this issue). Frequently, strong variations of velocities have been reported in the DH-CH velocity profiles at a local scale (within 1 m), explainable both in terms of arrival time picking errors and of the pumiceous and lapilli content of the Neapolitan pyroclastic soil. Then, V_s database was implemented with measurements in representative lithostratigraphic sites of Napoli obtained from the inversion, with the Hedgehog method (VALYUS *et al.*, 1968; PANZA, 1981), of the group velocity dispersion curve of the fundamental mode of Rayleigh waves, artificially generated. Such dispersion curve is extracted from a signal recorded in refraction seismic surveys, employing the FTAN method on single channels (LEVSHIN *et al.*, 1992). FTAN-Hedgehog V_s models represent average values over distances of 50–100 m and are more suitable than DH-CH point measurements for seismic response analysis. Beside this, the good agreement of FTAN-Hedgehog with cross-hole measurements, has allowed us to enrich the database and to acquire experience enough to select for each zone (Fig. 4) some V_s models for the evaluation of the spectral amplification. Shear quality factors Q_s have been attributed on the basis of laboratory measurements of damping (GUADAGNO *et al.*, 1992; VINALE, 1988), and compression quality factors Q_p have been computed as 2.5 Q_s.

Site amplification effects have been estimated in terms of spectral amplification and defined as the response spectrum at a site in the 2-D structural model, normalized to the response spectrum computed for the 1-D average reference model (VACCARI *et al.*, 1990). For the computation of the response spectra 2% and 5% dampings have been assumed, respectively, for masonry structures and reinforced concrete buildings.

In the following, V_s models and computed spectral amplifications are presented zone by zone.

4.1 Zone 1

About 20 down- and cross-hole tests (COMUNE DI NAPOLI, 1994) and 2 V_s velocity profiles from FTAN-Hedgehog measurements (NUNZIATA *et al.*, this issue) have been collected for Zone 1. A wide ranging variability of V_s velocities has resulted, even if the stratigraphy is laterally homogeneous and it consists of recent pyroclastic soil.

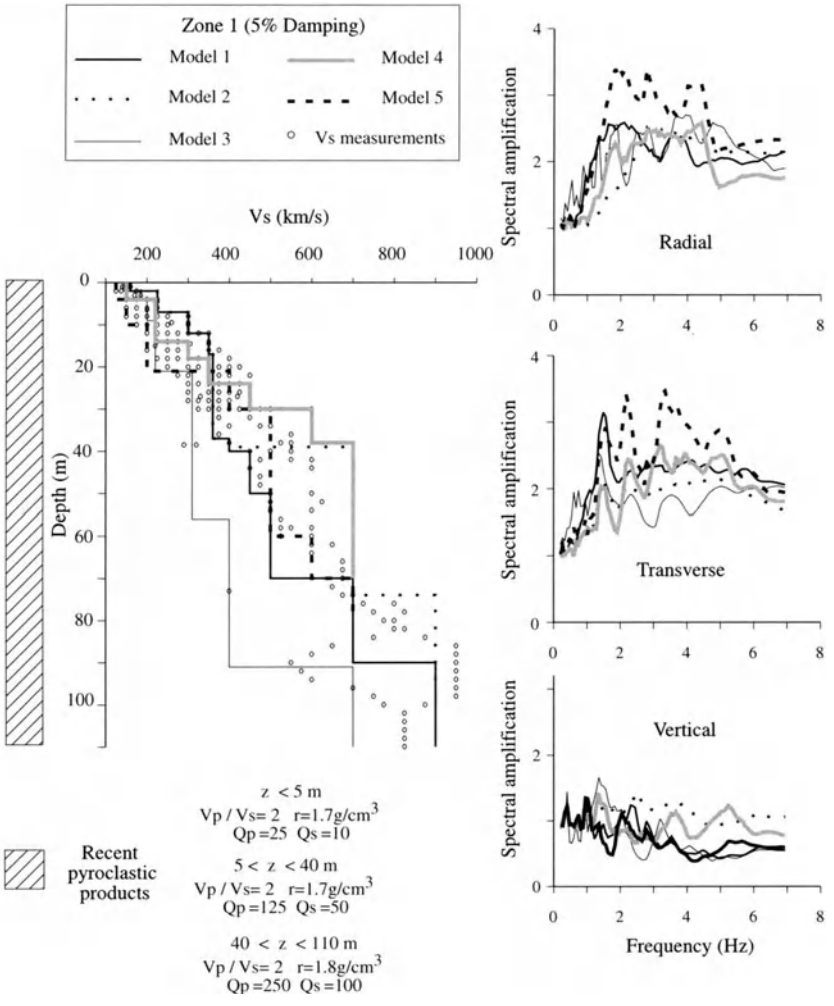

Figure 5
Representative stratigraphic column and V_s measurements (circles) at zone 1 (see Fig. 4 for location). A suite of 5 possible V_s models has been selected (lines) for which spectral amplifications for the *SH* and *P-SV* wave components have been computed.

Five different velocity profiles have been selected as being representative of the zone 1 (Fig. 5) to study their effect on the spectral amplification. In particular, models 1 and 3 are the average V_s profiles which were obtained from FTAN-Hedgehog measurements at Pianura and Soccavo quarters, respectively (see Fig. 1 for quarter location). Model 2 differs from model 1 at depths greater than 40 m, and can be considered as the envelope of the highest measured velocities. Models 4 and 5 are 2-DH velocity profiles and have been considered as a representation of the lowest and average shear velocities in the uppermost 20 m of subsoil. Model 1 is

representative of Pianura and Fuorigrotta, model 3 refers to Soccavo quarter, and models 4 and 5 are representative of Bagnoli quarter (Figs. 5 and 1).

Spectral amplifications have been computed for 5% damping, as the majority of houses, typically 5–7 floors, roughly corresponding to 1.5–2 Hz eigenfrequencies, have been built after 1950. They are similar along radial and transverse components and double that along vertical components (Fig. 5). Horizontal amplifications are about 2–3, and more than 3 for the V_s model 5. Transverse spectral amplifications show the same relative maximum peaks at about 1.5, 2.5 and 3.5 Hz with different amplitudes for the different V_s models. Average and maximum spectral amplifications have been computed for practical use (Fig. 6). The peak of the horizontal spectral amplification around 2 Hz is in correspondence with the building eigenfrequencies.

Average and maximum peak ground accelerations (PGA) of 0.04–0.05 g have been computed in the horizontal plane. Following the intensity-PGA correlations found for the Italian territory (PANZA *et al.*, 1999), predicted average peak ground accelerations correspond to the intensity range VII–VIII on the MCS scale, in agreement with the observed data. Concluding, average and maximum response spectra have been computed and are characterized in the horizontal plane by accelerations of 0.1–0.2 g in the 0.2–0.8 s period range (Fig. 6). A possible explanation of the different damage levels caused by the 1980 earthquake (Fig. 1) can be found in the prevailing presence of concrete buildings (70%) at Soccavo and Fuorigrotta quarters (low damage in Fig. 1), and of masonry structures (70%) at Bagnoli and Pianura (medium damage in Fig. 1). The sparse information regarding damage and floor number of buildings (RIPPA *et al.*, 1983) indicates more extensive damage for 6–7 floor concrete buildings at Bagnoli and Fuorigrotta quarters, which is in agreement with the peak of the spectral amplification at about 1.5 Hz (Fig. 6).

4.2 Zone 2

The 1980 earthquake caused minor damage at the quarters of Arenella, Vomero and Posillipo, medium and major damage at Chiaiano and S. Carlo quarters, respectively (Fig. 1). Tall concrete buildings prevail at Arenella quarter (> 5 floors) and are abundant in the northern area of S. Carlo quarter, at Vomero and Posillipo quarters. Instead masonry buildings (mostly 4–6 floors) are abundant at Chiaiano quarter and in the southern part of S.Carlo quarter.

Taking into account all down- and cross-hole V_s measurements, three V_s models can be assumed as representative of the different stratigraphic typologies (Fig. 7). Models 1 and 2 are referred to sites with very shallow NYT tuff horizon (statigraphy A), while model 3 also must be considered at typical stratigraphy B (average NYT tuff depth of 15 m) and sporadic stratigraphy C (NYT tuff depth of about 30 m). The selected V_s models have been used to compute spectral amplifications for 2% damping along plane-parallel cross sections (Fig. 8). As expected, V_s model 1 does not amplify. V_s model 2 is responsible for similar amplifications along radial and

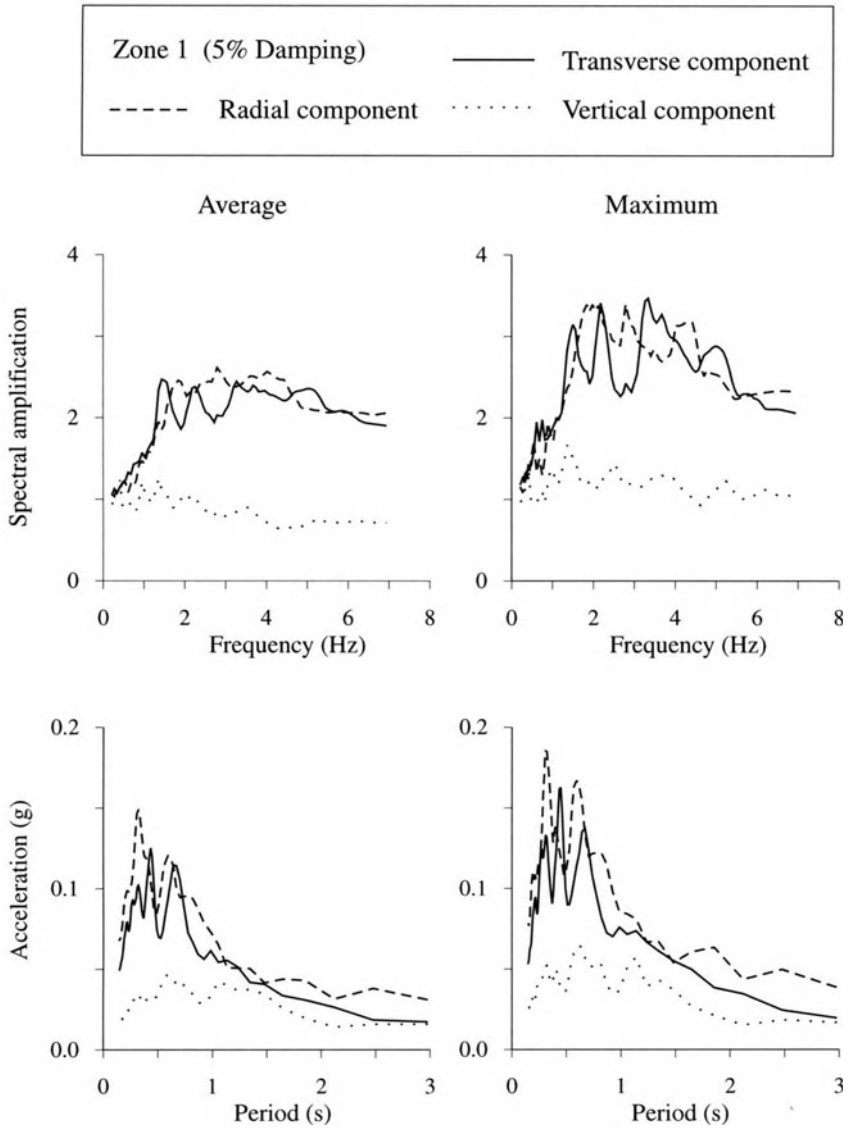

Figure 6
Average and maximum spectral amplifications and response spectra computed for the *SH* and *P-SV* wave components at zone 1 (see Fig. 4 for location).

transverse components of the ground motion, that is about 2 at 3.5–6 Hz frequency range. Spectral amplification computed for the V_s model 3 has a peak of 2–3 at 2–3 Hz, in the horizontal plane, and another peak at about 6 Hz along the radial component. Spectral amplification along the vertical component is negligible, except for the V_s model 3.

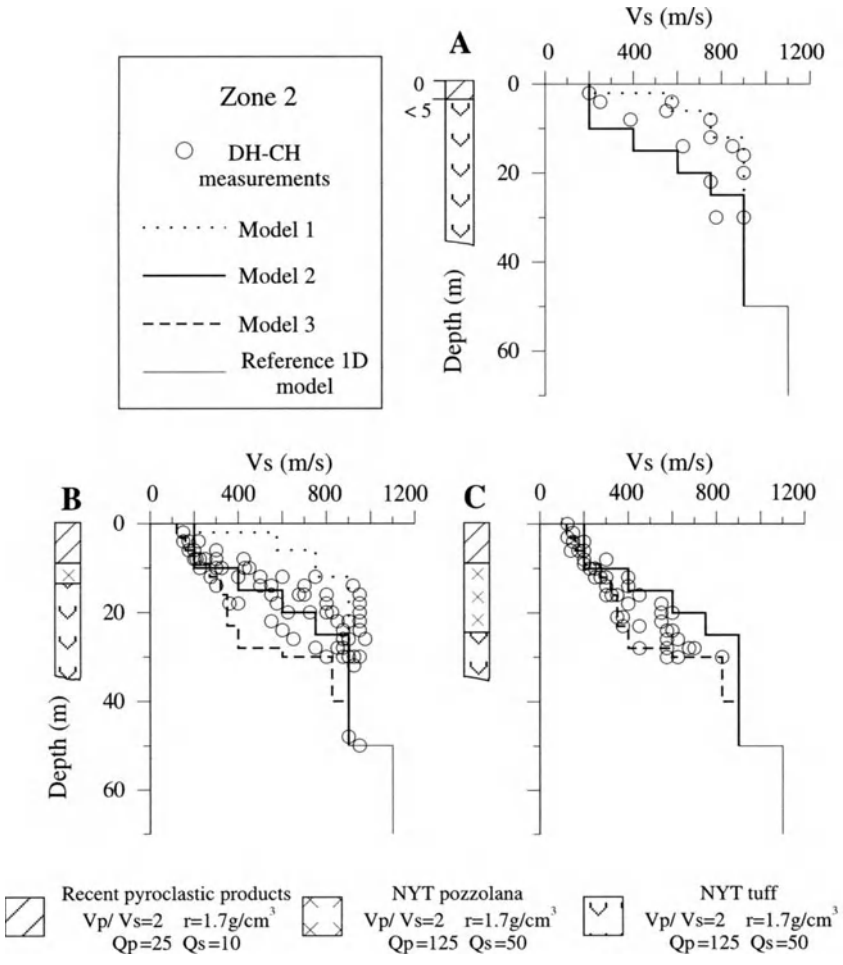

Figure 7
Representative stratigraphic columns and V_s measurements (circles) at zone 2 (see Fig. 4 for location). A suite of 3 possible V_s models has been selected (lines).

The horizontal spectral amplifications are consistent with the observed damage: low amplifications have been computed at low frequency (< 1.5 Hz), corresponding to the average building typology at Arenella, Vomero and Posillipo quarters; high peaks of amplifications have been computed corresponding to the eigenfrequencies of 4 floor buildings on soil with V_s model 3 and 1–2 floor buildings on soil with V_s model 2. The amplification at 2–3 Hz corresponds to the eigenfrequencies of buildings with medium and high damage. Since the chosen V_s models are more or less present at each quarter, average and maximum spectral amplifications have been assumed as being representative of the zone 2 (Fig. 9).

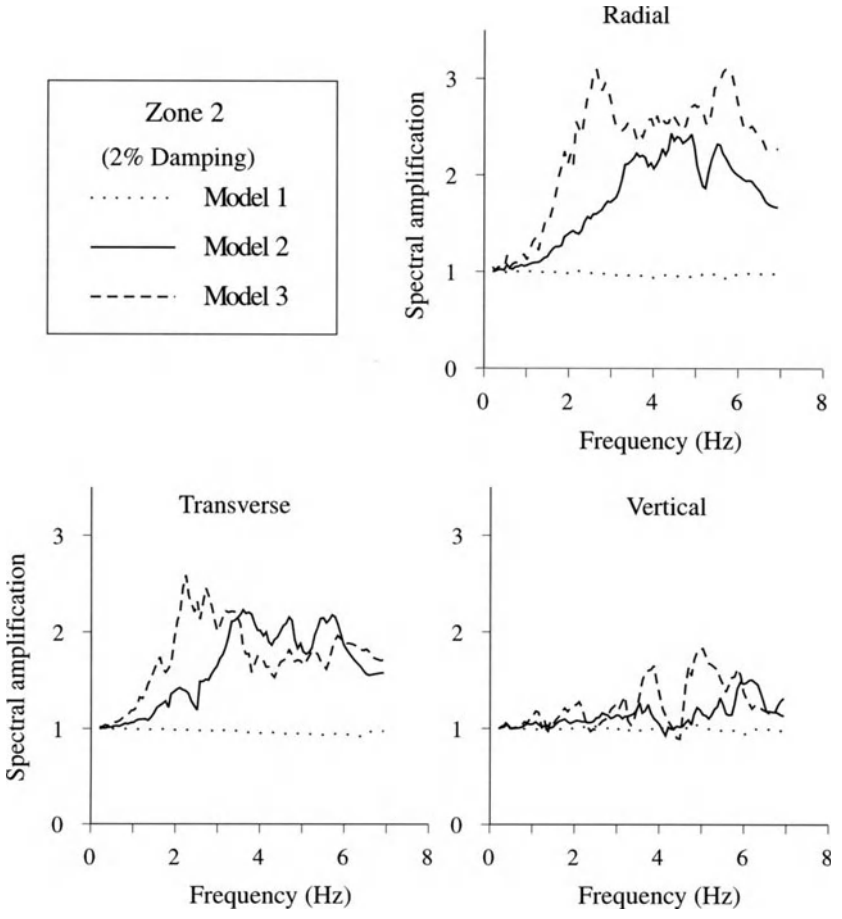

Figure 8
Spectral amplifications computed for the *SH* and *P-SV* wave components at zone 2 (see Fig. 4 for location) for the selected V_s models in Figure 7.

Response spectra have then been computed (Fig. 9). Average and maximum PGA of 0.04–0.06 g and 0.03–0.04 g, respectively along radial and transverse components of the ground motion, have been computed and, following the intensity-PGA correlation (PANZA *et al.*, 1999), correspond to I = VII–VIII on the MCS scale, being VIII relatively to V_s model 3.

4.3 Zone 3

DH and CH measurements have been collected and FTAN measurements have been carried out at three sites of zone 3 (Figs. 1 and 4). As regards the northern area, zone 3N, 4 V_s models have been taken into consideration (Fig. 10). Models 1 to 3 are the average Hedgehog solutions of the inversion of FTAN measurements, and model

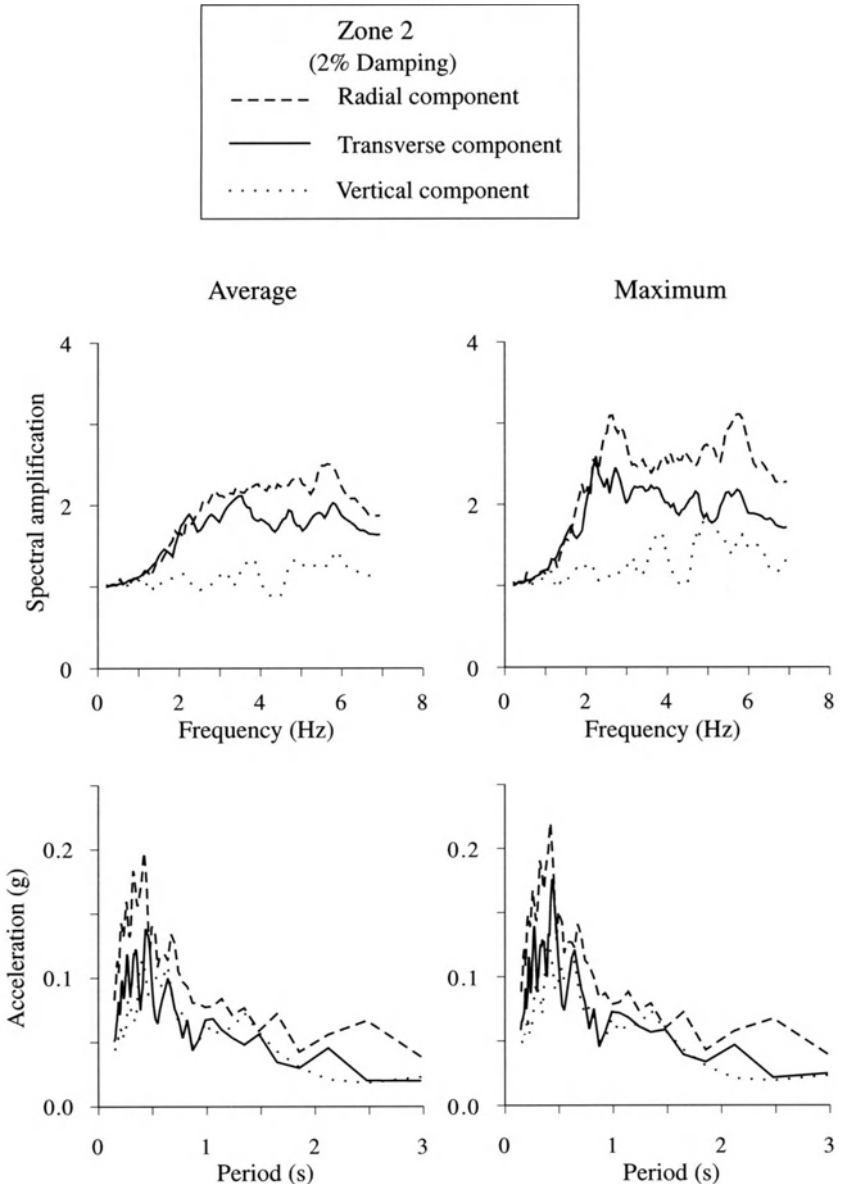

Figure 9
Average and maximum spectral amplifications and response spectra computed for the *SH* and *P-SV* wave components at zone 2 (see Fig. 4 for location).

4 represents an average V_s profile based on DH-CH measurements for the representative geological cross section. In particular, model 3 has been obtained at the site where a 8-floor building collapsed in the 1980 earthquake. Spectral

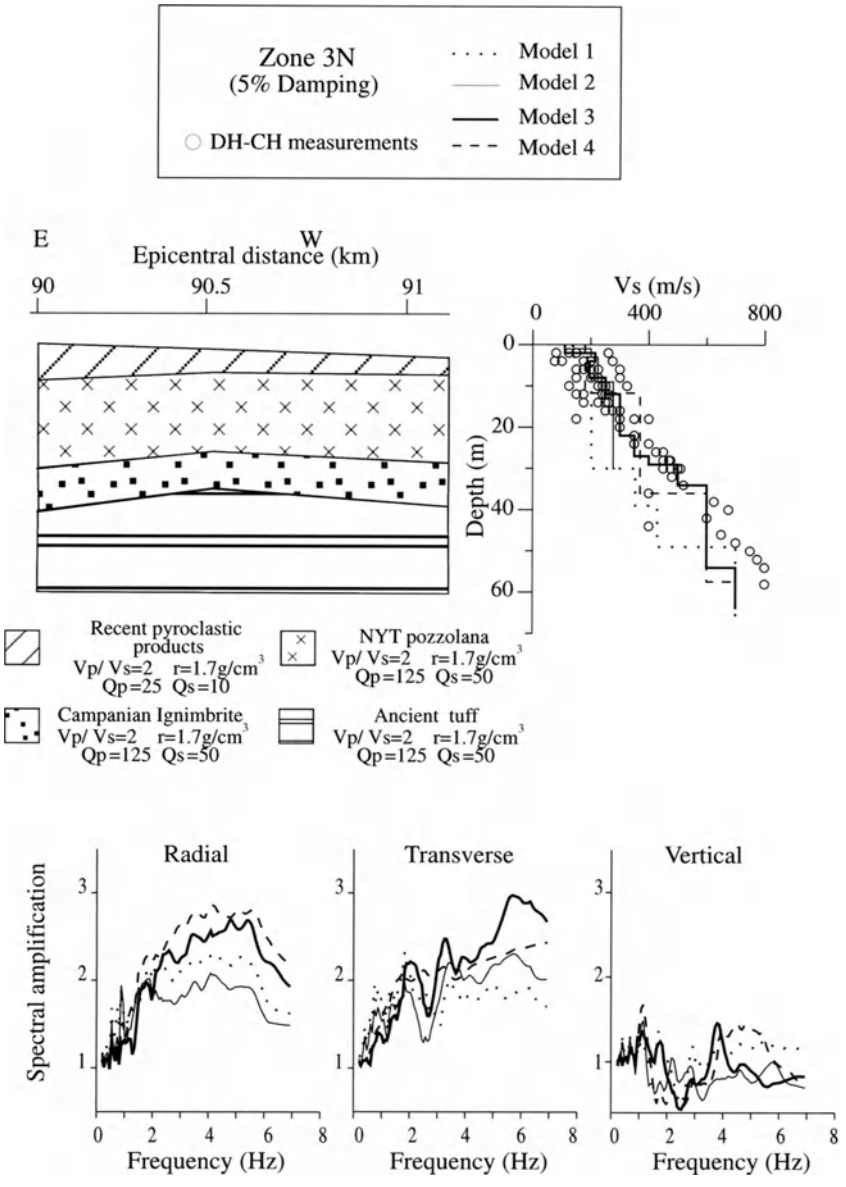

Figure 10
Geological cross section representative of zone 3N (see Fig. 4 for location) and physical parameters of the soil. Spectral amplifications have been computed for the *SH* and *P-SV* wave components for the selected V_s models.

amplification has been computed for the different V_s models by assuming 5% damping, due to the building typology. The only information about dependence of damage on number of floors regards the quarter of Secondigliano (Fig. 1) and

reports that the most damaged buildings had 5–6 floors (RIPPA and VINALE, 1983). Radial and transverse spectral amplifications exhibit similar features for the different V_s models, that is values between 2 and 3 at 2–7 Hz frequency range. The relative maximum peak at 2 Hz corresponds to the eigenfrequencies of the most damaged buildings. A negligible amplification has resulted at about 1 Hz, roughly corresponding to the eigenfrequency of the collapsed building ($T \sim 0.8$ s).

As regards the southern area of zone 3, zone 3S (Fig. 4), 2 V_s models have been assigned, based on lower and higher DH-CH measurements (Fig. 11). Average radial and transverse spectral amplifications show relative maximum peaks of about 2 at 3–6 Hz and 2–7 Hz frequency range, respectively, and they are similar to those computed at zone 3N. Spectral amplification along the vertical component is negligible at zone 3. The only data of correlation between damage and number of floors are relative to the quarter of Barra and indicate that the most damaged buildings were 4–8 floors high (RIPPA and VINALE, 1983). Only 4 floor buildings (about 2.5 Hz) have correspondence with peaks of spectral amplification. Average and maximum amplifications have been computed between zone 3N and zone 3S, and considered as representative of zone 3 (Fig. 12). Average and maximum response spectra also have been computed and they show a main peak at 0.3–0.5 s, and a second lower one at 0.5–0.7 s, close to the eigenperiods of the existing 6–8 floor buildings (Fig. 12). Peak ground accelerations of 0.05–0.07 g and 0.04–0.05 g have been computed along the radial and transverse components of the ground motion, respectively, corresponding to intensity range VII-VIII on the MCS scale.

4.4 Zone 4

Massive damage was caused by the 1980 earthquake at zone 4 (Fig. 1), characterized by old and ancient masonry houses (about 90%), generally with 4–6 floors. Velocity profiles of shear waves have been assigned, based on the analysis of the DH-CH measurements and a FTAN measurement. The resulting seismic and stratigraphic pattern is shown along a E-W cross section and can be considered as representative of zone 4 (Fig. 13). Water level is a few meters deep, below the layer of man-made ground material. V_s increases from 200 m/s to 400 m/s in the soil and reaches the value of 800 m/s in the compact NYT tuff. Lateral variations are quite smooth and the shape of the computed spectral amplifications changes only moderately along the cross section, except for the peak amplitudes. Thereafter, average and maximum spectral amplifications have been computed for 2% damping and they manifest similar features in the horizontal plane (Fig. 14), with a main peak of about 3 at 2 Hz. Instead, vertical amplification is negligible.

Data of correlations between floor numbers and damage percentage at Chiaia, S. Ferdinando and Pendino quarters (Fig. 1) have indicated a broad interval of severest damage between 2 and 6 floor buildings (RIPPA and VINALE, 1983). These

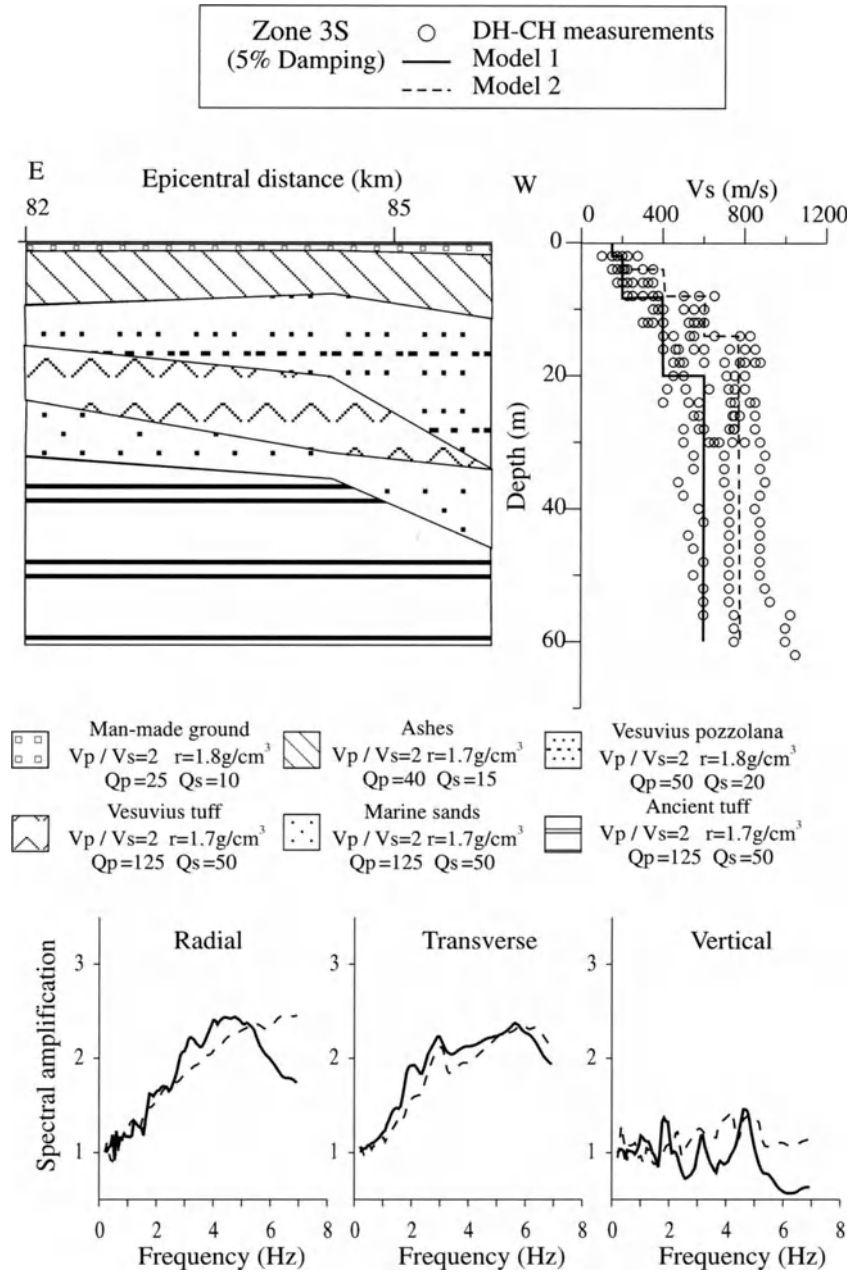

Figure 11
Geological cross section representative of zone 3S (see Fig. 4 for location) and physical parameters of the soil. Spectral amplifications have been computed for the *SH* and *P-SV* wave components for the selected V_s models.

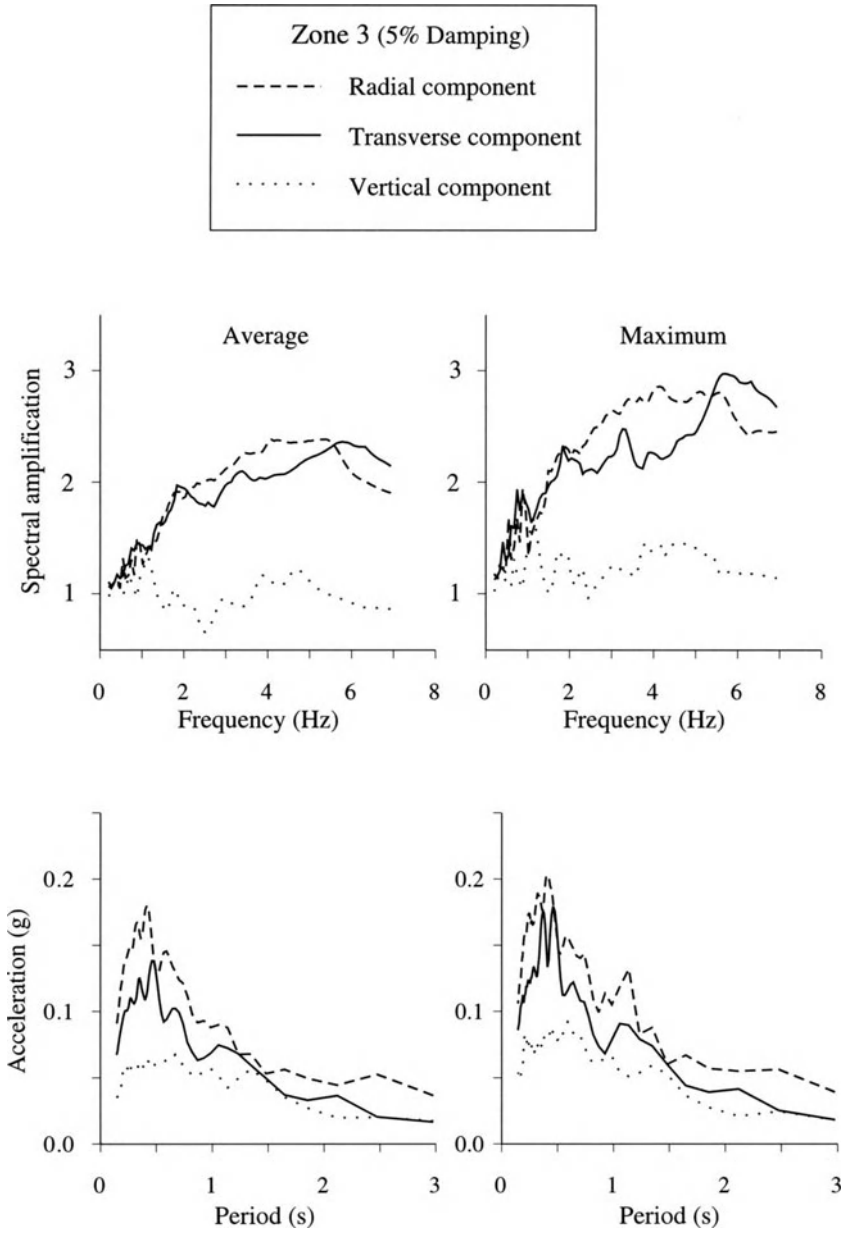

Figure 12
Average and maximum spectral amplifications and response spectra computed for the *SH* and *P-SV* wave components at zone 3 (see Fig. 4 for location).

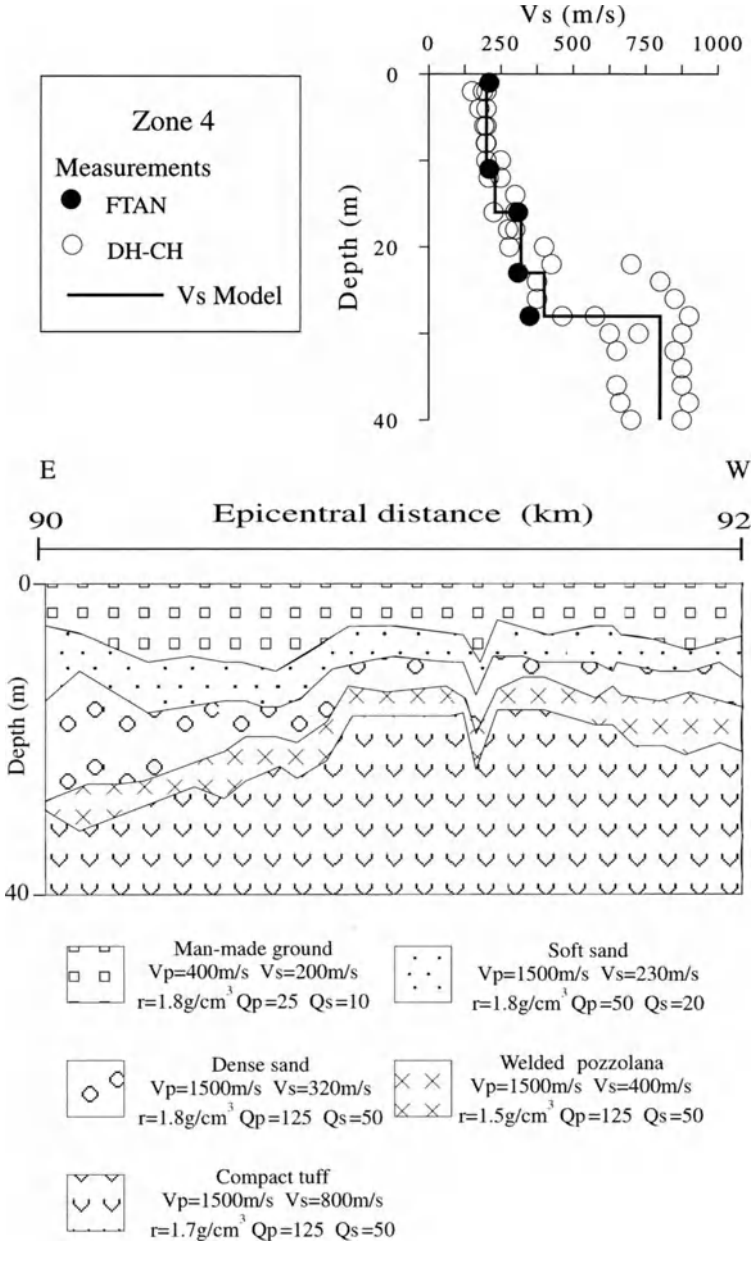

Figure 13
Geological cross section representative of zone 4 (see Fig. 4 for location) and physical parameters of the soil. The selected V_s model is shown at the top.

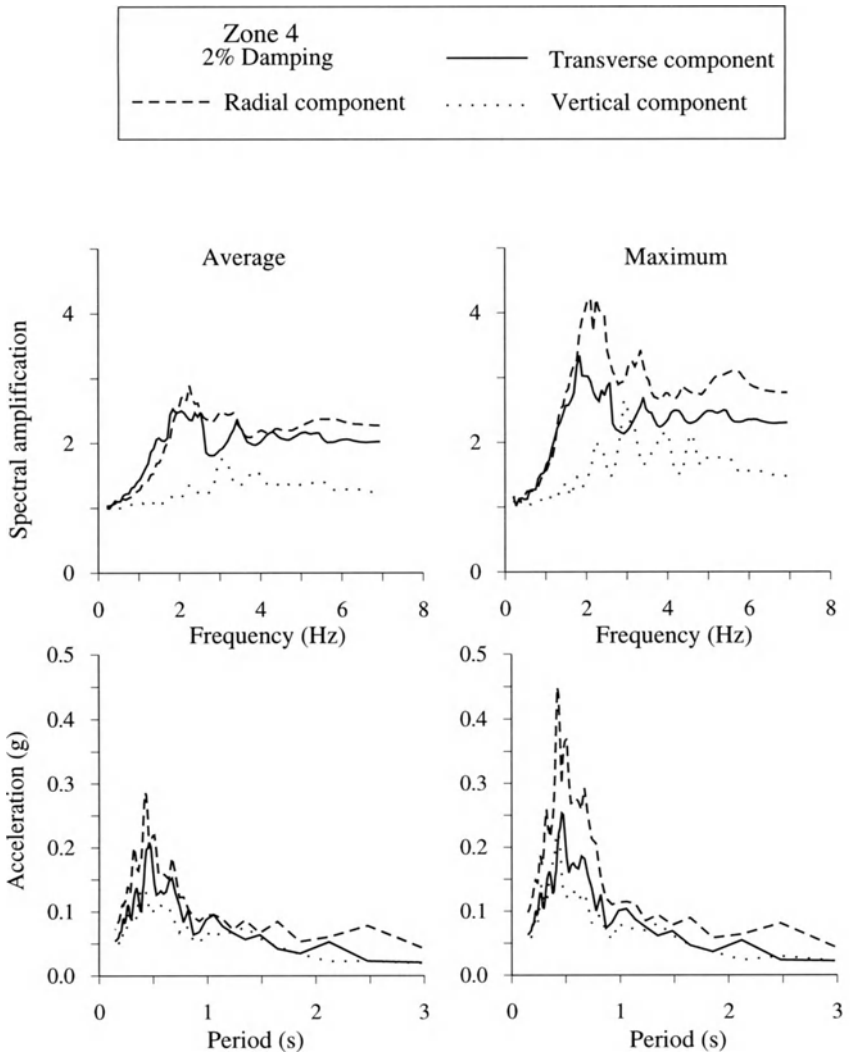

Figure 14
Average and maximum spectral amplifications and response spectra computed for the *SH* and *P-SV* wave components at zone 4 (see Fig. 4 for location), along the cross section shown in Figure 13.

data are in a good agreement with the peaks of the computed spectral amplifications. Computed average and maximum response spectra show horizontal maximum accelerations from 0.2 g to about 0.4 g at 0.4–0.6 s (Fig. 14). Average and maximum PGA of 0.04–0.05 g and 0.06–0.07 g, have been computed along transverse and radial components, respectively, and they correspond to about VIII intensity on the MCS scale (PANZA *et al.*, 1999).

4.5 Zone 5

Increasingly severe damage was reported at zone 5, characterized by ancient and old buildings of typically 3–6 floors.

Recently, NUNZIATA *et al.* (2002) computed the effect of the numerous cavities in the area, geometrically well-defined, on the SH-wave ground motion. In particular, it was evidenced that the presence of cavities in the tuff horizon (1–18 m wide and 7–16 m deep) causes a small reduction of the peak ground acceleration whereas their spatial distribution is of approximately one hundred meters, otherwise there is no effect. V_s model, which had been attributed on DH-CH measurements (COMUNE DI NAPOLI,

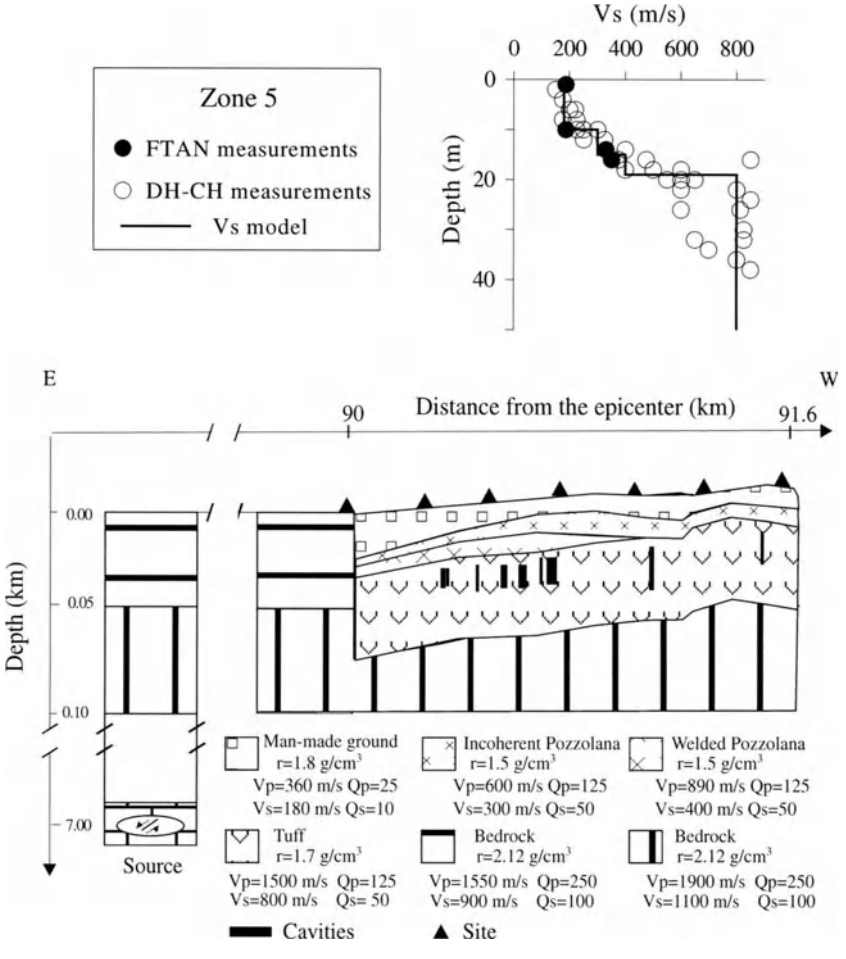

Figure 15
Geological cross-section representative of the historical center of Napoli (zone 5 in Fig. 4) and physical parameters of the soil. The selected V_s model is shown at the top. A schematic representation of the hybrid method is also shown.

1994), has been validated by recent FTAN measurements at Vicaria quarter (Figs. 15 and 1). Ground motion for *SH* and *P-SV* waves has been computed along the representative cross section (Fig. 15). Peak ground accelerations of 0.06–0.07 g and of 0.04–0.05 g have been computed along the radial and transverse components. These PGA values correspond to intensity VIII on the MCS scale (PANZA *et al.*, 1999). Average and maximum spectral amplifications, computed for 2% damping as more than 90% of buildings are masonry structures, are characterized by similar maximum peaks in the horizontal plane, which is between 2 and 4 at 2 Hz, with radial

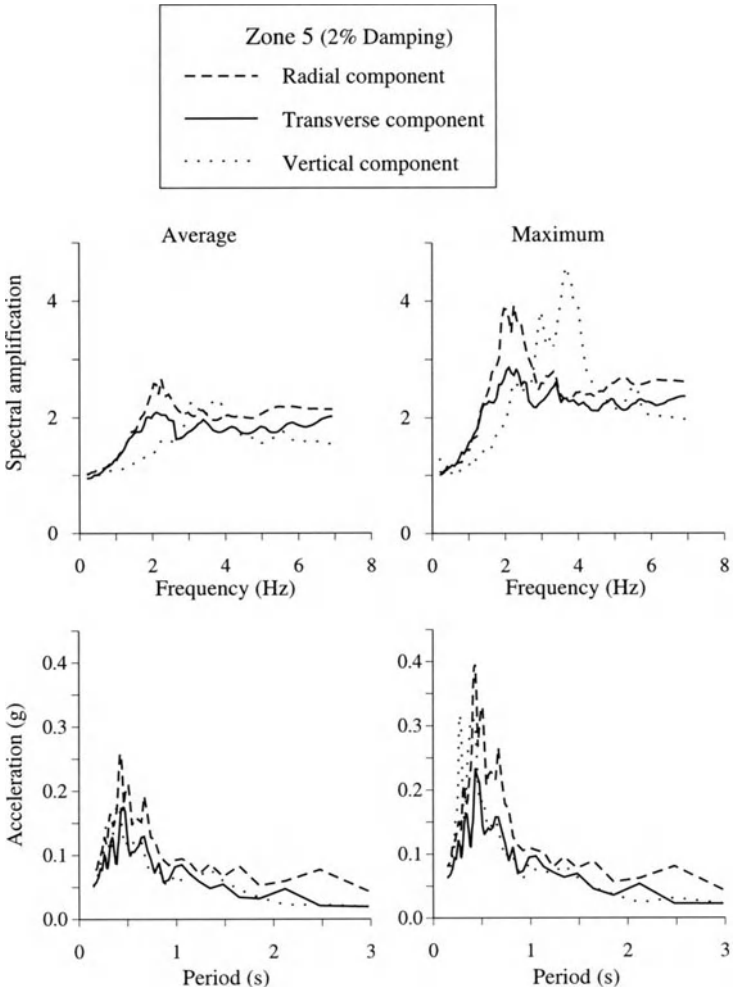

Figure 16
Average and maximum spectral amplifications and response spectra computed for the *SH* and *P-SV* wave components at zone 5 (see Fig. 4 for location), along the cross section shown in Figure 15.

amplification higher than the transverse one (Fig. 16). The maximum peak of the spectral amplifications is very close to the eigenfrequencies of the existing and most damaged buildings. As regards the vertical component, spectral amplification is characterized by a maximum peak of about 4 at 4 Hz. Finally, response spectra have been computed based on average and maximum spectral amplifications. The predominance of the radial component of the ground motion (Fig. 16) is even clearer.

4.6 Zone 6

Detailed knowledge of the stratigraphies and seismic velocity profiles already had been utilized to compute ground motion at zone 6 (NUNZIATA *et al.*, 1997; 2000). In particular, a parametric study was also done by considering different velocity profiles measured on very close sites. Ground motion modeling of complete *SH*- and *P-SV*-wave seismograms (NUNZIATA *et al.*, 2000) showed that the surficial soil deposits, which are composed of pyroclastic and alluvial materials with lateral discontinuities are responsible for an increase in amplitude of the radial and transverse components of the signal relative to the bedrock. Substantial variability of the ground motion resulted, mostly related to the presence of a discontinuous layer of peat with very low V_s values. In the light of the wide scattering of V_s velocities in the area, FTAN measurements have been carried out inside the zone. The obtained V_s models are characterized by similar ranges for ashes and sandy soil. Moreover, peat layers resemble the surrounding soils. The representative E-W cross section with geological and geophysical parameters is shown in Figure 17.

The unconsolidated sediments amplify of 2–4 some of the frequencies of the incoming wavetrain (Fig. 18). These frequencies range 1–2 Hz for the radial and transverse components, while the vertical component is negligibly amplified. Average and maximum spectral response spectra have been computed for 5% damping and they indicate that 7–10 floor buildings should face the highest horizontal accelerations. Concludingly, peak ground accelerations of 0.06–0.08 g and 0.08–0.10 g have been computed along the transverse and radial components, respectively. Taking into account the correlation obtained for the Italian territory between synthetic PGA on one side, and intensity on the other (PANZA *et al.*, 1999), we might expect macroseismic intensities VIII (MCS).

5. Conclusions

The validation of synthetic seismograms with the instrumental recording at Torre del Greco station, together with the detailed study of stratigraphies and V_s profiles, has allowed us to model the ground motion in Napoli. Sound average and maximum spectral amplifications have been computed based on selected V_s models. They are characterized by peaks of 2–4 at frequencies close to the eigenfrequencies of the

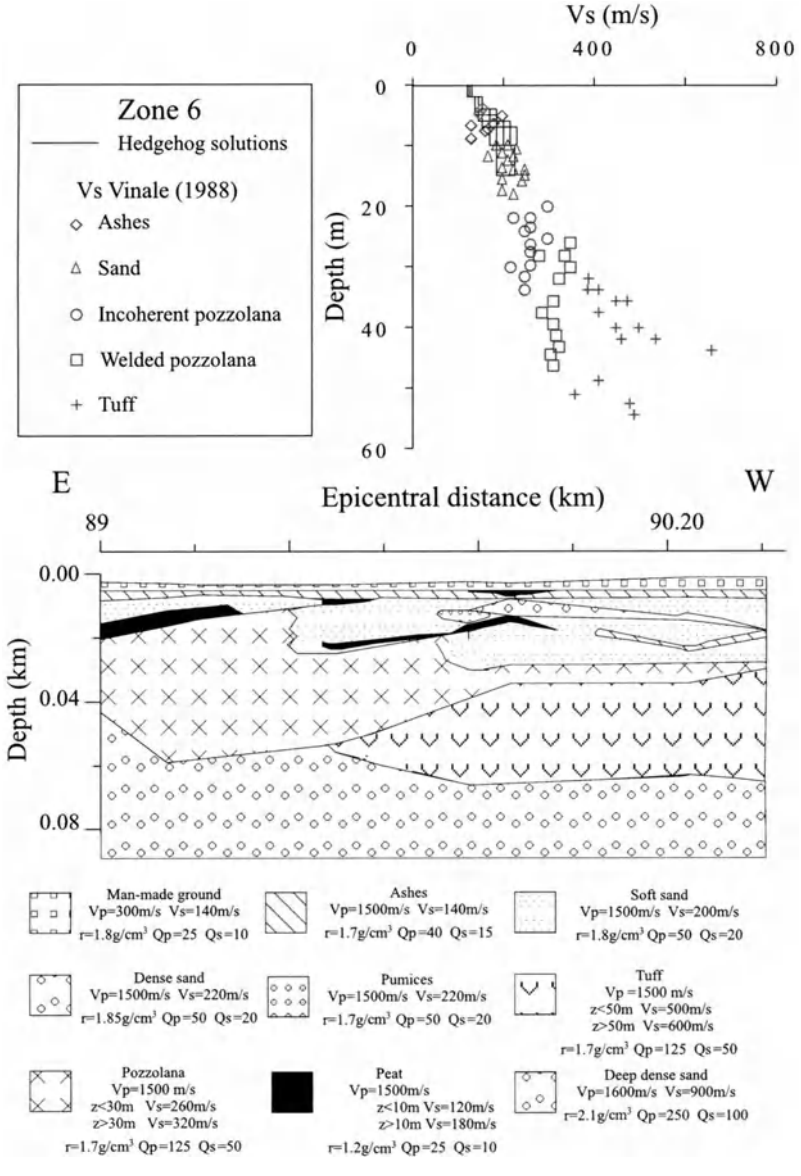

Figure 17
Geological cross section representative of the Centro Direzionale (zone 6 in Fig. 4) and physical parameters of the soil. V_s velocities have been assigned, based on measurements shown at the top.

damaged buildings, indicating that damage can be attributed not only to degradation of the buildings but also to site effects.

Following the correlation obtained for the Italian territory between synthetic PGA on one side, and intensity on the other (PANZA *et al.*, 1999), it resulted that the

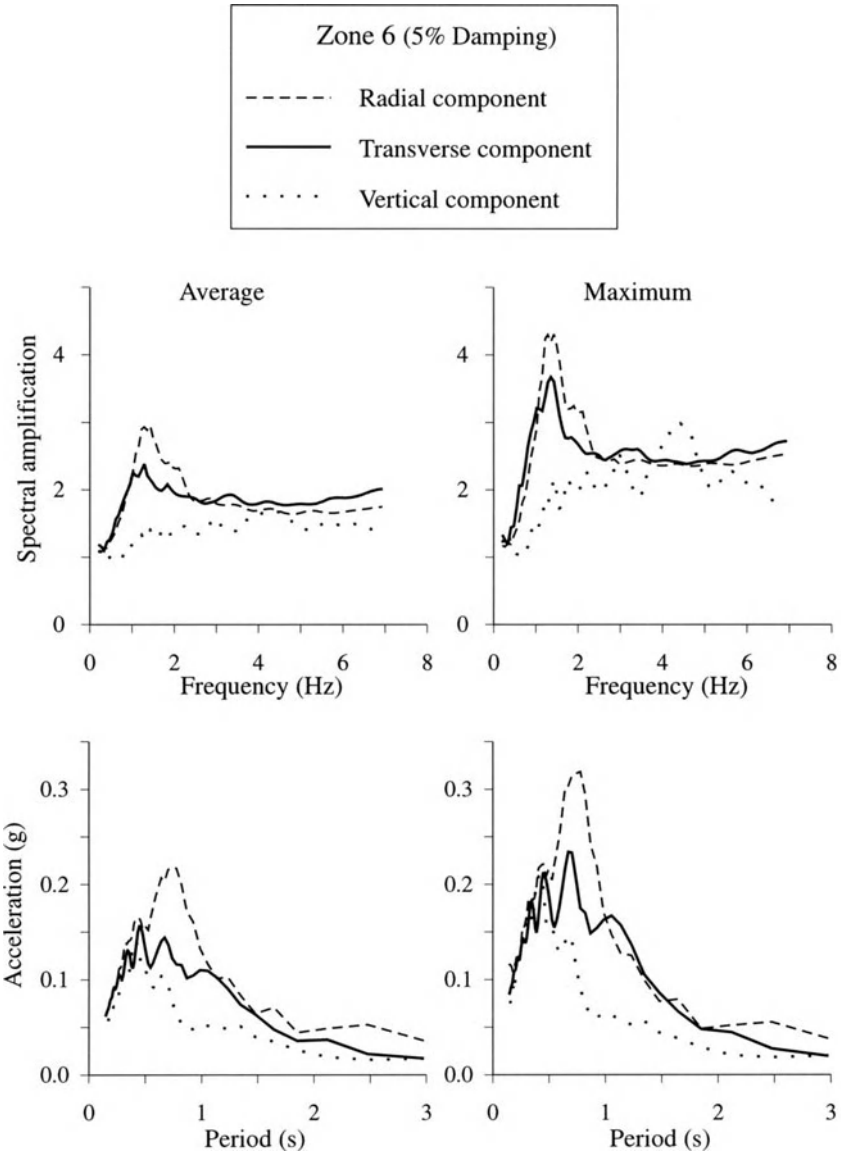

Figure 18
Average and maximum spectral amplifications and response spectra computed for the *SH* and *P-SV* wave components at zone 6 (see Fig. 4 for location), along the cross section shown in Figure 17.

zones with the highest intensity, VIII on the MCS scale, are the historical center (zone 5) and the Centro Direzionale (zone 6), followed by the zone 4, and then by all the other zones (I = VII–VIII MCS). Except for the Centro Direzionale, built after the 1980 earthquake, the computed intensities are in agreement with observed data.

Our results establish that a preventive definition of the seismic hazard in Napoli can be obtained immediately, without the need to wait for another strong event to occur, from the computation of time histories corresponding to possible seismotectonic scenarios for different sources and structural models. Then, the formulation of reliable building codes, based on the evaluation of the main potential earthquakes, will have a primary impact on the effective reduction of the seismic vulnerability of Napoli.

Acknowledgements

We are very grateful to Prof. G.F. Panza for the precious guide and for the use of computer programs, and to Prof. G. Luongo for useful suggestions and data.

Many thanks to Dr. M. NATALE and B. GAROFALO for collecting data and assisting in drawing figures.

REFERENCES

AA. VV. (1967), *Stratigrafie dei sondaggi riportati nella carta geologico-tecnica della città di Napoli*, A.G.I. VIII Convegno di Geotecnica "Il sottosuolo di Napoli". Appendice A, 86–104.

AKI, K., *Strong motion seismology: Strong Ground Motion Seismology*, NATO ASI Series, Series C: *Mathematical and Physical Sciences* (M.O. Erdik and M.N. Toksöz, eds.) (D. Reidel Publishing Company, Dordrecht 1987) *204*, pp. 3–39.

COMUNE DI NAPOLI (1994), *Indagini geologiche per l'adeguamento del P.R.G. alla legge regionale 07.01.1983 n. 9 in difesa del territorio dal rischio sismico.*

ESPOSITO, E., PORFIDO, S., LUONGO, G., and PETRAZZUOLI S.M. (1992), *Damage Scenarios Induced by the Major Seismic Events from XV to XIX Century in Naples City with Particular Reference to the Seismic Response*, Earthquake Engineering, Tenth World Conference, 1075–1080.

FÄH D. (1992), *A Hybrid Technique for the Estimation of Strong Ground Motion in Sedimentary Basin*, Ph.D. Thesis n. 9767, Swiss Federal Institute of Technology, Zürich.

FLORSCH, N., FÄH, D., SUHADOLC, P., and PANZA, G.F. (1991), *Complete Synthetic Seismograms for High-frequency Multimode SH-Waves*, Pure Appl. Geophys. *136*, 529–560.

GUADAGNO, F. M., NUNZIATA, C., and RAPOLLA, A., *Dynamic parameters of volcaniclastic soils and rocks of Campi Flegrei (Naples, Italy). Volcanic Seismology*, IAVCEI Proceedings in Volcanology, (Springer-Verlag 1992) pp. 533–546.

GUSEV, A.A. (1983), *Descriptive Statistical Model of Earthquake Source Radiation and its Application to an Estimation of Short-Period Strong Motion*, Geophys. J.R. Astron. Soc. *74*, 787–800.

KANAMORI, H. (1977), *The Energy Release in Great Earthquakes*, J. Geophys. Res. *82*, 2981–2987.

LEVSHIN, A., RATNIKOVA, L., and BERGER, J. (1992), *Peculiarities of Surface Wave Propagation Across Central Eurasia*, Bull. Seismol. Soc. Am. *82*, 2464–2493.

NUNZIATA, C., VACCARI, F., FÄH, D., LUONGO, G., and PANZA, G.F. (1997), *Seismic Ground Motion Expected for the Eastern District of Naples*, Natural Hazards *15*, 183–197.

NUNZIATA, C., MELE, R., and NATALE, M. (1999), *Shear-Wave Velocities of the Campi Flegrei- Neapolitan Deposits and the Primary Influencing Factors*, Engin. Geology *54*, 299–312.

NUNZIATA, C., COSTA, G., MARRARA, F., and PANZA, G.F. (2000), *Validated Estimation of the Response Spectra for the 1980 Irpinia Earthquake in the Eastern Area of Naples*. Earthquake Spectra *16* (3), 643–660.

NUNZIATA, C. and PANZA, G.F. (2002), *A Contribution to the Seismic Microzoning of Napoli*, Mem. Soc. Geol. It. *57* (2), 437–442.

NUNZIATA, C., NATALE, M., GAROFALO, B., and PANZA, G.F. (2004), *Seismic Characterization of Neapolitan Soils*, (this issue).

PANTOSTI, D. and VALENSISE, G. (1993), *Source Geometry and Long-term Behavior of the 1980, Irpinia Earthquake Fault Based on Field Geologic Observations*, Annali di Geofisica *XXXVI*, 41–49.

PANZA, G. F., *The Resolving Power of Seismic Surface Wave with Respect to Crust and Upper Mantle Structural Models*, In *The Solution of the Inverse Problem in Geophysical Interpretation* (R. Cassinis, ed., Plenum Press, 1993) pp. 39–77.

PANZA, G.F. (1985), *Synthetic Seismograms: The Rayleigh Waves Modal Summation*, J. Geophysics *58*, 125–145.

PANZA, G.F., VACCARI, F., and CAZZARO, R., *Deterministic Seismic Hazard Assessment.* In *Vrancea Earthquakes: Tectonics, Hazard and Risk Mitigation.* (F. Wenzel *et al.* eds.) (Kluwer Academy Publ 1999) pp. 269–286.

POSTPISCHL, D., BRANNO, A., ESPOSITO, E., FERRARI, G., MARTURANO, A., PORFIDO, S., RINALDIS, V., and STUCCHI, M. (1985), *The Irpinia Earthquakes of November 23, 1980.* Atlas of isoseismal maps of Italian earthquakes, CNR_PFG, n.114, 2A.

RIPPA, F. and VINALE, F. (1983), *Effetti del terremoto del 23 November 1980 sul patrimonio edilizio di Napoli.* Associazione Geotecnica Italiana, XV Convegno Nazionale di Geotecnica, 193–206.

VACCARI, F., SUHADOLC, P., and PANZA, G. F. (1990), *Irpinia, Italy, 1980 Earthquake; Waveform Modelling of Strong Motion Data*, Geophys. J. Int. *101*, 631–647.

VALYUS, V.P., KEILIS-BOROK, V.I., and LEVSHIN, A.L. (1968), *Determination of the Velocity Profile of the Upper Mantle in Europe*, Nauk SSR *l*, 185 (*8*), 564–567.

VINALE, F., (1988), *Caratterizzazione del sottosuolo di un'area campione di Napoli ai fini di una microzonazione sismica*, Rivista Italiana di Geotecnica *22*, 77–100.

(Received June 1, 2002, accepted January 30, 2003)

Pure appl. geophys. 161 (2004) 1265–1283
0033–4553/04/061265–19
DOI 10.1007/s00024-003-2490-1

Pure and Applied Geophysics

Expert Assessment of the Displacements Provoked by Seismic Events: Case Study for the Sofia Metropolitan Area

I. PASKALEVA[1], M. MATOVA[2] and G. FRANGOV[2]

Abstract—The paper discusses the very recent seismotectonic and geological investigations for the Sofia valley. It also reviews available historical and recent seismological data. One possible variant of seismic zoning (interpretation of available geological and seismological data) is used to evaluate uniform probability Fourier spectra of strong ground motion at Sofia City. The distribution of the maximum expected displacements, using 1-D models and SHAKE'91 techniques for 50 years of exposure time is mapped. The maps of eigensolution results for 30 m, 50 m depths to the rock are illustrated. These issues are important for definition of design parameters for evaluation of seismic safety of underground infrastructure, as well as for tall structures.

Key words: Displacements, accelerograms, eigensolution, seismograms, uniform risk.

Introduction

More than sixty types of destructive processes can be observed in the territory of Bulgaria (BRANKOV, 1983; BROUTCHEV, 1994; BROUTCHEV *et al.*, 1995). Earthquakes, landslides, erosion, abrasion, loess collapses or any phenomena associated with specific soils, non-resistant to pressure, are assumed to be the major destructive processes in Bulgaria.

The distribution of the processes is quite irregular over the territory of the country and is mostly concentrated at the land-water boundary and in the areas composed of "young" sediments with complex geological characteristics. The recent deterministic calculations (PANZA and VACCARI, 2000) show a significant range (15–30 cm) of the maximum displacements in the vicinity of the Sofia region. This study considers shallow seismicity, limiting the computations to epicentral distances shorter than 90 km. The hypocentral depth considered is 10 km for events with magnitude less than $M = 7$, and 15 km for larger events. The subject of this study is

[1] Central Laboratory Seismic Mechanics and Earthquake Engineering (CLSMEE, BAS) "Acad.G.Bonchev" str., Block 3, 1113 Sofia.
E-mail: Paskalev@geophys.bas.bg, Paskalev_2000@yahoo.com
[2] Geological Institute, BAS, Sofia 1113,"Acad. G.Boncev str.", bl.24.
E-mail: matova@geology.bas.bg, frangov@geology.bas.bg

to demonstrate assessments of the maximum expected displacements for the central part of the Sofia capital using the uniform risk spectrum (YOSSIFOV and PASKALEVA, 1999), taking into account recent manifestations of seismotectonic activity (MATOVA, 2001) and local geological conditions (IVANOV *et al.*, 1998; FRANGOV and IVANOV, 1999).

Seismicity in the Sofia Region

Historical view—Sofia city is situated in the Sofia valley, which is relatively flat with an average altitude of about 550 m. The city spreads over an area of about 12 km^2. The Sofia valley is part of a graben of the same name which is a structure of an approximately elliptic form in plan, with the long axis at 75 km and the short axis at 26 km and a NW-SE orientation. The graben is surrounded by mountainous horst-blocks. Numerous longitudinal, transversal and oblique faults cut the graben. A considerable part of them is included in the seismic movements (MATOVA, 1996, 2001; CHRISTOSKOV, 1988; OROZOVA-STANISHKOVA *et al.*, 1996), which create the seismic hazard.

In the city of Sofia the main seismic activity is caused by the fragments of the *Vitosha, Vladaya, Gorublyane, Gnilyane* and *Bozhurishte* faults. The concentration of faults and fault crossings in the territory of Sofia City is related to the graben-horst's evolution and the rising of the seismicity. Several historical descriptions support the fact that the Sofia region is an earthquake area. The first historical descriptions of local earthquakes date were back to the mid-XV century (WATZOV, 1902). Relatively reliable data were reported at the beginning of the XIX century (CHRISTOSKOV *et al.*, 1989). Two major events took place during this period, in 1818 and 1858, the latter of which with a very correct and detailed description from the macroseismic point of view (WATZOV, 1902). This event prompted an attempt for some, quite reliable, magnitude and intensity estimations (M = 6.5–7.0 and $I_o \sim$IX MSK) (SOLAKOV *et al.*, 2001). A long aftershock sequence was reported as well. Numerous site effects were reported as a consequence. Initially, the very important fact of surface rupture in the northern slope of the Vitosha mountain, with an approximate length of about 3–4 km and openings of several hundred centimeters. During this earthquake a new mineral spring broke out near *Ovcha Koupel*. It is depicted that big hot fountain water eruptions were observed by many people. There are also notes evocative for liquefaction and sand volcano effects in river valleys. Moreover, during the earthquake of 18 October 1917 (M = 5–5.5, $I_o \sim 7$) with its epicenter in the city, very strong effects of increasing intensity were observed in the Perlovska river belt. Damages, such as fallen chimneys and cracked walls, were reported for buildings and I_o = VII–VIII could be localized to the fault crossing points near the Bozhurishte quarter of the city and near the town of Elin Pelin. Based on the existing seismological and tectonic data, similar seismic events could be expected in the city of

Sofia. When earthquakes occur during heavy rain periods and when their effects are felt in the localities of shallow ground water level, and/or on areas of unconsolidated rocks (FRANGOV and IVANOV, 1999), their intensities could be stronger than that in earlier instances.

Recent seismicity—The observed epicenter distribution during the last 7–8 years delineates relatively clear epicenter concentrations. More than 280 relatively small seismic events ranging in magnitude between 1.2 and 3.6 have been observed. In comparison with the other seismogenic zones in Bulgaria, Sofia district has the lowest recent seismicity (BOTEV and RIZIKOVA 1982; RANGUELOV, 1996; RANGUELOV and TOTEVA, 1998). For example, it emits less than 10% of the total seismic energy emitted by the Kresna source and less than 15% of that in the Plovdiv zone. The location of the events shows active faults with SE-NW and SW-NE direction, with some concentration of the earthquakes to the south Sofia City (CHRISTOSKOV *et al.*, 1989). This coincidence between the epicenter concentration and the location of the Iskar dam (the biggest dam in Bulgaria) could be explained by induced events connected with the seasonal variations of the water level and activity of *Vitosha* fault. To the north of Sofia City another fault with NW-SE direction coincides with the base of the *Balkan Mts*. The zone is usually characterized by low-level seismic energy events. To the west of the city the seismicity shows more or less diffusive behavior. It is important to mention that within recent years the concentration of the epicenters to the south of Sofia City has been relatively weakest. But the most dangerous seismic source in this area is located along the area ruptured in the 1858 strong event. The magnitude-frequency relationship exhibits the behavior of the recent seismicity of the Sofia valley. Only one event with a magnitude greater than 3.5 was detected during the investigated period by GLAVCHEVA in 1993. An earthquake with a magnitude of $M = 3.6$ was registered on 20 April 1996, with an intensity of III-IV in the epicentral area. The city itself has a very small number of registered events. It is probably due to the registration conditions and the high levels of industrial noise.

Seismotectonic Information

Seismically active faults—Sofia City is situated on the active Sofia graben structure. The graben is a post-*Alpine* structural unit of the Neogene-Quaternary age. It has NW SE direction. Longitudinal, transversal and oblique faults (Fig. 1) cut the graben and the surrounding horsts. Numerous thermal sources are to be found in the graben. Their wide distribution could be interpreted as an additional indication for the recent activity of the faults. The faults in the southern part of the graben are of significant activity (Fig. 1). Considerable tectonic movements including the seismic manifestations of the region of Sofia City take place along several active faults. The latest are well represented in the Sofia graben and the adjacent block-horsts (Fig. 1).

Figure 1
The Sofia graben and the adjacent horsts-blocks: 1—fault (1—Negushevo fault zone, 2—Bozhurishte fault, 3—Vitosha fault zone, 4—Bankya fault, 5—Chepintsi fault, 6—Vladaya fault, 7—Ravno Pole fault, 8—Gnilyane fault, 9—Busmantsi fault, 10—Elin Pelin fault, 11—Draganovo fault, 12—Sub-Vitosha fault zone, 13—Gorublyane fault), 2—Sofia graben block, 3—horst block, 4—thermal source.

The spatial distribution of the epicenters of strong and moderate earthquakes shows some regularity (MATOVA, 1996, 2001). The seismic activity is related mainly to the following faults and fault zones: a) longitudinal faults (the *Bozhurishte* fault, the *Vitosha* fault zone) of the middle and southern parts of the Sofia graben, also the *Sub-Vitosha* fault zone of the southern part of the *Vitosha* blocks-horsts; b) transversal faults (the *Bankya*, the *Chepintsi*, the *Vladaya*, the *Ravno Pole* faults) of the middle and the eastern parts of the Sofia graben and the adjacent areas, c) oblique faults of two general directions: submeridional one (the *Gnilyane*, the *Busmantsi*, the *El. Pelin*, the *Draganovo* faults) of the central and the eastern parts of the graben; subequatorial direction (the *Gorublyane* fault zone) in the eastern part of the graben (Fig. 2). During the last ten years, the instrumental registration and the

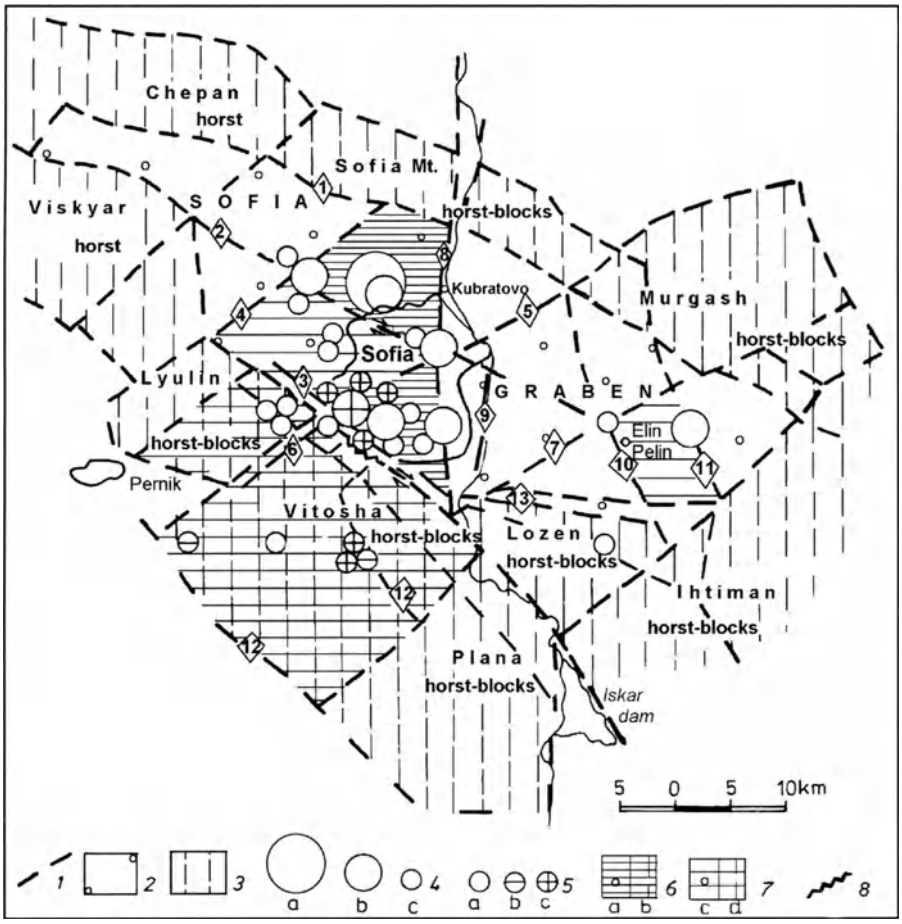

Figure 2

Seismic events with magnitude M = 4.00–7.00 in the blocks of the Sofia graben and the adjacent horsts: 1—faults: a—of the block boundary (the names are indicated in Fig. 4), b—sector of the Vitosha fault zone activated during the 1858 Sofia earthquake (M = 6.5–7.00); 2—block of the Sofia graben, 3—block of the adjacent horsts, 4—epicenters of earthquakes with magnitude: a—M = 6.0–7.0; b—M = 5.0–5.9, c—M = 4.0–4.9; 5--depths of earthquake hypocenters: a—up to 10 km, b—11–20 km, c—21–30 km; 6—blocks of considerable seismic mobility: a—of the graben, b—of the horsts; 7—blocks of moderate seismic mobility: a—of the graben, b—of the horsts; 8—seismic active sector of Vitosha fault during the 1858 Sofia earthquake.

publications of seismic data (BOTEV *et al.*, 1998, 1999) have enabled the analysis of the spatial distribution of the low seismicity in the investigated territory. The epicenters of numerous weak earthquakes (M < 3.5) are localized mainly along the *Negushevo* and the *Vitosha* fault zones of the northern and the southern boundaries of the Sofia graben. Some epicenters are along the *Bozhurishte*, the *Bankya*, the *Gnilyane*, the *Ravno Pole*, the *El. Pelin* faults and the *Sub-Vitosha* fault zone

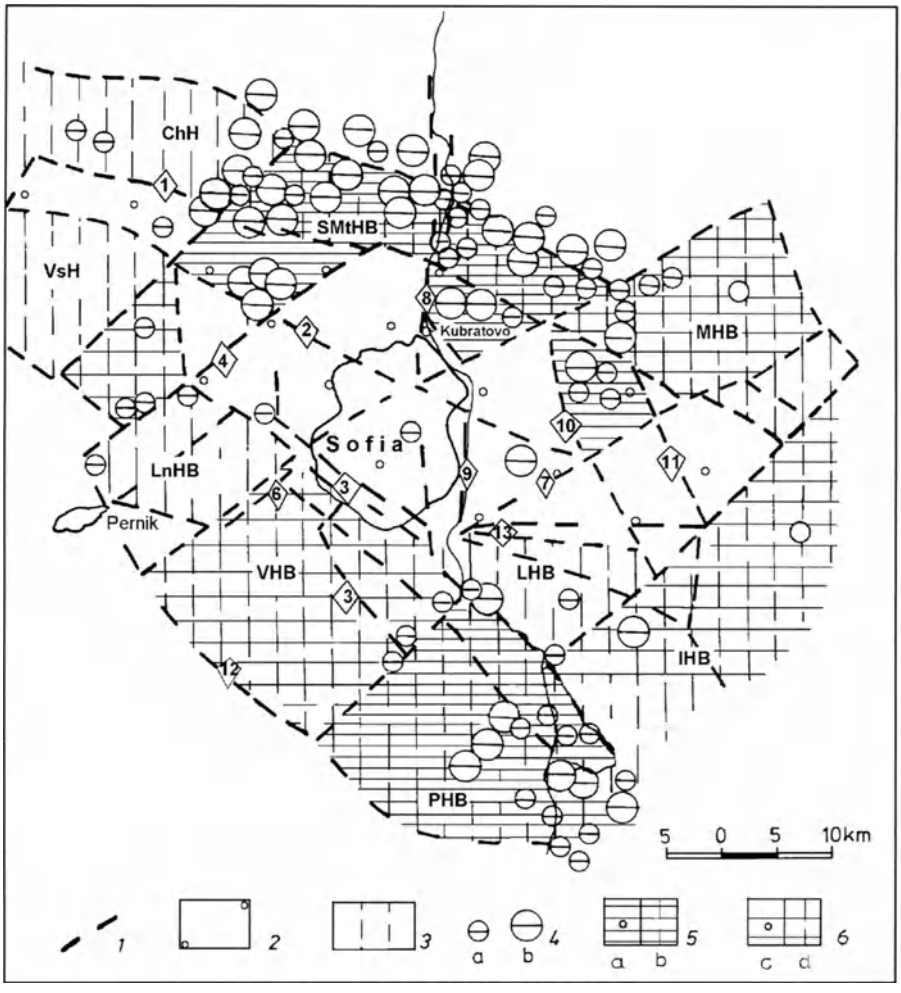

Figure 3
Weak earthquakes in the investigated territory during 1966–1979: 1—fault, 2—graben block, 3—horst-block, 4—earthquake epicenters (1966–1976): a—M < 1.5, b—M > 1.5; 5—blocks of relatively high seismic mobility: a—of the graben , b—of the horsts ; 6—blocks of considerable seismic mobility: a—of the graben, b—of the horsts.

(Figs. 3,4). The field study of the seismic active faults is a very difficult task, as the investigated territory is covered by numerous large settlements, as well as by some long-term cultivated terrains. The surface traces of the faults with seismic origin are established along the V*itosha* fault zone. The fault activity is historically documented. There is a mobile sector of the *Vitosha* faults in the vicinity of the *Boyana* quarter of the Sofia City (Fig. 2), whose occurrence is related to the 1858 Sofia earthquake (M = 6.5–7.0) (SOLAKOV *et al.*, 2001). That same earthquake triggered the activation

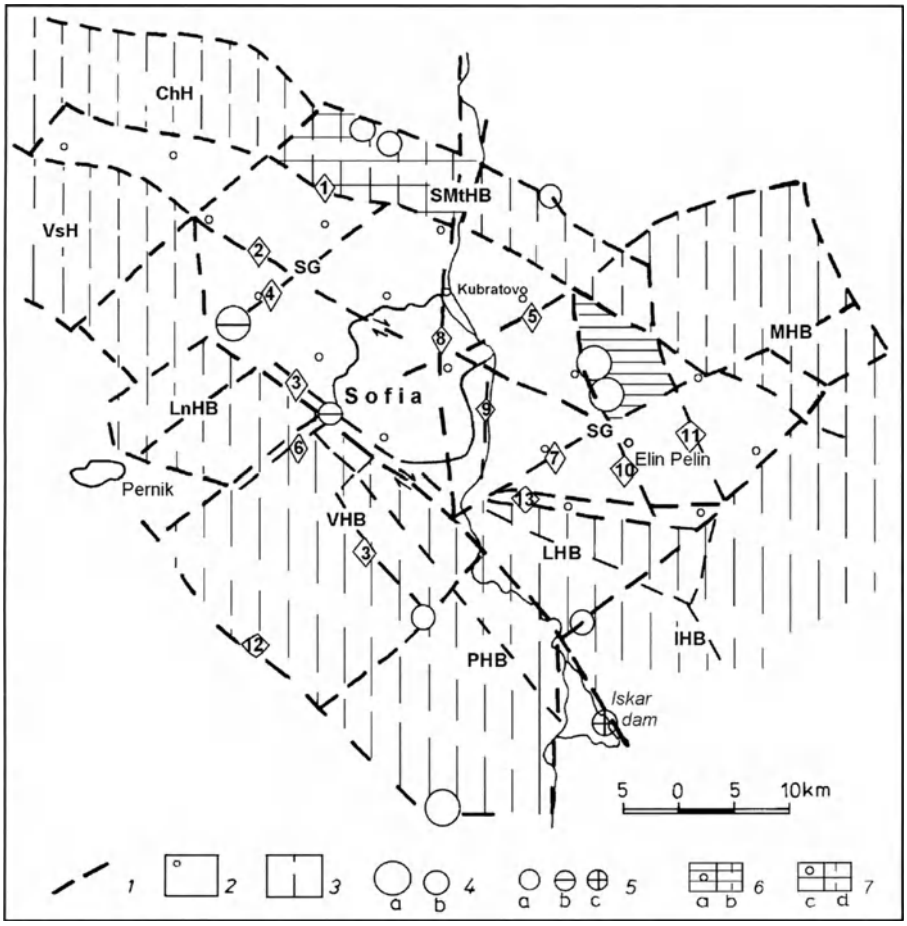

Figure 4
Weak earthquakes in the blocks of the Sofia graben and the adjacent horsts in the 1996–1999 period: 1—fault, 2—graben block, 3—horst-block, 4—earthquake epicenters: a—M = 3.0–3.6, b—M = 2.5–2.9; 5—depth of earthquake hypocenters: a—up to 10 km, b—11–20 km, c—21–31 km.

of old landslides and rockfalls, also the appearance of new ones along the *Vitosha* fault zone between the *Boyana* and *Dragalevtsi* quarters of the city. A considerable part of the above-mentioned landslides and rockfalls is still active, which is an indication of the long-time mobility of the *Vitosha* fault zone.

Several epicenters of earthquakes with $M < 3.5$ are concentrated near the fault crossings (Figs. 2–3). There is some considerable seismic mobility in the *Bozhurishte* crossing point as well.

The crossing is in the northwestern periphery of Sofia City, on the territory of the *Bozhurishte* quarter. There are epicenters of some earthquakes with $M > 5$,

with $M = 4.0$–4.9 and with $M < 3.5$ at the *Bozhurishte* crossing (Figs. 2, 3, 4). Another seismic active crossing point is placed on the territory of the *Gorublyane* quarter of Sofia City. The crossing is located in the southeastern periphery of the city, where the *Gnilyane*, the *Vitosha* and the *Gorublyane* faults cross. The *Gorublyane* crossing is a place of concentration of epicenters whose magnitude is of values $M < 3.5$ (Fig. 3). Some seismically mobile crossing points of faults also can be found on the eastern side of the Sofia graben. They are in the vicinity of the town of *El. Pelin* (crossing of the *El. Pelin* and the *Ravno Pole* faults) and of the *Draganovo* village (crossing of the *Draganovo* and the *Ravno pole* faults). A limited number of moderate and weak earthquakes have their epicenters in the crossings cited (Figs. 2–4). There are also seismically active crossings in the block-horsts of the *Plana*, the *Vitosha, the Ihtiman* and the *Sofia* Mountains. For the most part, the fault crossings in the investigated territory are related to weak earthquakes and manifestations of low seismicity. The influence of the seismic movement to the Sofia graben and Sofia City depends not only on the magnitude of the earthquakes, but also on the depth of their hypocenters. The earthquake information allows for the discovery of data about the depth of the faults included in the seismic movements (Figs. 2–4). The seismic active faults could be divided into three groups, based on the depth of their mobilization during the earthquakes. The groups, are the following: a) faults with seismic activation of up to 10 km (the *Bozhurishte*, *the El. Pelin*, the *Draganovo* faults), b) faults with seismic activation of up to 20 km (the Bankya fault), c) faults with seismic activation of up to 30 km (the *Vitosha*, the *Sub-Vitosha* fault zones, the *Chepintsi*, the *Vladaya*, the *Gnilyane* faults). The last group of hypocenters endangers large territories of Sofia City. The relatively shallow seismic active faults are placed in the northern and central parts of the studied territory and the relatively deep ones in its southern part. The seismically active *Sofia* graben and adjacent horsts are fragmented in a multifude of blocks with different sizes (Fig. 1).

The blocks of the graben and the horsts participate in horizontal and vertical movements of specific intensity. Both kinds of block movements are most impressive in the southern part of the *Sofia* graben. The southern periphery of the graben represents the contact between the low *Sofia* graben and the very high horst of the *Vitosha* Mountain. Sofia City is situated in the middle of the southern part of the graben. Its southern periphery is placed on the territory of the most contrast contacts of the blocks in the region studied. The tectonic interpretation of the spatial distribution of the strong and the moderate earthquake epicenters shows some peculiarities in the seismic mobility of the blocks of the Sofia graben and its adjacent horsts. The blocks of the *Sofia* graben between the *Bankya* and the *Gnilyane* faults are the most active (Fig. 2). The blocks of the graben to the west of the *Bankya* fault are the most passive. The blocks of the graben to the east of the *Gnilyane* fault, have limited mobility (Fig. 2). The blocks of the surrounding

horsts are involved very rarely in moderate earthquakes with the exception of the *Vitosha* and the *Lyulin* horst-blocks. The low seismicity has a large distribution in the blocks of the *Sofia* graben and the adjacent horsts. Two big blocks of the adjacent horsts and three small blocks of the graben are characterized by a very high concentration of weak earthquake epicenters (Figs. 3, 4). There are numerous epicenters in the big blocks of the *Plana* and the *Sofia* horsts (Fig. 3). Similar epicenter concentration is observed in the small blocks of the northern part of the *Sofia* graben. These blocks are situated to the southwest and to the southeast of the *Sofia* horst-block, also to the south of the *Murgash* horst-block (Fig. 3). The weak earthquake epicenters are in relatively significant concentration in the horst blocks of the *Murgash*, the *Ihtiman*, the *Vitosha*, and the *Lyulin* Mountains. No similar blocks with a moderate concentration of weak earthquake epicenters are represented in the *Sofia* graben. The low seismic activity also shows specific migration in the studied time periods. The weak earthquakes are localized in different blocks during the 1966–1976, 1976–1979 and 1996–1999 periods. The number of low seismic activity manifestations is the highest in the *Plana* Mountain horst-block during the 1966–1976 period (Fig. 3). The same quantity is the most significant in the *Sofia* Mountain horst-blocks and of the western *Lyulin* Mountain horst-block during the next period of 1976–1979 (Fig.3). The *Plana* and the *Sofia* Mountain horst-blocks are relatively active during the 1996–1999 period (Fig. 4). The seismotectonic study estabilishes that the blocks of the Sofia graben are impacted in more frequent and intense strong and moderate seismic movements than the blocks of the adjacent horsts (Fig. 2). It is the opposite in the instances of low seismicity, when the adjacent horst-blocks are more mobile than the Sofia graben blocks (Figs. 3, 4).

Specific involvement of the blocks and the faults in the seismic movements. The strong and moderate earthquake epicenters are concentrated along faults, also in fault crossing points and blocks of the middle and the southern parts of the Sofia graben (Figs. 2, 3). The *Vitosha* fault zone is the structure with the highest seismic mobility. It is situated in the southern periphery of the Sofia graben, in the southern part of Sofia City and its large hinterland. The weak earthquake epicenters have very impressive localization along the faults as well as in the horsts to the north, east and south of the *Sofia* graben (Figs. 3, 4). The epicenters of the weak earthquakes with $M < 4.00$ are localized generally along the *Negushevo* fault zone, which is located in the northern periphery of the *Sofia* graben. The mobility of the *Vitosha* fault zone of the southern graben periphery is also significant, although smaller than that at *Negushevo*. The influence of the low seismicity is limited. It could be detected mainly in the southern and the northern periphery of Sofia City. The local earthquakes have their sources in the crust. The shallow earthquakes emerge from hypocenters mainly at a depth of 10 km (Figs. 3, 4). The earthquake hypocenters situated in depths of 11–30 km are concentrated near the *Vitosha* fault zone, in its crossing with the *Chepintsi* and the

Vladaya faults. The hypocenters are in close proximity with the contact of the blocks of the *Sofia* graben and the *Vitosha* horst. The relatively deep seismic sources create a significant danger for larger Sofia City territories. The strong, moderate and weak seismicity is related specifically with the investigated faults and the blocks of the *Sofia* graben and the surrounding horsts. The mobility of the faults and the blocks changes with time. The seismotectonic conditions are most dangerous in the middle and the southern parts of the *Sofia* graben, where Sofia City is situated.

Geological Settings

Local geological conditions. The *Sofia* graben is filled with Neogene and Quaternary clay, sand and gravel of varying thickness. The maximal thickness of Pliocene and Quaternary sediments is 1200 m (near the town of *El. Pelin*) and 80 m respectively (Fig. 5) (IVANOV, 1997).

The water permeability of the sediments predetermines the high ground water levels as well as the specificity of the processes as suffusion and liquefaction of the fine water saturated sands. The Quaternary sediments represent the uppermost part of the geological sequence in the Sofia region. These deposits are widespread and lie over older rocks and soils. The Quaternary cover is thick from 3 m to 100 m and ground (FRANGOV and IVANOV, 1999). Quaternary deposits are characterized generally with their wide areas of spreading and great diversity in the composition and properties. In general, the Quaternary soil possesses relatively high pore volume and low deformation module. The thickness of Quaternary aquifer is provisionally accepted to be in the 20–30 m range in the western part of the *Sofia* graben and 50–70 m in the eastern part. A schematic geological profile of the *Sofia* graben and some physico-mechanical properties of Quaternary and Neogene (*Lozenec* Formation) sediments is presented in Figure 5. The map of the thickness of the *Lozenec* Formation sediments in Sofia basin is shown on Figure 6 (IVANOV, 1997).

The culture layer is composed of old structures, technogenic soil, and industrial and household waste. The first layer of old structure remnants is the thickest in the central parts of the town and reaches 10 m. Technogenic soil is distributed around opened pits, big city apartment buildings and power stations. It is composed of reworked rocks and soil and industrial waste. The Neogene sediments are represented to depths of the 25–30 m range by sands of various grain size distributions. The important feature of their granulometry is the high content of silty fraction (42–82%) which expands to a great degree the peculiarity in their physical and mechanical properties—low bulk density, high pore coefficient, high moisture content and plastic consistency (FRANGOV and IRANOV, 1999).

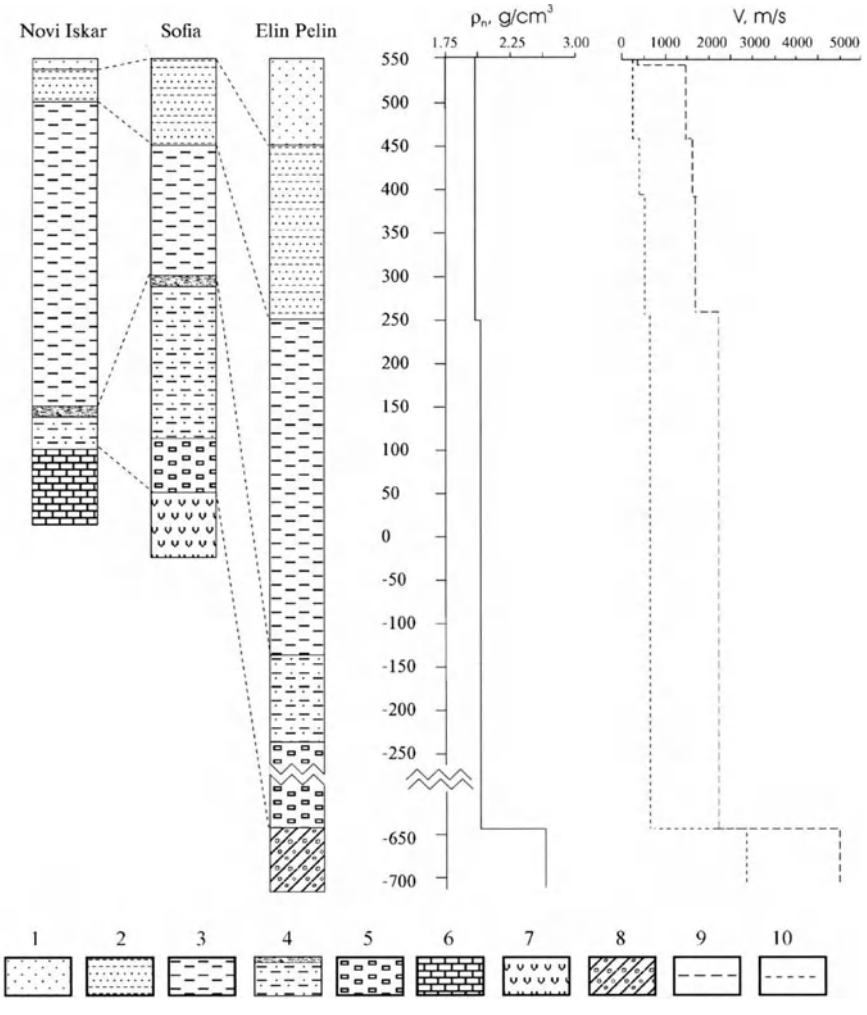

Figure 5
Schematic engineering seismogeological profiles in the Sofia area: 1—Quaternary sediments; 2—Lozenec Fm.; 3—Novi Iskar Fm.; 4—Gniljane Fm.; 5—Variegated terrigeneous Fm.; 6—Limestones (J3); 7—Andesites (K2 cn-st); 8—Volcano-terrigeneous Fm.; 9—velocity of the longitudinal waves; 10—velocity of the cross waves.

An Approach of Seismic hazard Assesment of the Sofia Region

Uniform Risk Spectra for the region. The concept of uniform seismic risk used in this work is a functional of shaking, S (T), which is represented by a Fourier amplitude spectrum computed by the NEQRISK program (LEE and TRIFUNAC, 1985). The above work (LEE and TRIFUNAC, 1985) also incorporated a realistic model to describe the seismicity and proposed two independent methods to obtain uniform

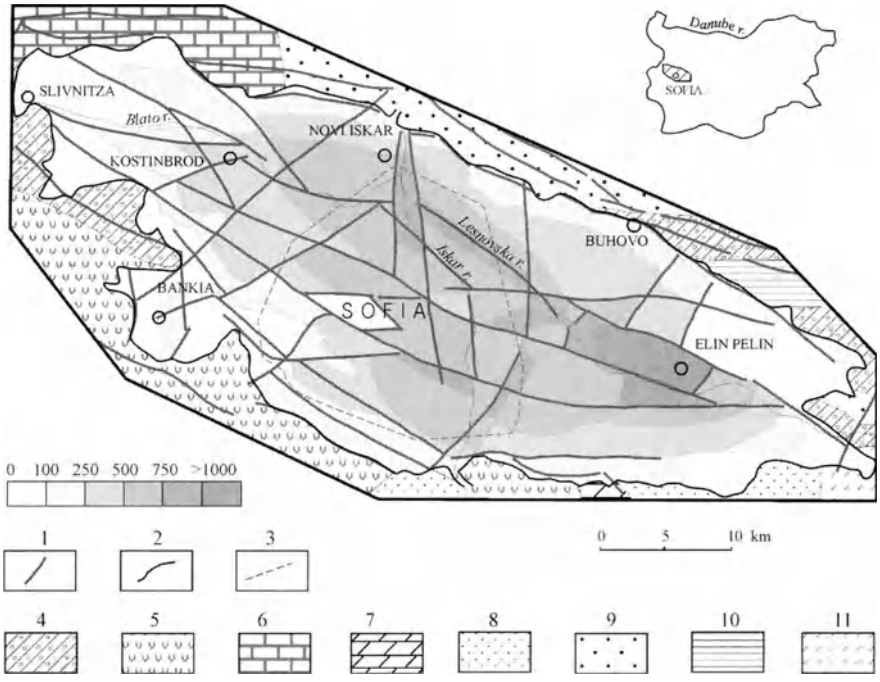

Figure 6
Map of the thickness of the Neogene and Quaternary sediments in the Sofia basin: 1—fault; 2—Sofia basin boundaries; 3—Sofia City boundaries; 4—Volcano-terrigeneous Fm.; 5—Andesites (K2 cn-st); 6—Limestones (J3); 7—Limestones and dolomites (T2); 8—Sandstones (T); 9—Sandstones (Pz-T1); 10—Argillites (O-S); 11—Gneisses and diabases (Pc).

risk functional: a) assuming that the seismicity, which is the input to the model, is treated as the mean of a Poisson sequence; b) assuming that it can be taken literally. Depending on the methods used, the outcome of a seismic risk analysis may be very sensitive to the description of the seismicity. In a large region the occurrence rate of earthquakes is often known. The analysis for a specific site is more difficult and depends on the conditions near the site, particularly within a range of 25 to 50 km. For smaller regions, "historical seismicity" based on felt reports is often incomplete and may not represent the true seismicity of the region (NENOV *et al.*, 1990). In such cases the knowledge of fault slip rates or regional strain rates from plate tectonics theory may be used to estimate "geological seismicity." This helps to increase the reliability of the seismicity description of a region. For the Sofia region a square of 25 $\times$ 25 km has been used. There are two sets of inputs for the NEQRISK seismic risk program: a) set of the inputs consists of descriptions of the seismicity in the region; b) inputs describing the attenuation of seismic waves from the seismic source to the site. A detailed seismic hazard assessment of a large Metropolitan area such as Sofia City will require very thorough studies of the activity and the distribution of all active

zones and will call for considerably more detailed knowledge of the local soil and geologic conditions and that is why we have adopted the use of an illustrative example in this study which is the seismicity model according to TODOROVSKA *et al.* (1995). Based on the map of the depth of sediments, a classification of the local soil conditions is made, using a modified scale: s = 0 to s = 3 (DUKE *et al.*, 1972). The target Sofia region has been divided into 1 × 1 km sections and an assessment of the soil conditions s = 3 for rock, s = 2-hard "rock" soil sites, s = 1-stiff soil sites, s = 0-for deep soil sites is carried out. Average soil velocity, V_s in the top-30–50 m beneath the surface, is taken for s = 3–V_s > 750 m/s; s = 2 V_s = 450–550 m/s; s = 1– V_s = 400–450 m/s; s = 0– V_s = 300–400 m/s, respectively. A map of surface geological conditions has been made (Fig. 7). It was used for the analytical assessment of the seismic hazard. Calculations of the frequency-dependent function of the risk as generated uniform Fourier spectrum FS (T) for point 42.70 N; 23.40 E are carried out. The Fourier spectrum for 50 years exposure time at five levels of probabilities of non exceedance p = 0.99; 0.90; 0.50; 0.1; 0.01 for periods 0.1–8 sec is given in Fig. 8.

We do believe that many overall features and trends of the map of surface geological conditions (Fig. 7) presented in this stydy will not change substantially when more detailed information becomes available.

1-D analyical approach for the central part of Sofia capital and eigenproblem solution

The higher degree of risk on the territory of Bulgaria and the expected development of the infrastructure forced the investigations of the seismic risk

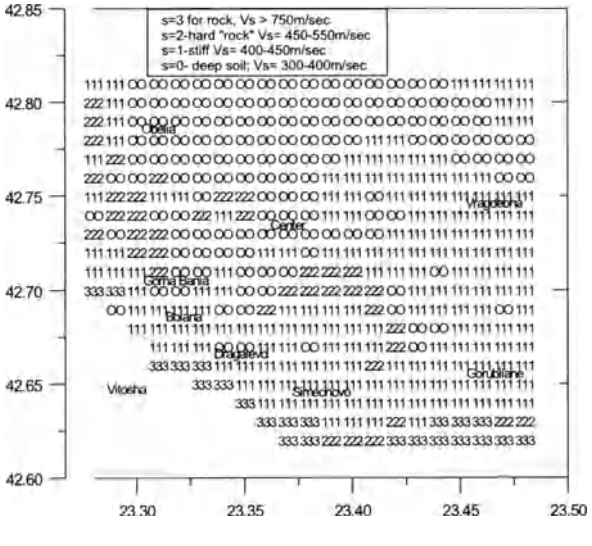

Figure 7
Classified surface geological conditions.

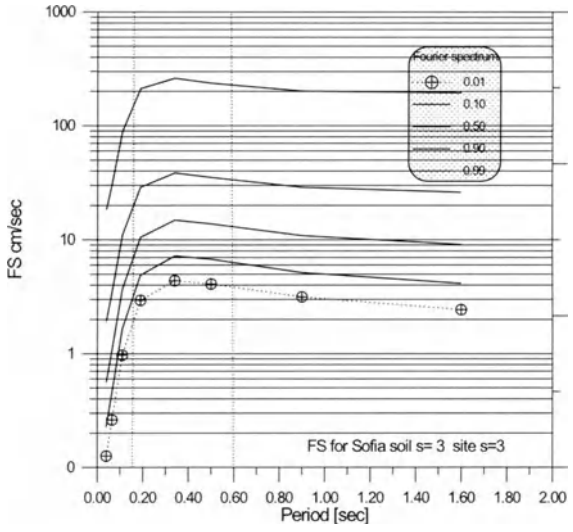

Figure 8
Uniform probability Fourier spectrum.

mitigation and safety management. Usually those efforts are concentrated on mapping the parameter of peak ground accelerations. The mapping of the displacements due to earthquake strong ground motion is neglected. The target of this analysis is to determine possible levels of the expected displacements on the territory of the Sofia region. On the basis of the generated uniform Fourier spectrum (Fig. 8), time histories have been generated for fourteen points (stations), positioned around the center of the city. The effect of the local geological conditions has been investigated analytically by a site response analysis for fourteen (up to 600 m deep) boreholes. The soil has been modeled in horizontally divided multilayers. The nonlinearity of the soil response has been considered in the analysis by using an equivalent linear complex model (SHNABEL *et al.*, 1976). Site response has been performed by SHAKE'91 techniques. The generated accelerograms, using uniform Fourier FS (T) response spectrum for point 42.70 N, 23.40 W for 50-years exposure time and probabilities of nonexceedance $p = 0.90$, have been scaled to the level of 0.15 g based on the models. The maximum displacements at target points are mapped in Figure 9 with in the framework of the generated seismograms. The biggest values of the surface displacements are oriented NE of the town and vary from 12 to 29 cm. The eigenproblem solution to determine the elastic vibration periods, implementing inverse iteration with Gram-Schmidt ortogonalization, has been carried out. Three models varying in depth have been used. Model M_{30}—depth to 30 m, M_{50}—depth to 50 m and model $M_{\&}$ with depth where shear-wave velocity reaches values of $V_s >$ 750 m/s. The models have been derived from combining Eurocode 8 soil classification and the national 1987 code. The results for the first four natural periods using those

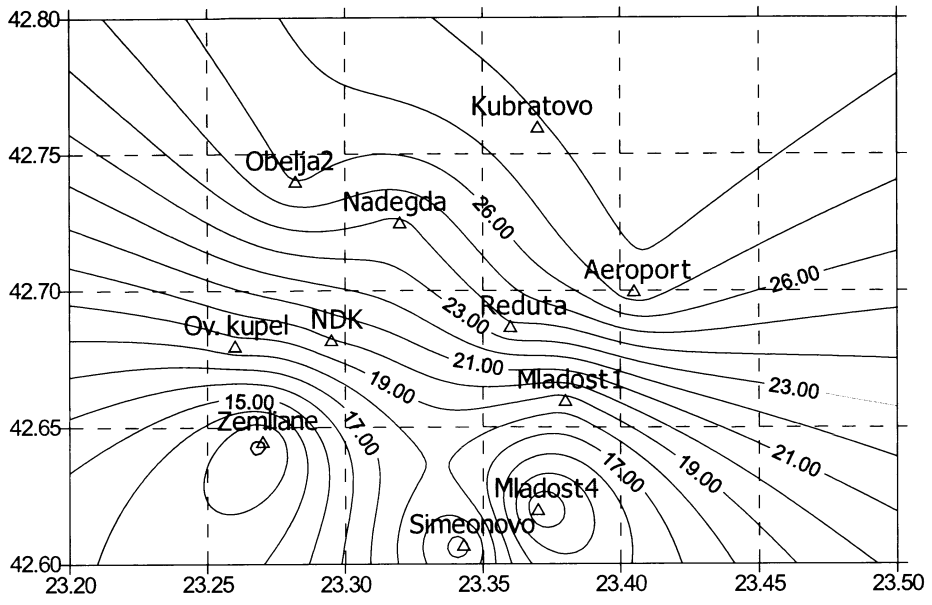

Figure 9
Maximum surface displacements [cm].

three models for fourteen sites have been obtained using the special purpose WAVES computer program for calculating the dynamic characteristics (HART and WILSON, 1989). The soil site is discretized into a finite-element mesh of one-dimensional shear elements. The models are represented dynamically by a viscously damped, lumped mass system. The analysis is very sensitive in subdividing geological column in layers. It is necessary to ensure spatial convergence (i.e., that the further mesh subdivision will not effect the solution). Plan distribution for the first natural period (in seconds) for the M_{30}, M_{50} and $M_{\&}$ models is given in Figures 10, 11, and 12, respectively. The first natural periods for the M_{30} models range 0.30–1.04 sec. The comparison with the first natural periods for the M_{50} models shows that they are bigger than the periods of Model M_{30} from 1.6 to 2 times for the central part of the city, and 1.4 times for the periphery. Those maps can keep designers aware of the types of structures that must be placed in the future. For example, the structures with relatively small natural periods ($T < 0.7$ sec) at a depth of 30 m and higher modes for 50 m depth will strongly influence their natural response.

Oppositely, for the structural systems with natural periods higher than $T > 0.8$ sec the response of the 50 m depth and higher modes for the depth up to the "rock" will influence their response. To achieve precise displacement distribution, future assessments of the seismic excitation of the metropolitan area of Sofia should be performed using more sophisticated models.

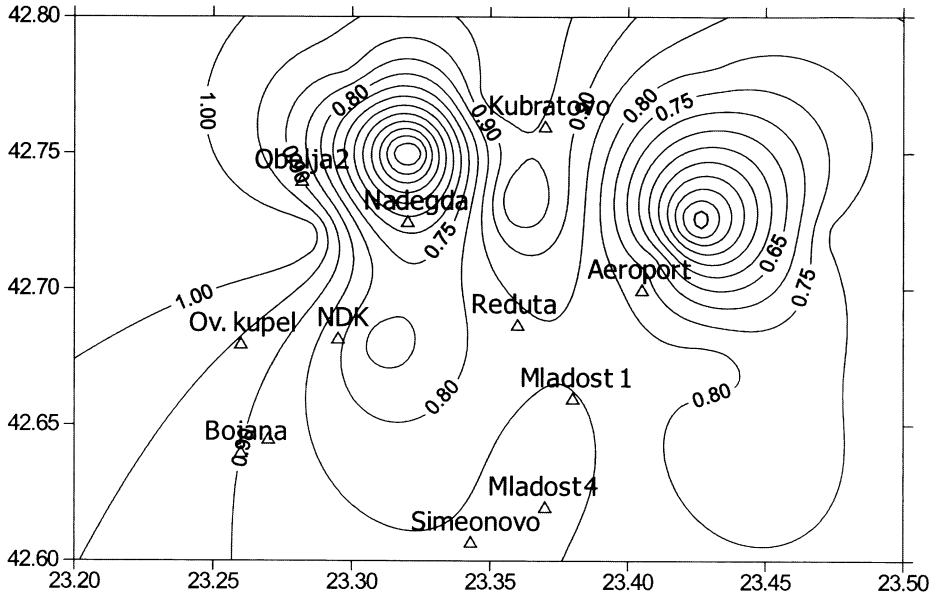

Figure 10
First natural period for 30 m depth.

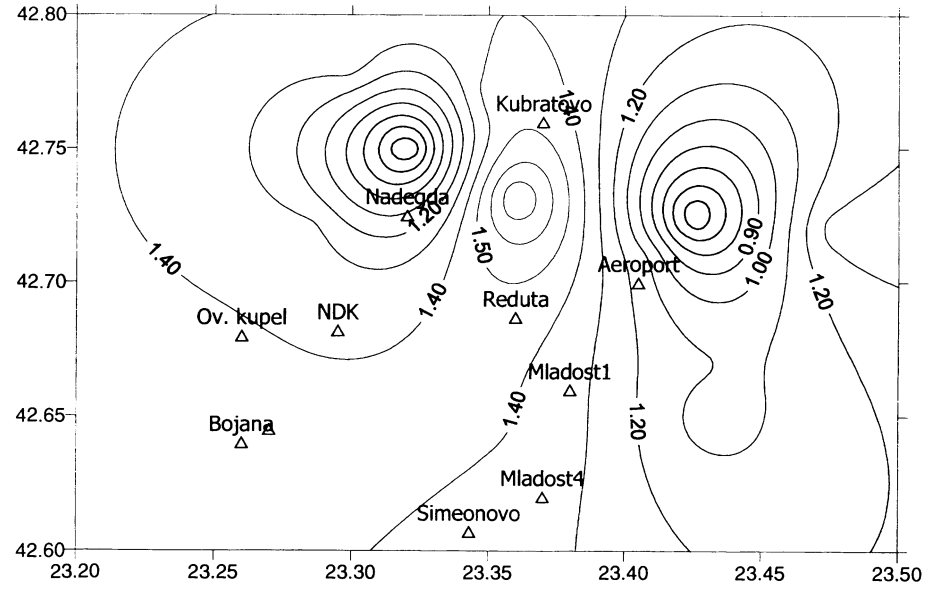

Figure 11
First natural period for 50 m depth.

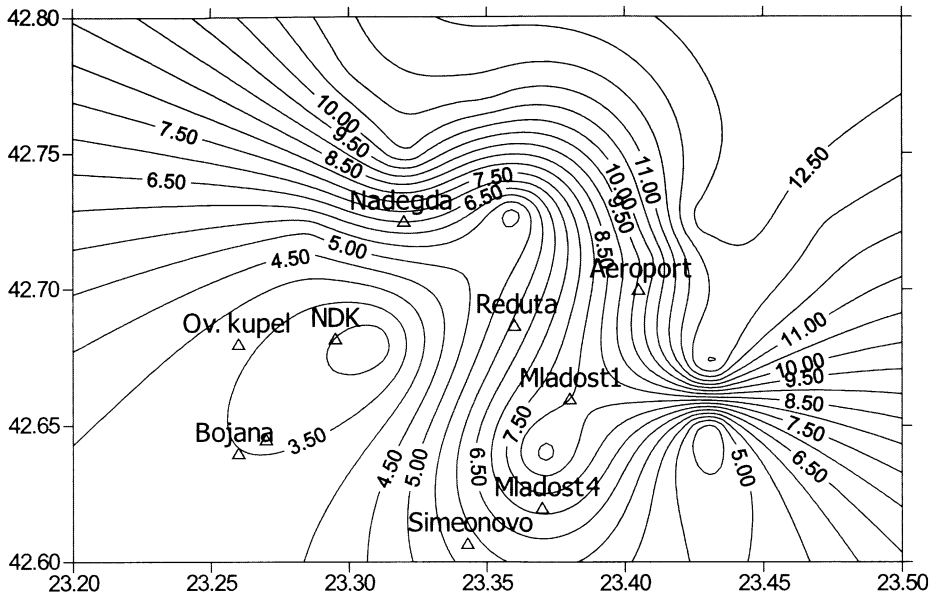

Figure 12
First natural period for depth to V_s > 750 m/s.

Conclusion

The work demonstrates the very recent investigations of the seismicity, seismotectonic and local geological conditions for the Sofia region. The concept of the uniform risk to calculate Fourier FS (T) response spectrum for point 42.70 N, 23.40 E for 50-years exposure time and probabilities of nonexceedance $p = 0.90$ is used to generate accelerograms and seismograms. The results from the performed investigations show that the variation of the depth of the soil profiles needs careful assessment in case of displacement calculations for the ground-built environment. The results based on one-dimensional models correspond to the tendencies shown by recent seismotectonic and geological investigations. When the recent intensive industrial and civil construction in the Sofia City region is taken into account, as well as the transport and agriculture development and the acceleration of the mine and stone-pit exploitation, it is important to keep in mind that the seismic influence on the surface could be stronger in the future.

Acknowledgements

This work is a contribution to the UNESCO-IUGS-IGCP Project 414 "Realistic Modeling of Seismic Input for Megacities and Large Urban Areas". Part of this

study has been supported by the National Science Foundation in Bulgaria, Project No. NZ 5/2001.

REFERENCES

BONCHEV, E., BUNE, V. I., CHRISTOSKOV, L., KARAJUILIVA, J., KOSTADINOV, V., REISNER, G. I., RIZIKOVA, S., SHEBALIN, N., SHOLPO, V., and SOKEROVA, D. (1982), *A Method for Compilation of Seismic Zoning Prognostic Maps for the Territory of Bulgaria,* Geologica Balkanica *12*(2), 3–48.

BOTEV, E. and RIZIKOVA, S. (1982), *Sofia Seismic Zone and Weak Earthquakes 1977–1979*, Bulg. Geoph. J. V. VIII, *3*, 98–105 (in Bulgarian with English abstract).

BOTEV, E., BABACHKOVA, B., DIMITROV, B., VELICHKOVA, S., TZONCHEVA, I., DONKOVA, K., and TOTEVA, T. (1998), *Preliminary Data on the Seismic Events Recorded by NOTSSI in July-December 1997,* J. Bulg. Geophys. *24*, 1–2, 170–178.

BOTEV, E., BABACHKOVA, B., DIMITROV, B., VELICHKOVA, S., TZONCHEVA, I., DONKOVA, K., and TOTEVA, T. (1999), *Preliminary Data on the Seismic Events Recorded by NOTSSI in July-December 1997,* J. Bulg. Geophys. *25*, 1–4, 215–224.

BRANKOV, G. (1983), *Vrancea Earthquake in 1977. Its After-effects in the People's Republic of Bulgaria.* (Publ. House of the Bulg. Acad. of Sciences, Sofia (Red.), 428 pp. (in Bulgarian with English and Russian abstracts).

BROUTCHEV, I. (1994), *Geological hazards in Bulgaria,* Bulgarian Academy of Sciences (Publishing House of the Bulgarian Academy of Sciences, Sofia, ed., 1994).

BROUTCHEV, I., TZANKOV, T., HRISTOSKOV, L., VAPTZAROV, I., PASKALEVA, I., and MILEV, G. (1995), *Natural Hazards in the Lithosphere on the Territory of Bulgaria*, J. Bulgarian Academy of Sciences, CVIII, Vol. *1*.

CHRISTOSKOV, L., GLAVCHEVA, R., GEORGIEV, Tz., HRISTOVA, Tz., DONKOVA, K., SIMEONOVA, St., SOLAKOV, D., DINEVA, S., MIHAILOV, D., DIMITROV, B., and SPASSOV, E. (1988), *Seismological Features of the Region of the 1986 Earthquake Sequence*, Bulgarian Geophys. J. *XIV*, 2, 73–89.

CHRISTOSKOV, L., GEORGIEV, T. Z., DINEVA, D., and BABACHKOVA, B. (1989), *On the Seismicity and Seismic Hazard of Sofia Valley*, Proc. 4th Int. Symp. 4–9 Sept. Bechine, 447–453.

DUKE, C., JONHNSEN, K., LARSON, L., and ENGMAN, D. (1972), *Effects of Site Classification and Distance on Instrumental Indices in the San Fernando Earthquak*e, USLA Engin. Report, No USLA-ENG-7247, June 1972.

FRANGOV, G.and IVANOV, P. L. (1999), *Engineering Geological Modeling of the Conditions in the Sofia Graben and Land Subsidence Prognoses*, Proc. 4th WG Meeting, Dec. 3–6, 1999, Sofia, 17–13.

GLAVCHEVA, R. (1993), *Atlas of Isoseismal Maps, Bulgaria 1981—1990*, Geoph. Inst., BAS.

GRIGOROVA, E. and GRIGOROV, B. (1964), *Epicenters and Seismic Lines*, BAS, 83.

HART, J. and WILSON, E. (1989), *Simplified Earthquake Analysis of Buildings Including Site Effects*, Rep. NUSB/SEMM-89/23, Structural Eng. and Mech. of Materials, Dep. of Civil Eng., Univ. of California, Berkeley.

IVANOV, P. (1997), *Assessment of the Geological Conditions in the Sofia Kettle under Seismic Impact*, Proc. Intern. Symp. on Eng. Geol. and the Env., IAEG, Athens, 23–27 June, BALKEMA, Rotterdam, 1265–1270.

IVANOV, PL., FRANGOV, G., and YANEVA, M. (1998), *Engineering Geological Characteristics of Quaternary Sediments in the Sofia Graben*, Proc. 3rd WG Meeting, Dec. 2–5, Sofia, 33–37.

LEE, V. and TRIFUNAC, M. (1985), *Uniform Risk Spectra of Strong Earthquake Ground Motion: NEQRISK*, Report No.85–05, Dep. of Civil Eng., Univ. of Southern California, Los Angeles.

LEE, V. and TRIFUNAC, M. (1985), *Frequency-dependent Attenuation of Strong Earthquake Ground Motion,* Rep. 85–02, Dep. of Civil Eng., Univ. of Southern California, Los Angeles.

MATOVA, M. (1996), *Seismic Active Faults in the Region of the Town of Sofia*, Proc. first WG Meeting, October 31-November3, 1996, Sofia, 45–50.

MATOVA, M. (2001), *Recent Manifestations of Seismotectonic Activity in Sofia Region and their Land Subsidence Potential*, Proc. Final Conf. of UNESCO-BAS Project on Land Subsidence, June 27–30, 2001, Sofia, pp. 93–98.

NENOV, D., GEORGIEV, G., PASKALEVA, I., LEE, V., and TRIFUNAC, M. (1990), *Strong Ground Motion Data in EQINFOS: Accelerograms Recorded in Bulgaria Between 1981–1987*, Bulgarian Academy of Sciences, Central Lab. Seismic Mech. and Earthq. Eng. and Dept. of Civil engineering, Rep. 90–02, Univ. of South. California.

OROZOVA-STANISHKOVA, I. M., VACCARI, F., and SUHADOLC, P. (1996), *Estimates of 1 Hz Maximum Acceleration in Bulgaria for Seismic Risk Reduction Purposes*, Tectonophysics, Internat. J. Geotectonics and Geology and Physics of the Interior of the Earth *258*, 263–274.

PANZA, G. and VACCARI, F. Introduction, Seismic Hazard of the Circum-Pannonian Region (Birkhäuser Verlag, Basel, Swizerland) (G.Panza *et al.* 2000 eds.) pp. 5–9.

PASKALEVA, I. and KOUTEVA, M. (2000) *An Approach of Microzonation of the Town of Russe in Connection of Recent Vrancea Earthquakes and Shabla Zone*; Report under Bilateral Co-operation, Trieste, 22 May-22 June, 2000.

RANGUELOV, B. (1996), *Seismicity and Site Effects on the Sofia Valley District.*, Proc. I-st WG meeting, 31 Oct.-3 Nov. 1996, Sofia, 28–31.

RANGUELOV, B. and TOTEVA, T. (1998), *Recent Seismicity Observed Around Sofia City*, Proc. 3rd WG Meeting, Dec. 2–5, 1998, Sofia, 7–9.

SHNABEL, P., LAYSMER, J., SEED, H. and UGAS, C. (1976), *SHAKE Equivalent Linear Seismic Response Analysis of Horizontally Layered Soil Deposits*, Report EERC 71–12, Dep. of Civ. Engineering, Univ. of California, Berkeley.

SOLAKOV, D., CHRISTOSKOV, L., and SIMEONOVA, S. (2001), *Possible Consequences from Strong Earthquakes in the Territory of Bulgaria.* MinnoDelo and Geologia J. 1, 52–57 (in Bulgarian, English abstract).

TODOROVSKA, M., PASKALEVA, I., and GLAVCHEVA, R. (1995), *Earthquake Source Parameters for Seismic Hazard Assessment: Examples of Bulgaria*, Proc. 10th ECEE, Aug.28-Sept.2, 1995, Vienna, Austria.

TRIFUNAC, M. (1990), *How to Model Amplification of Strong Earthquake Ground Motion by Local Soil and Geologic Site Conditions*, Earthq. Eng. Struct. Dynam. *19*(6), 833–846.

WATZOV, Sp. (1902), *Tremblements de terre en Bulgaria au XIX siecle*, IMPR. DE L'ETAT, Sofia, Bulg., 95 pp.

YOSSIFOV, D. and PASKALEVA, I. (1999), *Real Danger for Sofia*, J. Mining and Geology, *9*, 22–27.

(Received April 30, 2002, accepted July 10, 2002)

Pure appl. geophys. 161 (2004) 1285–1300
0033–4553/04/061285–16
DOI 10.1007/s00024-003-2492-z

Pure and Applied Geophysics

Seismic Characterization of Neapolitan Soils

C. NUNZIATA[1], M. NATALE[1], and G. F. PANZA[2,3]

Abstract—Detailed shear-wave velocity profiles versus depth have been obtained in typical lithostratigraphies of Napoli. FTAN and hedgehog methods have been applied to Rayleigh surface waves recorded in refraction seismic surveys. The comparison with literature measurements shows good agreement with nearby down- and cross-hole tests.

The pumiceous and lapilli content, and the different welding and alteration degree of the Neapolitan pyroclastic soils cause a strong scattering of the shear wave velocities (V_S) from bore-hole measurements, even for the same formation. Surface measurements, based on FTAN-hedgehog methods, determine average V_S along travel paths of about 100 m, give results that are comparable with down- and cross-hole velocity profiles, and have the additional advantage of being less scattered, and thus more representative of average properties than bore-hole measurements. The results of surface measurements should be preferred in the computation of realistic seismograms and are particularly suitable in urban areas, as they are not destructive and need just one receiver.

Key words: Napoli, pyroclastic materials. shear wave velocities, inversion.

1. Introduction

Napoli is located within the Campi Flegrei (CF), an active volcanic area, and is delimited on the eastern border by Somma-Vesuvius active volcano (Fig. 1). The CF area is a structural depression interpreted as a calderic system characterized by many Quaternary vents (ROSI and SBRANA, 1987; ORSI *et al.*, 1996). The subsoil structure of the CF caldera consists of incoherent volcanic products with different characteristics. Besides the alteration processes undergone after deposition, this is due to the differences of the primary magma composition, the mechanisms and environment of setting. As a consequence of these processes, the deposits are arranged in complex structural settings with vertical and lateral inhomogeneities, overlying a tufaceous formation.

The seismic hazard of Napoli is controlled both by Apennines tectonic earthquakes and by Vesuvius seismic activity. The last Apennines earthquake, November 23rd

[1] Dipartimento di Geofisica e Vulcanologia, Univ. Napoli "Federico II", Italy.
E-mails: conunzia@unina.it; manatale@unina.it
[2] Dipartimento di Scienze della Terra, Univ. Trieste, Italy. E-mail: panza@dst.units.it
[3] Abdus Salam International Center for Theoretical Physics, SAND Group, Trieste, Italy.

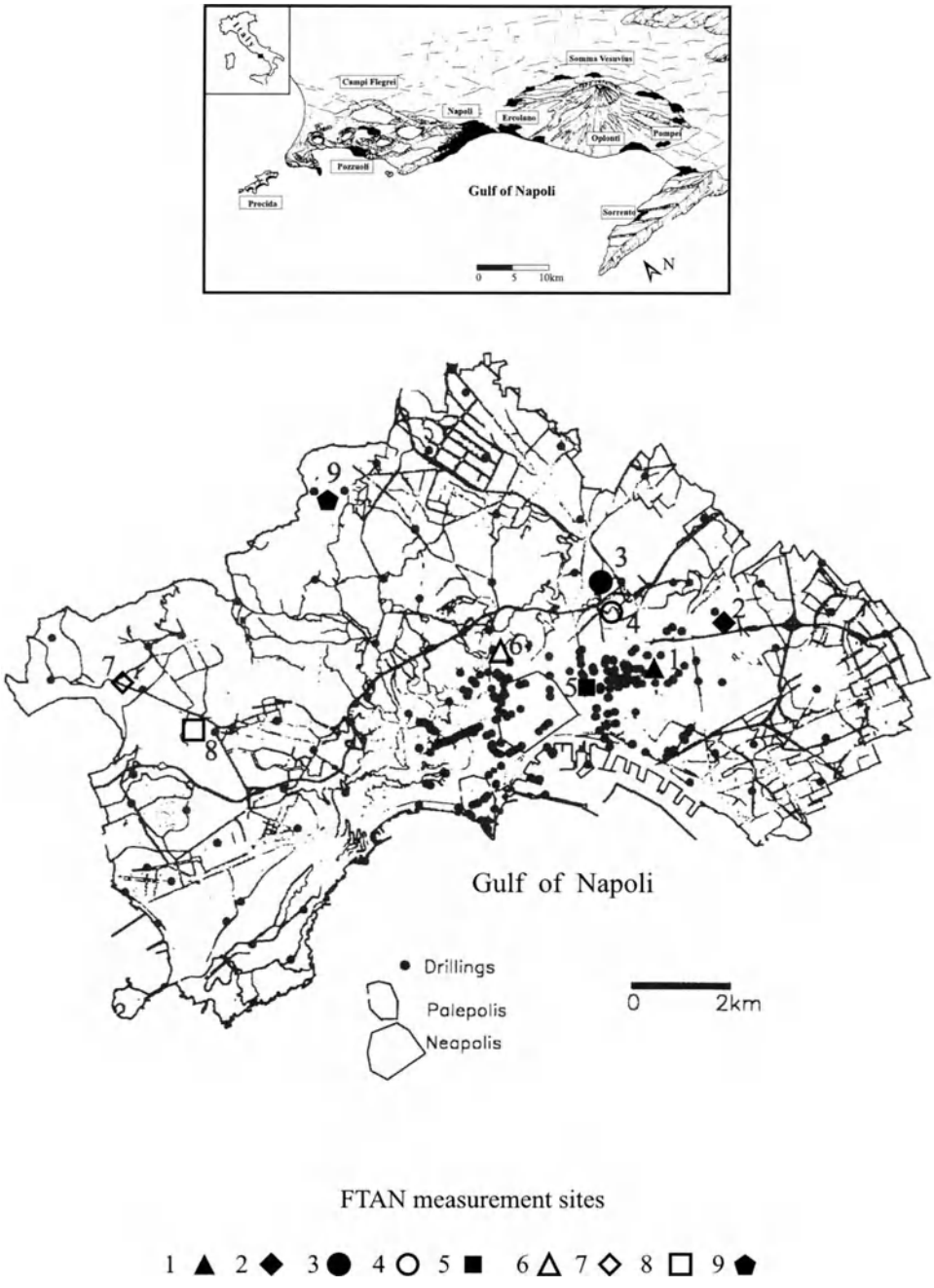

Figure 1
Location (top) and map of the urban area of Napoli with the location of collected drillings and FTAN measurement sites. The ancient Greek Palepolis and Neapolis are also shown.

1980, (M_S = 6.9) caused extensive damage corresponding to an intensity of VII-VIII on MCS (Mercalli-Cancani-Sieberg) scale. Even more damage is expected from the earthquakes connected to the volcanic activity of the Somma-Vesuvius complex, as testified by historical chronicles (ALFANO and FRIEDLANDER, 1929).

In this context, the definition of the shear wave velocities (V_S) of volcanic soils and rocks is fundamental for the evaluation of the site amplification effects in different stratigraphic conditions. Moreover, a better knowledge of the shear dynamic properties of the lithotypes and their variations associated with different deposition conditions may help in the stratigraphic modelling of seismic measurements.

The aim of this paper is twofold: the first one defines the ranges of V_S of the Neapolitan pyroclastic soils and rocks, based upon literature and original seismic measurements, and the second one defines V_S profiles in a highly urbanized city with a rich historical building heritage like Napoli, from the inversion of Rayleigh wave group velocities.

2. Geological Setting

Napoli is located on volcaniclastic soils and rocks (various types of tuffs) erupted by the Campi Flegrei (CF) volcanoes, and secondly by Vesuvius. The original material that forms the tuffs and the volcanic soils is in general the same, with the volcaniclastic rocks resulting from the hardening of the volcaniclastic soils by post depositional hydrothermal alteration. Such hardening is not homogeneous, thus intermediate facies may exist from lithoid (compact tuff) to incoherent (pozzolana), through welded incoherent facies (welded pozzolana). Beside the intense volcanic activity, Napoli has suffered extensively due to the influence of meteoric and marine agents, and the anthropic action of morphological modeling for urban settlement. In fact, the ancient Napoli, Palepolis and later Neapolis, in the middle of the city, was founded by Greek settlers, and was a tuff hill, separated from the neighbouring lands by several rivers and limited by the sea in the south (Fig. 1). Subsequently, the presence of so many rivers generated deep hollows filled with alluvial materials and bricks derived from the urban settlement. The sea receded and streets were built along the coastline. Numerous «vacua» of a different nature cross the Neapolitan underground. They include, besides present and ancient sewer systems and tunnels, tuff quarries, pits to extract the pumiceous lapilli and pozzolana, the canalisation of the ancient (Greek and Roman) aqueducts.

The volcanological study of the products of different explosive vents in the CF area (SCARPATI *et al.*, 1993; ORSI *et al.*, 1996), and the stratigraphic sequences from bore-holes (Fig. 1) (AA.VV., 1967; VINALE, 1988; COMUNE DI NAPOLI, 1994) have been very useful in reconstructing the volcanological and structural setting of the Neapolitan urban area. It results that below a cover of man-made ground material 10 m thick the most widespread pyroclastic products belong to the Neapolitan

Yellow Tuff (NYT) eruption (12,000 years old) and more recent volcanic activity (< 12,000 years old) of different CF eruptive centers (Fig. 2). The oldest product, that is the Campanian Ignimbrite tuff (33,000 years old), is sporadically present. Marine sands are present along the coast and organic materials are encountered locally. At last, Vesuvius tuff and ashes have been found in the eastern area of Napoli. The lithoid tuff horizon is, on average, 10–30 m deep, but deepens to more than 100 m in the western area and to more than 40 m in the southeastern area of Napoli (Fig. 3).

Laboratory measurements of geotechnical properties of several specimens, extracted from drillings and quarries (AA.VV., 1967; VINALE, 1988; COMUNE DI NAPOLI, 1994; NUNZIATA *et al.*, 1999a), show that the CF soil generally ranges from

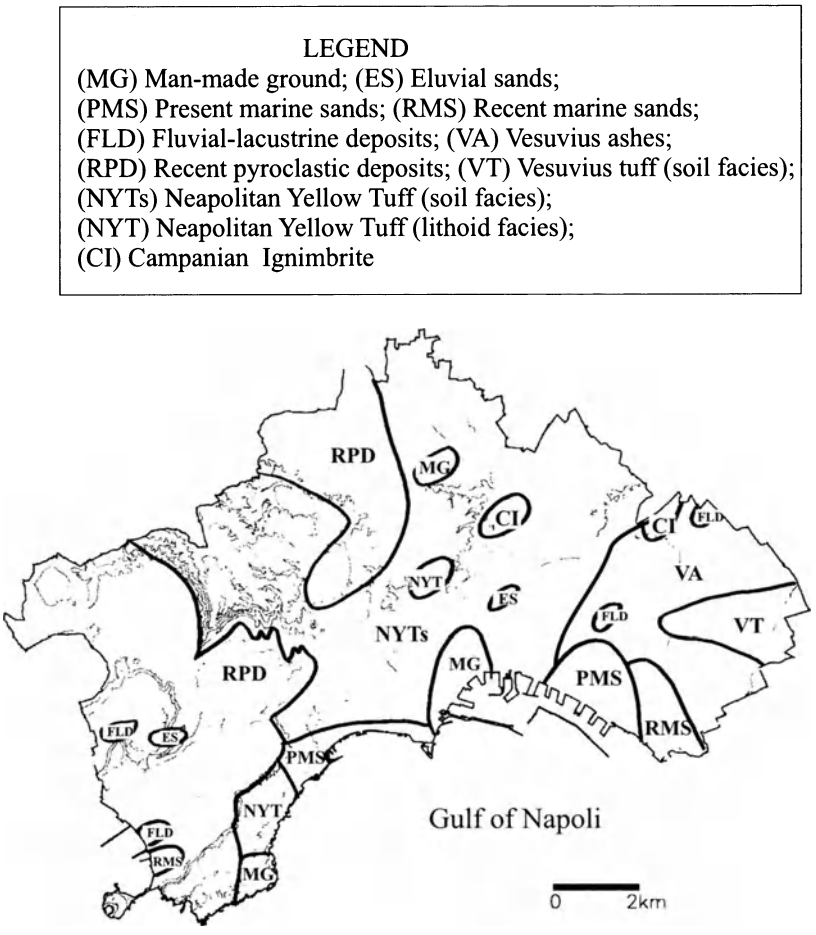

Figure 2
Volcanological map of Napoli at 10 m of depth from ground surface, placed on the topographic sketch map.

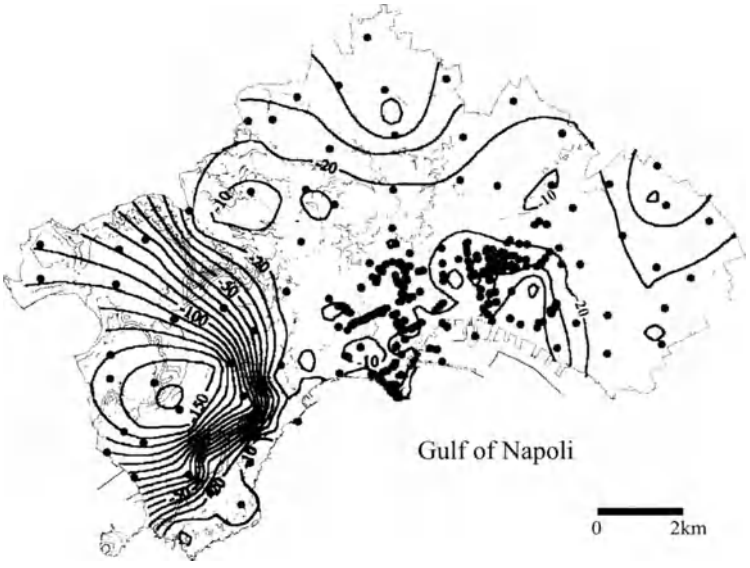

Figure 3
Map of isobaths of the lithoid tuff horizon in meters from ground surface (dots represent the drillings).

silty sand to sandy silt. The coarser deposits correspond to the pumiceous layers of the younger pyroclastic products. The unit weight of the soil solids (γ_s) ranges 17.5 ÷ 27.0 kN/m^3 and the natural unit weights (γ_n) vary between 9.4 and 21.7 kN/m^3. The shear resistance values ($\varphi°$) vary in the 18° ÷ 64° range, the porosity is between 30 and 90% and the water content varies between 6.5 and 62.3% (Table 1).

3. Shear wave Velocities of Neapolitan Soils and Rocks

The V_S of different deposits, determined in borehole, cross- and down- (VINALE, 1988; COMUNE DI NAPOLI, 1994) tests, have been collected. To define the ranges of variability for the Neapolitan soils and rocks, all V_S measurements have been analysed with the framework of the volcanological and geotechnical stratigraphies. A preliminary study of the V_S of NYT and of younger pyroclastic deposits of Campi Flegrei-Neapolitan area has been conducted, based on the comparative analysis of field and laboratory measurements by NUNZIATA *et al.* (1999a). Wide ranges of variations have been shown. They are the consequence of the profound differences of the physical properties and textural conditions that can be present even in the same formation. An additional important influencing factor is represented by the different hardening degree, due to the diagenetic process.

Down-hole (DH) and cross-hole (CH) measurements are point measurements, therefore average values of V_S, over some one hundred meters, are more suitable for any evaluation of seismic site amplification effects. With such aim, within the

Table 1

Geotechnical properties of the Neapolitan lithotypes

Lithotype	γ_s (kNm^{-3})	γ_n (kNm^{-3})	n (%)	$\varphi°$	W%
Eluvial deposit	23.0–25.8	11.0–20.7	34–66	32–41	18.8–53.7
Present marine sands	24.0–26.8	16.5–20.8	33–50	29–42	13.5–37.4
Recent marine sands	22.9–25.7	15.7–18.8	35–54	26–40	19.3–50.8
Fluvial-lacustre deposits	17.5–26.6	10.0–20.7	34–90	32–41	18.8–61.3
Vesuvius ashes	21.0–27.0	10.0–20.0	37–86	26–39	19.1–60.2
Recent pyroclastic deposits	23.5–26.3	13.5–14.5	40–64	21–45	9.9–62.3
NYT (soil facies)	22.1–26.0	10.6–18.6	38–64	18–41	6.5–47.5
NYT (lithoid facies)	22.3–24.5	9.4–15.3	38–58	no data	no data
Vesuvius tuff (soil facies)	20.5–26.8	11.0–20.3	30–41	36–64	18.1–50.8
Vesuvius tuff (lithoid facies)	24.7–26.3	16.0–17.6	44–54	30	26.9–41.3
Campanian Ignimbrite	23.3–26.9	11.0–21.7	no data	30–41	no data

γ_s = unit weight of the soil solids; γ_n = natural unit weights; n = porosity; $\varphi°$ = shear resistance values; W = content of water.

framework of the UNESCO-IUGS-IGCP project "Realistic Modelling of Seismic Input for Megacities and Large Urban Areas", detailed V_S velocity profiles with depth have been obtained in representative lithostratigraphic sites of Napoli by using Rayleigh waves recorded in refraction seismic surveys. The source was the vertical impact of a 20 Kg weight on the ground, the receivers were 1 Hz and 4.5 Hz vertical geophones (70% damping) and the source-receiver distance variable between 50 and 150 m. Group velocities of surface waves have been measured employing the FTAN method on single channels (LEVSHIN *et al.*, 1992). A nonlinear inversion, hedgehog method (VALYUS *et al.*, 1968; PANZA, 1981), of the group velocity dispersion curves defines the V_S distribution with depth. The average dispersion curves of the fundamental mode of Rayleigh wave group velocities typically fall in the 0.02 to 0.3 s period range.

Such an approach produces results well in agreement with DH and CH tests (NUNZIATA *et al.*, 1999b; NUNZIATA *et al.*, 2001a, b) and is substantially more reliable than the SASW method (NAZARIAN and STOKOE, 1985), often employed in engineering problems and based on phase velocity measurements.

In the following, the sets of V_S profiles obtained with hedgehog inversion are compared with bore-hole measurements given in literature, for the different formations and then, site by site, with the closest DH or CH velocity profile with depth. In such a way we improve our knowledge of the shear dynamic parameters of the Neapolitan pyroclastic products, and we test the possibilities offered by FTAN against bore-hole measurements, that are considered the most efficient by engineers.

3.1 Recent Pyroclastic Products

Volcanic products erupted by different vents of the CF area after the NYT tuff eruption ($<$ 12,000 y) are mainly concentrated on the western side of Napoli and, to

a lesser degree, on the northern side (Fig. 2). These deposits are represented by a proximal facies of pyroclastic-flow and -surge, in the CF caldera, and outside by distal fallout products (ORSI *et al.*, 1996). They are present as soil facies and are characterized by V_S velocities ranging between 80 m/s and more than 600 m/s (Fig. 4). FTAN measurements have been carried out at five sites (measurements at sites 7 and 8 are from GAROFALO, 2000) and they fall in the range defined by DH and CH tests (COMUNE DI NAPOLI, 1994), however they are always lower than 400 m/s, even at greater depths.

3.2 NYT Deposit

The NYT deposit is the most extensively present in Napoli, and consists of both lithoid (tuff) and soil (pozzolana) facies. The V_S of NYT pozzolana are strongly scattered, roughly between 100 m/s and 650 m/s (Fig. 5). The velocity range defined by the hedgehog nonlinear inversion is less scattered, between 150 m/s and 400 m/s.

Shear wave velocities of the NYT tuff range from about 300 m/s up to 1300 m/s (Fig. 5), and a continuity seems to exist between the velocity values of NYT pozzolana and tuff which may be interpreted as evidence of their origin. In fact, the NYT formation is the result of hardening processes due to hydrothermal alteration of the *pozzolana* deposit (DE' GENNARO *et al.*, 1983). The different degrees of these hardening processes have, as a consequence, a wide welding range of the volcanic products with strong variations of the physical properties, and consequently a wide range of V_S values. The wide range of tuff V_S can also be explained in terms of the different textural conditions, as the NYT tuff is present in facies with different

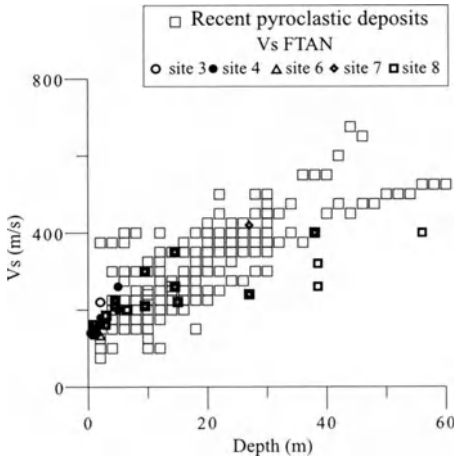

Figure 4
V_S velocities of recent pyroclastic deposits. Symbols indicate down- and cross-hole tests (COMUNE DI NAPOLI, 1994), and the velocity range defined by the hedgehog nonlinear inversion of FTAN measurements at sites located in Figure 1.

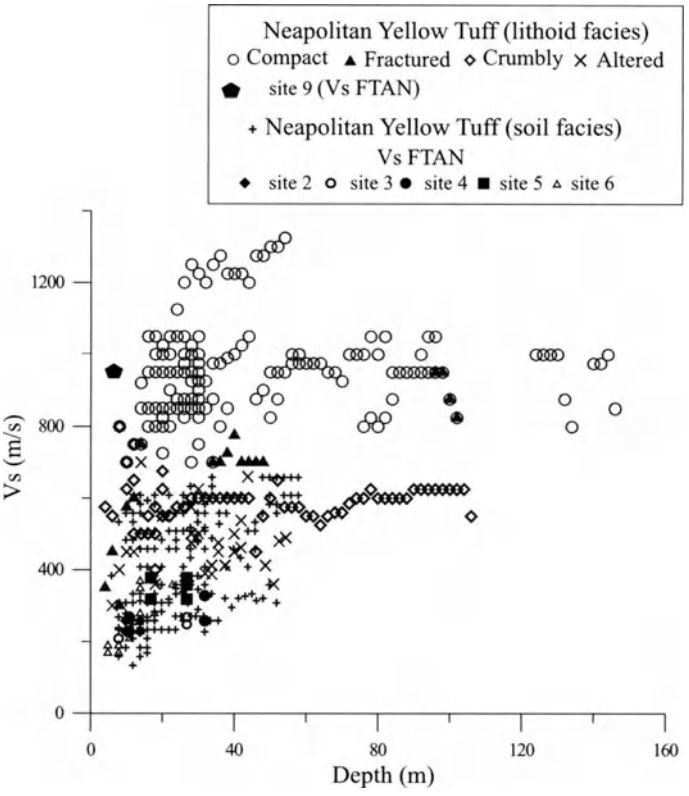

Figure 5
V_S velocities of Neapolitan Yellow Tuff, both soil and lithoid facies. Symbols indicate down- and cross-hole tests (VINALE, 1988; COMUNE DI NAPOLI, 1994), and the velocity range defined by the hedgehog nonlinear inversion of FTAN measurements at sites located in Figure 1.

degrees of lithification, porosity, and percentage of the pumiceous and/or lithic elements. The lowest values of V_S can be assigned to altered tuff which is always present in the shallower part of the tufaceous formation a few meters thick, and especially at the borders or where such bodies taper. Probably even at great depths (100 m), V_S velocities of altered tuff are similar to those of welded pozzolana. Altered NYT tuffs have wide ranges of V_S, from 300 m/s to 700 m/s (Fig. 5). Vacuous tuffs are characterized by the presence of pumiceous elements, and show a variability of V_S between 500 m/s and 650 m/s. The V_S of fractured NYT tuff increase with depth, nonetheless it is reasonable to think that fractures are already closed at 20 m of depth, since values higher than 700 m/s have been measured at those depths (Fig. 5). In compact NYT tuff V_S velocities higher than 700 m/s have been measured and FTAN experiments carried out in a NYT quarry have led to the definition of a V_S of about 950 m/s.

3.3 Vesuvius Products

Vesuvius tuffs and ashes are widespread in the eastern area. Ashes are characterized by V_S velocities in the range 100–450 m/s and such a wide range can be justified by the variable content of pumiceous and lithic elements (Fig. 6). Instead, hedgehog solutions show a narrow range between 150 m/s and 200 m/s.

Vesuvius tuff was erupted similarly in time as NYT tuff. Soil facies, pozzolana, is characterized by V_S ranging 300–600 m/s; lithoid facies, tuff, has V_S values between 650 m/s and 1100 m/s (Fig. 6). The transition V_S value of about 600 m/s from pozzolana to tuff facies is clearly evident. Physical characteristics of Vesuvius deposits are similar to those of NYT deposits and, consequently, the scattering of V_S measurements can be explained, also for these products, in terms of the different percentage of the pumiceous and/or lithic elements, and of welding process and alteration.

3.4 Campanian Ignimbrite Deposit

The oldest products include Campanian Ignimbrite (CI) deposit (33,000 years old), made by gross scoriae in a cinerite matrix. The variability can be clearly associated with the prevalence of scoriae on the cinerite matrix and/or the alteration of cinerite matrix, as it happens, for example, at the borders of the deposit. DH and CH measurements are

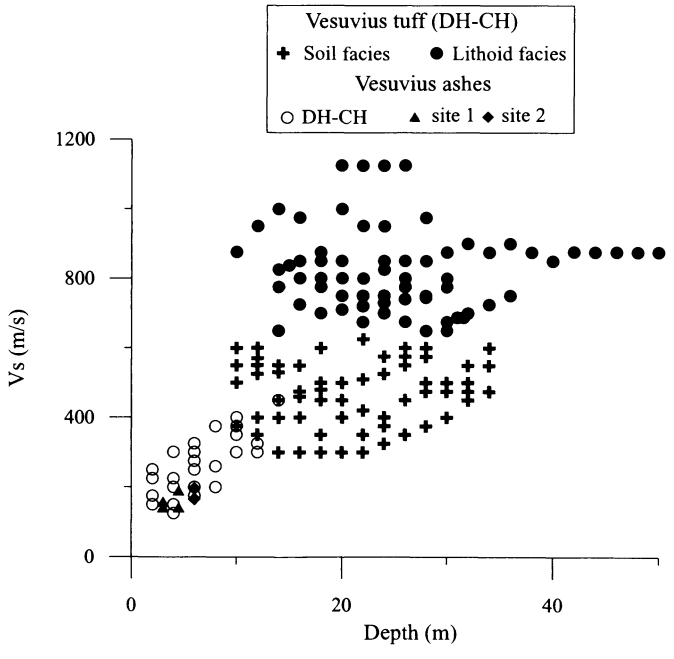

Figure 6

V_S velocities of Vesuvius ashes and tuff, both soil and lithoid facies. Symbols indicate down- and cross-hole tests (VINALE, 1988; COMUNE DI NAPOLI, 1994), and the velocity range defined by the hedgehog nonlinear inversion of FTAN measurements at sites located in Figure 1.

few, and give V_S velocities of 600–700 m/s (Fig. 7). The velocity range defined by the hedgehog nonlinear inversion obtained at two sites is characterized by V_S values of 250–450 m/s, typical of NYT (Fig. 5) and Vesuvius pozzolana (Fig. 6).

3.5 Sandy Deposits

The analysis of the lithostratigraphies has shown the presence of recent and present coastal sands along the coastline, and of eluvial and fluvial-lacustrine deposits with peat layers. In the western area the deposits are mainly constituted by the recent coastal sands and, to a minor extent, by the eluvial products made by reworked volcanic deposits. By contrast, in the eastern sector the outcropping deposits are formed by the ashy and sandy products, mainly of volcanic origin, reworked in marshy environment as testified by the presence of the peat layers (Fig. 2). These products are considered separately because they suffered different sedimentation processes, even though they have similar grain-size characteristics. As a consequence of the sedimentation environment and of the alteration processes, V_S are widely scattered and, on average, V_S of the eluvial and fluvial-lacustrine products are lower than those of the coastal sandy deposits (Figs. 8a–b). Regardless, it would seem that both eluvial and marine sands improve their mechanical behaviour with depth, reaching, at depths greater than 60 m, an average value for V_S of approximately 600 m/s.

4. Hedgehog and DH-CH Velocity Models

In order to test the V_S profiles versus depth obtained from the nonlinear inversion of Rayleigh wave group velocities, a comparison has been performed between FTAN-hedgehog V_S models and nearby DH and CH tests (Fig. 9).

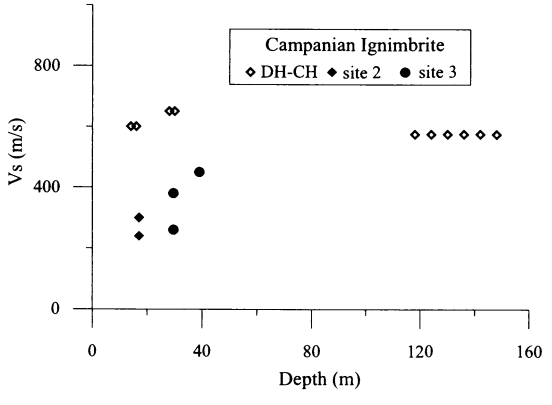

Figure 7
V_S velocities of Campanian Ignimbrite deposit. Symbols indicate down- and cross-hole tests (COMUNE DI NAPOLI, 1994), and the velocity range defined by the hedgehog nonlinear inversion of FTAN measurements at sites located in Figure 1.

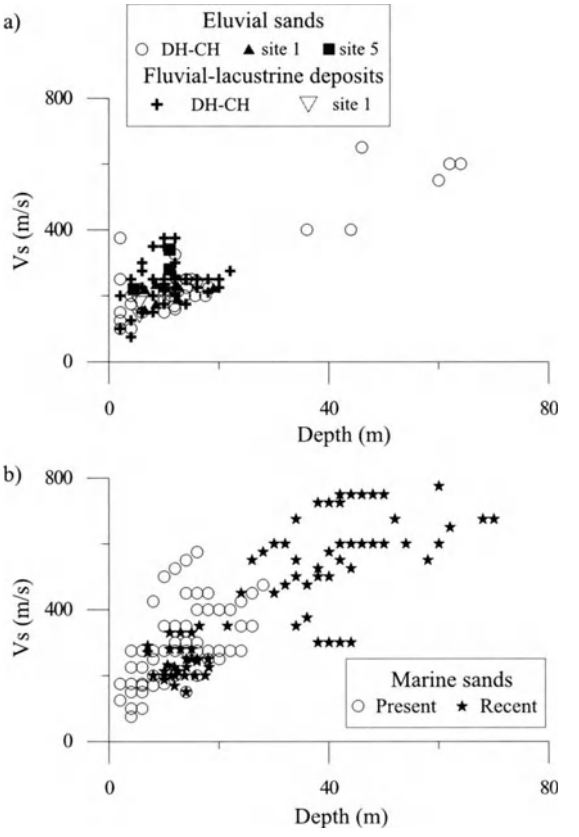

Figure 8
V_S velocities of sands. a) Eluvial sands and fluvial lacustrine deposits; b) Present and recent marine sands. Symbols indicate down- and cross-hole tests (VINALE, 1988; COMUNE DI NAPOLI, 1994), and the velocity range defined by the hedgehog nonlinear inversion of FTAN measurements at sites located in Figure 1.

Site 1 (Fig. 1 and Fig. 9) is located in the eastern sector of Napoli, about 400 m far from the nearest S20 cross-hole test. The subsoil is characterized by eluvial sands and Vesuvius ashes, with peat levels. Even if lateral inhomogeneities have been found in the area, mostly regarding the peat layer, good agreement exists between hedgehog solutions and cross-hole V_S profiles, in particular for the solution with a velocity inversion at 10 m of depth, surely to be attributed to the presence of the peat layer.

Site 2 (Fig. 1 and Fig. 9) is some meters from the building that collapsed during the last earthquake in 1980 (M_s = 6.9). The stratigraphy is characterized by Vesuvius ashes, NYT pozzolana and CI deposit. The agreement of the velocity range defined by the hedgehog nonlinear inversion with the DH test in the S67 drilling, located along the FTAN seismic spreading, is quite good for the uppermost 10 m. Below 10 m of depth, probably due to a bad borehole casing or to the presence of large scoriae or lavic lapilli, there is a large discrepancy.

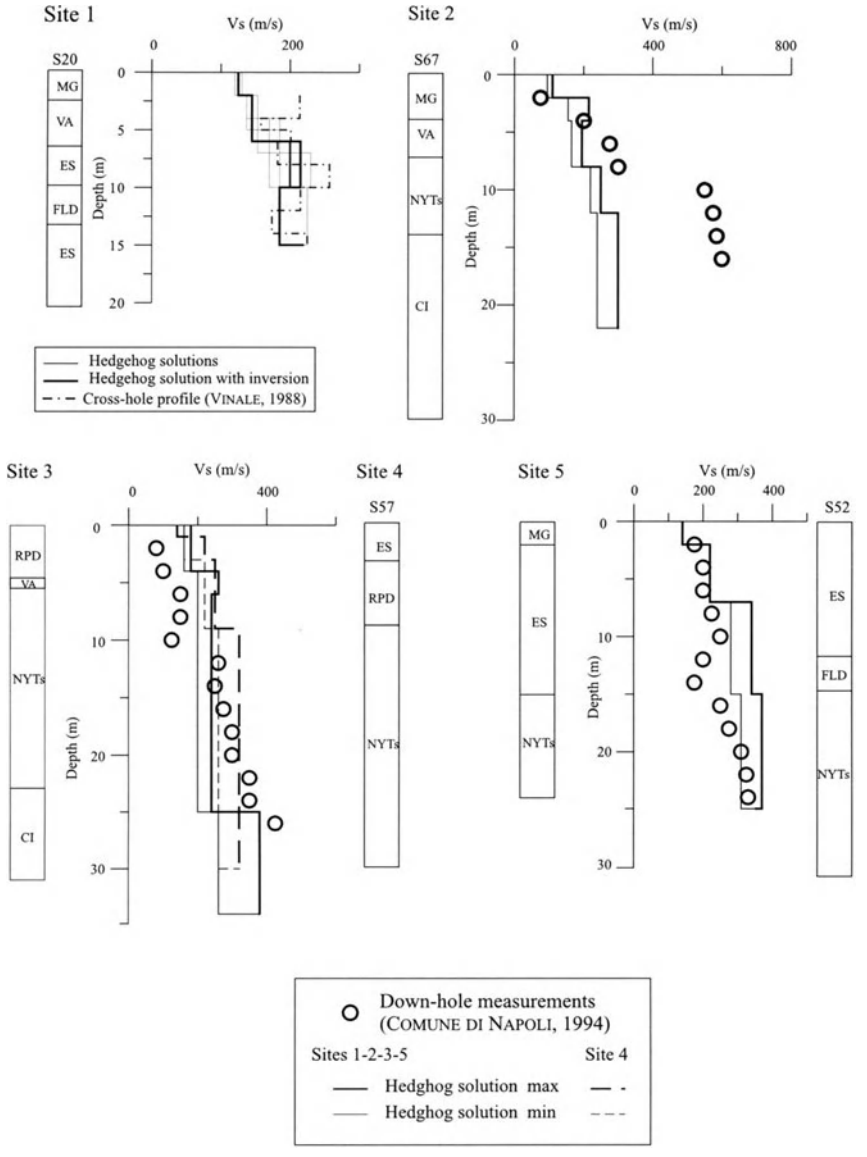

Figure 9
Comparison between down- and cross-hole V_S measurements and the velocity range defined by the hedgehog nonlinear inversion of FTAN measurements obtained at sites located in Figure 1.

Sites 3 and 4 (Fig. 1 and Fig. 9) are 400 m apart and 200 m and 400 m respectively from the drilling S57. The stratigraphy is mainly represented by NYT pozzolana and, at site 3, by CI deposit at depths greater than 20 m. Some discrepancy between the hedgehog velocity range and DH V_S profiles can be observed at depths

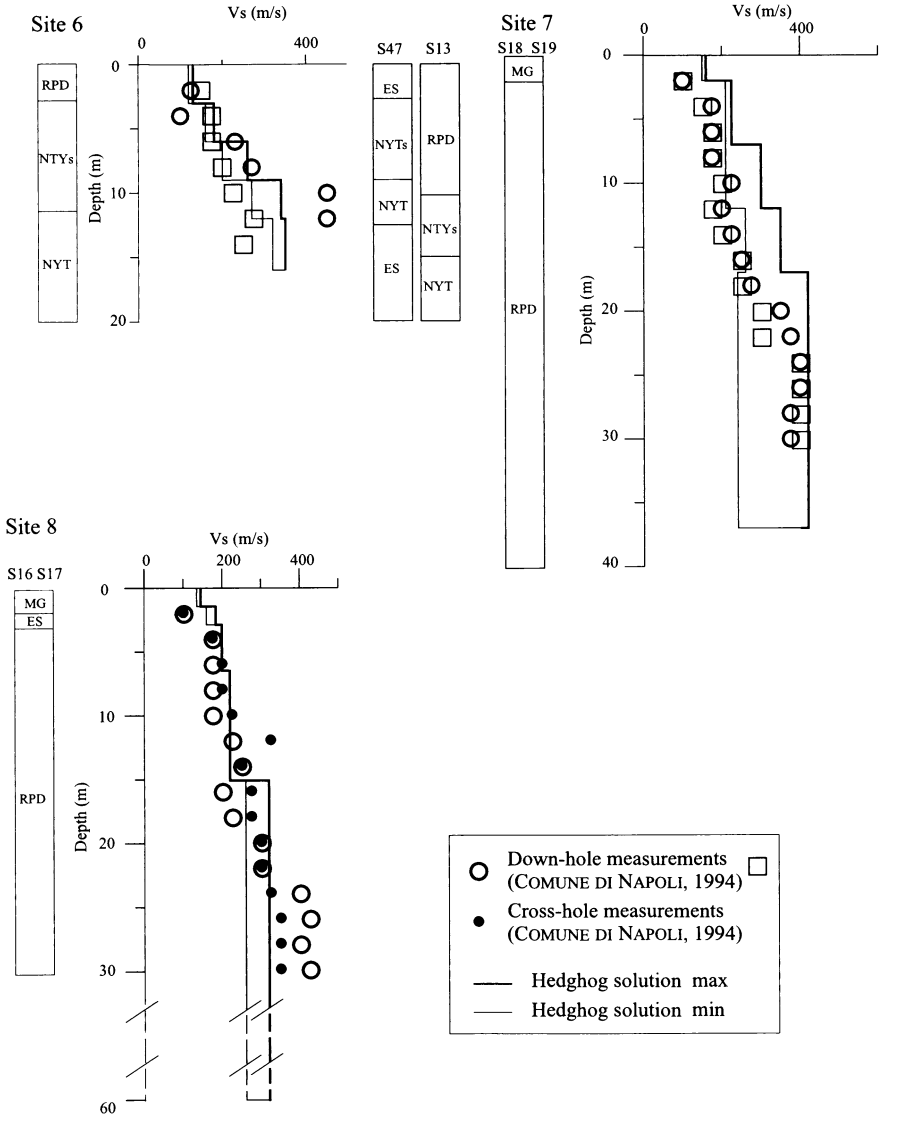

Figure 9
(Contd.)

lower than 10 m, however in the NYT pozzolana there is practically overlap between DH and the corresponding V_S measurements at site 4. Moreover, the hedgehog models obtained at the two sites differ by about 50 m/s, meaning that the NYT pozzolana horizon has the same characteristics.

Site 5 (Fig. 1 and Fig. 9) is characterized by the presence of eluvial sands on NYT pozzolana. The V_S DH measurements at the nearby S52 drilling, about 200 m

distant, are in good agreement with the velocity range defined by the hedgehog nonlinear inversion, except in the peat intercalation zone which is present only at drilling site S52.

Site 6 (Fig. 1 and Fig. 9) has a typical stratigraphy of the historical centre of Napoli, that is, recent pyroclastic products, NYT pozzolana and tuff. The pozzolana thickness changes within few hundred meters, as testified by S43 drilling, 350 m from the surface measurements site. A quite good agreement can be observed between DH and the velocity range defined by the hedgehog nonlinear inversion, except at depths exceeding 10 m.

Sites 7 and 8 (Fig. 1 and Fig. 9) are located in the western sector of Napoli and are both characterized by a cover of recent pyroclastic products. A good agreement exists between DH and the hedgehog velocity range, 400 m apart. The discrepancy between CH and DH measurements in site 8 is indicative of the reliability of such measurements.

5. *Conclusions*

Neapolitan pyroclastic soils can be classified as silty sands or sandy silts, originally deposited with different hardening degrees and textural conditions and often altered by the influence of the meteoric and marine agents, and the anthropic action. As a consequence of such a complex volcanological environment, we may expect soil and lithoid facies, with the lithoid facies depending on the degree of lithification, porosity, and percentage of the pumiceous and/or lithic elements. As a result lateral and vertical inhomogeneities, and consequently, wide scattering of V_S are found (Fig. 10), even for the same formation. Such scattering is particularly evident for DH and CH measurements, and it may be related to the pumiceous and scoriaceous nature of the Neapolitan soil and also to the peculiarity of borehole measurements, that are point measurements, strongly dependent on the casing quality. However, hedgehog solutions obtained from the inversion of FTAN group velocity dispersion curves, are representative of the average V_S over distances of about one hundred meters.

Compact tuff, both Vesuvius and NYT, and fractured NYT tuff, at a depth of 20 m, can be assumed as a soft rock basement characterized by V_S greater than 650 m/s. The same probably applies to eluvial and marine sands at depths greater than 60 m. Consequently, the isobath map of the compact tuffs (Fig. 3) can be considered as the isobath map of the bedrock seismic horizon of Napoli ($V_S > 650$ m/s) for any evaluation of site effects.

Surface measurements of V_S are requested for any evaluation of seismic response analysis at Napoli, and, for this purpose, FTAN measurements are preferable. In fact they give average values, comparable with borehole tests, are not destructive and request the use of just one receiver. All these properties are particularly important in

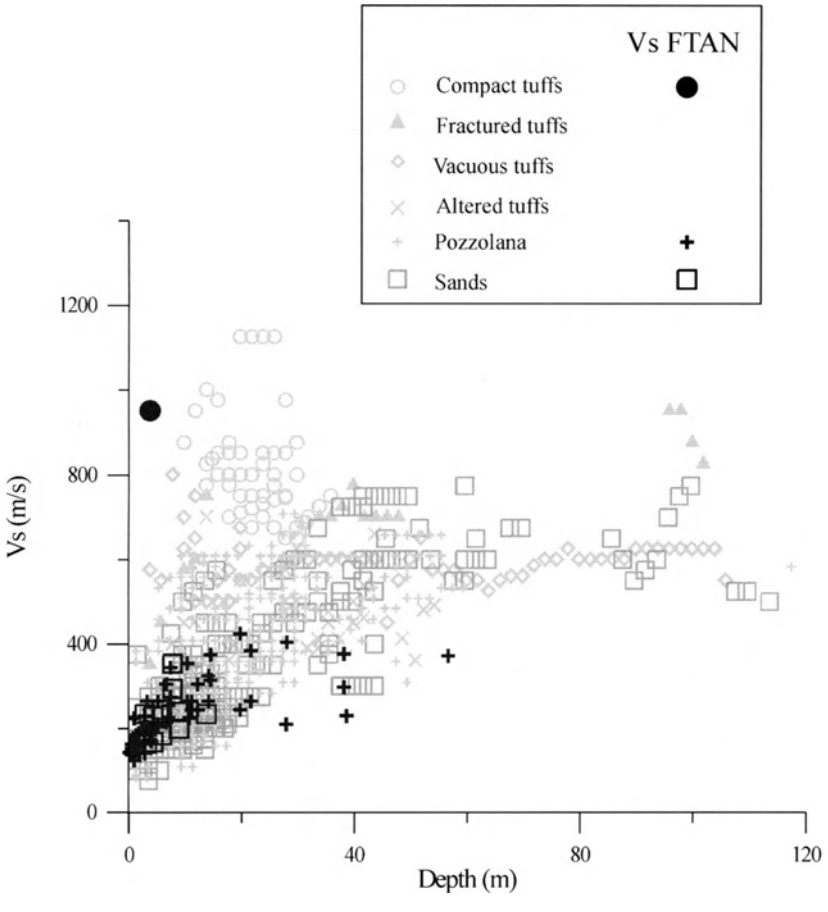

Figure 10
V_S velocities relative to all Neapolitan products obtained by down- and cross-hole measurements (grey symbols) and by the hedgehog nonlinear inversion of FTAN measurements (black symbols).

urban areas. Alternatively, a sound approach might be to make a parametric study of the ground motion by means of modeling (PANZA *et al.*, 2000) that allows us to take into account the wide range of variability of the Neapolitan pyroclastic products already determined (Fig. 10).

Acknowledgements

We thank Dr. B. Garofalo for collecting data and assisting in drawing figures 1 and 3.

References

AA. VV. (1967), *Stratigrafie dei sondaggi riportati nella carta geologico-tecnica della città di Napoli*, A.G.I. VIII Convegno di Geotecnica "Il sottosuolo di Napoli". Appendice A, 86–104.

ALFANO, G. B., and FRIEDLANDER, I. (1929), *La storia del Vesuvio illustrata dai documenti coevi*, Ulm a.d. Donau, K. Holm, 69.

COMUNE DI NAPOLI (1994), *Indagini geologiche per l'adeguamento del P.R.G. alla legge regionale 07.01.1983 n. 9 in difesa del territorio dal rischio sismico.*

DE' GENNARO, M., COLELLA, C., FRANCO, E., and AIELLO, R. (1983), *Italian Zeolites 1. Mineralogical and Technical Features of Neapolitan Yellow Tuff,* Industrial Minerals *186*, 47–53.

GAROFALO, B. (2000), *Misure Delle Velocità Sismiche di Taglio Nell'area Occidentale Napoletana (Pianura-Soccavo).* Degree Thesis.

LEVSHIN, A.L., RATNIKOVA, L., and BERGER, J. (1992), *Peculiarities of Surface Wave Propagation across Central Eurasia*, Bull. Seismol. Soc. Am. *82*, 2464–2493.

NAZARIAN, S., and STOKOE II, K. H. (1985), *Use of Rayleigh Waves in Liquefaction Studies*, Proceedings, Measurement and Use of Shear Wave Velocity for Evaluation Dynamic Soil Properties, held in Denver, Colorado, R.D. Woods, Ed., ASCEE, New York, NY, 1–17.

NUNZIATA, C., MELE, R., and NATALE, M. (1999a), *Shear-wave Velocities of the Campi Flegrei-Neapolitan Deposits and the Primary Influencing Factors,* Engineering Geology *54*, 299–312.

NUNZIATA, C., COSTA, G., NATALE, M., and PANZA, G. F. (1999b), *FTAN and SASW methods to evaluate V_S of Neapolitan pyroclastic soils.* In *Earthquake Geotechnical Engineering* (Balkema), *1*, 15–19.

NUNZIATA C., CHIMERA G., NATALE M., and PANZA G. F. (2001a), *V_S Velocities of Shallow Soils at Fabriano*, Rivista Italiana di Geotecnica XXXV *2*, 98–106.

NUNZIATA C., CHIMERA G., NATALE M., and PANZA G.F. (2001b), *Seismic Characterization of Shallow Soils at Nocera Umbra, for Seismic Response Analysis*, Rivista Italiana di Geotecnica XXXV *4*, 31–38.

ORSI, G., DE VITA, S., and DI VITO, M. (1996), *The Restless, Resurgent Campi Flegrei Nested Caldera (Italy): Constraints on its Evolution and Configuration*, J. Volcanol. Geotherm. Res. *74*, 179–214.

PANZA, G. F. (1981), *The resolving power of seismic surface wave with respect to crust and upper mantle structural models.* In *The Solution of the Inverse Problem in Geophysical Interpretation* (R. Cassinis, ed. Plenum Press 1981) 39–77.

PANZA, G. F., ROMANELLI, F., and VACCARI, F. (2000), *Seismic Wave Propagation in Laterally Heterogeneous Anelastic Media: Theory and Applications to the Seismic Zonation,* Advances in Geophysics, Academic Press, 43, 1–95.

ROSI, M., and SBRANA, A. (1987), *Phlegrean Fields. Quaderni de "La Ricerca Scientifica", 114 (8)* C.N.R. Prog. Fin. "Geod.," 1–175.

SCARPATI, C., COLE, P., and PERROTTA, A. (1993), *The Neapolitan Yellow Tuff – A Large Volume Multiphase Eruption from Campi Flegrei, Southern Italy*, Bull. Volcanol. *55*, 343–356.

VALYUS, V. P., KEILIS-BOROK, V. I., and LEVSHIN, A. L. (1968), *Determination of the Velocity Profile of the Upper Mantle in Europe,* Nauk SSR 1, 185 (*8*), 564–567.

VINALE, F. (1988), *Microzonazione sismica di un'area campione di Napoli*, Rivista Italiana di Geotecnica, vol. XXII, *3*, 141–162.

(Received May 20, 2002, accepted November 8, 2002)